

**2003 NEHRP
Recommended Provisions**
for Seismic Regulations for New Buildings and Other
Structures and Accompanying Commentary and Maps
FEMA 450-CD – 2003 Edition/June 2004



FEMA



NEHRP Recommended Provisions: Design Examples

FEMA 451 - August 2006



FEMA





of the National Institute of Building Sciences

NEHRP Recommended Provisions: Design Examples

FEMA 451 - August 2006

**Prepared by the
Building Seismic Safety Council
for the
Federal Emergency Management Agency
of the Department of Homeland Security**

National Institute of Building Sciences
Washington, D.C.

NOTICE: Any opinions, findings, conclusions, or recommendations expressed in this publication do not necessarily reflect the views of the Federal Emergency Management Agency. Additionally, neither FEMA nor any of its employees make any warranty, expressed or implied, nor assume any legal liability or responsibility for the accuracy, completeness, or usefulness of any information, product, or process included in this publication.

The opinions expressed herein regarding the requirements of the *International Residential Code* do not necessarily reflect the official opinion of the International Code Council. The building official in a jurisdiction has the authority to render interpretation of the code.

This report was prepared under Contract EMW-1998-CO-0419 between the Federal Emergency Management Agency and the National Institute of Building Sciences.

For further information on the Building Seismic Safety Council, see the Council's website -- www.bssconline.org -- or contact the Building Seismic Safety Council, 1090 Vermont, Avenue, N.W., Suite 700, Washington, D.C. 20005; phone 202-289-7800; fax 202-289-1092; e-mail bssc@nibs.org.

FOREWORD

One of the goals of the Department of Homeland Security's Federal Emergency Management Agency (FEMA) and the National Earthquake Hazards Reduction Program (NEHRP) is to encourage design and building practices that address the earthquake hazard and minimize the resulting risk of damage and injury. The 2003 edition of the *NEHRP Recommended Provisions for Seismic Regulation of New Buildings and Other Structures* and its *Commentary* affirmed FEMA's ongoing support to improve the seismic safety of construction in this country. The *NEHRP Recommended Provisions* serves as the basis for the seismic requirements in the ASCE 7 *Standard Minimum Design Loads for Buildings and Other Structures* as well as both the *International Building Code* and *NFPA 5000 Building Construction Safety Code*. FEMA welcomes the opportunity to provide this material and to work with these codes and standards organizations.

This product provides a series of design examples that will assist the user of the *NEHRP Recommended Provisions*. This material will also be of assistance to those using the ASCE 7 standard and the models codes that reference the standard.

FEMA wishes to express its gratitude to the authors listed elsewhere for their significant efforts in preparing this material and to the BSSC Board of Direction and staff who made this possible. Their hard work has resulted in a guidance product that will be of significant assistance for a significant number of users of the nation's seismic building codes and their reference documents.

*Department of Homeland Security/
Federal Emergency Management Agency*

PREFACE

This volume of design examples is intended for those experienced structural designers who are relatively new to the field of earthquake-resistant design and to application of seismic requirements of the *NEHRP (National Earthquake Hazards Reduction Program) Recommended Provisions for Seismic Regulations for New Buildings and Other Structures* and, by extension, the model codes and standards because the *Provisions* are the source of seismic design requirements in most of those documents including ASCE 7, *Standard Minimum Design Loads for Buildings and Other Structures*; the *International Building Code*; and the *NFPA 5000 Building Construction and Safety Code*.

This compilation of design examples is an expanded version of an earlier document (entitled *Guide to Application of the NEHRP Recommended Provisions*, FEMA 140) and reflects the expansion in coverage of the *Provisions* and the expanding application of the *Provisions* concepts in codes and standards. The widespread use of the *NEHRP Recommended Provisions* signals the success of the Federal Emergency Management Agency and Building Seismic Safety Council efforts to ensure that the nation's building codes and standards reflect the state of the art of earthquake-resistant design.

In developing this set of design examples, the BSSC first decided on the types of structures, types of construction and materials, and specific structural elements that needed to be included to provide the reader with at least a beginning grasp of the impact the *NEHRP Recommended Provisions* has on frequently encountered design problems. Some of the examples draw heavily on a BSSC trial design project conducted prior to the publication of the first edition of the *NEHRP Recommended Provisions* in 1985 but most were created by the authors to illustrate issues not covered in the trial design program. Further, the authors have made adjustments to those examples drawn from the trial design program as necessary to reflect the 2000 Edition of the *NEHRP Recommended Provisions*. Finally, because it obviously is not possible to present in a volume of this type complete building designs for all the situations and features that were selected, only portions of designs have been used.

The BSSC is grateful to all those individuals and organizations whose assistance made this set of design examples a reality:

- James Robert Harris, J. R. Harris and Company, Denver, Colorado, who served as the project manager, and Michael T. Valley, Magnusson Klemencic Associates, Seattle, Washington, who served as the technical editor of this volume
- The chapter authors – Robert Bachman, Finley A. Charney, Richard Drake, Charles A. Kircher, Teymour Manzouri, Frederick R. Rutz, Peter W. Somers, Harold O. Sprague, Jr., and Gene R. Stevens – for their unstinting efforts

- Greg Deierlein, J. Daniel Dolan, S. K. Ghosh, Robert D. Hanson, Neil Hawkins, and Thomas Murray for their insightful reviews
- William Edmands and Cambria Lambertson for their hard work behind the scenes preparing figures

Special thanks go to Mike Valley and Peter Somers for their work annotating the design examples to reflect the 2003 edition of the *Provisions* and updated versions of other standards referenced in the 2003 version. The BSSC Board is also grateful to FEMA Project Officer Michael Mahoney for his support and guidance and to Claret Heider and Carita Tanner of the BSSC staff for their efforts preparing this volume for publication and issuance as a CD-ROM.

Jim. W. Sealy, Chairman, BSSC Board of Direction

TABLE OF CONTENTS

1. FUNDAMENTALS by James Robert Harris, P.E., Ph.D.	1-1
1.1 Earthquake Phenomena	1-2
1.2 Structural Response to Ground Shaking	1-3
1.3 Engineering Philosophy	1-13
1.4 Structural Analysis	1-13
1.5 Nonstructural Elements of Buildings	1-15
1.6 Quality Assurance	1-16
2. GUIDE TO USE OF THE <i>PROVISIONS</i> by Michael Valley, P.E.	2-1
3 STRUCTURAL ANALYSIS by Finley A. Charney, Ph.D., P.E.	3-1
3.1 Irregular 12-Story Steel Frame Building, Stockton, California	3-3
3.1.1 Introduction	3-3
3.1.2 Description of Structure	3-3
3.1.3 <i>Provisions</i> Analysis Parameters	3-6
3.1.4 Dynamic Properties	3-7
3.1.5 Equivalent Lateral Force Analysis	3-11
3.1.6 Modal-Response-Spectrum Analysis	3-25
3.1.7 Modal-Time-History Analysis	3-35
3.1.8 Comparison of Results from Various Methods of Analysis	3-43
3.2 Six-Story Steel Frame Building, Seattle, Washington	3-51
3.2.1 Description of Structure	3-51
3.2.2 Loads	
3.2.3 Preliminaries to Main Structural Analysis	
3.2.4 Description of Model Used for Detailed Structural Analysis	3-65
3.2.5 Static Pushover Analysis	3-87
3.2.6 Time-History Analysis	3-115
3.2.7 Summary and Conclusions	3-143
4. FOUNDATION ANALYSIS AND DESIGN by Michael Valley, P.E.	4-1
4.1 Shallow Foundations for a Seven -Story Office Building, Los Angeles, California	4-4
4.1.1 Basic Information	4-4
4.1.2 Design for Gravity Loads	4-8
4.1.3 Design for Moment-Resisting Frame System	4-11
4.1.4 Design for Centrally Braced Frame System	4-17
4.1.5 Cost Comparison	4-24
4.2 Deep Foundations for a 12-Story Building, Seismic Design Category D	4-26
4.2.1 Basic Information	4-26
4.2.2 Pile Analysis, Design, and Detailing	4-34
4.2.3 Other Considerations	4-47

5. STRUCTURAL STEEL DESIGN by James R. Harris, P.E., Ph.D., Frederick R. Rutz, P.E., Ph.D., and Teymour Manzouri, P.E., Ph.D.	5-1
5.1 Industrial High-Clearance Building, Astoria, Oregon	5-3
5.1.1 Building Description	5-3
5.1.2 Design Parameters	5-6
5.1.3 Structural Design Criteria	5-7
5.1.4 Analysis	5-16
5.1.5 Proportioning and Details	5-16
5.2 Seven-Story Office Building, Los Angeles, California	5-29
5.2.1 Building Description	5-29
5.2.2 Basic Requirements	5-32
5.2.3 Structural Design Criteria	5-33
5.2.4 Analysis	5-38
5.2.5 Cost Comparison	5-74
5.3 Two-Story Building, Oakland, California	5-75
5.3.1 Building Description	5-75
5.3.2 Method	5-76
5.3.3 Analysis	5-77
5.3.4 Design of Eccentric Bracing	5-78
6. REINFORCED CONCRETE by Finley A. Charney, Ph.D., P.E.	6-1
6.1 Development of Seismic Loads and Design Requirements	6-6
6.1.1 Seismicity	6-6
6.1.2 Structural Design Requirements	6-7
6.1.3 Structural Configuration	6-8
6.2 Determination of Seismic Forces	6-8
6.2.1 Approximate Period of Vibration	6-9
6.2.2 Building Mass	6-10
6.2.3 Structural Analysis	6-11
6.2.4 Accurate Periods from Finite Element Analysis	6-12
6.2.5 Seismic Design Base Shear	6-14
6.2.6 Development of Equivalent Lateral Forces	6-15
6.3 Drift and P-delta Effects	6-19
6.3.1 Direct Drift and P-delta Check for the Berkeley Building	6-19
6.3.2 Test for Torsional Irregularity for Berkeley Building	6-23
6.3.3 Direct Drift and P-delta Check for the Honolulu Building	6-24
6.3.4 Test for Torsional Irregularity for the Honolulu Building	6-28
6.4 Structural Design of the Berkeley Building	6-28
6.4.1 Material Properties	6-28
6.4.2 Combination of Load Effects	6-28
6.4.3 Comments on the Structure's Behavior Under E-W Loading	6-31
6.4.4 Analysis of Frame-Only Structure for 25 Percent of Lateral Load	6-32
6.4.5 Design of Frame Members for the Berkeley Building	6-36
6.5 Structural Design of the Honolulu Building	6-76
6.5.1 Material Properties	6-77
6.5.2 Combination of Load Effects	6-77
6.5.3 Accidental Torsion and Orthogonal Loading (Seismic Versus Wind)	6-78
6.5.4 Design and Detailing of Members of Frame 1	6-80

6.5.5 Design of Members of Frame 3	6-92
7. PRECAST CONCRETE DESIGN by Gene R. Stevens, P.E. and James Robert Harris, P.E., Ph.D.	7-1
7.1 Horizontal Diaphragms	7-5
7.1.1 Untopped Precast Concrete Units for Five-Story Masonry Buildings Located in Birmingham, Alabama, and New York, New York	7-5
7.1.2 Topped Precast Concrete Units for Five-Story Masonry Building, Los Angeles, California (See <i>Guide</i> Sec. 9.2)	7-22
7.2 Three-Story Office Building With Precast Concrete Shear Walls	7-30
7.2.1 Building Description	7-30
7.2.2 Design Requirements	7-31
7.2.3 Load Combinations	7-34
7.2.4 Seismic Force Analysis	7-34
7.2.5 Proportioning and Detailing	7-37
7.3 One-Story Precast Shear Wall Building	7-49
7.3.1 Building Description	7-49
7.3.2 Design Requirements	7-51
7.3.3 Load Combinations	7-53
7.3.4 Seismic Force Analysis	7-54
7.3.5 Proportioning and Detailing	7-56
8. COMPOSITE STEEL AND CONCRETE by James Robert Harris, P.E., Ph.D. and Frederick R. Rutz, P.E., Ph.D.	8-1
8.1 Building Description	8-3
8.2 Summary of Design Procedure for Composite Partially Restrained Moment Frame System	8-6
8.3 Design Requirements	8-7
8.3.1 <i>Provisions</i> Parameters	8-7
8.3.2 Structural Design Considerations Per the <i>Provisions</i>	8-7
8.3.3 Building Weight and Base Shear Summary	8-8
8.4 Details of the PRC Connection and System	8-9
8.4.1 Connection <i>M-q</i> Relationships	8-9
8.4.2 Connection Design and Connection Stiffness Analysis	8-11
8.5 Analysis	8-19
8.5.1 Load Combinations	8-19
8.5.2 Drift and P-delta	8-21
8.5.3 Required and Provided Strength	8-22
8.6 Details of the Design	8-23
8.6.1 Overview	8-23
8.6.2 Width-Thickness Ratios	8-24
8.6.3 Column Axial Strength	8-24
8.6.4 Details of the Joint	8-25
9 MASONRY by James Robert Harris, P.E., Ph.D., Frederick R. Rutz, P.E., Ph.D. and Teymour Manzouri, P.E., Ph.D.	9-1
9.1 Warehouse with Masonry Walls and Wood Roof, Los Angeles, California	9-3
9.1.1 Building Description	9-3
9.1.2 Design Requirements	9-4

9.1.3	Load Combinations	9-6
9.1.4	Seismic Forces	9-9
9.1.5	Longitudinal Walls	9-10
9.1.6	Transverse Walls	9-25
9.1.7	Bond Beam	9-40
9.1.8	In-Plane Deflection	9-40
9.2	Five-story Masonry Residential Buildings in Birmingham, Alabama; New York, New York; and Los Angeles, California	9-42
9.2.1	Building Description	9-42
9.2.2	Design Requirements	9-44
9.2.3	Load Combinations	9-47
9.2.4	Seismic Design for Birmingham 1	9-49
9.2.5	Seismic Design for New York City	9-65
9.2.6	Birmingham 2 Seismic Design	9-77
9.2.7	Seismic Design for Los Angeles	9-84
9.3.1	Building Description	9-96
9.3.2	Design Requirements	9-97
9.3.3	Seismic Force Analysis	9-100
9.3.4	Deflections	9-126
9.3.5	Out-of-Plane Forces	9-131
9.3.6	Orthogonal Effects	9-132
9.3.7	Anchorage	9-132
9.3.8	Diaphragm Strength	9-132
10	WOOD DESIGN by Peter W. Somers, P.E. and Michael Valley, P.E.	10-1
10.1	Three-story Wood Apartment Building; Seattle, Washington	10-3
10.1.1	Building Description	10-3
10.1.2	Basic Requirements	10-5
10.1.3	Seismic Force Analysis	10-10
10.1.4	Basic Proportioning	10-16
10.2	Warehouse with Masonry Walls and Wood Roof, Los Angeles, California	10-44
10.2.1	Building Description	10-44
10.2.2	Basic Requirements	10-45
10.2.3	Seismic Force Analysis	10-46
10.2.4	Basic Proportioning of Diaphragm Elements	10-47
11	SEISMICALLY ISOLATED STRUCTURES by Charles A. Kircher, P.E., Ph.D.	11-1
11.1	Background and Basic Concepts	11-4
11.1.1	Types of Isolation Systems	11-5
11.1.2	Definition of Elements of an Isolated Structure	11-5
11.1.3	Design Approach	11-6
11.1.4	Effective Stiffness and Effective Damping	11-7
11.2	Criteria Selection	11-7
11.3	Equivalent Lateral Force Procedure	11-9
11.3.1	Isolation System Displacement	11-9
11.3.2	Design Forces	11-11
11.4	Dynamic Lateral Response Procedure	11-13
11.4.1	Minimum Design Criteria	11-13

11.4.2	Modeling Requirements	11-14
11.4.3	Response Spectrum Analysis	11-16
11.4.4	Time History Analysis	11-16
11.5	Emergency Operations Center Using Elastomeric Bearings, San Francisco, California ...	11-17
11.5.1	System Description	11-17
11.5.2	Basic Requirements	11-20
11.5.3	Seismic Force Analysis	11-27
11.5.4	Preliminary Design Based on the ELF Procedure	11-29
11.5.5	Design Verification Using Nonlinear Time History Analysis	11-41
11.5.6	Design and Testing Criteria for Isolator Units	11-45
12	NONBUILDING STRUCTURE DESIGN by Harold O. Sprague Jr., P.E.	12-1
12.1	Nonbuilding Structures Versus Nonstructural Components	12-2
12.1.1	Nonbuilding Structure	12-4
12.1.2	Nonstructural Component	12-4
12.2	Pipe Rack, Oxford, Mississippi	12-5
12.2.1	Description	12-5
12.2.2	<i>Provisions</i> Parameters	12-6
12.2.3	Design in the Transverse Direction	12-7
12.2.4	Design in the Longitudinal Direction	12-9
12.3	Steel Storage Rack, Oxford, Mississippi	12-11
12.3.1	Description	12-11
12.3.2	<i>Provisions</i> Parameters	12-12
12.3.3	Design of the System	12-12
12.4	Electric Generating Power Plant, Merna, Wyoming	12-16
12.4.1	Description	12-16
12.4.2	<i>Provisions</i> Parameters	12-17
12.4.3	Design in the North-South Direction	12-18
12.4.4	Design in the East-West Direction	12-19
12.5	Pier/Wharf Design, Long Beach, California	12-19
12.5.1	Description	12-19
12.5.2	<i>Provisions</i> Parameters	12-20
12.5.3	Design of the System	12-21
12.6	Tanks and Vessels, Everett, Washington	12-22
12.6.1	Flat-Bottom Water Storage Tank	12-23
12.6.2	Flat-bottom Gasoline Tank	12-26
12.7	Emergency Electric Power Substation Structure, Ashport, Tennessee	12-28
12.7.1	Description	12-29
12.7.2	<i>Provisions</i> Parameters	12-30
12.7.3	Design of the System	12-30
13	DESIGN FOR NONSTRUCTURAL COMPONENTS by Robert Bachman, P.E., and Richard Drake, P.E.	13-1
13.1	Development and Background of the Provisions for Nonstructural Components	13-2
13.1.1	Approach to Nonstructural Components	13-2
13.1.2	Force Equations	13-3
13.1.3	Load Combinations and Acceptance Criteria	13-4
13.1.4	Component Amplification Factor	13-4

13.1.5	Seismic Coefficient at Grade	13-5
13.1.6	Relative Location Factor	13-5
13.1.7	Component Response Modification Factor	13-5
13.1.8	Component Importance Factor	13-5
13.1.9	Accommodation of Seismic Relative Displacements	13-6
13.1.10	Component Anchorage Factors and Acceptance Criteria	13-7
13.1.11	Construction Documents	13-7
13.2	Architectural Concrete Wall Panel	13-7
13.2.1	Example Description	13-7
13.2.2	Design Requirements	13-9
13.2.3	Spandrel Panel	13-11
13.2.4	Column Cover	13-17
13.2.5	Additional Design Considerations	13-18
13.3	HVAC Fan Unit Support	13-19
13.3.1	Example Description	13-19
13.3.2	Design Requirements	13-20
13.3.3	Direct Attachment to Structure	13-21
13.3.4	Support on Vibration Isolation Springs	13-24
13.3.5	Additional Considerations for Support on Vibration Isolators	13-29
13.4	Analysis of Piping Systems	13-30
13.4.1	ASME Code Allowable Stress Approach	13-30
13.4.2	Allowable Stress Load Combinations	13-32
13.4.3	Application of the <i>Provisions</i>	13-33

Appendix A	THE BUILDING SEISMIC SAFETY COUNCIL	A-1
------------	-------------------------------------	-----

LIST OF CHARTS, FIGURES, AND TABLES

Figure 1.2-1	Earthquake ground acceleration in epicentral regions	1-4
Figure 1.2-2	Holiday Inn ground and building roof motion during the M6.4 1971 San Fernando earthquake	1-5
Figure 1.2-3	Response spectrum of North-South ground acceleration recorded at the Holiday Inn, approximately 5 miles from the causative fault in the 1971 San Fernando earthquake	1-6
Figure 1.2-4	Averaged spectrum	1-7
Figure 1.2-5	Force controlled resistance versus displacement controlled resistance	1-9
Figure 1.2-6	Initial yield load and failure load for a ductile portal frame	1-10
Chart 2.1	Overall Summary of Flow	2-3
Chart 2.2	Scope of Coverage	2-4
Chart 2.3	Application to Existing Structures	2-5
Chart 2.4	Basic Requirements	2-6
Chart 2.5	Structural Design	2-7
Chart 2.6	Equivalent Lateral Force	2-8
Chart 2.7	Soil-Structure Interaction	2-9
Chart 2.8	Modal Analysis	2-10
Chart 2.9	Response History Analysis	2-11
Chart 2.10	Seismically Isolated Structures	2-12

Chart 2.11	Strength Requirements	2-13
Chart 2.12	Deformation Requirements	2-14
Chart 2.13	Design and Detailing Requirements	2-15
Chart 2.14	Steel Structures	2-16
Chart 2.15	Concrete Structures	2-17
Chart 2.16	Precast Concrete Structures	2-18
Chart 2.17	Composite Steel and Concrete Structures	2-19
Chart 2.18	Masonry Structures	2-20
Chart 2.19	Wood Structures	2-21
Chart 2.20	Nonbuilding Structures	2-22
Chart 2.21	Foundations	2-23
Chart 2.22	Architectural, Mechanical, and Electrical Components	2-24
Chart 2.23	Quality Assurance	2-25
Table 2-1	Navigating Among the 2000 and 2003 <i>NEHRP Recommended Provisions</i> and ASCE 7	2-26
Figure 3.1-1	Various floor plans of 12-story Stockton building	3-4
Figure 3.1-2	Sections through Stockton building	3-5
Figure 3.1-3	Three-dimensional wire-frame model of Stockton building	3-6
Table 3.1-1	Area Masses on Floor Diaphragms	3-8
Table 3.1-2	Line Masses on Floor Diaphragms	3-9
Figure 3.1-4	Key Diagram for Computation of Floor Mass	3-9
Table 3.1-3	Floor Mass, Mass Moment of Inertia, and Center Mass Locations	3-10
Figure 3.1-5	Computed ELF total acceleration response system spectrum	3-12
Figure 3.1-6	Computed ELF relative displacement response spectrum	3-13
Table 3.1-4	Equivalent Lateral Forces for Building Responses in X and Y Directions	3-14
Figure 3.1-7	Amplification of accidental torsion	3-15
Table 3.1-5	Computation for Torsional Irregularity with ELF Loads Acting in X Direction	3-16
Table 3.1-6	Computation for Torsional Irregularity with ELF Loads Acting in Y Direction	3-16
Table 3.1-7	ELF Drift for Building Responding in X Direction	3-17
Table 3.1-8	ELF Drift for Building Responding in Y Direction	3-18
Table 3.1-9	Rayleigh Analysis for X-Direction Period of Vibration	3-19
Table 3.1-10	Rayleigh Analysis for Y-Direction Period of Vibration	3-20
Table 3.1-11	Computation of P-delta Effects for X-Direction Response	3-21
Figure 3.1-8	Basic load causes used in ELF analysis	3-24
Table 3.1-12	Seismic and Gravity Load Combinations as Run on SAP 2000	3-25
Figure 3.1-9	Seismic shears in girders (kips) as computed using ELF analysis	3-26
Figure 3.1-10	Mode shapes as computed using SAP2000	3-26
Table 3.1-13	Computed Periods and Directions Factors	3-29
Table 3.1-14	Computed Periods and Effective Mass Factors	3-29
Table 3.1-15	Response Structure Coordinates	3-30
Table 3.1-16	Story Shears from Modal-Response-Spectrum Analysis	3-32
Table 3.1-17	Response Spectrum Drift for Building Responding in X Direction	3-33
Table 3.1-18	Spectrum Response Drift for Building Responding in Y Direction	3-33
Table 3.1-19	Computation of P-delta Effects for X-Direction Response	3-34
Figure 3.1-12	Load combinations from response-spectrum analysis	3-35
Figure 3.1-13	Seismic shears in girders (kips) as computed using response-spectrum analysis	3-36
Table 3.1-20	Seattle Ground Motion Parameters	3-37

Figure 3.1-14	Unscaled SRSS of spectra of ground motion pairs	3-38
Figure 3.1-15	Ratio average scaled SRSS spectrum to <i>Provisions</i> spectrum	3-39
Table 3.1-21	Result Maxima from Time-History Analysis	3-40
Table 3.1-22	Result Maxima from Time-History Analysis	3-40
Table 3.1-23	Time-History Drift for Building Responding in X Direction to Motion	3-42
Table 3.1-24	Scaled Inertial Force and Story Shear Envelopes from Analysis A00X	3-42
Table 3.1-25	Computation of P-delta Effects for X-Direction Response	3-42
Figure 3.1-16	Combinations 1 and 2, beam shears (kips) as computed using time-history analysis	3-43
Figure 3.1-17	All combinations, beam shears (kips) as computed using time history analysis	3-44
Table 3.1-26	Summary of Results from Various Methods of Analysis: Story Shear	3-45
Table 3.1-27	Summary of Results from Various Methods of Analysis: Story Drift	3-46
Table 3.1-28	Summary of Results from Various Methods of Analysis: Beam Shear	3-47
Figure 3.2-1	Plan of structural system	3-52
Figure 3.2-2	Elevation of structural system	3-53
Table 3.2-1	Member Sizes Used in N-S Moment Frames	3-53
Table 3.2-2	Gravity Loads on Seattle Building	3-53
Figure 3.2-3	Element loads used in analysis	3-56
Table 3.2-3	Equivalent Lateral Forces for Seattle Building Responding in N-S Directions	3-58
Figure 3.2-4	Simple wire frame model used for preliminary analysis	3-60
Table 3.2-4	Results of Preliminary Analysis Using P-delta Effects	3-62
Table 3.2-5	Results of Preliminary Analysis Including P-delta Effects	3-62
Table 3.2-6	Periods of Vibration From Preliminary Analysis	3-62
Figure 3.2-5	Demand-to-capacity ratios for elements from analysis with P-delta effects included	3-63
Table 3.2-7	Lateral Strength on Basis of Rigid-Plastic Mechanism	3-65
Figure 3.2-6	Plastic mechanism for computing lateral strength	3-66
Figure 3.2-7	Detailed analytical model of 6-story frame	3-67
Figure 3.2-8	Model of girder and panel zone region	3-67
Figure 3.2-9	A compound node and attached spring	3-68
Figure 3.2-10	Krawinkler beam-column joint model	3-69
Figure 3.2-11	Column flange component of panel zone resistance	3-71
Figure 3.2-12	Column web component of panel zone resistance	3-72
Figure 3.2-13	Force-deformation behavior of panel zone region	3-73
Figure 3.4-14	Transforming shear deformation to rotational deformation in the Krawinkler model	3-74
Table 3.8-8	Properties for the Krawinkler Beam-Column Joint Model	3-75
Figure 3.2-15	Assumed stress-strain curve for modeling girders	3-78
Figure 3.2-16	Moment curvature diagram for W27x94 girder	3-79
Figure 3.2-17	Developing moment-deflection diagrams for a typical girder	3-80
Figure 3.2-18	Development of equations for deflection of moment-deflection curves	3-82
Table 3.2-9	Girder Properties as Modeled in DRAIN	3-84
Figure 3.2-19	Moment-deflection curve for W27x94 girder	3-85
Figure 3.2-20	Development of plastic hinge properties for the W27x97 girder	3-86
Figure 3.2-21	Yield surface used for modeling columns	3-87
Table 3.2-10	Lateral Load Patterns Used in Nonlinear Static Pushover Analysis	3-89
Figure 3.2-22	Two base shear components of pushover response	3-90
Figure 3.2-23	Response of strong panel model to three load pattern, excluding P-delta effects	3-91
Figure 3.2-24	Response of strong panel model to three loading patters, including P-delta effects	3-92
Figure 3.2-25	Response of strong panel model to ML loads, with and without P-delta effects	3-92
Figure 3.2-26	Tangent stiffness history for structure under ML loads, with and without	

	P-delta effects	3-93
Figure 3.2-27	Patterns of plastic hinge formation: SP model under ML load, including P-delta effects	3-95
Table 3.2-11	Strength Comparisons: Pushover vs. Rigid Plastic	3-96
Figure 3.2-28	Weak panel zone model under ML load	3-97
Figure 3.2-29	Comparison of weak panel zone model with strong panel zone model, excluding P-delta effects	3-97
Figure 3.2-30	Comparison of weak panel zone model with strong panel zone model, including P-delta effects	3-98
Figure 3.2-31	Tangent stiffness history for structure under ML loads, strong versus weak panels, including P-delta effects	3-98
Figure 3.2-32	Patterns of plastic hinge formation: weak panel zone model under ML load, including P-delta effects	3-99
Table 3.2-12	Modal Properties and Expected Inelastic Displacements for the Strong and Weak Panel Models Subjected to the Modal Load Pattern	3-100
Figure 3.2-33	A simple capacity spectrum	3-102
Figure 3.2-34	A simple demand spectrum	3-102
Figure 3.2-35	Capacity and demand spectra plotted together	3-103
Figure 3.2-36	Capacity spectrum showing control points	3-104
Table 3.2-13	Damping Modification Factors	3-105
Figure 3.2-37	Damping modification factors	3-106
Figure 3.2-38	Capacity spectrum used in iterative solution	3-107
Table 3.2-14	Results of Iteration for Maximum Expected Displacement	3-109
Table 3.2-15	Points on Capacity Spectrum Corresponding to Chosen Damping Values	3-110
Figure 3.2-39	Capacity spectrum with equivalent viscous damping points and secant stiffnesses	3-111
Figure 3.2-40	Demand spectra for several equivalent viscous damping values	3-112
Figure 3.2-41	Capacity and demand spectra on single plot	3-113
Figure 3.2-42	Close-up view of portion of capacity and demand spectra	3-114
Table 3.2-16	Summary of Results from Pushover Analysis	3-115
Table 3.2-17	Structural Frequencies and Damping Factors Used in Time-History Analysis	3-117
Table 3.2-18	Seattle Ground Motion Parameters	3-118
Figure 3.2-43	Time histories and response spectra for Record A	3-119
Figure 3.2-44	Time histories and response for Record B	3-120
Figure 3.2-45	Time histories and response spectra for Record C	3-121
Figure 3.2-46	Ground motion scaling parameters	3-123
Table 3.2-19	Maximum Base Shear in Frame Analyzed with 5 Percent Damping, Strong Panels, Excluding P-delta Effects	3-124
Table 3.2-20	Maximum Story Drifts from Time-History Analysis with 5 Percent Damping, Strong Panels, Excluding P-delta Effects	3-124
Table 3.2-21	Maximum Base Shear in Frame analyzed with 5 Percent Damping, Strong Panels, Excluding P-delta Effects	3-124
Table 3.2-22	Maximum Story Drifts from Time-History Analysis with 5 Percent Damping, Strong Panels, Including P-delta Effects	3-125
Figure 3.2-47	Time history of roof and first-story displacement, ground Motion A00, excluding P-delta effects	3-126
Figure 3.2-48	Time history of total base shear, Ground Motion A00, excluding P-delta effects	3-126
Figure 3.2-49	Energy time history, Ground Motion A00, excluding P-delta effects	3-127

Figure 3.2-50	Time history of roof and first story displacement	3-127
Figure 3.2-51	Time history of total base shear, Ground Motion B00, excluding P-delta effects	3-128
Figure 3.2-52	Energy time history, Ground Motion B00, excluding P-delta effects	3-128
Figure 3.2-53	Time history of roof and first-story displacement, Ground Motion C00, excluding P-delta effects	3-129
Figure 3.2-54	Time history of total base shear, Ground Motion C00, excluding P-delta effects	3-129
Figure 3.2-55	Energy time history, Ground Motion C00, excluding P-delta effects	3-130
Figure 3.2-56	Time history of roof and first-story displacement, Ground motion A00, including P-delta effects	3-130
Figure 3.2-57	Time history of total base shear, Ground Motion A00, including P-delta effects	3-131
Figure 3.2-58	Energy time history, Ground Motion A00, including P-delta effects	3-131
Figure 3.2-59	Time history of roof and first-story displacement, Ground Motion B00, including P-delta effects	3-132
Figure 3.2-60	Time history of total base shear, Ground motion B00, including P-delta effects	3-132
Figure 3.2-61	Energy time history, Ground Motion B00, including P-delta effects	3-133
Figure 3.2-62	Time history of roof and first-story displacement, Ground Motion C00, including P-delta effects	3-133
Figure 3.2-63	Time history of total base shear, Ground Motion C00, including P-delta effects	3-134
Figure 3.2-64	Energy time history, Ground Motion C00, including P-delta effects	3-134
Figure 3.2-65	Time-history of roof displacement, Ground Motion A00, with and without P-delta effect	3-135
Figure 3.2-66	Time history of base shear, Ground Motion A00, 135 with and without P-delta effects	3-135
Figure 3.2-67	Yielding locations for structure with strong panels subjected to Ground Motion A00, including P-delta effects	3-136
Table 3.2-23	Summary of All Analyses for Strong Panel Structure, Including P-delta Effects	3-137
Figure 3.2-68	Comparison of inertial force patterns	3-138
Table 3.2-24	Maximum Base Shear (kips) in Frame Analyzed Ground Motion A00, Strong Panels, Including P-delta Effects	3-138
Table 3.2-25	Maximum Story Drifts (in.) from Time-History Analysis Ground Motion A00, Strong Panels, Including P-delta Effects	3-139
Figure 3.2-69	Modeling a simple damper	3-140
Figure 3.2-70	Response of structure with discrete dampers and with equivalent viscous damping	3-141
Figure 3.2-71	Base shear time histories obtained from column forces	3-141
Figure 3.2-72	Base shear time histories as obtained from inertial forces	3-142
Figure 3.2-73	Energy time-history for structure with discrete added damping	3-143
Figure 4.1-1	Typical framing plan	4-4
Table 4.1-1	Geotechnical Parameters	4-5
Figure 4.1-2	Critical sections for isolated footings	4-7
Figure 4.1-3	Soil pressure distributions	4-7

Table 4.1-2	Footing Design for Gravity Loads	4-10
Figure 4.1-4	Foundation plan for gravity-load-resisting system	4-11
Figure 4.1-5	Framing plan for moment resisting frame system	4-12
Table 4.1-3	Demands for Moment-Resisting Frame System	4-12
Figure 4.1-6	Foundation plan for moment-resisting frame system	4-16
Figure 4.1-7	Framing plan for concentrically braced frame system	4-16
Figure 4.1-8	Soil Pressures for controlling bidirectional case	4-18
Figure 4.1-9	Foundation plan for concentrically braced frame system	4-19
Table 4.1-4	Mat Foundation Section Capacities	4-20
Figure 4.1-10	Envelope of mat foundation flexural demands	4-21
Figure 4.1-11	Mat foundation flexural reinforcement.	4-22
Figure 4.1-12	Section of mat foundation	4-23
Figure 4.1-13	Critical sections for shear and envelope of mat foundation shear demands	4-24
Table 4.1-5	Summary of Material Quantities and Cost Comparison	4-25
Figure 4.2-1	Design condition	4-26
Table 4.2-1	Geotechnical Parameters	4-27
Table 4.2-2	Gravity and Seismic Demands	4-28
Figure 4.2-2	Schematic model of deep foundation system	4-29
Figure 4.2-3	Pile cap free body diagram curves	4-30
Figure 4.2-4	Representative <i>p-y</i> curves	4-30
Figure 4.2-5	Passive pressure mobilization curve	4-31
Figure 4.2-6	Calculated group effect factors	4-34
Figure 4.2-7	Results of pile analysis – sheer versus depth	4-35
Figure 4.2-8	Results of pile analysis – moment versus depth	4-35
Figure 4.2-9	Results of pile analysis – displacement versus depth	4-35
Figure 4.2-10	Results of pile analysis – applied lateral load versus head moment	4-36
Figure 4.2-11	Results of pile – head displacement versus applied lateral load	4-36
Figure 4.2-12	P-M interaction diagram for Site Class C	4-38
Figure 4.2-13	P-M interaction diagram for Site Class E	4-39
Figure 4.2-14	Pile axial capacity as a function of length for Site Class C	4-41
Figure 4.2-15	Pile axial capacity as a function of length for Site Class E	4-42
Table 4.2-3	Pile Lengths Required for Axial Loads	4-42
Table 4.2-4	Summary of Pile Size, Length, and Longitudinal Reinforcement	4-43
Figure 4.2-16	Pile detailing for Site Class C	4-44
Figure 4.2-17	Pile detailing for Site Class E	4-45
Figure 4.2-18	Foundation tie section	4-47
Figure 5.1-1	Framing elevation and sections	5-4
Figure 5.1-2	Roof framing and mezzanine framing plan	5-5
Figure 5.1-3	Foundation plan	5-5
Table 5.1-1	ELF Vertical Distribution for N-S Analysis	5-11
Table 5.1-2	ELF Analysis in N-S Direction	5-12
Figure 5.1-4	Design response spectrum	5-12
Table 5.1-3	Design Response Spectra	5-12
Table 5.1-4	Moments in Gable Frame Members	5-16
Table 5.1-5	Axial Forces in Gable Frames Members	5-16
Figure 5.1-5	Moment diagram for seismic load combinations	5-16
Figure 5.1-6	Gable frame schematic	5-17

Table 5.1-6	Comparison of Standards	5-18
Figure 5.1-7	Arrangement at knee	5-19
Figure 5.1-8	Bolted stiffened connection at knee	5-20
Figure 5.2-9	End plate connection at ridge	5-24
Figure 5.1-10	Mezzanine framing	5-26
Figure 5.2-11	Shear force in roof deck diagram	5-28
Figure 5.2-1	Typical floor framing plan and building section	5-30
Figure 5.2-2	Framing plan for special moment frame	5-31
Figure 5.2-3	Concentrically braced frame elevations	5-31
Figure 5.2-4	Approximate effect of accidental of torsion	5-35
Table 5.2-1	Alternative A, Moment Frame Seismic Forces and Moments by Level	5-41
Table 5.2-2	Alternative B, Braced Frame Seismic Forces and Moments by Level	5-41
Table 5.2-3	Alternative C, Dual System Seismic Forces and Moments by Level	5-42
Figure 5.2-5	SMRF frame in E-W direction	5-44
Figure 5.2-6	SMRF frame in N-S direction	5-45
Table 5.2-4	Alternative A (Moment Frame) Story Drifts under Seismic Loads	5-45
Table 5.2-5	Alternative A Torsional Analysis	5-46
Figure 5.2-7	Projection of expected moment strength of beam	5-47
Figure 5.2-8	Story height and clear height	5-48
Figure 5.2-9	Free body diagram bounded by plastic hinges	5-48
Table 5.2-4	Column-Beam Moment Ratios for Seven-Bay Frame	5-49
Table 5.2-5	Column-Beam Moment Ratios for Five-Bay Frame	5-49
Figure 5.2-10	Illustration of AISC Seismic vs. FEMA 350 Methods for panel zone shear	5-50
Figure 5.2-11	Column shears for E-W direction	5-54
Figure 5.2-12	Column shears for N-S direction	5-54
Figure 5.2-13	Forces at beam/column connection	5-55
Figure 5.2-14	WUF-W connection, Second level, NS-direction	5-56
Figure 5.2-15	WUF-W weld detail	5-57
Figure 5.2-16	Braced frame in E-W direction	5-59
Figure 5.2-17	Braced frame in N-S direction	5-59
Table 5.2-6	Alternative B Amplification of Accidental Torison	5-61
Table 5.2-7	Alternative B Story Drifts under Seismic Load	5-62
Figure 5.2-18	Lateral force component in braces for N-S direction	5-63
Figure 5.2-19	Bracing connection detail	5-64
Figure 5.2-20	Whitmore section	5-65
Figure 5.2-21	Brace-to-brace connection	5-68
Figure 5.2-22	Moment frame of dual system in E-W direction	5-69
Figure 5.2-23	Moment frame of dual system in N-S direction	5-70
Table 5.2-8	Alternative C Amplification of Accidental Torsion	5-71
Figure 5.2-24	Braced frame of dual system in E-W-direction	5-72
Figure 5.2-25	Braced frame of dual system in N-S direction	5-72
Table 5.2-9	Alternative C Story Drifts under Seismic Load	5-73
Figure 5.3-1	Main floor framing plan	5-75
Figure 5.3-2	Section on Grid F	5-76
Table 5.3-1	Summary of Critical Member Design Forces	5-77
Figure 5.3-3	Diagram of eccentric braced beam	5-79
Figure 5.3-4	Typical eccentric braced frame	5-79
Figure 5.3-5	Link and upper brace connection	5-85

Figure 5.3-6	Lower brace connections	5-86
Figure 6-1	Typical floor plan of the Berkeley building	6-2
Figure 6-2	typical elevations of the Berkeley building	6-3
Table 6-1	Response Modification, Overstrength, and Deflection Amplification Coefficients for Structural Systems Used	6-7
Table 6-2	Story Weights, Masses, and Moments of Inertia	6-11
Table 6-3	Periods and Modal Response Characteristics for the Berkeley building	6-13
Table 6-4	Periods and Modal Response for the Honolulu Building	6-13
Table 6-5	Comparison of Approximate and “Exact” Periods	6-13
Table 6-6	Comparison of Periods, Seismic Shears Coefficients, and Base Shears for the Berkeley and Honolulu buildings	6-15
Table 6-7a	Vertical Distribution of N-S Seismic Forces for the Berkeley Building	6-16
Table 6-7b	Vertical Distribution of E-W Seismic Forces for the Berkeley Building	6-16
Table 6-8	Vertical Distribution of N-S and E-W Seismic Forces for the Honolulu Building	6-17
Figure 6-3	Comparison of wind and seismic story shears for the Berkeley building	6-18
Figure 6-4	Comparison of wind and seismic story shears for the Honolulu building	6-19
Figure 6-5	Drift profile for Berkeley building	6-20
Table 6-9a	Drift Computations for the Berkeley Building Loaded in the N-S Direction	6-21
Table 6-9b	Drift Computations for the Berkeley Building Loaded in the E-W Direction	6-21
Table 6-10a	P-delta Computations for the Berkeley Building Loaded in the N-S Direction	6-23
Table 6-10b	P-delta Computations for the Berkeley Building Loaded in the E-W Direction	6-23
Figure 6-6	Drift profile for the Honolulu building	6-25
Table 6-11a	Drift Computations for the Honolulu Building Loaded in the N-S Direction	6-26
Table 6-11b	Drift Computations for the Honolulu Building Loaded in the E-W Direction	6-26
Table 6-12a	P-delta Computations for the Honolulu Building Loaded in the N-S Direction	6-27
Table 6-12b	P-delta Computations for the Honolulu Building Loaded in the E-W Direction	6-28
Figure 6-7	Story forces in the E-W direction	6-32
Figure 6-8	Story shears in the E-W direction	6-33
Figure 6-9	Story overturning moments in the E-W direction	6-33
Figure 6-10	25 percent story shears, Frame 1 E-W direction	6-34
Figure 6-11	25 percent story shears, Frame 2 E-W direction	6-35
Figure 6-12	25 percent story shear, Frame 3 E-W direction	6-36
Figure 6-13	Layout for beam reinforcement	6-37
Table 6-13	Tension Development Length Requirements for Hooked Bars and Straight Bars in 4,000 psi LW Concrete	6-38
Figure 6-14	Bending moments Frame 1	6-40
Figure 6-15	Preliminary rebar layout for Frame 1	6-43
Table 6-14	Design and Maximum Probable Flexural Strength for Beams in Frame 1	6-43
Figure 6-16	Diagram for computing column shears	6-45
Figure 6-17	Computing joint shear stress	6-46
Figure 6-18	Loading for determination of rebar cutoffs	6-48
Figure 6-19	Free body diagrams	6-48
Figure 6-20	Development length for top bars	6-49
Figure 6-21	Final bar arrangement	6-50
Table 6-15	Design and Maximum Probable Flexural Strength For Beams in Frame 1	6-50
Figure 6-22	Shears forces for transverse reinforcement	6-52

Figure 6-23	Detailed shear force envelope in Span B-C	6-53
Figure 6-24	Layout and loads on column of Frame A	6-55
Figure 6-25	Design interaction diagram for column on Gridline A	6-56
Figure 6-26	Details of reinforcement for column	6-58
Figure 6-27	Design forces and detailing of haunched girder	6-59
Figure 6-28	Computing shear in haunched girder	6-63
Table 6-16	Design of Shear Reinforcement for Haunched Girder	6-64
Figure 6-29	Computation of column shears for use in joint	6-65
Figure 6-30	Computing joint shear force	6-66
Figure 6-31	Column loading	6-67
Figure 6-32	Interaction diagram and column design forces	6-68
Figure 6-33	Column detail	6-69
Table 6-17	Design Forces for Structural Wall	6-70
Table 6-18	Design of Structural Wall for Shear	6-71
Figure 6-34	Interaction diagram for structural wall	6-73
Figure 6-35	Variation of neutral axis depth with compressive force	6-74
Figure 6-36	Details of structural wall boundary element	6-75
Figure 6-37	Overall details of structural wall	6-76
Figure 6-38	With loading requirements from ASCE 7	6-79
Figure 6-39	Wind vs. seismic shears in exterior bay of Frame 1	6-81
Figure 6-40	Bending moment envelopes at Level 5 of Frame 1	6-82
Figure 6-41	Preliminary reinforcement layout for Level 5 of Frame 1	6-83
Figure 6-42	Shear strength envelopes for Span A-B of Frame 1	6-86
Figure 6-43	Isolated view of Column A	6-87
Figure 6-44	Interaction diagram for column	6-89
Figure 6-45	Column reinforcement	6-91
Figure 6-46	Loads, moments, and reinforcement for haunched girder	6-92
Figure 6-47	Shear force envelope for haunched girder	6-95
Figure 6-48	Loading for Column A, Frame 3	6-97
Figure 6-49	Interaction diagram for Column A	6-98
Figure 6-50	Details for Column A, Frame 3	6-99
Table 7.1-1	Design Parameters from Example 9.2	7-7
Table 7.2-2	Shear Wall Overstrength	7-8
Table 7.1-3	Birmingham 1 F_{px} Calculations	7-9
Figure 7.1-1	Diagram force distribution and analytical model	7-11
Figure 7.1-2	Diagram plan and critical design regions	7-12
Figure 7.1-3	Joint 3 chord reinforcement at the exterior edge	7-15
Figure 7.1-4	Interior joint reinforcement at the ends of plank and the collector reinforcement	7-16
Figure 7.1-5	Anchorage region of shear reinforcement and collector reinforcement	7-17
Figure 7.1-6	Joint 2 transverse wall joint reinforcement	7-19
Figure 7.1-7	Joint 4 exterior longitudinal walls to diaphragm reinforcement and out-of-plane anchorage	7-20
Figure 7.1-8	Wall-to-diaphragm reinforcement along interior longitudinal walls	7-21
Table 7.1-4	Design Parameters form Sec. 9.2	7-22
Table 7.1-5	F_{px} Calculations from Sec. 9.2	7-23
Figure 7.1-9	Diaphragm plan and section cuts	7-25
Figure 7.1-10	Boundary member and chord and collector reinforcement	7-26

Figure 7.1-11	Collector reinforcement at the end of the interior longitudinal walls	7-26
Figure 7.1-12	Wall-to-wall diaphragm reinforcement along interior longitudinal walls	7-27
Figure 7.1-13	Exterior longitudinal wall-to-diaphragm reinforcement and out-of-plane anchorage	7-28
Figure 7.2-1	Three-story building plan	7-30
Table 7.2-1	Design Parameters	7-31
Figure 7.2-2	Forces on the longitudinal walls	7-35
Figure 7.2-3	Forces on the transverse walls	7-36
Figure 7.2-4	Free-body diaphragm for longitudinal walls	7-37
Figure 7.2-5	Free-body diaphragm of the transverse walls	7-39
Figure 7.2-6	Overturning connection detail at the base of the walls	7-41
Figure 7.2-7	Shear connection at base	7-42
Figure 7.2-8	Shear connections on each side of the wall at the second and third floors	7-46
Figure 7.3-1	Single-story industrial warehouse building plan	7-49
Table 7.3-1	Design Parameters	7-50
Figure 7.3-2	Free-body diagram of a panel in the longitudinal direction	7-54
Figure 7.3-3	Free-body diagram of a panel in the transverse direction	7-55
Figure 7.3-4	Cross section of the DT dry-packed at the footing	7-57
Figure 7.3-5	Cross section of one DT leg showing the location of the bonded prestressing tendons or strand	7-58
Figure 7.3-6	Free-body of the angle and the fillet weld connecting the embedded plates in the DT and the footing	7-60
Figure 7.3-7	Free-body of angle with welds, top view, showing only shear forces and resisting moments	7-62
Figure 7.3-8	Section at the connection of the precast/prestressed shear wall panel and the footing	7-64
Figure 7.3-9	Details of the embedded plate in the DT at the base	7-66
Figure 7.3-11	Sketch of connection of load-bearing DT wall panel at the roof	7-66
Figure 7.3-10	Sketch of connection of non-load-bearing DT wall panel at the roof	7-67
Figure 8-1	Typical floor plan	8-3
Figure 8-2	Building and elevation	8-4
Figure 8-3	Building side elevation	8-4
Figure 8-4	Typical composite connection	8-5
Table 8-1	Design Parameters	8-7
Figure 8-5	M- θ Curve for W18x35 connection with 6-#5	8-10
Figure 8-6	M- θ Curve for W21x44 connection with 8-#5	8-11
Table 8-2	Partially Restrained Composite Connection Design	8-12
Figure 8-7	Analysis of seat-angle for tension	8-15
Figure 8-8	Moment diagram for typical beam	8-18
Figure 8-10	elevation of typical connection	8-19
Figure 8-11	Illustration of input for load combination for $1.2D + 0.5L + 1.0Q_E + 0.2S_{DS}D$	8-20
Figure 8-12	Illustration of input for load combination for $0.9D + 1.0Q_E - 0.2S_{DS}D$	8-21
Table 8-3	Story Drift (in.) and P-delta Analysis	8-22
Table 8-4	Maximum Connection Moments and Capacities	8-22
Table 8-5	Column Strength Check, for W10x77	8-23
Figure 8-13	Detail at column	8-25
Figure 8-14	Detail at spandrel	8-26
Figure 8-15	Detail at building corner	8-26

Figure 8-16	Force transfer from deck to column	8-27
Figure 9.1-1	Roof plan	9-3
Figure 9.1-2	End wall elevation	9-4
Table 9.1-1	Comparison of E_m	9-11
Figure 9.1-3	Trial design for 8-in.-thick CMU wall	9-12
Figure 9.1-4	Investigation of out-of-plane ductility for the 8-in.-thick CMU side wall	9-14
Table 9.1-2	Comparison of Variables	9-15
Figure 9.1-6	Basis for interpolation of modulus of rupture, f_x	9-17
Figure 9.1-7	Cracked moment of inertia (I_{cr}) for 8-in.-thick CMU side walls	9-17
Figure 9.1-8	Out-of-plane strength for 8-in.-thick CMU walls	9-20
Figure 9.1-9	In-plane ductility check for side walls	9-22
Figure 9.1-10	Grout cells solid within 10 ft of each end of side walls	9-23
Table 9.1-3	Combined Loads for Shear in Side Wall	9-25
Figure 9.1-11	Trial design for piers on end walls	9-26
Figure 9.1-12	In-plane loads on end walls	9-26
Figure 9.1-13	Out-of-plane load diagram and resultant of lateral loads	9-27
Figure 9.1-14	Investigation for out-of-plane ductility for end walls	9-28
Figure 9.1-15	Cracked moment of inertia for end walls	9-29
Figure 9.1-16	Out-of-plane seismic strength of pier on end wall	9-31
Figure 9.1-17	Input loads for in-plane and end wall analysis	9-32
Figure 9.1-18	In-plane design condition for 8-ft.-wide pier	9-32
Figure 9.1-19	In-plane ductility check for 8-ft.-wide pier	9-33
Figure 9.1-20	In-plane seismic strength of pier	9-35
Figure 9.1-21	In-plane $\Phi P_{11} - \Phi M_{11}$ diagram for pier	9-37
Table 9.1-4	Combined Loads for Flexure in End Pier	9-37
Figure 9.1-22	In-plane shear on end wall and pier	9-38
Table 9.1-5	Combined Loads for Shear in End Wall	9-40
Figure 9.1-23	In-plane deflection of end wall	9-41
Figure 9.2-1	Typical floor plan	9-42
Figure 9.2-2	Building elevation	9-43
Figure 9.2-3	Plan of walls	9-44
Table 9.2-1	Design Parameters	9-45
Table 9.2-2	Birmingham 1 Seismic Forces and moments by Level	9-51
Figure 9.2-4	Location of moments due to story shears	9-51
Table 9.2-3	Shear Strength Calculations for Birmingham 1 Wall D	9-54
Table 9.2-4	Demands for Birmingham 1 Wall D	9-54
Figure 9.2-5	Strength of Birmingham 1 Wall D	9-57
Figure 9.2-6	$\Phi P_{11} - \Phi M_{11}$ diagram for Birmingham 1 Wall D	9-60
Figure 9.2-7	Ductility check for Birmingham 1 Wall D	9-61
Table 9.2-5	Birmingham 1 Cracked Wall Determination	9-63
Figure 9.2-8	Shear wall deflections	9-63
Table 9.2-6	Deflections, Birmingham 1	9-64
Table 9.2-7	New York City Seismic Forces and Moments by Level	9-66
Table 9.2-8	New York City Shear Strength	9-69
Table 9.2-9	Demands for New York City Wall D	9-69
Figure 9.2-9	Strength of New York City and Birmingham 2 Wall D	9-70
Figure 9.2-10	$\Phi P_{11} - \Phi M_{11}$ Diagram for New York City and Birmingham 2 Wall D	9-72

Figure 9.2-11	Ductility check for New York City and Birmingham 2 Wall D	9-74
Table 9.2-10	New York City Cracked Wall Determination	9-75
Table 9.2-11	New York City Deflections	9-76
Table 9.2-12	Birmingham 2 Periods, Mass Participation Factors, and Modal Base Shears	9-79
Table 9.2-13	Birmingham 2 Seismic Forces and Moments by Level	9-80
Table 9.2-14	Birmingham Periods, Mass Participation Factors, and Modal Base	9-81
Table 9.2-15	Shear Strength Calculations for Wall D, Birmingham 2	9-82
Table 9.2-16	Birmingham 2 Demands for Wall D	9-82
Figure 9.2-12	Typical wall section from the Los Angeles location	9-85
Table 9.2-17	Los Angeles Seismic Forces and Moments by Level	9-86
Table 9.2-18	Los Angeles Shear Strength Calculations for Wall D	9-87
Table 9.2-19	Los Angeles Load Combinations for Wall D	9-88
Figure 9.2-13	Los Angeles: Strength of wall D	9-89
Figure 9.2-14	$\Phi P_{11} - \Phi M_{11}$ diagram for Los Angeles Wall D	9-91
Figure 9.2-15	Ductility check for Los Angeles Wall D	9-92
Table 9.2-20	Los Angeles Cracked Wall Determination	9-93
Table 9.2-21	Los Angeles Deflections	9-94
Table 9.2-22	Variation in Reinforcement and Grout by Location	9-95
Figure 9.3-1	Floor plan	9-96
Figure 9.3-2	Elevation	9-97
Table 9.3-1	Design Parameters	9-98
Table 9.3-2	Periods, Mass Participations Ratios, and Modal Base Shears	9-103
Table 9.3-3	Seismic Forces and Moments by Level	9-104
Table 9.3-4	Relative Rigidities	9-106
Figure 9.3-3	Wall dimensions	9-107
Table 9.3-5	Shear for Wall D	9-108
Table 9.3-6	Periods, Mass Participations Ratios, and Modal Base Shears	9-109
Table 9.3-7	Load Combinations for Wall D	9-110
Figure 9.3-4	Bulb reinforcement at lower levels	9-111
Figure 9.3-5	Strength of Wall D, Level 1	9-112
Figure 9.3-6	$\Phi P_{11} - \Phi M_{11}$ Diagram for Level 1	9-115
Figure 9.3-7	Ductility check for Wall D, Level 1	9-116
Figure 9.3-8	Bulb reinforcement at upper levels	9-118
Figure 9.3-9	Strength of Wall D at Level 7	9-119
Figure 9.3-10	$\Phi P_{11} - \Phi M_{11}$ Diagram for Level 7	9-122
Figure 9.3-11	Ductility check for Wall D, Level 7	9-123
Table 9.3-8	Shear Strength for Wall D	9-125
Table 9.3-9	Cracked Wall Determination	9-127
Table 9.3-10	Deflection for ELF Analysis	9-129
Table 9.3-11	Displacements from Modal Analysis	9-130
Figure 9.3-12	Floor anchorage to wall	9-132
Table 9.3-12	Diaphragm Seismic Forces	9-132
Figure 9.3-13	Shears and moments for diaphragm	9-134
Figure 10.1-1	Typical floor plan	10-4
Figure 10.1-2	Longitudinal section and elevation	10-4
Figure 10.1-3	Foundation plan	10-5
Figure 10.1-4	Load path and shear walls	10-7

Figure 10.1-5	Vertical shear distribution	10-11
Table 10.1-1	Seismic Coefficients, Forces, and Moments	10-12
Figure 10.1-6	Transverse section: end wall	10-18
Table 10.1-2	Fastener slip equations	10-20
Table 10.1-3	Wall Deflection	10-21
Figure 10.1-7	Force distribution for flexural deflections	10-21
Table 10.1-4	Wall Deflection (per story) Due to Bending and Anchorage Slip	10-22
Table 10.1-5	Total Elastic Deflection and Drift of End Wall	10-22
Figure 10.1-8	Shear wall tie down at suspended floor framing	10-25
Figure 10.1-9	Transverse wall: overturning	10-28
Figure 10.1-10	Bearing wall	10-29
Figure 10.1-11	Nonbearing wall	10-29
Figure 10.1-12	Foundation wall detail	10-30
Figure 10.1-13	Diaphragm chord splice	10-32
Table 10.1-6a	Total Deflection and Drift	10-36
Table 10.1-6b	Total Deflection and Drift (Structural I Plywood Shear Walls)	10-36
Table 10.1-7	P-delta Stability Coefficient	10-37
Figure 10.1-14	Perforated shear wall at exterior	10-39
Figure 10.1-15	Perforated shear wall detail at foundation	10-43
Figure 10.1-16	Perforated shear wall detail at floor framing	10-43
Figure 10.2-1	Building plan	10-44
Table 10.2-1	Roof Diaphragm Framing and Nailing Requirements	10-49
Figure 10.2-2	Diaphragm framing and nailing layout	10-49
Figure 10.2-3	Plywood layout	10-50
Figure 10.2-4	Chord splice detail	10-51
Figure 10.2-5	Adjustment for non-uniform nail spacing	10-52
Figure 10.2-6	Diaphragm at roof opening	10-54
Figure 10.2-7	Chord forces and Element 1 free-body diagram	10-55
Figure 10.2-8	Free-body diagram for Element 2	10-56
Figure 10.2-9	Anchorage of masonry wall perpendicular to joists	10-58
Figure 10.2-10	Chord tie at roof opening	10-59
Figure 10.2-11	Cross tie plan layout and subdiaphragm free-body diagram for side walls	10-60
Figure 10.2-12	Anchorage of masonry wall parallel to joists	10-61
Figure 10.2-13	Cross tie plan layout and subdiaphragm free-body diagram for end walls	10-62
Figure 11.1-1	Isolation system terminology	11-6
Figure 11.1-2	Effective stiffness and effective damping	11-8
Table 11.2-1	Acceptable Methods of Analysis	11-8
Figure 11.3-1	Isolation system capacity and earthquake demand	11-10
Figure 11.3-2	Design, maximum, and total maximum displacement	11-11
Figure 11.3-3	Isolation system displacement and shear force as function of period	11-13
Table 11.4-1	Summary of Minimum Design Criteria for Dynamic Analysis	11-14
Figure 11.4-1	Moments due to horizontal shear and P-delta effects	11-15
Figure 11.4-2	Bilinear idealization of isolator unit behavior	11-16
Figure 11.5-1	Three-dimensional model of the structural system	11-17
Figure 11.5-2	Typical floor framing plan	11-18
Figure 11.5-3	Penthouse roof framing plan	11-18
Figure 11.5-4	Longitudinal bracing elevation	11-19

Figure 11.5-5	Transverse bracing elevations	11-19
Table 11.5-1	Gravity Loads on Isolator Units	11-21
Figure 11.5-6	Example design spectra	11-23
Table 11.5-2	Earthquake Time History Records and Scaling Factors	11-24
Figures 11.5-7	Comparison of design earthquake spectra	11-25
Table 11.5-3	Vertical Distribution of Reduced Design Earthquake Forces	11-32
Table 11.5-4	Vertical Distribution of Unreduced DE and MCE Forces	11-32
Table 11.5-5	Maximum Downward Force for Isolator Design	11-33
Table 11.5-6	Minimum Downward Force for Isolator Design	11-33
Table 11.5-7	Maximum Downward Force on Isolator Units	11-34
Table 11.5-8	Maximum Uplift Displacement of Isolator Units	11-34
Figure 11.5-8	Elevation of framing on Column Line 2	11-35
Figure 11.5-9	Elevation of framing on Column Line B	11-36
Figure 11.5-10	First floor framing plan	11-36
Table 11.5-9	Summary of Key Design Parameters	11-38
Figure 11.5-11	Typical detail of the isolation system at columns	11-39
Figure 11.5-12	Stiffness and damping properties of EOC isolator units	11-42
Figure 11.5-13	Comparison of modeled isolator properties to test data	11-43
Table 11.5-10	Design Earthquake Response Parameters	11-44
Table 11.5-11	Maximum Considered Earthquake Response Parameters	11-44
Table 11.5-12	Maximum Downward Force (kips) on Isolator Units	11-45
Table 11.5-13	Maximum Uplift Displacement (in.) Of Isolator Units	11-45
Figure 11.5-14	Isolator dimensions	11-46
Table 11.5-14	Prototype Test Requirements	11-47
Table 12-1	Applicability of the Chapters of the <i>Provisions</i>	12-2
Figure 12-1	Combustion turbine building	12-3
Figure 12-2	Pipe rack	12-6
Figure 12-3	Steel storage rack	12-11
Table 12.3-1	Seismic Forces, Shears and Overturning Moments	12-14
Figure 12-4	Boiler building	12-16
Figure 12-5	Pier plan and elevation	12-20
Figure 12-6	Storage tank section	12-23
Figure 12-7	Platform for elevated transformer	12-29
Figure 13.2-1	Five-story building evaluation showing panel location	13-8
Figure 13.2-2	Detailed building elevation	13-9
Figure 13.2-3	Spandrel panel connection payout from interior	13-11
Figure 13.2-4	Spandrel panel moments	13-14
Figure 13.2-5	Spandrel panel connections forces	13-16
Figure 13.2-6	Column cover connection layout	13-17
Figure 13.3-1	Air handling fan unit	13-20
Figure 13.3-2	Free-body diagram for seismic force analysis	13-22
Figure 13.3-3	Anchor for direct attachment to structure	13-23
Figure 13.3-4	ASHRAE diagonal seismic force analysis for vibration isolation springs	13-25
Figure 13.3-5	Anchor and snubber loads for support on vibration isolation springs	13-27
Figure 13.3-6	Lateral restraint required to resist seismic forces	13-29

FUNDAMENTALS

James Robert Harris, P.E., Ph.D.

In introducing their well-known text, *Fundamentals of Earthquake Engineering*, Newmark and Rosenblueth (1971) comment:

In dealing with earthquakes, we must contend with appreciable probabilities that failure will occur in the near future. Otherwise, all the wealth of the world would prove insufficient to fill our needs: the most modest structures would be fortresses. We must also face uncertainty on a large scale, for it is our task to design engineering systems – about whose pertinent properties we know little – to resist future earthquakes and tidal waves – about whose characteristics we know even less. . . . In a way, earthquake engineering is a cartoon. . . . Earthquake effects on structures systematically bring out the mistakes made in design and construction, even the minutest mistakes.

Several points essential to an understanding of the theories and practices of earthquake-resistant design bear restating:

1. Ordinarily, a large earthquake produces the most severe loading that a building is expected to survive. The probability that *failure* will occur is very real and is greater than for other loading phenomena. Also, in the case of earthquakes, the definition of *failure* is altered to permit certain types of behavior and damage that are considered unacceptable in relation to the effects of other phenomena.
2. The levels of uncertainty are much greater than those encountered in the design of structures to resist other phenomena. This applies both to knowledge of the loading function and to the resistance properties of the materials, members, and systems.
3. The details of construction are very important because flaws of no apparent consequence often will cause systematic and unacceptable damage simply because the earthquake loading is so severe and an extended range of behavior is permitted.

The remainder of this chapter is devoted to a very abbreviated discussion of fundamentals that reflect the concepts on which earthquake-resistant design are based. When appropriate, important aspects of the *NEHRP Recommended Provisions for Seismic Regulations for New Buildings and Other Structures* are mentioned and reference is made to particularly relevant portions of the document. Note that through 2000, the *NEHRP Recommended Provisions* has been composed of two volumes of text and a separate set of maps. Part 1 (referred to herein as the *Provisions*) contains the actual requirements and Part 2 (referred to herein as the *Commentary*) provides a discussion of various aspects of the requirements.

Although the set of design examples is based on the 2000 *Provisions*, it is annotated to reflect changes made to the 2003 *Provisions*. Annotations within brackets, [], indicate both organizational changes (as a result of a reformat of all of the chapters of the 2003 *Provisions*) and substantive technical changes to the 2003 *Provisions* and its primary reference documents. While the general concepts of the changes are

described, the design examples and calculations in this book have not been revised to reflect the changes to the 2003 *Provisions*. Where related to the discussion in this chapter, significant changes to the 2003 *Provisions* and primary reference documents are noted. However, some minor changes to the 2003 *Provisions* and the reference documents may not be noted.

1.1 EARTHQUAKE PHENOMENA

According to the most widely held scientific belief, most earthquakes occur when two segments of the earth's crust suddenly move in relation to one another. The surface along which movement occurs is known as a fault. The sudden movement releases strain energy and causes seismic waves to propagate through the crust surrounding the fault. These waves cause the surface of the ground to shake violently, and it is this ground shaking that is the principal concern of structural engineering to resist earthquakes.

Earthquakes have many effects in addition to ground shaking. For various reasons, the other effects generally are not major considerations in the design of buildings and similar structures. For example, seismic sea waves or tsunamis can cause very forceful flood waves in coastal regions, and seiches (long-period sloshing) in lakes and inland seas can have similar effects along shorelines. These are outside the scope of the *Provisions*. This is not to say, however, that they should not be considered during site exploration and analysis. Designing structures to resist such hydrodynamic forces is a very specialized topic, and it is common to avoid constructing buildings and similar structures where such phenomena are likely to occur. Long-period sloshing of the liquid contents of tanks is addressed by the *Provisions*.

Abrupt ground displacements occur where a fault intersects the ground surface. (This commonly occurs in California earthquakes but apparently did not occur in the historic Charleston, South Carolina, earthquake or the very large New Madrid, Missouri, earthquakes of the nineteenth century.) Mass soil failures such as landslides, liquefaction, and gross settlement are the result of ground shaking on susceptible soil formations. Once again, design for such events is specialized, and it is common to locate structures so that mass soil failures and fault breakage are of no major consequence to their performance. Modification of soil properties to protect against liquefaction is one important exception; large portions of a few metropolitan areas with the potential for significant ground shaking are susceptible to liquefaction. Lifelines that cross faults require special design beyond the scope of the *Provisions*. The structural loads specified in the *Provisions* are based solely on ground shaking; they do not provide for ground failure. The *Commentary* includes a method for prediction of susceptibility to liquefaction as well as general guidelines for locating potential fault rupture zones.

Nearly all large earthquakes are *tectonic* in origin – that is, they are associated with movements of and strains in large segments of the earth's crust, called *plates*, and virtually all such earthquakes occur at or near the boundaries of these plates. This is the case with earthquakes in the far western portion of the United States where two very large plates, the North American continent and the Pacific basin, come together. In the central and eastern United States, however, earthquakes are not associated with such a plate boundary and their causes are not as completely understood. This factor, combined with the smaller amount of data about central and eastern earthquakes (because of their infrequency), means that the uncertainty associated with earthquake loadings is higher in the central and eastern portions of the nation than in the West. Even in the West, the uncertainty (when considered as a fraction of the predicted level) about the hazard level is probably greater in areas where the mapped hazard is low than in areas where the mapped hazard is high.

The amplitude of earthquake ground shaking diminishes with distance from the source, and the rate of attenuation is less for lower frequencies of motion than for higher frequencies. This effect is captured, to an extent, by the fact that the *Provisions* uses two sets of maps define the hazard of seismic ground shaking – one is pertinent for higher frequency motion (the S_5 maps) and the other for lower frequencies (the S_1 maps). There is evidence that extreme motions near the fault in certain types of large earthquakes

are not captured by the maps, but interim adjustments to design requirements for such a possibility are included in the *Provisions*.

Two basic data sources are used in establishing the likelihood of earthquake ground shaking, or seismicity, at a given location. The first is the historical record of earthquake effects and the second is the geological record of earthquake effects. Given the infrequency of major earthquakes, there is no place in the United States where the historical record is long enough to be used as a reliable basis for earthquake prediction – certainly not as reliable as with other phenomena such as wind and snow. Even on the eastern seaboard, the historical record is too short to justify sole reliance on the historical record. Thus, the geological record is essential. Such data require very careful interpretation, but they are used widely to improve knowledge of seismicity. Geological data have been developed for many locations as part of the nuclear power plant design process. On the whole, there are more geological data available for the far western United States than for other regions of the country. Both sets of data have been taken into account in the *Provisions* seismic hazard maps. Ground shaking, however, is known to vary considerably over small distances and the *Provisions* maps do not attempt to capture all such local variations (commonly called *microzoning*).

The *Commentary* provides a more thorough discussion of the development of the maps, their probabilistic basis, the necessarily crude lumping of parameters, and other related issues. In particular, note the description of the newest generation of maps introduced in 1997 and their close relationship to the development of a new design criterion. There are extended discussions of these issues in the appendices to the *Commentary*. Prior to its 1997 edition, the basis of the *Provisions* was to “provide *life safety* at the design earthquake motion,” which was defined as having a 10 percent probability of being exceeded in a 50-year reference period. As of the 1997 edition, the basis became to “avoid *structural collapse* at the maximum considered earthquake (MCE) ground motion,” which is defined as having a 2 percent probability of being exceeded in a 50-year reference period. In the long term, the change from life safety to structural collapse prevention as the limit state will create significant changes in procedures for design analysis. In the present interim, the ground motions for use with present design procedures are simply taken as being two-thirds of the MCE ground motions.

1.2 STRUCTURAL RESPONSE TO GROUND SHAKING

The first important difference between structural response to an earthquake and response to most other loadings is that the earthquake response is *dynamic*, not *static*. For most structures, even the response to wind is essentially static. Forces within the structure are due almost entirely to the pressure loading rather than the acceleration of the mass of the structure. But with earthquake ground shaking, the aboveground portion of a structure is not subjected to any applied force. The stresses and strains within the superstructure are created entirely by its dynamic response to the movement of its base, the ground. Even though the most used design procedure resorts to the use of a concept called the equivalent static force for actual calculations, some knowledge of the theory of vibrations of structures is essential.

1.2.1 Response Spectra

Figure 1.2-1 shows accelerograms, records of the acceleration at one point along one axis, for several representative earthquakes. Note the erratic nature of the ground shaking and the different characteristics of the different accelerograms. Precise analysis of the elastic response of an ideal structure to such a pattern of ground motion is possible; however, it is not commonly done for ordinary structures. The increasing power and declining cost of computational aids are making such analyses more common but, at this time, only a small minority of structures are analyzed for specific response to a specific ground motion.

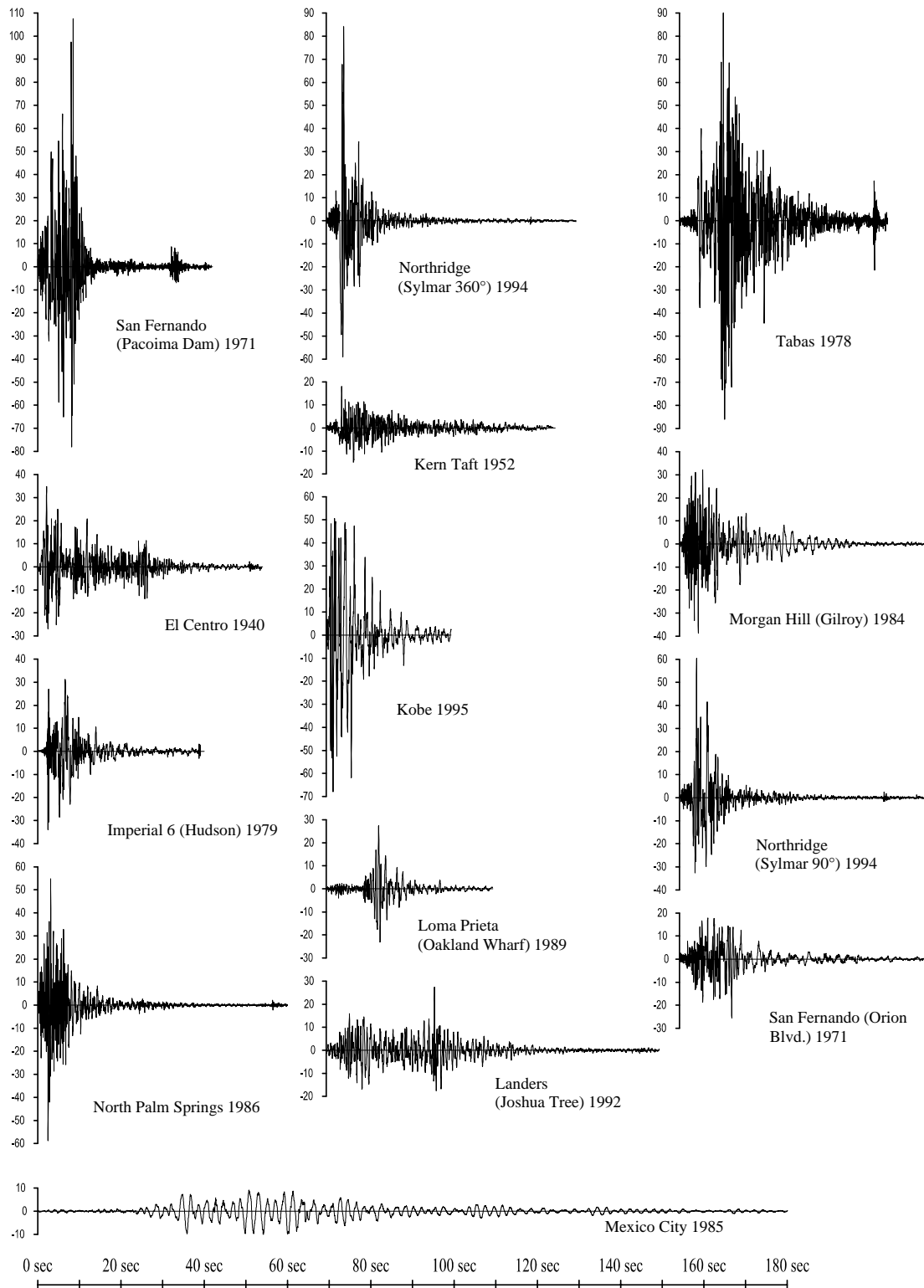
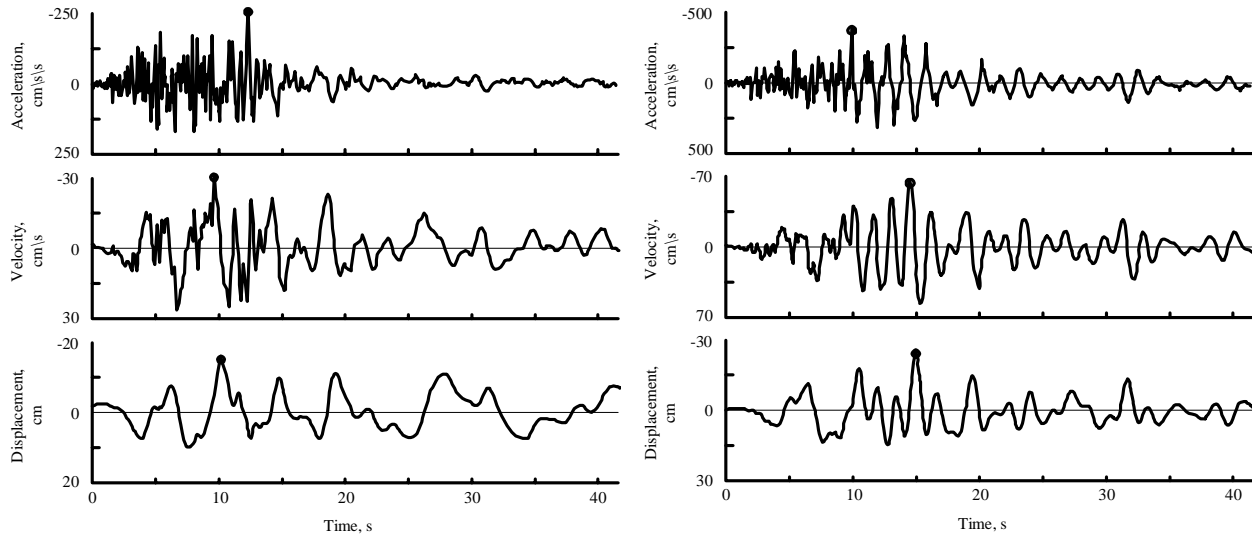


Figure 1.2-1 Earthquake ground acceleration in epicentral regions (all accelerograms are plotted to the same scale for time and acceleration). Great earthquakes extend for much longer periods of time.

Figure 1.2-2 shows further detail developed from an accelerogram. Part (a) shows the ground acceleration along with the ground velocity and ground displacement derived from it. Part (b) shows the

acceleration, velocity, and displacement for the same event at the roof of the building located where the ground motion was recorded. Note that the peak values are larger in the diagrams of Figure 1.2-2(b) (the vertical scales are different). This increase in response of the structure at the roof level over the motion of the ground itself is known as dynamic amplification. It depends very much on the vibrational characteristics of the structure and the characteristic frequencies of the ground shaking at the site.



(a) Ground acceleration, velocity, and displacement (b) Roof acceleration, velocity, and displacement

Figure 1.2-2 Holiday Inn ground and building roof motion during the M6.4 1971 San Fernando earthquake: (a) north-south ground acceleration, velocity, and displacement and (b) north-south roof acceleration, velocity, and displacement (Housner and Jennings 1982). Note that the vertical scale of (b) is different from (a). The Holiday Inn, a 7-story, reinforced concrete frame building, was approximately 5 miles from the closest portion of the causative fault. The recorded building motions enabled an analysis to be made of the stresses and strains in the structure during the earthquake.

In design, the response of a specific structure to an earthquake is ordinarily predicted from a design response spectrum such as is specified in the *Provisions*. The first step in creating a design response spectrum is to determine the maximum response of a given structure to a specific ground motion (see Figure 1.2-2). The underlying theory is based entirely on the response of a single-degree-of-freedom oscillator such as a simple one-story frame with the mass concentrated at the roof. The vibrational characteristics of such a simple oscillator may be reduced to two: the natural frequency and the amount of damping. By recalculating the record of response versus time to a specific ground motion for a wide range of natural frequencies and for each of a set of common amounts of damping, the family of response spectra for one ground motion may be determined. It is simply the plot of the maximum value of response for each combination of frequency and damping.

Figure 1.2-3 shows such a result for the ground motion of Figure 1.2-2(a) and illustrates that the erratic nature of ground shaking leads to a response that is very erratic in that a slight change in the natural period of vibration brings about a very large change in response. Different earthquake ground motions lead to response spectra with peaks and valleys at different points with respect to the natural frequency. Thus, computing response spectra for several different ground motions and then averaging them, based on some normalization for different amplitudes of shaking, will lead to a smoother set of spectra. Such smoothed spectra are an important step in developing a design spectrum.

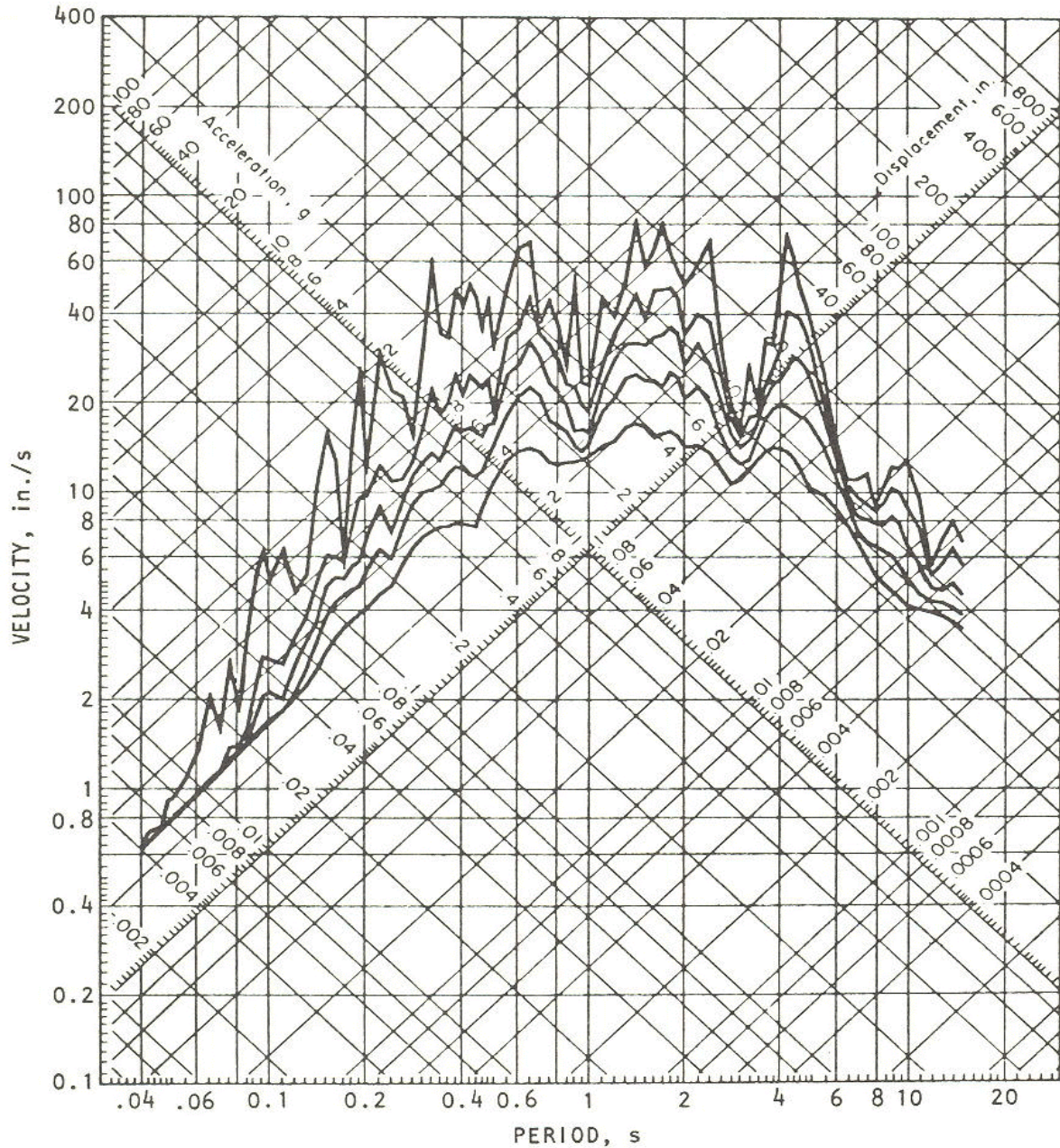


Figure 1.2-3 Response spectrum of north-south ground acceleration (0, 0.02, 0.05, 0.10, 0.20 of critical damping) recorded at the Holiday Inn, approximately 5 miles from the causative fault in the 1971 San Fernando earthquake (Housner and Jennings 1982).

Figure 1.2-4 is an example of an averaged spectrum. Note that the horizontal axes of Figures 1.2-3 and 1.2-4 are different, one being for the known frequency (period) while the other is for the cyclic frequency. Cyclic frequency is the inverse of period; therefore, Figure 1.2-4 should be rotated about the line $f = 1$ to compare it with Figure 1.2-3. Note that acceleration, velocity, or displacement may be obtained from Figure 1.2-3 or 1.2-4 for a structure with known frequency (period) and damping.

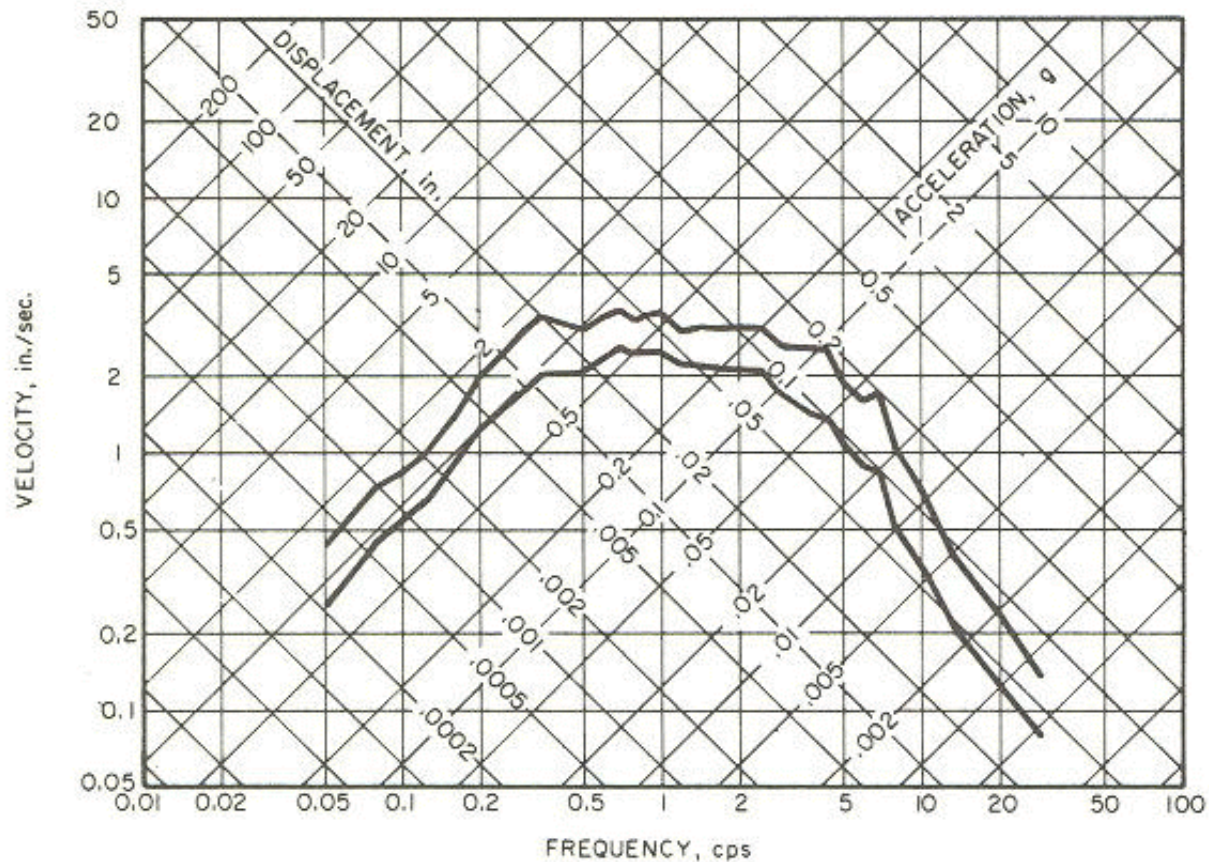


Figure 1.2-4 Averaged spectrum (Newmark, Blume, and Kapur 1973). Mean and mean plus one standard deviation acceleration, horizontal components (2.0 percent of critical damping). Reprinted with permission from the American Society of Civil Engineers.

Prior to the 1997 editions of the *Provisions*, the maps that characterized the ground shaking hazard were plotted in terms of peak ground acceleration, and design response spectra were created using expressions that amplified (or de-amplified) the ground acceleration as a function of period and damping. With the introduction of the MCE ground motions, this procedure changed. Now the maps present spectral response accelerations at two periods of vibration, 0.2 and 1.0 second, and the design response spectrum is computed more directly. This has removed a portion of the uncertainty in predicting response accelerations.

Few structures are so simple as to actually vibrate as a single-degree-of-freedom system. The principles of dynamic modal analysis, however, allow a reasonable approximation of the maximum response of a multi-degree-of-freedom oscillator, such as a multistory building, if many specific conditions are met. The procedure involves dividing the total response into a number of natural modes, modeling each mode as an equivalent single-degree-of-freedom oscillator, determining the maximum response for each mode from a single-degree-of-freedom response spectrum, and then estimating the maximum total response by statistically summing the responses of the individual modes. The *Provisions* does not require consideration of all possible modes of vibration for most buildings because the contribution of the higher modes (higher frequencies) to the total response is relatively minor.

The soil at a site has a significant effect on the characteristics of the ground motion and, therefore, on the structure's response. Especially at low amplitudes of motion and at longer periods of vibration, soft soils amplify the motion at the surface with respect to bedrock motions. This amplification is diminished somewhat, especially at shorter periods as the amplitude of basic ground motion increases, due to yielding in the soil. The *Provisions* accounts for this effect by providing amplifiers that are to be applied to the 0.2 and 1.0 second spectral accelerations for various classes of soils. (The MCE ground motion maps are drawn for sites on rock.) Thus, very different design response spectra are specified depending on the type of soil(s) beneath the structure. The *Commentary* contains a thorough explanation of this feature.

1.2.2 Inelastic Response

The preceding discussion assumes elastic behavior of the structure. The principal extension beyond ordinary behavior referenced at the beginning of this chapter is that structures are permitted to strain beyond the elastic limit in responding to earthquake ground shaking. This is dramatically different from the case of design for other types of loads in which stresses, and therefore strains, are not permitted to approach the elastic limit. The reason is economic. Figure 1.2-3 shows a peak acceleration response of about 1.0 g (the acceleration due to gravity) for a structure with moderately low damping – for only a moderately large earthquake! Even structures that are resisting lateral forces well will have a static lateral strength of only 20 to 40 percent of gravity.

The dynamic nature of earthquake ground shaking means that a large portion of the shaking energy can be dissipated by inelastic deformations if some damage to the structure is accepted. Figure 1.2-5 illustrates the large amount of strain energy that may be stored by a ductile system in a displacement-controlled event such as an earthquake. The two graphs are plotted with the independent variables on the horizontal axis and the dependent response on the vertical axis. Thus, part (b) of the figure is characteristic of the response to forces such as gravity weight or wind pressure, while part (c) is characteristic of induced displacements such as foundation settlement or earthquake ground shaking. The figures should not be interpreted as a horizontal beam and a vertical column. Figure 1.2-5(a) would represent a beam if the load W were small and a column if W were large. The point being made with the figures is that ductile structures have the ability to resist displacements much larger than those that first cause yield.

The degree to which a member or structure may deform beyond the elastic limit is referred to as ductility. Different materials and different arrangements of structural members lead to different ductilities. Response spectra may be calculated for oscillators with different levels of ductility. At the risk of gross oversimplification, the following conclusions may be drawn:

1. For structures with very low natural frequencies, the acceleration response is reduced by a factor equivalent to the ductility ratio (the ratio of maximum usable displacement to effective yield displacement – note that this is displacement and not strain).
2. For structures with very high natural frequencies, the acceleration response of the ductile structure is essentially the same as that of the elastic structure, but the displacement is increased.
3. For intermediate frequencies (which applies to nearly all buildings), the acceleration response is reduced, but the displacement response is generally about the same for the ductile structure as for the elastic structure strong enough to respond without yielding.

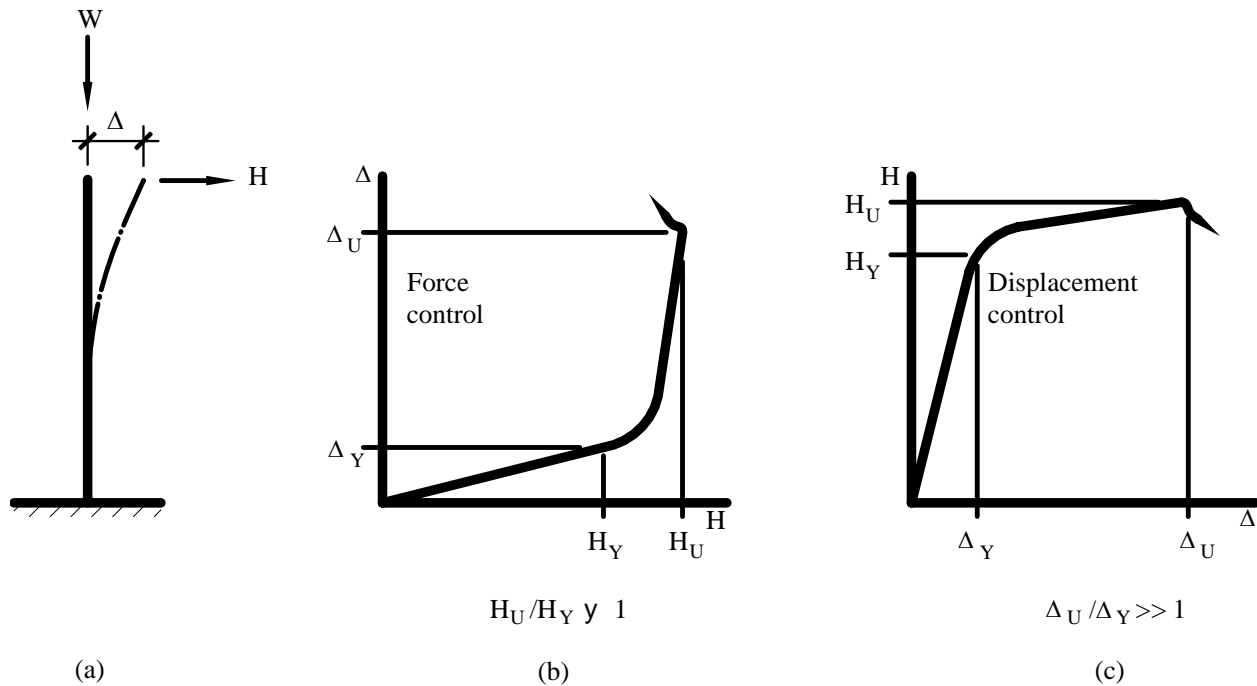


Figure 1.2-5 Force controlled resistance versus displacement controlled resistance (after Housner and Jennings 1982). In part (b) the force H is the independent variable. As H is increased, the displacement increases until the yield point stress is reached. If H is given an additional increment (about 15 percent), a plastic hinge forms giving large displacements. For this kind of system, the force producing the yield point stress is close to the force producing collapse. The ductility does not produce a large increase in load capacity. In part (c) the displacement is the independent variable. As the displacement is increased, the base moment ($F\ell$) increases until the yield point is reached. As the displacement increases still more, the base moment increases only a small amount. For a ductile element, the displacement can be increased 10 to 20 times the yield point displacement before the system collapses under the weight W . (As W increases, this ductility is decreased dramatically.) During an earthquake, the oscillator is excited into vibrations by the ground motion and it behaves essentially as a displacement-controlled system and can survive displacements much beyond the yield point. This explains why ductile structures can survive ground shaking that produces displacements much greater than yield point displacement.

Inelastic response is quite complex. Earthquake ground motions involve a significant number of reversals and repetitions of the strains. Therefore, observation of the inelastic properties of a material, member, or system under a monotonically increasing load until failure can be very misleading. Cycling the deformation can cause degradation of strength, stiffness, or both. Systems that have a proven capacity to maintain a stable resistance to a large number of cycles of inelastic deformation are allowed to exercise a greater portion of their ultimate ductility in designing for earthquake resistance. This property is often referred to as toughness, but this is not the same as the classic definition used in mechanics of materials.

Most structures are designed for seismic response using a linear elastic analysis with the strength of the structure limited by the strength at its critical location. Most structures possess enough complexity so that the peak strength of a ductile structure is not accurately captured by such an analysis. Figure 1.2-6 shows the load versus displacement relation for a simple frame. Yield must develop at four locations before the peak resistance is achieved. The margin from the first yield to the peak strength is referred to as overstrength and it plays a significant role in resisting strong ground motion. Note that a few key design standards (for example, ACI 318 for the design of concrete structures) do allow for some redistribution of internal forces from the critical locations based upon ductility; however, the redistributions allowed therein are minor compared to what occurs in response to strong ground motion.

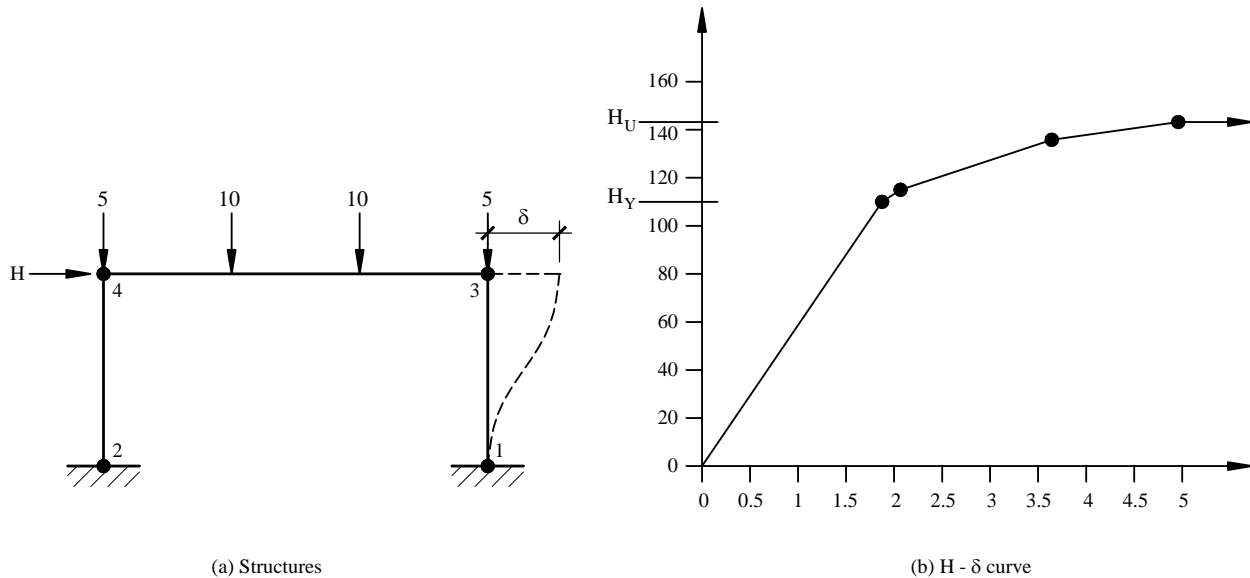


Figure 1.2-6 Initial yield load and failure load for a ductile portal frame. The margin from initial yield to failure (mechanism in this case) is known as overstrength.

To summarize, the characteristics important in determining a building's seismic response are natural frequency, damping, ductility, stability of resistance under repeated reversals of inelastic deformation, and overstrength. The natural frequency is dependent on the mass and stiffness of the building. Using the *Provisions*, the designer calculates, or at least approximates, the natural period of vibration (the inverse of natural frequency). Damping, ductility, toughness, and overstrength depend primarily on the type of building system, but not the building's size or shape. Three coefficients – R , C_d , and Ω_0 – are provided to encompass damping, ductility, stability of resistance, and overstrength. R is intended to be a conservatively low estimate of the reduction of acceleration response in a ductile system from that for an elastic oscillator with a certain level of damping. It is used to compute a required strength. Computations of displacement based upon ground motion reduced by the factor R will underestimate the actual displacements. C_d is intended to be a reasonable mean for the amplification necessary to convert the elastic displacement response computed for the reduced ground motion to actual displacements. Ω_0 is intended to deliver a reasonably high estimate of the peak force that would develop in the structure. Sets of R , C_d , and Ω_0 are specified in the *Provisions* for the most common structural materials and systems.

1.2.3 Building Materials

The following brief comments about building materials and systems are included as general guidelines only, not for specific application.

1.2.3.1 Wood

Timber structures nearly always resist earthquakes very well, even though wood is a brittle material as far as tension and flexure are concerned. It has some ductility in compression (generally monotonic), and its strength increases significantly for brief loadings, such as earthquake. Conventional timber structures (plywood or board sheathing on wood framing) possess much more ductility than the basic material primarily because the nails and other steel connection devices yield and the wood compresses against the connector. These structures also possess a much higher degree of damping than the damping that is assumed in developing the basic design spectrum. Much of this damping is caused by slip at the connections. The increased strength, connection ductility, and high damping combine to give timber

structures a large reduction from elastic response to design level. This large reduction should not be used if the strength of the structure is actually controlled by bending or tension of the gross timber cross sections. The large reduction in acceleration combined with the light weight timber structures make them very efficient with regard to earthquake ground shaking when they are properly connected. This is confirmed by their generally good performance in earthquakes.

1.2.3.2 Steel

Steel is the most ductile of the common building materials. The moderate-to-large reduction from elastic response to design response allowed for steel structures is primarily a reflection of this ductility and the stability of the resistance of steel. Members subject to buckling (such as bracing) and connections subject to brittle fracture (such as partial penetration welds under tension) are much less ductile and are addressed in the *Provisions* in various ways. Other defects, such as stress concentrations and flaws in welds, also affect earthquake resistance as demonstrated in the Northridge earthquake. The basic and applied research program that grew out of that demonstration has greatly increased knowledge of how to avoid low ductility details in steel construction.

1.2.3.3 Reinforced Concrete

Reinforced concrete achieves ductility through careful limits on steel in tension and concrete in compression. Reinforced concrete beams with common proportions can possess ductility under monotonic loading even greater than common steel beams, in which local buckling is usually a limiting factor. Providing stability of the resistance to reversed inelastic strains, however, requires special detailing. Thus, there is a wide range of reduction factors from elastic response to design response depending on the detailing for stable and assured resistance. The *Commentary* and the commentary with the ACI 318 standard for design of structural concrete explain how controlling premature shear failures in members and joints, buckling of compression bars, concrete compression failures (through confinement with transverse reinforcement), the sequence of plastification, and other factors lead to larger reductions from the elastic response.

1.2.3.4 Masonry

Masonry is a more diverse material than those mentioned above, but less is known about its inelastic response characteristics. For certain types of members (such as pure cantilever shear walls), reinforced masonry behaves in a fashion similar to reinforced concrete. The nature of the masonry construction, however, makes it difficult, if not impossible, to take some of the steps (e.g., confinement of compression members) used with reinforced concrete to increase ductility and stability. Further, the discrete differences between mortar and the masonry unit create additional failure phenomena. Thus, the reduction factors for reinforced masonry are not quite as large as those for reinforced concrete. Unreinforced masonry possesses little ductility or stability, except for rocking of masonry piers on a firm base, and very little reduction from the elastic response is permitted.

1.2.3.5 Precast Concrete

Precast concrete obviously can behave quite similarly to reinforced concrete, but it also can behave quite differently. The connections between pieces of precast concrete commonly are not as strong as the members being connected. Clever arrangements of connections can create systems in which yielding under earthquake motions occurs away from the connections, in which case the similarity to reinforced concrete is very real. Some carefully detailed connections also can mimic the behavior of reinforced concrete. Many common connection schemes, however, will not do so. Successful performance of such systems requires that the connections perform in a ductile manner. This requires some extra effort in design, but it can deliver successful performance. As a point of reference, the most common wood

seismic resisting systems perform well yet have connections (nails) that are significantly weaker than the connected elements (structural wood panels). The *Provisions* includes guidance, some only for trial use and comment, for seismic design of precast structures.

1.2.3.6 Composite Steel and Concrete

Reinforced concrete is a composite material. In the context of the *Provisions*, *composite* is a term reserved for structures with elements consisting of structural steel and reinforced concrete acting in a composite manner. These structures generally are an attempt to combine the most beneficial aspects of each material.

1.2.4 Building Systems

Three basic lateral-load-resisting elements – walls, braced frames, and unbraced frames (moment resisting frames) – are used to build a classification of structural types in the *Provisions*. Unbraced frames generally are allowed greater reductions from elastic response than walls and braced frames. In part, this is because frames are more redundant, having several different locations with approximately the same stress levels, and common beam-column joints frequently exhibit an ability to maintain a stable response through many cycles of reversed inelastic deformations. Systems using connection details that have not exhibited good ductility and toughness, such as unconfined concrete and the welded steel joint used before the Northridge earthquake, are penalized with small reduction factors.

Connection details often make development of ductility difficult in braced frames, and buckling of compression members also limits their inelastic response. Eccentrically braced steel frames and new proportioning and detailing rules for concentrically braced frames have been developed to overcome these shortcomings. [The 2003 *Provisions* include proportioning and detailing rules for buckling-restrained braced frames. This new system has the advantages of a special steel concentrically braced frame, but with performance that is superior as brace buckling is prevented. Design provisions appear in 2003 *Provisions* Sec. 8.6.] Walls that are not load bearing are allowed a greater reduction than walls that are load bearing. Redundancy is one reason; another is that axial compression generally reduces the flexural ductility of concrete and masonry elements (although small amounts of axial compression usually improve the performance of materials weak in tension, such as masonry and concrete). Systems that combine different types of elements are generally allowed greater reductions from elastic response because of redundancy.

Redundancy is frequently cited as a desirable attribute for seismic resistance. A quantitative measure of redundancy has been introduced in recent editions of the *Provisions* in an attempt to prevent use of large reductions from elastic response in structures that actually possess very little redundancy. As with many new empirical measures, it is not universally accepted and is likely to change in the future. [In the 2003 *Provisions*, a radical change was made to the requirements related to redundancy. Only two values of the redundancy factor, ρ , are defined: 1.0 and 1.3. Assignment of a value for ρ is based on explicit consideration of the consequence of failure of a single element of the seismic-force-resisting system. A simple, deemed-to-comply exception is provided for certain structures.]

1.3 ENGINEERING PHILOSOPHY

The *Provisions*, under “Purpose,” states:

The design earthquake ground motion levels specified herein could result in both structural and nonstructural damage. For most structures designed and constructed according to the *Provisions*, structural damage from the design earthquake ground motion would be repairable although perhaps not economically so. For essential facilities, it is expected that the damage from the design earthquake ground motion would not be so severe as to preclude continued occupancy and function of the facility. . . . For ground motions larger than the design levels, the intent of the *Provisions* is that there be low likelihood of structural collapse.

The two points to be emphasized are that damage is to be expected when an earthquake (equivalent to the design earthquake) occurs and that the probability of collapse is not zero. The design earthquake ground motion level mentioned is two-thirds of the MCE ground motion.

The basic structural criteria are strength, stability, and distortion. The yield-level strength provided must be at least that required by the design spectrum (which is reduced from the elastic spectrum as described previously). Structural elements that cannot be expected to perform in a ductile manner are to have strengths greater than those required by the Ω_0 amplifier on the design spectral response. The stability criterion is imposed by amplifying the effects of lateral forces for the destabilizing effect of lateral translation of the gravity weight (the P-delta effect). The distortion criterion as a limit on story drift and is calculated by amplifying the linear response to the (reduced) design spectrum by the factor C_d to account for inelastic behavior.

Yield-level strengths for steel and concrete structures are easily obtained from common design standards. The most common design standards for timber and masonry are based on allowable stress concepts that are not consistent with the basis of the reduced design spectrum. Although strength-based standards for both materials have been introduced in recent years, the engineering profession has not yet embraced these new methods. In the past, the *Provisions* stipulated adjustments to common reference standards for timber and masonry to arrive at a strength level equivalent to yield and compatible with the basis of the design spectrum. Most of these adjustments were simple factors to be applied to conventional allowable stresses. With the deletion of these methods from the *Provisions*, methods have been introduced into model building codes and the ASCE standard *Minimum Design Loads for Buildings and Other Structures* to factor downward the seismic load effects based on the *Provisions* for use with allowable stress design methods.

The *Provisions* recognizes that the risk presented by a particular building is a combination of the seismic hazard at the site and the consequence of failure, due to any cause, of the building. Thus, a classification system is established based on the use and size of the building. This classification is called the Seismic Use Group (SUG). A combined classification called the Seismic Design Category (SDC) incorporates both the seismic hazard and the SUG. The SDC is used throughout the *Provisions* for decisions regarding the application of various specific requirements. The flow charts in Chapter 2 illustrate how these classifications are used to control application of various portions of the *Provisions*.

1.4 STRUCTURAL ANALYSIS

The *Provisions* sets forth several procedures for determining the force effect of ground shaking. Analytical procedures are classified by two facets: linear versus nonlinear and dynamic versus equivalent static. The two most fully constrained and frequently used are both linear methods: an equivalent static force procedure and a dynamic modal response spectrum analysis procedure. A third linear method, a full history of dynamic response (often referred to as a time-history or response-history analysis), and a nonlinear method are also permitted, subject to certain limitations. These methods use real or synthetic ground motion histories as input but require them to be scaled to the basic response spectrum at the site

for the range of periods of interest for the structure in question. Nonlinear analyses are very sensitive to assumptions made in the analysis and a peer review is required. A nonlinear static method, also known as a pushover analysis, is described in an appendix for trial use and comment. [In the 2003 *Provisions*, substantial changes were made to the appendix for the nonlinear static procedure based, in part, on the results of the Applied Technology Council's Project 55.]

The two most common linear methods make use of the same design spectrum. The entire reduction from the elastic spectrum to design spectrum is accomplished by dividing the elastic spectrum by the coefficient R , which ranges from 1-1/4 to 8. The specified elastic spectrum is based on a damping level at 5 percent of critical damping, and a part of the R factor accomplishes adjustments in the damping level. The *Provisions* define the total effect of earthquake actions as a combination of the response to horizontal motions (or forces for the equivalent static force method) with response to vertical ground acceleration. The resulting internal forces are combined with the effects of gravity loads and then compared to the full strength of the members, which are not reduced by a factor of safety.

With the equivalent static force procedure, the level of the design spectrum is set by determining the appropriate values of basic seismic acceleration, the appropriate soil profile type, and the value for R . The particular acceleration for the building is determined from this spectrum by selecting a value for the natural period of vibration. Equations that require only the height and type of structural system are given to approximate the natural period for various building types. (The area and length of shear walls come into play with an optional set of equations.) Calculation of a period based on an analytical model of the structure is encouraged, but limits are placed on the results of such calculations. These limits prevent the use of a very flexible model in order to obtain a large period and correspondingly low acceleration. Once the overall response acceleration is found, the base shear is obtained by multiplying it by the total effective mass of the building, which is generally the total permanent load.

Once the total lateral force is determined, the equivalent static force procedure specifies how this force is to be distributed along the height of the building. This distribution is based on the results of dynamic studies of relatively uniform buildings and is intended to give an envelope of shear force at each level that is consistent with these studies. This set of forces will produce, particularly in tall buildings, an envelope of gross overturning moment that is larger than the dynamic studies indicate is necessary. Dynamic analysis is encouraged, and the modal procedure is required for structures with large periods (essentially this means tall structures) in the higher seismic design categories.

With one exception, the remainder of the equivalent static force analysis is basically a standard structural analysis. That exception accounts for uncertainties in the location of the center of mass, uncertainties in the strength and stiffness of the structural elements, and rotational components in the basic ground shaking. This concept is referred to as horizontal torsion. The *Provisions* requires that the center of force be displaced from the calculated center of mass by an arbitrary amount in either direction (this torsion is referred to as accidental torsion). The twist produced by real and accidental torsion is then compared to a threshold, and if the threshold is exceeded, the torsion must be amplified.

In many respects, the modal analysis procedure is very similar to the equivalent static force procedure. The primary difference is that the natural period and corresponding deflected shape must be known for several of the natural modes of vibration. These are calculated from a mathematical model of the structure. The procedure requires inclusion of enough modes so that the dynamic model represents at least 90 percent of the mass in the structure that can vibrate. The base shear for each mode is determined from a design spectrum that is essentially the same as that for the static procedure. The distribution of forces, and the resulting story shears and overturning moments, are determined for each mode directly from the procedure. Total values for subsequent analysis and design are determined by taking the square root of the sum of the squares for each mode. This summation gives a statistical estimate of maximum response when the participation of the various modes is random. If two or more of the modes have very

similar periods, more advanced techniques for summing the values are required; these procedures must account for coupling in the response of close modes. The sum of the absolute values for each mode is always conservative.

A lower limit to the base shear determined from the modal analysis procedure is specified based on the static procedure and the approximate periods specified in the static procedure. When this limit is violated, which is common, all results are scaled up in direct proportion. The consideration of horizontal torsion is the same as for the static procedure. Because the forces applied at each story, the story shears, and the overturning moments are separately obtained from the summing procedure, the results are not statically compatible (that is, the moment calculated from the story forces will not match the moment from the summation). Early recognition of this will avoid considerable problems in later analysis and checking.

For structures that are very uniform in a vertical sense, the two procedures give very similar results. The modal analysis method is better for buildings having unequal story heights, stiffnesses, or masses. The modal procedure is required for such structures in higher seismic design categories. Both methods are based on purely elastic behavior and, thus, neither will give a particularly accurate picture of behavior in an earthquake approaching the design event. Yielding of one component leads to redistribution of the forces within the structural system. This may be very significant; yet, none of the linear methods can account for it.

Both of the common methods require consideration of the stability of the building as a whole. The technique is based on elastic amplification of horizontal displacements created by the action of gravity on the displaced masses. A simple factor is calculated and the amplification is provided for in designing member strengths when the amplification exceeds about 10 percent. The technique is referred to as the P-delta analysis and is only an approximation of stability at inelastic response levels.

1.5 NONSTRUCTURAL ELEMENTS OF BUILDINGS

Severe ground shaking often results in considerable damage to the nonstructural elements of buildings. Damage to nonstructural elements can pose a hazard to life in and of itself, as in the case of heavy partitions or facades, or it can create a hazard if the nonstructural element ceases to function, as in the case of a fire suppression system. Some buildings, such as hospitals and fire stations, need to be functional immediately following an earthquake; therefore, many of their nonstructural elements must remain undamaged.

The *Provisions* treats damage to and from nonstructural elements in three ways. First, indirect protection is provided by an overall limit on structural distortion; the limits specified, however, may not offer enough protection to brittle elements that are rigidly bound by the structure. More restrictive limits are placed upon those SUGs for which better performance is desired given the occurrence of strong ground shaking. Second, many components must be anchored for an equivalent static force. Third, the explicit design of some elements (the elements themselves, not just their anchorage) to accommodate specific structural deformations or seismic forces is required.

The dynamic response of the structure provides the dynamic input to the nonstructural component. Some components are rigid with respect to the structure (light weights and small dimensions often lead to fundamental periods of vibration that are very short). Application of the response spectrum concept would indicate that the time history of motion of a building roof to which mechanical equipment is attached looks like a ground motion to the equipment. The response of the component is often amplified above the response of the supporting structure. Response spectra developed from the history of motion of a point on a structure undergoing ground shaking are called floor spectra and are a useful in understanding the demands upon nonstructural components.

The *Provisions* simplifies the concept greatly. The force for which components are checked depends on:

1. The component mass;
2. An estimate of component acceleration that depends on the structural response acceleration for short period structures, the relative height of the component within the structure, and a crude approximation of the flexibility of the component or its anchorage;
3. The available ductility of the component or its anchorage; and
4. The function or importance of the component or the building.

Also included in the *Provisions* is a quantitative measure for the deformation imposed upon nonstructural components. The inertial force demands tend to control the seismic design for isolated or heavy components whereas the imposed deformations are important for the seismic design for elements that are continuous through multiple levels of a structure or across expansion joints between adjacent structures, such as cladding or piping.

1.6 QUALITY ASSURANCE

Since strong ground shaking has tended to reveal hidden flaws or *weak links* in buildings, detailed requirements for assuring quality during construction are contained in the *Provisions*. Loads experienced during construction provide a significant test of the likely performance of ordinary buildings under gravity loads. Tragically, mistakes occasionally will pass this test only to cause failure later, but it is fairly rare. No comparable proof test exists for horizontal loads, and experience has shown that flaws in construction show up in a disappointingly large number of buildings as distress and failure due to earthquakes. This is coupled with the fact that the design is based on excursions into inelastic straining, which is not the case for response to other loads.

The quality assurance provisions require a systematic approach with an emphasis on documentation and communication. The designer who conceives the systems to resist the effects of earthquake forces must identify the elements that are critical for successful performance as well as specify the testing and inspection necessary to ensure that those elements are actually built to perform as intended. Minimum levels of testing and inspection are specified in the *Provisions* for various types of systems and components.

The *Provisions* also requires that the contractor and building official be aware of the requirements specified by the designer. Furthermore, those individuals who carry out the necessary inspection and testing must be technically qualified and must communicate the results of their work to all concerned parties. In the final analysis, there is no substitute for a sound design, soundly executed.

GUIDE TO USE OF THE *PROVISIONS*

Michael Valley, P.E.

The flow charts and table that follow are provided to assist the user of the *NEHRP Recommended Provisions* and, by extension, the seismic provisions of ASCE 7, *Minimum Design Loads for Buildings and Other Structures*, the *International Building Code*, and *NFPA 5000*. The flow charts provide an overview of the complete process for satisfying the *Provisions*, including the content of all technical chapters. The table that concludes this chapter provides cross references for ASCE 7 and the 2000 and 2003 editions of the *NEHRP Recommended Provisions*.

The flow charts are expected to be of most use to those who are unfamiliar with the scope of the *NEHRP Recommended Provisions*, but they cannot substitute for a careful reading of the *Provisions*. Notes indicate discrepancies and errors in the *Provisions*. Both editions of the *Provisions* can be obtained free from the FEMA Publications Distribution Center by calling 1-800-480-2520. Order by FEMA Publication number; the 2003 *Provisions* is available as FEMA 450 in CD form (only a limited number of paper copies are available) and the 2000 *Provisions* are available as FEMA 368 and 369 (2 volumes and maps).

Although the examples in this volume are based on the 2000 *Provisions*, they have been annotated to reflect changes made to the 2003 *Provisions*. Annotations within brackets, [], indicate both organizational changes (as a result of a reformat of all of the chapters of the 2003 *Provisions*) and substantive technical changes to the 2003 *Provisions* and its primary reference documents. For those readers coming from ASCE 7-05, see the cross reference table at the end of this chapter.

The level of detail shown varies, being greater where questions of applicability of the *Provisions* are pertinent and less where a standard process of structural analysis or detailing is all that is required. The details contained in the many standards referenced in the *Provisions* are not included; therefore, the actual flow of information when proportioning structural members for the seismic load effects specified in the *Provisions* will be considerably more complex.

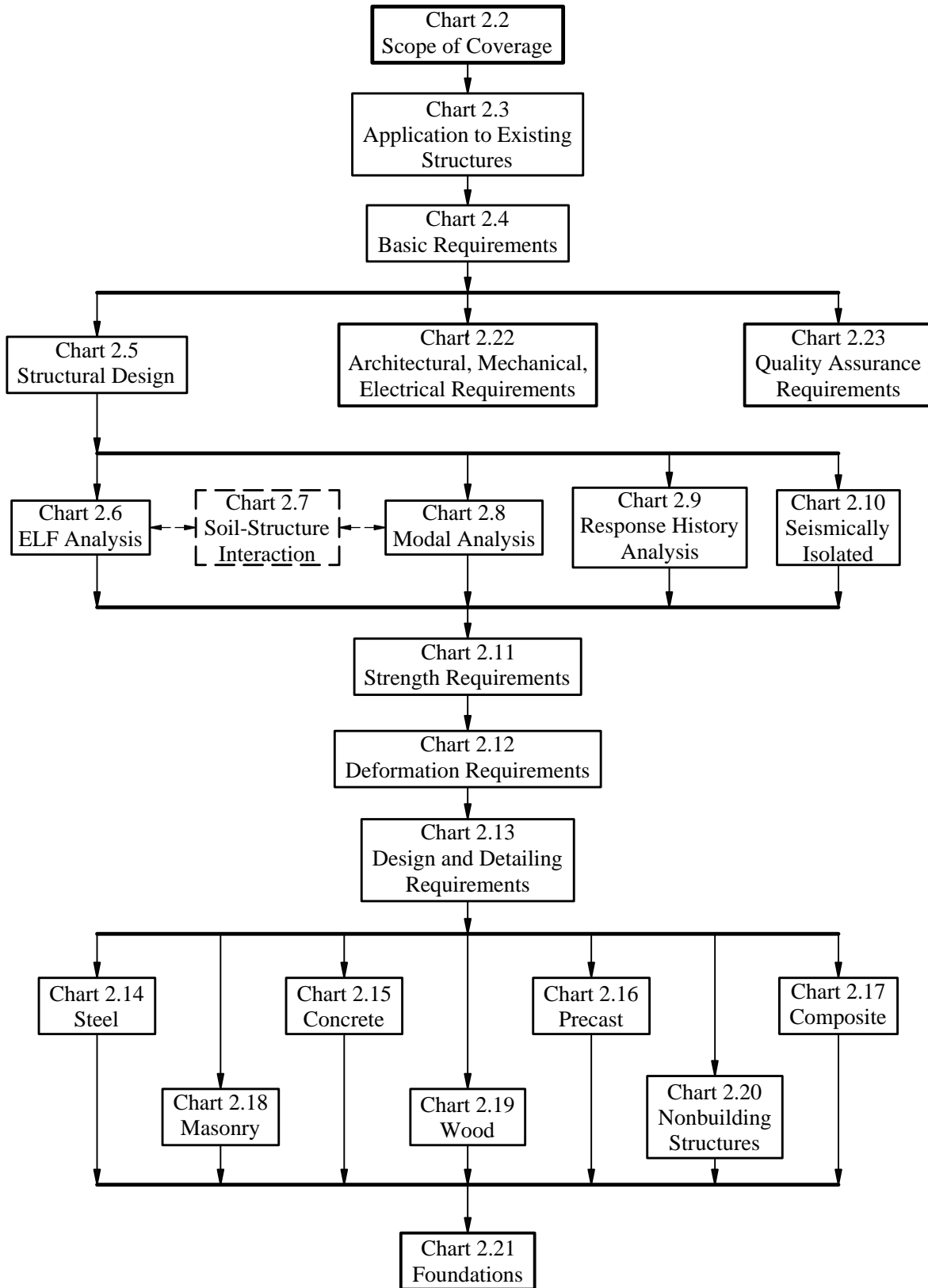
On each chart the flow generally is from a heavy-weight box at the top-left to a medium-weight box at the bottom-right. User decisions are identified by six-sided cells. Optional items and modified flow are indicated by dashed lines.

Chart 2.1 provides an overall summary of the process which begins with consideration of the Scope of Coverage and ends with Quality Assurance Requirements. All of the specific provisions pertaining to nonbuilding structures are collected together on one page (Chart 2.20); application for nonbuilding structures requires the use of various portions of the *Provisions* with appropriate modification.

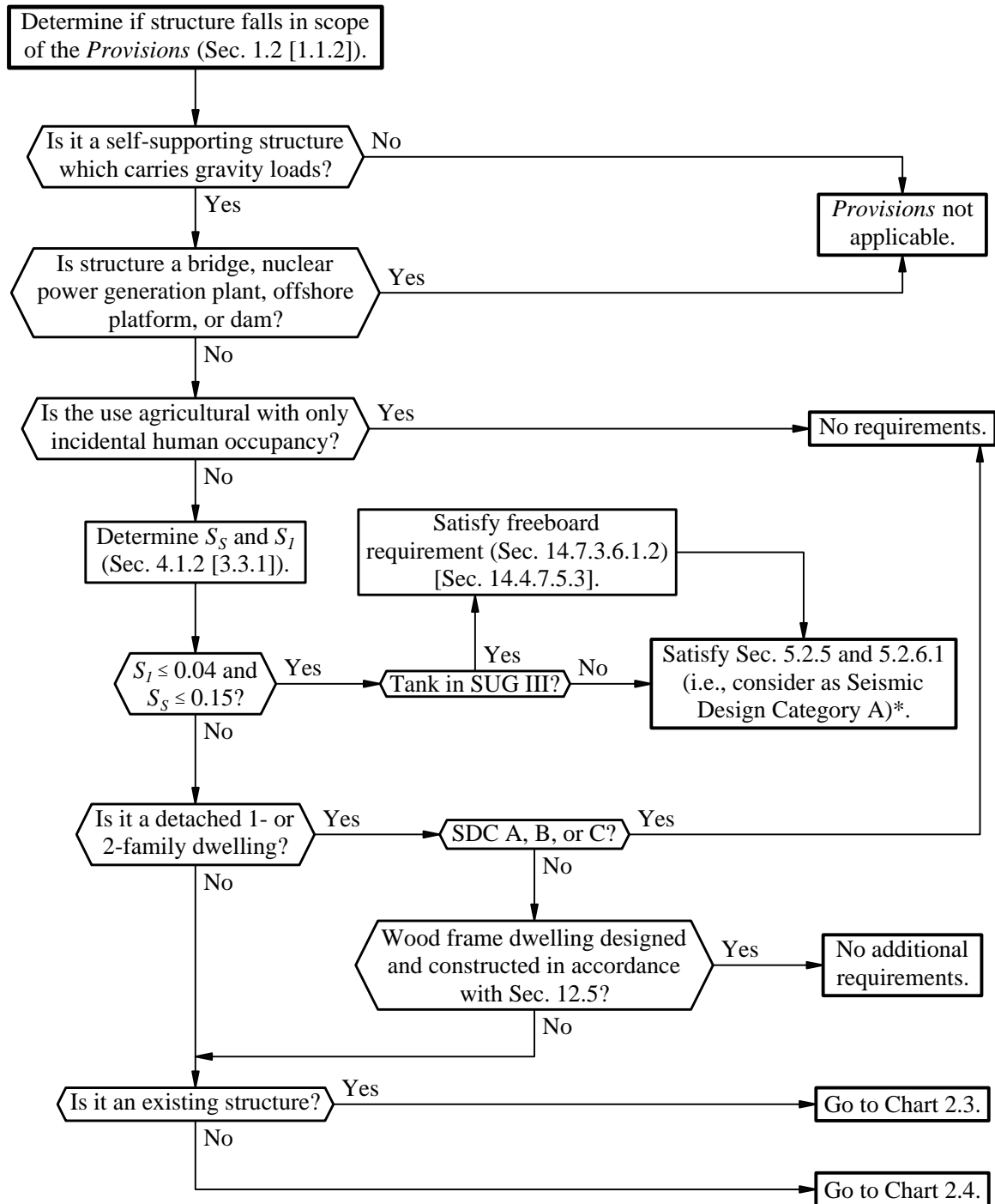
Additions to, changes of use in, and alterations of existing structures are covered by the *NEHRP Recommended Provisions* (see Chart 2.3), but evaluation and rehabilitation of existing structures is not.

In recent years FEMA has sponsored several coordinated efforts dealing with seismic safety in existing buildings. A *Handbook for Seismic Evaluation of Buildings* (FEMA 310) was developed as an update to the original FEMA 178, although this document has since been replaced by the ASCE 31 Standard (*Seismic Evaluation of Existing Buildings*). *Guidelines for the Seismic Rehabilitation of Buildings* (FEMA 273) and a corresponding *Commentary* (FEMA 274) have also been developed. A prestandard (FEMA 356, *Prestandard and Commentary for the Seismic Rehabilitation of Buildings*) based on FEMA 273 has been developed and is in balloting as ASCE 41. In addition, specific recommendations have been developed for the evaluation, repair, and rehabilitation of earthquake-damaged concrete and masonry wall buildings (FEMA 306, 307, and 308) and for the evaluation, rehabilitation, post-earthquake assessment, and repair of steel moment frame structures (FEMA 351 and 352).

**Chart 2.1
Overall Summary of Flow**

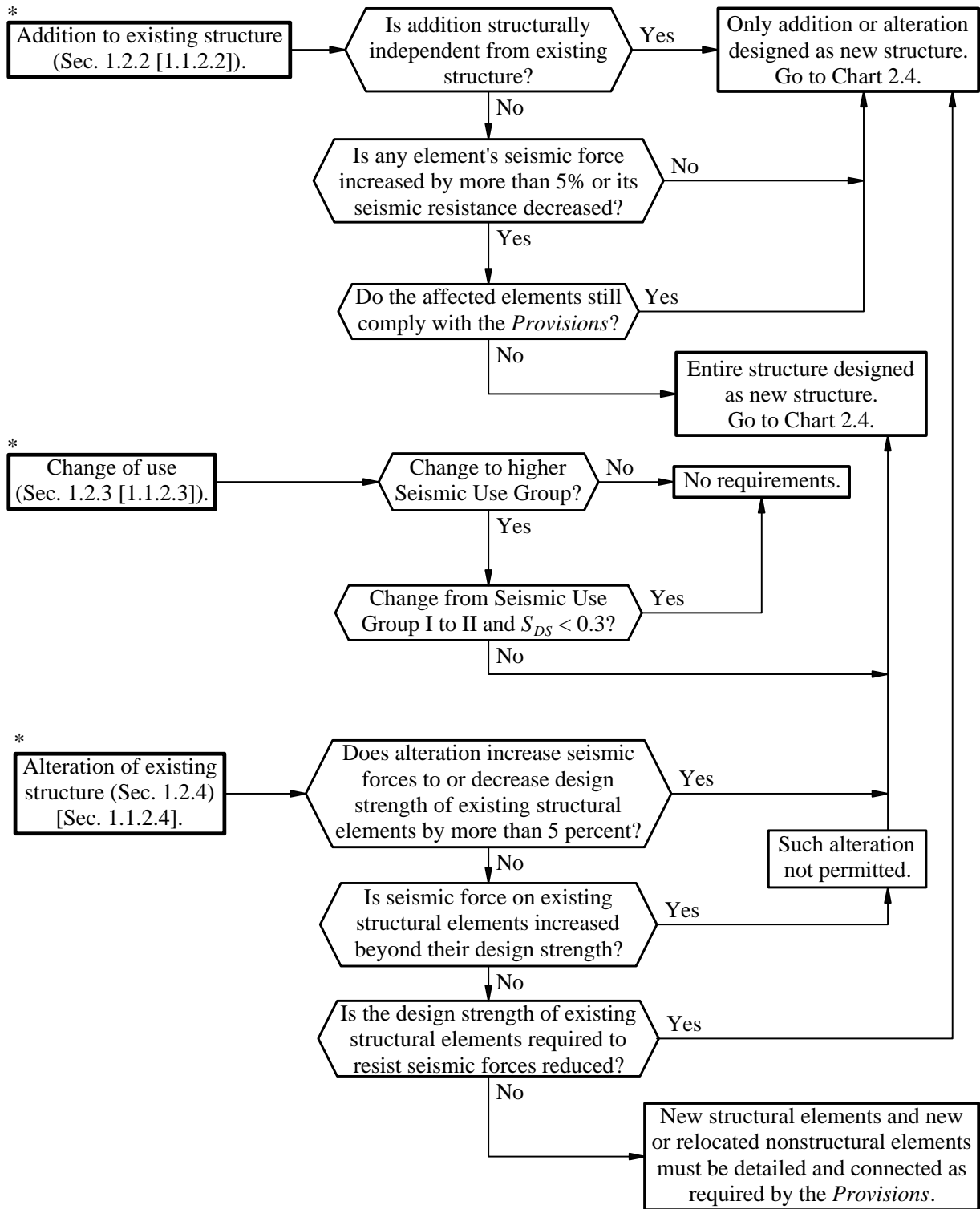


**Chart 2.2
Scope of Coverage**



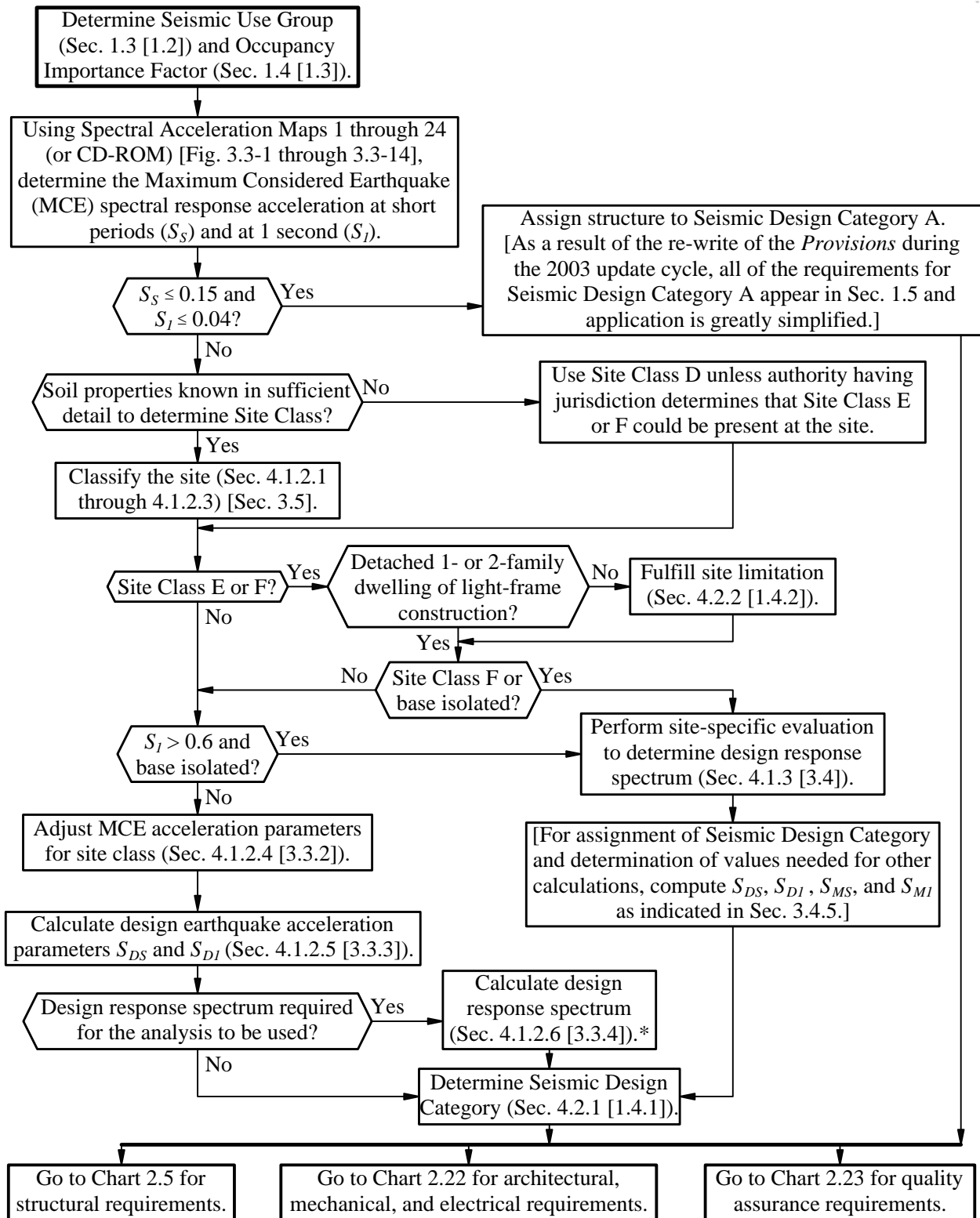
*The *Provisions* has never defined clearly the scope of application for structures assigned to Seismic Design Category A. Although the framers of the *Provisions* intended application of only a few simple requirements in Seismic Design Category A, a strict reading of the 2000 *Provisions* would lead to a substantial list of items that remain within the scope. [As a result of the complete re-write of the *Provisions* at the beginning of the 2003 update cycle, this situation is improved considerably as the requirements for Seismic Design Category A all appear in Sec. 1.5.]

Chart 2.3
Application to Existing Structures



* The *Provisions* applies to existing structures only in the cases of additions to, changes of use in, and alterations of such structures.

**Chart 2.4
Basic Requirements**



* [Sec. 3.3.4 of the 2003 Provisions defines reduced spectral ordinates for periods greater than T_L .]

**Chart 2.5
Structural Design**

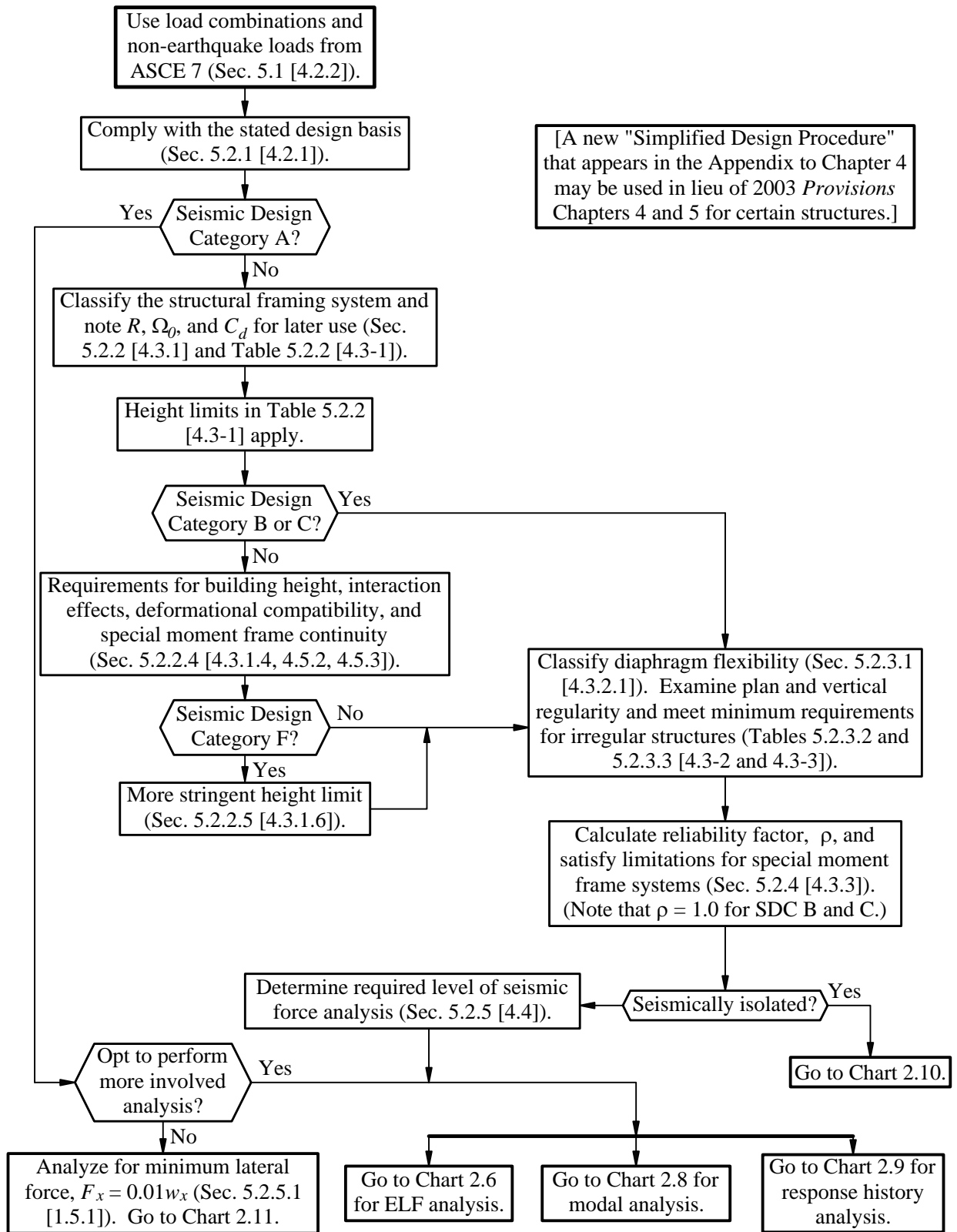


Chart 2.6
Equivalent Lateral Force (ELF) Analysis

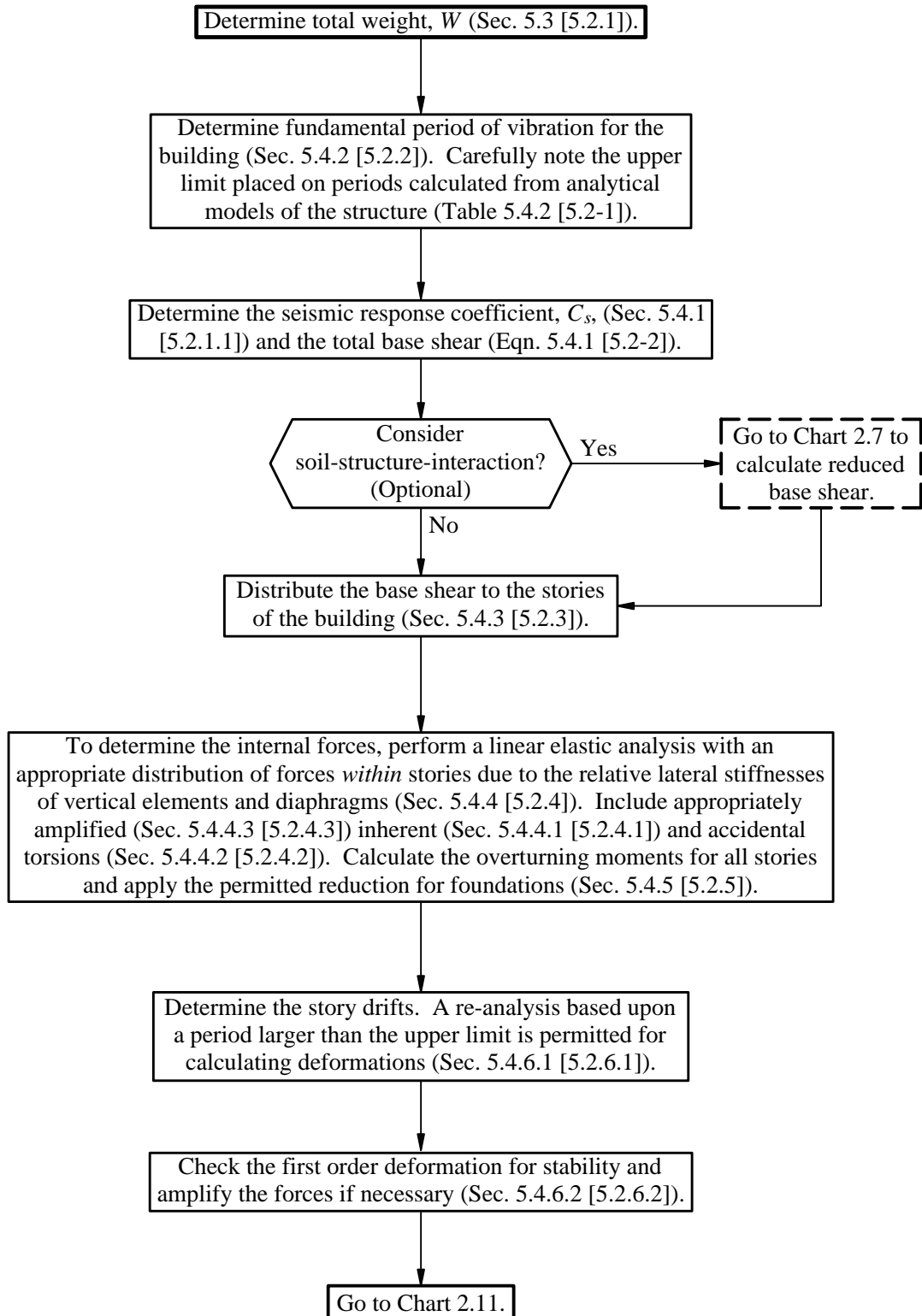
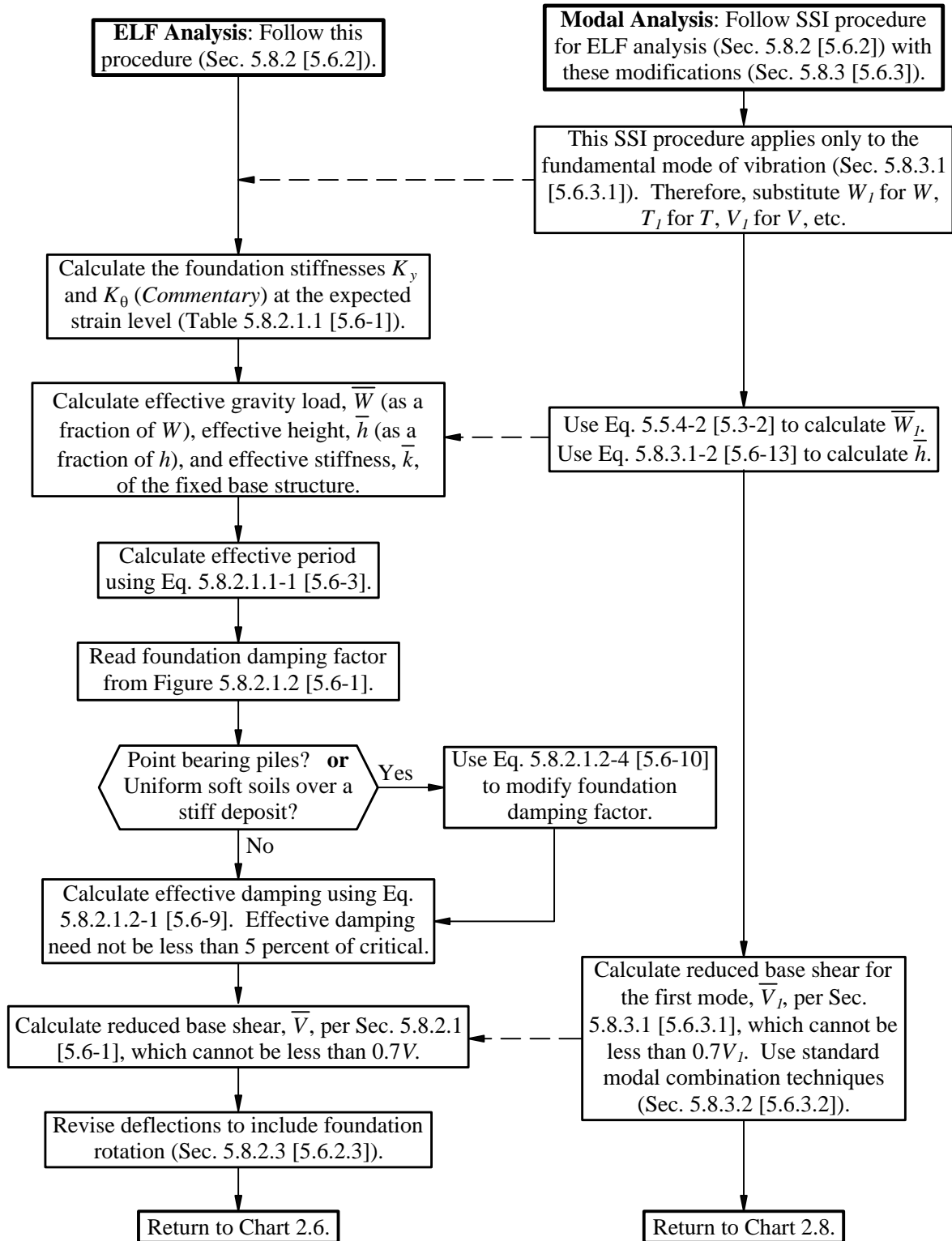
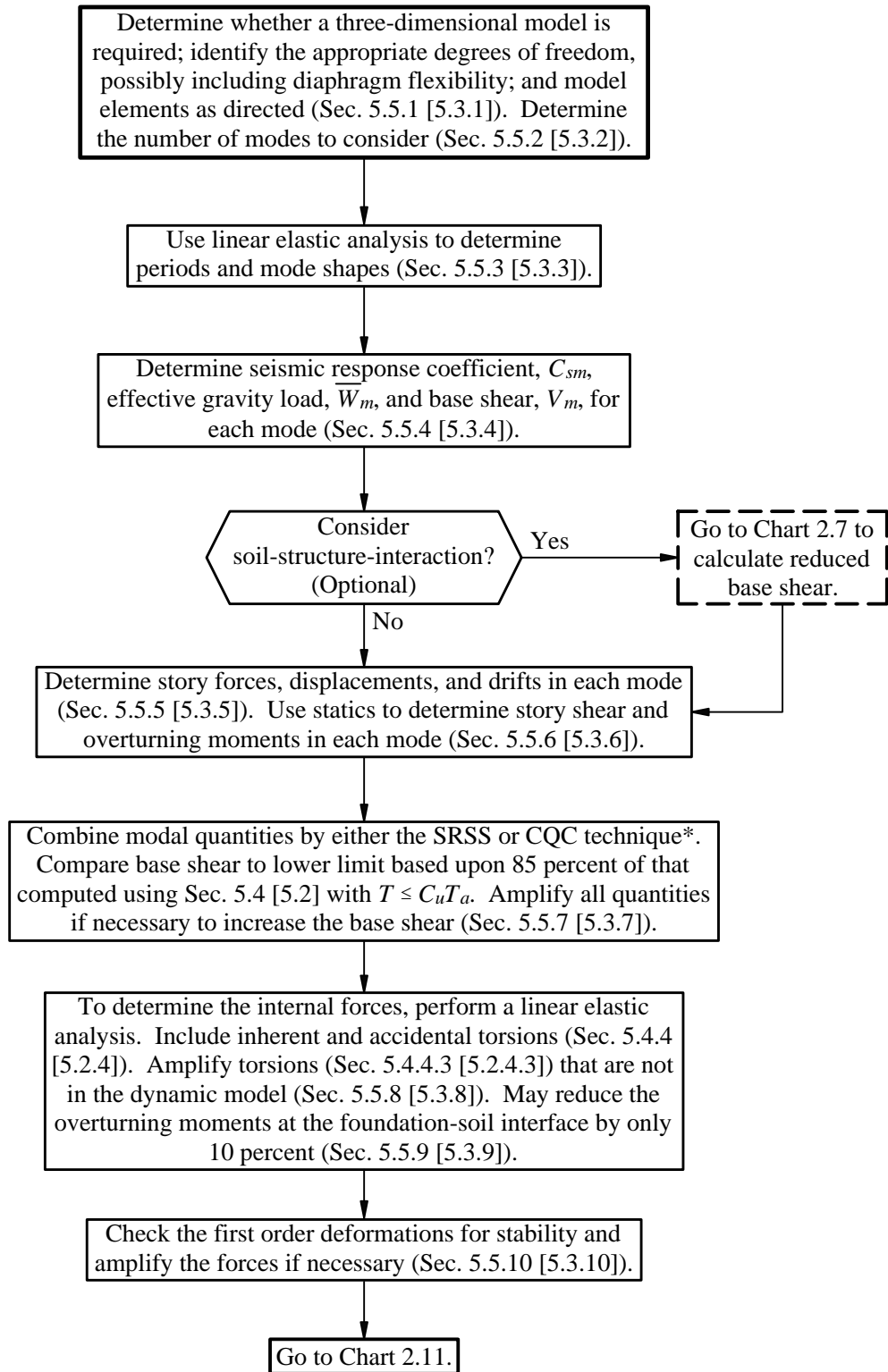


Chart 2.7
Soil-Structure Interaction (SSI)



**Chart 2.8
Modal Analysis**



*As indicated in the text, use of the CQC technique is required where closely spaced periods in the translational and torsional modes will result in cross-correlation of the modes.

Chart 2.9
Response History Analysis

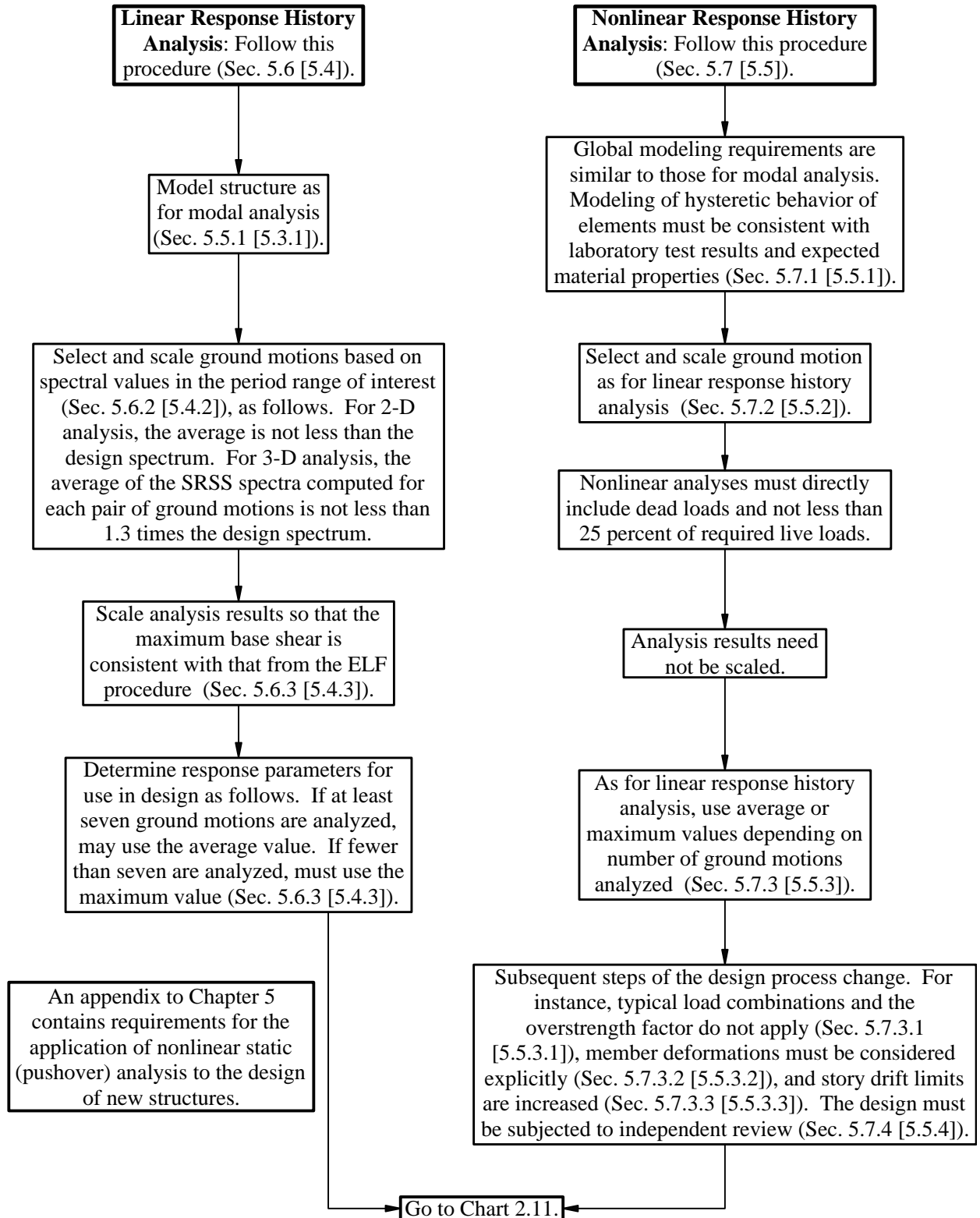
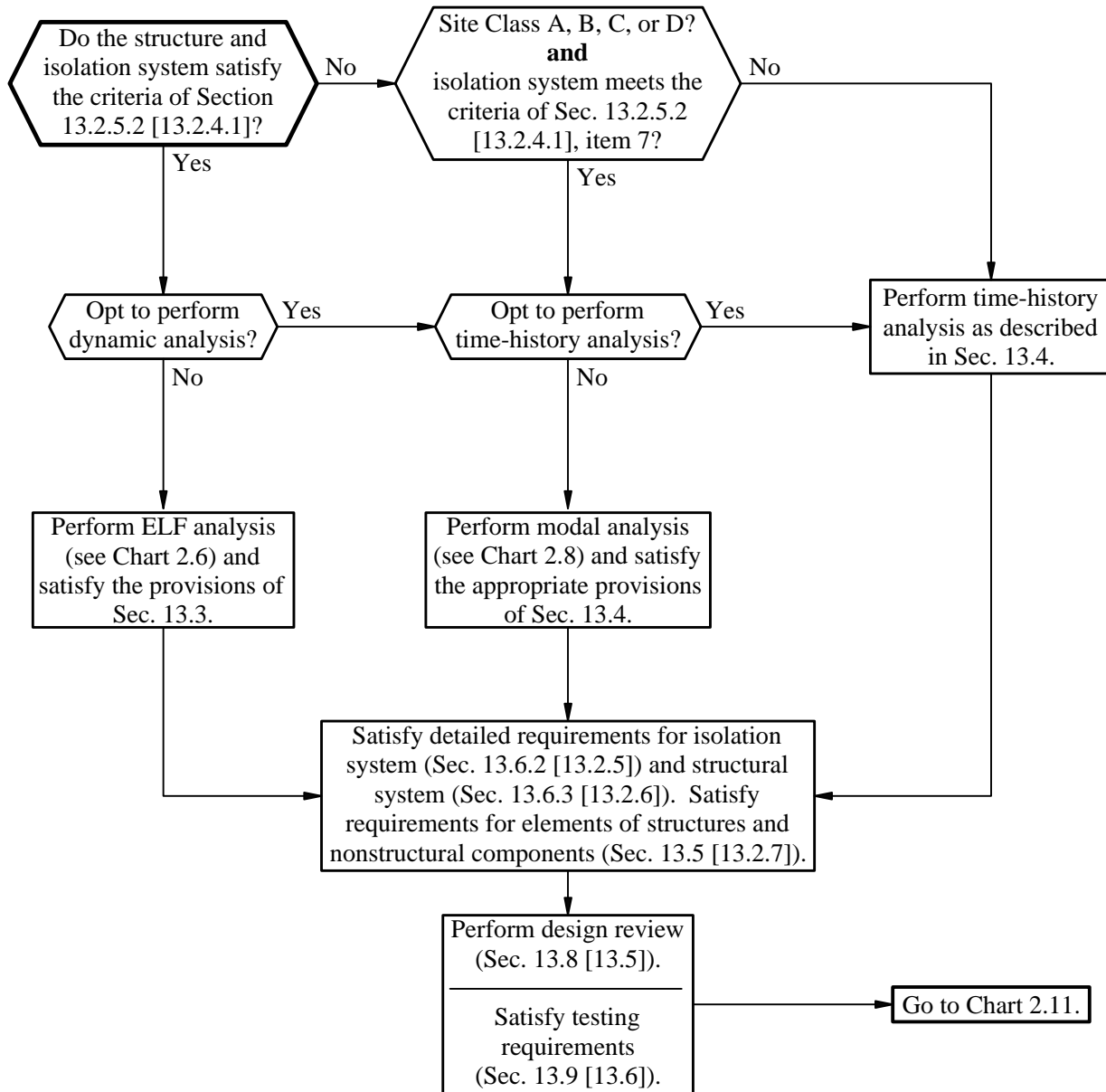


Chart 2.10
Seismically Isolated Structures



[In the 2003 Provisions, requirements for structures with damping systems appear in Chapter 15 (rather than in an appendix to Chapter 13).]

Chart 2.11 Strength Requirements

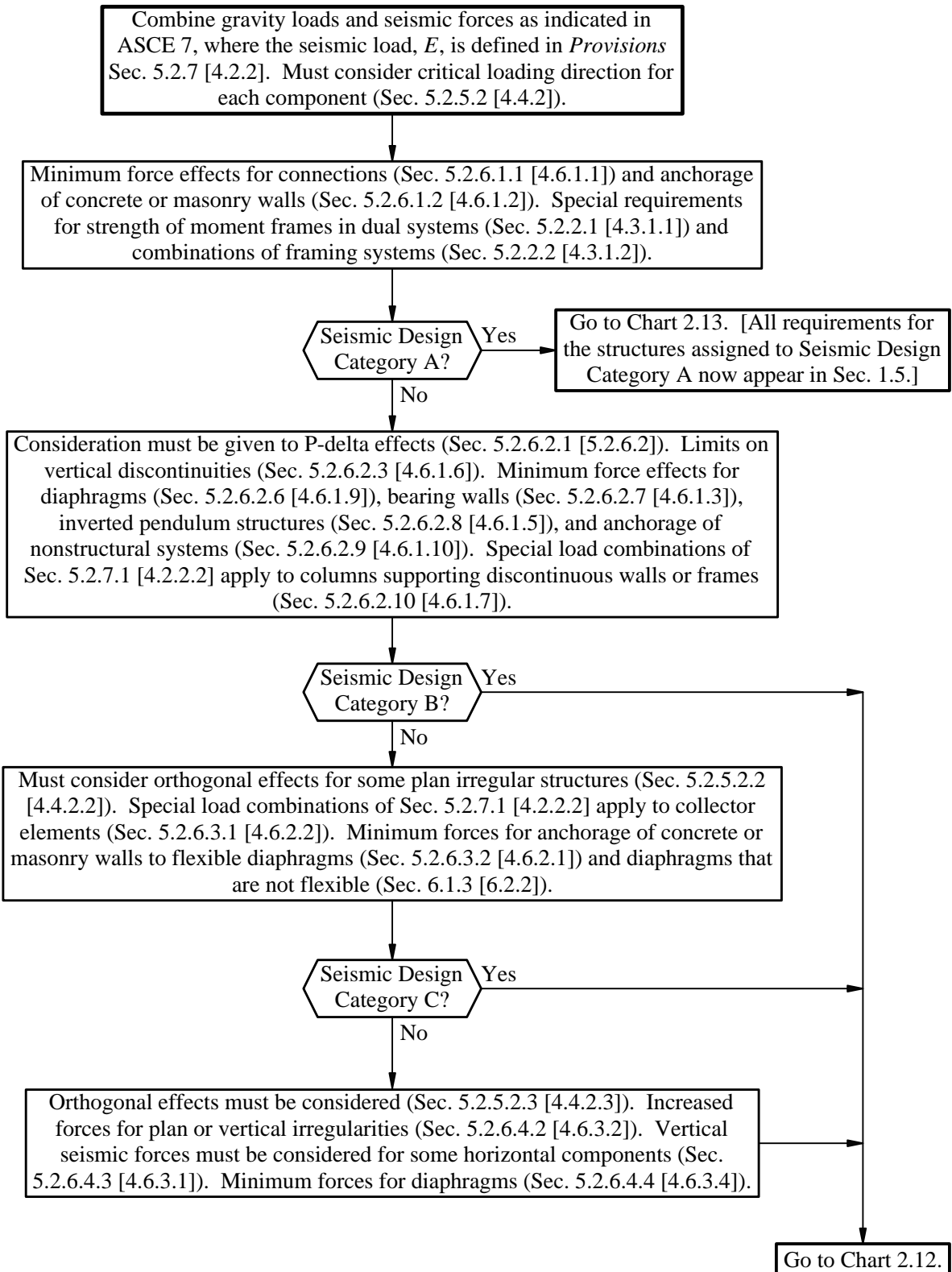


Chart 2.12 Deformation Requirements

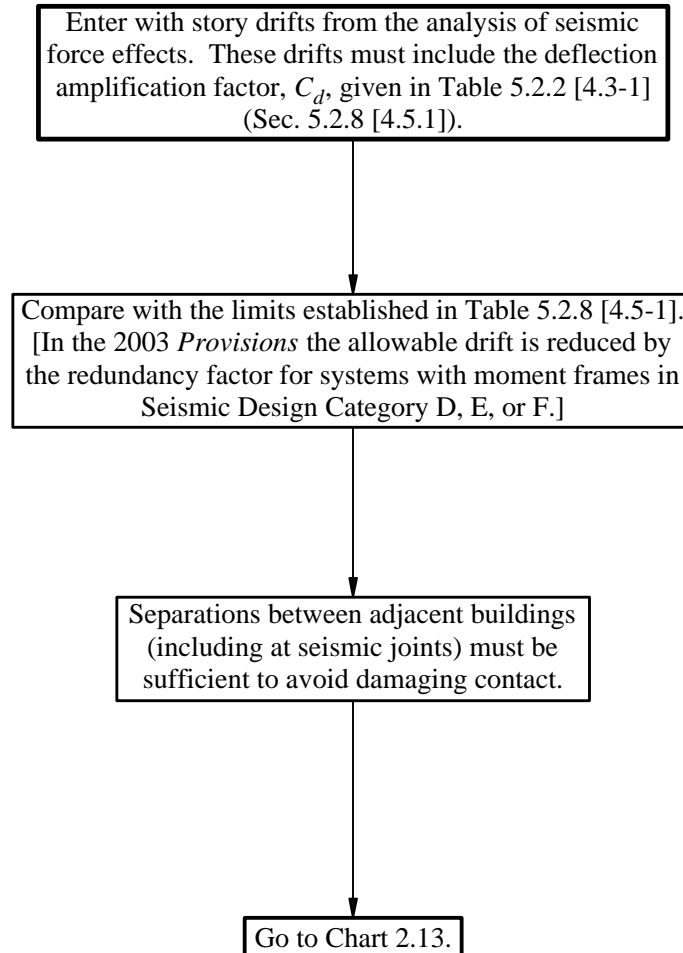


Chart 2.13
Design and Detailing Requirements

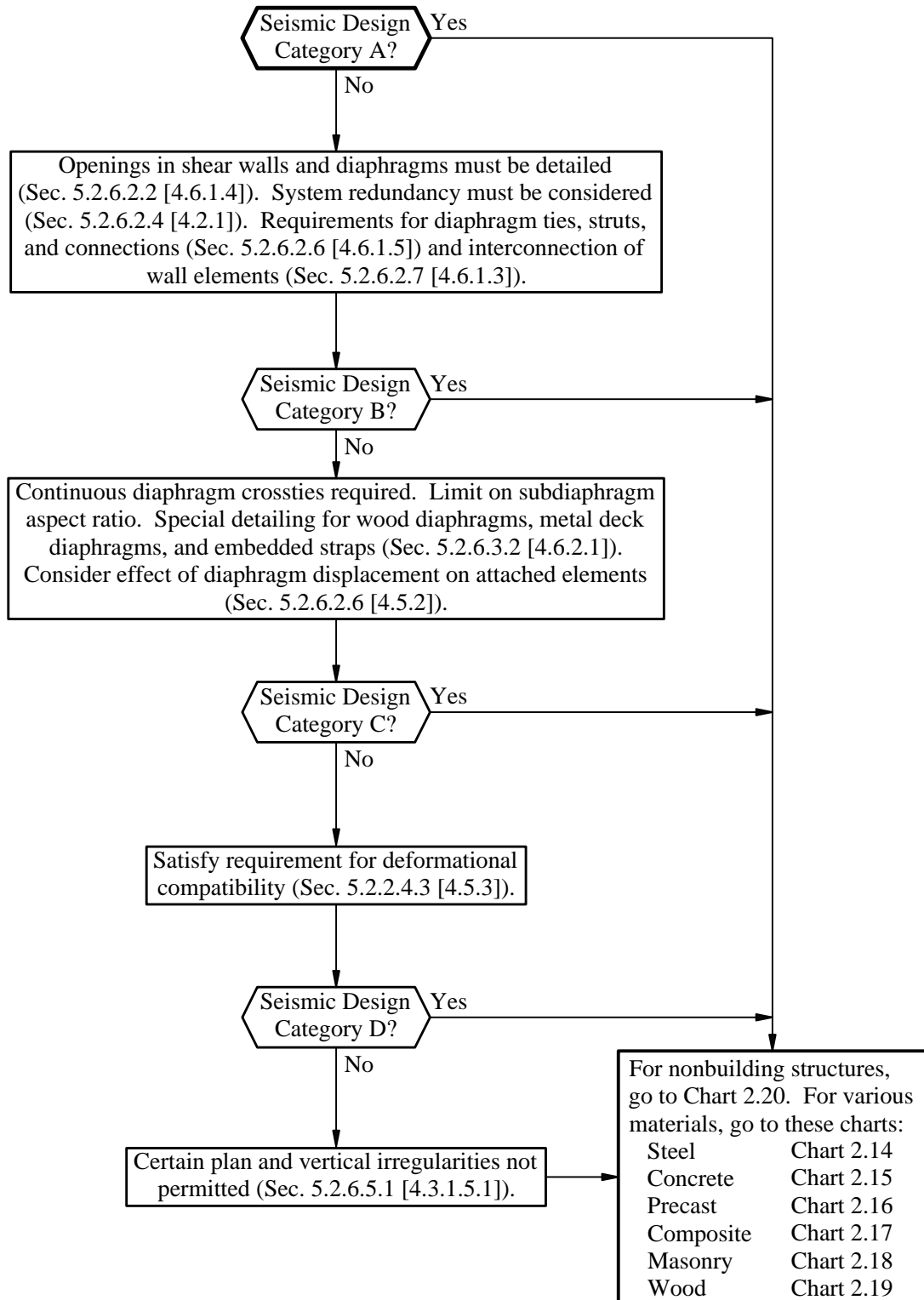


Chart 2.14
Steel Structures

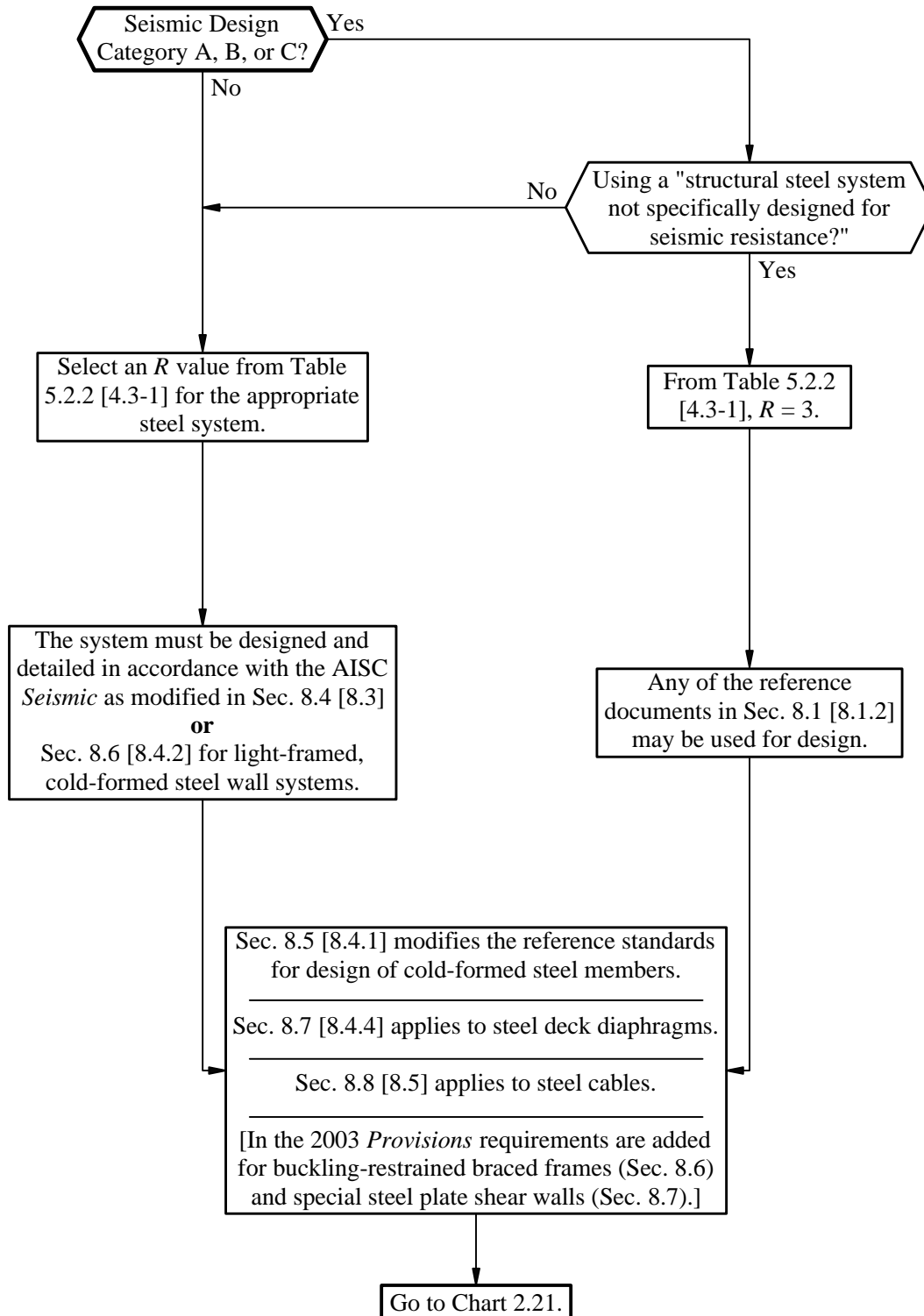


Chart 2.15
Concrete Structures

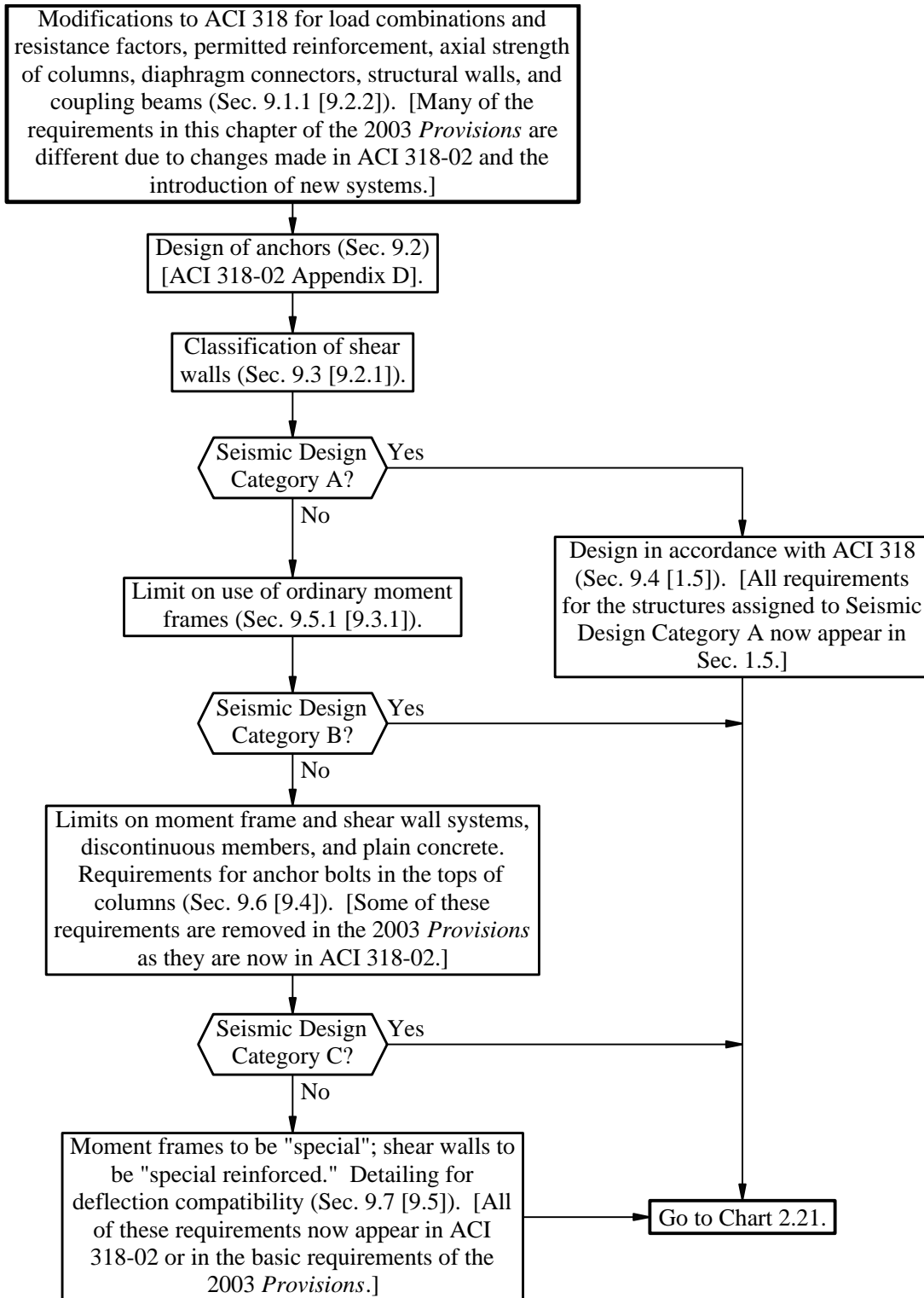


Chart 2.16
Precast Concrete Structures

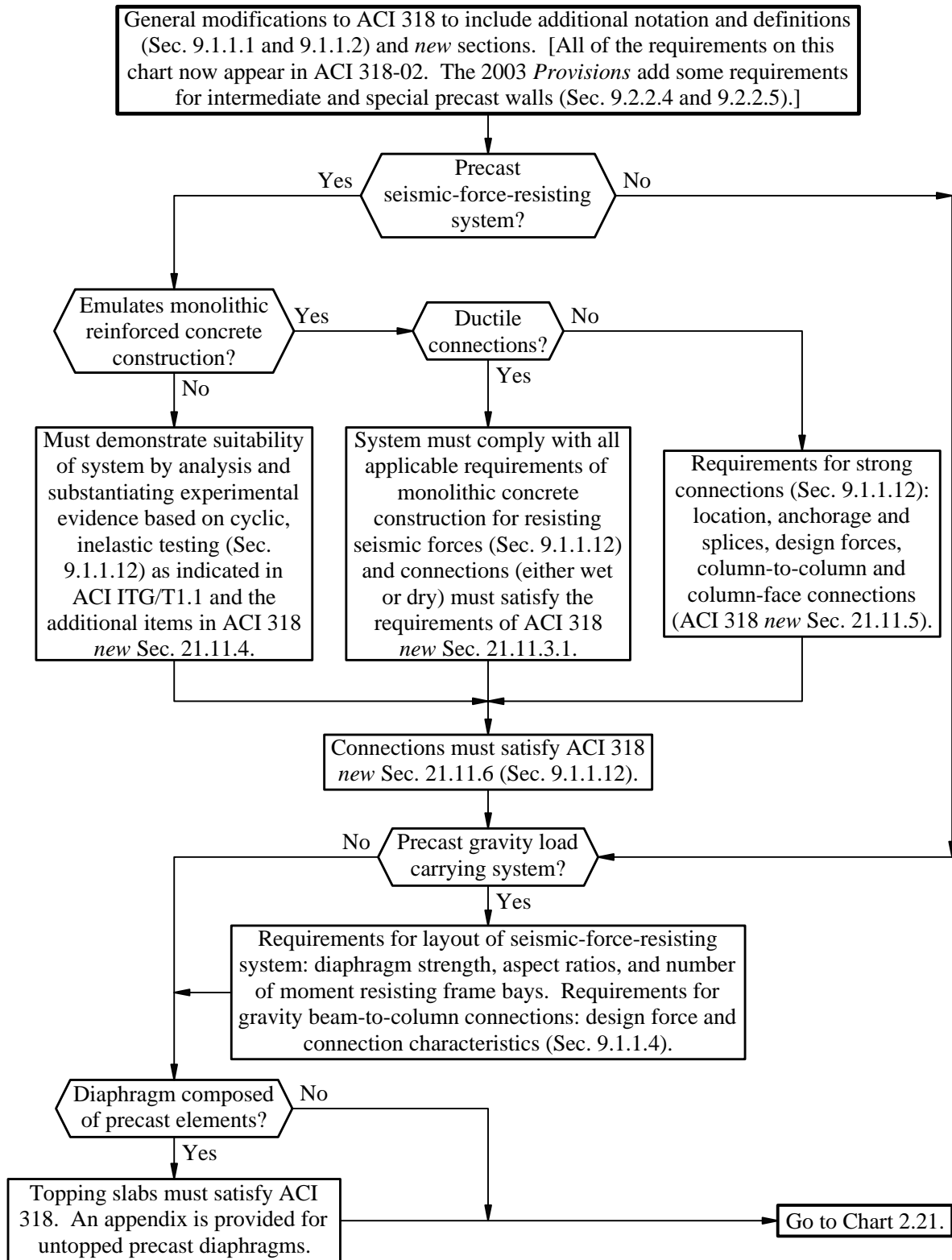


Chart 2.17
Composite Steel and Concrete Structures

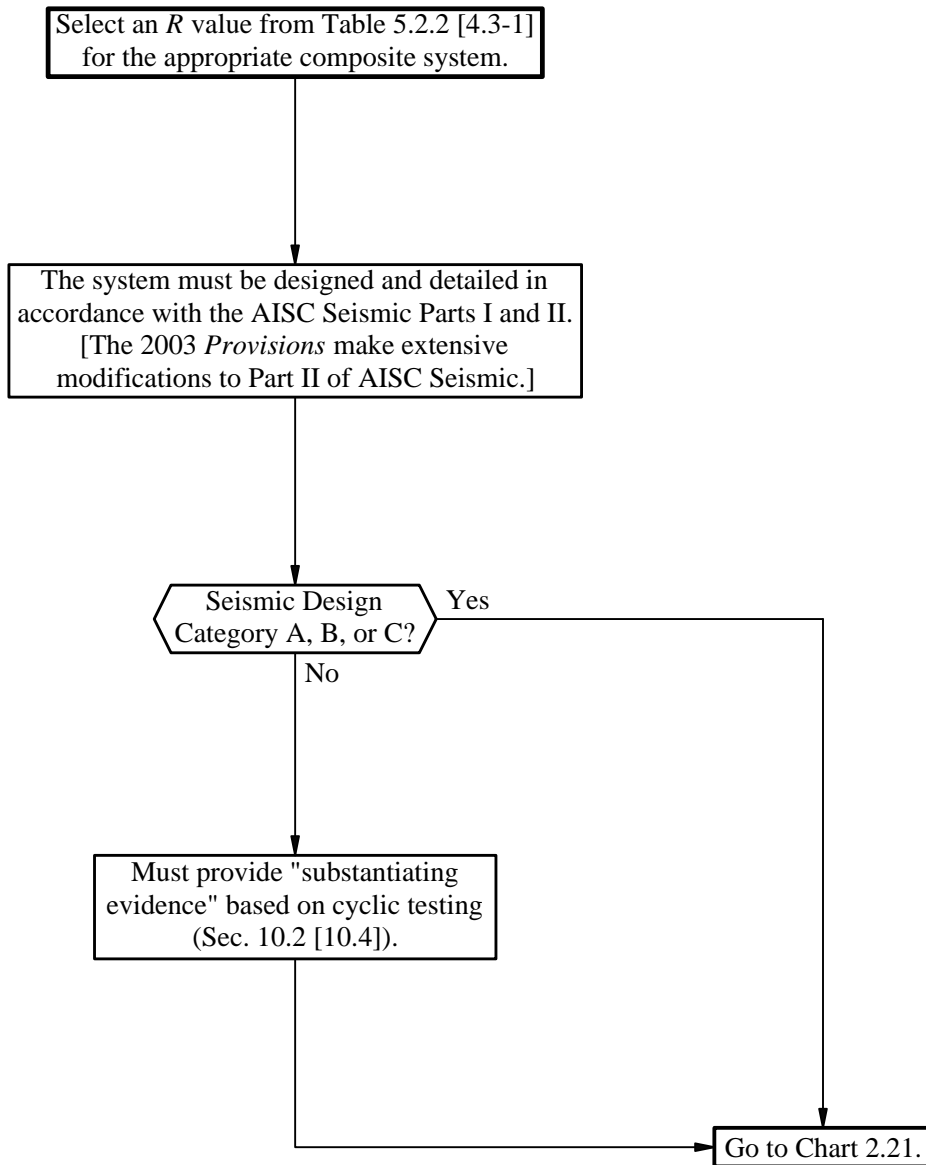


Chart 2.18
Masonry Structures

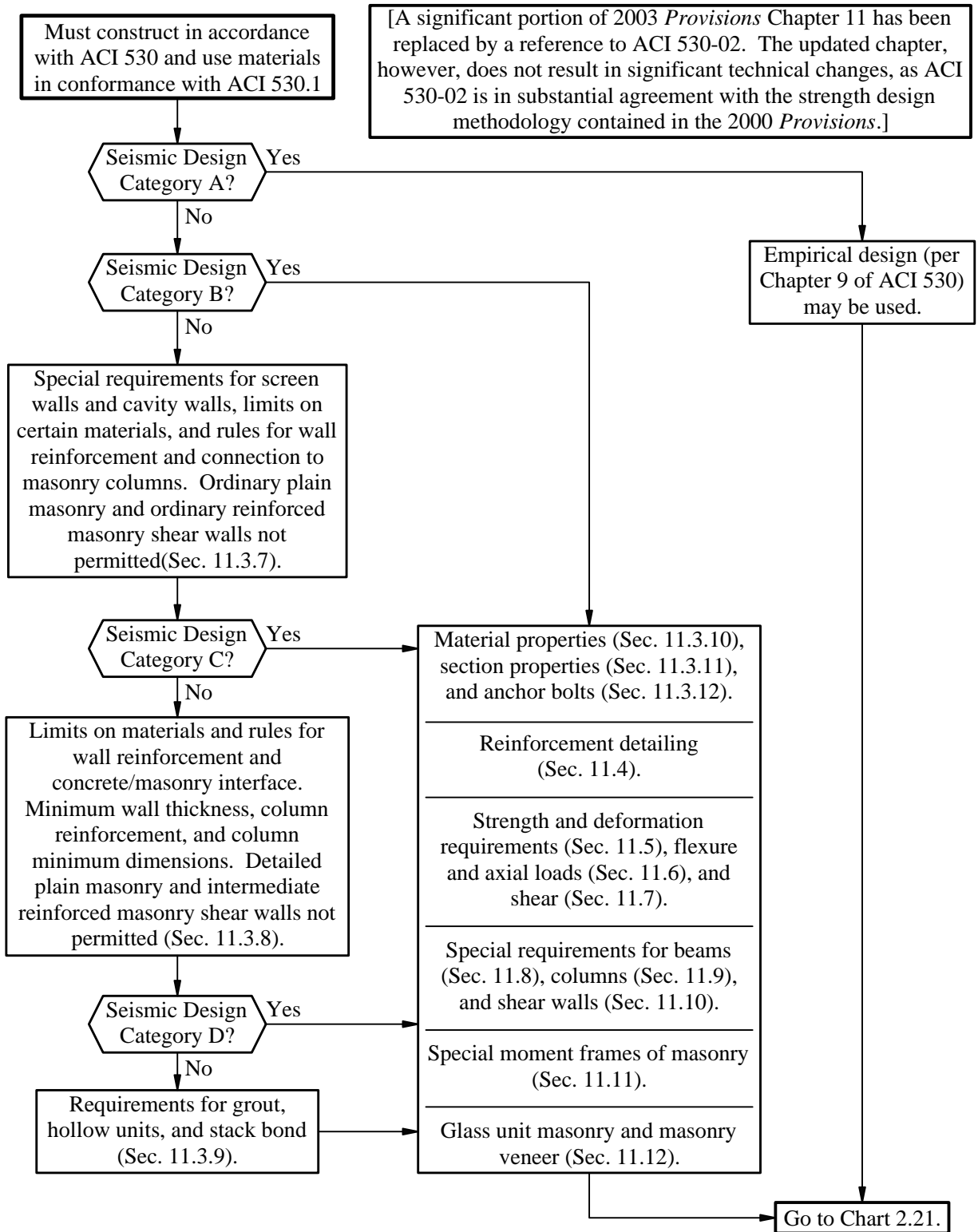


Chart 2.19
Wood Structures

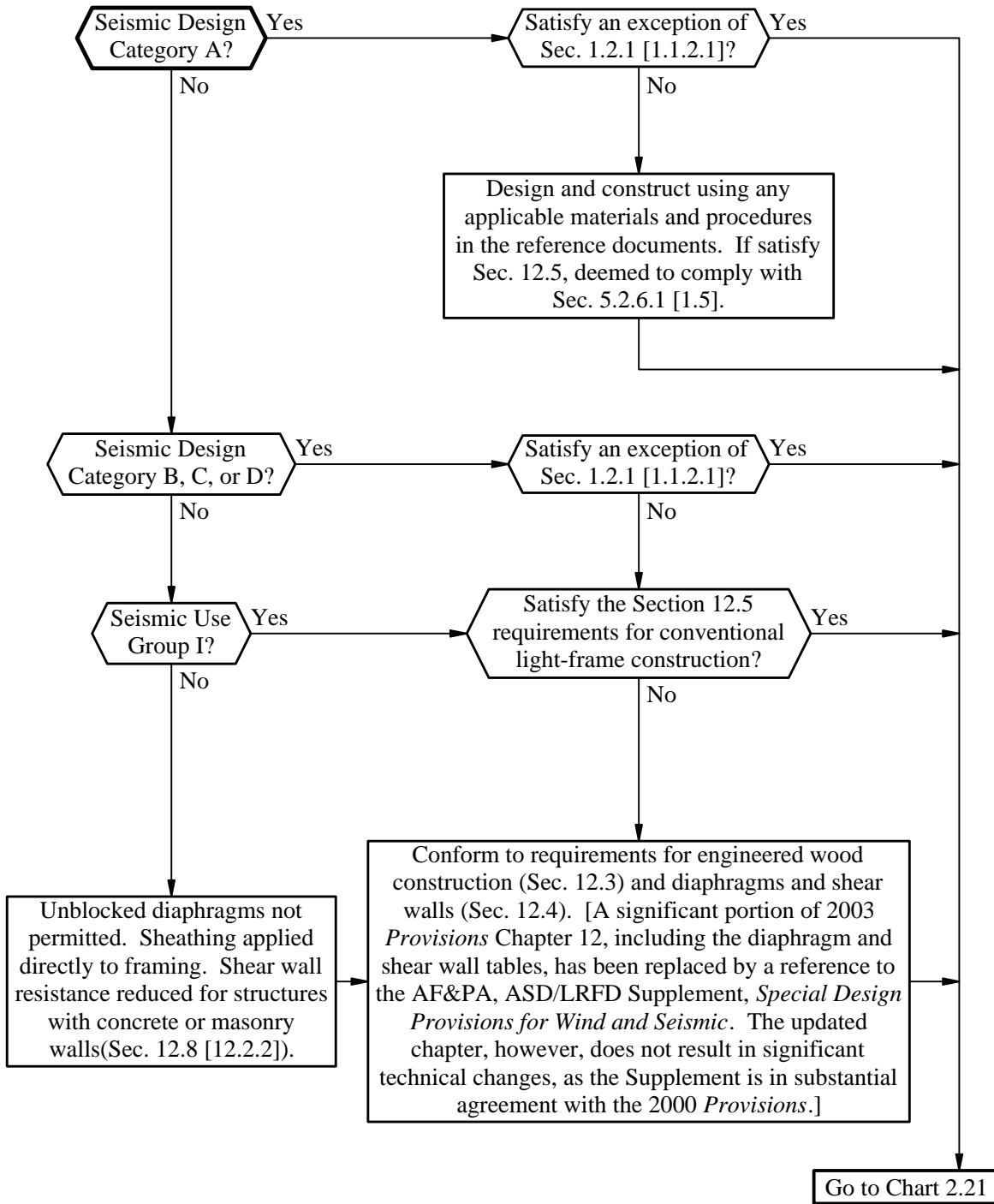
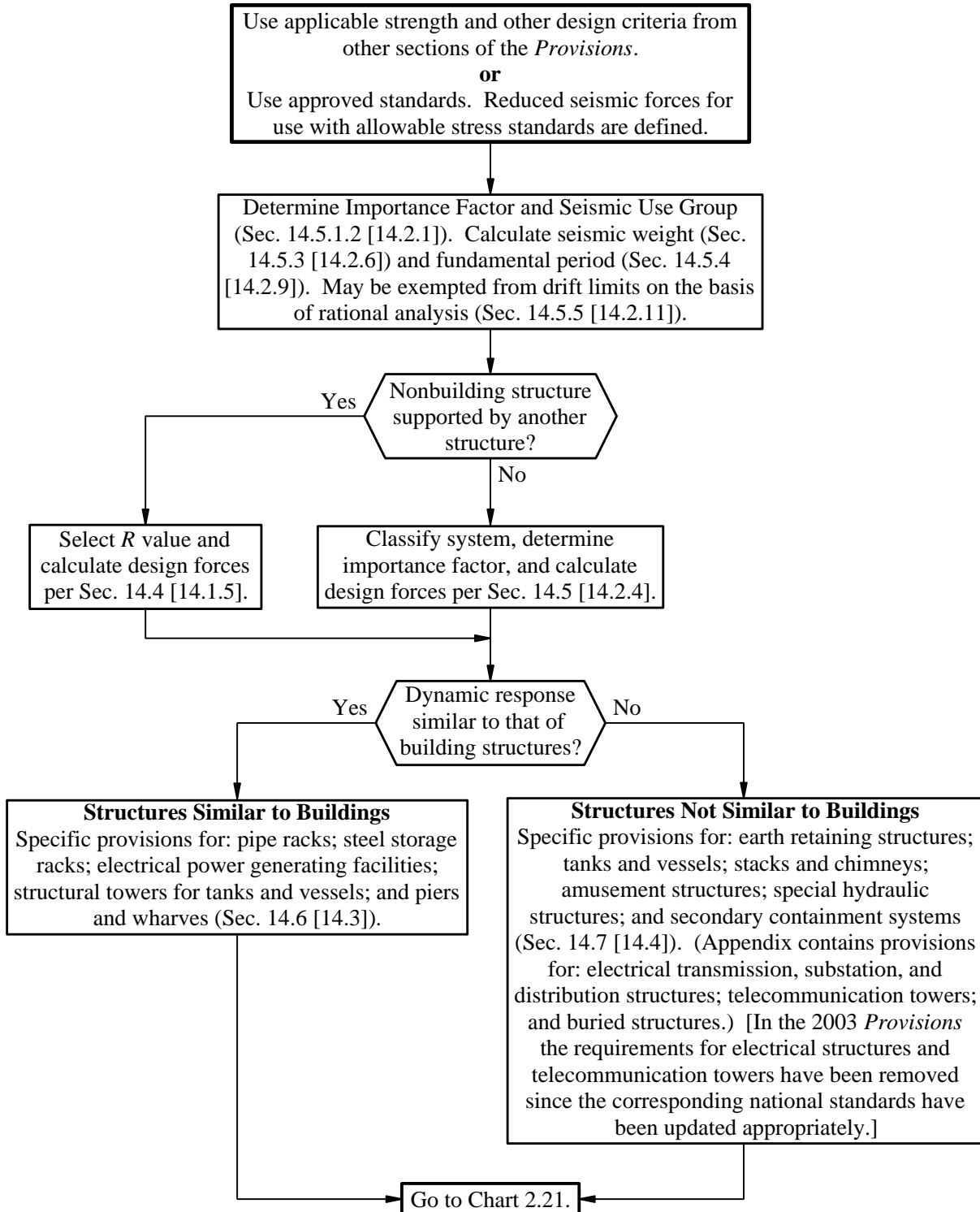


Chart 2.20 Nonbuilding Structures



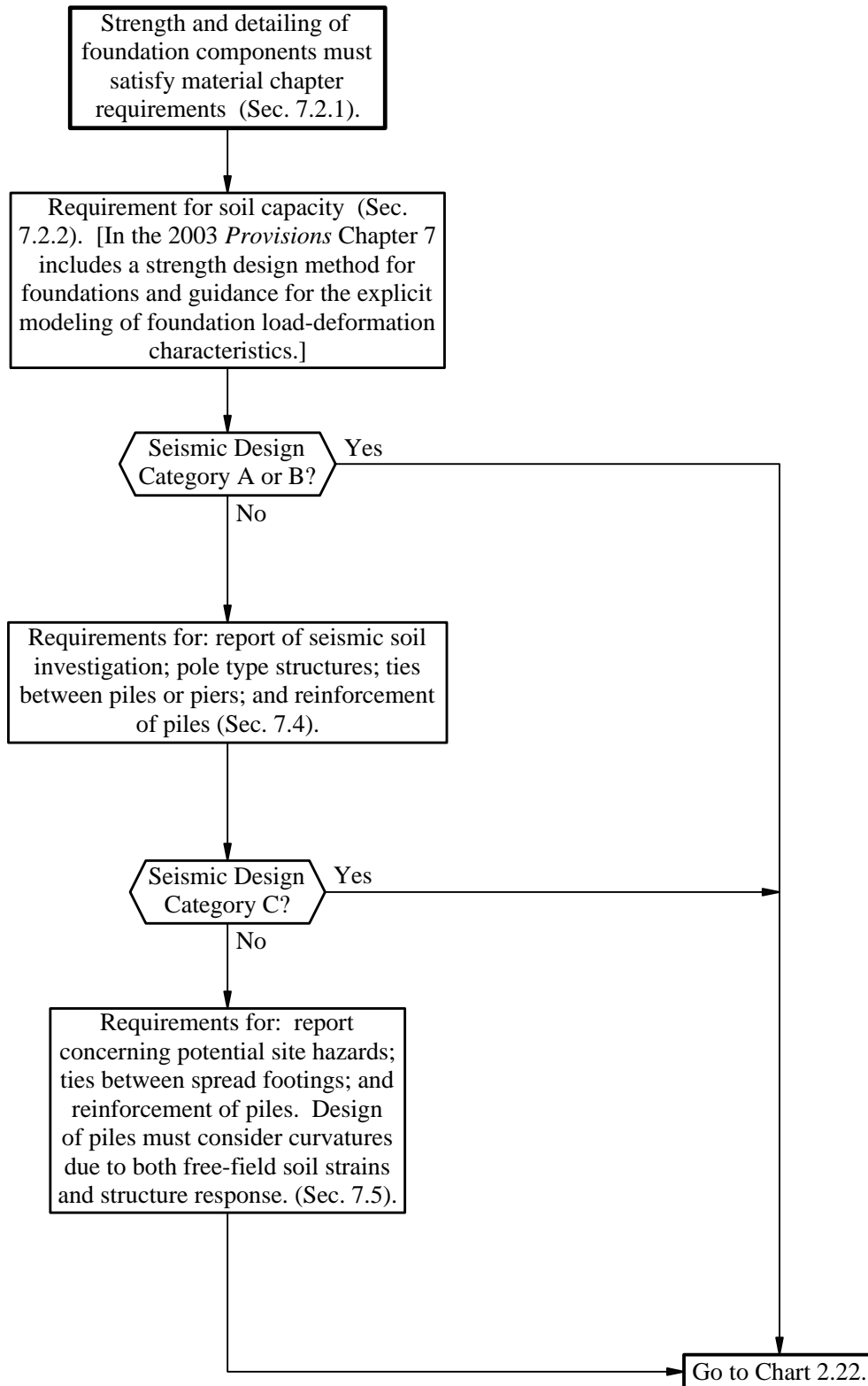
**Chart 2.21
Foundations**

Chart 2.22
Architectural, Mechanical, and Electrical Components

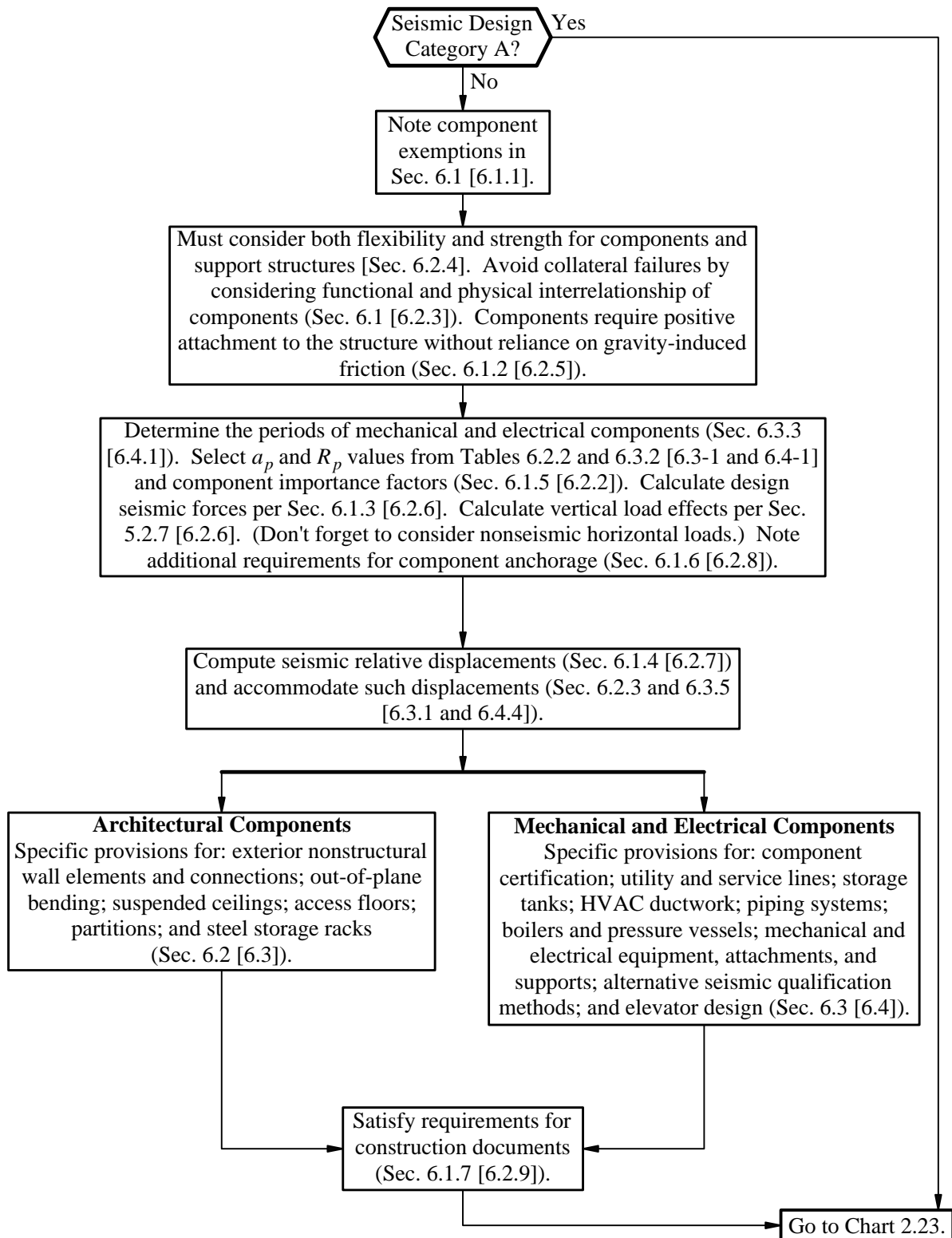


Chart 2.23
Quality Assurance

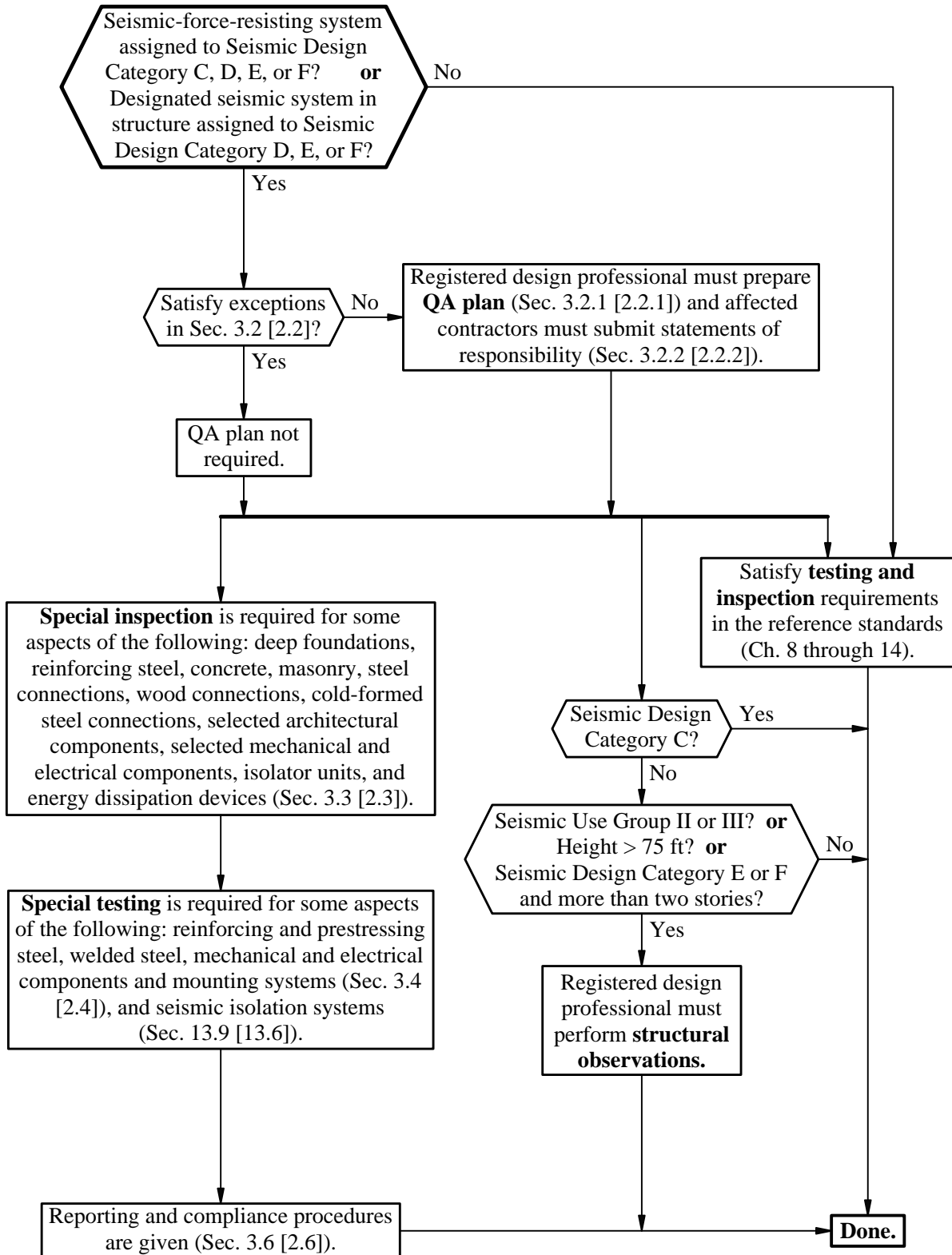


Table 2-1 Navigating Among the 2000 and 2003 NEHRP Recommended Provisions and ASCE 7

ASCE 7 Section	NEHRP 2000 Section	NEHRP 2003 Section	Topic
Chapter 11			SEISMIC DESIGN CRITERIA
11.1	1.1, 1.2	1.1	General
11.2	2.1	1.1.4	Definitions
11.3	2.2	1.1.5	Notation
11.4	4.1	3.3	Seismic Ground Motion Values
11.5	1.3, 1.4	1.2, 1.3	Importance Factor and Occupancy Category
11.6	4.2	1.4	Seismic Design Category
11.7	5.2.6.1	1.5	Design Requirements for Seismic Design Category A
11.8	4.2, 7.4, 7.5	1.4.2, 7.4, 7.5	Geologic hazards and Geotechnical Investigation
Chapter 12	5	4, 5	SEISMIC DESIGN REQUIREMENTS FOR BUILDING STRUCTURES
12.1	5.2	4.2.1	Structural Design Basis
12.2	5.2.2	4.3.1	Structural System Selection
12.3	5.2.3, 5.2.6, 5.2.4	4.3.2	Diaphragm Flexibility, Configuration Irregularities and Redundancy
12.4	5.2.7, 5.2.6	4.2.2	Seismic Load Effects and Combinations
12.5	5.2.5	4.4.2	Direction of Loading
12.6	5.2.5	4.4.1	Analysis Procedure Selection
12.7	5.2, 5.6.2		Modeling Criteria
12.8	5.5	5.2	Equivalent Lateral Force Procedures
12.9	5.6	5.3	Modal Response Spectrum Analysis
12.10	5.2.6	4.6	Diaphragms, Chords and Collectors
12.11	5.2.6	4.6	Structural Walls and Their Anchorage
12.12	5.2.8	4.5	Drift and Deformation
12.13	7	7	Foundation Design
12.14	5.4	4 Alt.	Simplified Alternative Structural Design Criteria for Simple Bearing Wall of Building Frame System
Chapter 13			SEISMIC REQUIREMENTS FOR NONSTRUCTURAL COMPONENTS
13.1	6.1	6.1	General
13.2	6.1	6.2	General Design Requirements
13.3	6.1.3, 6.1.4	6.2	Seismic Demands on Nonstructural Components
13.4	6.1.2	6.2	Nonstructural Component Anchorage
13.5	6.2	6.3	Architectural Components
13.6	6.3	6.4	Mechanical and Electrical Components
Chapter 14			MATERIAL SPECIFIC SEISMIC DESIGN AND DETAILING REQUIREMENTS
14			Scope
14.1	8	8	Steel
14.2	9	9	Concrete
14.3	10	10	Composite Steel and Concrete Structures
14.4	11	11	Masonry
14.5	12	12	Wood

Chapter 15	14	14	SEISMIC DESIGN REQUIREMENTS FOR NONBUILDING STRUCTURES
15.1	14.1	14.1	General
15.2	14.2,14.3	14.1.2	Reference Documents
15.3	14.4	14.1.5	Nonbuilding Structures Supported by Other Structures
15.4	14.5	14.2	Structural Design Requirements
15.5	14.6	14.3	Nonbuilding Structures Similar to Buildings
15.6	14.7	14.4	General Requirements for Nonbuilding Structures Not Similar to Buildings
15.7	14.7.3	14.4.7	Tanks and Vessels
Chapter 16			SEISMIC RESPONSE HISTORY PROCEDURES
16.1	5.7	5.4	Linear Response History Analysis
16.2	5.8	5.5	Nonlinear Response History Procedure
Chapter 17	13	13	SEISMIC DESIGN REQUIREMENTS FOR SEISMICALLY ISOLATED STRUCTURES
17.1	13.1	13.1	General
17.2	13.5, 13.6	13.2	General design Requirements
17.3	13.4.4	13.2.3	Ground Motion for Isolated Systems
17.4	13.2.5	13.2.4	Analysis Procedure Selection
17.5	13.3	13.3	Equivalent Lateral Force Procedure
17.6	13.4	13.4	Dynamic Analysis Procedures
17.7	13.8	13.5	Design Review
17.8	13.9	13.6	Testing
Chapter 18	13A	15	SEISMIC DESIGN REQUIREMENTS FOR STRUCTURES WITH DAMPING SYSTEMS
18.1	13A.1	15.1	General
18.2	13A.2, 13A.8	15.2	General Design Requirements
18.3	13A.6	15.3	Nonlinear Procedures
18.4	13A.5	15.4	Response Spectrum Procedure
18.5	13A.4	15.5	Equivalent Lateral Force Procedure
18.6	13A.3	15.6	Damped Response Modification
18.7	13A.7	15.7	Seismic Load Conditions and Acceptance
18.8	13A.9	15.8	Design Review
18.9	13A.10	15.9	Testing
Chapter 19			SOIL STRUCTURE INTERACTION FOR SEISMIC DESIGN
19.1	5.8.1	5.6.1	General
19.2	5.8.2	5.6.2	Equivalent Lateral Force Procedure
19.3	5.8.3	5.6.3	Modal Analysis Procedure
Chapter 20			SITE CLASSIFICATION PROCEDURE FOR SEISMIC DESIGN
20.1	4.1	3.5	Site Classification
20.2	4.1	3.5	Site Response Analysis for Site Class F Soil
20.3	4.1	3.5	Site Class Definitions
20.4	4.1	3.5	Definitions of Site Class Parameters

Chapter 21			SITE-SPECIFIC GROUND MOTION PROCEDURES FOR SEISMIC DESIGN
21.1	4.1	3.4	Site Response Analysis
21.2	4.1	3.4	Ground Motion Hazard Analysis
21.3	4.1	3.4	Design Response Spectrum
21.4	4.1	3.4	Design Acceleration Parameters
Chapter 22	4.1	3.3	SEISMIC GROUND MOTION AND LONG PERIOD TRANSITION MAPS
Chapter 23			SEISMIC DESIGN REFERENCE DOCUMENTS
23.1			Consensus Standards and Other Reference Documents
11A	3	2	QUALITY ASSURANCE PROVISIONS
11A.1	3.1, 3.2, 3.3	2.1, 2.2, 2.3	Quality Assurance
11A.2	3.4	2.4	Testing
11A.3	3.5	2.5	Structural Observations
11A.4	3.6	2.6	Reporting and Compliance Procedures
11B			EXISTING BUILDING PROVISIONS
11B.1	1.2.1	1.1.2	Scope
11B.2	1.2.2.1	1.1.2.2	Structurally Independent Additions
11B.3	1.2.2.2	1.1.2.2	Structurally Dependent Additions
11B.4	1.2.4	1.1.2.4	Alterations
11B.5	1.2.3	1.1.2.3	Change of Use

STRUCTURAL ANALYSIS

Finley A. Charney, Ph.D., P.E.

This chapter presents two examples that focus on the dynamic analysis of steel frame structures:

1. A 12-story steel frame building in Stockton, California – The highly irregular structure is analyzed using three techniques: equivalent lateral force (ELF) analysis, modal-response-spectrum analysis, and modal time-history analysis. In each case, the structure is modeled in three dimensions, and only linear elastic response is considered. The results from each of the analyses are compared, and the accuracy and relative merits of the different analytical approaches are discussed.
2. A six-story steel frame building in Seattle, Washington. This regular structure is analyzed using both linear and nonlinear techniques. Due to limitations of available software, the analyses are performed for only two dimensions. For the nonlinear analysis, two approaches are used: static pushover analysis in association with the capacity-demand spectrum method and direct time-history analysis. In the nonlinear analysis, special attention is paid to the modeling of the beam-column joint regions of the structure. The relative merits of pushover analysis versus time-history analysis are discussed.

Although the Seattle building, as originally designed, responds reasonably well under the design ground motions, a second set of time-history analyses is presented for the structure augmented with added viscous fluid damping devices. As shown, the devices have the desired effect of reducing the deformation demands in the critical regions of the structure.

Although this volume of design examples is based on the 2000 *Provisions*, it has been annotated to reflect changes made to the 2003 *Provisions*. Annotations within brackets, [], indicate both organizational changes (as a result of a reformat of all of the chapters of the 2003 *Provisions*) and substantive technical changes to the 2003 *Provisions* and its primary reference documents. While the general concepts of the changes are described, the design examples and calculations have not been revised to reflect the changes to the 2003 *Provisions*.

A number of noteworthy changes were made to the analysis requirements of the 2003 *Provisions*. These include elimination of the minimum base shear equation in areas without near-source effects, a change in the treatment of P-delta effects, revision of the redundancy factor, and refinement of the pushover analysis procedure. In addition to changes in analysis requirements, the basic earthquake hazard maps were updated and an approach to defining long-period ordinates for the design response spectrum was developed. Where they affect the design examples in this chapter, significant changes to the 2003 *Provisions* and primary reference documents are noted. However, some minor changes to the 2003 *Provisions* and the reference documents may not be noted.

In addition to the 2000 *NEHRP Recommended Provisions* (herein, the *Provisions*), the following documents are referenced:

- AISC Seismic American Institute of Steel Construction. 1997 [2002]. *Seismic Provisions for Structural Steel Buildings*.
- ATC-40 Applied Technology Council. 1996. *Seismic Evaluation and Retrofit of Concrete Buildings*.
- Bertero Bertero, R. D., and V.V. Bertero. 2002. "Performance Based Seismic Engineering: The Need for a Reliable Comprehensive Approach," *Earthquake Engineering and Structural Dynamics* 31, 3 (March).
- Chopra 1999 Chopra, A. K., and R. K. Goel. 1999. *Capacity-Demand-Diagram Methods for Estimating Seismic Deformation of Inelastic Structures: SDF Systems*. PEER-1999/02. Berkeley, California: Pacific Engineering Research Center, College on Engineering, University of California, Berkeley.
- Chopra 2001 Chopra, A. K., and R. K. Goel. 2001. *A Modal Pushover Procedure to Estimate Seismic Demands for Buildings: Theory and Preliminary Evaluation*, PEER-2001/03. Berkeley, California: Pacific Engineering Research Center, College on Engineering, University of California, Berkeley.
- FEMA 356 American Society of Civil Engineers. 2000. *Prestandard and Commentary for the Seismic Rehabilitation of Buildings*.
- Krawinkler Krawinkler, Helmut. 1978. "Shear in Beam-Column Joints in Seismic Design of Frames," *Engineering Journal*, Third Quarter.

3.1 IRREGULAR 12-STORY STEEL FRAME BUILDING, STOCKTON, CALIFORNIA

3.1.1 Introduction

This example presents the analysis of a 12-story steel frame building under seismic effects acting alone. Gravity forces due to live and dead load are not computed. For this reason, member stress checks, member design, and detailing are not discussed. For detailed examples of the seismic-resistant design of structural steel buildings, see Chapter 5 of this volume of design examples.

The analysis of the structure, shown in Figures 3.1-1 through 3.1-3, is performed using three methods:

1. Equivalent lateral force (ELF) procedure based on the requirements of *Provisions* Chapter 5,
2. Three-dimensional, modal-response-spectrum analysis based on the requirements of *Provisions* Chapter 5, and
3. Three-dimensional, modal time-history analysis using a suite of three different recorded ground motions based on the requirements of *Provisions* Chapter 5.

In each case, special attention is given to applying the *Provisions* rules for orthogonal loading and accidental torsion. All analyses were performed using the finite element analysis program SAP2000 (developed by Computers and Structures, Inc., Berkeley, California).

3.1.2 Description of Structure

The structure is a 12-story special moment frame of structural steel. The building is laid out on a rectangular grid with a maximum of seven 30-ft-wide bays in the X direction, and seven 25-ft bays in the Y direction. Both the plan and elevation of the structure are irregular with setbacks occurring at Levels 5 and 9. All stories have a height of 12.5 ft except for the first story which is 18 ft high. The structure has a full one-story basement that extends 18.0 ft below grade. Reinforced 1-ft-thick concrete walls form the perimeter of the basement. The total height of the building above grade is 155.5 ft.

Gravity loads are resisted by composite beams and girders that support a normal weight concrete slab on metal deck. The slab has an average thickness of 4.0 in. at all levels except Levels G, 5, and 9. The slabs on Levels 5 and 9 have an average thickness of 6.0 in. for more effective shear transfer through the diaphragm. The slab at Level G is 6.0 in. thick to minimize pedestrian-induced vibrations, and to support heavy floor loads. The low roofs at Levels 5 and 9 are used as outdoor patios, and support heavier live loads than do the upper roofs or typical floors.

At the perimeter of the base of the building, the columns are embedded into pilasters cast into the basement walls, with the walls supported on reinforced concrete tie beams over piles. Interior columns are supported by concrete caps over piles. All tie beams and pile caps are connected by a grid of reinforced concrete grade beams.

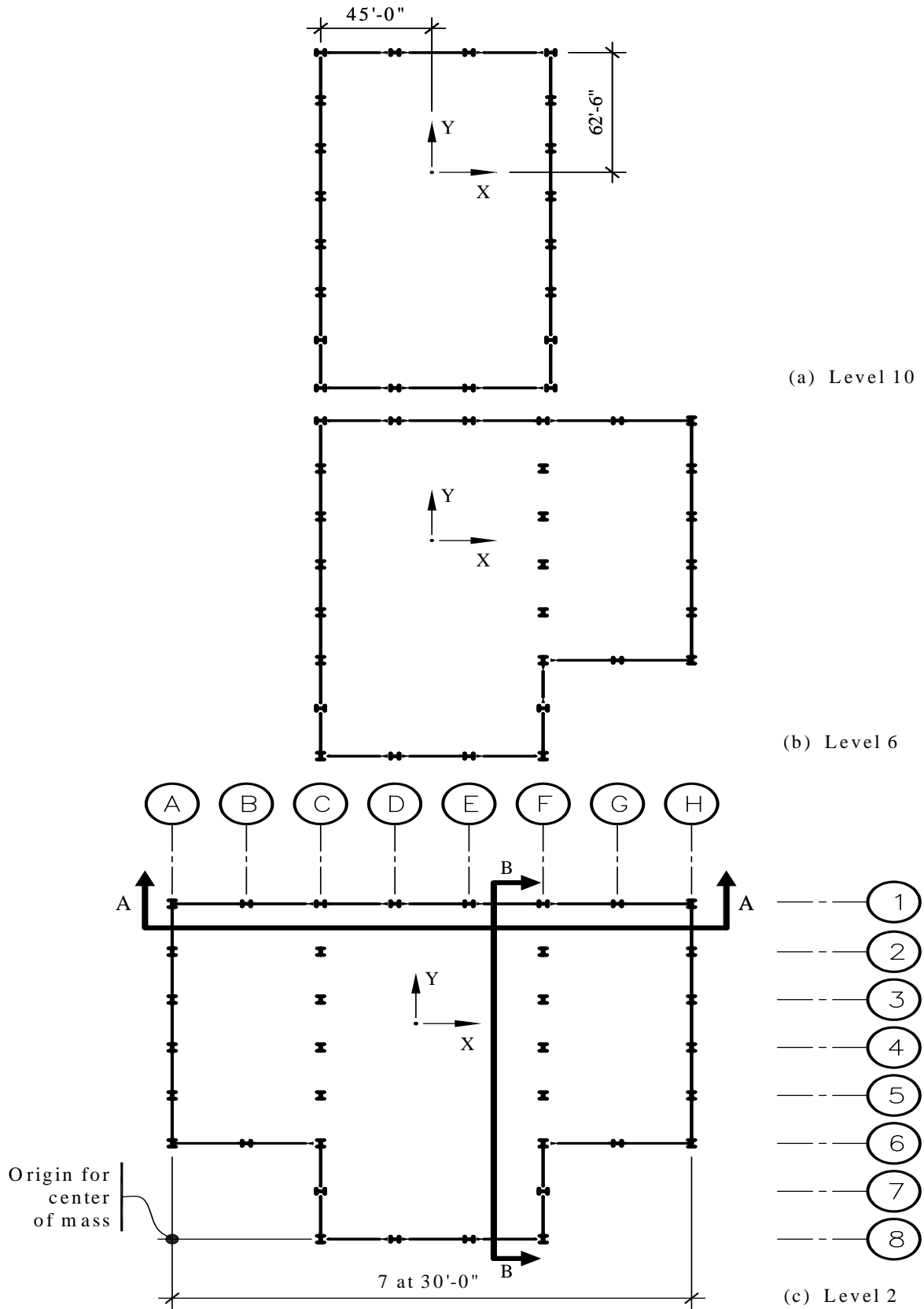


Figure 3.1-1 Various floor plans of 12-story Stockton building (1.0 ft = 0.3048 m).

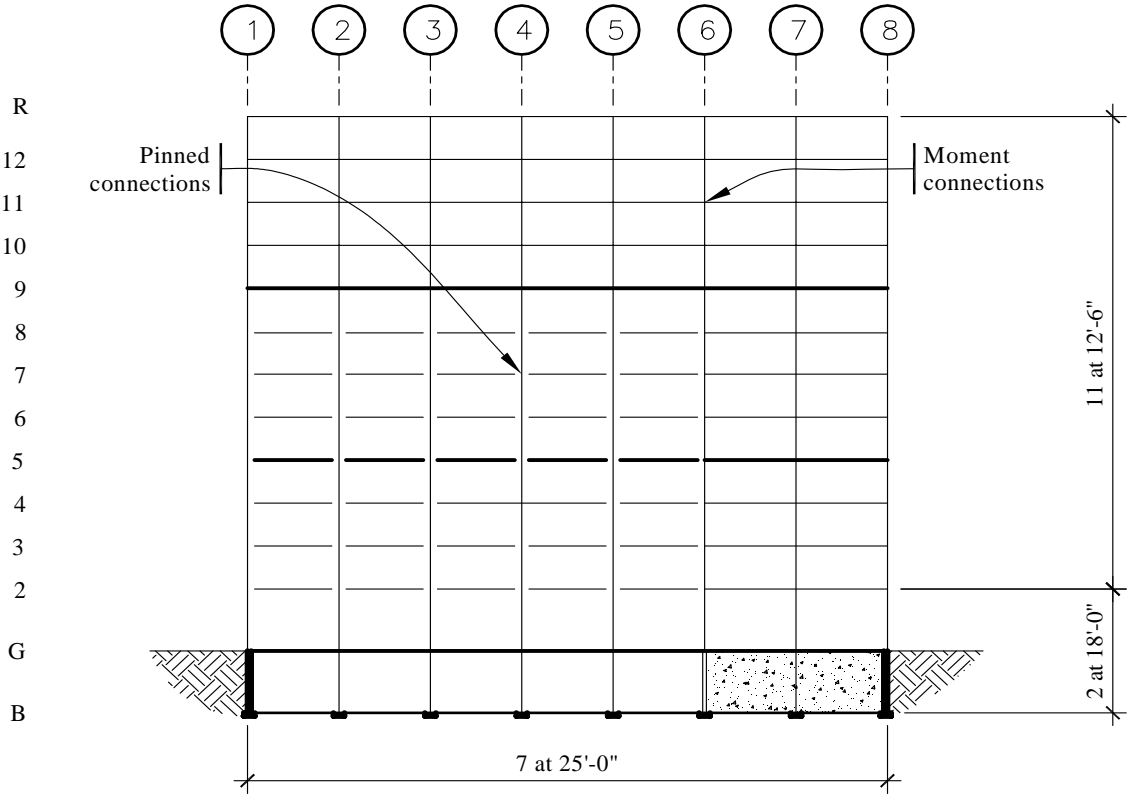
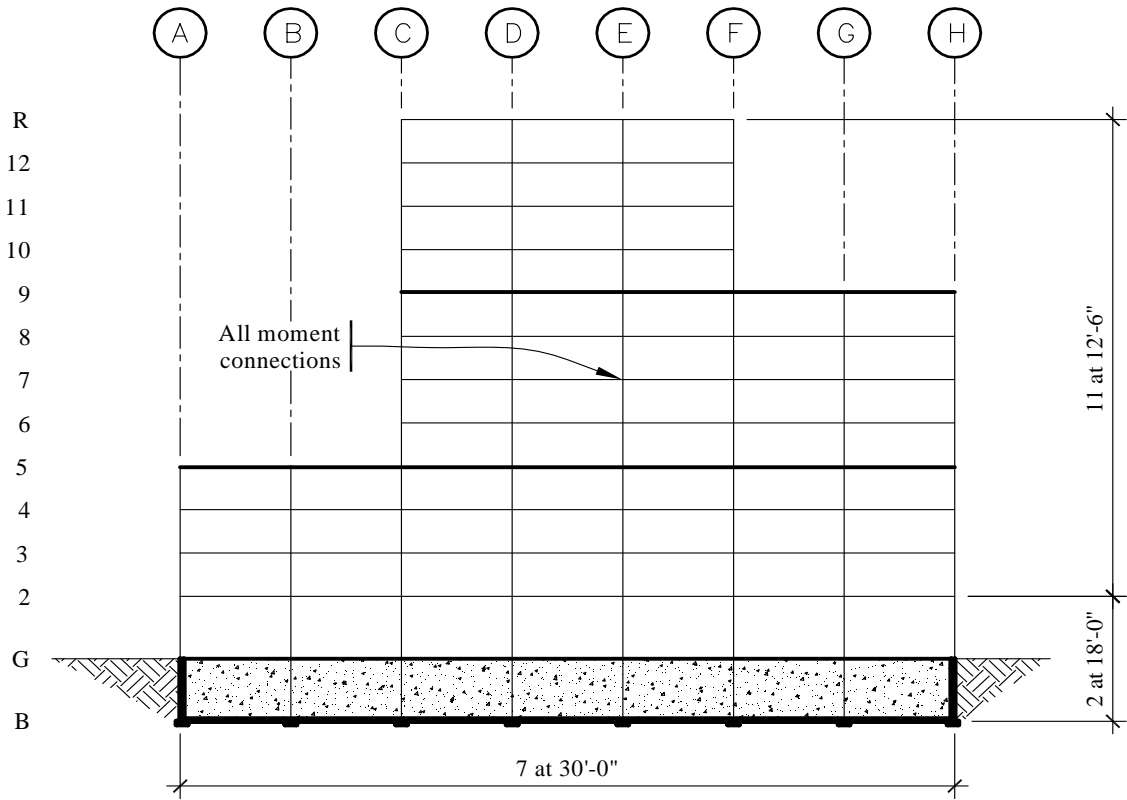


Figure 3.1-2 Sections through Stockton building (1.0 ft. = 0.3048 m).

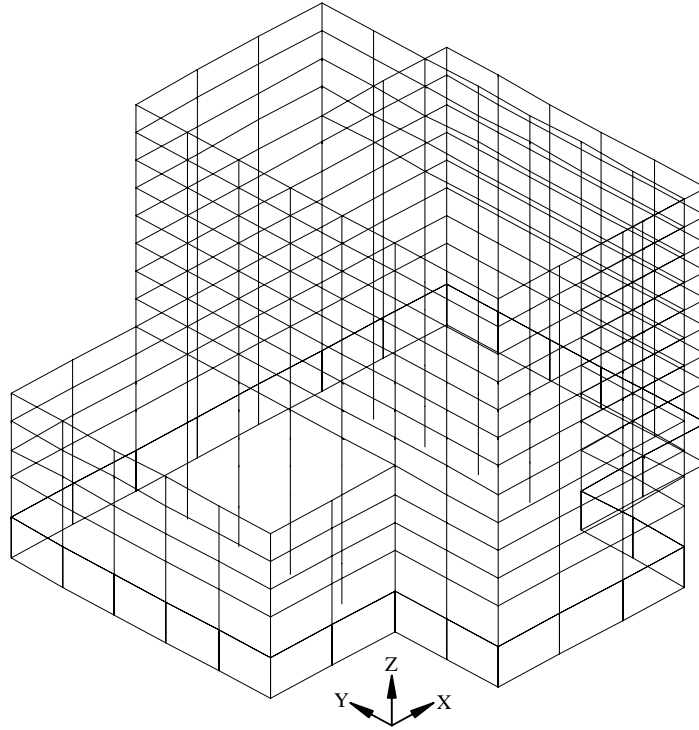


Figure 3.1-3 Three-dimensional wire-frame model of Stockton building.

The lateral-load-resisting system consists of special moment frames at the perimeter of the building and along Grids C and F. For the frames on Grids C and F, the columns extend down to the foundation, but the lateral-load-resisting girders terminate at Level 5 for Grid C and Level 9 for Grid F. Girders below these levels are simply connected. Due to the fact that the moment-resisting girders terminate in Frames C and F, much of the Y-direction seismic shears below Level 9 are transferred through the diaphragms to the frames on Grids A and H. Overturning moments developed in the upper levels of these frames are transferred down to the foundation by outriggering action provided by the columns. Columns in the moment-resisting frame range in size from W24x146 at the roof to W24x229 at Level G. Girders in the moment frames vary from W30x108 at the roof to W30x132 at Level G. Members of the moment resisting frames have a yield strength of 36 ksi, and floor members and interior columns that are sized strictly for gravity forces are 50 ksi.

3.1.3 Provisions Analysis Parameters

Stockton, California, is in San Joaquin County approximately 60 miles east of Oakland. According to *Provisions* Maps 7 and 8, the short-period and 1-second mapped spectral acceleration parameters are:

$$S_s = 1.25$$

$$S_1 = 0.40$$

[The 2003 *Provisions* have adopted the 2002 USGS probabilistic seismic hazard maps, and the maps have been added to the body of the 2003 *Provisions* as figures in Chapter 3 (instead of being issued in a separate map package).]

Assuming Site Class C, the adjusted maximum considered 5-percent-damped spectral accelerations are obtained from *Provisions* Eq. 4.1.2.4-1 and Eq. 4.1.2.4-2 [3.3-1 and 3.3-2]:

$$S_{MS} = F_a S_S = 1.0(1.25) = 1.25$$

$$S_{MI} = F_v S_I = 1.4(0.4) = 0.56$$

where the coefficients $F_a = 1.0$ and $F_v = 1.4$ come from *Provisions* Tables 4.1.2.4(a) and 4.1.2.4(b) [3.3-1 and 3.3-2], respectively.

According to *Provisions* Eq. 4.1.2.5-1 and 4.1.2.5-2 [3.3-3 and 3.3-4], the design level spectral acceleration parameters are 2/3 of the above values:

$$S_{DS} = \frac{2}{3} S_{MS} = \frac{2}{3} (1.25) = 0.833$$

$$S_{DI} = \frac{2}{3} S_{MI} = \frac{2}{3} (0.56) = 0.373$$

As the primary occupancy of the building is business offices, the Seismic Use Group (SUG) is I and, according to *Provisions* Table 1.4 [1.3-1], the importance factor (I) is 1. According to *Provisions* Tables 4.2.1(a) and 4.2.1(b) [1.4-1 and 1.4-2], the Seismic Design Category (SDC) for this building is D.

The lateral-load-resisting system of the building is a special moment-resisting frame of structural steel. For this type of system, *Provisions* Table 5.2.2 [4.3-1] gives a response modification coefficient (R) of 8 and a deflection amplification coefficient (C_d) of 5.5. Note that there is no height limit placed on special moment frames.

According to *Provisions* Table 5.2.5.1 [4.4-1] if the building has certain types of irregularities or if the computed building period exceeds 3.5 seconds where $T_s = S_{DI}/S_{DS} = 0.45$ seconds, the minimum level of analysis required for this structure is modal-response-spectrum analysis. This requirement is based on apparent plan and vertical irregularities as described in *Provisions* Tables 5.2.3.2 and 5.2.3.3 [4.3-2 and 4.3-3]. The ELF procedure would not be allowed for a final design but, as explained later, certain aspects of an ELF analysis are needed in the modal-response-spectrum analysis. For this reason, and for comparison purposes, a complete ELF analysis is carried out and described herein.

3.1.4 Dynamic Properties

Before any analysis can be carried out, it is necessary to determine the dynamic properties of the structure. These properties include mass, periods of vibration and their associated mode shapes, and damping.

3.1.4.1 Mass

For two-dimensional analysis, only the translational mass is required. To perform a three-dimensional modal or time-history analysis, it is necessary to compute the mass moment of inertia for floor plates rotating about the vertical axis and to find the location of the center of mass of each level of the structure. This may be done two different ways:

1. The mass moments of inertia may be computed “automatically” by SAP2000 by modeling the floor diaphragms as shell elements and entering the proper mass density of the elements. Line masses, such as window walls and exterior cladding, may be modeled as point masses. The floor diaphragms

may be modeled as rigid in-plane by imposing displacement constraints or as flexible in-plane by allowing the shell elements to deform in their own plane. Modeling the diaphragms as flexible is not necessary in most cases and may have the disadvantage of increasing solution time because of the additional number of degrees of freedom required to model the diaphragm.

2. The floor is assumed to be rigid in-plane but is modeled without explicit diaphragm elements. Displacement constraints are used to represent the in-plane rigidity of the diaphragm. In this case, floor masses are computed by hand (or an auxiliary program) and entered at the “master node” location of each floor diaphragm. The location of the master node should coincide with the center of mass of the floor plate. (Note that this is the approach traditionally used in programs such as ETABS which, by default, assumed rigid in-plane diaphragms and modeled the diaphragms using constraints.)

In the analysis performed herein, both approaches are illustrated. Final analysis used Approach 1, but the frequencies and mode shapes obtained from Approach 1 were verified with a separate model using Approach 2. The computation of the floor masses using Approach 2 is described below.

Due to the various sizes and shapes of the floor plates and to the different dead weights associated with areas within the same floor plate, the computation of mass properties is not easily carried out by hand. For this reason, a special purpose computer program was used. The basic input for the program consists of the shape of the floor plate, its mass density, and definitions of auxiliary masses such as line, rectangular, and concentrated mass.

The uniform area and line masses associated with the various floor plates are given in Tables 3.1-1 and 3.1-2. The line masses are based on a cladding weight of 15.0 psf, story heights of 12.5 or 18.0 ft, and parapets 4.0 ft high bordering each roof region. Figure 3.1-4 shows where each mass type occurs. The total computed floor mass, mass moment of inertia, and locations of center of mass are shown in Table 3.1-3. The reference point for center of mass location is the intersection of Grids A and 8. Note that the dimensional units of mass moment of inertia (in.-kip-sec²/radian), when multiplied by angular acceleration (radians/sec²), must yield units of torsional moment (in.-kips).

Table 3.1-3 includes a mass computed for Level G of the building. This mass is associated with an extremely stiff story (the basement level) and is not dynamically excited by the earthquake. As shown later, this mass is not included in equivalent lateral force computations.

Table 3.1-1 Area Masses on Floor Diaphragms

Mass Type	Area Mass Designation				
	A	B	C	D	E
Slab and Deck (psf)	50	75	50	75	75
Structure (psf)	20	20	20	20	50
Ceiling and Mechanical (psf)	15	15	15	15	15
Partition (psf)	10	10	0	0	10
Roofing (psf)	0	0	15	15	0
Special (psf)	<u>0</u>	<u>0</u>	<u>0</u>	<u>60</u>	<u>25</u>
TOTAL (psf)	95	120	100	185	175

See Figure 3.1-4 for mass location.

1.0 psf = 47.9 N/m².

Table 3.1-2 Line Masses on Floor Diaphragms

Mass Type	Line Mass Designation				
	1	2	3	4	5
From Story Above (plf)	60.0	93.8	93.8	93.8	135.0
From Story Below (plf)	<u>93.8</u>	<u>93.8</u>	<u>0.0</u>	<u>135.0</u>	<u>1350.0</u>
TOTAL (plf)	153.8	187.6	93.8	228.8	1485.0

See Figure 3.1-4 for mass location.

1.0 plf = 14.6 N/m.

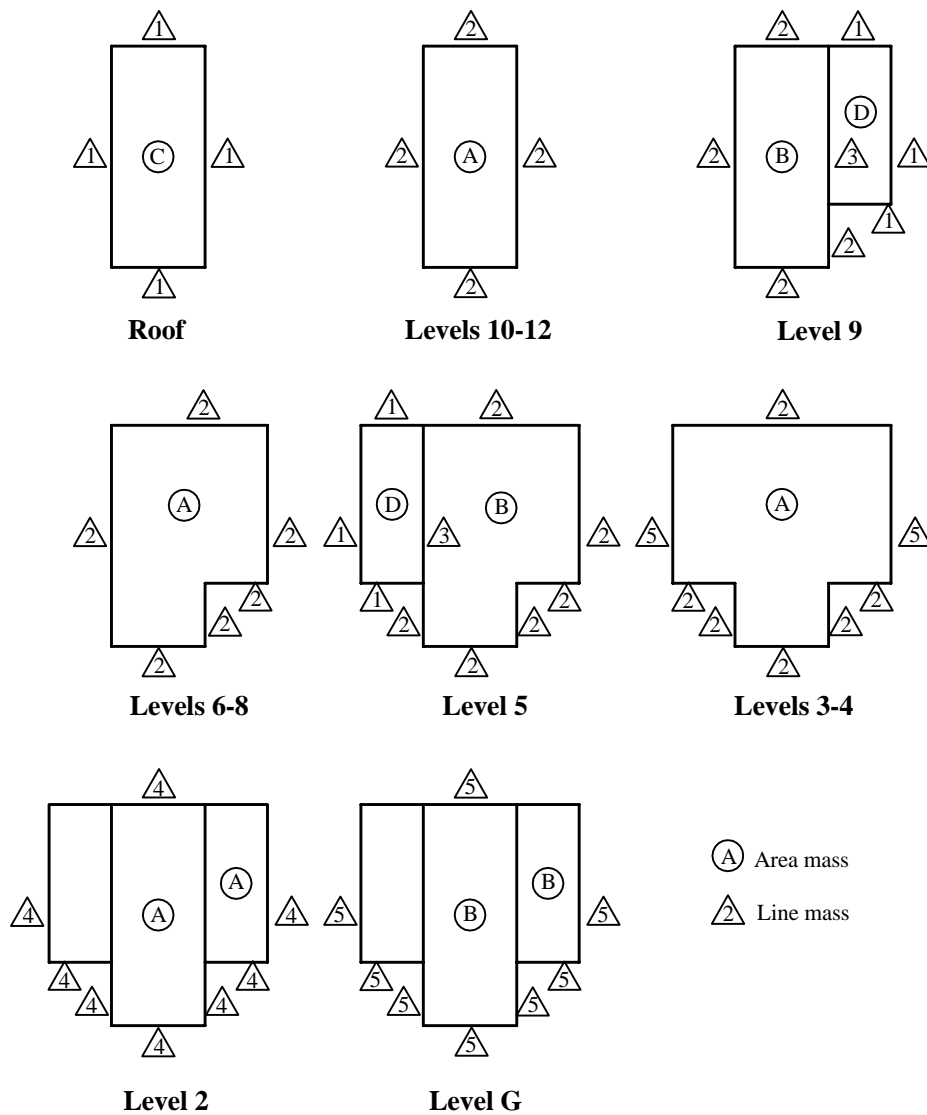


Figure 3.1-4 Key diagram for computation of floor mass.

Table 3.1-3 Floor Mass, Mass Moment of Inertia, and Center of Mass Locations

Level	Weight (kips)	Mass (kip-sec ² /in.)	Mass Moment of Inertia (in.-kip- sec ² /radian)	X Distance to C.M. (in.)	Y Distance to C.M. (in.)
R	1656.5	4.287	2.072x10 ⁶	1260	1050
12	1595.8	4.130	2.017x10 ⁶	1260	1050
11	1595.8	4.130	2.017x10 ⁶	1260	1050
10	1595.8	4.130	2.017x10 ⁶	1260	1050
9	3403.0	8.807	5.309x10 ⁶	1637	1175
8	2330.8	6.032	3.703x10 ⁶	1551	1145
7	2330.8	6.032	3.703x10 ⁶	1551	1145
6	2330.8	6.032	3.703x10 ⁶	1551	1145
5	4323.8	11.190	9.091x10 ⁶	1159	1212
4	3066.1	7.935	6.356x10 ⁶	1260	1194
3	3066.1	7.935	6.356x10 ⁶	1260	1194
2	3097.0	8.015	6.437x10 ⁶	1260	1193
G	<u>6526.3</u>	16.890	1.503x10 ⁷	1260	1187
Σ	36918.6				

1.0 in. = 25.4 mm, 1.0 kip = 4.45 kN.

3.1.4.2 Period of Vibration

3.1.4.2.1 Approximate Period of Vibration

The formula in *Provisions* Eq. 5.4.2.1-1 [5.2-6] is used to estimate the building period:

$$T_a = C_r h_n^x$$

where $C_r = 0.028$ and $x = 0.8$ for a steel moment frame from *Provisions* Table 5.4.2.1 [5.2-2]. Using $h_n =$ the total building height (above grade) = 155.5 ft, $T_a = 0.028(155.5)^{0.8} = 1.59$ sec.

When the period is computed from a properly substantiated analysis, the *Provisions* requires that the computed period not exceed $C_u T_a$ where $C_u = 1.4$ (from *Provisions* Table 5.4.2 [5.2-1] using $S_{DI} = 0.373g$). For the structure under consideration, $C_u T_a = 1.4(1.59) = 2.23$ seconds. When a modal-response spectrum is used, *Provisions* Sec. 5.5.7 [5.3.7] requires that the displacements, drift, and member design forces be scaled to a value consistent with 85 percent of the equivalent lateral force base shear computed using the period $C_u T_a = 2.23$ sec. *Provisions* Sec. 5.6.3 [5.4.3] requires that time-history analysis results be scaled up to an ELF shear consistent with $T = C_u T_a$ (without the 0.85 factor).¹

Note that when the accurately computed period (such as from a Rayleigh analysis) is less than the approximate value shown above, the computed period should be used. In no case, however, must a period less than $T_a = 1.59$ seconds be used. The use of the Rayleigh method and the eigenvalue method of determining accurate periods of vibration are illustrated in a later part of this example.

¹This requirements seems odd to the writer since the *Commentary* to the *Provisions* states that time-history analysis is superior to response-spectrum analysis. Nevertheless, the time-history analysis performed later will be scaled as required by the *Provisions*.

3.1.4.3 Damping

When a modal-response-spectrum analysis is performed, the structure's damping is included in the response spectrum. A damping ratio of 0.05 (5 percent of critical) is appropriate for steel structures. This is consistent with the level of damping assumed in the development of the mapped spectral acceleration values.

When recombining the individual modal responses, the square root of the sum of the squares (SRSS) technique has generally been replaced in practice by the complete quadratic combination (CQC) approach. Indeed, *Provisions* Sec. 5.5.7 [5.3.7] requires that the CQC approach be used when the modes are closely spaced. When using CQC, the analyst must correctly specify a damping factor. This factor must match that used in developing the response spectrum. It should be noted that if zero damping is used in CQC, the results are the same as those for SRSS.

For time-history analysis, SAP2000 allows an explicit damping ratio to be used in each mode. For this structure, a damping of 5 percent of critical was specified in each mode.

3.1.5 Equivalent Lateral Force Analysis

Prior to performing modal or time-history analysis, it is often necessary to perform an equivalent lateral force (ELF) analysis of the structure. This analysis typically is used for preliminary design and for assessing the three-dimensional response characteristics of the structure. ELF analysis is also useful for investigating the behavior of drift-controlled structures, particularly when a virtual force analysis is used for determining member displacement participation factors.² The virtual force techniques cannot be used for modal-response-spectrum analysis because signs are lost in the CQC combinations.

In anticipation of the “true” computed period of the building being greater than 2.23 seconds, the ELF analysis is based on a period of vibration equal to $C_u T_a = 2.23$ seconds. For the ELF analysis, it is assumed that the structure is “fixed” at grade level. Hence, the total effective weight of the structure (see Table 3.1-3) is the total weight minus the grade level weight, or $36918.6 - 6526.3 = 30392.3$ kips.

3.1.5.1 Base Shear and Vertical Distribution of Force

Using *Provisions* Eq. 5.4.1 [5.2-1], the total seismic shear is:

$$V = C_S W$$

where W is the total weight of the structure. From *Provisions* Eq. 5.4.1.1-1 [5.2-2], the maximum (constant acceleration region) spectral acceleration is:

$$C_{S_{max}} = \frac{S_{DS}}{(R/I)} = \frac{0.833}{(8/1)} = 0.104$$

²For an explanation of the use of the virtual force technique, see “Economy of Steel Framed Structures Through Identification of Structural Behavior” by F. Charney, *Proceedings of the 1993 AISC Steel Construction Conference*, Orlando, Florida, 1993.

Provisions Eq. 5.4.1.1-2 [5.2-3] controls in the constant velocity region:

$$C_s = \frac{S_{DI}}{T(R/I)} = \frac{0.373}{2.23(8/1)} = 0.021$$

However, the acceleration must not be less than that given by Provisions Eq. 5.4.1.1-3 [replaced by 0.010 in the 2003 Provisions]:

$$C_{S_{min}} = 0.044I_{DS} = 0.044(1)(0.833) = 0.037$$

[With the change of this base shear equation, the result of Eq. 5.2-3 would control, reducing the design base shear significantly. This change would also result in removal of the horizontal line in Figure 3.1-5 and the corresponding segment of Figure 3.1-6.]

The value from Eq. 5.4.1.1-3 [not applicable in the 2003 Provisions] controls for this building. Using $W = 30,392$ kips, $V = 0.037(30,392) = 1,124$ kips. The acceleration response spectrum given by the above equations is plotted in Figure 3.1-5.

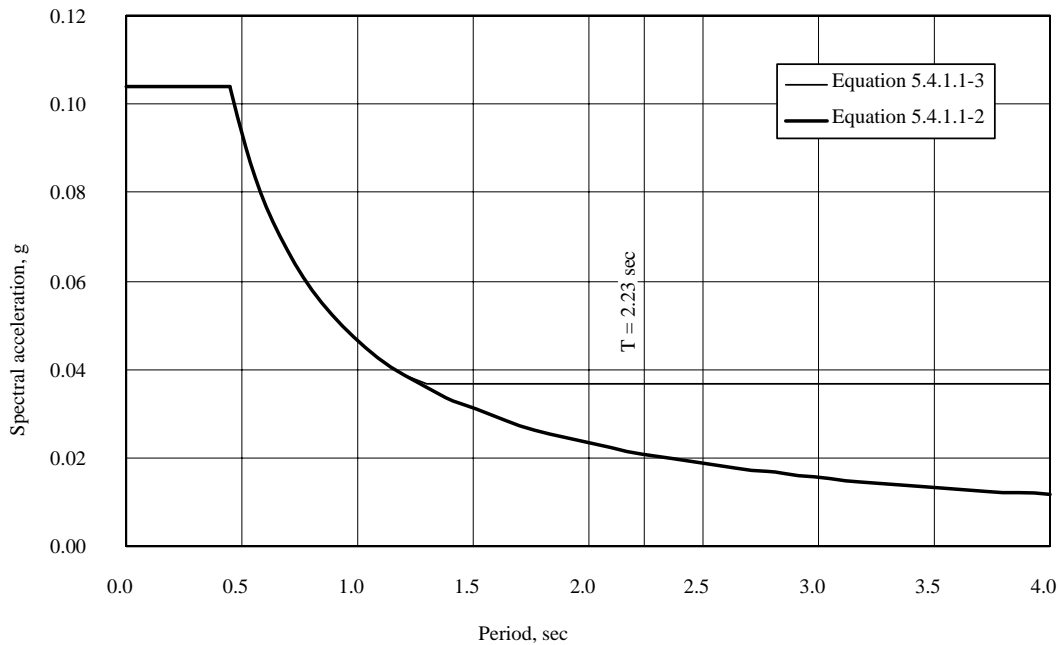


Figure 3.1-5 Computed ELF total acceleration response spectrum.

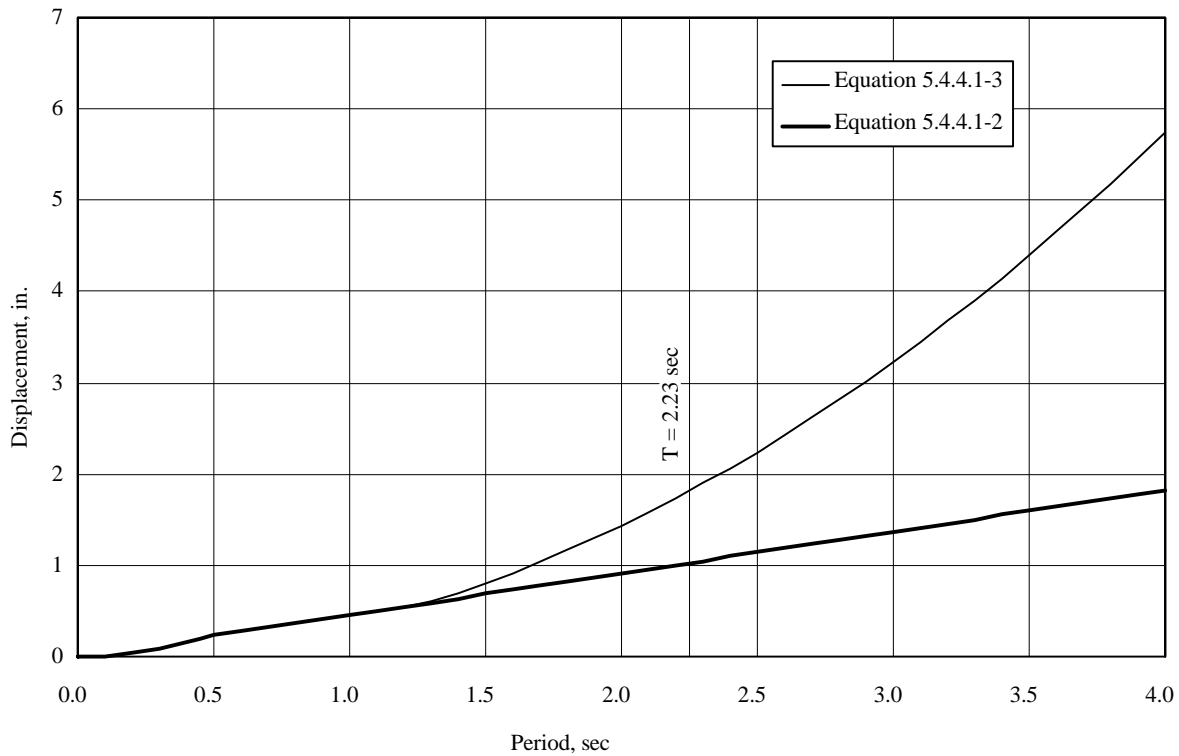


Figure 3.1-6 Computed ELF relative displacement response spectrum (1.0 in. = 25.4 mm).

While it is certainly reasonable to enforce a minimum base shear, *Provisions* Sec. 5.4.6.1 has correctly recognized that displacements predicted using Eq. 5.4.1.1-3 are not reasonable. Therefore, it is very important to note that *Provisions* Eq. 5.4.1.1-3, when it controls, should be used for determining member forces, but should not be used for computing drift. For drift calculations, forces computed according to Eq. 5.4.1.1-2 [5.2-3] should be used. The effect of using Eq. 5.4.1.1-3 for drift is shown in Figure 3.1-6, where it can be seen that the fine line, representing Eq. 5.4.1.1-3, will predict significantly larger displacements than Eq. 5.4.1.1-2 [5.2-3].

[The minimum base shear is 1% of the weight in the 2003 *Provisions* ($C_s = 0.01$). For this combination of S_{D1} and R , the new minimum controls for periods larger than 4.66 second. The minimum base shear equation for near-source sites (now triggered in the *Provisions* by S_1 greater than or equal to 0.6) has been retained.]

In this example, all ELF analysis is performed using the forces obtained from Eq. 5.4.1.1-3, but for the purposes of computing drift, the story deflections computed using the forces from Eq. 5.4.1.1-3 are multiplied by the ratio ($0.021/0.037 = 0.568$).

The base shear computed according to *Provisions* Eq. 5.4.1.1-3 is distributed along the height of the building using *Provisions* Eq. 5.4.3.1 and 5.4.3.2 [5.2-10 and 5.2-11]:

$$F_x = C_{vx} V$$

and

$$C_{vx} = \frac{w_x h^k}{\sum_{i=1}^n w_i h_i^k}$$

where $k = 0.75 + 0.5T = 0.75 + 0.5(2.23) = 1.86$. The story forces, story shears, and story overturning moments are summarized in Table 3.1-4.

Table 3.1-4 Equivalent Lateral Forces for Building Responding in X and Y Directions

Level x	w_x (kips)	h_x (ft)	$w_x h_x^k$	C_{vx}	F_x (kips)	V_x (kips)	M_x (ft-kips)
R	1656.5	155.5	20266027	0.1662	186.9	186.9	2336
12	1595.8	143.0	16698604	0.1370	154.0	340.9	6597
11	1595.8	130.5	14079657	0.1155	129.9	470.8	12482
10	1595.8	118.0	11669128	0.0957	107.6	578.4	19712
9	3403.0	105.5	20194253	0.1656	186.3	764.7	29271
8	2330.8	93.0	10932657	0.0897	100.8	865.5	40090
7	2330.8	80.5	8352458	0.0685	77.0	942.5	51871
6	2330.8	68.0	6097272	0.0500	56.2	998.8	64356
5	4323.8	55.5	7744119	0.0635	71.4	1070.2	77733
4	3066.1	43.0	3411968	0.0280	31.5	1101.7	91505
3	3066.1	30.5	1798066	0.0147	16.6	1118.2	103372
2	<u>3097.0</u>	18.0	<u>679242</u>	<u>0.0056</u>	<u>6.3</u>	1124.5	120694
Σ	30392.3	-	121923430	1.00	1124.5		

1.0 ft = 0.3048 m, 1.0 kip = 4.45 kN.

3.1.5.2 Accidental Torsion and Orthogonal Loading Effects

When using the ELF method as the basis for structural design, two effects must be added to the direct lateral forces shown in Table 3.1-4. The first of these effects accounts for the fact that the earthquake can produce inertial forces that act in any direction. For SDC D, E, and F buildings, *Provisions* Sec. 5.2.5.2.3 [4.4.2.3] requires that the structure be investigated for forces that act in the direction that causes the “critical load effect.” Since this direction is not easily defined, the *Provisions* allows the analyst to load the structure with 100 percent of the seismic force in one direction (along the X axis, for example) simultaneous with the application of 30 percent of the force acting in the orthogonal direction (the Y axis).

The other requirement is that the structure be modeled with additional forces to account for uncertainties in the location of center of mass and center of rigidity, uneven yielding of vertical systems, and the possibility of torsional components of ground motion. This requirement, given in *Provisions* Sec. 5.4.4.2 [5.2.4.2], can be satisfied for torsionally regular buildings by applying the equivalent lateral force at an eccentricity, where the eccentricity is equal to 5 percent of the overall dimension of the structure in the direction perpendicular to the line of the application of force.

For structures in SDC C, D, E, or F, these accidental eccentricities (and inherent torsion) must be amplified if the structure is classified as torsionally irregular. According to *Provisions* Table 5.2.3.2, a torsional irregularity exists if:

$$\frac{\delta_{max}}{\delta_{avg}} \geq 1.2$$

where, as shown in Figure 3.1-7, δ_{max} is the maximum displacement at the edge of the floor diaphragm, and δ_{avg} is the average displacement of the diaphragm. If the ratio of displacements is greater than 1.4, the torsional irregularity is referred to as “extreme.” In computing the displacements, the structure must be loaded with the basic equivalent lateral forces applied at a 5 percent eccentricity.

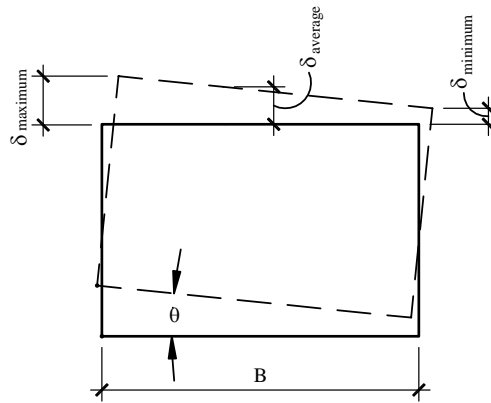


Figure 3.1-7 Amplification of accidental torsion.

The analysis of the structure for accidental torsion was performed on SAP2000. The same model was used for ELF, modal-response-spectrum, and modal-time-history analysis. The following approach was used for the mathematical model of the structure:

1. The floor diaphragm was modeled as infinitely rigid in-plane and infinitely flexible out-of-plane. Shell elements were used to represent the diaphragm mass. Additional point masses were used to represent cladding and other concentrated masses.
2. Flexural, shear, axial, and torsional deformations were included in all columns. Flexural, shear, and torsional deformations were included in the beams. Due to the rigid diaphragm assumption, axial deformation in beams was neglected.
3. Beam-column joints were modeled using centerline dimensions. This approximately accounts for deformations in the panel zone.
4. Section properties for the girders were based on bare steel, ignoring composite action. This is a reasonable assumption in light of the fact that most of the girders are on the perimeter of the building and are under reverse curvature.
5. Except for those lateral-load-resisting columns that terminate at Levels 5 and 9, all columns were assumed to be fixed at their base.

The results of the accidental torsion analysis are shown in Tables 3.1-5 and 3.1-6. As may be observed, the largest ratio of maximum to average floor displacements is 1.16 at Level 5 of the building under Y direction loading. Hence, this structure is not torsionally irregular and the story torsions do not need to be amplified.

Table 3.1-5 Computation for Torsional Irregularity with ELF Loads Acting in X Direction

Level	δ_1 (in.)	δ_2 (in.)	δ_{avg} (in.)	δ_{max} (in.)	$\delta_{max}/\delta_{avg}$	Irregularity
R	6.04	7.43	6.74	7.43	1.10	none
12	5.75	7.10	6.43	7.10	1.11	none
11	5.33	6.61	5.97	6.61	1.11	none
10	4.82	6.01	5.42	6.01	1.11	none
9	4.26	5.34	4.80	5.34	1.11	none
8	3.74	4.67	4.21	4.67	1.11	none
7	3.17	3.96	3.57	3.96	1.11	none
6	2.60	3.23	2.92	3.23	1.11	none
5	2.04	2.52	2.28	2.52	1.11	none
4	1.56	1.91	1.74	1.91	1.10	none
3	1.07	1.30	1.19	1.30	1.10	none
2	0.59	0.71	0.65	0.71	1.09	none

Tabulated displacements are not amplified by C_d . Analysis includes accidental torsion. 1.0 in. = 25.4 mm.

Table 3.1-6 Computation for Torsional Irregularity with ELF Loads Acting in Y Direction

Level	δ_1 (in.)	δ_2 (in.)	δ_{avg} (in.)	δ_{max} (in.)	$\delta_{max}/\delta_{avg}$	Irregularity
R	5.88	5.96	5.92	5.96	1.01	none
12	5.68	5.73	5.71	5.73	1.00	none
11	5.34	5.35	5.35	5.35	1.00	none
10	4.92	4.87	4.90	4.92	1.01	none
9	4.39	4.29	4.34	4.39	1.01	none
8	3.83	3.88	3.86	3.88	1.01	none
7	3.19	3.40	3.30	3.40	1.03	none
6	2.54	2.91	2.73	2.91	1.07	none
5	1.72	2.83	2.05	2.38	1.16	none
4	1.34	1.83	1.59	1.83	1.15	none
3	0.93	1.27	1.10	1.27	1.15	none
2	0.52	0.71	0.62	0.71	1.15	none

Tabulated displacements are not amplified by C_d . Analysis includes accidental torsion. 1.0 in. = 25.4 mm.

3.1.5.3 Drift and P-Delta Effects

Using the basic structural configuration shown in Figure 3.1-1 and the equivalent lateral forces shown in Table 3.1-4, the total story deflections were computed as shown in the previous section. In this section, story drifts are computed and compared to the allowable drifts specified by the *Provisions*.

The results of the analysis are shown in Tables 3.1-7 and 3.1-8. The tabulated drift values are somewhat different from those shown in Table 3.1-5 because the analysis for drift did not include accidental torsion, whereas the analysis for torsional irregularity did. In Tables 3.1-7 and 3.1-8, the values in the first numbered column are the *average* story displacements computed by the SAP2000 program using the lateral forces of Table 3.1-4. Average story drifts are used here instead of maximum story drifts because this structure does not have a “significant torsional response.” If the torsional effect were significant, the maximum drifts at the extreme edge of the diaphragm would need to be checked.

The values in column 2 of Tables 3.1-7 and 3.1-8 are the story drifts as reported by SAP2000. These drift values, however, are much less than those that will actually occur because the structure will respond inelastically to the earthquake. The true inelastic story drift, which by assumption is equal to $C_d = 5.5$

times the SAP2000 drift, is shown in Column 3. As discussed above in Sec. 3.1.5.1, the values in column 4 are multiplied by 0.568 to scale the results to the base shear calculated ignoring *Provisions* Eq. 5.4.1.1-3 since that limit does not apply to drift checks. [Recall that the minimum base shear is different in the 2003 *Provisions*.] The allowable story drift of 2.0 percent of the story height per *Provisions* Table 5.2-8 is shown in column 5. (Recall that this building is assigned to Seismic Use Group I.) It is clear from Tables 3.1-7 and 3.1-8 that the allowable drift is not exceeded at any level.

Table 3.1-7 ELF Drift for Building Responding in X Direction

Level	1 Total Drift from SAP2000 (in.)	2 Story Drift from SAP2000 (in.)	3 Inelastic Story Drift (in.)	4 Inelastic Drift Times 0.568 (in.)	5 Allowable Drift (in.)
R	6.71	0.32	1.73	0.982	3.00
12	6.40	0.45	2.48	1.41	3.00
11	5.95	0.56	3.08	1.75	3.00
10	5.39	5.39	3.38	1.92	3.00
9	4.77	0.59	3.22	1.83	3.00
8	4.19	0.64	3.52	2.00	3.00
7	3.55	0.65	3.58	2.03	3.00
6	2.90	0.63	3.44	1.95	3.00
5	2.27	0.55	3.00	1.70	3.00
4	1.73	0.55	3.00	1.70	3.00
3	1.18	0.54	2.94	1.67	3.00
2	0.65	0.65	3.55	2.02	4.32

Column 4 adjusts for *Provisions* Eq. 5.4.1.1-2 (for drift) vs 5.4.1.1-3 (for strength). [Such a modification is not necessary when using the 2003 *Provisions* because the minimum base shear is different. Instead, the design forces applied to the model, which produce the drifts in Columns 1 and 2, would be lower by a factor of 0.568.]

1.0 in. = 25.4 mm.

Table 3.1-8 ELF Drift for Building Responding in Y Direction

Level	1 Total Drift from SAP2000 (in.)	2 Story Drift from SAP2000 (in.)	3 Inelastic Story Drift (in.)	4 Inelastic Drift Times 0.568 (in.)	5 Allowable Drift (in.)
R	6.01	0.22	1.21	0.687	3.00
12	5.79	0.36	1.98	1.12	3.00
11	5.43	0.45	2.48	1.41	3.00
10	4.98	0.67	3.66	2.08	3.00
9	4.32	0.49	2.70	1.53	3.00
8	3.83	0.57	3.11	1.77	3.00
7	3.26	0.58	3.19	1.81	3.00
6	2.68	0.64	3.49	1.98	3.00
5	2.05	0.46	2.53	1.43	3.00
4	1.59	0.49	2.67	1.52	3.00
3	1.10	0.49	2.70	1.53	3.00
2	0.61	0.61	3.36	1.91	4.32

Column 4 adjusts for *Provisions* Eq. 5.4.1.1-2 (for drift) vs 5.4.1.1-3 (for strength). [Such a modification is not necessary when using the 2003 *Provisions* because the minimum base shear is different. Instead, the design forces applied to the model, which produce the drifts in Columns 1 and 2, would be lower by a factor of 0.568.]
1.0 in. = 25.4 mm.

3.1.5.3.1 Using ELF Forces and Drift to Compute Accurate Period

Before continuing with the example, it is helpful to use the computed drifts to more accurately estimate the fundamental periods of vibration of the building. This will serve as a check on the “exact” periods computed by eigenvalue extraction in SAP2000. A Rayleigh analysis will be used to estimate the periods. This procedure, which is usually very accurate, is derived as follows:

The exact frequency of vibration ω (a scalar), in units of radians/second, is found from the following eigenvalue equation:

$$K\phi = \omega^2 M\phi$$

where K is the structure stiffness matrix, M is the (diagonal) mass matrix, and ϕ , is a vector containing the components of the mode shape associated with ω .

If an approximate mode shape δ is used instead of ϕ , where δ is the deflected shape under the equivalent lateral forces F , the frequency ω can be closely approximated. Making the substitution of δ for ϕ , premultiplying both sides of the above equation by δ^T (the transpose of the displacement vector), noting that $F = K\delta$, and $M = (1/g)W$, the following is obtained:

$$\delta^T F = \omega^2 \delta^T M \delta = \frac{\omega^2}{g} \delta^T W \delta$$

where W is a vector containing the story weights and g is the acceleration due to gravity (a scalar). After rearranging terms, this gives:

$$\omega = \sqrt{g \frac{\delta^T F}{\delta^T W \delta}}$$

Using the relationship between period and frequency, $T = \frac{2\pi}{\omega}$.

Using F from Table 3.1-4 and δ from Column 1 of Tables 3.1-7 and 3.1-8, the periods of vibration are computed as shown in Tables 3.1-9 and 3.1-10 for the structure loaded in the X and Y directions, respectively. As may be seen from the tables, the X-direction period of 2.87 seconds and the Y-direction period of 2.73 seconds are much greater than the approximate period of $T_a = 1.59$ seconds and also exceed the upper limit on period of $C_u T_a = 2.23$ seconds.

Table 3.1-9 Rayleigh Analysis for X-Direction Period of Vibration

Level	Drift, δ (in.)	Force, F (kips)	Weight, W (kips)	δF (in.-kips)	$\delta^2 W/g$ (in.-kips-sec ²)
R	6.71	186.9	1656	1259.71	194.69
12	6.40	154.0	1598	990.22	170.99
11	5.95	129.9	1598	775.50	147.40
10	5.39	107.6	1598	583.19	121.49
9	4.77	186.3	3403	894.24	202.91
8	4.19	100.8	2330	424.37	106.88
7	3.55	77.0	2330	274.89	76.85
6	2.90	56.2	2330	164.10	51.41
5	2.27	71.4	4323	162.79	58.16
4	1.73	31.5	3066	54.81	24.02
3	1.18	16.6	3066	19.75	11.24
2	0.65	6.3	3097	4.10	3.39
Σ				5607.64	1169.42

$\omega = (5607/1169)^{0.5} = 2.19$ rad/sec. $T = 2\pi/\omega = 2.87$ sec. 1.0 in. = 25.4 mm, 1.0 kip = 4.45 kN.

Table 3.1-10 Rayleigh Analysis for Y-Direction Period of Vibration

Level	Drift, δ (in.)	Force, F (kips)	Weight, W (kips)	δF	$\delta^2 W/g$
R	6.01	186.9	1656	1123.27	154.80
12	5.79	154.0	1598	891.66	138.64
11	5.43	129.9	1598	705.36	121.94
10	4.98	107.6	1598	535.85	102.56
9	4.32	186.3	3403	804.82	164.36
8	3.83	100.8	2330	386.06	88.45
7	3.26	77.0	2330	251.02	64.08
6	2.68	56.2	2330	150.62	43.31
5	2.05	71.4	4323	146.37	47.02
4	1.59	31.5	3066	50.09	20.06
3	1.10	16.6	3066	18.26	9.60
2	0.61	6.3	3097	3.84	2.98
Σ				5067.21	957.81

$\omega = (5067/9589)^{0.5} = 2.30$ rad/sec. $T = 2\pi/\omega = 2.73$ sec. 1.0 in. = 25.4 mm, 1.0 kip = 4.45 kN.

3.1.5.3.2 P-Delta Effects

P-delta effects are computed for the X-direction response in Table 3.1-11. The last column of the table shows the story stability ratio computed according to *Provisions* Eq. 5.4.6.2-1 [5.2-16]:

$$\theta = \frac{P_x \Delta}{V_x h_{sx} C_d}$$

[In the 2003 *Provisions*, the equation for the story stability ratio was changed by introducing the importance factor (I) to the numerator. As previously formulated, larger axial loads (P_x) would be permitted where the design shears (V_x) included an importance factor greater than 1.0; that effect was unintended.]

Provisions Eq. 5.4.6.2-2 places an upper limit on θ :

$$\theta_{max} = \frac{0.5}{\beta C_d}$$

where β is the ratio of shear demand to shear capacity for the story. Conservatively taking $\beta = 1.0$ and using $C_d = 5.5$, $\theta_{max} = 0.091$. [In the 2003 *Provisions*, this upper limit equation has been eliminated. Instead, the *Provisions* require that where $\theta > 0.10$ a special analysis be performed in accordance with Sec. A5.2.3. This example constitutes a borderline case as the maximum stability ratio (at Level 3, as shown in Table 3.1-11) is 0.103.]

The Δ terms in Table 3.1-11 below are taken from Column 3 of Table 3.1-7 because these are consistent with the ELF story shears of Table 3.1-4 and thereby represent the true lateral stiffness of the system. (If 0.568 times the story drifts were used, then 0.568 times the story shears also would need to be used. Hence, the 0.568 factor would cancel out as it would appear in both the numerator and denominator.)

Table 3.1-11 Computation of P-Delta Effects for X-Direction Response

Level	h_{sx} (in.)	Δ (in.)	P_D (kips)	P_L (kips)	P_T (kips)	P_X (kips)	V_X (kips)	θ_x
R	150	1.73	1656.5	315.0	1971.5	1971.5	186.9	0.022
12	150	2.48	1595.8	315.0	1910.8	3882.3	340.9	0.034
11	150	3.08	1595.8	315.0	1910.8	5793.1	470.8	0.046
10	150	3.38	1595.8	315.0	1910.8	7703.9	578.4	0.055
9	150	3.22	3403.0	465.0	3868.0	11571.9	764.7	0.059
8	150	3.52	2330.8	465.0	2795.8	14367.7	865.8	0.071
7	150	3.58	2330.8	465.0	2795.8	17163.5	942.5	0.079
6	150	3.44	2330.8	465.0	2795.8	19959.3	998.8	0.083
5	150	3.00	4323.8	615.0	4938.8	24898.1	1070.2	0.085
4	150	3.00	3066.1	615.0	3681.1	28579.2	1101.7	0.094
3	150	2.94	3066.1	615.0	3681.1	32260.3	1118.2	0.103
2	216	3.55	3097.0	615.0	3712.0	35972.3	1124.5	0.096

1.0 in. = 25.4 mm, 1.0 kip = 4.45 kN.

The gravity force terms include a 20 psf uniform live load over 100 percent of the floor and roof area. The stability ratio just exceeds 0.091 at Levels 2 through 4. However, β was very conservatively taken as 1.0. Because a more refined analysis would most likely show a lower value of β , we will proceed assuming that P-delta effects are not a problem for this structure. Calculations for the Y direction produced similar results, but are not included herein.

3.1.5.4 Computation of Member Forces

Before member forces may be computed, the proper load cases and combinations of load must be identified such that all critical seismic effects are captured in the analysis.

3.1.5.4.1 Orthogonal Loading Effects and Accidental Torsion

For a nonsymmetric structure such as the one being analyzed, four directions of seismic force (+X, -X, +Y, -Y) must be considered and, for each direction of force, there are two possible directions for which the accidental eccentricity can apply (causing positive or negative torsion). This requires a total of eight possible combinations of direct force plus accidental torsion. When the 30 percent orthogonal loading rule is applied, the number of load combinations increases to 16 because, for each direct application of load, a positive or negative orthogonal loading can exist. Orthogonal loads are applied without accidental eccentricity.

Figure 3.1-8 illustrates the basic possibilities of application of load. Although this figure shows 16 different load combinations, it may be observed that eight of these combinations – 7, 8, 5, 6, 15, 16, 13, and 14 – are negatives of one of Combinations 1, 2, 3, 4, 9, 10, 11, and 12, respectively.

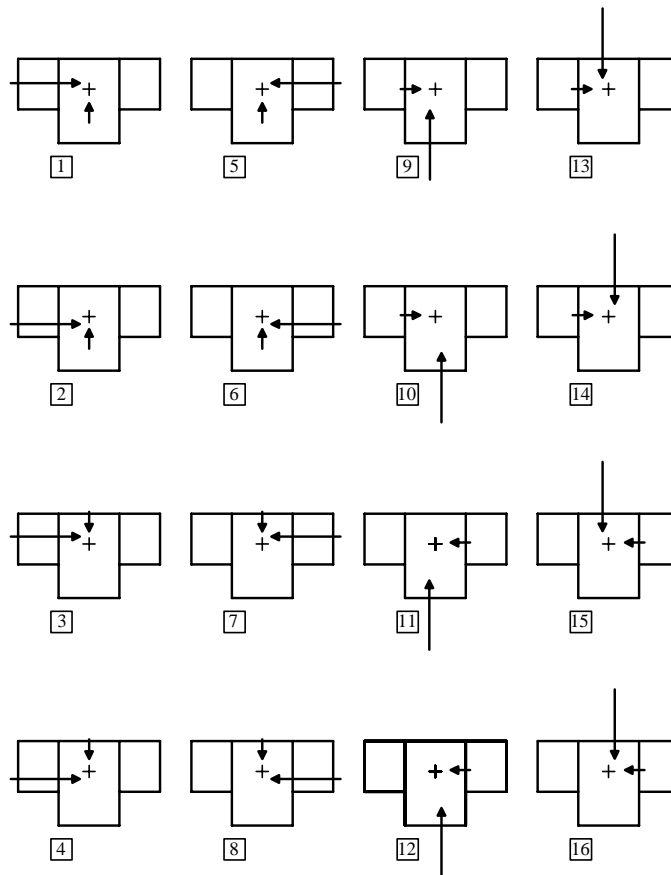


Figure 3.1-8 Basic load cases used in ELF analysis.

3.1.5.4.2 Load Combinations

The basic load combinations for this structure come from ASCE 7 with the earthquake loadings modified according to *Provisions* Sec. 5.2.7 [4.2.2.1].

The basic ASCE 7 load conditions that include earthquake are:

$$1.4D + 1.2L + E + 0.2S$$

and

$$0.9D + E$$

From *Provisions* Eq. 5.2.7-1 and Eq. 5.2.7-2 [4.2-1 and 4.2-2]:

$$E = \rho Q_E + 0.2S_{DS}Q_D$$

and

$$E = \rho Q_E - 0.2S_{DS}Q_D$$

where ρ is a redundancy factor (explained later), Q_E is the earthquake load effect, Q_D is the dead load effect, and S_{DS} is the short period spectral design acceleration.

Using $S_{DS} = 0.833$ and assuming the snow load is negligible in Stockton, California, the basic load combinations become:

$$1.37D + 0.5L + \rho E$$

and

$$0.73D + \rho E$$

[The redundancy requirements have been changed substantially in the 2003 *Provisions*. Instead of performing the calculations that follow, 2003 *Provisions* Sec. 4.3.3.2 would require that an analysis determine the most severe effect on story strength and torsional response of loss of moment resistance at the beam-to-column connections at both ends of any single beam. Where the calculated effects fall within permitted limits, or the system is configured so as to satisfy prescriptive requirements in the exception, the redundancy factor is 1.0. Otherwise, $\rho = 1.3$. Although consideration of all possible single beam failures would require substantial effort, in most cases an experienced analyst would be able to identify a few critical elements that would be likely to produce the maximum effects and then explicitly consider only those conditions.]

Based on *Provisions* Eq. 5.2.4.2, the redundancy factor (ρ) is the largest value of ρ_x computed for each story:

$$\rho_x = 2 - \frac{20}{r_{max_x} \sqrt{A_x}}$$

In this equation, r_{max_x} is a ratio of element shear to story shear, and A_x is the area of the floor diaphragm immediately above the story under consideration; ρ_x need not be taken greater than 1.5, but it may not be less than 1.0. [In the 2003 *Provisions*, ρ is either 1.0 or 1.3.]

For this structure, the check is illustrated for the lower level only where the area of the diaphragm is 30,750 ft². Figure 3.1-1 shows that the structure has 18 columns resisting load in the X direction and 18 columns resisting load in the Y direction. If it is assumed that each of these columns equally resists base shear and the check, as specified by the *Provisions*, is made for any two adjacent columns:

$$r_{max_x} = 2/18 = 0.111 \text{ and } \rho_x = 2 - \frac{20}{0.111\sqrt{30750}} = 0.963.$$

Checks for upper levels will produce an even lower value of ρ_x ; therefore, ρ_x may be taken a 1.0 for this structure. Hence, the final load conditions to be used for design are:

$$1.37D + 0.5L + E$$

and

$$0.73D + E$$

The first load condition will produce the maximum negative moments (tension on the top) at the face of the supports in the girders and maximum compressive forces in columns. The second load condition will produce the maximum positive moments (or minimum negative moment) at the face of the supports of the girders and maximum tension (or minimum compression) in the columns. In addition to the above load condition, the gravity-only load combinations as specified in ASCE 7 also must be checked. Due to the relatively short spans in the moment frames, however, it is not expected that the non-seismic load combinations will control.

3.1.5.4.3 Setting up the Load Combinations in SAP2000

The load combinations required for the analysis are shown in Table 3.1-12.

It should be noted that 32 different load combinations are required only if one wants to maintain the signs in the member force output, thereby providing complete design envelopes for all members. As mentioned later, these signs are lost in response-spectrum analysis and, as a result, it is possible to capture the effects of dead load plus live load plus-or-minus earthquake load in a single SAP2000 run containing only four load combinations.

Table 3.1-12 Seismic and Gravity Load Combinations as Run on SAP 2000

Run	Combination	Lateral*		Gravity	
		A	B	1 (Dead)	2 (Live)
One	1	[1]		1.37	0.5
	2	[1]		0.73	0.0
	3	[-1]		1.37	0.5
	4	[-1]		0.73	0.0
	5		[2]	1.37	0.5
	6		[2]	0.73	0.0
	7		[-2]	1.37	0.5
	8		[-2]	0.73	0.0
Two	1	[3]		1.37	0.5
	2	[3]		0.73	0.0
	3		[4]	1.37	0.5
	4		[4]	0.73	0.0
	5	[-3]		1.37	0.5
	6	[-3]		0.73	0.0
	7		[-4]	1.37	0.5
	8		[-4]	0.73	0.0
Three	1	[9]		1.37	0.5
	2	[9]		0.73	0.0
	3		[10]	1.37	0.5
	4		[10]	0.73	0.0
	5	[-9]		1.37	0.5
	6	[-9]		0.73	0.0
	7		[-10]	1.37	0.5
	8		[-10]	0.73	0.0
Four	1	[11]		1.37	0.5
	2	[11]		0.73	0.0
	3		[12]	1.37	0.5
	4		[12]	0.73	0.0
	5	[-11]		1.37	0.5
	6	[-11]		0.73	0.0
	7		[-12]	1.37	0.5
	8		[-12]	0.73	0.0

* Numbers in brackets [#] represent load conditions shown in Figure 3.1-8. A negative sign [-#] indicates that all lateral load effects act in the direction opposite that shown in the figure.

3.1.5.4.4 Member Forces

For this portion of the analysis, the earthquake shears in the girders along Gridline 1 are computed. This analysis considers only 100 percent of the X-direction forces applied in combination with 30 percent of the (positive or negative) Y-direction forces. The X-direction forces are applied with a 5 percent accidental eccentricity to produce a clockwise rotation of the floor plates. The Y-direction forces are applied without eccentricity.

The results of the member force analysis are shown in Figure 3.1-9. In a later part of this example, the girder shears are compared to those obtained from modal-response-spectrum and modal-time-history analyses.

			8.31	9.54	9.07		
R-12			16.1	17.6	17.1		
12-11			25.8	26.3	26.9		
11-10			31.2	31.0	32.9		
10-9			32.7	32.7	30.4	28.9	12.5
9-8			34.5	34.1	32.3	36.0	22.4
8-7			39.1	38.1	36.5	39.2	24.2
7-6			40.4	38.4	37.2	39.6	24.8
6-5	13.1	30.0	31.7	34.3	33.1	34.9	22.2
5-4	22.1	33.6	29.1	31.0	30.1	31.6	20.4
4-3	22.0	33.0	30.5	31.7	31.1	32.2	21.4
3-2	20.9	33.0	30.9	31.8	31.1	32.4	20.4
2-G							

Figure 3.1-9 Seismic shears in girders (kips) as computed using ELF analysis. Analysis includes orthogonal loading and accidental torsion. (1.0 kip = 4.45 kn)

3.1.6 Modal-Response-Spectrum Analysis

The first step in the modal-response-spectrum analysis is the computation of the structural mode shapes and associated periods of vibration. Using the Table 3.1-4 structural masses and the same mathematical model as used for the ELF and the Rayleigh analyses, the mode shapes and frequencies are automatically computed by SAP2000.

The computed periods of vibration for the first 10 modes are summarized in Table 3.1-13, which also shows values called the modal direction factor for each mode. Note that the longest period, 2.867 seconds, is significantly greater than $C_u T_a = 2.23$ seconds. Therefore, displacements, drift, and member forces as computed from the true modal properties may have to be scaled up to a value consistent with 85 percent of the ELF base shear using $T = C_u T_a$. The smallest period shown in Table 3.1-13 is 0.427 seconds.

The modal direction factors shown in Table 3.1-13 are indices that quantify the direction of the mode. A direction factor of 100.0 in any particular direction would indicate that this mode responds entirely along one of the orthogonal (X, Y or θ_z axes) of the structure.³ As Table 3.1-13 shows, the first mode is predominantly X translation, the second mode is primarily Y translation, and the third mode is largely

³It should be emphasized that, in general, the principal direction of structural response will not coincide with one of the axes used to describe the structure in three-dimensional space.

torsional. Modes 4 and 5 also are nearly unidirectional, but Modes 6 through 10 have significant lateral-torsional coupling. Plots showing the first eight mode shapes are given in Figure 3.1-10.

It is interesting to note that the X-direction Rayleigh period (2.87 seconds) is virtually identical to the first mode predominately X-direction period (2.867 seconds) computed from the eigenvalue analysis. Similarly, the Y-direction Rayleigh period (2.73 seconds) is very close to second mode predominantly Y-direction period (2.744 seconds) from the eigenvalue analysis. The closeness of the Rayleigh and eigenvalue periods of this building arises from the fact that the first and second modes of vibration act primarily along the orthogonal axes. Had the first and second modes not acted along the orthogonal axes, the Rayleigh periods (based on loads and displacements in the X and Y directions) would have been somewhat less accurate.

In Table 3.1-14, the effective mass in Modes 1 through 10 is given as a percentage of total mass. The values shown in parentheses in Table 3.1-14 are the accumulated effective masses and should total 100 percent of the total mass when all modes are considered. By Mode 10, the accumulated effective mass value is approximately 80 percent of the total mass for the translational modes and 72 percent of the total mass for the torsional mode. *Provisions* Sec. 5.5.2 [5.3.2] requires that a sufficient number of modes be represented to capture at least 90 percent of the total mass of the structure. On first glance, it would seem that the use of 10 modes as shown in Table 3.1-14 violates this rule. However, approximately 18 percent of the total mass for this structure is located at grade level and, as this level is extremely stiff, this mass does not show up as an effective mass until Modes 37, 38, and 39 are considered. In the case of the building modeled as a 13-story building with a very stiff first story, the accumulated 80 percent of effective translational mass in Mode 10 actually represents almost 100 percent of the dynamically excitable mass. In this sense, the *Provisions* requirements are clearly met when using only the first 10 modes in the response spectrum or time-history analysis. For good measure, 14 modes were used in the actual analysis.

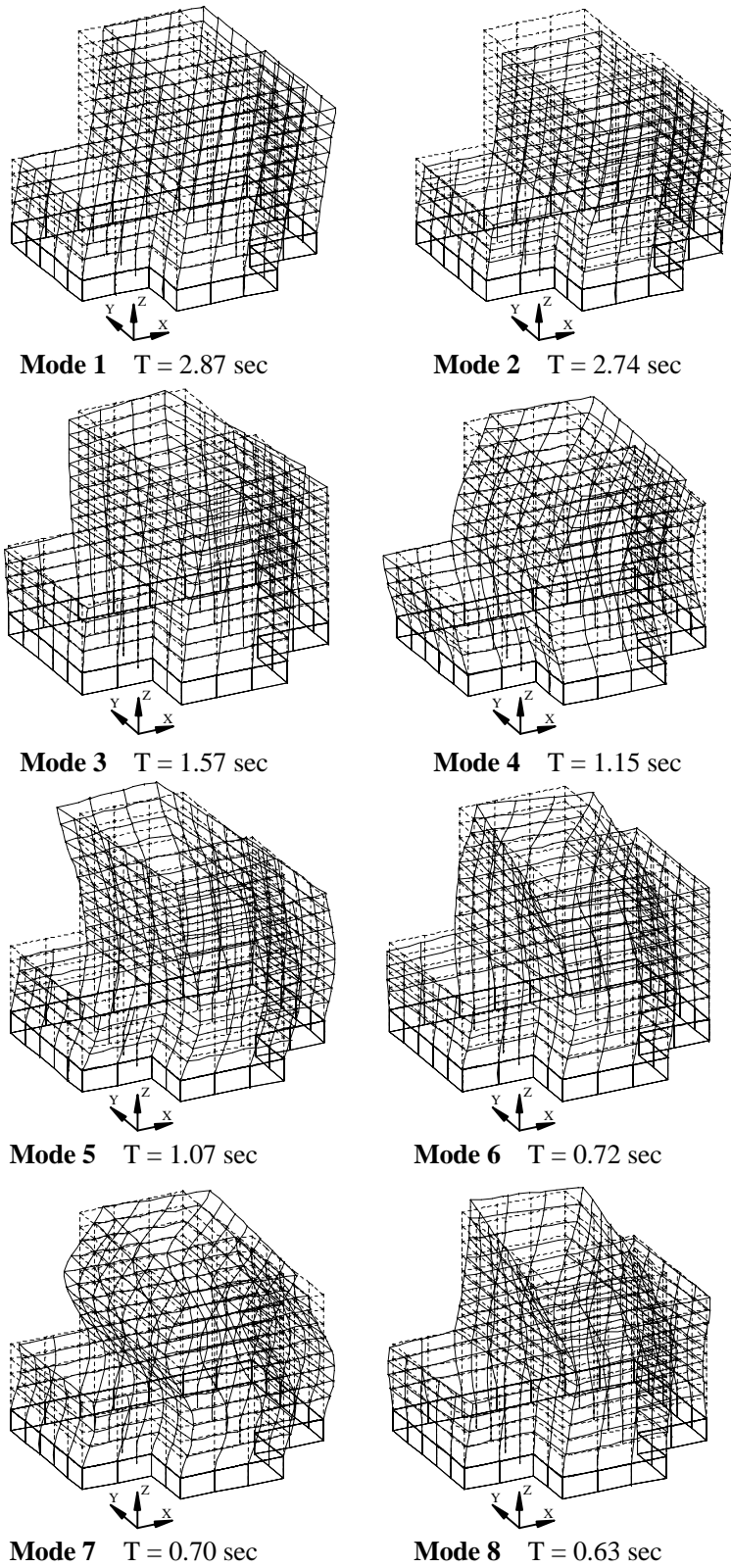


Figure 3.1-10 Mode shapes as computed using SAP2000.

Table 3.1-13 Computed Periods and Direction Factors

Mode	Period (seconds)	Modal Direction Factor		
		X Translation	Y Translation	Z Torsion
1	2.867	99.2	0.7	0.1
2	2.745	0.8	99.0	0.2
3	1.565	1.7	9.6	88.7
4	1.149	98.2	0.8	1.0
5	1.074	0.4	92.1	7.5
6	0.724	7.9	44.4	47.7
7	0.697	91.7	5.23	3.12
8	0.631	0.3	50.0	49.7
9	0.434	30.0	5.7	64.3
10	0.427	70.3	2.0	27.7

Table 3.1-14 Computed Periods and Effective Mass Factors

Mode	Period (seconds)	Effective Mass Factor		
		X Translation	Y Translation	Z Torsion
1	2.867	64.04 (64.0)	0.46 (0.5)	0.04 (0.0)
2	2.744	0.51 (64.6)	64.25 (64.7)	0.02 (0.1)
3	1.565	0.34 (64.9)	0.93 (65.6)	51.06 (51.1)
4	1.149	10.78 (75.7)	0.07 (65.7)	0.46 (51.6)
5	1.074	0.04 (75.7)	10.64 (76.3)	5.30 (56.9)
6	0.724	0.23 (75.9)	1.08 (77.4)	2.96 (59.8)
7	0.697	2.94 (78.9)	0.15 (77.6)	0.03 (59.9)
8	0.631	0.01 (78.9)	1.43 (79.0)	8.93 (68.8)
9	0.434	0.38 (79.3)	0.00 (79.0)	3.32 (71.1)
10	0.427	1.37 (80.6)	0.01 (79.0)	1.15 (72.3)

3.1.6.1 Response Spectrum Coordinates and Computation of Modal Forces

The coordinates of the response spectrum are based on *Provisions* Eq. 4.1.2.6-1 and 4.1.2.6-2 [3.3-5 and 3.3-6]. [In the 2003 *Provisions*, the design response spectrum has reduced ordinates at very long periods as indicated in Sec. 3.3.4. The new portion of the spectrum reflects a constant ground displacement at periods greater than T_L , the value of which is based on the magnitude of the source earthquake that dominates the probabilistic ground motion at the site.]

For periods less than T_0 :

$$S_a = 0.6 \frac{S_{DS}}{T_0} T + 0.4 S_{DS}$$

and for periods greater than T_S :

$$S_a = \frac{S_{D1}}{T}$$

where $T_0 = 0.2S_{DS} / S_{D1}$ and $T_s = S_{D1} / S_{DS}$.

Using $S_{DS} = 0.833$ and $S_{D1} = 0.373$, $T_0 = 0.089$ seconds and $T_s = 0.448$ seconds. The computed response-spectrum coordinates for several period values are shown in Table 3.1-15 and the response spectrum, shown with and without the $I/R = 1/8$ modification, is plotted in Figure 3.1-11. The spectrum does not include the high period limit on C_s ($C_{s, min} = 0.044IS_{DS}$), which controlled the ELF base shear for this structure and which ultimately will control the scaling of the results from the response-spectrum analysis. (Recall that if the computed base shear falls below 85 percent of the ELF base shear, the computed response must be scaled up such that the computed base shear equals 85 percent of the ELF base shear.)

Table 3.1-15 Response Spectrum Coordinates

T_m (seconds)	C_{sm}	$C_{sm}(I/R)$
0.000	0.333	0.0416
0.089 (T_0)	0.833	0.104
0.448 (T_s)	0.833	0.104
1.000	0.373	0.0446
1.500	0.249	0.0311
2.000	0.186	0.0235
2.500	0.149	0.0186
3.000	0.124	0.0155

$I = 1, R = 8.7$.

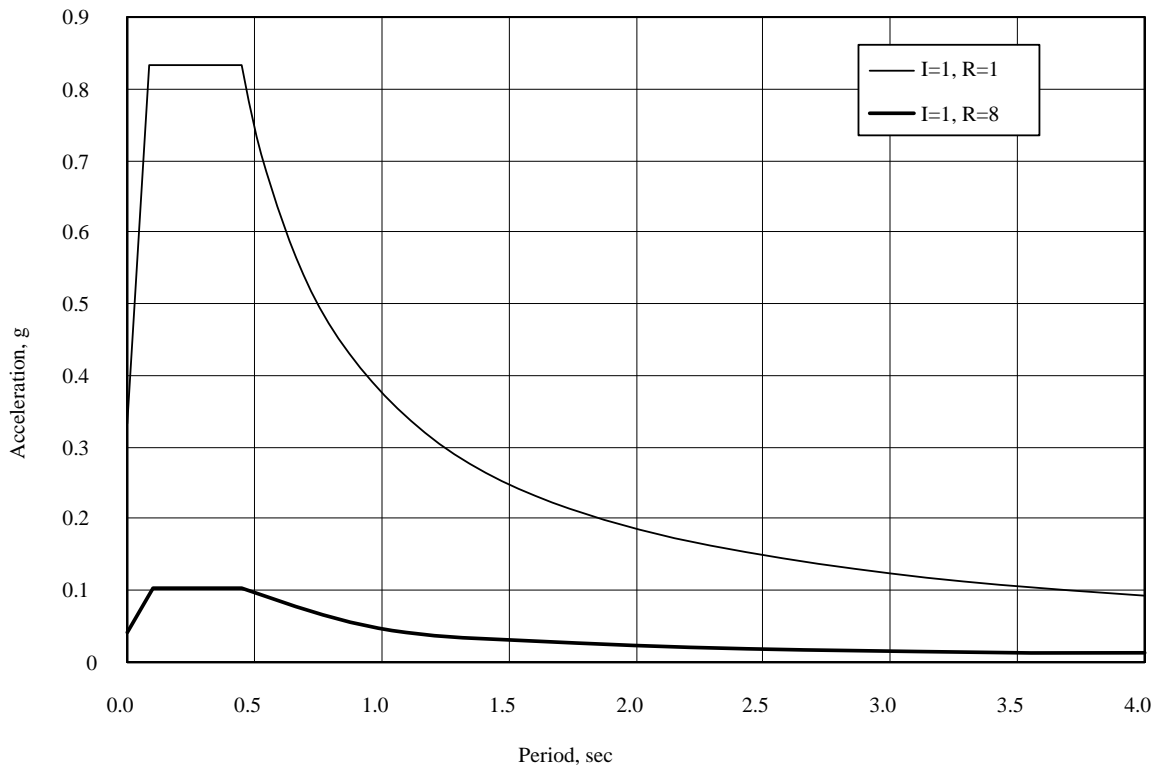


Figure 3.1-11 Total acceleration response spectrum used in analysis.

Using the response spectrum coordinates of Table 3.1-15, the response-spectrum analysis was carried out using SAP2000. As mentioned above, the first 14 modes of response were computed and superimposed using complete quadratic combination (CQC). A modal damping ratio of 5 percent of critical was used in the CQC calculations.

Two analyses were carried out. The first directed the seismic motion along the X axis of the structure, and the second directed the motion along the Y axis. Combinations of these two loadings plus accidental torsion are discussed later. The response spectrum used in the analysis did include *I/R*.

3.1.6.1.1 Dynamic Base Shear

After specifying member “groups,” SAP2000 automatically computes and prints the CQC story shears. Groups were defined such that total shears would be printed for each story of the structure. The base shears were printed as follows:

X-direction base shear = 437.7 kips

Y-direction base shear = 454.6 kips

These values are much lower than the ELF base shear of 1124 kips. Recall that the ELF base shear was controlled by *Provisions* Eq. 5.4.1.1-3. The modal-response-spectrum shears are less than the ELF shears because the fundamental period of the structure used in the response-spectrum analysis is 2.87 seconds (vs 2.23) and because the response spectrum of Figure 3.1-11 does not include the minimum base shear limit imposed by *Provisions* Eq. 5.4.1.1-3. [Recall that the equation for minimum base shear coefficient does not appear in the 2003 *Provisions*.]

According to *Provisions* Sec. 5.5.7 [5.3.7], the base shears from the modal-response-spectrum analysis must not be less than 85 percent of that computed from the ELF analysis. If the response spectrum shears are lower than the ELF shear, then the computed shears and displacements must be scaled up such that the response spectrum base shear is 85 percent of that computed from the ELF analysis.

Hence, the required scale factors are:

X-direction scale factor = $0.85(1124)/437.7 = 2.18$

Y-direction scale factor = $0.85(1124)/454.6 = 2.10$

The computed and scaled story shears are as shown in Table 3.1-16. Since the base shears for the ELF and the modal analysis are different (due to the 0.85 factor), direct comparisons cannot be made between Table 3.1-11 and Table 3.1-4. However, it is clear that the vertical distribution of forces is somewhat similar when computed by ELF and modal-response spectrum.

Table 3.1-16 Story Shears from Modal-Response-Spectrum Analysis

Story	X Direction (SF = 2.18)		Y Direction (SF = 2.10)	
	Unscaled Shear (kips)	Scaled Shear (kips)	Unscaled Shear (kips)	Scaled Shear (kips)
R-12	82.5	180	79.2	167
12-11	131.0	286	127.6	268
11-10	163.7	358	163.5	344
10-9	191.1	417	195.0	410
9-8	239.6	523	247.6	521
8-7	268.4	586	277.2	583
7-6	292.5	638	302.1	635
6-5	315.2	688	326.0	686
5-4	358.6	783	371.8	782
4-3	383.9	838	400.5	843
3-2	409.4	894	426.2	897
2-G	437.7	956	454.6	956

1.0 kip = 4.45 kN.

3.1.6.2 Drift and P-Delta Effects

According to *Provisions* Sec. 5.5.7 [5.3.7], the computed displacements and drift (as based on the response spectrum of Figure 3.1-11) must also be scaled by the base shear factors (SF) of 2.18 and 2.10 for the structure loaded in the X and Y directions, respectively.

In Tables 3.1-17 and 3.1-18, the story displacement from the response-spectrum analysis, the scaled story displacement, the scaled story drift, the amplified story drift (as multiplied by $C_d = 5.5$), and the allowable story drift are listed. As may be observed from the tables, the allowable drift is not exceeded at any level.

P-delta effects are computed for the X-direction response as shown in Table 3.1-19. Note that the scaled story shears from Table 3.1-16 are used in association with the scaled story drifts (including C_d) from Table 3.1-17. The story stability factors are above the limit ($\theta_{max} = 0.091$) only at the bottom two levels of the structure and are only marginally above the limit. As the β factor was conservatively set at 1.0 in computing the limit, it is likely that a refined analysis for β would indicate that P-delta effects are not of particular concern for this structure.

Table 3.1-17 Response Spectrum Drift for Building Responding in X Direction

Level	1 Total Drift from R.S. Analysis (in.)	2 Scaled Total Drift [Col-1 \times 2.18] (in.)	3 Scaled Drift (in.)	4 Scaled Story Drift $\times C_d$ (in.)	5 Allowable Story Drift (in.)
R	1.96	4.28	0.18	0.99	3.00
12	1.88	4.10	0.26	1.43	3.00
11	1.76	3.84	0.30	1.65	3.00
10	1.62	3.54	0.33	1.82	3.00
9	1.47	3.21	0.34	1.87	3.00
8	1.32	2.87	0.36	1.98	3.00
7	1.15	2.51	0.40	2.20	3.00
6	0.968	2.11	0.39	2.14	3.00
5	0.789	1.72	0.38	2.09	3.00
4	0.615	1.34	0.38	2.09	3.00
3	0.439	0.958	0.42	2.31	3.00
2	0.245	0.534	0.53	2.91	4.32

1.0 in. = 25.4 mm.

Table 3.1-18 Spectrum Response Drift for Building Responding in Y Direction

Level	1 Total Drift from R.S. Analysis (in.)	2 Scaled Total Drift [Col-1 \times 2.18] (in.)	3 Scaled Drift (in.)	4 Scaled Story Drift $\times C_d$ (in.)	5 Allowable Story Drift (in.)
R	1.84	3.87	0.12	0.66	3.00
12	1.79	3.75	0.20	1.10	3.00
11	1.69	3.55	0.24	1.32	3.00
10	1.58	3.31	0.37	2.04	3.00
9	1.40	2.94	0.29	1.60	3.00
8	1.26	2.65	0.33	1.82	3.00
7	1.10	2.32	0.35	1.93	3.00
6	0.938	1.97	0.38	2.09	3.00
5	0.757	1.59	0.32	1.76	3.00
4	0.605	1.27	0.36	2.00	3.00
3	0.432	0.908	0.39	2.14	3.00
2	0.247	0.518	0.52	2.86	4.32

1.0 in. = 25.4 mm.

Table 3.1-19 Computation of P-Delta Effects for X-Direction Response

Level	h_{sx} (in.)	Δ (in.)	P_D (kips)	P_L (kips)	P_T (kips)	P_X (kips)	V_X (kips)	θ_X
R	150	0.99	1656.5	315.0	1971.5	1971.5	180	0.013
12	150	1.43	1595.8	315.0	1910.8	3882.3	286	0.024
11	150	1.65	1595.8	315.0	1910.8	5793.1	358	0.032
10	150	1.82	1595.8	315.0	1910.8	7703.9	417	0.041
9	150	1.87	3403.0	465.0	3868.0	11571.9	523	0.050
8	150	1.98	2330.8	465.0	2795.8	14367.7	586	0.059
7	150	2.20	2330.8	465.0	2795.8	17163.5	638	0.072
6	150	2.14	2330.8	465.0	2795.8	19959.3	688	0.075
5	150	2.09	4323.8	615.0	4938.8	24898.1	783	0.081
4	150	2.09	3066.1	615.0	3681.1	28579.2	838	0.086
3	150	2.31	3066.1	615.0	3681.1	32260.3	894	0.101
2	216	2.91	3097.0	615.0	3712.0	35972.3	956	0.092

1.0 in. = 25.4 mm, 1.0 kip = 4.45 kN.

3.1.6.3 Torsion, Orthogonal Loading, and Load Combinations

To determine member design forces, it is necessary to add the effects of accidental torsion and orthogonal loading into the analysis. When including accidental torsion in modal-response-spectrum analysis, there are generally two approaches that can be taken:

1. Displace the center of mass of the floor plate plus or minus 5 percent of the plate dimension perpendicular to the direction of the applied response spectrum. As there are four possible mass locations, this will require four separate modal analyses for torsion with each analysis using a different set of mode shapes and frequencies.
2. Compute the effects of accidental torsion by creating a load condition with the story torques applied as static forces. Member forces created by the accidental torsion are then added directly to the results of the response-spectrum analysis. Since the sign of member forces in the response-spectrum analysis is lost as a result of SRSS or CQC combinations, the absolute value of the member forces resulting from accidental torsion should be used. As with the displaced mass method, there are four possible ways to apply the accidental torsion: plus and minus torsion for primary loads in the X or Y directions. Because of the required scaling, the static torsional forces should be based on 85 percent of the ELF forces.

Each of the above approaches has advantages and disadvantages. The primary disadvantage of the first approach is a practical one: most computer programs do not allow for the extraction of member force maxima from more than one run when the different runs incorporate a different set of mode shapes and frequencies. For structures that are torsionally regular and will not require amplification of torsion, the second approach is preferred. For torsionally flexible structures, the first approach may be preferred because the dynamic analysis will automatically amplify the torsional effects. In the analysis that follows, the second approach has been used because the structure has essentially rigid diaphragms and high torsional rigidity and amplification of accidental torsion is not required.

There are three possible methods for applying the orthogonal loading rule:

1. Run the response-spectrum analysis with 100 percent of the scaled X spectrum acting in one direction, concurrent with the application of 30 percent of the scaled Y spectrum acting in the orthogonal direction. Use CQC for combining modal maxima. Perform a similar analysis for the larger seismic forces acting in the Y direction.
2. Run two separate response-spectrum analyses, one in the X direction and one in the Y direction, with CQC being used for modal combinations in each analysis. Using a direct sum, combine 100 percent of the scaled X-direction results with 30 percent of the scaled Y-direction results. Perform a similar analysis for the larger loads acting in the Y direction.
3. Run two separate response-spectrum analyses, one in the X direction and one in the Y-direction, with CQC being used for modal combinations in each analysis. Using SRSS, combine 100 percent of the scaled X-direction results with 100 percent of the scaled Y-direction results.⁴

All seismic effects can be considered in only two load cases by using Approach 2 for accidental torsion and Approach 2 for orthogonal loading. These are shown in Figure 3.1-12. When the load combinations required by *Provisions* Sec. 5.2.7 [4.2.2.1] are included, the total number of load combinations will double to four.

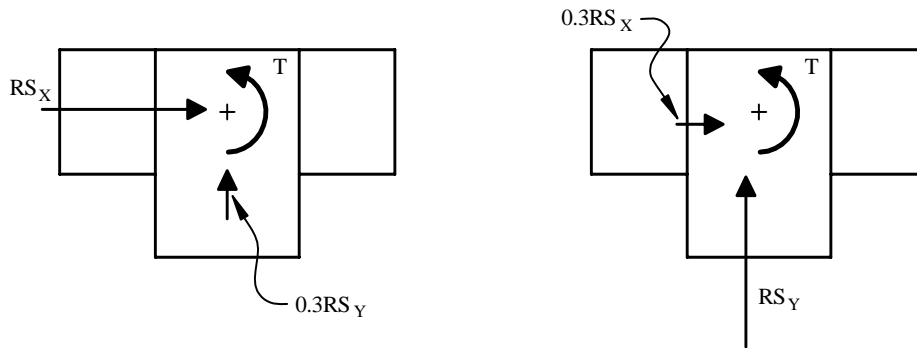


Figure 3.1-12 Load combinations from response-spectrum analysis.

3.1.6.4 Member Design Forces

Earthquake shear forces in the beams of Frame 1 are given in Figure 3.1-13 for the X direction of response. These forces include 100 percent of the scaled X-direction spectrum added to the 30 percent of the scaled Y-direction spectrum. Accidental torsion is then added to the combined spectral loading. The design force for the Level 12 beam in Bay 3 (shown in bold type in Figure 3.1-13) was computed as follows:

⁴This method has been forwarded in the unpublished paper *A Seismic Analysis Method Which Satisfies the 1988 UBC Lateral Force Requirements*, written in 1989 by Wilson, Suharwardy, and Habibullah. The paper also suggests the use of a single scale factor, where the scale factor is based on the total base shear developed along the principal axes of the structure. As stated in the paper, the major advantage of the method is that one set of dynamic design forces, including the effect of accidental torsion, is produced in one computer run. In addition, the resulting structural design has equal resistance to seismic motions in all possible directions.

Force from 100 percent X-direction spectrum = 6.94 kips (as based on CQC combination for structure loaded with X spectrum only).

Force from 100 percent Y-direction spectrum = 1.26 kips (as based on CQC combination for structure loaded with Y spectrum only).

Force from accidental torsion = 1.25 kips.

Scale factor for X-direction response = 2.18.

Scale factor for Y-direction response = 2.10.

$$\text{Earthquake shear force} = (2.18 \times 6.94) + (2.10 \times 0.30 \times 1.26) + (0.85 \times 1.25) = 17.0 \text{ kips}$$

			9.4	9.7	9.9		
R-12			17.0	17.7	17.8		
12-11			25.0	24.9	26.0		
11-10			28.2	27.7	29.8		
10-9			26.6	26.5	24.8	22.9	10.2
9-8			27.2	26.7	25.5	28.0	18.0
8-7			30.9	28.8	28.8	30.5	19.4
7-6			32.3	30.4	29.8	31.1	20.1
6-5	11.1	24.4	26.0	27.7	27.1	27.9	18.6
5-4	19.0	28.8	25.7	27.0	26.6	27.1	18.6
4-3	20.1	29.7	28.0	28.8	28.4	29.0	20.2
3-2	20.0	31.5	30.1	30.6	30.4	31.1	20.1
2-G							

Figure 3.1-13 Seismic shears in girders (kips) as computed using response-spectrum analysis. Analysis includes orthogonal loading and accidental torsion (1.0 kip = 4.45 kN).

3.1.7 Modal-Time-History Analysis

In modal-time-history analysis, the response in each mode is computed using step-by-step integration of the equations of motion, the modal responses are transformed to the structural coordinate system, linearly superimposed, and then used to compute structural displacements and member forces. The displacement and member forces for each time step in the analysis or minimum and maximum quantities (response envelopes) may be printed.

Requirements for time-history analysis are provided in *Provisions* Sec. 5.6 [5.4]. The same mathematical model of the structure used for the ELF and response-spectrum analysis is used for the time-history analysis.

As allowed by *Provisions* Sec. 5.6.2 [5.4.2], the structure will be analyzed using three different pairs of ground motion time-histories. The development of a proper suite of ground motions is one of the most critical and difficult aspects of time-history approaches. The motions should be characteristic of the site and should be from real (or simulated) ground motions that have a magnitude, distance, and source mechanism consistent with those that control the maximum considered earthquake.

For the purposes of this example, however, the emphasis is on the *implementation* of the time-history approach rather than on selection of realistic ground motions. For this reason, the motion suite developed for Example 3.2 is also used for the present example.⁵ The structure for Example 3.2 is situated in Seattle, Washington, and uses three pairs of motions developed specifically for the site. The use of the Seattle motions for a Stockton building analysis is, of course, not strictly consistent with the requirements of the *Provisions*. However, a realistic comparison may still be made between the ELF, response spectrum, and time-history approaches.

3.1.7.1 The Seattle Ground Motion Suite

It is beneficial to provide some basic information on the Seattle motion suites in Table 3.1-20 below. Refer to Figures 3.2-40 through 3.2-42 for additional information, including plots of the ground motion time histories and 5-percent-damped response spectra for each motion.

Table 3.1-20 Seattle Ground Motion Parameters (Unscaled)

Record Name	Orientation	Number of Points and Time Increment	Peak Ground Acceleration (g)	Source Motion
Record A00	N-S	8192 @ 0.005 seconds	0.443	Lucern (Landers)
Record A90	E-W	8192 @ 0.005 seconds	0.454	Lucern (Landers)
Record B00	N-S	4096 @ 0.005 seconds	0.460	USC Lick (Loma Prieta)
Record B90	E-W	4096 @ 0.005 seconds	0.435	USC Lick (Loma Prieta)
Record C00	N-S	1024 @ 0.02 seconds	0.460	Dayhook (Tabas, Iran)
Record C90	E-W	1024 @ 0.02 seconds	0.407	Dayhook (Tabas, Iran)

Before the ground motions may be used in the time-history analysis, they must be scaled using the procedure described in *Provisions* Sec. 5.6.2.2 [5.4.2.2]. One scale factor will be determined for each pair of ground motions. The scale factors for record sets A, B, and C will be called S_A , S_B , and S_C , respectively.

The scaling process proceeds as follows:

1. For each pair of motions (A, B, and C):
 - a. Assume an initial scale factor (S_A , S_B , S_C),
 - b. Compute the 5-percent-damped elastic response spectrum for each component in the pair,
 - c. Compute the SRSS of the spectra for the two components, and
 - d. Scale the SRSS using the factor from (a) above.
2. Adjust scale factors (S_A , S_B , and S_C) such that the average of the three scaled SRSS spectra over the period range $0.2T_l$ to $1.5T_l$ is not less than 1.3 times the 5-percent-damped spectrum determined in accordance with *Provisions* Sec. 4.1.2.6 [3.3.4]. T_l is the fundamental mode period of vibration of

⁵See Sec. 3.2.6.2 of this volume of design examples for a detailed discussion of the selected ground motions.

the structure. (The factor of 1.3 more than compensates for the fact that taking the SRSS of the two components of a ground motion effectively increases their magnitude by a factor of 1.414.) Note that the scale factors so determined are not unique. An infinite number of different scale factors will satisfy the above requirements, and it is up to the engineer to make sure that the selected scale factors are reasonable.⁶ Because the original ground motions are similar in terms of peak ground acceleration, the same scale factor will be used for each motion; hence, $S_A = S_B = S_C$. This equality in scale factors would not necessarily be appropriate for other suites of motions.

Given the 5-percent-damped spectra of the ground motions, this process is best carried out using an Excel spreadsheet. The spectra themselves were computed using the program *NONLIN*.⁷ The results of the analysis are shown in Figures 3.1-14 and 3.1-15. Figure 3.1-14 shows the average of the SRSS of the *unscaled* spectra together with the *Provisions* response spectrum using $S_{DS} = 0.833g$ (322 in./sec²) and $S_{D1} = 0.373g$ (144 in./sec²). Figure 3.1-15 shows the ratio of the average SRSS spectrum to the *Provisions* spectrum over the period range 0.573 seconds to 4.30 seconds, where a scale factor $S_A = S_B = S_C = 0.922$ has been applied to each original spectrum. As can be seen, the minimum ratio of 1.3 occurs at a period of approximately 3.8 seconds.

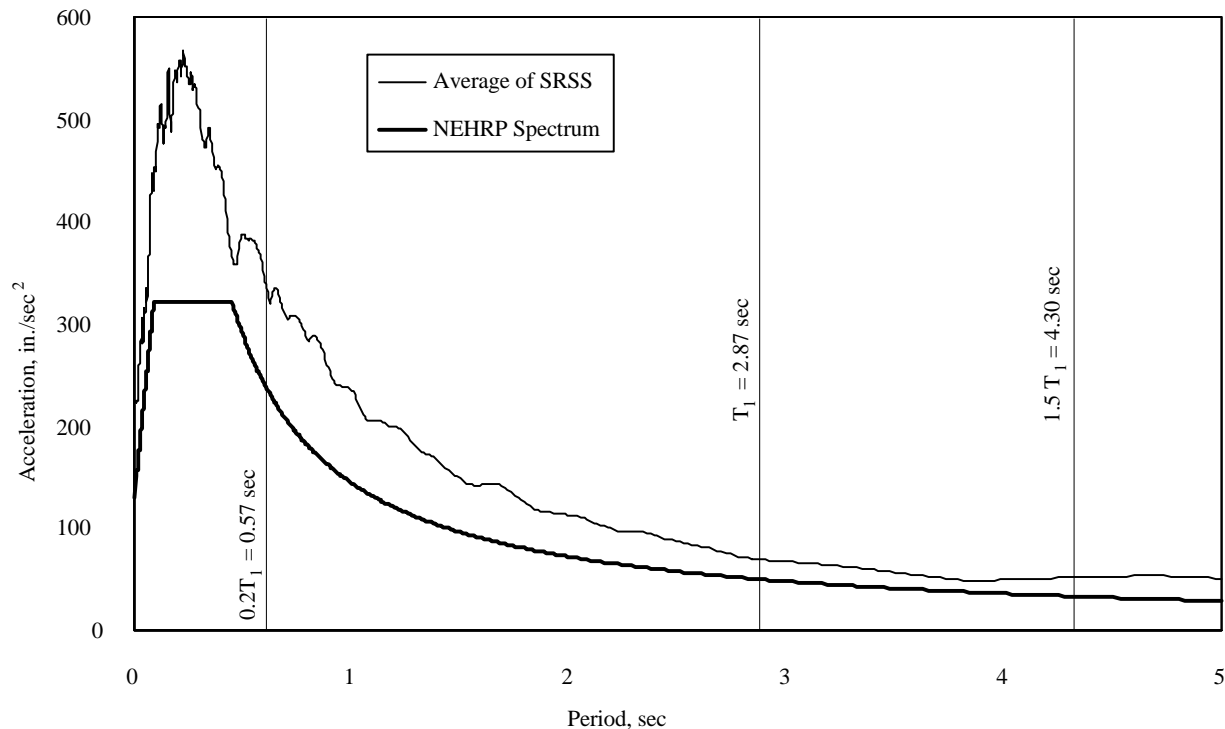


Figure 3.1-14 Unscaled SRSS of spectra of ground motion pairs together with *Provisions* spectrum (1.0 in. = 25.4 mm).

At all other periods, the effect of using the 0.922 scale factor to provide a minimum ratio of 1.3 over the target period range is to have a relatively higher scale factor at all other periods if those periods significantly contribute to the response. For example, at the structure’s fundamental mode, with $T = 2.867$ sec, the ratio of the scaled average SRSS to the *Provisions* spectrum is 1.38, not 1.30. At the higher modes, the effect is even more pronounced. For example, at the second translational X mode, $T = 1.149$

⁶The “degree of freedom” in selecting the scaling factors may be used to reduce the effect of a particularly demanding motion.

⁷*NONLIN*, developed by Finley Charney, may be downloaded at no cost at www.fema.gov/emi. To find the latest version, do a search for *NONLIN*.

seconds and the computed ratio is 1.62. This, of course, is an inherent difficulty of using a single scale factor to scale ground motion spectra to a target code spectrum.

When performing linear-time-history analysis, the ground motions also should be scaled by the factor I/R . In this case, $I = 1$ and $R = 8$, so the actual scale factor applied to each ground motion will be $0.922(1/8) = 0.115$.

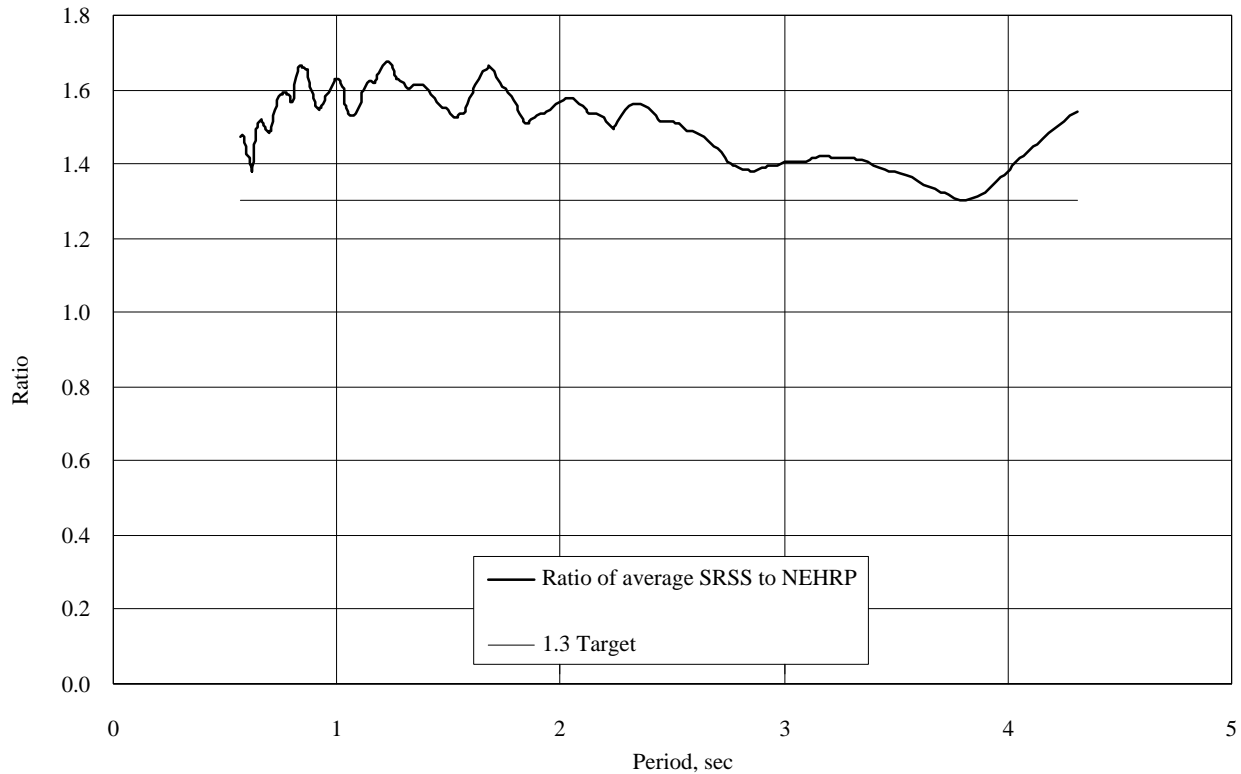


Figure 3.1-15 Ratio of average scaled SRSS spectrum to *Provisions* spectrum.

If the maximum base shear from any of the analyses is less than that computed from *Provisions* Eq. 5.4.1.1-3 ($C_s = 0.044I S_{DS}$), all forces and displacements⁸ computed from the time-history analysis must again be scaled such that peak base shear from the time-history analysis is equal to the minimum shear computed from Eq. 5.4.1.1-3. This is stated in *Provisions* Sec. 5.6.3 [5.4.3]. Recall that the base shear controlled by Eq. 5.4.1.1-3 is 1124 kips in each direction. [In the 2003 *Provisions* base shear scaling is still required, but recall that the minimum base shear has been revised.]

The second paragraph of *Provisions* Sec. 5.6.3 [5.4.3] states that if fewer than seven ground motion pairs are used in the analysis, the design of the structure should be based on the maximum scaled quantity among all analyses.

The *Provisions* is not particularly clear regarding the scaling of displacements in time-history analysis. The first paragraph of Sec. 5.6.3 states that member forces should be scaled, but displacements are not mentioned. The second paragraph states that member forces and displacements should be scaled. In this example, the displacements will be scaled, mainly to be consistent with the response spectrum procedure which, in *Provisions* Sec. 5.5.7, explicitly states that forces and displacements should be scaled. See Sec. 3.1.8 of this volume of design examples for more discussion of this apparent inconsistency in the *Provisions*.

Twelve individual time-history analyses were carried out using SAP2000: one for each N-S ground motion acting in the X direction, one for each N-S motion acting in the Y direction, one for each E-W motion acting in the X direction, and one for each E-W motion acting in the Y direction. As with the response-spectrum analysis, 14 modes were used in the analysis. Five percent of critical damping was used in each mode. The integration time-step used in all analyses was 0.005 seconds. The results from the analyses are summarized Tables 3.1-21 and 3.1-22.

As may be observed from Table 3.1-21, the maximum scaled base shears computed from the time-history analysis are significantly less than the ELF minimum of 1124 kips. This is expected because the ELF base shear was controlled by *Provisions* Eq. 5.4.1.1-3. Hence, each of the analyses will need to be scaled up. The required scale factors are shown in Table 3.1-22. Also shown in that table are the scaled maximum deflections with and without $C_d = 5.5$.

Table 3.1-21 Result Maxima from Time-History Analysis (Unscaled)

Analysis	Maximum Base Shear (S.F. = 0.115) (kips)	Time of Maximum Shear (sec)	Maximum Roof Displacement (S.F. = 0.115) (in.)	Time of Maximum Displacement (sec)
A00-X	394.5	12.73	2.28	11.39
A00-Y	398.2	11.84	2.11	11.36
A90-X	473.8	15.42	2.13	12.77
A90-Y	523.9	15.12	1.91	10.90
B00-X	393.5	15.35	2.11	14.17
B00-Y	475.1	14.29	1.91	19.43
B90-X	399.6	13.31	1.77	16.27
B90-Y	454.2	12.83	1.68	12.80
C00-X	403.1	6.96	1.86	7.02
C00-Y	519.2	6.96	1.70	7.02
C90-X	381.5	19.40	1.95	19.38
C90-Y	388.5	19.38	1.85	19.30

1.0 in. = 25.4 mm, 1.0 kip = 4.45 kN.

Table 3.1-22 Result Maxima from Time-History Analysis (Scaled)

Analysis	Maximum Base Shear (SF = 0.115) (kips)	Required Additional Scale Factor for $V = 1124$ kips	Adjusted Maximum Roof Displacement (in.)	Adjusted Max Roof Disp. $\times C_d$ (in.)
A00-X	394.5	2.85	6.51	35.7
A00-Y	398.2	2.82	5.95	32.7
A90-X	473.8	2.37	5.05	27.8
A90-Y	523.9	2.15	4.11	22.6
B00-X	393.5	2.86	6.03	33.2
B00-Y	475.1	2.37	4.53	24.9
B90-X	399.6	2.81	4.97	27.4
B90-Y	454.2	2.48	4.17	22.9
C00-X	403.1	2.79	5.19	28.5
C00-Y	519.2	2.16	3.67	20.2
C90-X	381.5	2.95	5.75	31.6
C90-Y	388.5	2.89	5.35	29.4

Scaled base shear = 1124 kips for all cases. 1.0 in. = 25.4 mm, 1.0 kip = 4.45 kN.

3.1.7.2 Drift and P-Delta Effects

In this section, drift and P-delta effects are checked only for the structure subjected to Motion A00 acting in the X direction of the building. As can be seen from Table 3.1-22, this analysis produced the largest roof displacement, but not necessarily the maximum story drift. To be sure that the maximum drift has been determined, it would be necessary to compute the scaled drifts histories from each analysis and then find the maximum drift among all analyses.

As may be observed from Table 3.1-23, the allowable drift has been exceeded at several levels. For example, at Level 11, the computed drift is 4.14 in. compared to the limit of 3.00 inches.

Before computing P-delta effects, it is necessary to determine the story shears that exist at the time of maximum displacement. These shears, together with the inertial story forces, are shown in the first two columns of Table 3.1-24. The maximum base shear at the time of maximum displacement is only 668.9 kips, significantly less than the peak base shear of 1124 kips. For comparison purposes, Table 3.1-24 also shows the story shears and inertial forces that occur at the time of peak base shear.

As may be seen from Table 3.1-25, the P-delta effects are marginally exceeded at the lower three levels of the structure, as the maximum allowable stability ratio for the structure is 0.091 (see Sec. 3.1.5.3 of this example). As mentioned earlier, the fact that the limit has been exceeded is probably of no concern because the factor β was conservatively taken as 1.0.

Table 3.1-23 Time-History Drift for Building Responding in X Direction to Motion A00X

Level	1 Elastic Total Drift (in.)	2 Elastic Story Drift (in.)	3 Inelastic Story Drift (in.)	4 Allowable Drift (in.)
R	6.51	0.47	2.57	3.00
12	6.05	0.66	3.63	3.00
11	5.39	0.75	4.14	3.00
10	4.63	0.75	4.12	3.00
9	3.88	0.62	3.40	3.00
8	3.27	0.61	3.34	3.00
7	2.66	0.58	3.20	3.00
6	2.08	0.54	2.95	3.00
5	1.54	0.42	2.32	3.00
4	1.12	0.39	2.12	3.00
3	0.74	0.34	1.89	3.00
2	0.39	0.39	2.13	4.32

Computations are at time of maximum roof displacement from analysis A00X. 1.0 in. = 25.4 mm.

Table 3.1-24 Scaled Inertial Force and Story Shear Envelopes from Analysis A00X

Level	At Time of Maximum Roof Displacement ($T = 11.39$ sec)		At Time of Maximum Base Shear ($T = 12.73$ sec)	
	Story Shear (kips)	Inertial Force (kips)	Story Shear (kips)	Inertial Force (kips)
R	307.4	307.4	40.2	40.2
12	529.7	222.3	44.3	4.1
11	664.9	135.2	45.7	1.4
10	730.5	65.6	95.6	49.9
9	787.9	57.4	319.0	223.4
8	817.5	29.6	468.1	149.1
7	843.8	26.3	559.2	91.1
6	855.0	11.2	596.5	37.3
5	828.7	-26.3	662.7	66.2
4	778.7	-50.0	785.5	122.8
3	716.1	-62.6	971.7	186.2
2	668.9	-47.2	1124.0	148.3

1.0 kip = 4.45 kN.

Table 3.1-25 Computation of P-Delta Effects for X-Direction Response

Level	h_{sx} (in.)	Δ (in.)	P_D (kips)	P_L (kips)	P_T (kips)	P_X (kips)	V_X (kips)	θ_x
R	150	2.57	1656.5	315.0	1971.5	1971.5	307.4	0.020
12	150	3.63	1595.8	315.0	1910.8	3882.3	529.7	0.032
11	150	4.14	1595.8	315.0	1910.8	5793.1	664.9	0.044
10	150	4.12	1595.8	315.0	1910.8	7703.9	730.5	0.053
9	150	3.40	3403.0	465.0	3868.0	11571.9	787.9	0.061
8	150	3.34	2330.8	465.0	2795.8	14367.7	817.5	0.071
7	150	3.20	2330.8	465.0	2795.8	17163.5	843.8	0.079
6	150	2.95	2330.8	465.0	2795.8	19959.3	855.0	0.083
5	150	2.32	4323.8	615.0	4938.8	24898.1	828.7	0.084
4	150	2.12	3066.1	615.0	3681.1	28579.2	778.7	0.094
3	150	1.89	3066.1	615.0	3681.1	32260.3	716.1	0.103
2	216	2.13	3097.0	615.0	3712.0	35972.3	668.9	0.096

Computations are at time of maximum roof displacement from analysis A00X. 1.0 in. = 25.4 mm, 1.0 kip = 4.45 kN.

3.1.7.3 Torsion, Orthogonal Loading, and Load Combinations

As with ELF or response-spectrum analysis, it is necessary to add the effects of accidental torsion and orthogonal loading into the analysis. Accidental torsion is applied in exactly the same manner as done for the response spectrum approach, except that the factor 0.85 is not used. Orthogonal loading is automatically accounted for by concurrently running one ground motion in one principal direction with

30 percent of the companion motion being applied in the orthogonal direction. Because the signs of the ground motions are arbitrary, it is appropriate to add the absolute values of the responses from the two directions. Six dynamic load combinations result:

- Combination 1: A00X + 0.3 A90Y + Torsion
 Combination 2: A90X + 0.3 A00Y + Torsion

 Combination 3: B00X + 0.3 B90Y + Torsion
 Combination 4: B90X + 0.3 B00Y + Torsion

 Combination 5: C00X + 0.3 C90Y + Torsion
 Combination 6: C90X + 0.3 C00Y + Torsion

3.1.7.4 Member Design Forces

Using the method outlined above, the individual beam shear maxima developed in Fame 1 were computed for each load combination. The envelope values from only the first two combinations are shown in Figure 3.1-16. Envelope values from all combinations are shown in Figure 3.1-17. Note that some of the other combinations (Combinations 3 through 8) control the member shears at the lower levels of the building. These forces are compared to the forces obtained using ELF and modal-response-spectrum analysis in the following discussion.

			16.2	17.5	17.6		
R-12			30.4	32.3	32.3		
12-11			45.5	45.6	47.6		
11-10			50.0	49.3	52.8		
10-9			43.9	44.4	40.9	37.8	16.3
9-8			42.0	41.9	39.6	44.4	28.4
8-7			44.9	44.3	42.1	45.4	28.9
7-6			43.4	42.0	40.2	43.7	27.9
6-5	13.7	30.3	32.3	34.2	33.5	34.9	23.0
5-4	23.2	35.6	31.1	32.9	32.4	33.2	22.8
4-3	23.7	35.6	32.6	34.0	33.6	34.4	24.0
3-2	23.1	36.2	35.1	35.3	35.4	35.8	23.4
2-G							

Figure 3.1-16 For Combinations 1 and 2, beam shears (kips) as computed using time-history analysis; analysis includes orthogonal loading and accidental torsion (1.0 kip = 4.45 kN).

			16.2	17.5	17.6		
R-12			30.4	32.3	32.3		
12-11			45.5	45.6	47.6		
11-10			50.0	49.3	52.8		
10-9			44.7	44.5	41.7	38.5	17.3
9-8			43.9	43.5	41.3	45.8	29.6
8-7			46.6	45.4	43.6	46.7	29.6
7-6			45.2	42.9	41.8	44.1	28.5
6-5	14.9	32.4	34.4	36.4	35.6	36.7	24.2
5-4	24.9	37.9	33.5	35.3	34.8	35.6	24.2
4-3	25.3	37.1	35.6	36.1	36.0	36.2	25.3
3-2	24.6	38.2	36.9	37.3	37.3	37.8	24.6
2-G							

Figure 3.1-17 For all combinations, beam shears (kips) as computed using time-history analysis; analysis includes orthogonal loading and accidental torsion (1.0 kip = 4.45 kN).

3.1.8 Comparison of Results from Various Methods of Analysis

A summary of the results from all of the analyses is provided in Tables 3.1-26 through 3.1-28.

3.1.8.1 Comparison of Base Shear and Story Shear

The maximum story shears are shown in Table 3.1-26. For the time-history analysis, the shears computed at the time of maximum displacement and time of maximum base shear (from analysis A00X only) are provided. Also shown from the time-history analysis is the envelope of story shears computed among all analyses. As may be observed, the shears from ELF and response-spectrum analysis seem to differ primarily on the basis of the factor 0.85 used in scaling the response spectrum results. ELF does, however, produce relatively larger forces at Levels 6 through 10.

The difference between ELF shears and time-history envelope shears is much more pronounced, particularly at the upper levels where time-history analysis gives larger forces. One reason for the difference is that the scaling of the ground motions has greatly increased the contribution of the higher modes of response.

The time-history analysis also gives shears larger than those computed using the response spectrum procedure, particularly for the upper levels.

3.1.8.2 Comparison of Drift

Table 3.1-27 summarizes the drifts computed from each of the analyses. The time-history drifts are from a single analysis, A00X; envelope values would be somewhat greater. As with shear, the ELF and modal-response-spectrum approaches appear to produce similar results, but the drifts from time-history analysis are significantly greater. Aside from the fact that the 0.85 factor is not applied to time-history response, it is not clear why the time-history drifts are as high as they are. One possible explanation is that the drifts are dominated by one particular pulse in one particular ground motion. As mentioned above, it is also possible that the effect of scaling has been to artificially enhance the higher mode response.

3.1.8.3 Comparison Member Forces

The shears developed in Bay D-E of Frame 1 are compared in Table 3.1-28. The shears from the time-history (TH) analysis are envelope values among all analyses, including torsion and orthogonal load effects. The time-history approach produced larger beam shears than the ELF and response spectrum (RS) approaches, particularly in the upper levels of the building. The effect of higher modes on the response is again the likely explanation for the noted differences.

Table 3.1-26 Summary of Results from Various Methods of Analysis: Story Shear

Level	Story Shear (kips)				
	ELF	RS	TH at Time of Maximum Displacement	TH at Time of Maximum Base Shear	TH. at Envelope
R	187	180	307	40.2	325
12	341	286	530	44.3	551
11	471	358	664	45.7	683
10	578	417	731	95.6	743
9	765	523	788	319	930
8	866	586	818	468	975
7	943	638	844	559	964
6	999	688	856	596	957
5	1070	783	829	663	1083
4	1102	838	779	786	1091
3	1118	894	718	972	1045
2	1124	956	669	1124	1124

1.0 kip = 4.45 kN.

Table 3.1-27 Summary of Results from Various Methods of Analysis: Story Drift

Level	X-Direction Drift (in.)		
	ELF	RS	TH
R	0.982	0.99	2.57
12	1.41	1.43	3.63
11	1.75	1.65	4.14
10	1.92	1.82	4.12
9	1.83	1.87	3.40
8	2.00	1.98	3.34
7	2.03	2.20	3.20
6	1.95	2.14	2.95
5	1.70	2.09	2.32
4	1.70	2.09	2.12
3	1.67	2.31	1.89
2	2.02	2.91	2.13

1.0 in. = 25.4 mm.

Table 3.1-28 Summary of Results from Various Methods of Analysis: Beam Shear

Level	Beam Shear Force in Bay D-E of Frame 1 (kips)		
	ELF	RS	TH
R	9.54	9.70	17.5
12	17.6	17.7	32.3
11	26.3	24.9	45.6
10	31.0	27.7	49.3
9	32.7	26.5	44.5
8	34.1	26.7	43.5
7	38.1	28.8	45.4
6	38.4	30.4	42.9
5	34.3	27.7	36.4
4	31.0	27.0	35.3
3	31.7	28.8	36.1
2	31.8	30.6	37.3

1.0 kip = 4.45 kN.

3.1.8.4 A Commentary on the Provisions Requirements for Analysis

From the writer's perspective, there are two principal inconsistencies between the requirements for ELF, modal-response-spectrum, and modal-time-history analyses:

1. In ELF analysis, the *Provisions* allows displacements to be computed using base shears consistent with Eq. 5.4.1.4-2 [5.2-3] ($C_s = S_{D1}/T(R/I)$) when Eq. 5.4.1.4-3 ($C_s = 0.044I S_{DS}$) controls for strength. For both modal-response-spectrum analysis and modal time-history analysis, however, the computed

shears and displacements must be scaled if the computed base shear falls below the ELF shear computed using Eq. 5.1.1.1-3. [Because the minimum base shear has been revised in the 2003 *Provisions*, this inconsistency would not affect this example.]

2. The factor of 0.85 is allowed when scaling modal-response-spectrum analysis, but not when scaling time-history results. This penalty for time-history analysis is in addition to the penalty imposed by selecting a scale factor that is controlled by the response at one particular period (and thus exceeding the target at other periods). [In the 2003 *Provisions* these inconsistencies are partially resolved. The minimum base shear has been revised, but time-history analysis results are still scaled to a higher base shear than are modal response spectrum analysis results.]

The effect of these inconsistencies is evident in the results shown in Tables 3.1-26 through 3.1-28 and should be addressed prior to finalizing the 2003 edition of the *Provisions*.

3.1.8.5 Which Method Is Best?

In this example, an analysis of an irregular steel moment frame was performed using three different techniques: equivalent-lateral-force, modal-response-spectrum, and modal-time-history analyses. Each analysis was performed using a linear elastic model of the structure even though it is recognized that the structure will repeatedly yield during the earthquake. Hence, each analysis has significant shortcomings with respect to providing a reliable prediction of the actual response of the structure during an earthquake.

The purpose of analysis, however, is not to predict response but rather to provide information that an engineer can use to proportion members and to estimate whether or not the structure has sufficient stiffness to limit deformations and avoid overall instability. In short, the analysis only has to be “good enough for design.” If, on the basis of any of the above analyses, the elements are properly designed for strength, the stiffness requirements are met and the elements and connections of the structure are detailed for inelastic response according to the requirements of the *Provisions*, the structure will likely survive an earthquake consistent with the maximum considered ground motion. The exception would be if a highly irregular structure were analyzed using the ELF procedure. Fortunately, the *Provisions* safeguards against this by requiring three-dimensional dynamic analysis for highly irregular structures.

For the structure analyzed in this example, the irregularities were probably not so extreme such that the ELF procedure would produce a “bad design.” However, when computer programs (e.g., SAP2000 and ETABS) that can perform modal-response-spectrum analysis with only marginally increased effort over that required for ELF are available, the modal analysis should always be used for final design in lieu of ELF (even if ELF is allowed by the *Provisions*). As mentioned in the example, this does not negate the need or importance of ELF analysis because such an analysis is useful for preliminary design and components of the ELF analysis are necessary for application of accidental torsion.

The use of time-history analysis is limited when applied to a linear elastic model of the structure. The amount of additional effort required to select and scale the ground motions, perform the time-history analysis, scale the results, and determine envelope values for use in design is simply not warranted when compared to the effort required for modal-response-spectrum analysis. This might change in the future when “standard” suites of ground motions are developed and are made available to the earthquake engineering community. Also, significant improvement is

needed in the software available for the preprocessing and particularly, for the post-processing of the huge amounts of information that arise from the analysis.

Scaling ground motions used for time-history analysis is also an issue. The *Provisions* requires that the selected motions be consistent with the magnitude, distance, and source mechanism of a maximum considered earthquake expected at the site. If the ground motions satisfy this criteria, then why scale at all? Distant earthquakes may have a lower peak acceleration but contain a frequency content that is more significant. Near-source earthquakes may display single damaging pulses. Scaling these two earthquakes to the *Provisions* spectrum seems to eliminate some of the most important characteristics of the ground motions. The fact that there is a degree of freedom in the *Provisions* scaling requirements compensates for this effect, but only for very knowledgeable users.

The main benefit of time-history analysis is in the nonlinear dynamic analysis of structures or in the analysis of non-proportionally damped linear systems. This type of analysis is the subject of Example 3.2.

3.2 SIX-STORY STEEL FRAME BUILDING, SEATTLE, WASHINGTON

In this example, the behavior of a simple, six-story structural steel moment-resisting frame is investigated using a variety of analytical techniques. The structure was initially proportioned using a preliminary analysis, and it is this preliminary design that is investigated. The analysis will show that the structure falls short of several performance expectations. In an attempt to improve performance, viscous fluid dampers are considered for use in the structural system. Analysis associated with the added dampers is performed in a very preliminary manner.

The following analytical techniques are employed:

1. Linear static analysis,
2. Plastic strength analysis (using virtual work),
3. Nonlinear static (pushover) analysis,
4. Linear dynamic analysis, and
5. Nonlinear dynamic analysis.

The primary purpose of this example is to highlight some of the more advanced analytical techniques; hence, more detail is provided on the last three analytical techniques. The *Provisions* provides some guidance and requirements for the advanced analysis techniques. Nonlinear static analysis is covered in the Appendix to Chapter 5, nonlinear dynamic analysis is covered in Sec. 5.7 [5.5], and analysis of structures with added damping is prescribed in the Appendix to Chapter 13 [new Chapter 15].

3.2.1 Description of Structure

The structure analyzed for this example is a 6-story office building in Seattle, Washington. According to the descriptions in *Provisions* Sec. 1.3 [1.2], the building is assigned to Seismic Use Group I. From *Provisions* Table 1.4 [1.3-1], the occupancy importance factor (I) is 1.0. A plan and elevation of the building are shown in Figures 3.2-1 and 3.2-2, respectively. The lateral-load-resisting system consists of steel moment-resisting frames on the perimeter of the building. There are five bays at 28 ft on center in the N-S direction and six bays at 30 ft on center in the E-W direction. The typical story height is 12 ft-6 in. with the exception of the first story, which has a height of 15 ft. There are a 5-ft-tall perimeter parapet at the roof and one basement level that extends 15 ft below grade. For this example, it is assumed that the columns of the moment-resisting frames are embedded into pilasters formed into the basement wall.

For the moment-resisting frames in the N-S direction (Frames A and G), all of the columns bend about their strong axes, and the girders are attached with fully welded moment-resisting connections. It is assumed that these and all other fully welded connections are constructed and inspected according to post-Northridge protocol. Only the demand side of the required behavior of these connections is addressed in this example.

For the frames in the E-W direction (Frames 1 and 6), moment-resisting connections are used only at the interior columns. At the exterior bays, the E-W girders are connected to the weak axis of the exterior (corner) columns using non-moment-resisting connections.

All interior columns are gravity columns and are not intended to resist lateral loads. A few of these

columns, however, would be engaged as part of the added damping system described in the last part of this example. With minor exceptions, all of the analyses in this example will be for lateral loads acting in the N-S direction. Analysis for lateral loads acting in the E-W direction would be performed in a similar manner.

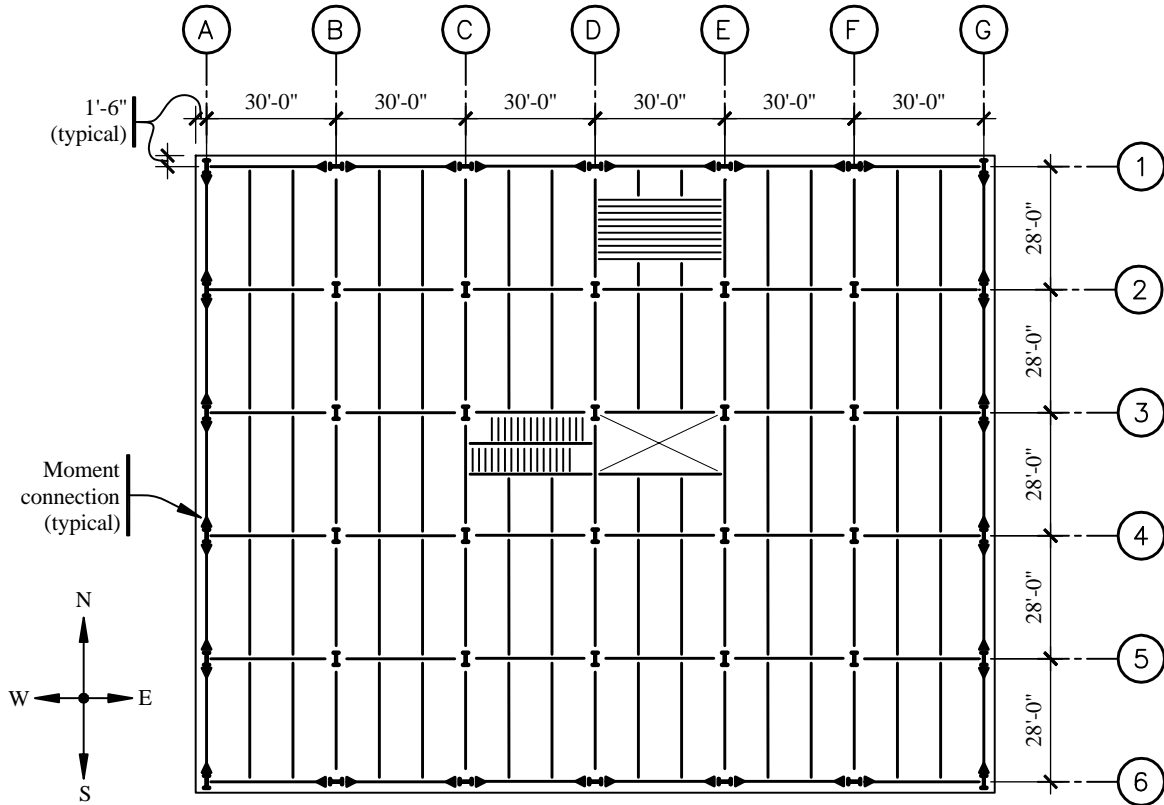


Figure 3.2-1 Plan of structural system.

The sections shown in Table 3.2-1 meet the width-to-thickness requirements for special moment frames, and the size of the column relative to the girders should ensure that plastic hinges will form in the girders. Doubler plates 0.875 in. thick are used at each of the interior columns at Levels 2 and 3, and 1.00 in. thick plates are used at the interior columns at Levels 4, 5, 6, and R. Doubler plates were not used in the exterior columns.

3.2.2 Loads

3.2.2.1 Gravity Loads

It is assumed that the floor system of the building consists of a normal weight composite concrete slab on formed metal deck. The slab is supported by floor beams that span in the N-S direction. These floor beams have a span of 28 ft and are spaced 10 ft on center.

The dead weight of the structural floor system is estimated at 70 psf. Adding 15 psf for ceiling and mechanical, 10 psf for partitions at Levels 2 through 6, and 10 psf for roofing at Level R, the total dead load at each level is 95 psf. The cladding system is assumed to weigh 15 psf. A basic live load of 50 psf is used over the full floor. Twenty-five percent of this load, or 12.5 psf, is assumed to act concurrent with seismic forces. A similar reduced live load is used for the roof.

Based on these loads, the total dead load, live load, and dead plus live load applied to each level are given in Table 3.2-2. The slight difference in loads at Levels R and 2 is due to the parapet and the tall first story, respectively.

Tributary areas for columns and girders as well as individual element gravity loads used in the analysis are illustrated in Figure 3.2-3. These are based on a total dead load of 95 psf, a cladding weight of 15 psf, and a live load of $0.25(50) = 12.5$ psf.

Table 3.2-2 Gravity Loads on Seattle Building

Level	Dead Load (kips)		Reduced Live Load (kips)		Total Load (kips)	
	Story	Accumulated	Story	Accumulated	Story	Accumulated
R	2,549	2,549	321	321	2,870	2,870
6	2,561	5,110	321	642	2,882	5,752
5	2,561	7,671	321	963	2,882	8,634
4	2,561	10,232	321	1,284	2,882	11,516
3	2,561	12,792	321	1,605	2,882	14,398
2	2,573	15,366	321	1,926	2,894	17,292

3.2.2.2 Earthquake Loads

Although the main analysis in this example is nonlinear, equivalent static forces are computed in accordance with the *Provisions*. These forces are used in a preliminary static analysis to determine whether the structure, as designed, conforms to the drift requirements of the *Provisions*.

The structure is situated in Seattle, Washington. The short period and the 1-second mapped spectral

acceleration parameters for the site are:

$$\begin{aligned} S_s &= 1.63 \\ S_l &= 0.57 \end{aligned}$$

The structure is situated on Site Class C materials. From *Provisions* Tables 4.1.2.4(a) and 4.1.2.4(b) [Tables 3.3-1 and 3.3-2]:

$$\begin{aligned} F_a &= 1.00 \\ F_v &= 1.30 \end{aligned}$$

From *Provisions* Eq. 4.1.2.4-1 and 4.1.2.4-2 [3.3-1 and 3.3-2], the maximum considered spectral acceleration parameters are:

$$\begin{aligned} S_{MS} &= F_a S_s = 1.00(1.63) \\ &= 1.63 \end{aligned}$$

$$\begin{aligned} S_{MI} &= F_v S_l = 1.30(0.57) \\ &= 0.741 \end{aligned}$$

And from *Provisions* Eq. 4.1.2.5-1 and Eq. 4.1.2.5-2 [3.3-3 and 3.3-4], the design acceleration parameters are:

$$\begin{aligned} S_{DS} &= (2/3)S_{MI} = (2/3)1.63 \\ &= 1.09 \end{aligned}$$

$$\begin{aligned} S_{DI} &= (2/3)S_{MI} = (2/3)0.741 \\ &= 0.494 \end{aligned}$$

Based on the above coefficients and on *Provisions* Tables 4.2.1a and 4.2.1b [1.4-1 and 1.4-2], the structure is assigned to Seismic Design Category D. For the purpose of analysis, it is assumed that the structure complies with the requirements for a special moment frame, which, according to *Provisions* Table 5.2.2 [4.3-1], has $R = 8$, $C_d = 5.5$, and $\Omega_0 = 3.0$.

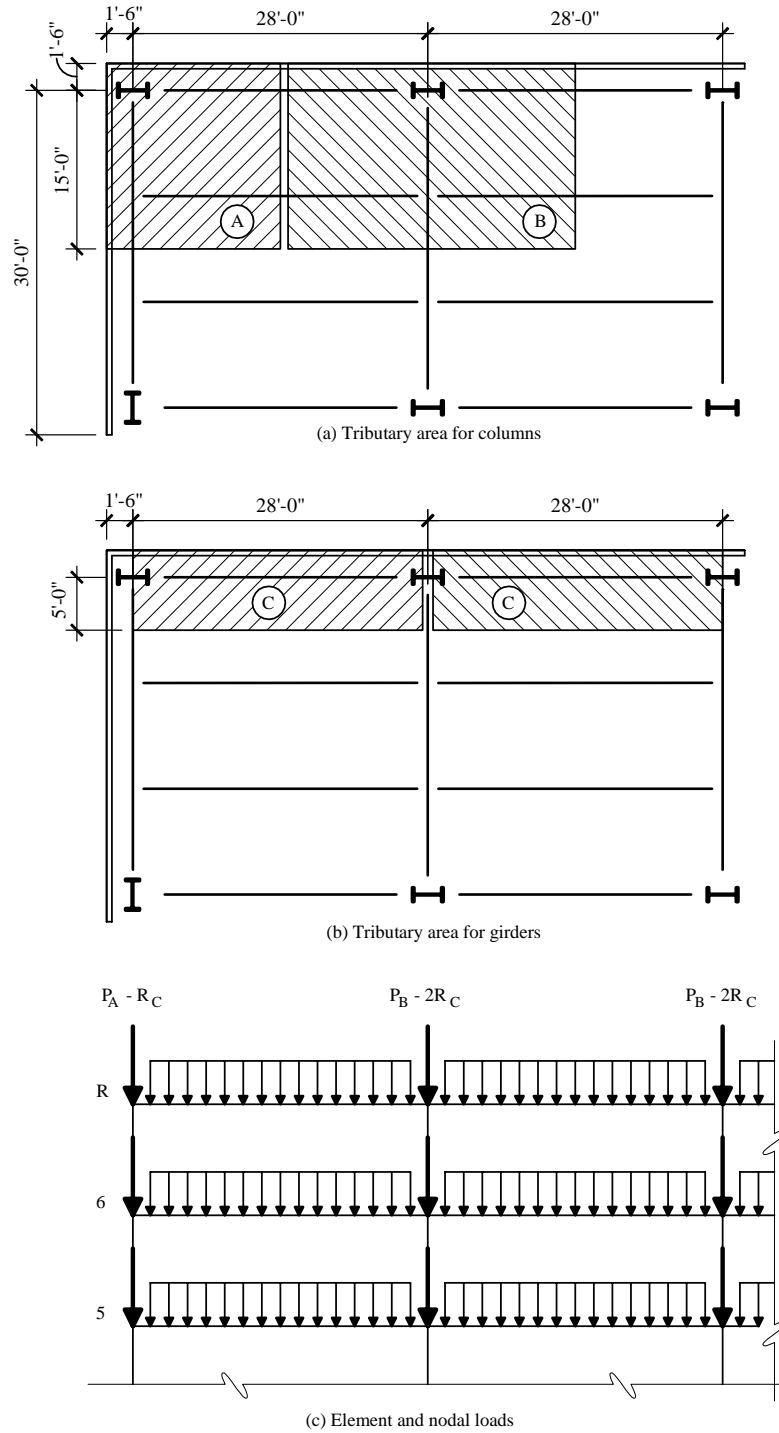


Figure 3.2-3 Element loads used in analysis.

3.2.2.2.1 Approximate Period of Vibration

Provisions Eq. 5.4.2.1-1 [5.2-6] is used to estimate the building period:

$$T_a = C_r h_n^x$$

where, from *Provisions* Table 5.4.2.1 [5.5-2], $C_r = 0.028$ and $x = 0.8$ for a steel moment frame. Using h_n (the total building height above grade) = 77.5 ft, $T_a = 0.028(77.5)^{0.8} = 0.91$ sec.

When the period is determined from a properly substantiated analysis, the *Provisions* requires that the period used for computing base shear not exceed $C_u T_a$ where, from *Provisions* Table 5.4.2 [5.2-1] (using $S_{DI} = 0.494$), $C_u = 1.4$. For the structure under consideration, $C_u T_a = 1.4(0.91) = 1.27$ sec.

3.2.2.2.2 Computation of Base Shear

Using *Provisions* Eq. 5.4.1 [5.2-1], the total seismic shear is:

$$V = C_s W$$

where W is the total weight of the structure. From *Provisions* Eq. 5.4.1.1-1 [5.2-2], the maximum (constant acceleration region) seismic response coefficient is:

$$C_{S_{max}} = \frac{S_{DS}}{(R/I)} = \frac{1.09}{(8/1)} = 0.136$$

Provisions Eq. 5.4.1.1-2 [5.2-3] controls in the constant velocity region:

$$C_s = \frac{S_{DI}}{T(R/I)} = \frac{0.494}{1.27(8/1)} = 0.0485$$

The seismic response coefficient, however, must not be less than that given by Eq. 5.4.1.1-3 [revised for the 2003 *Provisions*]:

$$C_{S_{min}} = 0.044 I S_{DS} = 0.044(1)(1.09) = 0.0480 .$$

[In the 2003 *Provisions*, this equation for minimum base shear coefficient has been revised. The results of this example problem would not be affected by the change.]

Thus, the value from Eq. 5.4.1.1-2 [5.2-3] controls for this building. Using $W = 15,366$ kips, $V = 0.0485(15,366) = 745$ kips.

3.2.2.2.3 Vertical Distribution of Forces

The Provisions Eq. 5.4.1.1-2 [5.2-3] base shear is distributed along the height of the building using Provisions Eq. 5.4.3.1 and 5.4.3.2 [5.2-10 and 5.2-11]:

$$F_x = C_{vx}V$$

and

$$C_{vx} = \frac{w_x h_x^k}{\sum_{i=1}^n w_i h_i^k}$$

where $k = 0.75 + 0.5T = 0.75 + 0.5(1.27) = 1.385$. The lateral forces acting at each level and the story shears and story overturning moments acting at the bottom of the story below the indicated level are summarized in Table 3.2-3. These are the forces acting on the whole building. For analysis of a single frame, one-half of the tabulated values are used.

Table 3.2-3 Equivalent Lateral Forces for Seattle Building Responding in N-S Direction

Level x	w_x (kips)	h_x (ft)	$w_x h_x^k$	C_{vx}	F_x (kips)	V_x (kips)	M_x (ft-kips)
R	2,549	77.5	1,060,663	0.321	239.2	239.2	2,990
6	2,561	65.0	835,094	0.253	188.3	427.5	8,334
5	2,561	52.5	621,077	0.188	140.1	567.6	15,429
4	2,561	40.0	426,009	0.129	96.1	663.7	23,725
3	2,561	27.5	253,408	0.077	57.1	720.8	32,735
2	<u>2,561</u>	15.0	<u>109,882</u>	<u>0.033</u>	<u>24.8</u>	745.6	43,919
Σ	15,366		3,306,133	1.000	745.6		

3.2.3 Preliminaries to Main Structural Analysis

Performing a nonlinear analysis of a structure is an incremental process. The analyst should first perform a linear analysis to obtain some basic information on expected behavior and to serve later as a form of verification for the more advanced analysis. Once the linear behavior is understood (and extrapolated to expected nonlinear behavior), the anticipated nonlinearities are introduced. If more than one type of nonlinear behavior is expected to be of significance, it is advisable to perform a preliminary analysis with each nonlinearity considered separately and then to perform the final analysis with all nonlinearities considered. This is the approach employed in this example.

3.2.3.1 The Computer Program DRAIN-2Dx

The computer program DRAIN-2Dx (henceforth called DRAIN) was used for all of the analyses described in this example. DRAIN allows linear and nonlinear static and dynamic analysis of two-dimensional (planar) structures only.

As with any finite element analysis program, DRAIN models the structure as an assembly of nodes and elements. While a variety of element types is available, only three element types were used:

- Type 1, inelastic bar (truss) element
- Type 2, beam-column element
- Type 4, connection element

Two models of the structure were prepared for DRAIN. The first model, used for preliminary analysis and for verification of the second (more advanced) model, consisted only of Type 2 elements for the main structure and Type 1 elements for modeling P-delta effects. All analyses carried out using this model were linear.

For the second more detailed model, Type 1 elements were used for modeling *P*-delta effects, the braces in the damped system, and the dampers in the damped system. It was assumed that these elements would remain linear elastic throughout the response. Type 2 elements were used to model the beams and columns as well as the rigid links associated with the panel zones. Plastic hinges were allowed to form in all columns. The column hinges form through the mechanism provided in DRAIN's Type 2 element. Plastic behavior in girders and in the panel zone region of the structure was considered through the use of Type 4 connection elements. Girder yielding was forced to occur in the Type 4 elements (in lieu of the main span represented by the Type 2 elements) to provide more control in hinge location and modeling. A complete description of the implementation of these elements is provided later.

3.2.3.2 Description of Preliminary Model and Summary of Preliminary Results

The preliminary DRAIN model is shown in Figure 3.2-4. Important characteristics of the model are as follows:

1. Only a single frame was modeled. Hence one-half of the loads shown in Tables 3.2-2 and 3.2-3 were applied.
2. Columns were fixed at their base.
3. Each beam or column element was modeled using a Type 2 element. For the columns, axial, flexural, and shear deformations were included. For the girders, flexural and shear deformations were included but, because of diaphragm slaving, axial deformation was not included. Composite action in the floor slab was ignored for all analysis.
4. Members were modeled using centerline dimensions without rigid end offsets. This allows, in an approximate but reasonably accurate manner, deformations to occur in the beam-column joint region. Note that this model does not provide any increase in beam-column joint stiffness due to the presence of doubler plates.
5. P-delta effects were modeled using the leaner column shown in Figure 3.2-4 at the right of the main frame. This column was modeled with an axially rigid Type 1 (truss) element. *P*-delta effects were activated for this column only (P-delta effects were turned off for the columns of the main frame). The lateral degree of freedom at each level of the P-delta column was slaved to the floor diaphragm at

the matching elevation. When P-delta effects were included in the analysis, a special initial load case was created and executed. This special load case consisted of a vertical force equal to one-half of the total story weight (dead load plus fully reduced live load) applied to the appropriate node of the P-delta column. P-delta effects were modeled in this manner to avoid the inconsistency of needing true column axial forces for assessing strength and requiring total story forces for assessing stability.

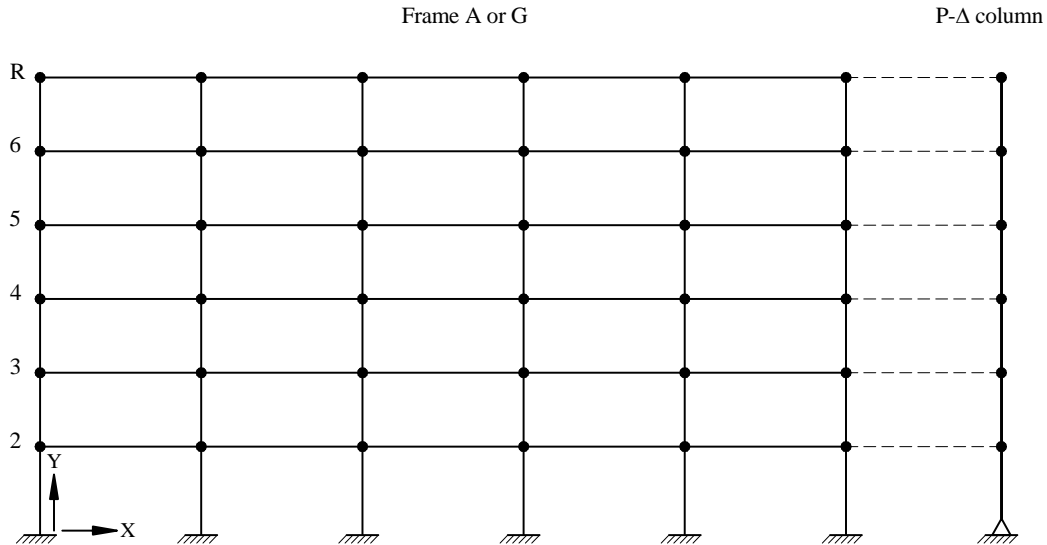


Figure 3.2-4 Simple wire frame model used for preliminary analysis.

3.2.3.2.1 Results of Preliminary Analysis: Drift and Period of Vibration

The results of the preliminary analysis for drift are shown in Tables 3.2-4 and 3.2-5 for the computations excluding and including P-delta effects, respectively. In each table, the deflection amplification factor (C_d) equals 5.5, and the acceptable story drift (story drift limit) is taken as 1.25 times the limit provided by *Provisions* Table 5.2.8. This is in accordance with *Provisions* Sec. 5.7.3.3 [5.5.3.3] which allows such an increase in drift when a nonlinear analysis is performed. This increased limit is used here for consistency with the results from the following nonlinear time-history analysis.

When P-delta effects are not included, the computed story drift is less than the allowable story drift at each level of the structure. The largest magnified story drift, including $C_d = 5.5$, is 3.45 in. in Story 2. If the 1.25 multiplier were not used, the allowable story drift would reduce to 3.00 in., and the computed story drift at Levels 3 and 4 would exceed the limit.

As a preliminary estimate of the importance of P-delta effects, story stability coefficients (θ) were computed in accordance with *Provisions* Sec. 5.4.6.2 [5.2.6.2]. At Story 2, the stability coefficient is 0.0839. *Provisions* Sec. 5.4.6.2 [5.2.6.2] allows P-delta effects to be ignored when the stability coefficient is less than 0.10. For this example, however, analyses are performed with and without P-delta effects. [In the 2003 *Provisions*, the stability coefficient equation has been revised to include the importance factor in the numerator and the calculated result is used simply to determine whether a special

analysis (in accordance with Sec. A5.2.3) is required.]

When P-delta effects are included, the drifts at the lower stories increase by about 10 percent as expected from the previously computed stability ratios. (Hence, the stability ratios provide a useful check.²) Recall that this analysis ignored the stiffening effect of doubler plates.

Table 3.2-4 Results of Preliminary Analysis Excluding P-delta Effects

Story	Total Drift (in.)	Story Drift (in.)	Magnified Story Drift (in.)	Drift Limit (in.)	Story Stability Ratio
6	3.14	0.33	1.82	3.75	0.0264
5	2.81	0.50	2.75	3.75	0.0448
4	2.31	0.54	2.97	3.75	0.0548
3	1.77	0.61	3.36	3.75	0.0706
2	1.16	0.63	3.45	3.75	0.0839
1	0.53	0.53	2.91	4.50	0.0683

Table 3.2-5 Results of Preliminary Analysis Including P-delta Effects

Story	Total Drift (in.)	Story Drift (in.)	Magnified Story Drift (in.)	Drift Limit (in.)
6	3.35	0.34	1.87	3.75
5	3.01	0.53	2.91	3.75
4	2.48	0.57	3.15	3.75
3	1.91	0.66	3.63	3.75
2	1.25	0.68	3.74	3.75
1	0.57	0.57	3.14	4.50

The computed periods for the first three natural modes of vibration are shown in Table 3.2-6. As expected, the period including P-delta effects is slightly larger than that produced by the analysis without such effects. More significant is the fact that the first mode period is considerably longer than that predicted from *Provisions* Eq. 5.4.2.1-1 [5.2-6]. Recall from previous calculations that this period (T_a) is 0.91 seconds, and the upper limit on computed period $C_u T_a$ is $1.4(0.91) = 1.27$ seconds. When doubler plate effects are included in the analysis, the period will decrease slightly, but it remains obvious that the structure is quite flexible.

²The story drifts including P-delta effects can be estimated as the drifts without P-delta times the quantity $1/(1-\theta)$, where θ is the stability coefficient for the story.

Table 3.2-6 Periods of Vibration From Preliminary Analysis (sec)

Mode	P-delta Excluded	P-delta Included
1	1.985	2.055
2	0.664	0.679
3	0.361	0.367

3.2.3.2.2 Results of Preliminary Analysis: Demand-to-Capacity Ratios

To determine the likelihood of and possible order of yielding, demand-to-capacity ratios were computed for each element. The results are shown in Figure 3.2-5. For this analysis, the structure was subjected to full dead load plus 25 percent of live load followed by the equivalent lateral forces of Table 3.2-3. P-delta effects were included.

For girders, the demand-to-capacity ratio is simply the maximum moment in the member divided by the member’s plastic moment capacity where the plastic capacity is $Z_{girder}F_y$. For columns, the ratio is similar except that the plastic flexural capacity is estimated to be $Z_{col}(F_y - P_u/A_{col})$ where P_u is the total axial force in the column. The ratios were computed at the end of the member, not at the face of the column or girder. This results in slightly conservative ratios, particularly for the columns, because the columns have a smaller ratio of clear span to total span than do the girders.

Level R	0.176	0.177	0.169	0.172	0.164	
	0.066	0.182	0.177	0.177	0.170	0.135
Level 6	0.282	0.281	0.277	0.282	0.280	
	0.148	0.257	0.255	0.255	0.253	0.189
Level 5	0.344	0.333	0.333	0.333	0.354	
	0.133	0.274	0.269	0.269	0.269	0.175
Level 4	0.407	0.394	0.394	0.394	0.420	
	0.165	0.314	0.308	0.308	0.309	0.211
Level 3	0.452	0.435	0.435	0.434	0.470	
	0.162	0.344	0.333	0.333	0.340	0.223
Level 2	0.451	0.425	0.430	0.424	0.474	
	0.413	0.492	0.485	0.485	0.487	0.492

Figure 3.2-5 Demand-to-capacity ratios for elements from analysis with P-delta effects included.

It is very important to note that the ratios shown in Figure 3.2-5 are based on the inelastic seismic forces (using $R = 8$). Hence, a ratio of 1.0 means that the element is just at yield, a value less than 1.0 means the element is still elastic, and a ratio greater than 1.0 indicates yielding.³

Several observations are made regarding the likely inelastic behavior of the frame:

1. The structure has considerable overstrength, particularly at the upper levels.
2. The sequence of yielding will progress from the lower level girders to the upper level girders. Because of the uniform demand-to-capacity ratios in the girders of each level, all the hinges in the girders in a level will form almost simultaneously.
3. With the possible exception of the first level, the girders should yield before the columns. While not shown in the table, it should be noted that the demand-to-capacity ratios for the lower story columns were controlled by the moment at the base of the column. It is usually very difficult to prevent yielding of the base of the first story columns in moment frames, and this frame is no exception. The column on the leeward (right) side of the building will yield first because of the additional axial compressive force arising from the seismic effects.

3.2.3.2.3 Results of Preliminary Analysis: Overall System Strength

The last step in the preliminary analysis was to estimate the total lateral strength (collapse load) of the frame using virtual work. In the analysis, it is assumed that plastic hinges are perfectly plastic. Girders hinge at a value $Z_{girder}F_y$ and the hinges form 5.0 in. from the face of the column. Columns hinge only at the base, and the plastic moment capacity is assumed to be $Z_{col}(F_y - P_u/A_{col})$. The fully plastic mechanism for the system is illustrated in Figure 3.2-6. The inset to the figure shows how the angle modification term σ was computed. The strength (V) for the total structure is computed from the following relationships (see Figure 3.2-6 for nomenclature):

Internal Work = External Work

$$\text{Internal Work} = 2[20\sigma\theta M_{PA} + 40\sigma\theta M_{PB} + \theta(M_{PC} + 4M_{PD} + M_{PE})]$$

$$\text{External Work} = V\theta \left[\sum_{i=1}^{nLevels} F_i H_i \right] \quad \text{where} \quad \sum_{i=1}^{nLevels} F_i = 1.0$$

Three lateral force patterns were used: uniform, upper triangular, and *Provisions* where the *Provisions* pattern is consistent with the vertical force distribution of Table 3.2-3 in this volume of design examples. The results of the analysis are shown in Table 3.2-7. As expected, the strength under uniform load is significantly greater than under triangular or *Provisions* load. The closeness of the *Provisions* and triangular load strengths is due to the fact that the vertical-load-distributing parameter (k) was 1.385, which is close to 1.0. The difference between the uniform and the triangular or *Provisions* patterns is an

³To determine the demand-to-capacity ratio on the basis of an elastic analysis, multiply all the values listed in Table 3.2-6 by $R = 8$. With this modification, the ratios are an approximation of the ductility demand for the individual elements.

indicator that the results of a capacity-spectrum analysis of the system will be quite sensitive to the lateral force pattern applied to the structure when performing the pushover analysis.

The equivalent-lateral-force (ELF) base shear, 746 kips (see Table 3.2-3), when divided by the *Provisions* pattern capacity, 2886 kips, is 0.26. This is reasonably consistent with the demand to capacity ratios shown in Figure 3.2-5.

Before proceeding, three important points should be made:

1. The rigid-plastic analysis did not include strain hardening, which is an additional source of overstrength.
2. The rigid-plastic analysis did not consider the true behavior of the panel zone region of the beam-column joint. Yielding in this area can have a significant effect on system strength.
3. Slightly more than 10 percent of the system strength comes from plastic hinges that form in the columns. If the strength of the column is taken simply as M_p (without the influence of axial force), the “error” in total strength is less than 1 percent.

Table 3.2-7 Lateral Strength on Basis of Rigid-Plastic Mechanism

Lateral Load Pattern	Lateral Strength (kips)	Lateral Strength (kips)
	Entire Structure	Single Frame
Uniform	3,850	1,925
Upper Triangular	3,046	1,523
<i>Provisions</i>	2,886	1,443

3.2.4 Description of Model Used for Detailed Structural Analysis

Nonlinear-static and -dynamic analyses require a much more detailed model than was used in the linear analysis. The primary reason for the difference is the need to explicitly represent yielding in the girders, columns, and panel zone region of the beam-column joints.

The DRAIN model used for the nonlinear analysis is shown in Figure 3.2-7. A detail of a girder and its connection to two interior columns is shown in Figure 3.2-8. The detail illustrates the two main features of the model: an explicit representation of the panel zone region and the use of concentrated (Type 4 element) plastic hinges in the girders.

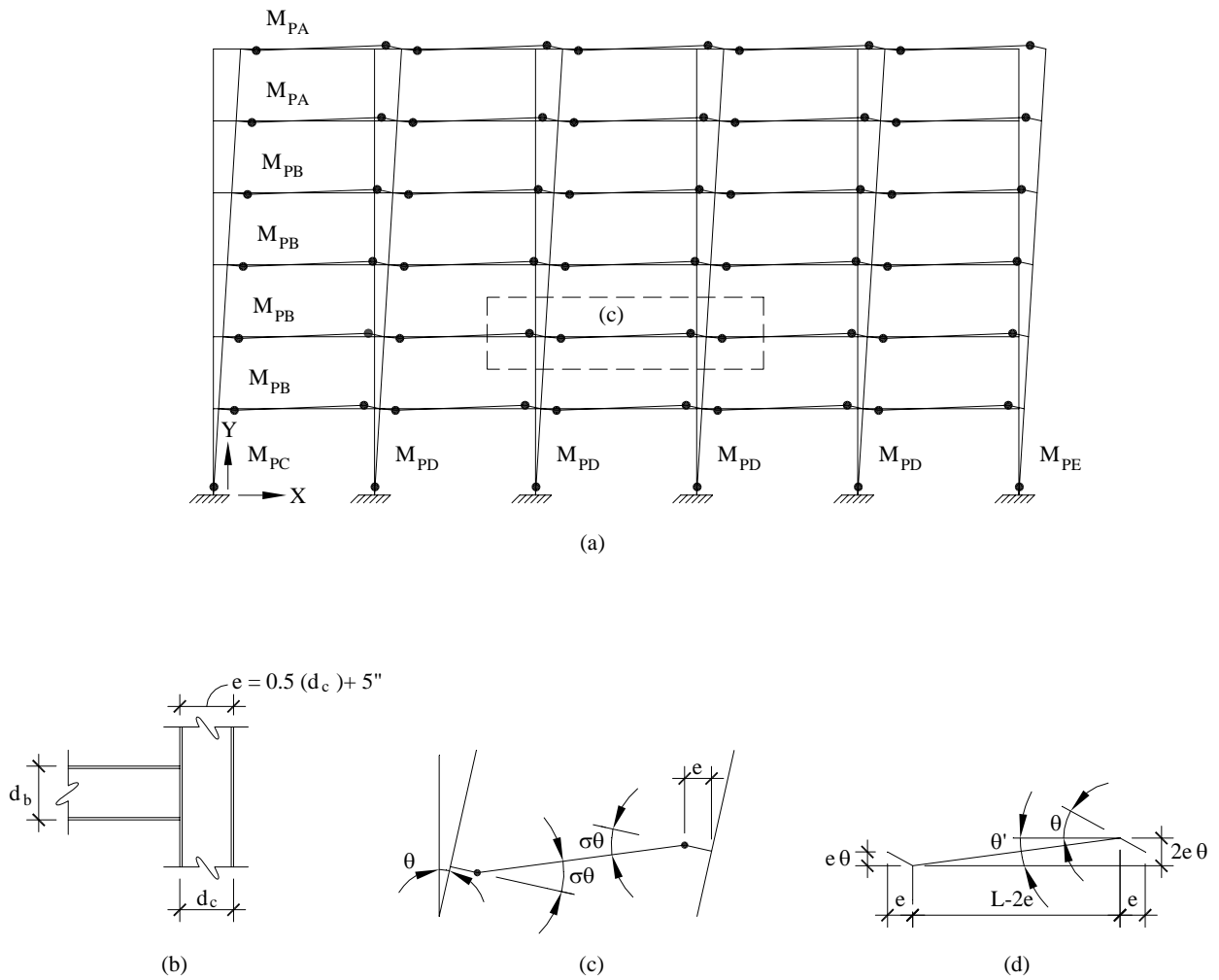


Figure 3.2-6 Plastic mechanism for computing lateral strength.

In Figure 3.2-7, the column shown to the right of the structure is used to represent P-delta effects. See Sec. 3.2.3.2 of this example for details.

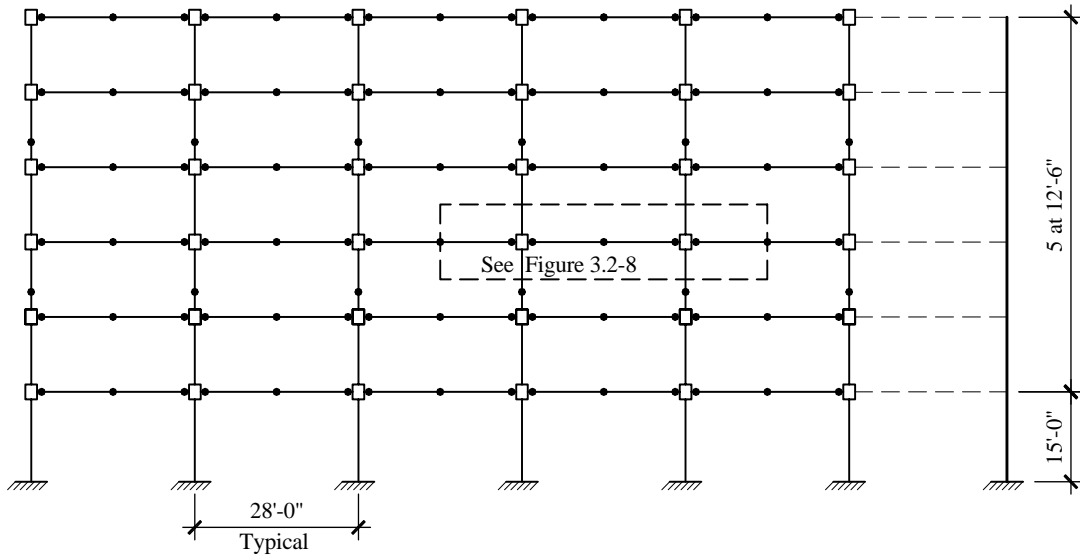


Figure 3.2-7 Detailed analytical model of 6-story frame.

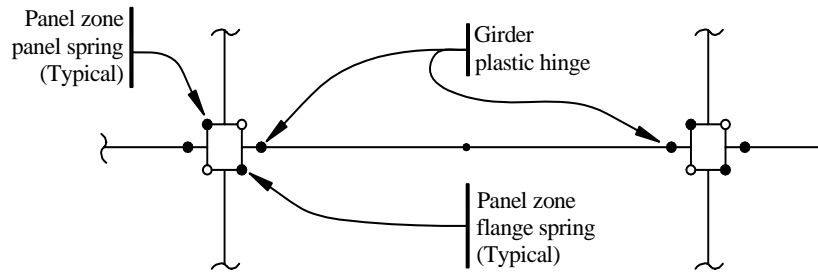


Figure 3.2-8 Model of girder and panel zone region.

The development of the numerical properties used for panel zone and girder hinge modeling is not straightforward. For this reason, the following theoretical development is provided before proceeding with the example.

3.2.4.1 Plastic Hinge Modeling and Compound Nodes

In the analysis described below, much use is made of compound nodes. These nodes are used to model plastic hinges in girders and, through a simple transformation process, deformations in the panel zone region of beam-column joints.

A compound node typically consists of a pair of single nodes with each node sharing the same point in space. The X and Y degrees of freedom of the first node of the pair (the slave node) are constrained to be equal to the X and Y degrees of freedom of the second node of the pair (the master node), respectively. Hence, the compound node has four degrees of freedom: an X displacement, a Y displacement, and two independent rotations.

In most cases, one or more rotational spring connection elements (DRAIN element Type 4) are placed between the two single nodes of the compound node, and these springs develop bending moment in resistance to the relative rotation between the two single nodes. If no spring elements are placed between the two single nodes, the compound node acts as a moment-free hinge. A typical compound node with a single rotational spring is shown in Figure 3.2-9. The figure also shows the assumed bilinear, inelastic moment-rotation behavior for the spring.

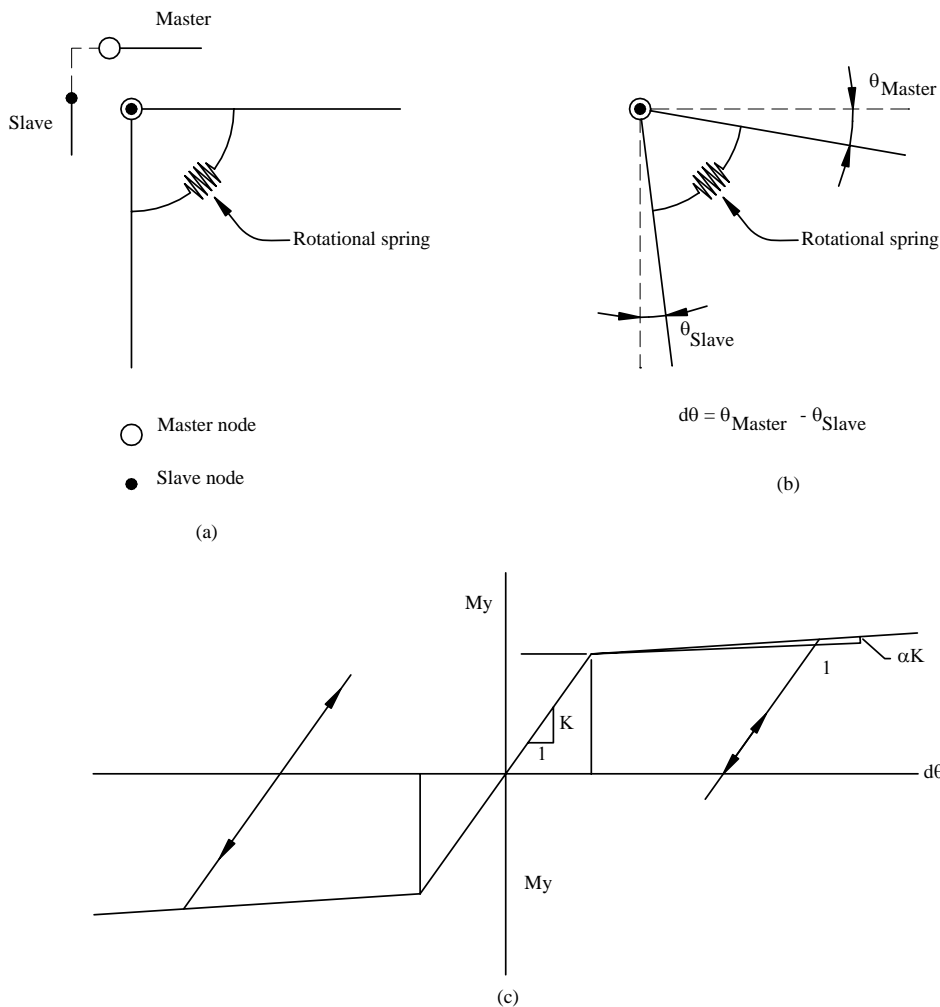


Figure 3.2-9 A compound node and attached spring.

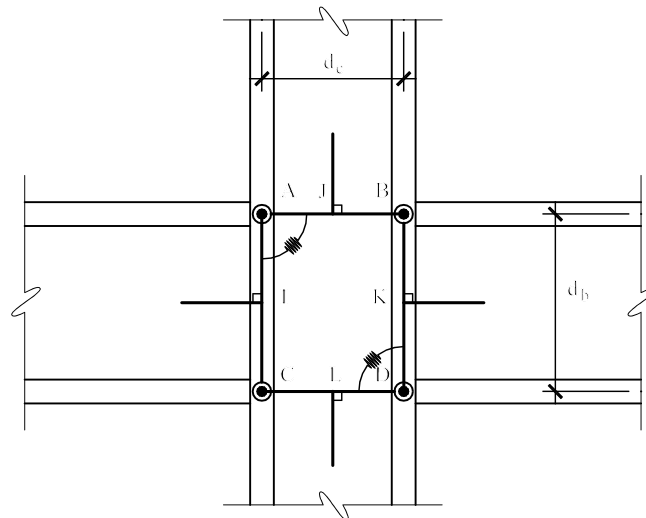


Figure 3.2-10 Krawinkler beam-column joint model.

3.2.4.2 Modeling of Beam-Column Joint Regions

A very significant portion of the total story drift of a moment-resisting frame may be due to deformations that occur in the panel zone region of the beam-column joint. In this example, panel zones are modeled using an approach developed by Krawinkler (1978). This model, illustrated in Figure 3.2-10, has the advantage of being conceptually simple, yet robust. The disadvantage of the approach is that the number of degrees of freedom required to model a structure is significantly increased.

A simpler model, often referred to as the scissors model, also has been developed to represent panel zone behavior. The scissors model has the advantage of using fewer degrees of freedom. However, due to its simplicity, it is generally considered to inadequately represent the kinematics of the problem.⁴ For this reason, the scissors model is not used here.

The Krawinkler model assumes that the panel zone area has two resistance mechanisms acting in parallel:

1. Shear resistance of the web of the column, including doubler plates and
2. Flexural resistance of the flanges of the column.

These two resistance mechanisms are apparent in AISC Seismic Eq. (9-1), which is used for determining panel zone shear strength:

⁴The author of this example is completing research at Virginia Tech to determine whether the scissors model is adequate to model steel moment frames. Preliminary results indicate that the kinematics error is not significant and that very good results may be obtained by a properly formulated scissors model.

$$R_v = 0.6F_y d_c t_p \left[1 + \frac{3b_{cf} t_{cf}^2}{d_b d_c t_p} \right].$$

The equation can be rewritten as:

$$R_v = 0.6F_y d_c t_p + 1.8 \frac{F_y b_{cf} t_{cf}^2}{d_b} \equiv V_{Panel} + 1.8V_{Flanges}$$

where the first term is the panel shear resistance and the second term is the plastic flexural resistance of the column flange. The terms in the equations are defined as follows:

- F_y = yield strength of the column and the doubler plate,
- d_c = total depth of column,
- t_p = thickness of panel zone region = column web thickness plus doubler plate thickness,
- b_{cf} = width of column flange,
- t_{cf} = thickness of column flange, and
- d_b = total depth of girder.

Additional terms used in the subsequent discussion are:

- t_{bf} = girder flange thickness and
- G = shear modulus of steel.

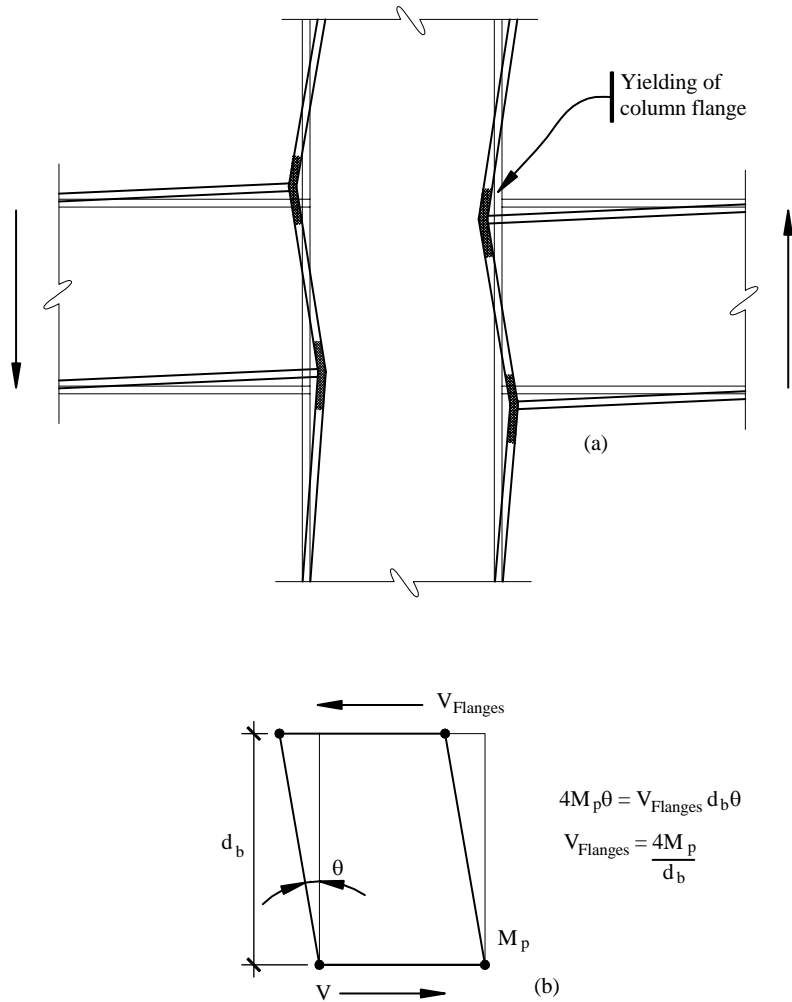


Figure 3.2-11 Column flange component of panel zone resistance.

The panel zone shear resistance (V_{panel}) is simply the effective shear area of the panel $d_c t_p$ multiplied by the yield stress in shear, assumed as $0.6F_y$. (The 0.6 factor is a simplification of the Von Mises yield criterion that gives the yield stress in shear as $1/\sqrt{3} = 0.577$ times the strength in tension.)

The second term, $1.8V_{Flanges}$, is based on experimental observation. Testing of simple beam-column subassemblies show that a “kink” forms in the column flanges as shown in Figure 3.2-11(a). If it can be assumed that the kink is represented by a plastic hinge with a plastic moment capacity of $M_p = F_y Z = F_y b_{cf} t_{cf}^2/4$, it follows from virtual work (see Figure 3.2-11b) that the equivalent shear strength of the column flanges is:

$$V_{Flanges} = \frac{4M_p}{d_b}$$

and by simple substitution for M_p :

$$V_{Flanges} = \frac{F_y b_{cf} t_{cf}^2}{d_b}$$

This value does not include the 1.8 multiplier that appears in the AISC equation. This multiplier is based on experimental results. It should be noted that the flange component of strength is small compared to the panel component unless the column has very thick flanges.

The shear stiffness of the panel is derived as shown in Figure 3.2-12:

$$K_{Panel,\gamma} = \frac{V_{Panel}}{\gamma} = \frac{V_{Panel}}{\delta/d_b}$$

noting that the displacement δ can be written as:

$$\delta = \frac{V_{Panel} d_b}{G t_p d_c},$$

$$K_{Panel,\gamma} = \frac{V_{Panel}}{\left(\frac{V_{Panel} d_b}{G t_p d_c} \right) \frac{1}{d_b}} = G t_p d_c$$

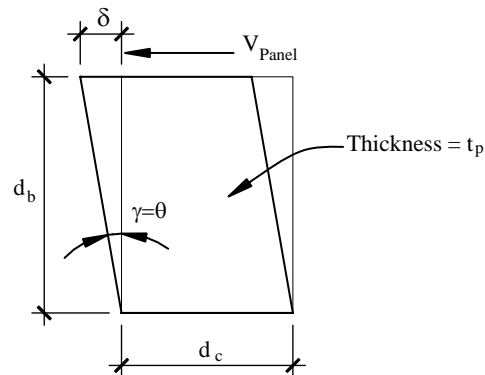


Figure 3.2-12 Column web component of panel zone resistance.

Krawinkler assumes that the column flange component yields at four times the yield deformation of the panel component, where the panel yield deformation is:

$$\gamma_y = \frac{V_{Panel}}{K_{Panel,\gamma}} = \frac{0.6F_y d_c t_p}{G d_c t_p} = \frac{0.6F_y}{G}$$

At this deformation, the panel zone strength is $V_{Panel} + 0.25 V_{Flanges}$; at four times this deformation, the strength is $V_{Panel} + V_{Flanges}$. The inelastic force-deformation behavior of the panel is illustrated in Figure 3.2-13. This figure is applicable also to exterior joints (girder on one side only), roof joints (girders on both sides, column below only), and corner joints (girder on one side only, column below only).

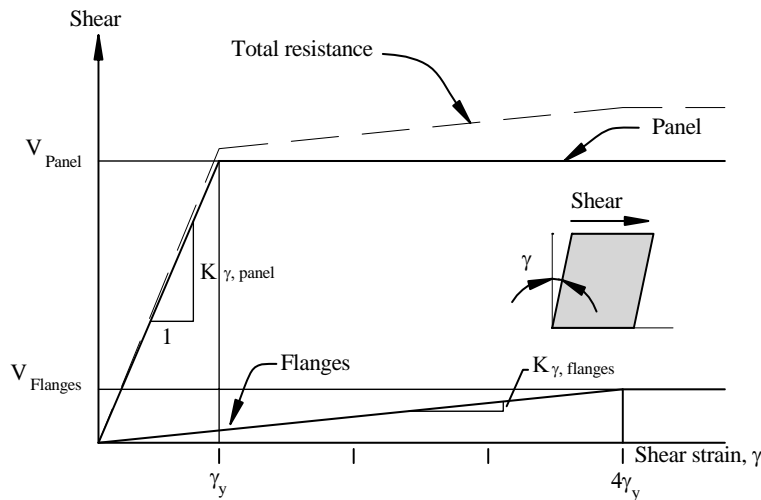


Figure 3.2-13 Force-deformation behavior of panel zone region.

The actual Krawinkler model is shown in Figure 3.2-10. This model consists of four rigid links, connected at the corners by compound nodes. The columns and girders frame into the links at right angles at Points I through L. These are moment-resisting connections. Rotational springs are used at the upper left (point A) and lower right (point D) compound nodes. These springs are used to represent the panel resistance mechanisms described earlier. The upper right and lower left corners (points B and C) do not have rotational springs and thereby act as real hinges.

The finite element model of the joint requires 12 individual nodes: one node each at Points I through L, and two nodes (compound node pairs) at Points A through D. It is left to the reader to verify that the total number of degrees of freedom in the model is 28 (if the only constraints are associated with the corner compound nodes).

The rotational spring properties are related to the panel shear resistance mechanisms by a simple transformation, as shown in Figure 3.2-14. From the figure it may be seen that the moment in the rotational spring is equal to the applied shear times the beam depth. Using this transformation, the properties of the rotational spring representing the panel shear component of resistance are:

$$M_{Panel} = V_{Panel}d_b = 0.6F_y d_c d_b t_p$$

$$K_{Panel,\theta} = K_{Panel,\gamma} d_b = Gd_c d_b t_p$$

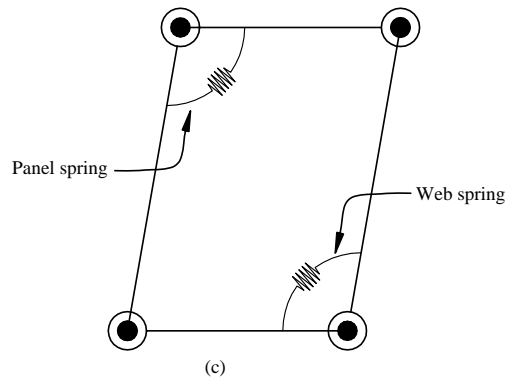
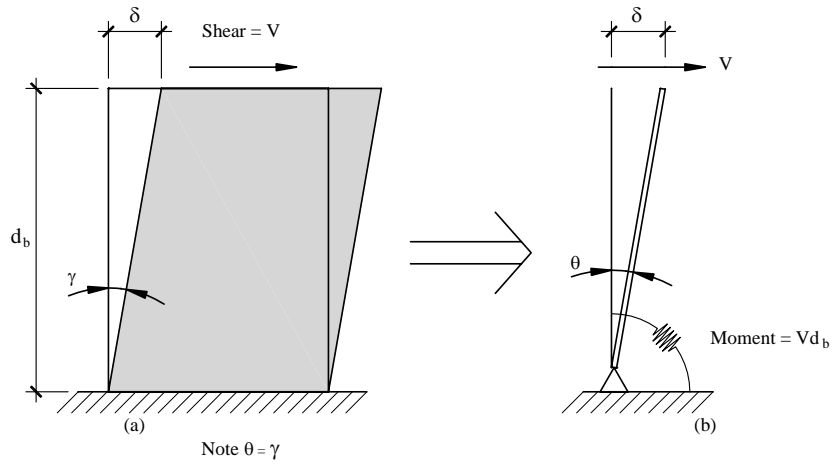


Figure 3.2-14 Transforming shear deformation to rotational deformation in the Krawinkler model.

It is interesting to note that the shear strength in terms of the rotation spring is simply $0.6F_y$ times the volume of the panel, and the shear stiffness in terms of the rotational spring is equal to G times the panel volume.

The flange component of strength in terms of the rotational spring is determined in a similar manner:

$$M_{Flanges} = 1.8V_{Flanges}d_b = 1.8F_y b_{cf} t_{cf}^2$$

Because of the equivalence of rotation and shear deformation, the yield rotation of the panel is the same as the yield strain in shear:

$$\theta_y = \gamma_y = \frac{M_{Panel}}{K_{Panel,\theta}} = \frac{0.6F_y}{G}.$$

To determine the initial stiffness of the flange spring, it is assumed that this spring yields at four times the yield deformation of the panel spring. Hence,

$$K_{Flanges,\theta} = \frac{M_{Flanges}}{4\theta_y} = 0.75Gb_{cf}t_{cf}^2.$$

The complete resistance mechanism, in terms of rotational spring properties, is shown in Figure 3.2-13. This trilinear behavior is represented by two elastic-perfectly plastic springs at the opposing corners of the joint assemblage.

If desired, strain-hardening may be added to the system. Krawinkler suggests using a strain-hardening stiffness equal to 3 percent of the initial stiffness of the joint. In this analysis, the strain-hardening component was simply added to both the panel and the flange components:

$$K_{SH,\theta} = 0.03(K_{Panel,\theta} + K_{Flanges,\theta}).$$

Before continuing, one minor adjustment is made to the above derivations. Instead of using the nominal total beam and girder depths in the calculations, the distance between the center of the flanges was used as the effective depth. Hence:

$$d_c \equiv d_{c,nom} - t_{cf}$$

where the *nom* part of the subscript indicates the property listed as the total depth in the *AISC Manual of Steel Construction*.

The Krawinkler properties are now computed for a typical interior subassembly of the 6-story frame. A summary of the properties used for all connections is shown in Table 3.2-8.

Table 3.2-8 Properties for the Krawinkler Beam-Column Joint Model

Connection	Girder	Column	Doubler Plate (in.)	$M_{panel,\theta}$ (in.-k)	$K_{panel,\theta}$ (in.-k/rad)	$M_{flanges,\theta}$ (in.-k/rad)	$K_{flanges,q}$ (in.-k/rad)
A	W24x84	W21x122	–	8,701	3,480,000	1,028	102,800
B	W24x84	W21x122	1.00	23,203	9,281,000	1,028	102,800
C	W27x94	W21x147	–	11,822	4,729,000	1,489	148,900
D	W27x94	W21x147	1.00	28,248	11,298,000	1,489	148,900
E	W27x94	W21x201	–	15,292	6,117,000	3,006	300,600
F	W27x94	W21x201	0.875	29,900	11,998,000	3,006	300,600

Example calculations shown for row in **bold** type.

The sample calculations below are for Connection D in Table 3.2-8.

Material Properties:

$$F_y = 50.0 \text{ ksi (girder, column, and doubler plate)}$$

$$G = 12,000 \text{ ksi}$$

Girder:

W27x94

$$d_{b,nom} = 26.92 \text{ in.}$$

$$t_f = 0.745 \text{ in.}$$

$$d_b = 26.18 \text{ in.}$$

Column:

W21x147

$$d_{c,nom} = 22.06 \text{ in.}$$

$$t_w = 0.72 \text{ in.}$$

$$t_{cf} = 1.150 \text{ in.}$$

$$d_c = 20.91 \text{ in.}$$

$$b_{cf} = 12.51 \text{ in.}$$

Doubler plate: 1.00 in.

$$\text{Total panel zone thickness} = t_p = 0.72 + 1.00 = 1.72 \text{ in.}$$

$$V_{Panel} = 0.6F_y d_c t_p = 0.6(50)(20.91)(1.72) = 1,079 \text{ kips}$$

$$V_{Flanges} = 1.8 \frac{F_y b_{cf} t_{cf}^2}{d_b} = 1.8 \frac{50(12.51)(1.15^2)}{26.18} = 56.9 \text{ kips}$$

$$K_{Panel,\gamma} = Gt_p d_c = 12,000(1.72)(20.91) = 431,582 \text{ kips/unit shear strain}$$

$$\gamma_y = \theta_y = \frac{0.6F_y}{G} = \frac{0.6(50,000)}{12,000} = 0.0025$$

$$M_{Panel} = V_{Panel} d_b = 1,079(26.18) = 28,248 \text{ in.-kips}$$

$$K_{Panel,\theta} = K_{Panel,\gamma} d_b = 431,582(26.18) = 11,298,000 \text{ in.-kips/radian}$$

$$M_{Flanges} = V_{Flanges} d_b = 56.9(26.18) = 1,489 \text{ in.-kips}$$

$$K_{Flanges,\theta} = \frac{M_{Flanges}}{4\gamma_y} = \frac{1,489}{4(0.0025)} = 148,900 \text{ in.-kips/radian}$$

3.2.4.3 Modeling Girders

Because this structure is designed in accordance with the strong-column/weak-beam principle, it is anticipated that the girders will yield in flexure. Although DRAIN provides special yielding beam elements (Type 2 elements), more control over behavior is obtained through the use of the Type 4 connection element.

The modeling of a typical girder is shown in Figure 3.2-8. This figure shows an interior girder, together with the panel zones at the ends. The portion of the girder between the panel zones is modeled as four segments with one simple node at mid span and one compound node near each end. The mid-span node is used to enhance the deflected shape of the structure.⁵ The compound nodes are used to represent inelastic behavior in the hinging region.

The following information is required to model each plastic hinge:

1. The initial stiffness (moment per unit rotation),
2. The effective yield moment,
3. The secondary stiffness, and
4. The location of the hinge with respect to the face of the column.

Determination of the above properties, particularly the location of the hinge, is complicated by the fact that the plastic hinge grows in length during increasing story drift. Unfortunately, there is no effective way to represent a changing hinge length in DRAIN, so one must make do with a fixed hinge length and location. Fortunately, the behavior of the structure is relatively insensitive to the location of the hinges.

⁵A graphic post-processor was used to display the deflected shape of the structure. The program represents each element as a straight line. Although the computational results are unaffected, a better graphical representation is obtained by subdividing the member.

To determine the hinge properties, it is necessary to perform a moment-curvature analysis of the cross section, and this, in turn, is a function of the stress-strain curve of the material. In this example, a relatively simple stress-strain curve is used to represent the 50 ksi steel in the girders. This curve does not display a yield plateau, which is consistent with the assumption that the section has yielded in previous cycles, with the Baushinger effect erasing any trace of the yield plateau. The idealized stress-strain curve is shown in Figure 3.2-15.

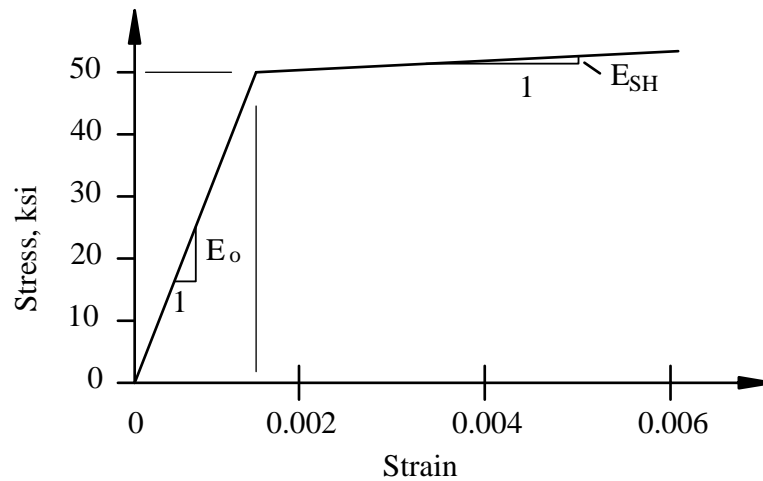


Figure 3.2-15 Assumed stress-strain curve for modeling girders.

To compute the moment-curvature relationship, the girder cross section was divided into 50 horizontal slices, with 10 slices in each flange and 30 slices in the web. The girder cross section was then subjected to gradually increasing rotation. For each value of rotation, strain compatibility (plane sections remain plane) was used to determine fiber strain. Fiber stress was obtained from the stress-strain law and stresses were multiplied by fiber area to determine fiber force. The forces were then multiplied by the distance to the neutral axis to determine that fiber's contribution to the section's resisting moment. The fiber contributions were summed to determine the total resisting moment. Analysis was performed using a Microsoft Excel worksheet. Curves were computed for an assumed strain hardening ratio of 1, 3, and 5 percent of the initial stiffness. The resulting moment-curvature relationship is shown for the W27x94 girder in Figure 3.2-16. Because of the assumed bilinear stress-strain curve, the moment-curvature relationships are essentially bilinear. Residual stresses due to section rolling were ignored, and it was assumed that local buckling of the flanges or the web would not occur.

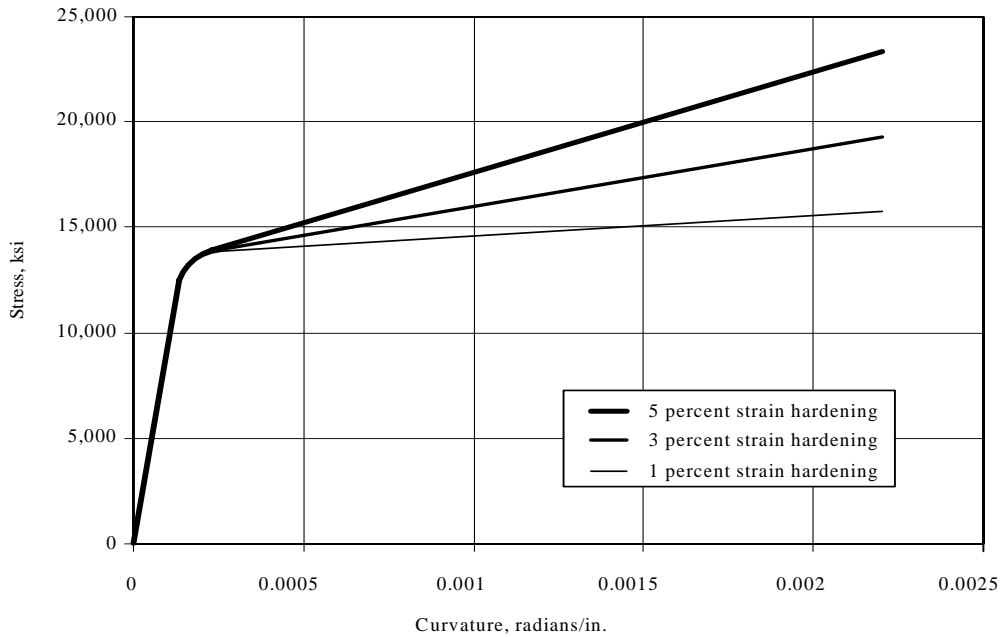


Figure 3.2-16 Moment curvature diagram for W27x94 girder.

To determine the parameters for the plastic hinge in the DRAIN model, a separate analysis was performed on the structure shown in Figure 3.2-17(a). This structure represents half of the clear span of the girder supported as a cantilever. The purpose of the special analysis was to determine a moment-deflection relationship for the cantilever loaded at the tip with a vertical force V . A similar moment-deflection relationship was determined for the structure shown in Figure 3.2-17(b), which consists of a cantilever with a compound node used to represent the inelastic rotation in the plastic hinge. Two Type-4 DRAIN elements were used at each compound node. The first of these is rigid-perfectly plastic and the second is bilinear. The resulting behavior is illustrated in Figure 3.2-17(c).

If the moment-curvature relationship is idealized as bilinear, it is a straightforward matter to compute the deflections of the structure of Figure 3.2-17(a). The method is developed in Figure 3.2-18. Figure 3.2-18(a) is a bilinear moment-curvature diagram. The girder is loaded to some moment M , which is greater than the yield moment. The moment diagram for the member is shown in Figure 3.2-18(b). At some distance x the moment is equal to the yield moment:

$$x = \frac{M_y L}{M}$$

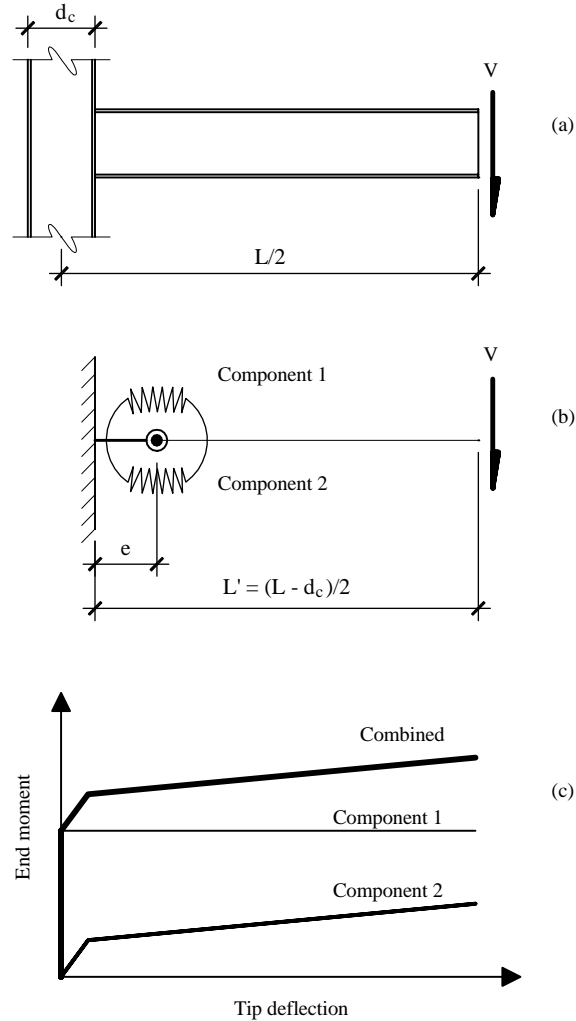


Figure 3.2-17 Developing moment-deflection diagrams for a typical girder.

The curvature along the length of the member is shown in Figure 3.2-18(c). At the distance x , the curvature is the yield curvature (ϕ_y), and at the support, the curvature (ϕ_M) is the curvature corresponding to the Point M on the moment-curvature diagram. The deflection is computed using the moment-area method, and consists of three parts:

$$\Delta_1 = \frac{\phi_y x}{2} \cdot \frac{2x}{3} = \frac{\phi_y x^2}{3}$$

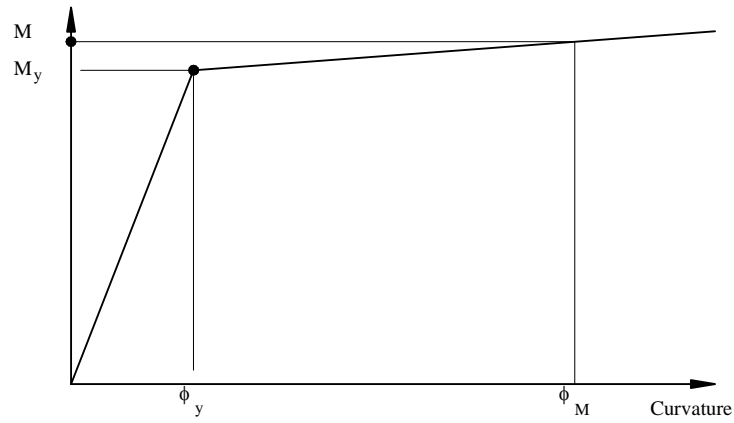
$$\Delta_2 = \phi_y (L' - x) \frac{L' + x}{2} = \frac{\phi_y (L' - x)(L' + x)}{2}$$

$$\begin{aligned}\Delta_3 &= \frac{(\phi_M - \phi_y)(L' - x)}{2} \cdot \left[x + \frac{2(L' - x)}{3} \right] \\ &= \frac{(\phi_M - \phi_y)(L' - x)(2L' + x)}{6}\end{aligned}$$

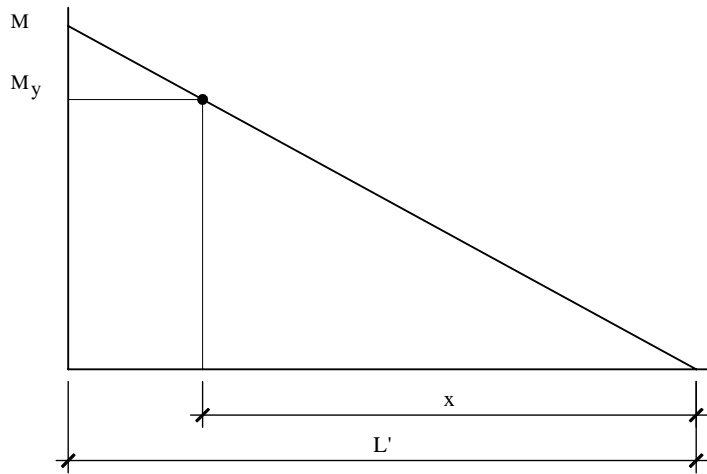
The first two parts of the deflection are for elastic response and the third is for inelastic response. The elastic part of the deflection is handled by the Type-2 elements in Figure 3.2-17(b). The inelastic part is represented by the two Type-4 elements at the compound node of the structure.

The development of the moment-deflection relationship for the W27x94 girder is illustrated in Figure 3.2-19. Part (a) of the figure is the idealized bilinear moment-curvature relationship for 3 percent strain hardening. Displacements were computed for 11 points on the structure. The resulting moment-deflection diagram is shown in Figure 3.2-19(b), where the total deflection ($\Delta_1 + \Delta_2 + \Delta_3$) is indicated. The inelastic part of the deflection (Δ_3 only) is shown separately in Figure 3.2-19(c), where the moment axis has been truncated below 12,000 in.-kips.

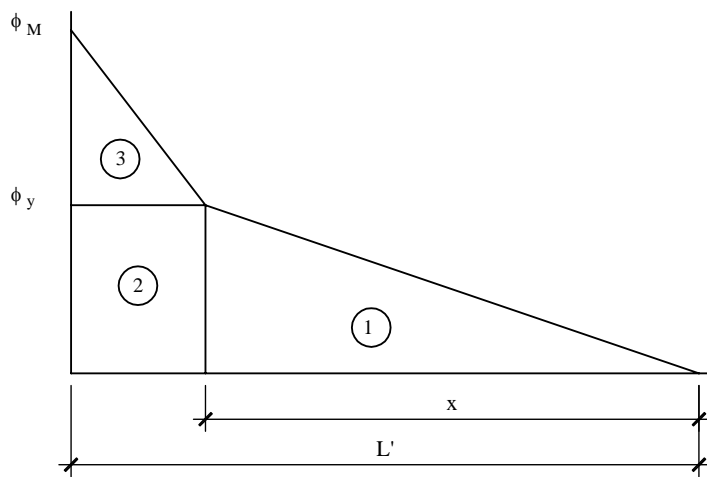
Finally, the simple DRAIN cantilever model of Figure 3.2-17(b) is analyzed. The compound node has arbitrarily been placed a distance $e = 5$ in. from the face of the support. (The analysis is relatively insensitive to the assumed hinge location.)



(a)



(b)



(c)

Figure 3.2-18 Development of equations for deflection of moment-deflection curves.

The moment diagram is shown in Figure 3.2-20(a) for the model subjected to a load producing a support moment, M_s , greater than the yield moment. The corresponding curvature diagram is shown in Figure 3.2-20(b). At the location of the plastic hinge, the moment is:

$$M_H = M_s \frac{(L' - e)}{L'}$$

and all inelastic curvature is concentrated into a plastic hinge with rotation θ_H . The tip deflection of the structure of Figure 3.2-20(c) consists of two parts:

$$\Delta_E = \frac{M_{Support} L'^2}{3EI}$$

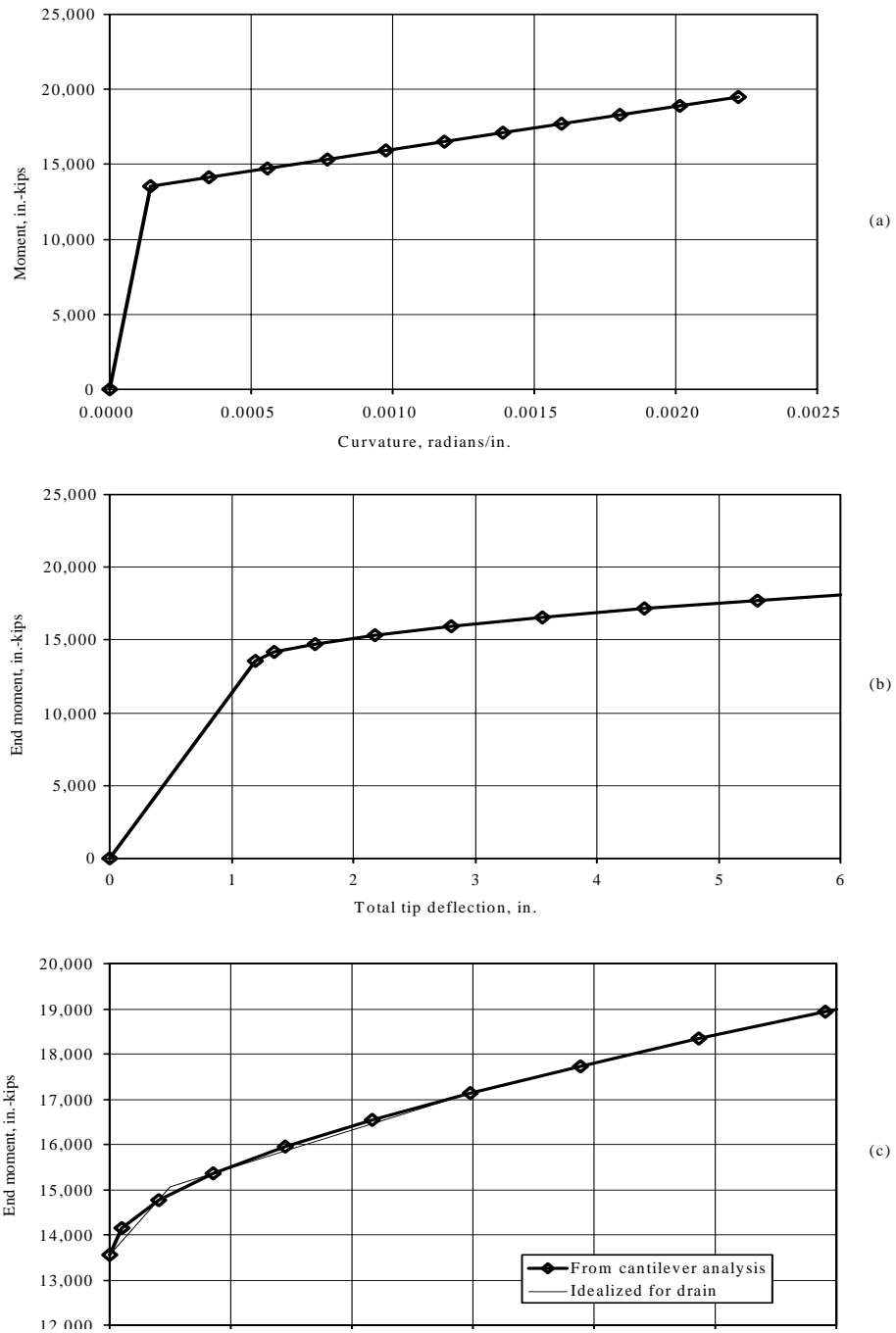


Figure 3.2-19 Moment-deflection curve for W27x94 girder with 3 percent strain hardening.

$$\Delta_I = \theta_H(L' - e) .$$

The first part is the elastic deflection and the second part is the inelastic deflection. Note that Δ_E and $(\Delta_1 + \Delta_2)$ are not quite equal because the shapes of the curvature diagram used to generate the deflections are not the same. For the small values of strain hardening assumed in this analysis, however, there is little error in assuming that the two deflections are equal. As Δ_E is simply the elastic displacement of a simple cantilever beam, it is possible to model the main portion of the girder using its nominal moment of inertia. The challenge is to determine the properties of the two Type-4 elements such that the deflections predicted using Δ_I are close to those produced using Δ_3 . This is a trial-and-error procedure, which is difficult to reproduce in this example. However, the development of the hinge properties is greatly facilitated by the fact that one component of the hinge must be rigid-plastic, with the second component being bilinear. The resulting “fit” for the W27x94 girder is shown in Figure 3.2-19. The resulting properties for the model are shown in Table 3.2-9. The properties for the W24x84 girder are also shown in the table. Note that the first yield of the model will be the yield moment from Component 1, and that this moment is roughly equal to the fully plastic moment of the section.

Table 3.2-9 Girder Properties as Modeled in DRAIN

Property	Section		
	W24x84	W27x94	
Elastic Properties	Moment of Inertia (in. ⁴)	2,370	3,270
	Shear Area (in. ²)	11.3	13.2
Inelastic Component 1 (see note below)	Yield Moment (in.-kip)	11,025	13,538
	Initial Stiffness (in.-kip/radian)	10E10	10E10
	S.H. Ratio	0.0	0.0
Inelastic Component 2	Yield Moment (in.-kip)	1,196	1,494
	Initial Stiffness (in.-kip/radian)	326,000	450,192
	S.H. Ratio	0.284	0.295
Comparative Property	Yield Moment = $S_x F_y$	9,800	12,150
	Plastic Moment = $Z_x F_y$	11,200	13,900

In some versions of DRAIN the strain hardening stiffness of the Type-4 springs is set to some small value (e.g. 0.001) if a zero value is entered in the appropriate data field. This may cause very large artificial strain hardening moments to develop in the hinge after it yields. It is recommended, therefore, to input a strain hardening value of 10^{-20} to prevent this from happening.

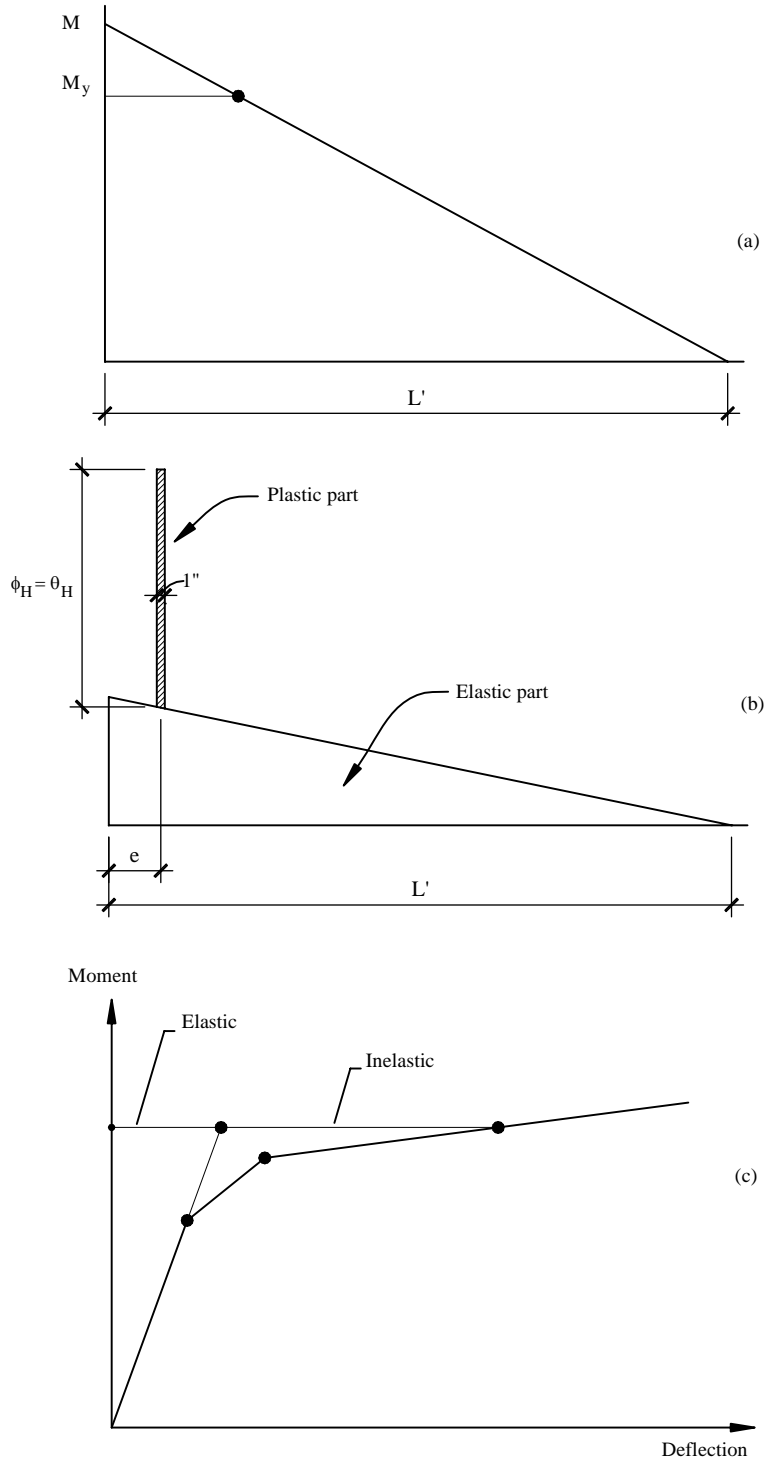


Figure 3.2-20 Development of plastic hinge properties for the W27x97 girder.

3.2.4.4 Modeling Columns

All columns in the analysis were modeled as Type-2 elements. Preliminary analysis indicated that columns should not yield, except at the base of the first story. Subsequent analysis showed that the columns will yield in the upper portion of the structure as well. For this reason, column yielding had to be activated in all of the Type-2 column elements. The columns were modeled using the built-in yielding functionality of the DRAIN program, wherein the yield moment is a function of the axial force in the column. The yield surface used by DRAIN is shown in Figure 3.2-21.

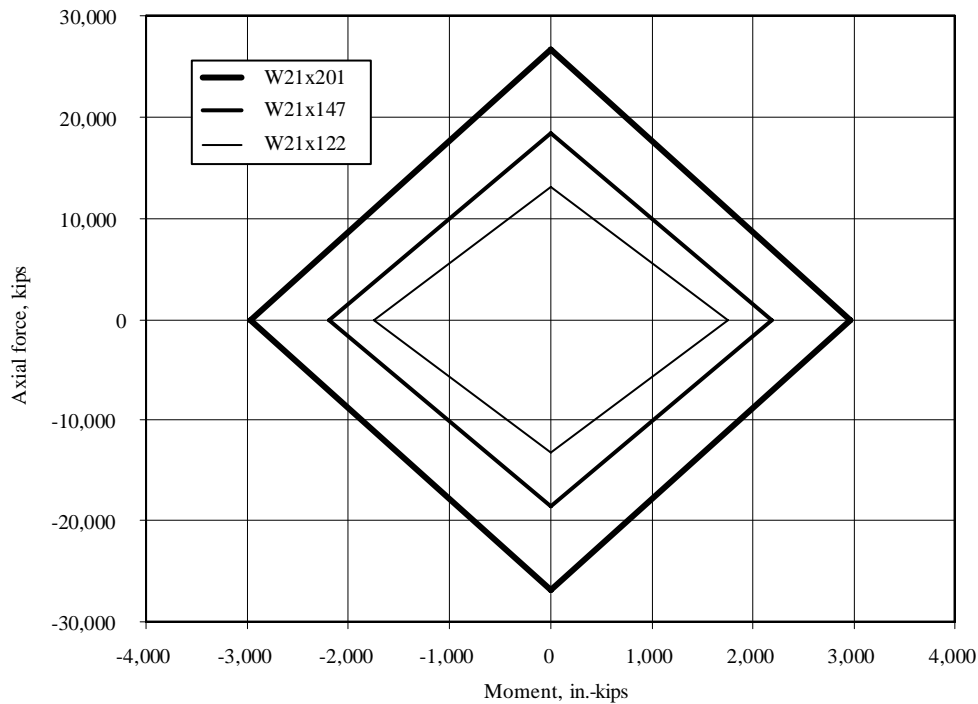


Figure 3.2-21 Yield surface used for modeling columns.

The rules employed by DRAIN to model column yielding are adequate for event-to-event nonlinear static pushover analysis, but leave much to be desired when dynamic analysis is performed. The greatest difficulty in the dynamic analysis is adequate treatment of the column when unloading and reloading. An assessment of the effect of these potential problems is beyond the scope of this example.

3.2.5 Static Pushover Analysis

Nonlinear static analysis is covered for the first time in the Appendix to Chapter 5 of the 2000 *Provisions*. Inclusion of these requirements in an appendix rather than the main body indicates that pushover analysis is in the developmental stage and may not be “ready for prime time.” For this reason, some liberties are taken in this example; however, for the most part, the example follows the appendix. [In the 2003

Provisions, a number of substantive technical changes have been made to the appendix, largely as a result of work performed by the Applied Technology Council in Project 55, Evaluation and Improvement of Inelastic Seismic Analysis Procedures.)]

Nonlinear static pushover analysis, in itself, provides the location and sequence of expected yielding in a structure. Additional analysis is required to estimate the amount of inelastic deformation that may occur during an earthquake. These inelastic deformations may then be compared to the deformations that have been deemed acceptable under the ground motion parameters that have been selected. *Provisions* Sec. 5A.1.3 [Appendix to Chapter 5] provides a simple methodology for estimating the inelastic deformations but does not provide specific acceptance criteria.

Another well-known method for determining maximum inelastic displacement is based on the capacity spectrum approach. This method is described in some detail in ATC 40 (Applied Technology Council, 1996). The capacity spectrum method is somewhat controversial and, in some cases may produce unreliable results (Chopra and Goel, 1999). However, as the method is still very popular and is incorporated in several commercial computer programs, it will be utilized here, and the results obtained will be compared to those computed using the simple approach.

Provisions Sec. 5A1.1 [A5.2.1] discusses modeling requirements for the pushover analysis in relatively vague terms, possibly reflecting the newness of the approach. However, it is felt that the model of the structure described earlier in this example is consistent with the spirit of the *Provisions*.⁶

The pushover curve obtained from a nonlinear static analysis is a function of the way the structure is both modeled and loaded. In the analysis reported herein, the structure was first subjected to the full dead load plus reduced live load followed by the lateral loads. The *Provisions* states that the lateral load pattern should follow the shape of the first mode. In this example, four different load patterns were initially considered:

- UL = uniform load (equal force at each level)
- TL = triangular (loads proportional to height)
- ML = modal load (lateral loads proportional to first mode shape)
- BL = *Provisions* load distribution (using the forces indicated in Table 3.2-3)

Relative values of these load patterns are summarized in Table 3.2-10. The loads have been normalized to a value of 15 kips at Level 2. Because of the similarity between the TL and ML distributions, the results from the TL distribution are not presented.

DRAIN analyses were run with P-delta effects included and, for comparison purposes, with such effects excluded. The *Provisions* requires “the influence of axial loads” to be considered when the axial load in the column exceeds 15 percent of the buckling load but presents no guidance on exactly how the buckling load is to be determined nor on what is meant by “influence.” In this analysis the influence was taken as inclusion of the story-level P-delta effect. This effect may be easily represented through linearized geometric stiffness, which is the basis of the outrigger column shown in Figure 3.2-4. Consistent

⁶The mathematical model does not represent strength loss due to premature fracture of welded connections. If such fracture is likely, the mathematical model must be adjusted accordingly.

geometric stiffness, which may be used to represent the influence of axial forces on the flexural flexibility of individual columns, may not be used directly in DRAIN. Such effects may be approximated in DRAIN by subdividing columns into several segments and activating the linearized geometric stiffness on a column-by-column basis. That approach was not used here.

Table 3.2-10 Lateral Load Patterns Used in Nonlinear Static Pushover Analysis

Level	Uniform Load	Triangular Load	Modal Load	BSSC Load
	UL (kips)	TL (kips)	ML (kips)	BL (kips)
R	15.0	77.5	88.4	150.0
6	15.0	65.0	80.4	118.0
5	15.0	52.5	67.8	88.0
4	15.0	40.0	50.3	60.0
3	15.0	27.5	32.0	36.0
2	15.0	15.0	15.0	15.0

As described later, the pushover analysis indicated all yielding in the structure occurred in the clear span of the girders and columns. Panel zone hinging did not occur. For this reason, the ML analysis was repeated for a structure with thinner doubler plates and without doubler plates. Because the behavior of the structure with thin doubler plates was not significantly different from the behavior with the thicker plates, the only comparison made here will be between the structures with and without doubler plates. These structures are referred to as the strong panel (SP) and weak panel (WP) structures, respectively.

The analyses were carried out using the DRAIN-2Dx computer program. Using DRAIN, an analysis may be performed under “load control” or under “displacement control.” Under load control, the structure is subjected to gradually increasing lateral loads. If, at any load step, the tangent stiffness matrix of the structure has a negative on the diagonal, the analysis is terminated. Consequently, loss of strength due to P-delta effects cannot be tracked. Using displacement control, one particular point of the structure (the control point) is forced to undergo a monotonically increasing lateral displacement and the lateral forces are constrained to follow the desired pattern. In this type of analysis, the structure can display loss of strength because the displacement control algorithm adds artificial stiffness along the diagonal to overcome the stability problem. Of course, the computed response of the structure after strength loss is completely fictitious in the context of a static loading environment. Under a dynamic loading, however, structures can display strength loss and be incrementally stable. It is for this reason that the post-strength-loss realm of the pushover response is of interest.

When performing a displacement controlled pushover analysis in DRAIN with *P*-Delta effects included, one must be careful to recover the base-shear forces properly.⁷ At any displacement step in the analysis, the true base shear in the system consists of two parts:

⁷If *P*-delta effects have been included, this procedure needs to be used when recovering base shear from column shear forces. This is true for displacement controlled static analysis, force controlled static analysis, and dynamic time-history analysis.

$$V = \sum_{i=1}^n V_{C,i} - \frac{P_1 \Delta_1}{h_1}$$

where the first term represents the sum of all the column shears in the first story and the second term represents the destabilizing P-delta shear in the first story. The P-delta effects for this structure were included through the use of the outrigger column shown at the right of Figure 3.2-4. Figure 3.2-22 plots two base shear components of the pushover response for the SP structure subjected to the ML loading. Also shown is the total response. The kink in the line representing P-delta forces results because these forces are based on first-story displacement, which, for an inelastic system, will not generally be proportional to the roof displacement.

For all of the pushover analyses reported for this example, the maximum displacement at the roof is 42.0 in. This value is slightly greater than 1.5 times the total drift limit for the structure where the total drift limit is taken as 1.25 times 2 percent of the total height. The drift limit is taken from *Provisions* Table 5.2.8 [4.5-1] and the 1.25 factor is taken from *Provisions* Sec. 5A.1.4.3. [In the 2003 *Provisions*, Sec. A5.2.6 requires multiplication by $0.85R/C_d$ rather than by 1.25.] As discussed below in Sec. 3.2.5.3, the Appendix to Chapter 5 of the *Provisions* requires only that the pushover analysis be run to a maximum displacement of 1.5 times the expected inelastic displacement. If this limit were used, the pushover analysis of this structure would only be run to a total displacement of about 13.5 in.

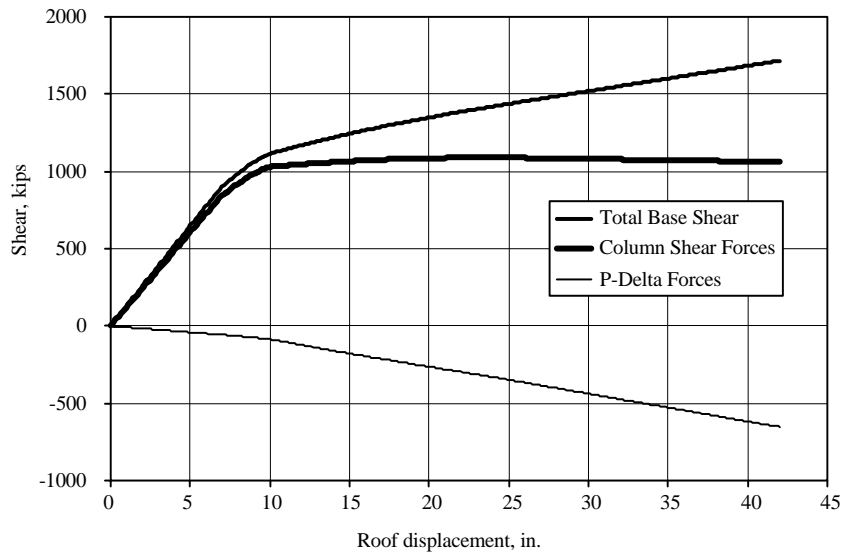


Figure 3.2-22 Two base shear components of pushover response.

3.2.5.1 Pushover Response of Strong Panel Structure

Figure 3.2-23 shows the pushover response of the SP structure to all three lateral load patterns when P-delta effects are excluded. In each case, gravity loads were applied first and then the lateral loads were applied using the displacement control algorithm. Figure 3.2-24 shows the response curves if P-delta effects are included. In Figure 3.2-25, the response of the structure under ML loading with and without

P-delta effects is illustrated. Clearly, P-delta effects are an extremely important aspect of the response of this structure, and the influence grows in significance after yielding. This is particularly interesting in the light of the *Provisions*, which ignore P-delta effects in elastic analysis if the maximum stability ratio is less than 0.10 (see *Provisions* Sec. 5.4.6.2 [5.2.6.2]). For this structure, the maximum computed stability ratio was 0.0839 (see Table 3.2-4), which is less than 0.10 and is also less than the upper limit of 0.0901. The upper limit is computed according to *Provisions* Eq. 5.4.6.2-2 and is based on the very conservative assumption that $\beta = 1.0$. While the *Provisions* allow the analyst to exclude P-delta effects in an elastic analysis, this clearly should not be done in the pushover analysis (or in time-history analysis). [In the 2003 *Provisions*, the upper limit for the stability ratio is eliminated. Where the calculated θ is greater than 0.10 a special analysis must be performed in accordance with Sec. A5.2.3. Sec. A5.2.1 requires that P-delta effects be considered for all pushover analyses.]

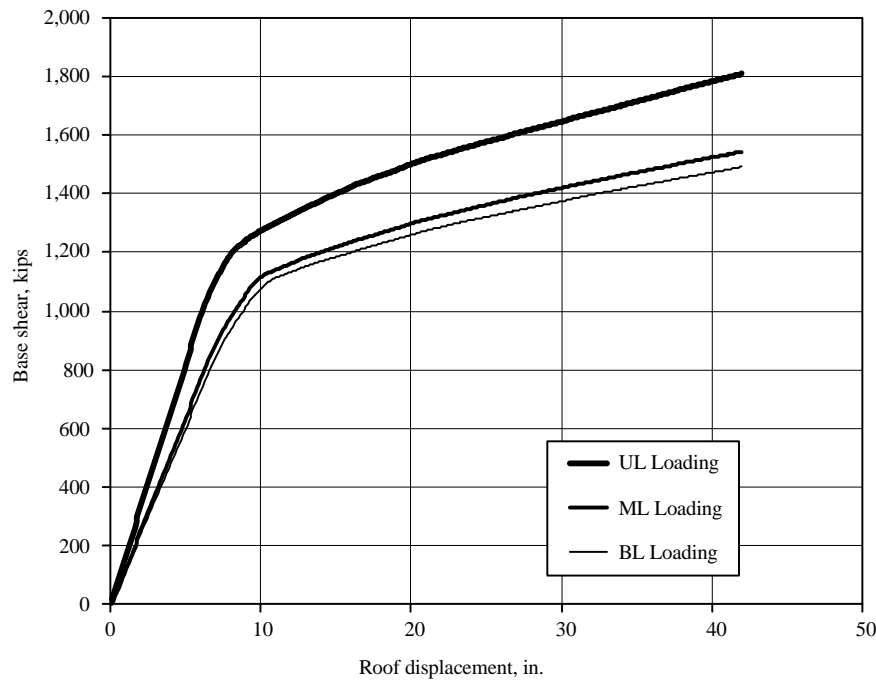


Figure 3.2-23 Response of strong panel model to three load pattern, excluding P-delta effects.

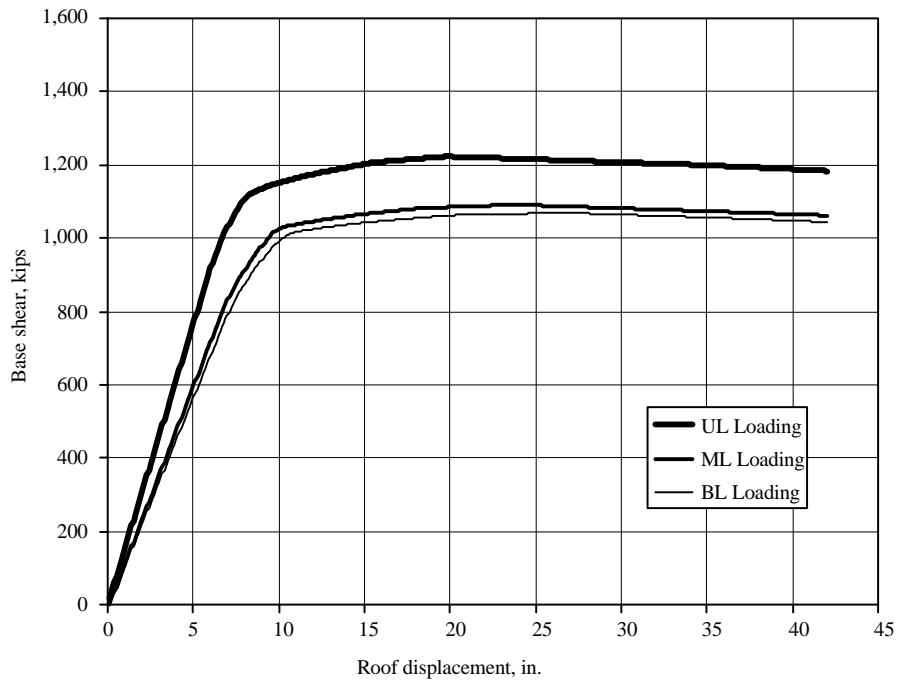


Figure 3.2-24 Response of strong panel model to three load patterns, including P-delta effects.

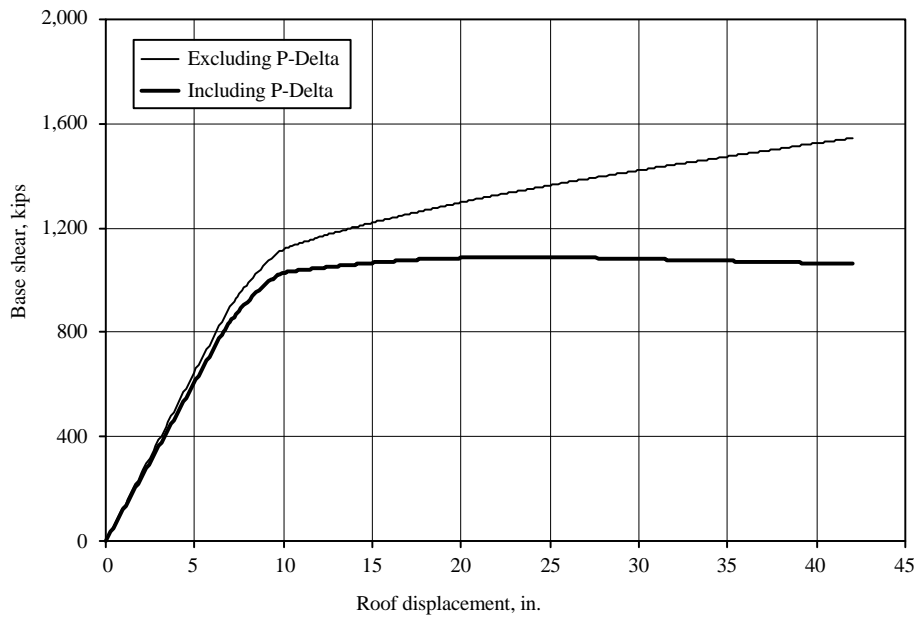


Figure 3.2-25 Response of strong panel model to ML loads, with and without P-delta effects.

In Figure 3.2-26, a plot of the tangent stiffness versus roof displacement is shown for the SP structure with ML loading, and with P-delta effects excluded or included. This plot, which represents the slope of the pushover curve at each displacement value, is more effective than the pushover plot in determining when yielding occurs. As Figure 3.2-26 illustrates, the first significant yield occurs at a roof displacement of approximately 6.5 in. and that most of the structure's original stiffness is exhausted by the time the roof drift reaches 10 in.

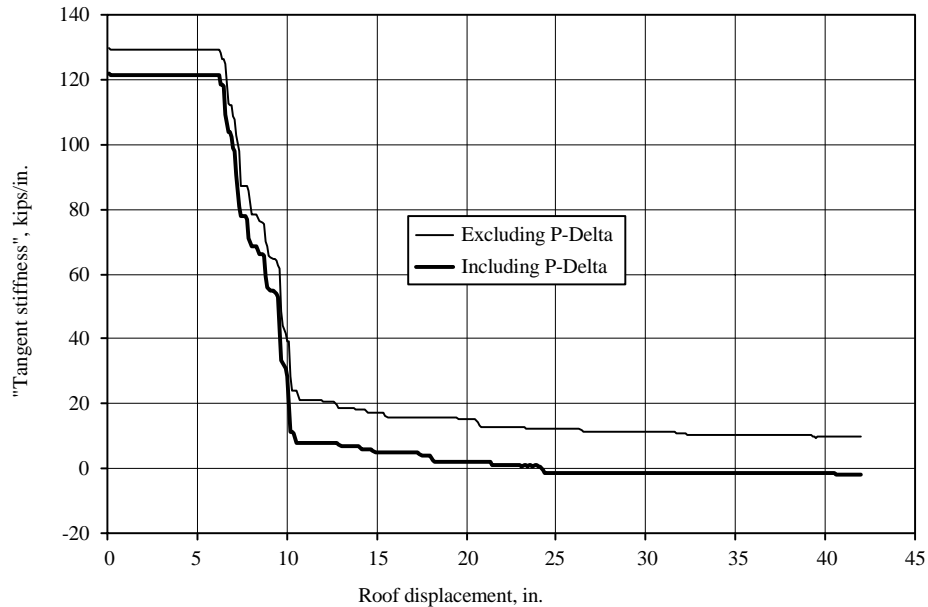


Figure 3.2-26 Tangent stiffness history for structure under ML loads, with and without *P*-delta effects.

For the case with *P*-delta effects excluded, the final stiffness shown in Figure 3.2-26 is approximately 10 kips/in., compared to an original value of 133 kips/in. Hence, the strain-hardening stiffness of the structure is 0.075 times the initial stiffness. This is somewhat greater than the 0.03 (3.0 percent) strain hardening ratio used in the development of the model because the entire structure does not yield simultaneously.

When *P*-delta effects are included, the final stiffness is -1.6 kips per in. The structure attains this negative residual stiffness at a displacement of approximately 23 in.

3.2.5.1.1 Sequence and Pattern of Plastic Hinging

The sequence of yielding in the structure with ML loading and with *P*-delta effects included is shown in Figure 3.2-27. Part (a) of the figure shows an elevation of the structure with numbers that indicate the sequence of plastic hinge formation. For example, the numeral “1” indicates that this was the first hinge to form. Part (b) of the figure shows a pushover curve with several hinge formation events indicated. These events correspond to numbers shown in part (a) of the figure. The pushover curve only shows selected events because an illustration showing all events would be difficult to read.

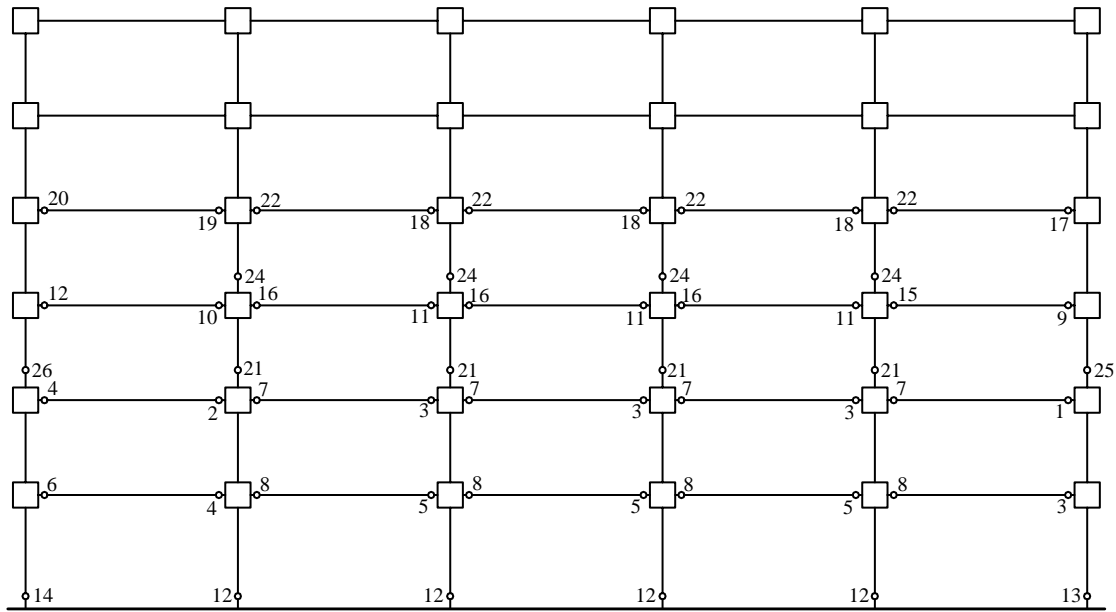
Several important observations are made from Figure 3.2-27:

1. There was no hinging in Levels 6 and R,
2. There was no hinging in any of the panel zones,
3. Hinges formed at the base of all the first-story columns,
4. All columns on Story 3 and all the interior columns on Story 4 formed plastic hinges, and
5. Both ends of all the girders at Levels 2 through 5 yielded.

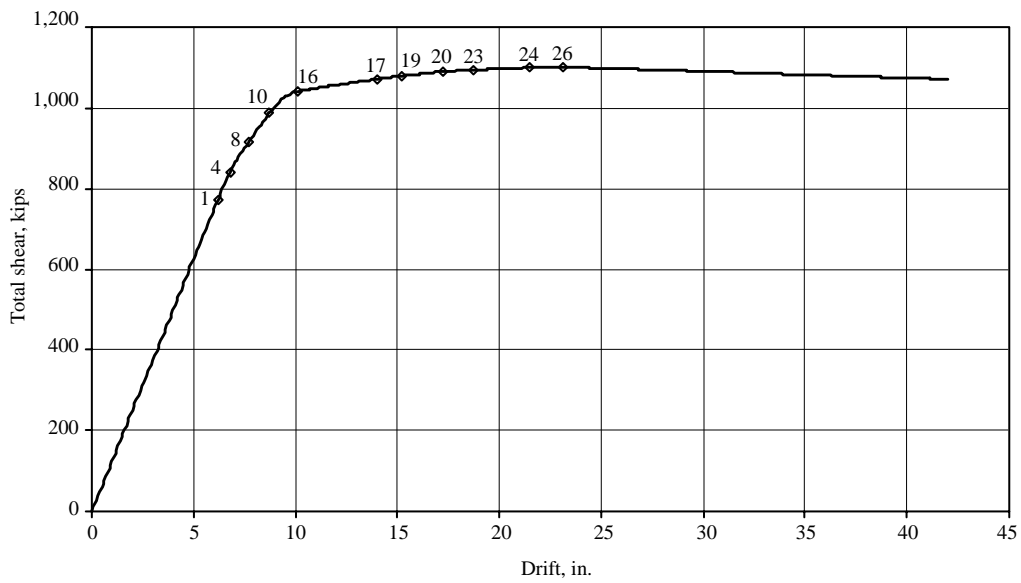
It appears the structure is somewhat weak in the middle two stories and is too strong at the upper stories. The doubler plates added to the interior columns prevented panel zone yielding (even at the extreme roof displacement of 42 in.).

The presence of column hinging at Levels 3 and 4 is a bit troublesome because the structure was designed as a strong-column/weak-beam system. This design philosophy, however, is intended to prevent the formation of complete story mechanisms, not to prevent individual column hinging. While hinges did form at the bottom of each column in the third story, hinges did not form at the top of these columns, and a complete story mechanism was avoided.

Even though the pattern of hinging is interesting and useful as an evaluation tool, the performance of the structure in the context of various acceptance criteria cannot be assessed until the expected inelastic displacement can be determined. This is done below in Sec. 3.2.5.3.



(a)



(b)

Figure 3.2-27 Patterns of plastic hinge formation: SP model under ML load, including P-delta effects.

3.2.5.1.2 Comparison with Strength from Plastic Analysis

It is interesting to compare the strength of the structure from pushover analysis with that obtained from the rigid-collapse analysis performed using virtual work. These values are summarized in Table 3.2-11. The strength from the case with P-delta excluded was estimated from the curves shown in Figure 3.2-23 and is taken as the strength at the principal bend in the curve (the estimated yield from a bilinear representation of the pushover curve). Consistent with the upper bound theorem of plastic analysis, the strength from virtual work is significantly greater than that from pushover analysis. The reason for the difference in predicted strengths is related to the pattern of yielding that actually formed in the structure, compared to that assumed in the rigid-plastic analysis.

Table 3.2-11 Strength Comparisons: Pushover vs Rigid Plastic

Pattern	Lateral Strength (kips)		
	P-delta Excluded	P-delta Included	Rigid-Plastic
Uniform	1220	1223	1925
Modal (Triangular)	1137	1101	1523
BSSC	1108	1069	1443

3.2.5.2 Pushover Response of Weak Panel Structure

Before continuing, the structure should be re-analyzed without panel zone reinforcing and the behavior compared with that determined from the analysis described above. For this exercise, only the modal load pattern d is considered but the analysis is performed with and without P-delta effects.

The pushover curves for the structure under modal loading and with weak panels are shown in Figure 3.2-28. Curves for the analyses run with and without P-delta effects are included. Figures 3.2-29 and 3.2-30 are more informative because they compare the response of the structures with and without panel zone reinforcement. Figure 3.2-31 shows the tangent stiffness history comparison for the structures with and without doubler plates. In both cases P-delta effects have been included.

From Figures 3.2-28 through 3.2-31 it may be seen that the doubler plates, which represent approximately 2.0 percent of the volume of the structure, increase the strength by approximately 12 percent and increase the initial stiffness by about 10 percent.

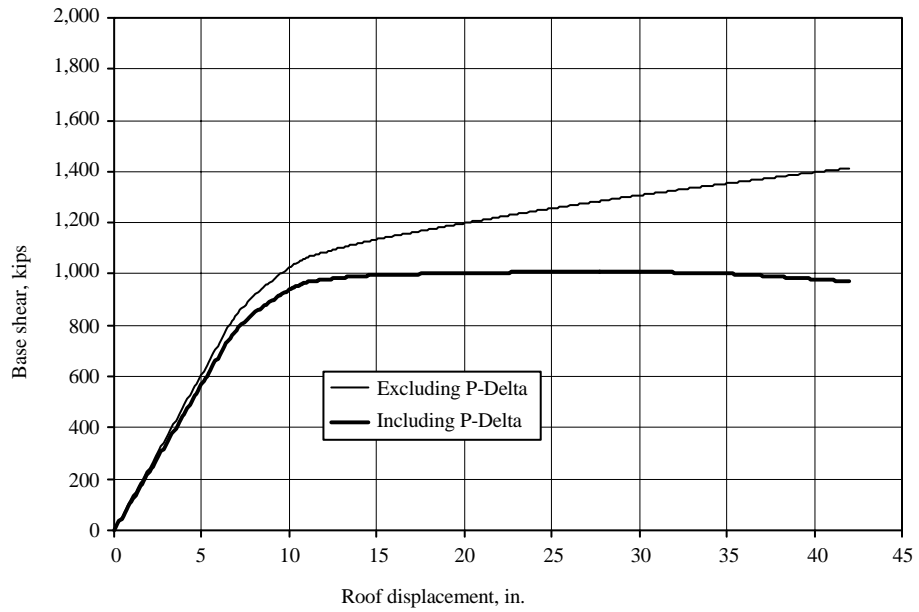


Figure 3.2-28 Weak panel zone model under ML load.

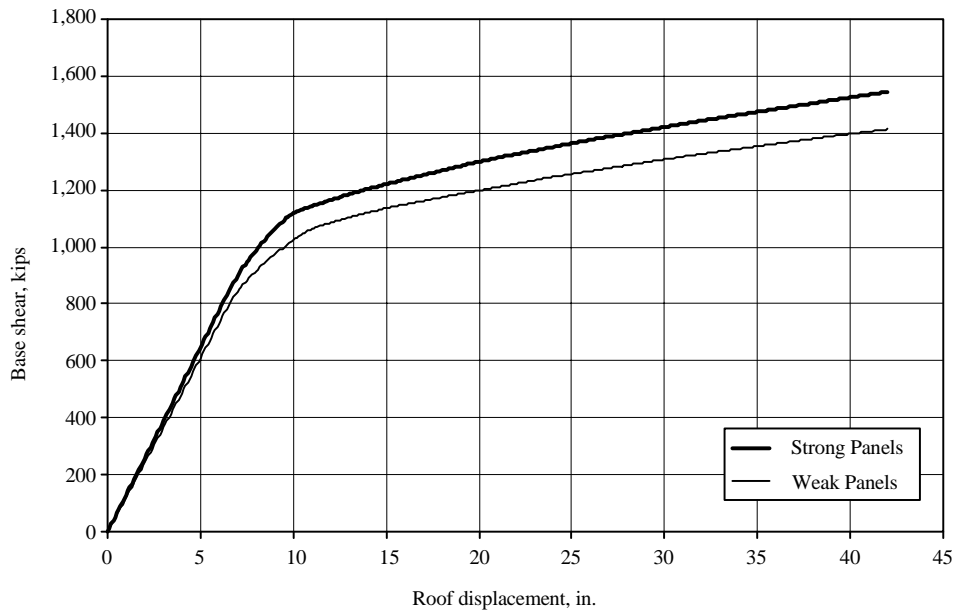


Figure 3.2-29 Comparison of weak panel zone model with strong panel zone model, excluding P-delta effects.

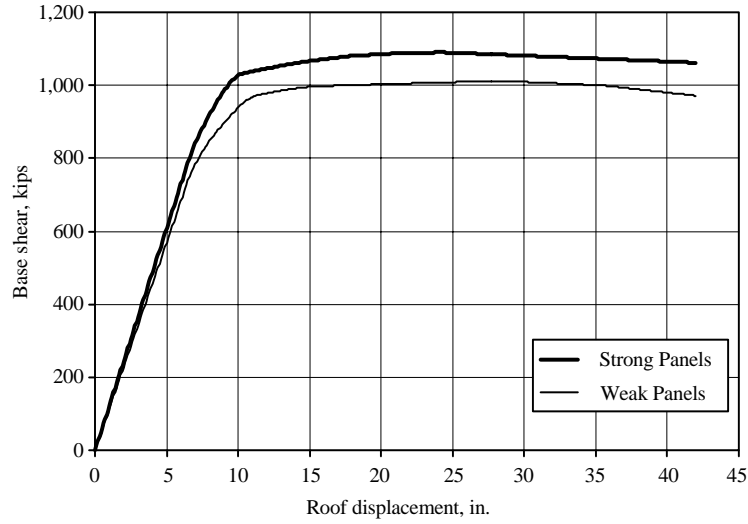


Figure 3.2-30 Comparison of weak panel zone model with strong panel zone model, including P-delta effects.

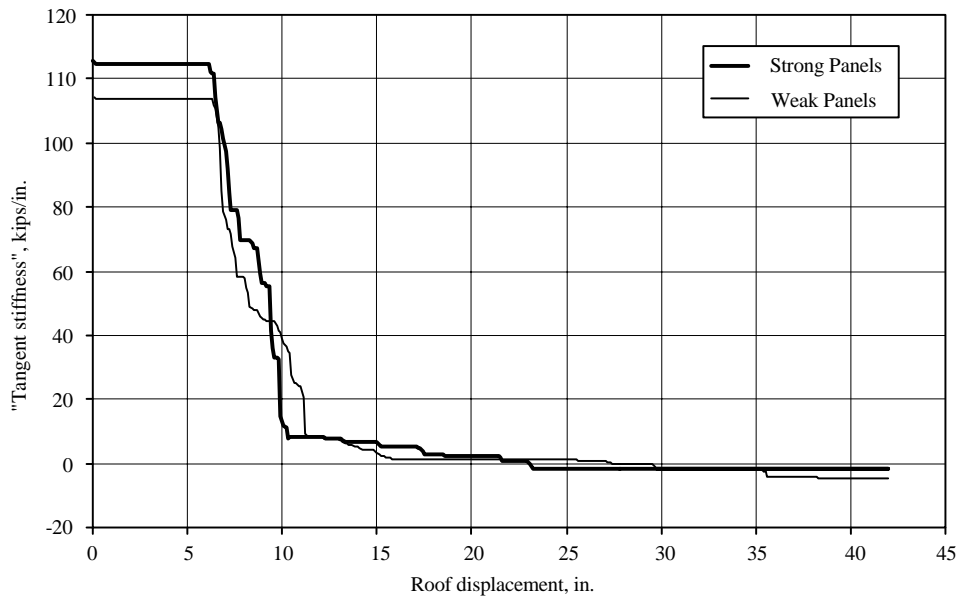
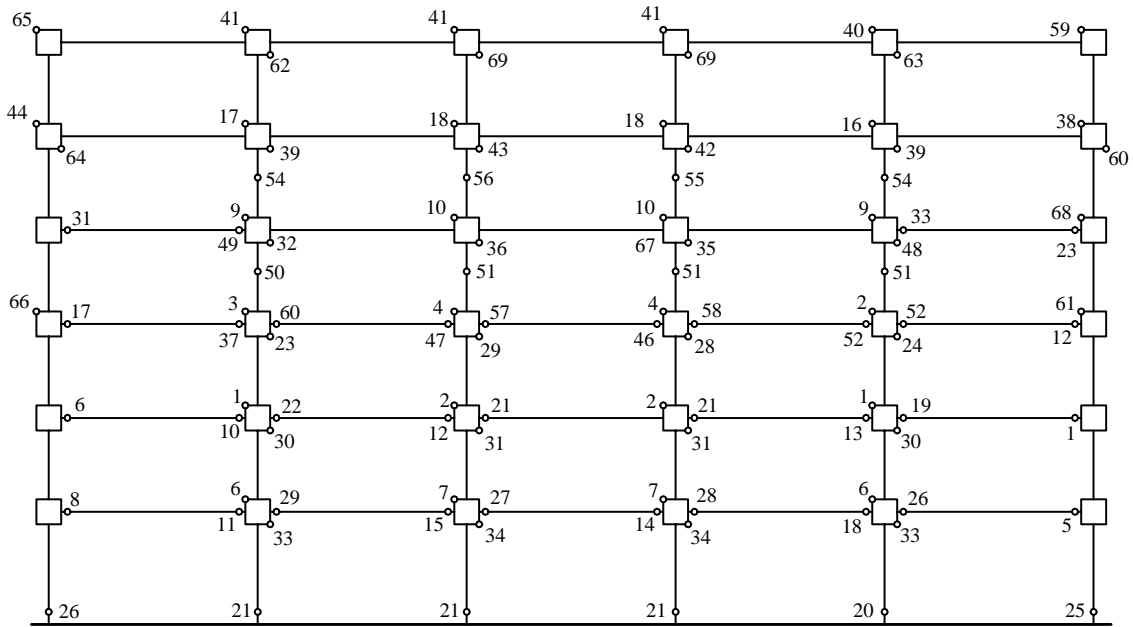
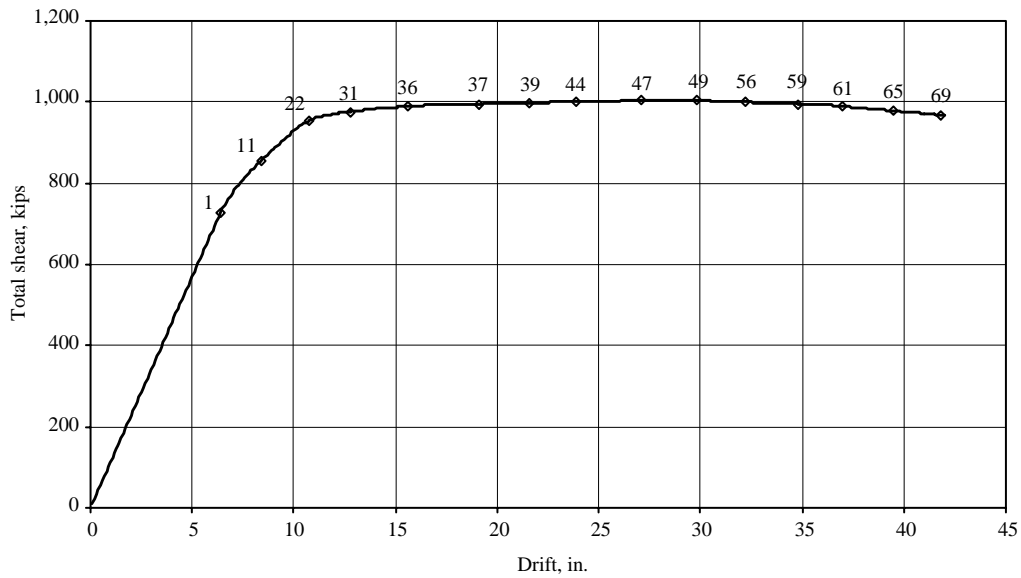


Figure 3.2-31 Tangent stiffness history for structure under ML loads, strong versus weak panels, including P-delta effects.



(a)



(b)

Figure 3.2-32 Patterns of plastic hinge formation: weak panel zone model under ML load, including P-delta effects.

The difference between the behavior of the structures with and without doubler plates is attributed to the yielding of the panel zones in the structure without panel zone reinforcement. The sequence of hinging is illustrated in Figure 3.2-32. Part (a) of this figure indicates that panel zone yielding occurs early. (Panel zone yielding is indicated by a numeric sequence label in the corner of the panel zone.) In fact, the first yielding in the structure is due to yielding of a panel zone at the second level of the structure.

It should be noted that under very large displacements, the flange component of the panel zone yields. Girder and column hinging also occurs, but the column hinging appears relatively late in the response. It is also significant that the upper two levels of the structure display yielding in several of the panel zones.

Aside from the relatively marginal loss in stiffness and strength due to removal of the doubler plates, it appears that the structure without panel zone reinforcement is behaving adequately. Of course, actual performance cannot be evaluated without predicting the maximum inelastic panel shear strain and assessing the stability of the panel zones under these strains.

3.2.5.3 Predictions of Total Displacement and Story Drift from Pushover Analysis

In the following discussion, the only loading pattern considered is the modal load pattern discussed earlier. This is consistent with the requirements of *Provisions* Sec. 5A.1.2 [A5.2.2]. The structure with both strong and weak panel zones is analyzed, and separate analyses are performed including and excluding P-delta effects.

3.2.5.3.1 Expected Inelastic Displacements Computed According to the Provisions

The expected inelastic displacement was computed using the procedures of *Provisions* Sec. 5.5 [5.3]. In the *Provisions*, the displacement is computed using response-spectrum analysis with only the first mode included. The expected roof displacement will be equal to the displacement computed from the 5-percent-damped response spectrum multiplied by the modal participation factor which is multiplied by the first mode displacement at the roof level of the structure. In the present analysis, the roof level first mode displacement is 1.0.

Details of the calculations are not provided herein. The relevant modal quantities and the expected inelastic displacements are provided in Table 3.2-12. Note that only those values associated with the ML lateral load pattern were used.

Table 3.2-12 Modal Properties and Expected Inelastic Displacements for the Strong and Weak Panel Models Subjected to the Modal Load Pattern

Computed Quantity	Strong Panel w/o P-Delta	Strong Panel with P-Delta	Weak Panel w/o P-Delta	Weak Panel with P-Delta
Period (seconds)	1.950	2.015	2.028	2.102
Modal Participation Factor	1.308	1.305	1.315	1.311
Effective Modal Mass (%)	82.6	82.8	82.1	82.2
Expected Inelastic Disp. (in.)	12.31	12.70	12.78	13.33
Base Shear Demand (kips)	1168	1051	1099	987
6 th Story Drift (in.)	1.09	1.02	1.12	1.11
5 th Story Drift (in.)	1.74	1.77	1.84	1.88
4 th Story Drift (in.)	2.28	2.34	2.44	2.53
3 rd Story Drift (in.)	2.10	2.73	2.74	2.90
2 nd Story Drift (in.)	2.54	2.73	2.56	2.71
1 st Story Drift (in.)	2.18	2.23	2.09	2.18

As the table indicates, the modal quantities are only slightly influenced by P-delta effects and the inclusion or exclusion of doubler plates. The maximum inelastic displacements are in the range of 12.2 to 13.3 in. The information provided in Figures 3.2-23 through 3.2-32 indicates that at a target displacement of, for example, 13.0 in., some yielding has occurred but the displacements are not of such a magnitude that the slope of the pushover curve is negative when P-delta effects are included.

It should be noted that FEMA 356, *Prestandard and Commentary for the Seismic Rehabilitation of Buildings*, provides a simplified methodology for computing the target displacement that is similar to but somewhat more detailed than the approach illustrated above. See Sec. 3.3.3.3.2 of FEMA 356 for details.

3.2.5.3.2 Inelastic Displacements Computed According to the Capacity Spectrum Method

In the capacity spectrum method, the pushover curve is transformed to a capacity curve that represents the first mode inelastic response of the full structure. Figure 3.2-33 shows a bilinear capacity curve. The horizontal axis of the capacity curve measures the first mode displacement of the simplified system. The vertical axis is a measure of simplified system strength to system weight. When multiplied by the acceleration due to gravity (g), the vertical axis represents the acceleration of the mass of the simple system.

Point E on the horizontal axis is the value of interest, the expected inelastic displacement of the simplified system. This displacement is often called the target displacement. The point on the capacity curve directly above Point E is marked with a small circle, and the line passing from the origin through this point represents the secant stiffness of the simplified system. If the values on the vertical axis are multiplied by the acceleration due to gravity, the slope of the line passing through the small circle is equal to the acceleration divided by the displacement. This value is the same as the square of the circular frequency of the simplified system. Thus, the sloped line is also a measure of the secant period of the simplified structure. As will be shown later, an equivalent viscous damping value (ζ_E) can be computed for the simple structure deformed to Point E.

Figure 3.2-34 shows a response spectrum with the vertical axis representing spectral acceleration as a ratio of the acceleration due to gravity and the horizontal axis representing displacement. This spectrum, called a demand spectrum, is somewhat different from the traditional spectrum that uses period of vibration as the horizontal axis. The demand spectrum is drawn for a particular damping value (ζ). Using the demand spectrum, the displacement of a SDOF system may be determined if its period of vibration is known and the system's damping matches the damping used in the development of the demand spectrum. If the system's damping is equal to ζ_E , and its stiffness is the same as that represented by the sloped line in Figure 3.2-33, the displacement computed from the demand spectrum will be the same as the expected inelastic displacement shown in Figure 3.2-33.

The capacity spectrum and demand spectrum are shown together in Figure 3.2-35. The demand spectrum is drawn for a damping value exactly equal to ζ_E , but ζ_E is not known *a priori* and must be determined by the analyst. There are several ways to determine ζ_E . In this example, two different methods will be demonstrated: an iterative approach and a semigraphical approach.

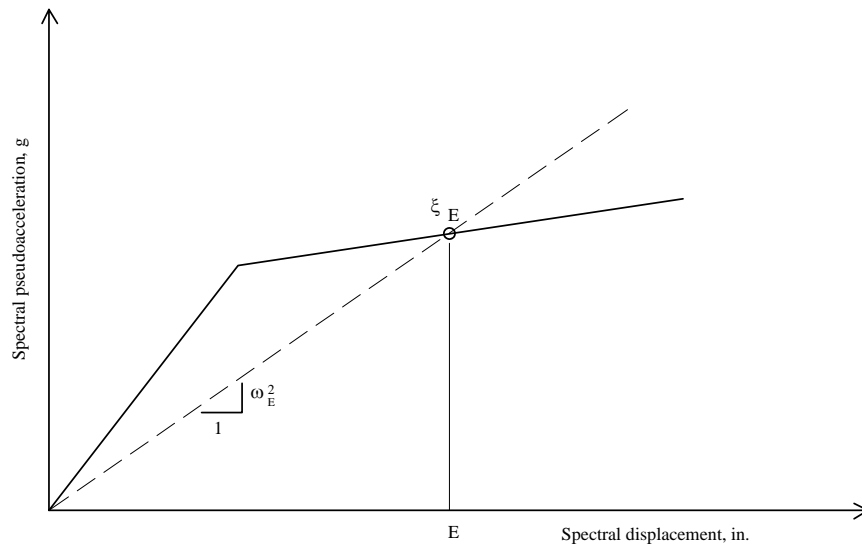


Figure 3.2-33 A simple capacity spectrum.

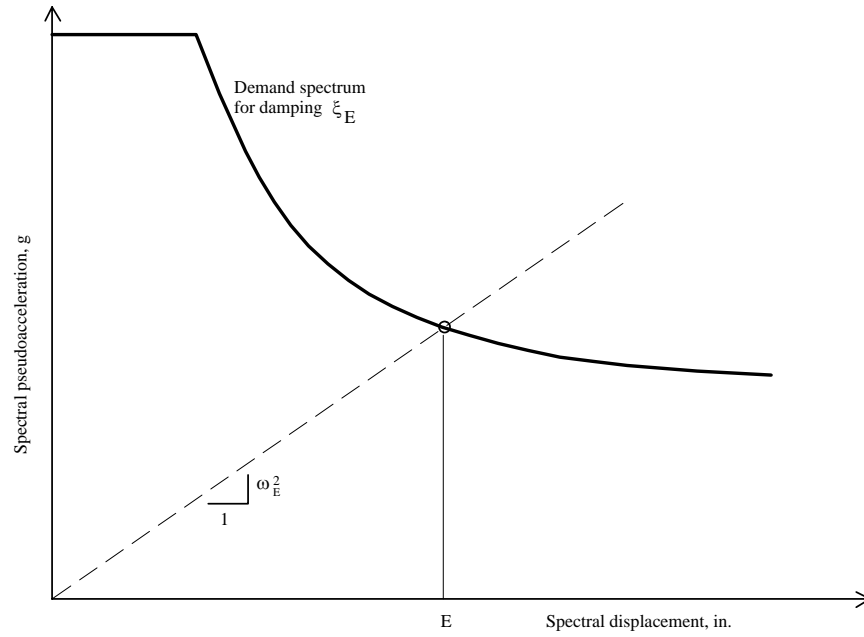


Figure 3.2-34 A simple demand spectrum.

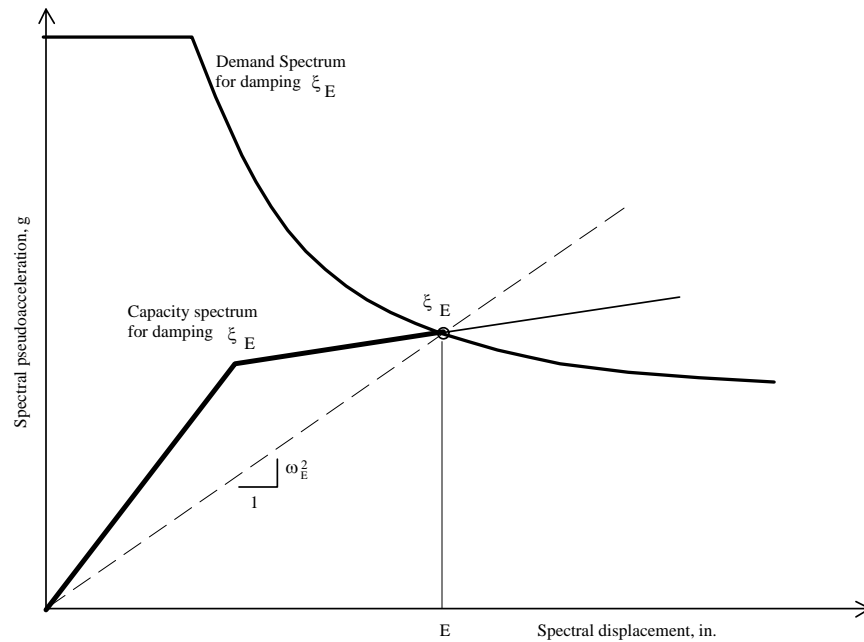


Figure 3.2-35 Capacity and demand spectra plotted together.

The first step in either approach is to convert the pushover curve into a capacity spectrum curve. This is done using the following two transformations:⁸

1. To obtain spectral displacement, multiply each displacement value in the original pushover curve by the quantity:

$$\frac{1}{PF_1\phi_{Roof,1}}$$

where PF_1 is the modal participation factor for the fundamental mode and $\phi_{Roof,1}$ is the value of the first mode shape at the top level of the structure. The modal participation factor and the modal displacement must be computed using a consistent normalization of the mode shapes. One must be particularly careful when using DRAIN because the printed mode shapes and the printed modal participation factors use inconsistent normalizations – the mode shapes are normalized to a maximum value of 1.0 and the modal participation factors are based on a normalization that produces a unit generalized mass matrix. For most frame-type structures, the first mode participation factor will be in the range of 1.3 to 1.4 if the mode shapes are normalized for a maximum value of 1.0.

2. To obtain spectral pseudoacceleration, divide each force value in the pushover curve by the total weight of the structure, and then multiply by the quantity:

$$\frac{1}{\alpha_1}$$

where α_1 is the ratio of the effective mass in the first mode to the total mass in the structure. For frame structures, α_1 will be in the range of 0.8 to 0.85. Note that α_1 is not a function of mode shape normalization.

After performing the transformation, convert the smooth capacity curve into a simple bilinear capacity curve. This step is somewhat subjective in terms of defining the effective yield point, but the results are typically insensitive to different values that could be assumed for the yield point. Figure 3.2-36 shows a typical capacity spectrum in which the yield point is represented by points a_Y and d_Y . The displacement and acceleration at the expected inelastic displacement are d_E and a_E , respectively. The two slopes of the demand spectrum are K_1 and K_2 , and the intercept on the vertical axis is a_r .

⁸Expressions in this section are taken from ATC40 but have been modified to conform to the nomenclature used herein.

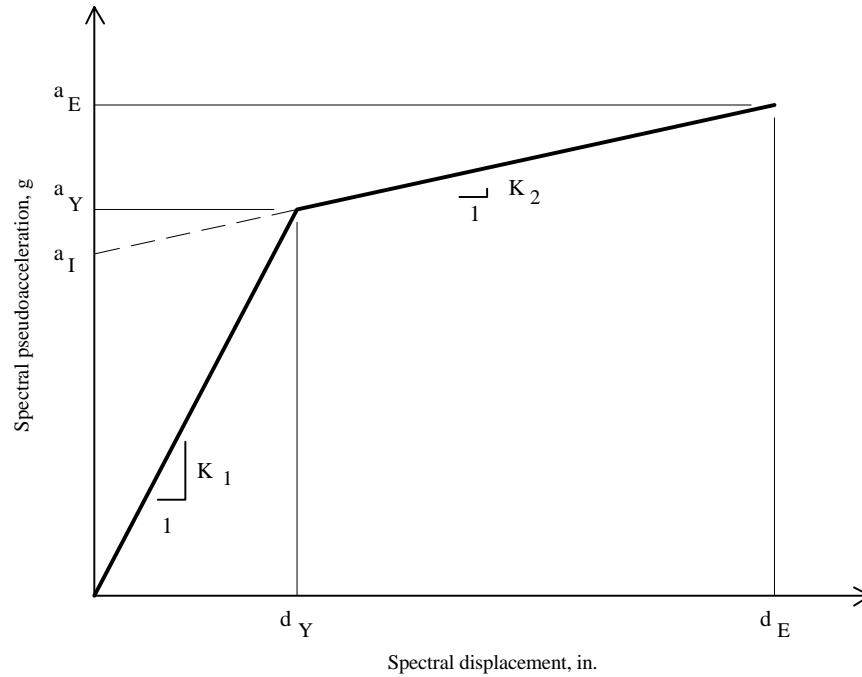


Figure 3.2-36 Capacity spectrum showing control points.

At this point the iterative method and the direct method diverge somewhat. The iterative method will be presented first, followed by the direct method.

Given the capacity spectrum, the iterative approach is as follows:

- I-1. Guess the expected inelastic displacement d_E . The displacement computed from the simplified procedure of the *Provisions* is a good starting point.
- I-2. Compute the equivalent viscous damping value at the above displacement. This damping value, in terms of percent critical, may be estimated as:

$$\xi_E = 5 + \frac{63.7(a_Y d_E - d_Y a_E)}{a_E d_E}$$

- I-3. Compute the secant period of vibration:

$$T_E = \frac{2\pi}{\sqrt{\frac{g \times a_E}{d_E}}}$$

where g is the acceleration due to gravity.

I-4. An estimated displacement must now be determined from the demand spectrum. A damping value of ζ_E will be assumed in the development of the spectrum. The demand spectrum at this damping value is adapted from the response spectrum given by *Provisions* Sec. 4.1.2.6 [3.3.4]. This spectrum is based on 5 percent of critical damping; therefore, it must be modified for the higher equivalent damping represented by ζ_E . For the example presented here, the modification factors for systems with higher damping values are obtained from *Provisions* Table 13.3.3.1 [13.3-1], which is reproduced in a somewhat different form as Table 3.2-13 below. In Table 3.2-13, the modification factors are shown as multiplying factors instead of dividing factors as is done in the *Provisions*. The use of the table can be explained by a simple example: the spectral ordinate for a system with 10 percent of critical damping is obtained by multiplying the 5-percent-damped value by 0.833.

The values in Table 3.2-13 are intended for use only for ductile systems without significant strength loss. They are also to be used only in the longer period constant velocity region of the response spectrum. This will be adequate for our needs because the initial period of vibration of our structure is in the neighborhood of 2.0 seconds. See ATC 40 for conditions where the structure does have strength loss or where the period of vibration is such that the constant acceleration region of the spectrum controls. During iteration it may be more convenient to use the information from Table 3.2-13 in graphic form as shown in Figure 3.2-37.

Table 3.2-13 Damping Modification Factors

Effective Damping (% critical)	Damping Modification Factor
5	1.000
10	0.833
20	0.667
30	0.588
40	0.526
50 or greater	0.500

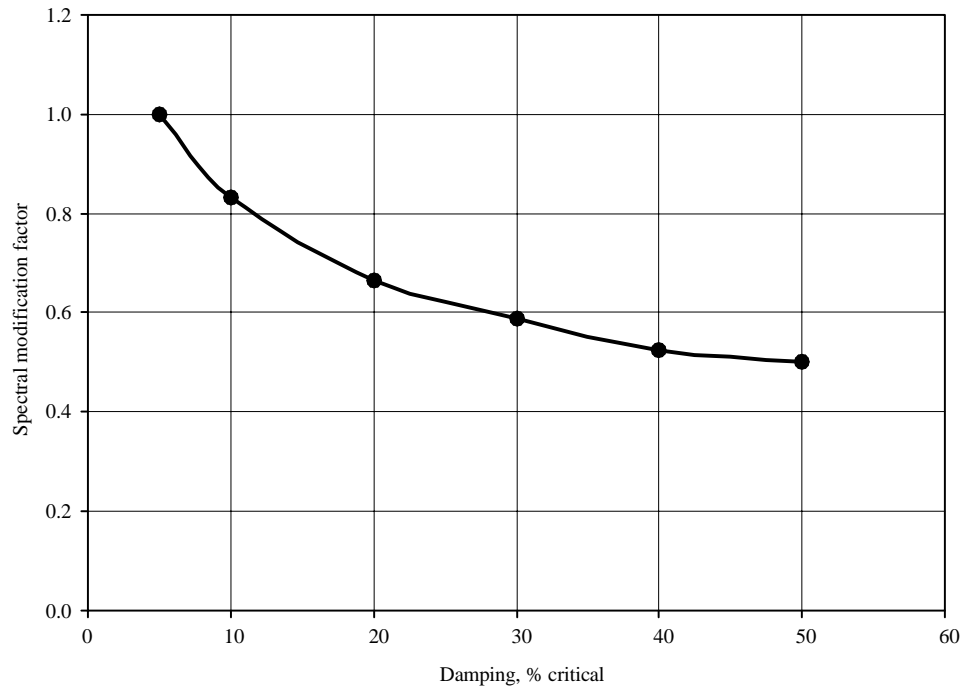


Figure 3.2-37 Damping modification factors.

- I-5. Using the period of vibration computed in Step 3 and the damping computed in Step 4, compute the updated estimate of spectral acceleration a_E^{new} and convert to displacement using the following expression:

$$d_E^{new} = \frac{g \times a_E^{new}}{[2\pi/T_E]^2}$$

If this displacement is the same as that estimated in Step 1, the iteration is complete. If not, set the displacement in Step 1 to d_E^{new} and perform another cycle. Continue iterating until the desired level of accuracy is achieved.

- I-6. Convert the displacement for the simple system to the expected inelastic displacement for the complete structure by multiplying by the product of the modal participation factor and the first mode roof displacement.

The procedure will now be demonstrated for the strong panel structure subjected to the ML load pattern. P-delta effects are *excluded*.

For this structure, the modal participation factor and effective modal mass factor for the first mode are:

$$\phi_1 = 1.308 \text{ and } \alpha_1 = 0.826$$

The original pushover curve is shown in Figure 3.2-23. The capacity spectrum version of the curve is shown in Figure 3.2-38 as is a bilinear representation of the capacity curve.

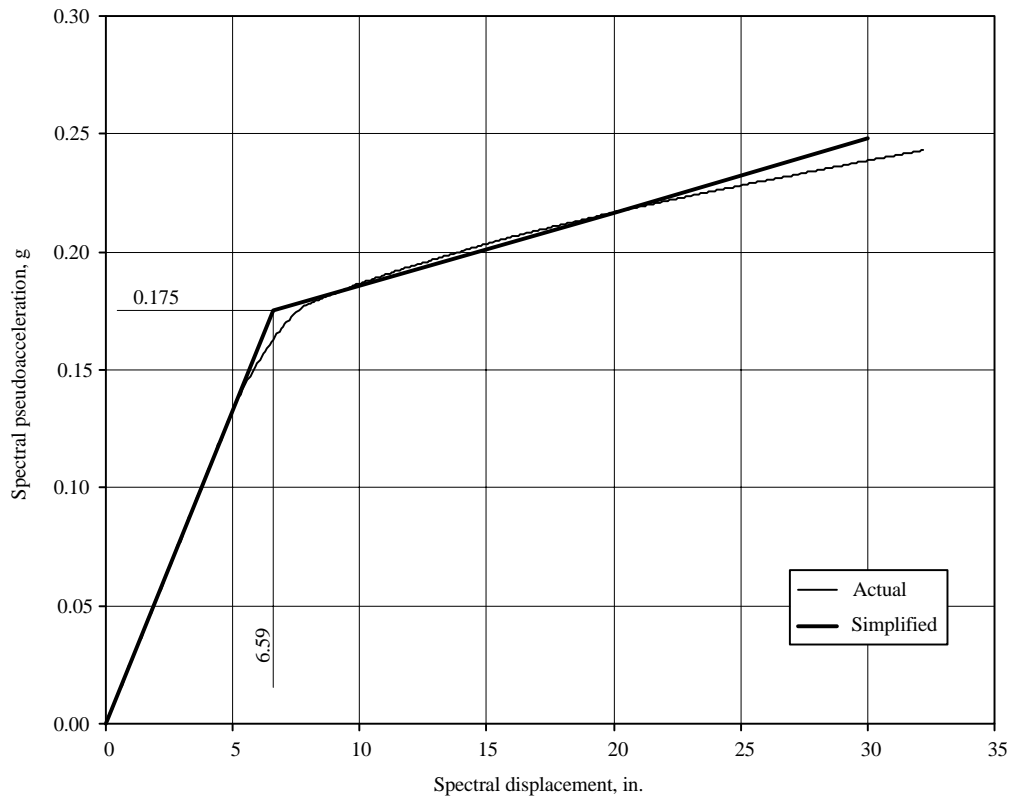


Figure 3.2-38 Capacity spectrum used in iterative solution.

The control values for the bilinear curve are:

$$d_y = 6.592 \text{ in.}$$

$$a_y = 0.1750 \text{ g}$$

$$a_1 = 0.1544 \text{ g}$$

$$K_1 = 0.0265 \text{ g/in.}$$

$$K_2 = 0.00311 \text{ g/in.}$$

The initial period of the structure (from DRAIN) is 1.95 sec. The same period may be recovered from the demand curve as follows:

$$T = \frac{2\pi}{\sqrt{\frac{g \times a_Y}{d_Y}}} = \frac{2\pi}{\sqrt{\frac{386.1 \times 0.175}{6.659}}} \cong 1.95 \text{ sec.}$$

The 5-percent-damped demand spectrum for this example is based on *Provisions* Figure 4.1.2.6 [3.3-15]. Since the initial period is nearly 2.0 seconds, the only pertinent part of the spectrum is the part that is inversely proportional to period. Using a value of S_{DI} of 0.494 (see Sec. 3.2.2.2), the spectral acceleration as a function of period T is $a = 0.494/T$ where a is in terms of the acceleration due to gravity. For higher damping values, the acceleration will be multiplied by the appropriate value from Table 3.2-13 of this example.

At this point the iteration may commence. Assume an initial displacement d_E of 8.5 in. This is the value computed earlier (see Table 3.2-12) from the simplified procedure in the *Provisions*. At this displacement, the acceleration a_E is:

$$a_E = a_I + K_2 d_E = 0.1544 + 0.00311(8.5) = 0.1808 \text{ g.}$$

At this acceleration and displacement, the equivalent damping is:

$$\xi_E = 5 + \frac{63.7(a_Y d_E - d_Y a_E)}{a_E d_E} = 5 + \frac{63.7(0.175 \times 8.5 - 6.592 \times 0.1808)}{0.1808 \times 8.5} = 17.2\% \text{ critical.}$$

The updated secant period of vibration is:

$$T = \frac{2\pi}{\sqrt{\frac{g \times a_E}{d_E}}} = \frac{2\pi}{\sqrt{\frac{386.4 \times 0.1808}{8.5}}} = 2.19 \text{ sec.}$$

From Table 3.2-13 (or Figure 3.2-37), the damping modification factor for $\xi_E = 17.2$ percent is 0.71. Therefore, the updated acceleration is:

$$a_E^{new} = 0.71(0.494) / 2.19 = 0.160 \text{ g.}$$

Using this acceleration, the updated displacement for the next iteration is:

$$d_E^{new} = \frac{g \times a_E^{new}}{[2\pi / T_E]^2} = \frac{386.4 \times 0.160}{[2\pi / 2.19]^2} = 7.52 \text{ in.}$$

The complete iteration is summarized in Table 3.2-14, where the final displacement from the iteration is 7.82 in. This must be multiplied by the modal participation factor, 1.308, to obtain the actual roof displacement. This value is $7.82(1.308) = 10.2$ in. and is somewhat greater than the value of 8.5 in. predicted from the simplified method of the *Provisions*.

This example converged even though some of the accelerations from the demand spectrum were less than the yield value in the development of the capacity spectrum (e.g., 0.161 in iteration 1 is less than 0.175). This particular example predicts displacements very close to the yield displacement d_Y ; consequently, there may be some influence of the choice of a_Y and d_Y on the computed displacement.

Table 3.2-14 Results of Iteration for Maximum Expected Displacement

Iteration	a^* (g)	d_E (in.)	a_E (g)	Damping (%)	Damping Mod. Factor	T_E (sec.)
		8.50	0.181	17.2	0.71	2.19
1	0.161	7.52	0.178	11.8	0.80	2.08
2	0.189	8.01	0.179	14.7	0.75	2.14
3	0.173	7.70	0.179	12.9	0.78	2.10
4	0.183	7.88	0.179	14.0	0.76	2.12
5	0.176	7.77	0.179	13.4	0.77	2.12
6	0.180	7.84	0.179	13.7	0.76	2.12
7	0.178	7.80	0.179	13.5	0.77	2.11
8	0.179	7.82	0.179	13.6	0.76	2.11
9	0.178	7.81	0.179	13.6	0.76	2.11
10	0.179	7.82	0.179	13.6	0.76	2.11

Note: a^* is from demand spectrum at period T_E .

In the direct approach, a family of demand spectra are plotted together with the capacity spectrum and the desired displacement is found graphically. The steps in the procedure are as follows:

- D-1. Develop a bilinear capacity spectrum for the structure.
- D-2. Find the points on the capacity spectrum that represent 5, 10, 15, 20, 25, and 30 percent damping.
- D-3. Draw a series of secant stiffness lines, one for each damping value listed above.
- D-4. Develop demand spectra for damping values of 5, 10, 15, 20, 25, and 30 percent of critical.
- D-5. Draw the demand spectra on the same plot as the capacity spectrum.
- D-6. Find the points where the secant stiffness lines (from Step 3) for each damping value cross the demand spectrum line for the same damping value.
- D-7. Draw a curve connecting the points found in Step 6.
- D-8. Find the point where the curve from Step 7 intersects the capacity spectrum. This is the target displacement, but it is still in SDOF spectrum space.
- D-9. Convert the target displacement to structural space.

This procedure is now illustrated for the strong panel structure subjected to the modal load pattern. For this example, P-delta effects are excluded.

1. The original pushover curve for this structure is shown in Figure 3.2-23. The effective mass in the first mode is 0.826 times the total mass, and the first mode participation factor is 1.308. The first mode displacement at the roof of the building is 1.0. Half of the dead weight of the structure was used in the conversion because the pushover curve represents the response of one of the two frames. The resulting capacity curve and its bilinear equivalent are shown in Figure 3.2-38. For this example, the yield displacement (d_y) is taken as 6.59 in. and the corresponding yield strength (a_y) is 0.175g. The secant stiffness through the yield point is 0.0263g/in. or 10.2 (rad/sec)². Note that the secant stiffness through this point is mathematically equivalent to the circular frequency squared of the structure; therefore, the frequency is 3.19 rad/sec and the period is 1.96 seconds. This period, as required, is the same as that obtained from DRAIN. (The main purpose of computing the period from the initial stiffness of the capacity spectrum is to perform an intermediate check on the analysis.)
- 2-3. The points on the capacity curve representing β_{eff} values of 5, 10, 15, 20, 25, and 30 percent critical damping are shown in Table 3.2-15. The points are also shown as small diamonds on the capacity spectrum of Figure 3.2-39. The secant lines through the points are also shown.

Table 3.2-15 Points on Capacity Spectrum Corresponding to Chosen Damping Values

Effective Damping (% critical)	Displacement d_{pi} (in.)	Spectral Acceleration a_{pi} (g)
5	6.59	0.175
10	7.25	0.177
15	8.07	0.180
20	9.15	0.183
25	10.7	0.188
30	13.1	0.195

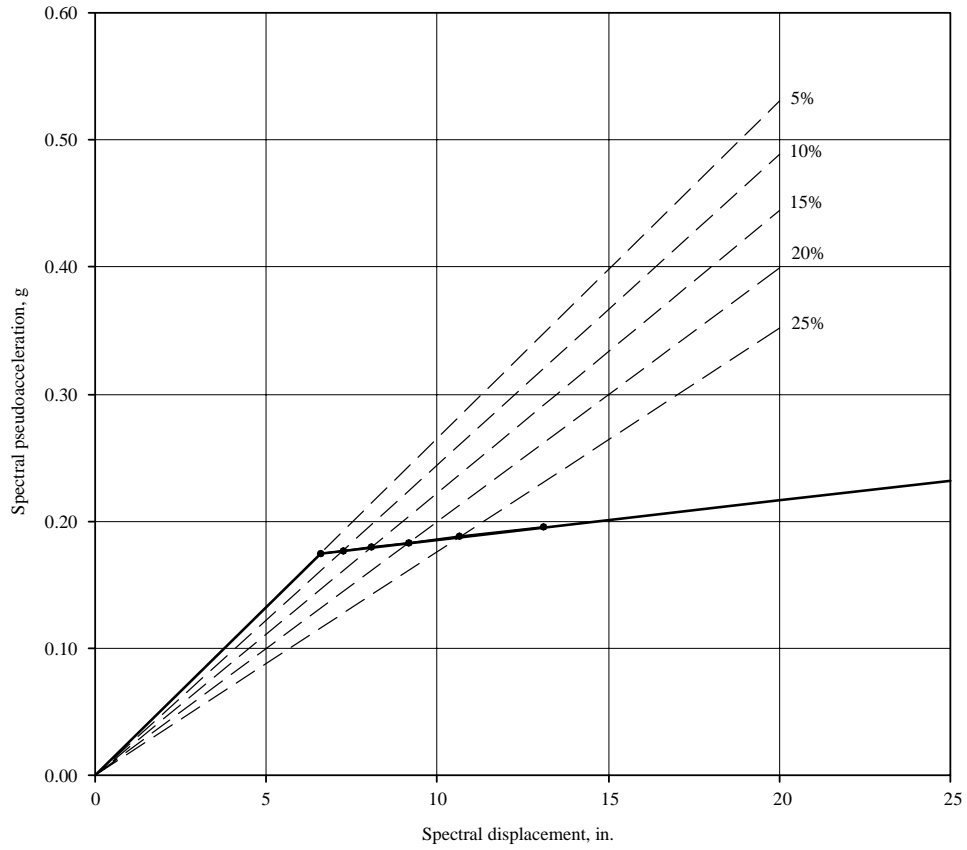


Figure 3.2-39 Capacity spectrum with equivalent viscous damping points and secant stiffnesses.

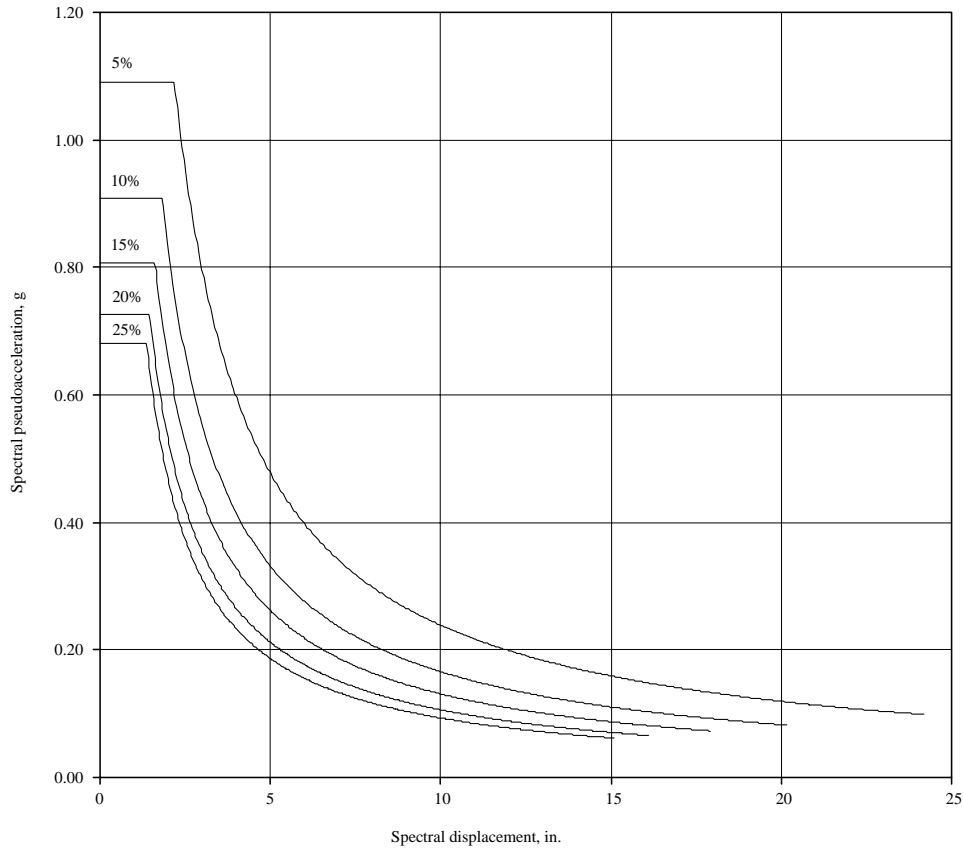


Figure 3.2-40 Demand spectra for several equivalent viscous damping values.

- 4-5. The demand spectra are based on the short period and 1-second period accelerations obtained in Sec. 3.2.2.2e. These values are $S_{DS} = 1.09$ and $S_{DI} = 0.494$. Plots for these spectra are shown individually in Figure 3.2-37. The damping modification factors used to obtain the curves were taken directly or by interpolation from Table 3.2-13. The demand spectra are shown on the same plot as the capacity spectrum in Figure 3.2-41.
- 6-8. The final steps of the analysis are facilitated by Figure 3.2-42, which is a close-up of the relevant portion of Figure 3.2-41. The expected inelastic roof displacement, still in spectral space, is approximately 7.8 in. This is the same as that found from the iterative solution.
9. The expected inelastic roof displacement for the actual structure is 1.308(7.8) or 10.2 in. This is 20 percent greater than the value of 8.5 in. obtained from the first mode elastic response-spectrum analysis.

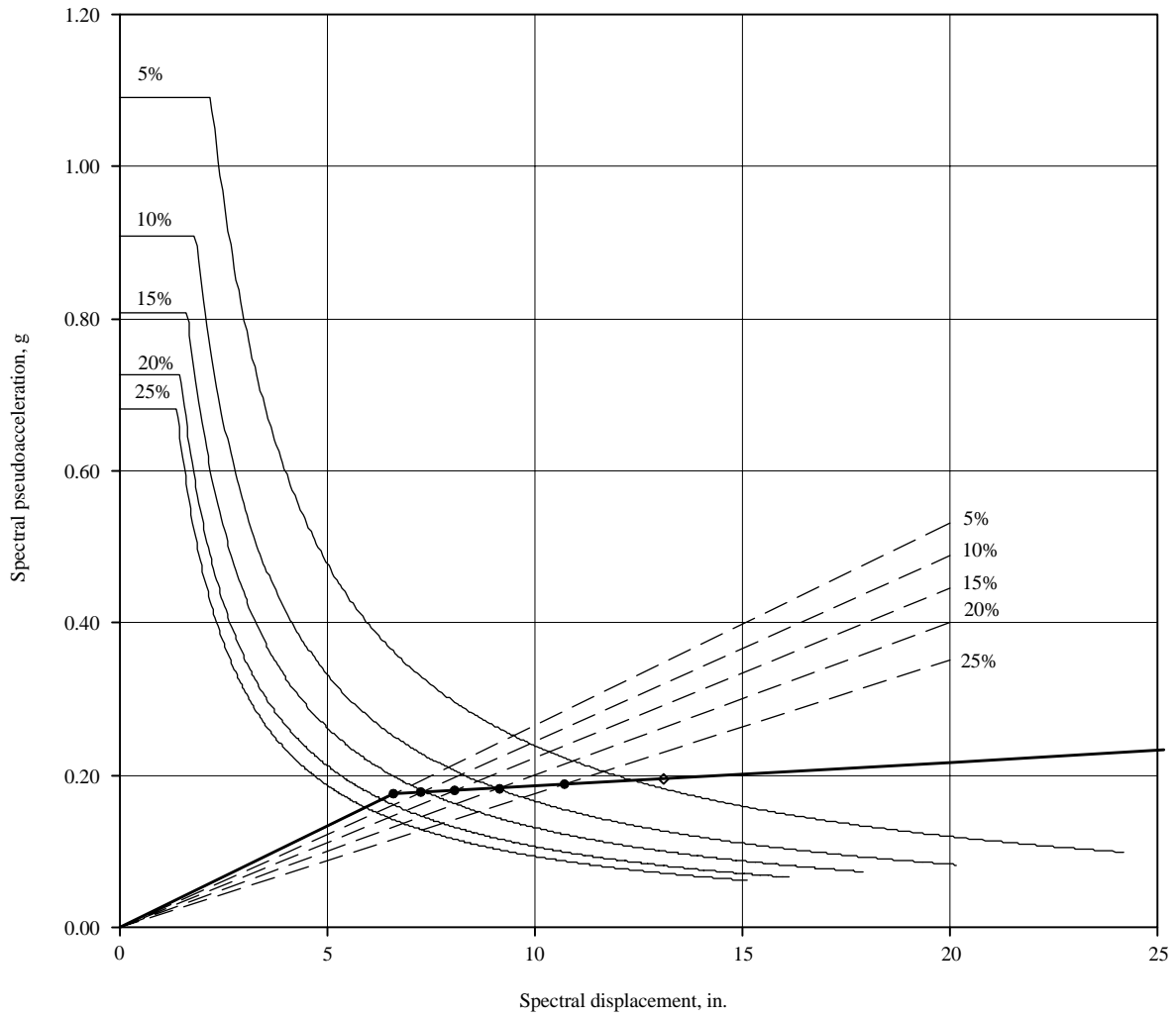


Figure 3.2-41 Capacity and demand spectra on single plot.

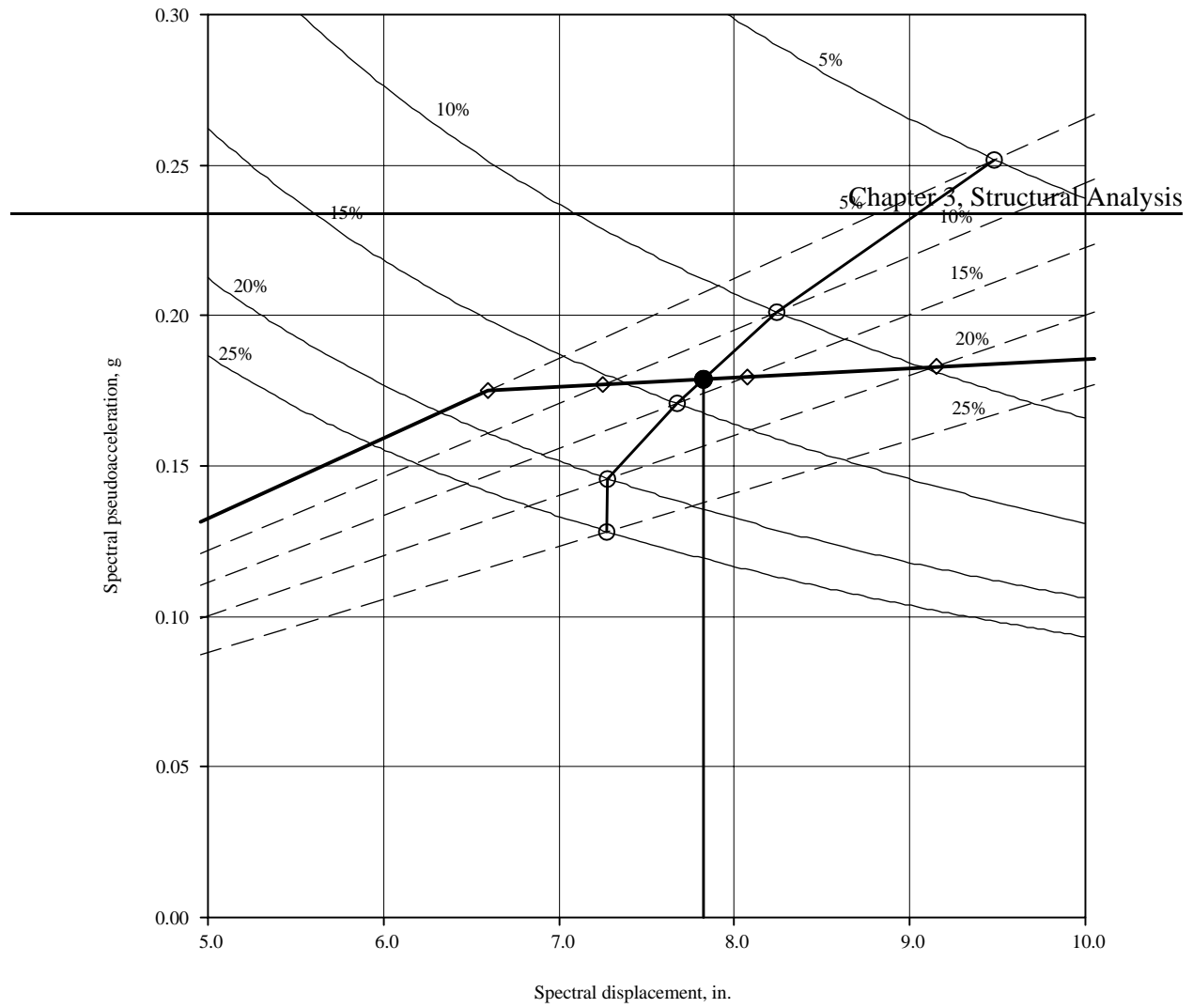


Figure 3.2-42 Close-up view of portion of capacity and demand spectra.

Results for all the strong and weak panel structures under modal load are summarized in Table 3.2-16. All drifts and rotations are consistent with the expected inelastic roof displacement shown at the top of the table.

Table 3.2-16 Summary of Results from Pushover Analysis

Computed Quantity	Strong Panel w/o P-Delta	Strong Panel with P-Delta	Weak Panel w/o P-Delta	Weak Panel with P-Delta
Expected Inelastic Disp. (in.)	10.2	10.3	10.2	10.4
Base Shear Demand (kips)	1125	1031	1033	953
6 th Story Drift (in.)	0.81	0.78	0.87	0.84
5 th Story Drift (in.)	1.35	1.31	1.55	1.45
4 th Story Drift (in.)	1.82	1.81	1.96	2.00
3 rd Story Drift (in.)	2.19	2.23	2.21	2.29
2 nd Story Drift (in.)	2.20	2.27	2.06	2.14
1 st Story Drift (in.)	1.83	1.90	1.64	1.68
Max beam plastic hinge rot. (rad)	0.00522	0.00564	0.00511	0.00524
Max column plastic hinge rot. (rad)	0.0	0.0	0.0	0.0
Max panel zone hinge rot. (rad)	0.0	0.0	0.00421	0.00437

3.2.5.4 Summary and Observations from Pushover Analysis

1. The simplified approach from the *Provisions* predicts maximum expected displacements about 8 to 10 percent lower than the much more complicated capacity spectrum method. Conclusions cannot be drawn from this comparison, however, as only one structure has been analyzed.
2. P-delta effects had a small but significant effect on the response of the system. In particular, base shears for the structure with P-delta effects included were about 8 percent lower than for the structure without P-delta effects. If the maximum expected displacement was larger, the differences between response with and without P-delta effects would have been much more significant.
3. The inelastic deformation demands in the hinging regions of the beams and in the panel zones of the beam-column joints were small and are certainly within acceptable limits. The small inelastic deformations are attributed to the considerable overstrength provided when preliminary member sizes were adjusted to satisfy story drift limits.
4. The structure without panel zone reinforcement appears to perform as well as the structure with such reinforcement. This is again attributed to the overstrength provided.

3.2.6 Time-History Analysis

Because of the many assumptions and uncertainties inherent in the capacity spectrum method, it is reasonable to consider the use of time-history analysis for the computation of global and local deformation demands. A time-history analysis, while by no means perfect, does eliminate two of the main problems with static pushover analysis: selection of the appropriate lateral load pattern and use of equivalent linear

viscous damping in the demand spectrum to represent inelastic hysteretic energy dissipation. However, time-history analysis does introduce its own problems, most particularly selection and scaling of ground motions, choice of hysteretic model, and inclusion of inherent (viscous) damping.

The time-history analysis of Example 2 is used to estimate the deformation demands for the structure shown in Figures 3.2-1 and 3.2-2. The analysis, conducted only for the structure with panel zone reinforcement, is carried out for a suite of three ground motions specifically prepared for the site. Analyses included and excluded P-delta effects.

3.2.6.1 Modeling and Analysis Procedure

The DRAIN-2Dx program was used for each of the time-history analyses. The structural model was identical to that used in the static pushover analysis. Second order effects were included through the use of the outrigger element shown to the right of the actual frame in Figure 3.2-4.

Inelastic hysteretic behavior was represented through the use of a bilinear model. This model exhibits neither a loss of stiffness nor a loss of strength and, for this reason, it will generally have the effect of overestimating the hysteretic energy dissipation in the yielding elements. Fortunately, the error produced by such a model will not be of great concern for this structure because the hysteretic behavior of panel zones and flexural plastic hinges should be very robust for this structure when inelastic rotations are less than about 0.02 radians. (Previous analysis has indicated a low likelihood of rotations significantly greater than 0.02 radians.) At inelastic rotations greater than 0.02 radians it is possible for local inelastic buckling to reduce the apparent strength and stiffness.

Rayleigh proportional damping was used to represent viscous energy dissipation in the structure. The mass and stiffness proportional damping factors were set to produce 5 percent damping in the first and third modes. This was done primarily for consistency with the pushover analysis, which use a baseline damping of 5 percent of critical. Some analysts would use a lower damping, say 2.5 percent, to compensate for the fact that bilinear hysteretic models tend to overestimate energy dissipation in plastic hinges.

In Rayleigh proportional damping, the damping matrix (D) is a linear combination of the mass matrix M and the initial stiffness matrix K :

$$D = \alpha M + \beta K$$

where α and β are mass and stiffness proportionality factors, respectively. If the first and third mode frequencies, ω_1 and ω_3 , are known, the proportionality factors may be computed from the following expression:⁹

$$\begin{Bmatrix} \alpha \\ \beta \end{Bmatrix} = \frac{2\xi}{\omega_1 + \omega_3} \begin{Bmatrix} \omega_1 \omega_3 \\ 1 \end{Bmatrix}$$

⁹See Ray W. Clough and Joseph Penzien, *Dynamics of Structures*, 2nd Edition.

Note that α and β are directly proportional to ζ . To increase ζ from 5 percent to 10 percent of critical requires only that α and β be increased by a factor of 2.0. The structural frequencies and damping proportionality factors are shown in Table 3.2-17 for the models analyzed by the time-history method.

Table 3.2-17 Structural Frequencies and Damping Factors Used in Time-History Analysis.
(Damping Factors that Produce 5 Percent Damping in Modes 1 and 3)

Model/Damping Parameters	ω_1 (Hz.)	ω_3 (Hz.)	α	β
Strong Panel with P-Delta	3.118	18.65	0.267	0.00459
Strong Panel without P-Delta	3.223	18.92	0.275	0.00451

It is very important to note that the stiffness proportional damping factor must *not* be included in the Type-4 elements used to represent rotational plastic hinges in the structure. These hinges, particularly those in the girders, have a very high initial stiffness. Before the hinge yields there is virtually no rotational velocity in the hinge. After yielding, the rotational velocity is significant. If a stiffness proportional damping factor is used for the hinge, a viscous moment will develop in the hinge. This artificial viscous moment – the product of the rotational velocity, the initial rotational stiffness of the hinge, and the stiffness proportional damping factor – can be quite large. In fact, the viscous moment may even exceed the intended plastic capacity of the hinge. These viscous moments occur in phase with the plastic rotation; hence, the plastic moment and the viscous moments are additive. These large moments transfer to the rest of the structure, effecting the sequence of hinging in the rest of the structure, and produce artificially high base shears. The use of stiffness proportional damping in discrete plastic hinges can produce a totally inaccurate analysis result.

The structure was subjected to dead load and full reduced live load, followed by ground acceleration. The incremental differential equations of motion were solved in a step-by-step manner using the Newmark constant average acceleration approach. Time steps and other integration parameters were carefully controlled to minimize errors. The minimum time step used for analysis was 0.00025 seconds. Later analyses used time steps as large as 0.001 seconds.

3.2.6.2 Development of Ground Motion Records

The ground motion time histories used in the analysis were developed specifically for the site. Basic information for the records was shown previously in Table 3.1-20 and is repeated as Table 3.2-18.

Table 3.2-18 Seattle Ground Motion Parameters (Unscaled)

Record Name	Orientation	Number of Points and Time Increment	Peak Ground Acceleration (g)	Source Motion
Record A00	N-S	8192 @ 0.005 seconds	0.443	Lucern (Landers)
Record A90	E-W	8192 @ 0.005 seconds	0.454	Lucern (Landers)
Record B00	N-S	4096 @ 0.005 seconds	0.460	USC Lick (Loma Prieta)
Record B90	E-W	4096 @ 0.005 seconds	0.435	USC Lick (Loma Prieta)
Record C00	N-S	1024 @ 0.02 seconds	0.460	Dayhook (Tabas, Iran)
Record C90	E-W	1024 @ 0.02 seconds	0.407	Dayhook (Tabas, Iran)

Time histories and 5-percent-damped response spectra for each of the motions are shown in Figures 3.2-43 through 3.2-45.

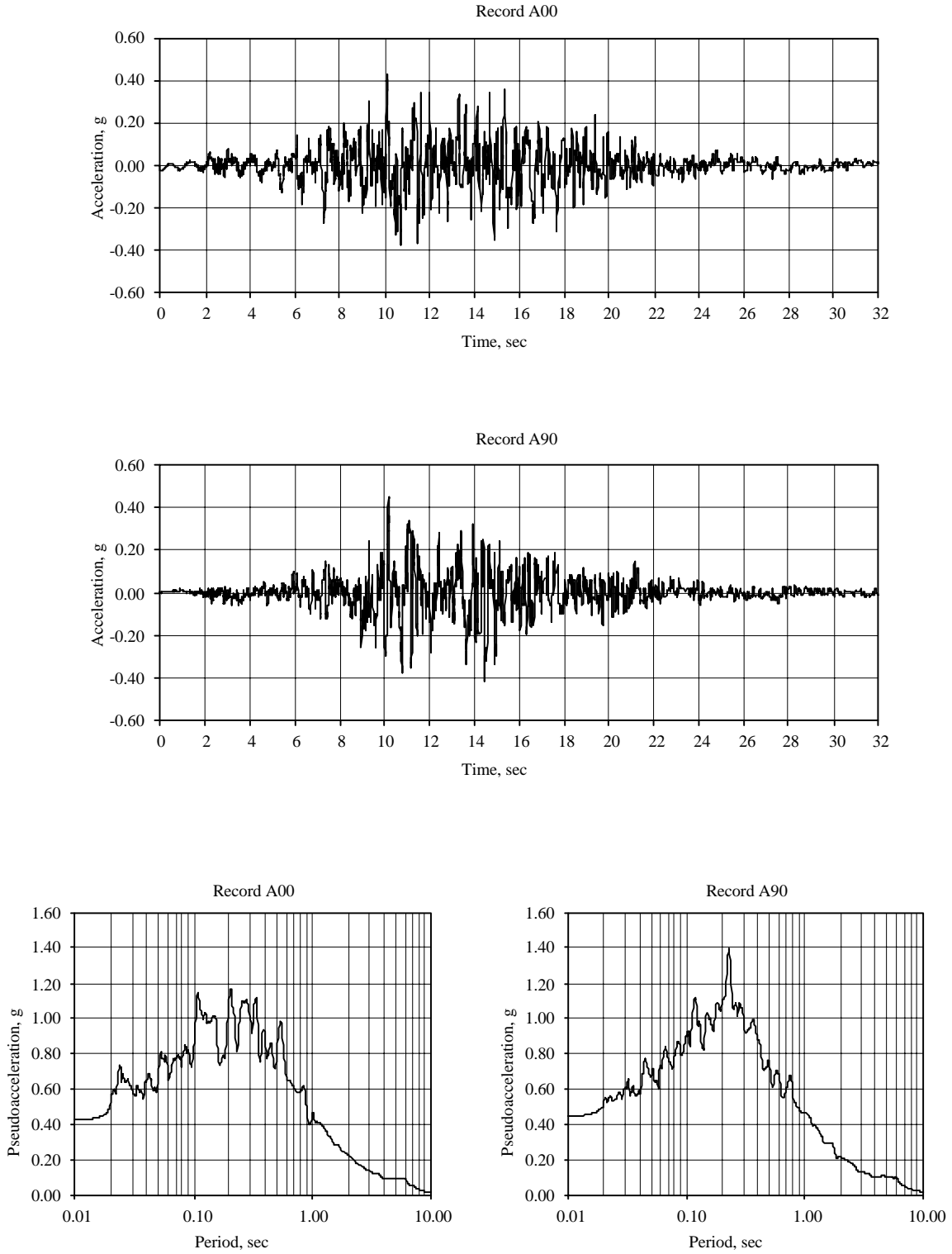


Figure 3.2-43 Time histories and response spectra for Record A.

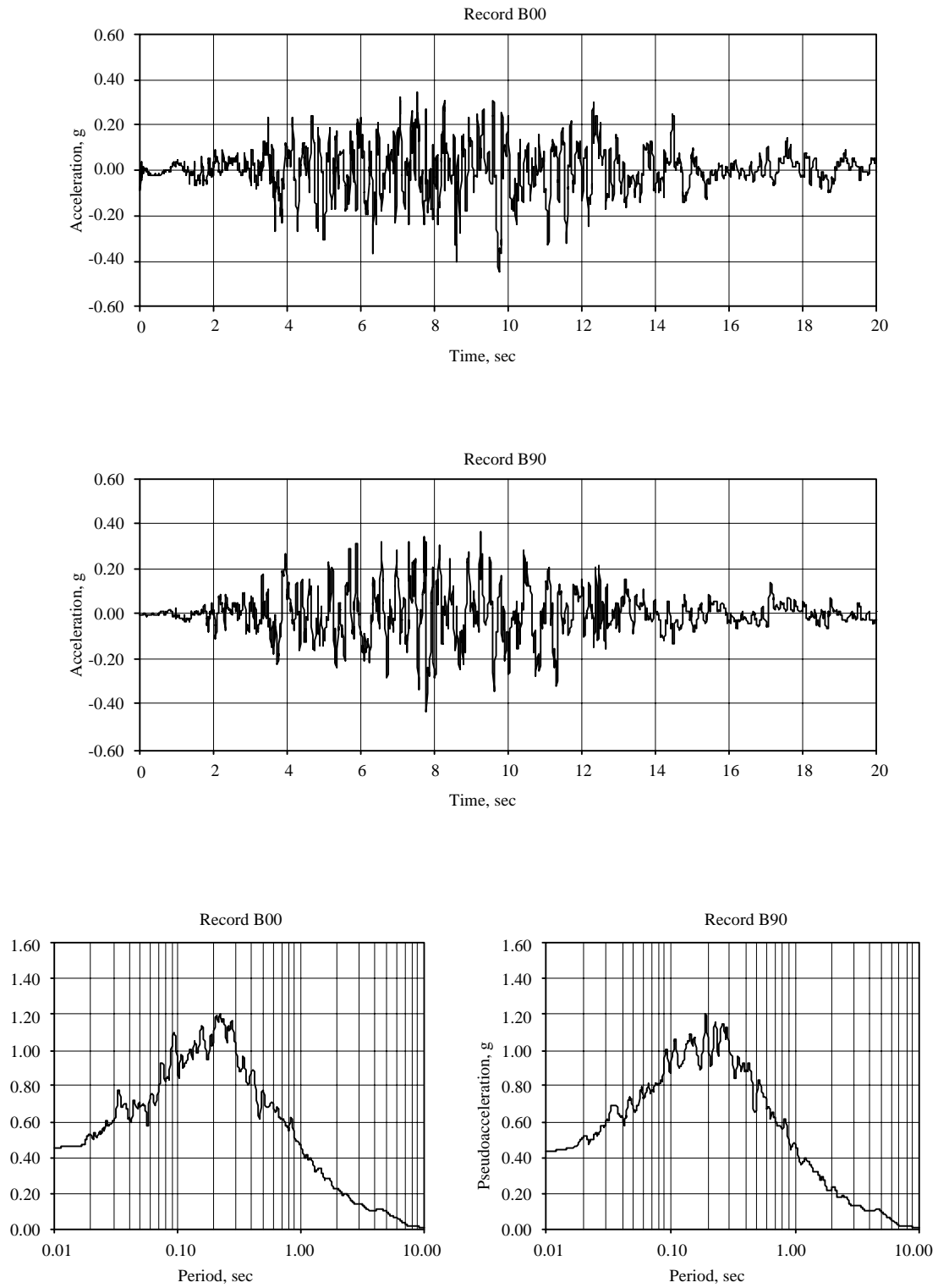


Figure 3.2-44 Time histories and response spectra for Record B.

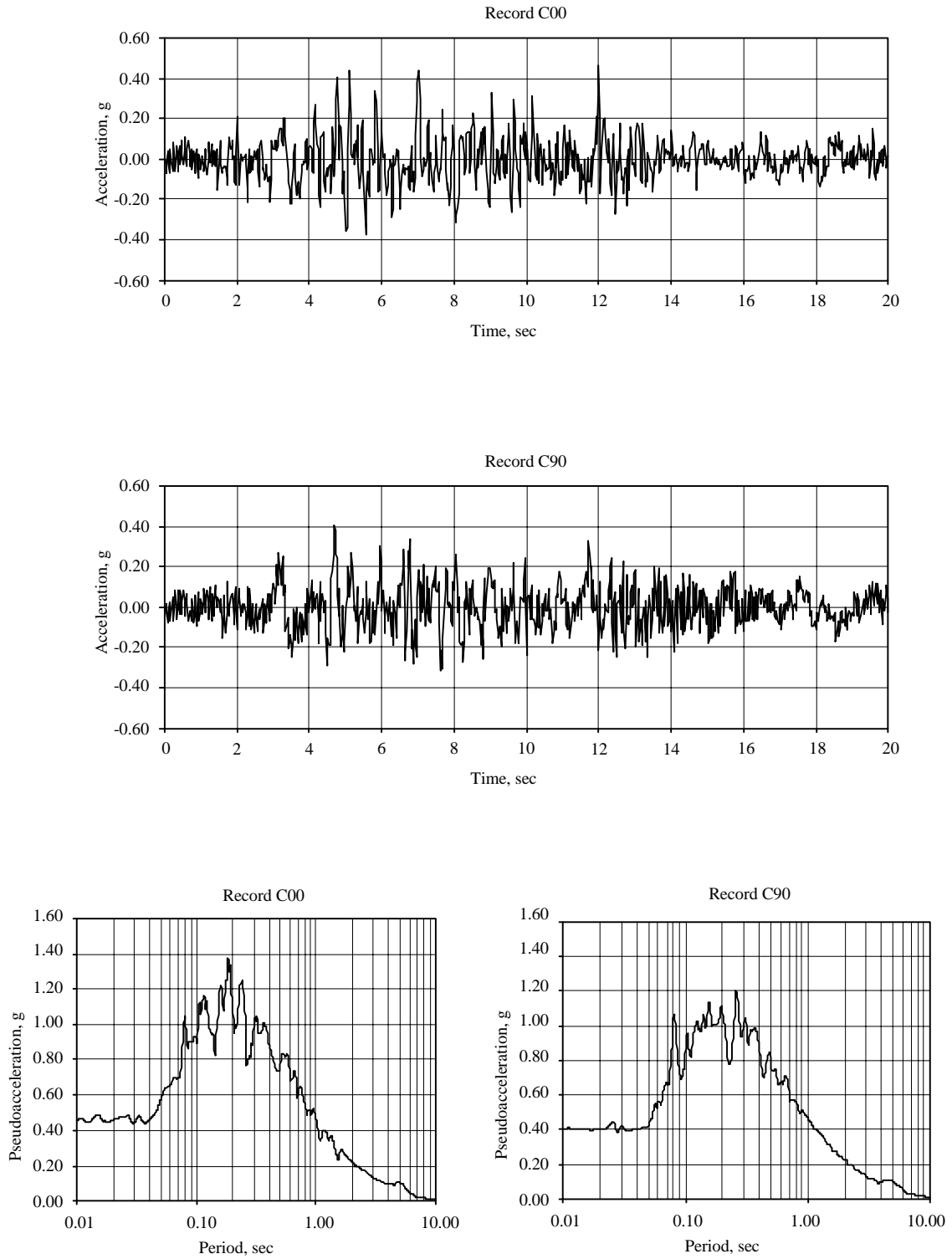


Figure 3.2-45 Time histories and response spectra for Record C.

Because only a two-dimensional analysis of the structure is performed using DRAIN, only a single component of ground motion is applied at one time. For the analyses reported herein, only the N-S (00) records of each ground motion were utilized. A complete analysis would require consideration of both sets of ground motions.

When analyzing structures in two dimensions, *Provisions* Sec. 5.6.2.1 [5.4.2.1] gives the following instructions for scaling:

1. For each pair of motions:
 - a. Assume an initial scale factor for each motion pair (for example, S_A for ground motion A00).
 - b. Compute the 5-percent-damped elastic response spectrum for each component in the pair.
2. Adjust scale factors S_A , S_B , and S_C such that the average of the scaled response spectra over the period range $0.2T_1$ to $1.5 T_1$ is not less than the 5-percent-damped spectrum determined in accordance with *Provisions* Sec. 4.1.3. T_1 is the fundamental mode period of vibration of the structure.

As with the three-dimensional time-history analysis for the first example in this chapter, it will be assumed that the scale factors for the three earthquakes are to be the same. If a scale factor of 1.51 is used, Figure 3.2-46 indicates that the criteria specified by the *Provisions* have been met for all periods in the range $0.2(2.00) = 0.40$ sec to $1.5(2.00) = 3.0$ seconds.¹⁰ The scale factor of 1.51 is probably conservative because it is controlled by the period at 0.47 seconds, which will clearly be in the higher modes of response of the structure. If the *Provisions* had called for a cutoff of $0.25T$ instead of the (somewhat arbitrary) value of $0.2T$, the required scale factor would be reduced to 1.26.

3.2.6.3 Results of Time-History Analysis

Time-history analyses were performed for the structure subjected to the first 20 seconds of the three different ground motions described earlier. The 20-second cutoff was based on a series of preliminary analyses that used the full duration.

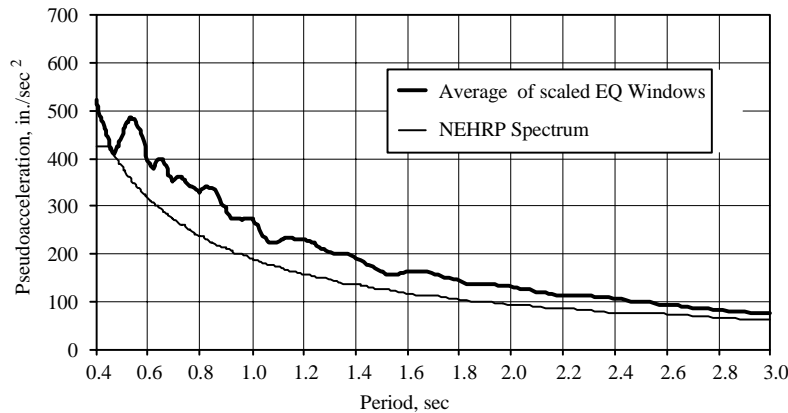
The following parameters were varied to determine the sensitivity of the response to the particular variation:

1. Analysis was run with and without P-delta effects for all three ground motions.
2. Analysis was run with 2.5, 5, 10, and 20 percent damping (Ground Motion A00, including P-delta effects). These analyses were performed to assess the potential benefit of added viscous fluid damping devices.

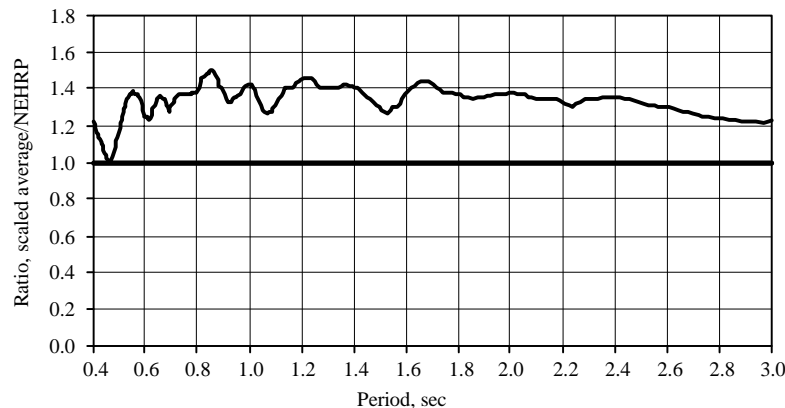
3.2.6.3.1 Response of Structure with 5 Percent of Critical Damping

¹⁰2.00 seconds is approximately the average of the period of the strong panel model with and without P-delta effects. See Table 3.2-12.

The results from the first series of analyses, all run with 5 percent of critical damping, are summarized in Tables 3.2-19 through 3.2-22. Selected time-history traces are shown in Figures 3.2-47 through 3.2-64. Energy time histories are included for each analysis.



(a) Comparison of Average of Scaled Spectra and NEHRP Spectrum (S.F.=1.51)



(b) Ratio of Average of Scaled Spectra to NEHRP Spectrum (S.F.=1.51)

Figure 3.2-46 Ground motion scaling parameters.

The tabulated shears in Tables 3.2-19 and 3.2-21 are for the single frame analyzed and should be doubled to obtain the total shear in the structure. The tables of story shear also provide two values for each ground motion. The first value is the maximum total elastic column story shear, including P-delta effects if applicable. The second value represents the maximum total inertial force for the structure. The inertial base shear, which is not necessarily concurrent with the column shears, was obtained as sum of the products of the total horizontal accelerations and nodal mass of each joint. For a system with no damping, the story shears obtained from the two methods should be identical. For a system with damping, the base shear obtained from column forces generally will be less than the shear from inertial forces because the

viscous component of column shear is not included. Additionally, the force absorbed by the mass proportional component of damping will be lost (as this is not directly recoverable in DRAIN).

The total roof drift and the peak story drifts listed in Tables 3.2-20 and 3.2-22 are peak (envelope) values at each story and are not necessarily concurrent.

Tables 3.2-19 and 3.2-20 summarize the global response of the structure with *excluding* P-delta effects. Time-history traces are shown in Figures 3.2-47 through 3.2-55. Significant yielding occurred in the girders, columns, and panel zone regions for each of the ground motions. Local quantification of such effects is provided later for the structure responding to Ground Motion A00.

Table 3.2-19 Maximum Base Shear (kips) in Frame Analyzed with 5 Percent Damping, Strong Panels, Excluding P-Delta Effects

Level	Motion A00	Motion B00	Motion C00
Column Forces	1559	1567	1636
Inertial Forces	1307	1370	1464

Table 3.2-20 Maximum Story Drifts (in.) from Time-History Analysis with 5 percent Damping, Strong Panels, Excluding P-Delta Effects

Level	Motion A00	Motion B00	Motion C00	Limit
Total Roof	16.7	13.0	11.4	NA
R-6	1.78	1.60	1.82	3.75
6-5	3.15	2.52	2.63	3.75
5-4	3.41	2.67	2.65	3.75
4-3	3.37	2.75	2.33	3.75
3-2	3.98	2.88	2.51	3.75
2-G	4.81	3.04	3.13	4.50

Table 3.2-21 Maximum Base Shear (kips) in Frame Analyzed with 5 Percent Damping, Strong Panels, Including P-Delta Effects

Level	Motion A00	Motion B00	Motion C00
Column Forces	1426	1449	1474
Inertial Forces	1282	1354	1441

Table 3.2-22 Maximum Story Drifts (in.) from Time-History Analysis with 5 Percent Damping, Strong Panels, Including P-Delta Effects

Level	Motion A00	Motion B00	Motion C00	Limit
Total Roof	17.4	14.2	10.9	NA
R-6	1.90	1.59	1.78	3.75
6-5	3.31	2.48	2.61	3.75
5-4	3.48	2.66	2.47	3.75
4-3	3.60	2.89	2.31	3.75
3-2	4.08	3.08	2.78	3.75
2-G	4.84	3.11	3.75	4.50

The peak base shears (for a single frame), taken from the sum of column forces, are very similar for each of the ground motions and range from 1307 kips to 1464 kips. There is, however, a pronounced difference in the recorded peak displacements. For Ground Motion A00 the roof displacement reached a maximum value of 16.7 in., while the peak roof displacement from Ground Motion C00 was only 11.4 in. Similar differences occurred for the first-story displacement. For Ground Motion A00, the maximum story drift was 4.81 in. for Level 1 and 3.98 in. for Levels 2 through 6. The first-story drift of 4.81 in. exceeds the allowable drift of 4.50 in. Recall that the allowable drift includes a factor of 1.25 that is permitted when nonlinear analysis is performed.

As shown in Figure 3.2-47, the larger displacements observed in Ground Motion A00 are due to a permanent inelastic displacement offset that occurs at about 10.5 seconds into the earthquake. The sharp increase in energy at this time is evident in Figure 3.2-49. Responses for the other two ground motions shown in Figures 3.2-50 and 3.2-53 do not have a significant residual displacement. The reason for the differences in response to the three ground motions is not evident from their ground acceleration time-history traces (see Figures 3.2-43 through 3.2-45).

The response of the structure *including* P-delta effects is summarized in Tables 3.2-21 and 3.2-22. Time-history traces are shown in Figures 3.2-56 through 3.2-64. P-delta effects have a significant influence on the response of the structure to each of the ground motions. This is illustrated in Figures 3.2-65 and 3.2-66, which are history traces of roof displacement and base shear, respectively, in response to Ground Motion A00. Responses for analysis with and without P-delta effects are shown in the same figure. The P-delta effect is most evident after the structure has yielded.

Table 3.2-21 summarizes the base shear response and indicates that the maximum base shear from the column forces, 1441 kips, occurs during Ground Motion C00. This shear is somewhat less than the shear of 1464 kips which occurs under the same ground motion when P-delta effects are excluded. A reduction in base shear is to be expected for yielding structures when P-delta effects are included.

Table 3.2-22 shows that inclusion of P-delta effects led to a general increase in displacements with the peak roof displacement of 17.4 in. occurring during ground motion A00. The story drift at the lower level of the structure is 4.84 in. when P-delta effects are included and this exceeds the limit of 4.5 in. The larger drifts recorded during Ground Motion A00 are again associated with residual inelastic deformations. This may be seen clearly in the time-history trace of roof and first-story displacement shown in Figure 3.2-56.

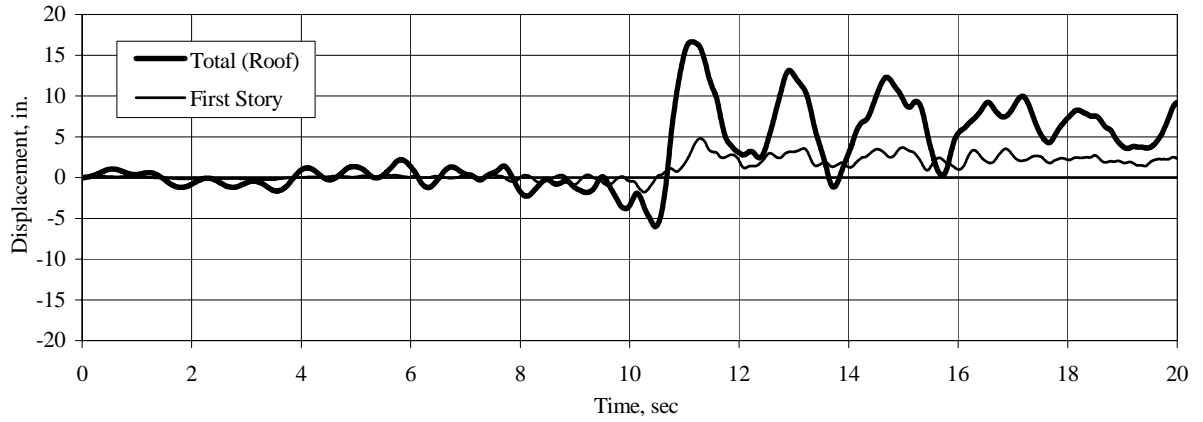


Figure 3.2-47 Time history of roof and first-story displacement, Ground Motion A00, excluding P-delta effects.

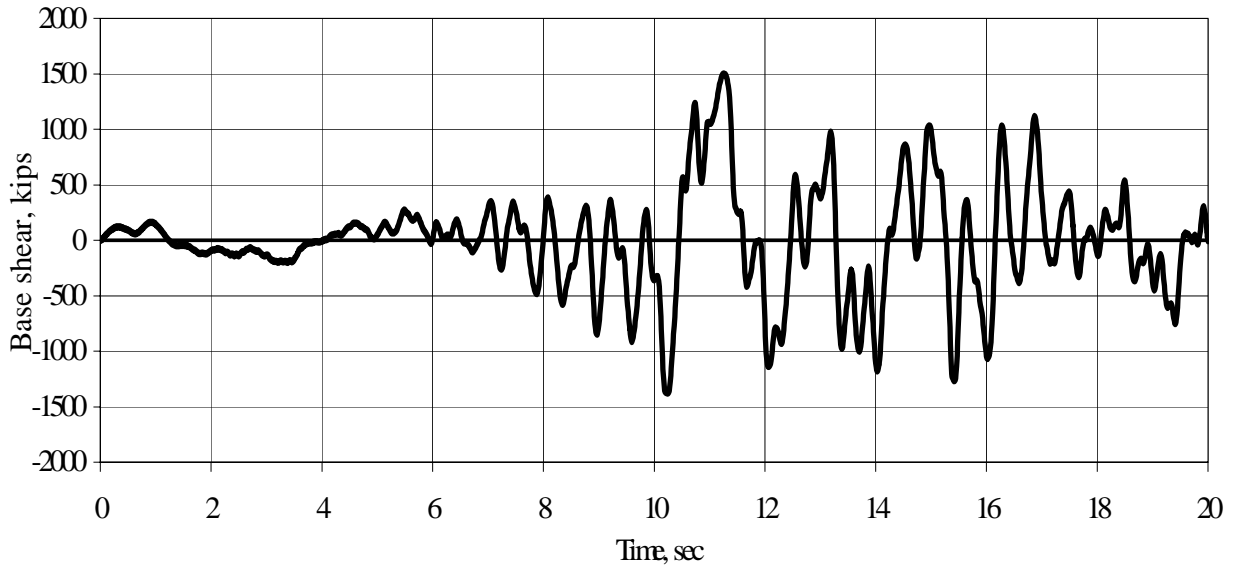


Figure 3.2-48 Time history of total base shear, Ground Motion A00, excluding P-delta effects.

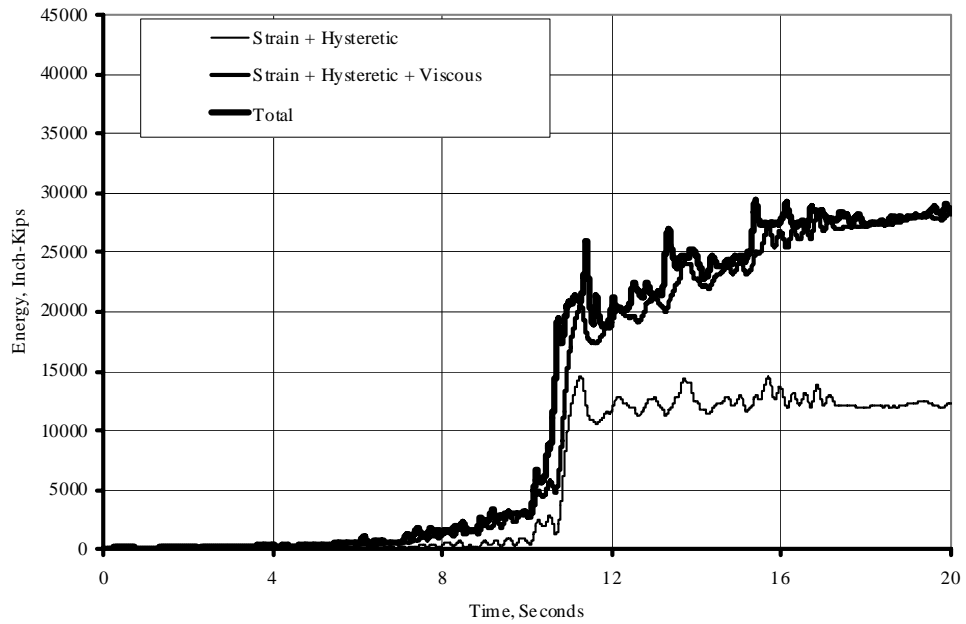


Figure 3.2-49 Energy time history, Ground MotionA00, excluding P-delta effects.

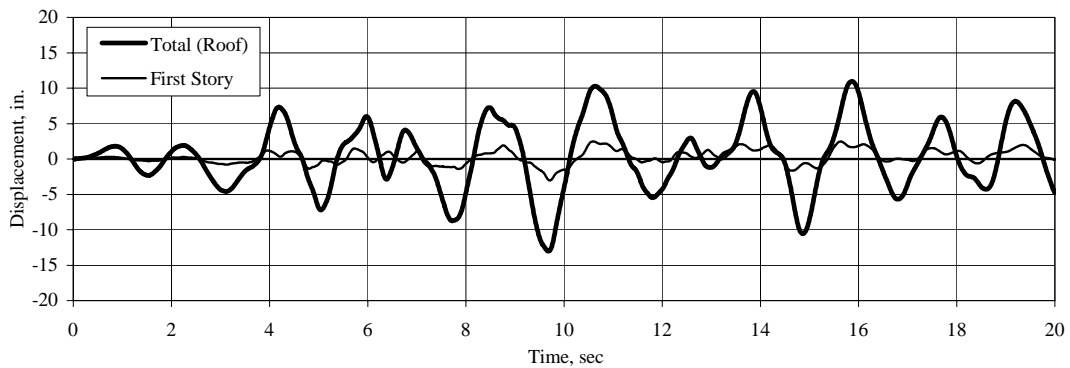


Figure 3.2-50 Time history of roof and first-story displacement. Ground Motion B00, excluding P-delta effects.

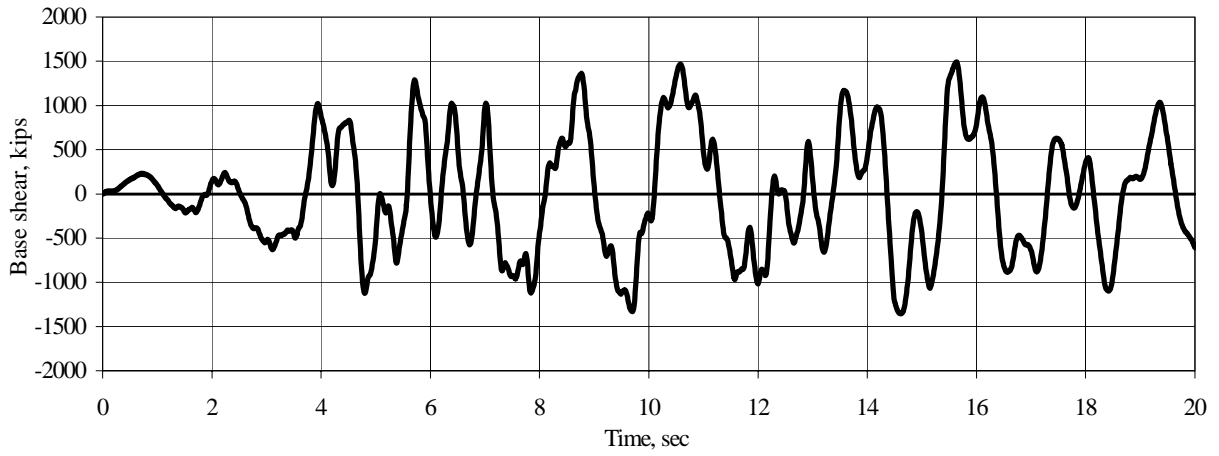


Figure 3.2-51 Time history of total base shear, Ground Motion B00, excluding P-delta effects.

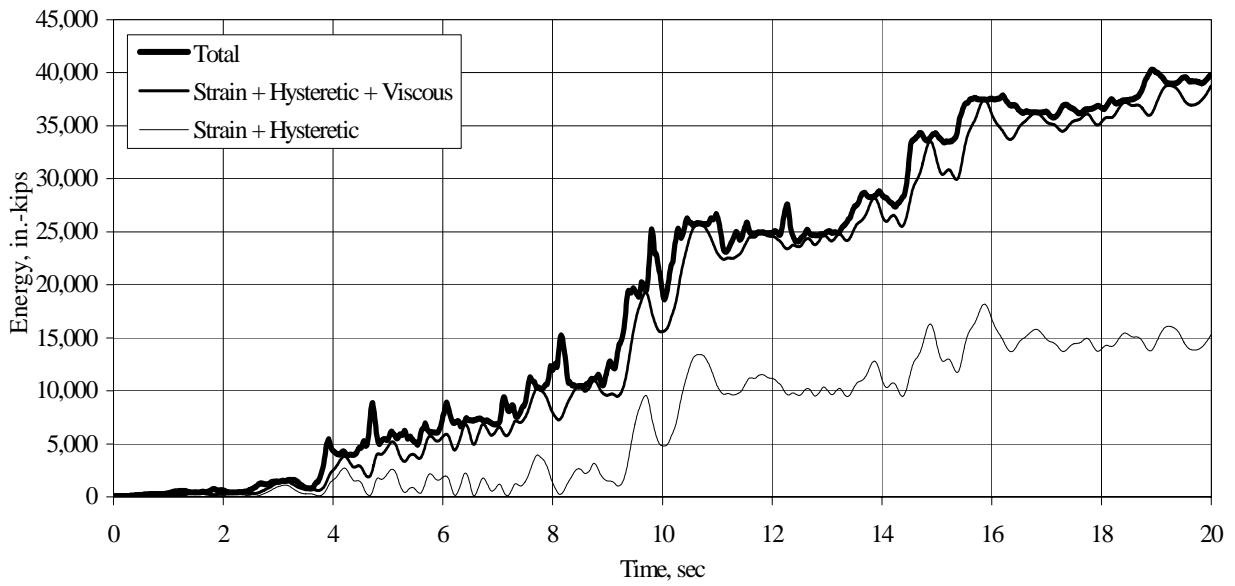


Figure 3.2-52 Energy time history, Ground Motion B00, excluding P-delta effects.

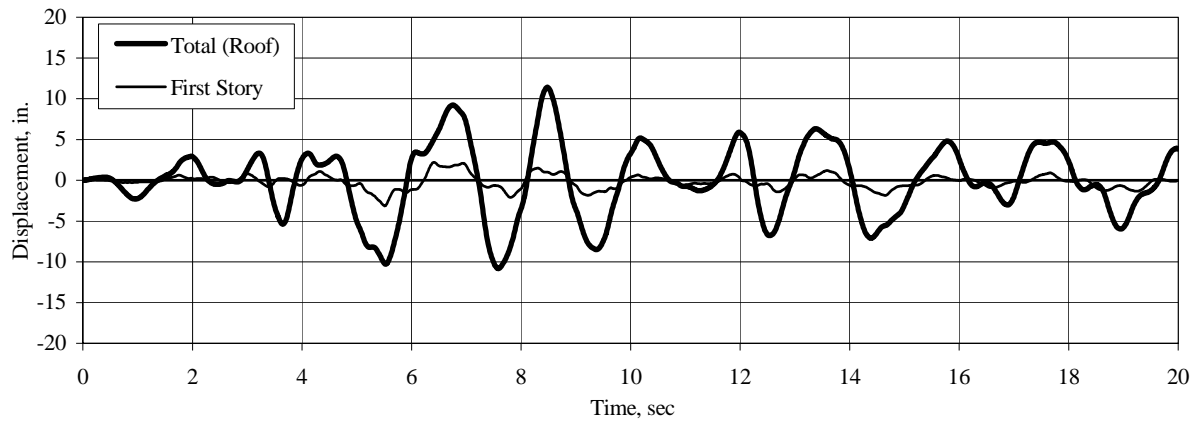


Figure 3.2-53 Time history of roof and first-story displacement, Ground Motion C00, excluding P-delta effects.

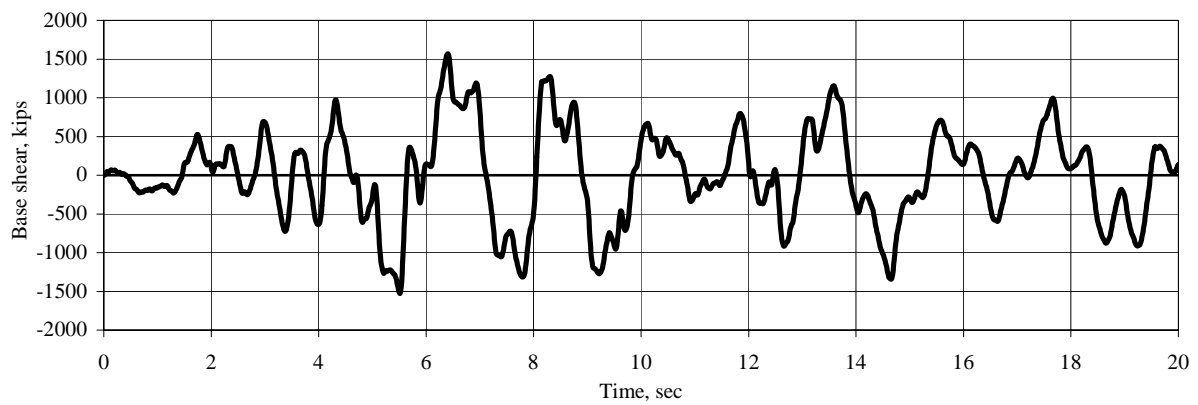


Figure 3.2-54 Time history of total base shear, Ground Motion C00, excluding P-delta effects.

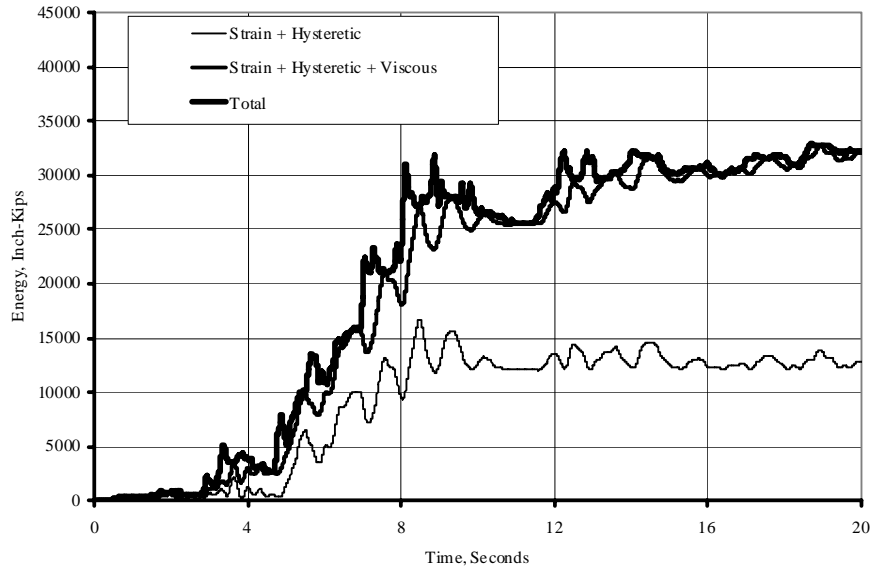


Figure 3.2-55 Energy time history, Ground Motion C00, excluding P-delta effects.

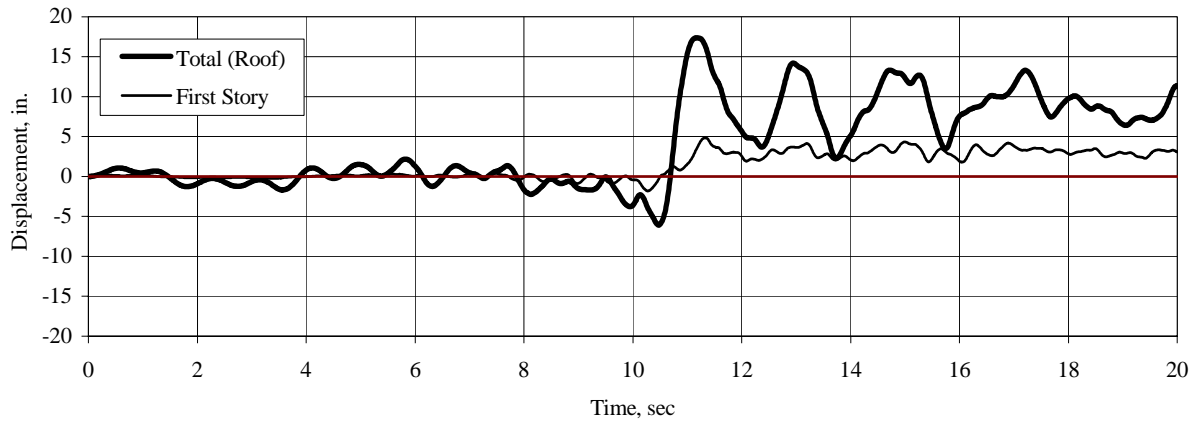


Figure 3.2-56 Time history of roof and first-story displacement, Ground Motion A00, including P-delta effects.

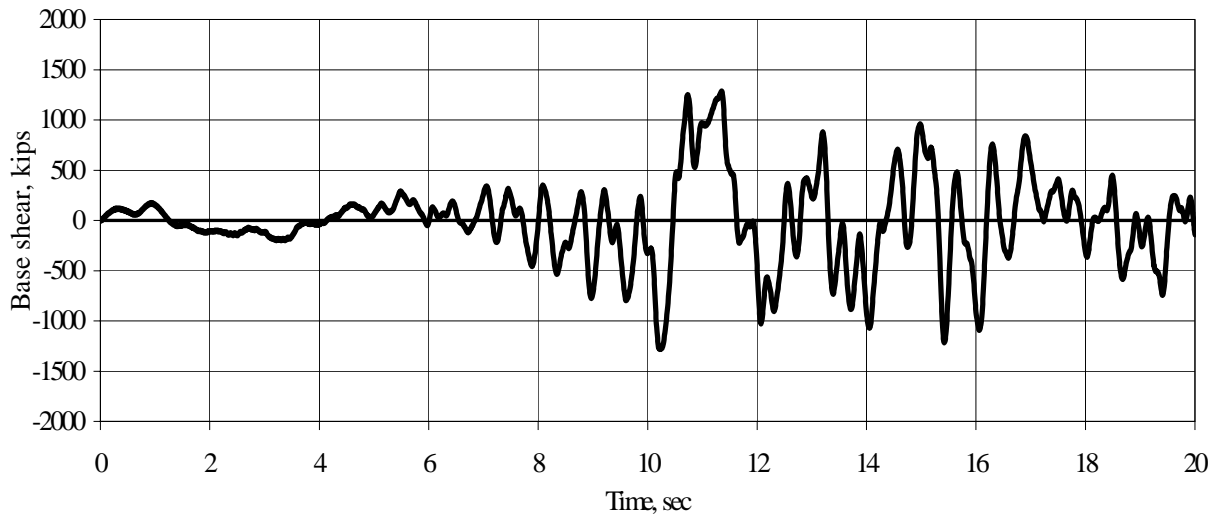


Figure 3.2-57 Time history of total base shear, Ground Motion A00, including P-delta effects.

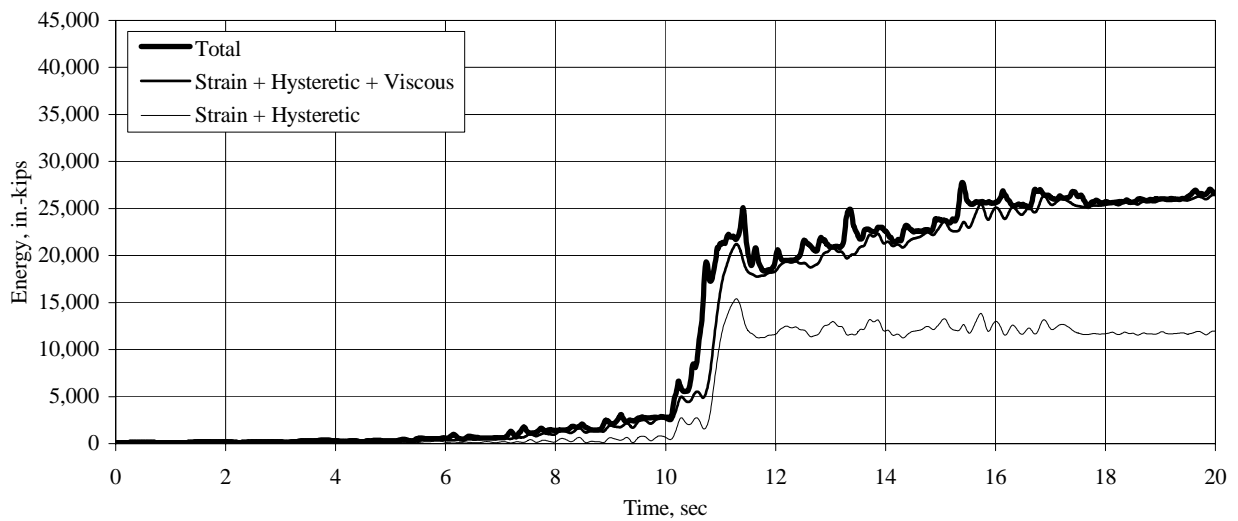


Figure 3.2-58 Energy time history, Ground Motion A00, including P-delta effects.

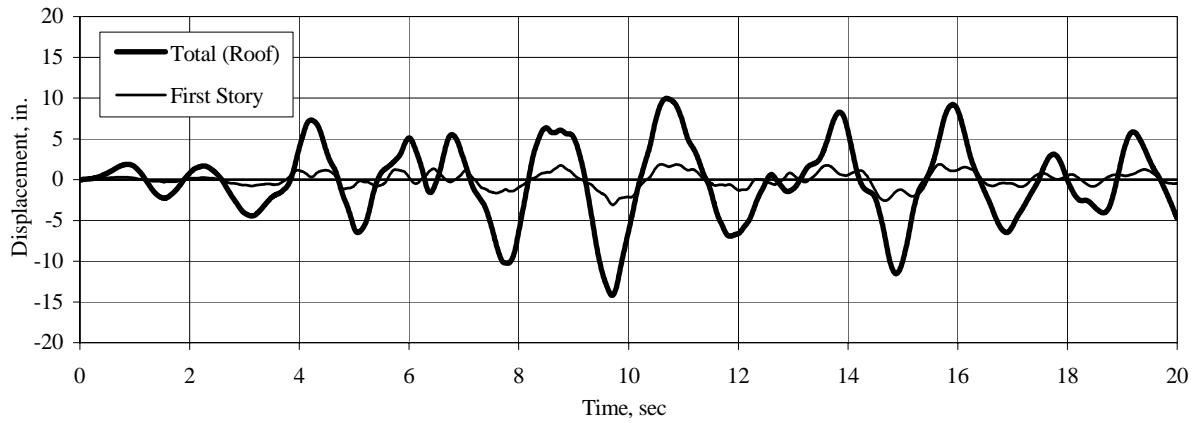


Figure 3.2-59 Time history of roof and first-story displacement, Ground Motion B00, including P-delta effects.

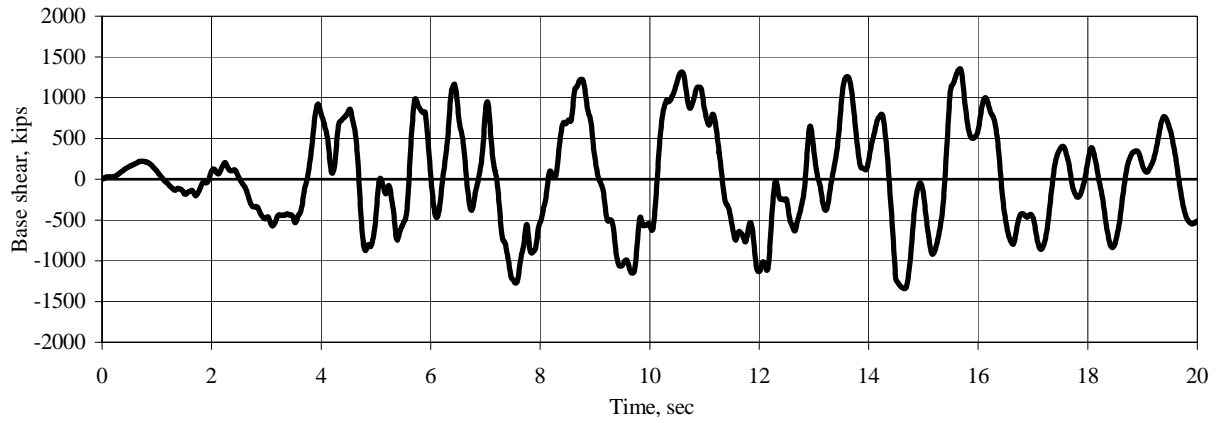


Figure 3.2-60 Time history of total base shear, Ground Motion B00, including P-delta effects.

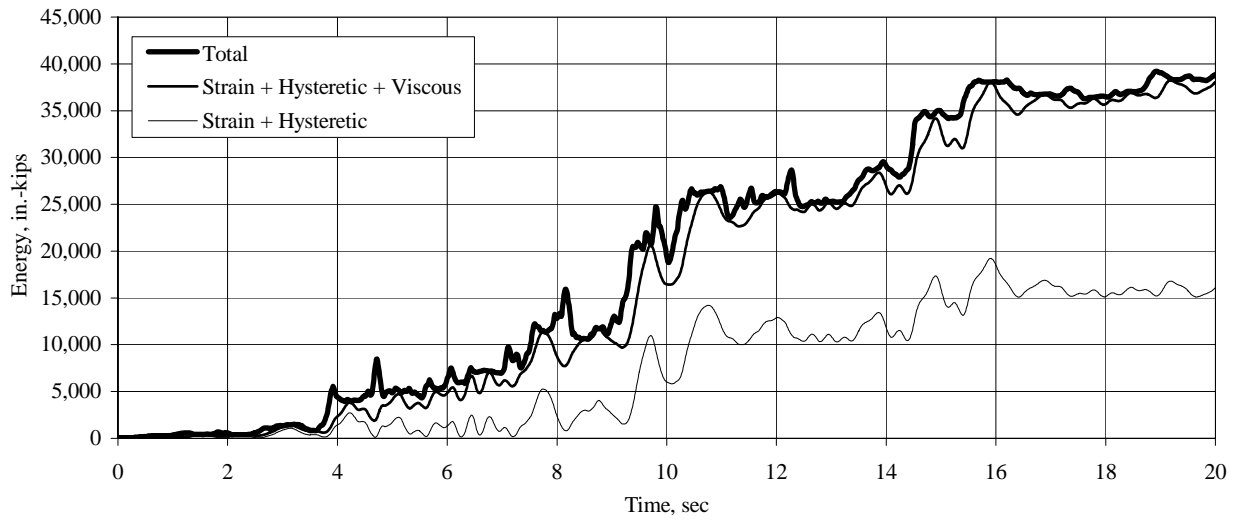


Figure 3.2-61 Energy time history, Ground Motion B00, including P-delta effects.

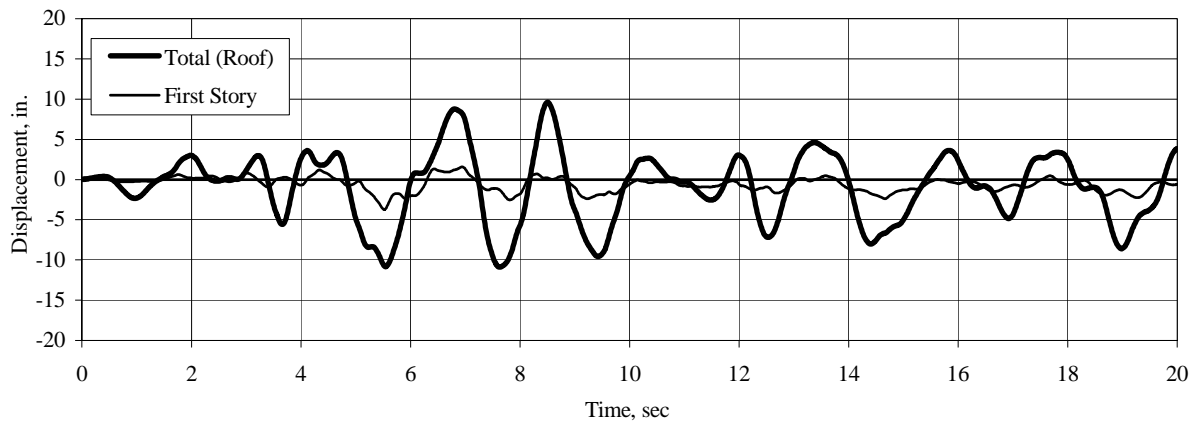


Figure 3.2-62 Time history of roof and first-story displacement, Ground Motion C00, including P-delta effects.

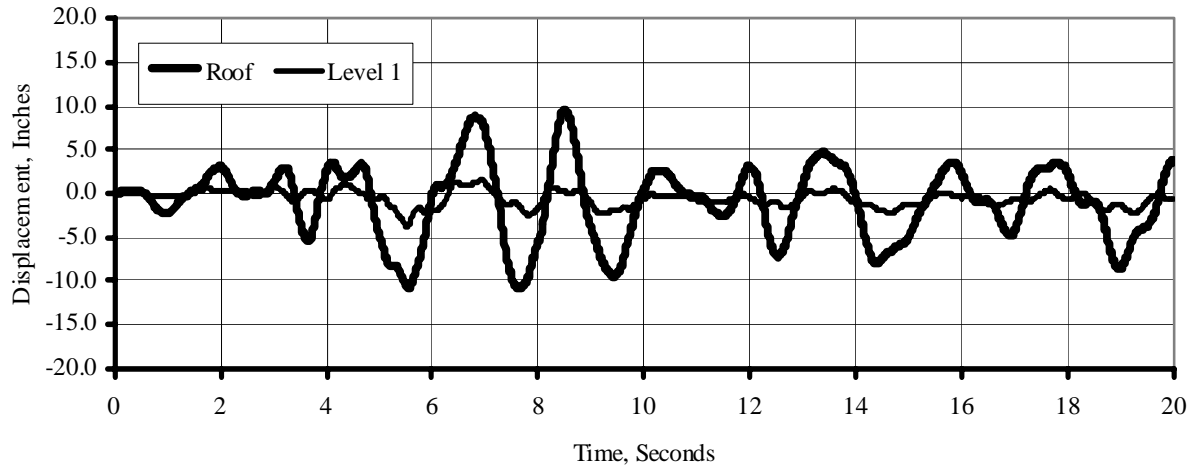


Figure 3.2-63 Time history of total base shear, Ground Motion C00, including P-delta effects.

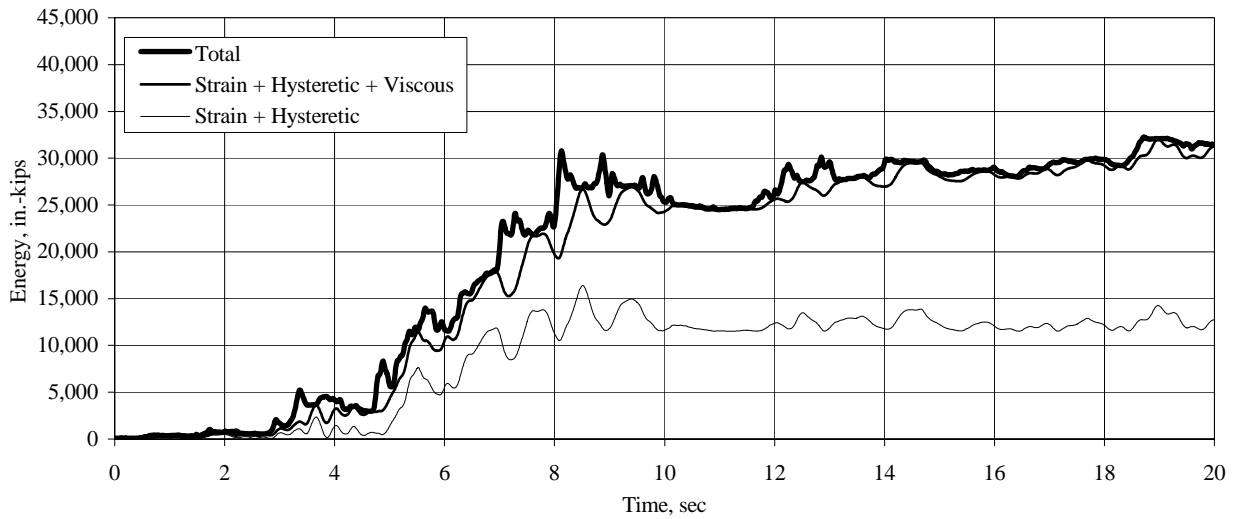


Figure 3.2-64 Energy time history, Ground Motion C00, including P-delta effects.

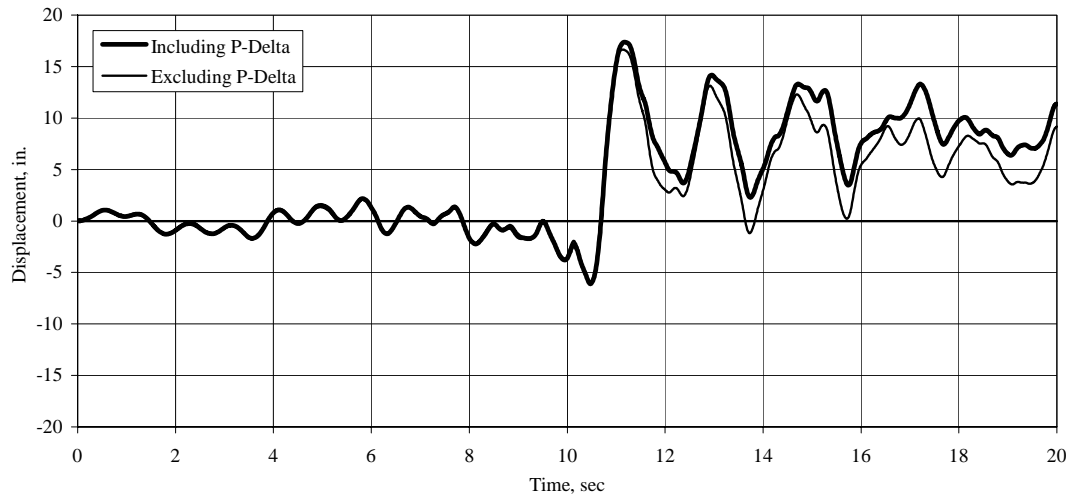


Figure 3.2-65 Time-history of roof displacement, Ground Motion A00, with and without P-delta effect.

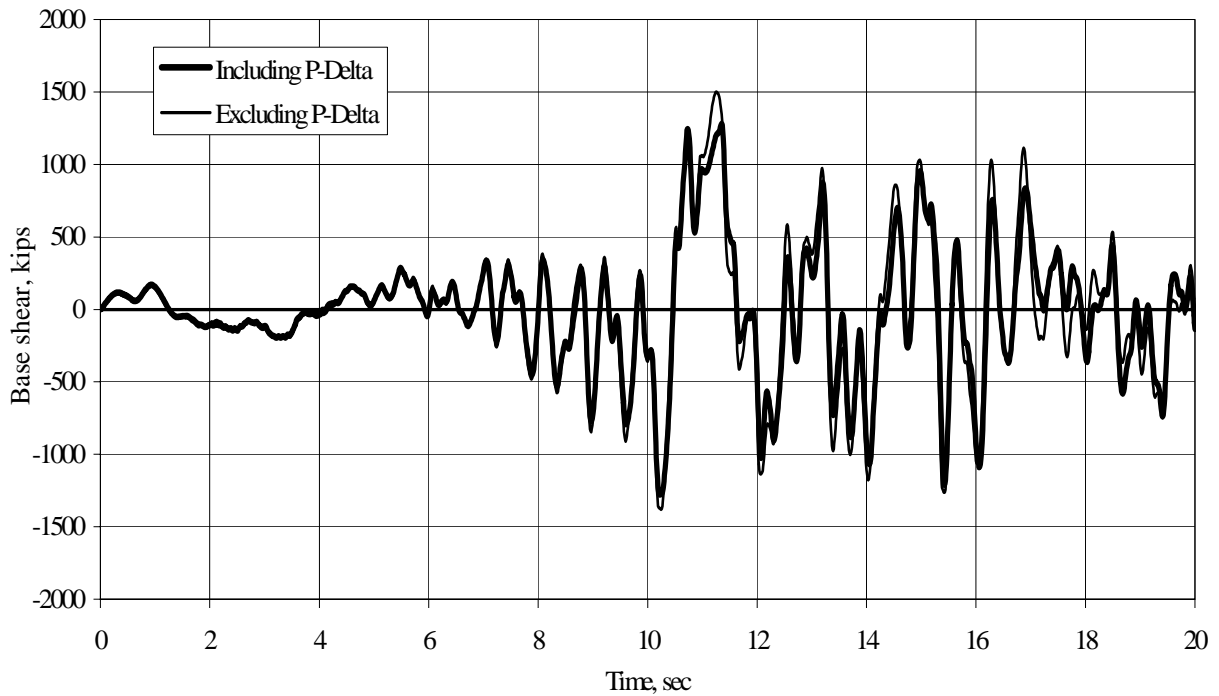


Figure 3.2-66 Time history of base shear, Ground Motion A00, with and without P-delta effects.

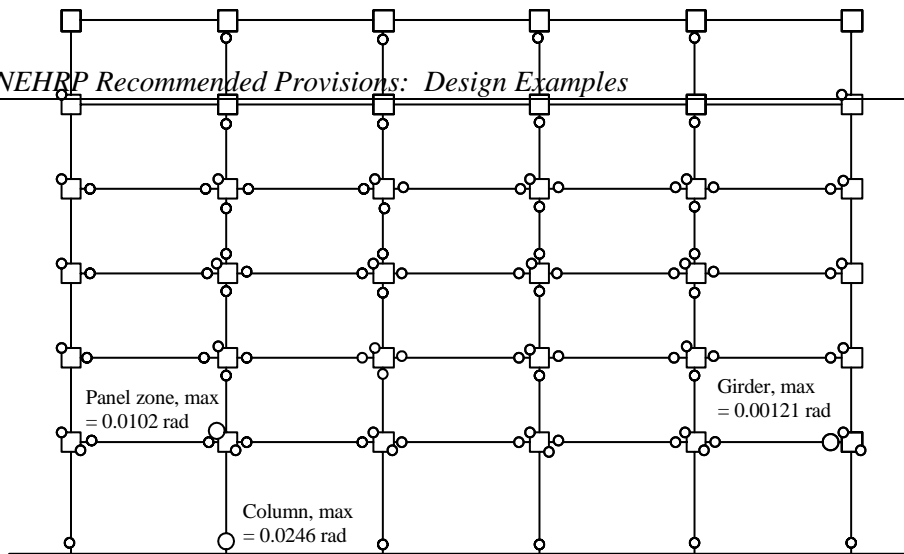


Figure 3.2-67 Yielding locations for structure with strong panels subjected to Ground Motion A00, including P-delta effects.

Figure 3.2-67 shows the pattern of yielding in the structure subjected to Ground Motion A00 including P-delta effects. Recall that the model analyzed incorporated panel zone reinforcement at the interior beam-column joints. Yielding patterns for the other ground motions and for analyses run with and without P-delta effects were similar but are not shown here. The circles on the figure represent yielding at any time during the response; consequently, yielding does not necessarily occur at all locations simultaneously. Circles shown at the upper left corner of the beam-column joint region indicate yielding in the rotational spring that represents the web component of panel zone behavior. Circles at the lower right corner of the panel zone represent yielding of the flange component.

Figure 3.2-67 shows that yielding occurred at both ends of each of the girders at Levels 2, 3, 4, 5, and 6, and in the columns at Stories 1 and 5. The panels zones at the exterior joints of Levels 2 and 6 also yielded. The maximum plastic hinge rotations are shown at the locations they occur for the columns, girders, and panel zones. Tabulated values are shown in Table 3.2-23. The maximum plastic shear strain in the web of the panel zone is identical to the computed hinge rotation in the panel zone spring.

3.2.6.3.2 Comparison with Results from Other Analyses

Table 3.2-23 compares the results obtained from the time-history analysis with those obtained from the ELF and the nonlinear static pushover analyses. Recall that the base shears in the table represent half of the total shear in the building. The differences shown in the results are quite striking:

1. The base shear from nonlinear dynamic analysis is more than four times the value computed from the ELF analysis, but the predicted displacements and story drifts are similar. Due to the highly empirical nature of the ELF approach, it is difficult to explain these differences. The ELF method also has no mechanism to include the overstrength that will occur in the structure although it is represented explicitly in the static and dynamic nonlinear analyses.
2. The nonlinear static pushover analysis predicts base shears and story displacements that are significantly less than those obtained from time-history analysis. It is also very interesting to note that

the pushover analysis indicates no yielding in the panel zones, even at an applied roof displacement of 42 in.

While part of the difference in the pushover and time-history response is due to the scale factor of 1.51 that was required for the time-history analysis, the most significant reason for the difference is the use of the first-mode lateral loading pattern in the nonlinear static pushover response. Figure 3.2-68 illustrates this by plotting the inertial forces that occur in the structure at the time of peak base shear and comparing this pattern to the force system applied for nonlinear static analysis. The differences are quite remarkable. The higher mode effects shown in the Figure 3.2-68 are the likely cause of the different hinging patterns and are certainly the reason for the very high base shear developed in the time-history analysis. (If the inertial forces were constrained to follow the first mode response, the maximum base shear that could be developed in the system would be in the range of 1100 kips. See, for example, Figure 3.2-24.)

Table 3.2-23 Summary of All Analyses for Strong Panel Structure, Including P-Delta Effects

Response Quantity	Analysis Method			
	Equivalent Lateral Forces	Static Pushover Provisions Method	Static Pushover Capacity-Spectrum	Nonlinear Dynamic
Base Shear (kips)	373	1051	1031	1474
Roof Disp. (in.)	18.4	12.7	10.3	17.4
Drift R-6 (in.)	1.87	1.02	0.78	1.90
Drift 6-5 (in.)	2.91	1.77	1.31	3.31
Drift 5-4 (in.)	3.15	2.34	1.81	3.48
Drift 4-3 (in.)	3.63	2.73	2.23	3.60
Drift 3-2 (in.)	3.74	2.73	2.27	4.08
Drift 2-1 (in.)	3.14	2.23	1.90	4.84
Girder Hinge Rot. (rad)	NA	0.0065	0.00732	0.0140
Column Hinge Rot. (rad)	NA	0.00130	0.00131	0.0192
Panel Hinge Rot. (rad)	NA	No Yielding	No Yielding	0.00624
Panel Plastic Shear Strain	NA	No Yielding	No Yielding	0.00624

Note: Shears are for half of total structure.

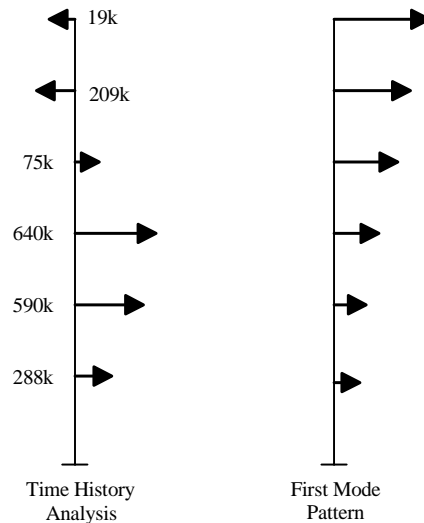


Figure 3.2-68 Comparison of inertial force patterns.

3.2.6.3.3 Effect of Increased Damping on Response

The time-history analysis of the structure with panel zone reinforcement indicates that excessive drift may occur in the first story. The most cost effective measure to enhance the performance of the structure would probably be to provide additional strength and/or stiffness at this story. However, added damping is also a viable approach.

To determine the effect of added damping on the behavior of the structure, preliminary analysis was performed by simply increasing the damping ratio from 5 percent to 20 percent of critical in 5-percent increments. For comparison purposes, an additional analysis was performed for a system with only 2.5 percent damping. In each case, the structure was subjected to Ground Motion A00, the panel zones were reinforced, and P-delta effects were included. A summary of the results is shown in Tables 3.2-24 and 3.2-25. As may be seen, an increase in damping from 5 to 10 percent of critical eliminates the drift problem. Even greater improvement is obtained by increasing damping to 20 percent of critical. In is interesting to note, however, that an increase in damping had little effect on the inertial base shear, which is the true shear in the system.

Table 3.2-24 Maximum Base Shear (kips) in Frame Analyzed Ground Motion A00, Strong Panels, Including P-Delta Effects

Item	Damping Ratio				
	2.5%	5%	10%	20%	28%
Column Forces	1354	1284	1250	1150	1132
Inertial Forces	1440	1426	1520	1421	1872

Table 3.2-25 Maximum Story Drifts (in.) from Time-History Analysis Ground Motion A00, Strong Panels, Including P-Delta Effects

Level	Damping Ratio				
	2.5%	5%	10%	20%	28%
Total Roof	18.1	17.4	15.8	12.9	11.4
R-6	1.81	1.90	1.74	1.43	1.21
6-5	3.72	3.31	2.71	2.08	1.79
5-4	3.87	3.48	3.00	2.42	2.13
4-3	3.70	3.60	3.33	2.77	2.40
3-2	4.11	4.08	3.69	2.86	2.37
2-G	4.93	4.84	4.21	2.90	2.18

If added damping were a viable option, additional analysis that treats the individual dampers explicitly would be required. This is easily accomplished in DRAIN by use of the stiffness proportional component of Rayleigh damping; however, only linear damping is possible in DRAIN. In practice, added damping systems usually employ devices with a “softening” nonlinear relationship between the deformational velocity in the device and the force in the device.

If a linear viscous fluid damping device (Figure 3.2-69) were to be used in a particular story, it could be modeled through the use of a Type-1 (truss bar) element. If a damping constant C_{device} were required, it would be obtained as follows:

Let the length of the Type-1 damper element be L_{device} , the cross sectional area A_{device} , and modulus of elasticity E_{device} .

The elastic stiffness of the damper element is simply:

$$k_{device} = \frac{A_{device} E_{device}}{L_{device}}$$

As stiffness proportional damping is used, the damping constant for the element is:

$$C_{device} = \beta_{device} k_{device}$$

The damper elastic stiffness should be negligible so set $k_D = 0.001$ kips/in. Thus:

$$\beta_{device} = \frac{C_{device}}{0.001} = 1000 C_{device}$$

When modeling added dampers in this manner, the author typically sets $E_{device} = 0.001$ and A_{device} = the damper length L_{device} .

This value of β_{device} is for the added damper element *only*. Different dampers may require different values. Also, a different (global) value of β will be required to model the stiffness proportional component of damping in the remaining nondamper elements.

Modeling the dynamic response using Type-1 elements is *exact* within the typical limitations of finite element analysis. Using the modal strain energy approach, DRAIN will report a damping value in each mode. These modal damping values are approximate and may be poor estimates of actual modal damping, particularly when there is excessive flexibility in the mechanism that connects the damper to the structure.

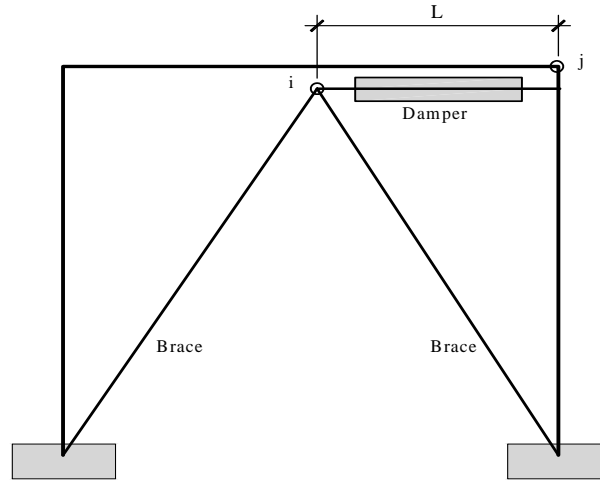


Figure 3.2-69 Modeling a simple damper.

In order to compare the response of the structure with fictitiously high Rayleigh damping to the response with actual discrete dampers, dampers were added in a chevron configuration along column lines C and D, between Bays 3 and 4 (see Figure 3.2-1). As before, the structure is subjected to Ground Motion A00, has strong panels, and has P-delta effects included.

Devices with a damping constant (C) of 80 kip-sec/in. were added in Stories 1 and 2, devices with $C = 70$ kip-sec/in. were added in Stories 3 and 4, and dampers with $C = 60$ kip-sec/in. were added at Stories 5 and 6. The chevron braces used to connect the devices to the main structure had sufficient stiffness to eliminate any loss of efficiency of the devices. Using these devices, an equivalent viscous damping of approximately 28 percent of critical was obtained in the first mode, 55 percent of critical damping was obtained in the second mode, and in excess of 70 percent of critical damping was obtained in modes three through six..

The analysis was repeated using Rayleigh damping wherein the above stated modal damping ratios were approximately obtained. The peak shears and displacements obtained from the analysis with Rayleigh damping are shown at the extreme right of Tables 3.2-24 and 3.2-25. As may be observed, the trend of decreased displacements and increased inertial shears with higher damping is continued.

Figure 3.2-70 shows the time history of roof displacements for the structure without added damping, with true viscous dampers, and with equivalent Rayleigh damping. As may be seen, there is a dramatic

decrease in roof displacement. It is also clear that the discrete dampers and the equivalent Rayleigh damping produce very similar results.

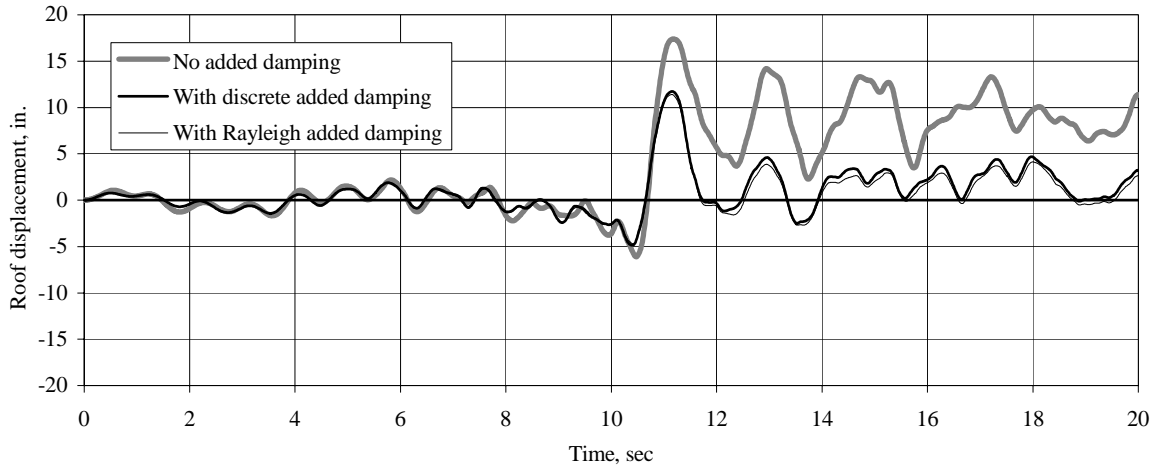


Figure 3.2-70 Response of structure with discrete dampers and with equivalent viscous damping (1.0 in. = 25.4 mm).

Figure 3.2-71 shows the time history of base shears for the structure without added damping, with discrete dampers, and with equivalent viscous damping. These base shears were obtained from the summation of column forces, including P-delta effects. For the discrete damper case, the base shears include the horizontal component of the forces in the chevron braces. The base shears for the discretely damped system are greater than the shears for the system without added damping. The peak base shear for the system with equivalent viscous damping is less than the shear in the system without added damping.

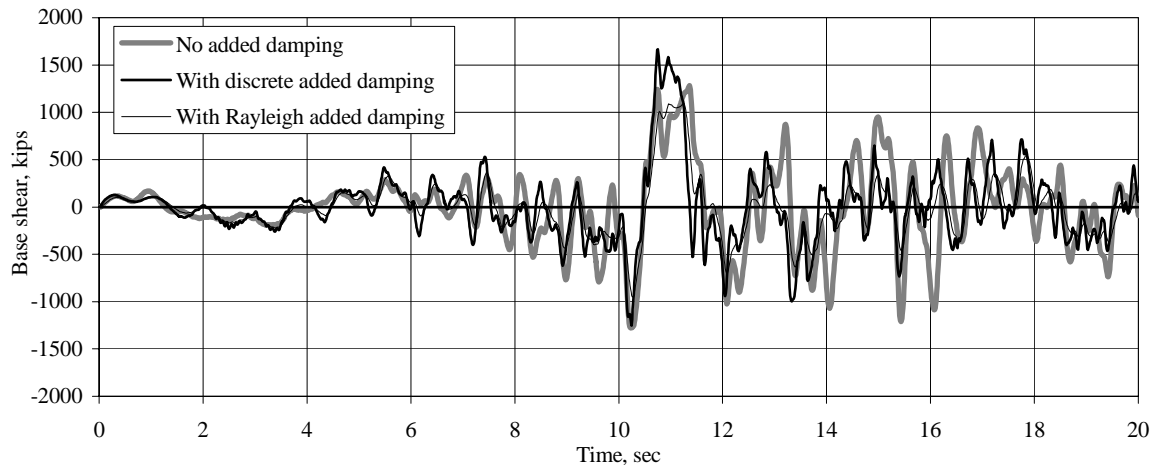


Figure 1Figure 3.2-71 Base shear time histories obtained from column forces (1.0 kip = 4.45 kN).

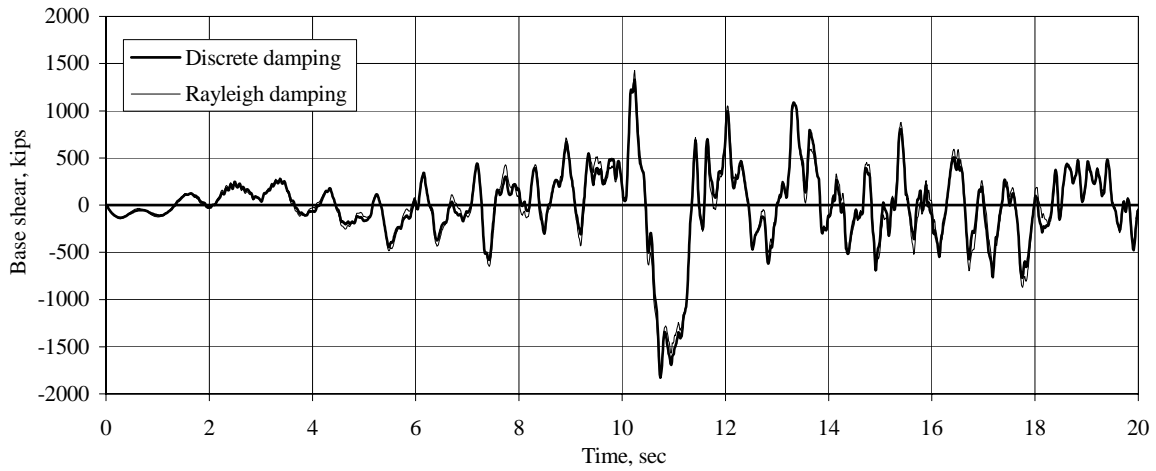


Figure 3.2-72 Base shear time histories as obtained from inertial forces (1.0 kip = 4.45 kN).

The inertial base shears in the system with discrete damping and with equivalent viscous damping are shown in Figure 3.2-72. As may be observed, the responses are almost identical. The inertial forces represent the true base shear in the structure, and should always be used in lieu of the sum of column forces.

As might be expected, the use of added discrete damping reduces the hysteretic energy demand on the structure. This effect is shown in Figure 3.2-73, which is an energy time history for the structure with added discrete damping (which yields equivalent viscous damping of 28 percent of critical). This figure should be compared to Figure 3.2-58, which is the energy history for the structure without added damping. The reduction in hysteretic energy demand for the system with added damping will reduce the damage in the structure.

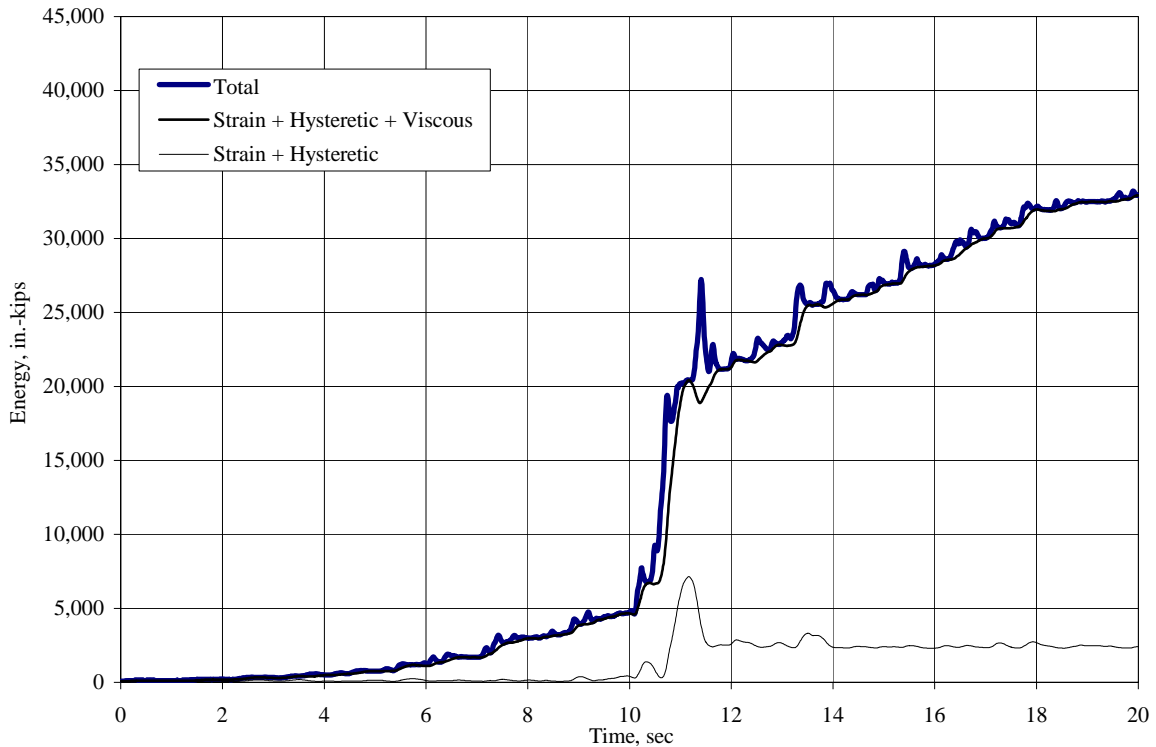


Figure 3.2-73 Energy time-history for structure with discrete added damping (1.0 in.-kip = 0.113 kN-m).

3.2.7 Summary and Conclusions

In this example, five different analytical approaches were used to estimate the deformation demands in a simple unbraced steel frame structure:

1. Linear static analysis (the equivalent lateral force method)
2. Plastic strength analysis (using virtual work)
3. Nonlinear static pushover analysis
4. Linear dynamic analysis
5. Nonlinear dynamic time-history analysis

Approaches 1, 3, and 5 were carried to a point that allowed comparison of results. In modeling the structure, particular attention was paid to representing possible inelastic behavior in the panel-zone regions of the beam-column joints.

The results obtained from the three different analytical approaches were quite dissimilar. Because of the influence of the higher mode effects on the response, pushover analysis, when used alone, is inadequate.¹¹ [In the 2003 *Provisions*, a number of substantive technical changes have been made to the appendix,

¹¹Improved methods are becoming available for pushover analysis (see, for example, Chopra and Goel 2001).

largely as a result of work performed in the development of ATC 55. That report outlines numerous other technical modifications that could be considered in application of nonlinear static analysis methods.] Except for preliminary design, the ELF approach should not be used in explicit performance evaluation as it has no mechanism for determining location and extent of yielding in the structure.

This leaves time-history analysis as the most viable approach. Given the speed and memory capacity of personal computers, it is expected that time-history analysis will eventually play a more dominant role in the seismic analysis of buildings. However, significant shortcomings, limitations, and uncertainties in time-history analysis still exist.

Among the most pressing problems is the need for a suitable suite of ground motions. All ground motions must adequately reflect site conditions and, where applicable, the suite must include near-field effects. Through future research and the efforts of code writing bodies, it may be possible to develop standard suites of ground motions that could be published together with tools and scaling methodologies to make the motions represent the site. The scaling techniques that are currently recommended in the *Provisions* are a start but need improving.

Systematic methods need to be developed for identifying uncertainties in the modeling of the structure and for quantifying the effect of such uncertainties on the response. While probabilistic methods for dealing with such uncertainties seem like a natural extension of the analytical approach, the author believes that deterministic methods should not be abandoned entirely.

In the context of performance-based design, improved methods for assessing the effect of inelastic response and acceptance criteria based on such measures need to be developed. Methods based on explicit quantification of damage should be seriously considered.

The ideas presented above are certainly not original. They have been presented by many academics and practicing engineers. What is still lacking is a comprehensive approach for seismic-resistant design based on these principles. Bertero and Bertero (2002) have presented valuable discussions in these regards.

FOUNDATION ANALYSIS AND DESIGN

Michael Valley, P.E.

This chapter illustrates application of the 2000 Edition of the *NEHRP Recommended Provisions* to the design of foundation elements. Example 4.1 completes the analysis and design of shallow foundations for two of the alternate framing arrangements considered for the building featured in Example 5.2. Example 4.2 illustrates the analysis and design of deep foundations for a building similar to the one highlighted in Chapter 6 of this volume of design examples. In both cases, only those portions of the designs necessary to illustrate specific points are included.

The force-displacement response of soil to loading is highly nonlinear and strongly time dependent. Control of settlement is generally the most important aspect of soil response to gravity loads. However, the strength of the soil may control foundation design where large amplitude transient loads, such as those occurring during an earthquake, are anticipated.

Foundation elements are most commonly constructed of reinforced concrete. As compared to design of concrete elements that form the superstructure of a building, additional consideration must be given to concrete foundation elements due to permanent exposure to potentially deleterious materials, less precise construction tolerances, and even the possibility of unintentional mixing with soil.

Although the application of advanced analysis techniques to foundation design is becoming increasingly common (and is illustrated in this chapter), analysis should not be the primary focus of foundation design. Good foundation design for seismic resistance requires familiarity with basic soil behavior and common geotechnical parameters, the ability to proportion concrete elements correctly, an understanding of how such elements should be detailed to produce ductile response, and careful attention to practical considerations of construction.

Although this chapter is based on the 2000 *Provisions*, it has been annotated to reflect changes made to the 2003 *Provisions*. Annotations within brackets, [], indicate both organizational changes (as a result of a reformat of all of the chapters of the 2003 *Provisions*) and substantive technical changes to the 2003 *Provisions* and its primary reference documents. While the general concepts of the changes are described, the design examples and calculations have not been revised to reflect the changes to the 2003 *Provisions*. The most significant change to the foundation chapter in the 2003 *Provisions* is the addition of a strength design method for foundations. Another change was made to introduce guidance for the explicit modeling of foundation load-deformation characteristics. Where they affect the design examples in this chapter, other significant changes to the 2003 *Provisions* and primary reference documents are noted. However, some minor changes to the 2003 *Provisions* and the reference documents may not be noted.

In addition to the 2000 *NEHRP Recommended Provisions and Commentary* (referred to herein as *Provisions and Commentary*), the following documents are either referenced directly or provide useful information for the analysis and design of foundations for seismic resistance:

- ACI 318 American Concrete Institute. 1999 [2002]. *Building Code Requirements and Commentary for Structural Concrete*.
- ASCE 7 American Society of Civil Engineers. 1998 [2002]. *Minimum Design Loads for Buildings and Other Structures*.
- Bowles Bowles, J. E. 1988. *Foundation Analysis and Design*. McGraw-Hill.
- Brown 1987 Brown, D. A., L. C. Reese, and M. W. O'Neill. 1987. "Cyclic Lateral Loading of a Large-Scale Pile Group," *Journal of Geotechnical Engineering*, Vol. 113, No. 11 (November). ASCE.
- Brown 1988 Brown, D. A., C. Morrison, and L. C. Reese. 1988. "Lateral Load Behavior of Pile Group in Sand." *Journal of Geotechnical Engineering*, Vol 114, No. 11, (November). ASCE.
- CRSI Concrete Reinforcing Steel Institute. 1996. *CRSI Design Handbook*. Concrete Reinforcing Steel Institute.
- FEMA 356 ASCE. 2000. *Prestandard and Commentary for the Seismic Rehabilitation of Buildings*, FEMA 356, prepared by the American Society of Civil Engineers for the Federal Emergency Management Agency.
- GROUP Reese, L. C., and S. T. Wang. 1996. *Manual for GROUP 4.0 for Windows*. Ensoft.
- Kramer Kramer, S. L. 1996. *Geotechnical Earthquake Engineering*. Prentice Hall.
- LPILE Reese, L. C., and S. T. Wang. 1997. *Technical Manual for LPILE Plus 3.0 for Windows*. Ensoft.
- Martin Martin, G. R., and I. PoLam. 1995. "Seismic Design of Pile Foundations: Structural and Geotechnical Issues." *Proceedings: Third International Conference on Recent Advances in Geotechnical Earthquake Engineering and Soil Dynamics*.
- Pender Pender, M. J. 1993. "Aseismic Pile Foundation Design Analysis." *Bulletin of the New Zealand National Society for Earthquake Engineering*, Vol. 26, No. 1 (March).
- PoLam PoLam, I., M. Kapuskar, and D. Chaudhuri. 1998. *Modeling of Pile Footings and Drilled Shafts for Seismic Design*, MCEER-98-0018. Multidisciplinary Center for Earthquake Engineering Research.
- Wang & Salmon Wang, C.-K., and C. G. Salmon. 1992. *Reinforced Concrete Design*. HarperCollins.

Youd
Youd, T. L., Idriss, I. M., and et al. 2001. "Liquefaction Resistance of Soils: Summary Report from the 1996 NCEER and 1998 NCEER/NSF Workshops on Evaluation of Liquefaction Resistance of Soils." *Journal of Geotechnical and Geoenvironmental Engineering* (October). ASCE.

Several commercially available programs were used to perform the calculations described in this chapter. RISA: 3D is used to determine the shears and moments in a concrete mat foundation; LPILE, in the analysis of laterally loaded single piles; and PCACOL, to determine concrete pile section capacities.

4.1 SHALLOW FOUNDATIONS FOR A SEVEN-STORY OFFICE BUILDING, LOS ANGELES, CALIFORNIA

This example features the analysis and design of shallow foundations for two of the three framing arrangements for the seven-story steel office building described in Sec. 5.2 of this volume of design examples. Refer to that example for more detailed building information and for the design of the superstructure; because Chapter 4 was completed after Chapter 5, some values may differ slightly between the two chapters.

4.1.1 Basic Information

4.1.1.1 Description

The framing plan in Figure 4.1-1 shows the gravity-load-resisting system for a representative level of the building. The site soils, consisting of medium dense sands, are suitable for shallow foundations. Table 4.1-1 shows the design parameters provided by a geotechnical consultant. Note the distinction made between *bearing pressure* and *bearing capacity*. If the long-term, service-level loads applied to foundations do not exceed the noted bearing pressure, differential and total settlements are expected to be within acceptable limits. Settlements are more pronounced where large areas are loaded, so the bearing pressure limits are a function of the size of the loaded area. The values identified as bearing capacity are related to gross failure of the soil mass in the vicinity of loading. Where loads are applied over smaller areas, punching into the soil is more likely.

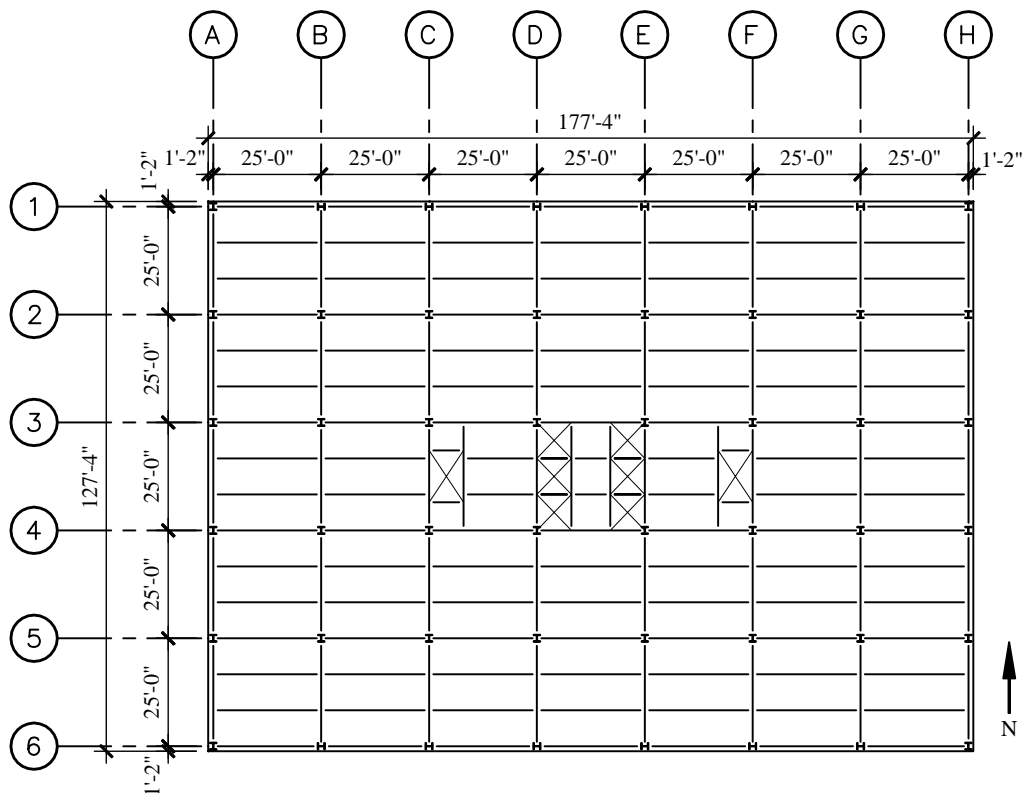


Figure 4.1-1 Typical framing plan.

Because bearing capacities are generally expressed as a function of the minimum dimension of the loaded area and are applied as limits on the maximum pressure, foundations with significantly non-square loaded areas (tending toward strip footings) and those with significant differences between average pressure and maximum pressure (as for eccentrically loaded footings) have higher calculated bearing capacities. The recommended values are consistent with these expectations.

[The 2003 *Provisions* discuss the settlement and strength limit states in Sec. 7.2.2.2 using slightly different nomenclature.]

Table 4.1-1 Geotechnical Parameters

Parameter	Value
Basic soil properties	Medium dense sand (SPT) $N = 20$ $\gamma = 125$ pcf angle of internal friction = 33 deg
Net bearing pressure (to control settlement due to sustained loads)	≤ 4000 psf for $B \leq 20$ ft ≤ 2000 psf for $B \geq 40$ ft (may interpolate for intermediate dimensions)
Bearing capacity (for plastic equilibrium strength checks with factored loads)	2000 B psf for concentrically loaded square footings 3000 B' psf for eccentrically loaded footings where B and B' are in feet, B is the footing width and B' is an average width for the compressed area. Resistance factor, $\phi = 0.6$ [In the 2003 <i>Provisions</i> , the ϕ factor for cohesionless soil is explicitly defined; the value is set at 0.7 for vertical, lateral, and rocking resistance.]
Lateral properties	Earth pressure coefficients Active, $K_A = 0.3$ At-rest, $K_0 = 0.46$ Passive, $K_p = 3.3$ “Ultimate” friction coefficient at base of footing = 0.65 Resistance factor, $\phi = 0.8$ [In the 2003 <i>Provisions</i> , the ϕ factor for cohesionless soil is explicitly defined; the value is set at 0.7 for vertical, lateral, and rocking resistance.]

The structural material properties assumed for this example are:

$$f'_c = 4,000 \text{ psi}$$

$$f_y = 60,000 \text{ psi}$$

4.1.1.2 Provisions Parameters

The complete set of parameters used in applying the *Provisions* to design of the superstructure is described in Sec. 5.2.2.1 of this volume of design examples. The following parameters, which are used during foundation design, are duplicated here.

$$\text{Site Class} = D$$

$$S_{DS} = 1.0$$

Seismic Design Category = D

4.1.1.3 Design Approach

4.1.1.3.1 *Selecting Footing Size and Reinforcement*

Most foundation failures are related to excessive movement rather than loss of load-carrying capacity. Settlement control should be addressed first. In recognition of this fact, settlement control should be the first issue addressed. Once service loads have been calculated, foundation plan dimensions should be selected to limit bearing pressures to those that are expected to provide adequate settlement performance. Maintaining a reasonably consistent level of service load bearing pressures for all of the individual footings is encouraged as it will tend to reduce differential settlements, which are usually of more concern than are total settlements.

When a preliminary footing size that satisfies serviceability criteria has been selected, bearing capacity can be checked. It would be rare for bearing capacity to govern the size of footings subjected to sustained loads. However, where large transient loads are anticipated, consideration of bearing capacity may become important.

The thickness of footings is selected for ease of construction and to provide adequate shear capacity for the concrete section. The common design approach is to increase footing thickness as necessary to avoid the need for shear reinforcement, which is uncommon in shallow foundations.

Design requirements for concrete footings are found in Chapters 15 and 21 of ACI 318. Chapter 15 provides direction for the calculation of demands and includes detailing requirements. Section capacities are calculated in accordance with Chapters 10 (for flexure) and 11 (for shear). Figure 4.1-2 illustrates the critical sections (dashed lines) and areas (hatched) over which loads are tributary to the critical sections. For elements that are very thick with respect to the plan dimensions (as at the pile caps), these critical section definitions become less meaningful and other approaches (e.g., strut-and-tie modeling) should be employed. Chapter 21 provides the minimum requirements for concrete foundations in Seismic Design Categories D, E, and F, which are similar to those provided in prior editions of the *Provisions*.

For shallow foundations, reinforcement is designed to satisfy flexural demands. ACI 318 Sec. 15.4 defines how flexural reinforcement is to be distributed for footings of various shapes.

Sec. 10.5 of ACI 318 prescribes the minimum reinforcement for flexural members where tensile reinforcement is required by analysis. Provision of the minimum reinforcement assures that the strength of the cracked section is not less than that of the corresponding unreinforced concrete section, thus preventing sudden, brittle failures. Less reinforcement may be used as long as “the area of tensile reinforcement provided is at least one-third greater than that required by analysis.” Sec. 10.5.4 relaxes the minimum reinforcement requirement for footings of uniform thickness. Such elements need only satisfy the shrinkage reinforcement requirements of Sec. 7.12. Sec. 10.5.4 also imposes limits on the maximum spacing of bars.

4.1.1.3.2 *Additional Considerations for Eccentric Loads*

The design of eccentrically loaded footings follows the approach outlined above with one significant addition – consideration of overturning stability. Stability calculations are sensitive to the characterization of soil behavior. For sustained eccentric loads a linear distribution of elastic soil stresses is generally assumed and uplift is usually avoided. If the structure is expected to remain elastic when subjected to short-term eccentric loads (as for wind loading), uplift over a portion of the footing is acceptable to most designers. Where foundations will be subjected to short-term loads and inelastic

response is acceptable (as for earthquake loading), plastic soil stresses may be considered. It is most common to consider stability effects on the basis of statically applied loads even where the loading is actually dynamic; that approach simplifies the calculations at the expense of increased conservatism. Figure 4.1-3 illustrates the distribution of soil stresses for the various assumptions. Most textbooks on foundation design provide simple equations to describe the conditions shown in parts b, c, and d of the figure; finite element models of those conditions are easy to develop. Simple hand calculations can be performed for the case shown in part f. Practical consideration of the case shown in part e would require modeling with inelastic elements, but offers no advantage over direct consideration of the plastic limit. (All of the discussion in this section focuses on the common case in which foundation elements may be assumed to be rigid with respect to the supporting soil. For the interested reader, Chapter 4 of FEMA 356 provides a useful discussion of foundation compliance, rocking, and other advanced considerations.)

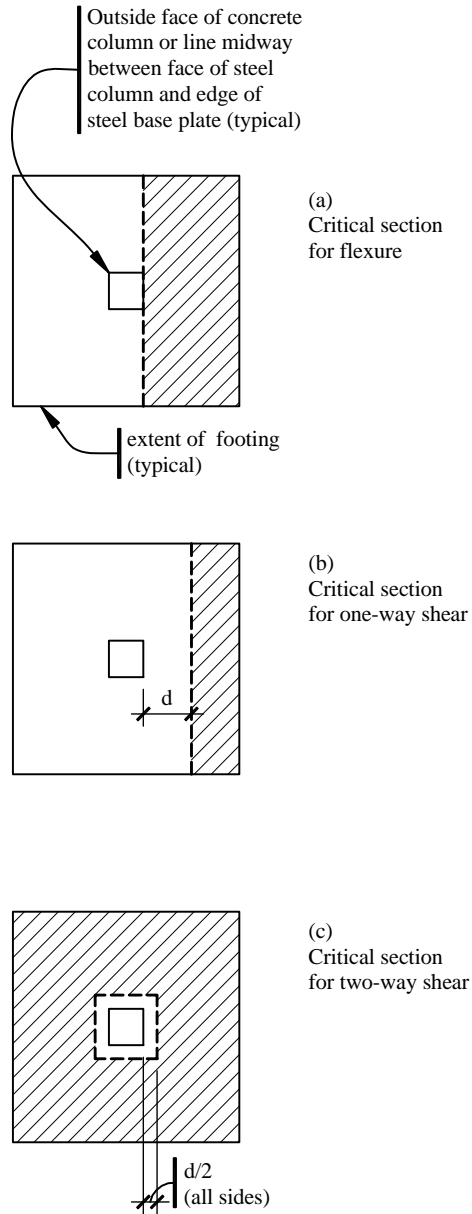


Figure 4.1-2 Critical sections for isolated footings.

4.1.2 Design for Gravity Loads

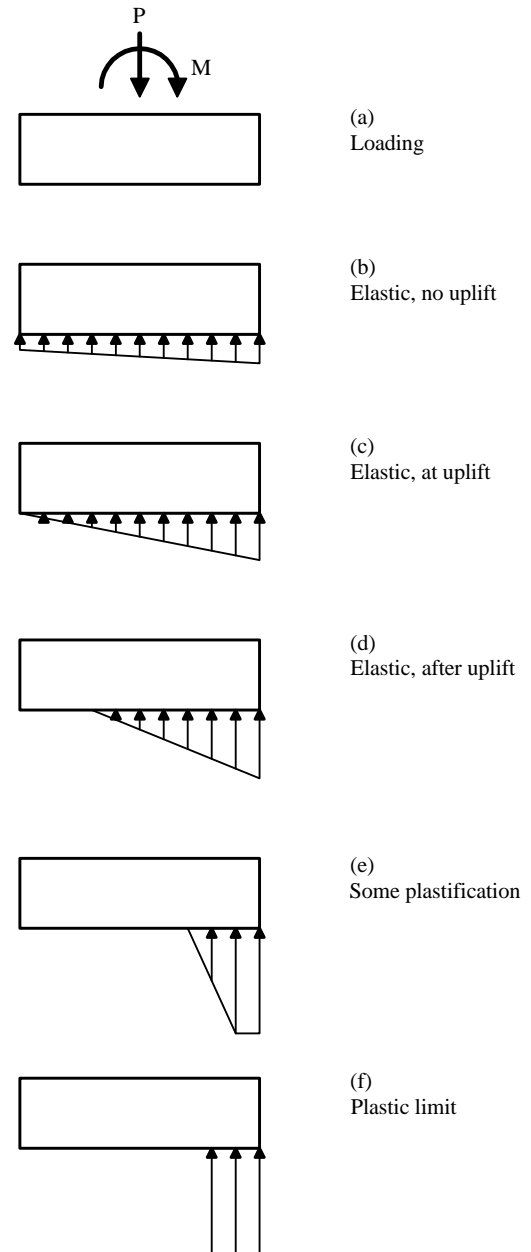


Figure 4.1-3 Soil pressure distributions.

Although most of the examples in the volume do not provide detailed design for gravity loads, it is provided in this section for two reasons. First, most of the calculation procedures used in designing shallow foundations for seismic loads are identical to those used for gravity design. Second, a complete gravity design is needed to make the cost comparisons shown in Sec. 4.1.5 below meaningful.

Detailed calculations are shown for a typical interior footing. The results for all three footing types are summarized in Sec. 4.1.2.5.

4.1.2.1 Demands

Dead and live load reactions are determined as part of the three-dimensional analysis described in Sec. 5.2 of this volume of design examples. Although there are slight variations in the calculated reactions, the foundations are lumped into three groups (interior, perimeter, and corner) for gravity load design and the maximum computed reactions are applied to all members of the group, as follows:

$$\begin{aligned}\text{Interior: } D &= 387 \text{ kips} \\ L &= 98 \text{ kips}\end{aligned}$$

$$\begin{aligned}\text{Perimeter: } D &= 206 \text{ kips} \\ L &= 45 \text{ kips}\end{aligned}$$

$$\begin{aligned}\text{Corner: } D &= 104 \text{ kips} \\ L &= 23 \text{ kips}\end{aligned}$$

The service load combination for consideration of settlement is $D + L$. Considering the load combinations for strength design defined in Sec. 2.3.2 of ASCE 7, the controlling gravity load combination is $1.2D + 1.6L$. Because ASCE 7 load combinations are employed, the alternate strength reduction factors found in ACI 318 Appendix C must be used. [The 2003 *Provisions* refer to ACI 318-02, in which the basic resistance factors have been revised to be consistent with the load combinations in ASCE 7. These new resistance factors (not those found in the ACI 318 Appendix) are used for seismic design. This change would affect slightly the results of the example calculations in this chapter.]

4.1.2.2 Footing Size

The preliminary size of the footing is determined considering settlement. The service load on a typical interior footing is calculated as:

$$P = D + L = 387 \text{ kips} + 98 \text{ kips} = 485 \text{ kips.}$$

Since the footing dimensions will be less than 20 ft, the allowable bearing pressure (see Table 4.1-1) is 4000 psf. Therefore, the required footing area is $487,000 \text{ lb}/4000 \text{ psf} = 121.25 \text{ ft}^2$.

Check a footing that is 11'-0" by 11'-0":

$$P_{allow} = 11 \text{ ft}(11 \text{ ft})(4000 \text{ psf}) = 484,000 \text{ lb} = 484 \text{ kips} \approx 485 \text{ kips (demand)}. \quad \text{OK}$$

The strength demand is:

$$P_u = 1.2(387 \text{ kips}) + 1.6(98 \text{ kips}) = 621 \text{ kips.}$$

As indicated in Table 4.1-1, the bearing capacity (q_c) is $2000 B = 2000 \times 11 = 22000 \text{ psf} = 22 \text{ ksf}$.

The design capacity for the foundation is:

$$\phi P_n = \phi q_c B^2 = 0.6(22 \text{ ksf})(11 \text{ ft})^2 = 1597 \text{ kips} \gg 621 \text{ kips.} \quad \text{OK}$$

For use in subsequent calculations, the factored bearing pressure $q_u = 621 \text{ kips}/(11 \text{ ft})^2 = 5.13 \text{ ksf}$.

4.1.2.3 Footing Thickness

Once the plan dimensions of the footing are selected, the thickness is determined such that the section satisfies the one-way and two-way shear demands without the addition of shear reinforcement. Because the demands are calculated at critical sections (see Figure 4.1-2) that depend on the footing thickness, iteration is required.

Check a footing that is 26 in. thick:

For the W14 columns used in this building, the side dimensions of the loaded area (taken halfway between the face of the column and the edge of the base plate) are about 16 in. Accounting for cover and expected bar sizes, $d = 26 - (3 + 1.5(1)) = 21.5 \text{ in}$.

One-way shear:

$$V_u = 11 \left(\frac{11 - \frac{16}{12}}{2} - \frac{21.5}{12} \right) (5.13) = 172 \text{ kips.}$$

$$\phi V_n = \phi V_c = (0.75) 2 \sqrt{4000} (11 \times 12) (21.5) \left(\frac{1}{1000} \right) = 269 \text{ kips} > 172 \text{ kips.} \quad \text{OK}$$

Two-way shear:

$$V_u = 621 - \left(\frac{16 + 21.5}{12} \right)^2 (5.13) = 571 \text{ kips.}$$

$$\phi V_n = \phi V_c = (0.75) 4 \sqrt{4000} [4 \times (16 + 21.5)] (21.5) \left(\frac{1}{1000} \right) = 612 \text{ kips} > 571 \text{ kips.} \quad \text{OK}$$

4.1.2.4 Footing Reinforcement

Footing reinforcement is selected considering both flexural demands and minimum reinforcement requirements. The following calculations treat flexure first because it usually controls:

$$M_u = \frac{1}{2} (11) \left(\frac{11 - \frac{16}{12}}{2} \right)^2 (5.13) = 659 \text{ ft-kips.}$$

Try 10 #8 bars each way. The distance from the extreme compression fiber to the center of the top layer of reinforcement, $d = t - \text{cover} - 1.5d_b = 26 - 3 - 1.5(1) = 21.5 \text{ in}$.

$$T = A_s f_y = 10(0.79)(60) = 474 \text{ kips.}$$

Noting that $C = T$ and solving the expression $C = 0.85 f'_c b a$ for a produces $a = 1.06 \text{ in}$.

$$\phi M_n = \phi T \left(d - \frac{a}{2} \right) = 0.80(474) \left(21.5 - \frac{1.06}{2} \right) \left(\frac{1}{12} \right) = 663 \text{ ft-kips} > 659 \text{ ft-kips.} \quad \text{OK}$$

The ratio of reinforcement provided $\rho = 10(0.79)/[(11)(12)(21.5)] = 0.00278$. The distance between bars spaced uniformly across the width of the footing $s = [(11)(12)-2(3+0.5)]/(10-1) = 13.9$ in.

According to ACI 318 Sec. 7.12, the minimum reinforcement ratio = $0.0018 < 0.00278$. OK

and the maximum spacing is the lesser of 3×26 in. or $18 = 18$ in. > 13.9 in. OK

4.1.2.5 Design Results

The calculations performed in Sec. 4.1.2.2 through 4.1.2.4 are repeated for typical perimeter and corner footings. The footing design for gravity loads is summarized in Table 4.1-2; Figure 4.1-4 depicts the resulting foundation plan.

Table 4.1-2 Footing Design for Gravity Loads

Location	Loads	Footing Size and Reinforcement; Soil Capacity	Critical Section Demands and Design Strengths	
Interior	$D = 387$ kip $L = 98$ kip	$11'-0" \times 11'-0" \times 2'-2"$ deep 10-#8 bars each way	One-way shear:	$V_u = 172$ kip $\phi V_n = 269$ kip
	$P = 485$ kip $P_u = 621$ kip	$P_{allow} = 484$ kip $\phi P_n = 1597$ kip	Two-way shear:	$V_u = 571$ kip $\phi V_n = 612$ kip
			Flexure:	$M_u = 659$ ft-kip $\phi M_n = 663$ ft-kip
Perimeter	$D = 206$ kip $L = 45$ kip	$8'-0" \times 8'-0" \times 1'-6"$ deep 10-#6 bars each way	One-way shear:	$V_u = 88.1$ kip $\phi V_n = 123$ kip
	$P = 251$ kip $P_u = 319$ kip	$P_{allow} = 256$ kip $\phi P_n = 614$ kip	Two-way shear:	$V_u = 289$ kip $\phi V_n = 302$ kip
			Flexure:	$M_u = 222$ ft-kip $\phi M_n = 230$ ft-kip
Corner	$D = 104$ kip $L = 23$ kip	$6'-0" \times 6'-0" \times 1'-2"$ deep 7-#5 bars each way	One-way shear:	$V_u = 41.5$ kip $\phi V_n = 64.9$ kip
	$P = 127$ kip $P_u = 162$ kip	$P_{allow} = 144$ kip $\phi P_n = 259$ kip	Two-way shear:	$V_u = 141$ kip $\phi V_n = 184$ kip
			Flexure:	$M_u = 73.3$ ft-kip $\phi M_n = 80.2$ ft-kip

[Use of the new resistance factors in ACI 318-02 would change these results.]

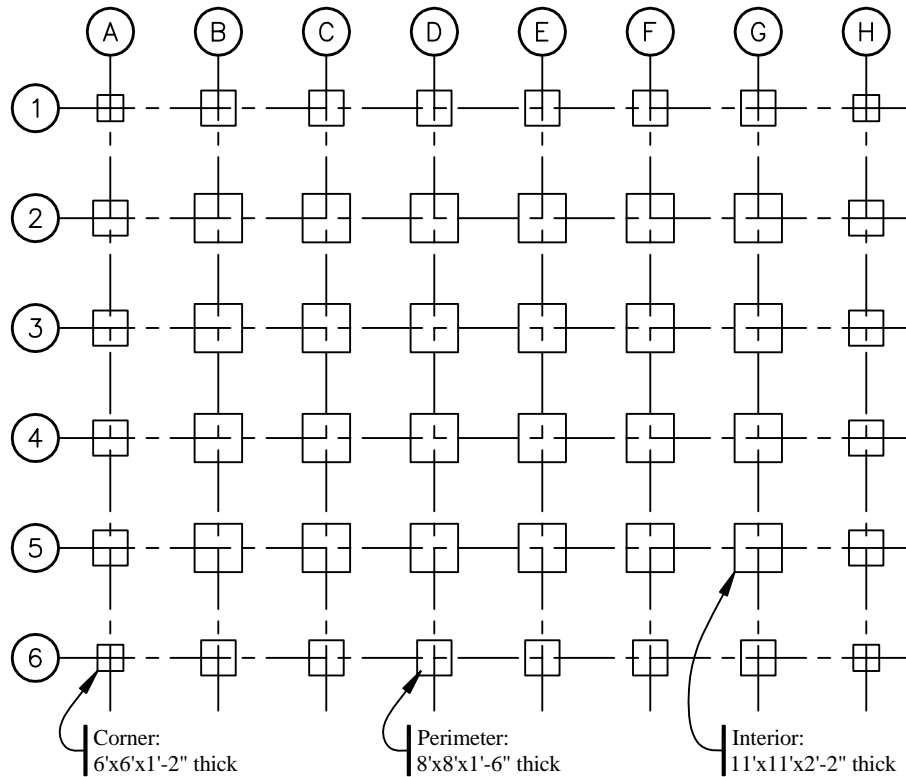


Figure 4.1-4 Foundation plan for gravity-load-resisting system.

4.1.3 Design for Moment-Resisting Frame System

Framing Alternate A in Sec. 5.2 of this volume of design examples includes a perimeter moment resisting frame as the seismic-force-resisting system. A framing plan for the system is shown in Figure 4.1-5. Detailed calculations are provided in this section for a combined footing at the corner and focus on overturning and sliding checks for the eccentrically loaded footing; settlement checks and design of concrete sections would be similar to the calculations shown in Sec. 4.1.2. The results for all footing types are summarized in Sec. 4.1.3.4.

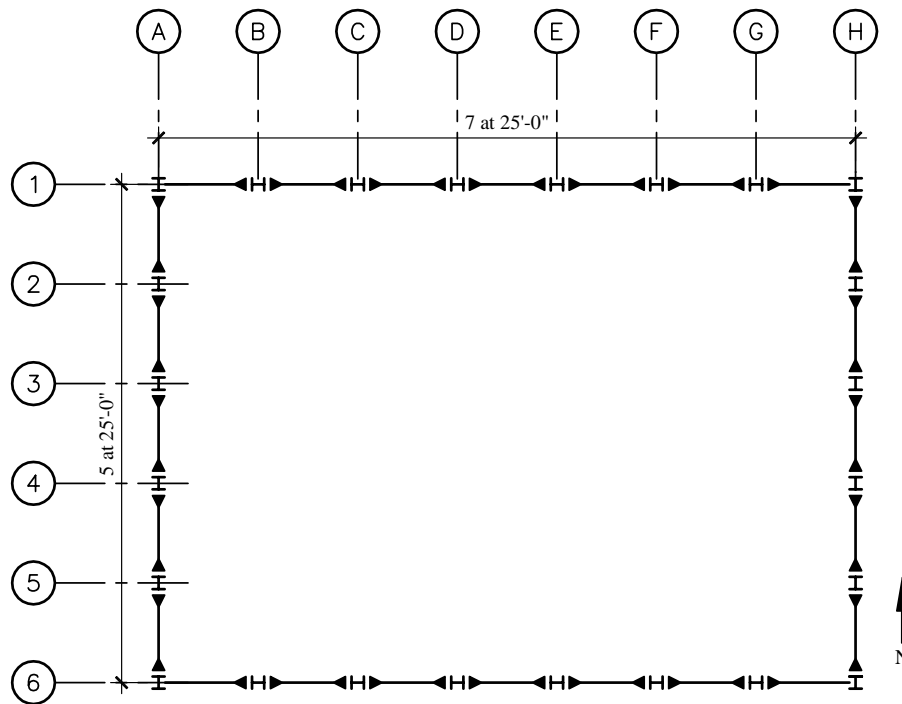


Figure 4.1-5 Framing plan for moment resisting frame system.

4.1.3.1 Demands

A three-dimensional analysis of the superstructure, in accordance with the requirements for the equivalent lateral force (ELF) procedure, is performed using the RAMFRAME program. Foundation reactions at selected grids are reported in Table 4.1-3.

Table 4.1-3 Demands from Moment-Resisting Frame System

Location	Load	R_x	R_y	R_z	M_{xx}	M_{yy}
A-5	D			-203.8		
	L			-43.8		
	Ex	-13.8	4.6	3.8	53.6	-243.1
	Ey	0.5	-85.1	-21.3	-1011.5	8.1
A-6	D			-103.5		
	L			-22.3		
	Ex	-14.1	3.7	51.8	47.7	-246.9
	Ey	0.8	-68.2	281.0	-891.0	13.4

Note: Units are kips and feet. Load Ex is for loads applied toward the east, including appropriately amplified counter-clockwise accidental torsion. Load Ey is for loads applied toward the north, including appropriately amplified clockwise accidental torsion.

Sec. 5.2.3.5 of this volume of design examples outlines the design load combinations, which include the redundancy factor as appropriate. Considering two senses of accidental torsion for loading in each direction and including orthogonal effects results in a large number of load cases. The detailed calculations presented here are limited to two primary conditions, both for a combined foundation for columns at Grids A-5 and A-6: the downward case ($1.4D + 0.5L + 0.32Ex + 1.11Ey$) and the upward case

$(0.7D + 0.32Ex + 1.11Ey)$. [Because the redundancy factor is changed substantially in the 2003 *Provisions*, the factors in these load combinations would change.]

Before loads can be computed, attention must be given to *Provisions* Sec. 5.4.5 [5.2.5]. That section permits “foundations of structures . . . to be designed for three-fourths of the foundation overturning design moment, M_p .” Because the overturning moment in question is the global overturning moment for the *system*, judgment must be used in determining which design actions may be reduced. If the seismic-force-resisting system consists of isolated shear walls, the shear wall overturning moment at the base best fits that description. For a perimeter moment-resisting frame, most of the global overturning resistance is related to axial loads in columns. Therefore, in this example column axial loads (R_z) from load cases Ex and Ey will be multiplied by 0.75 and all other load effects will remain unreduced.

4.1.3.2 Downward Case ($1.4D + 0.5L + 0.32Ex + 1.11Ey$)

In order to perform the overturning checks a footing size must be assumed. Preliminary checks (not shown here) confirmed that isolated footings under single columns were untenable. Check overturning for a footing that is 10 ft wide by 40 ft long by 5 ft thick. Further, assume that the top of the footing is 2 ft below grade (the overlying soil contributes to the resisting moment). (In these calculations the $0.2S_{Ds}D$ modifier for vertical accelerations is used for the dead loads *applied to the foundation* but not for the weight of the foundation and soil. This is the author’s interpretation of the *Provisions*. The footing and soil overburden are not subject to the same potential for dynamic amplification as the dead load of the superstructure, and it is not common practice to include the vertical acceleration on the weight of the footing and the overburden. Furthermore, for footings that resist significant overturning, this issue makes a significant difference in design.) Combining the loads from columns at Grids A-5 and A-6 and including the weight of the foundation and overlying soil produces the following loads at the foundation-soil interface:

$$\begin{aligned} P &= \text{applied loads} + \text{weight of foundation and soil} \\ &= 1.4(-203.8 - 103.5) + 0.5(-43.8 - 22.3) + 0.75[0.32(3.8 + 51.8) + 1.11(-21.3 + 281)] \\ &\quad - 1.2[10(40)(5)(0.15) + 10(40)(2)(0.125)] \\ &= -714 \text{ kips.} \end{aligned}$$

$$\begin{aligned} M_{xx} &= \text{direct moments} + \text{moment due to eccentricity of applied axial loads} \\ &= 0.32(53.6 + 47.7) + 1.11(-1011.5 - 891.0) \\ &\quad + [1.4(-203.8) + 0.5(-43.8) + 0.75(0.32)(3.8) + 0.75(1.11)(-21.3)](12.5) \\ &\quad + [1.4(-103.5) + 0.5(-22.3) + 0.75(0.32)(51.8) + 0.75(1.11)(281)](-12.5) \\ &= -7258 \text{ ft-kips.} \end{aligned}$$

$$\begin{aligned} M_{yy} &= 0.32(-243.1 - 246.9) + 1.11(8.1 + 13.4) \\ &= -133 \text{ ft-kips. (The resulting eccentricity is small enough to neglect here, which simplifies the} \\ &\quad \text{problem considerably.)} \end{aligned}$$

$$\begin{aligned} V_x &= 0.32(-13.8 - 14.1) + 1.11(0.5 + 0.8) \\ &= -7.49 \text{ kips.} \end{aligned}$$

$$\begin{aligned} V_y &= 0.32(4.6 + 3.7) + 1.11(-85.1 - 68.2) \\ &= -167.5 \text{ kips.} \end{aligned}$$

Note that the above load combination does not yield the maximum downward load. Reversing the direction of the seismic load results in $P = -1173$ kips and $M_{xx} = 3490$ ft-kips. This larger axial load does not control the design because the moment is so much less that the resultant is within the kern and no uplift occurs.

The soil calculations that follow use a different sign convention than that in the analysis results noted above; compression is positive for the soil calculations. The eccentricity is:

$$e = |M/P| = 7258/714 = 10.17 \text{ ft.}$$

Where e is less than $L/2$, a solution to the overturning problem exists; however, as e approaches $L/2$, the bearing pressures increase without bound. Since e is greater than $L/6 = 40/6 = 6.67$ ft, uplift occurs and the maximum bearing pressure is:

$$q_{\max} = \frac{2P}{3B\left(\frac{L}{2} - e\right)} = \frac{2(714)}{3(10)\left(\frac{40}{2} - 10.17\right)} = 4.84 \text{ ksf}$$

and the length of the footing in contact with the soil is:

$$L' = 3\left(\frac{L}{2} - e\right) = 3\left(\frac{40}{2} - 10.17\right) = 29.5 \text{ ft.}$$

The bearing capacity $q_c = 3000 B' = 3000 \times \min(B, L'/2) = 3000 \times \min(10, 29.5/2) = 30,000 \text{ psf} = 30 \text{ ksf}$. ($L'/2$ is used as an adjustment to account for the gradient in the bearing pressure in that dimension.)

The design bearing capacity $\phi q_c = 0.6(30 \text{ ksf}) = 18 \text{ ksf} > 4.84 \text{ ksf}$. OK

The foundation satisfies overturning and bearing capacity checks. The upward case, which follows, will control the sliding check.

4.1.3.3 Upward Case (0.7D + 0.32Ex + 1.1Ey)

For the upward case the loads are:

$$\begin{aligned} P &= -346 \text{ kips} \\ M_{xx} &= -6240 \text{ ft-kips} \\ M_{yy} &= -133 \text{ ft-kips (negligible)} \\ V_x &= -7.5 \text{ kips} \\ V_y &= -167 \text{ kips} \end{aligned}$$

The eccentricity is:

$$e = |M/P| = 6240/346 = 18.0 \text{ ft.}$$

Again, e is greater than $L/6$, so uplift occurs and the maximum bearing pressure is:

$$q_{\max} = \frac{2(346)}{3(10)\left(\frac{40}{2} - 18.0\right)} = 11.5 \text{ ksf}$$

and the length of the footing in contact with the soil is:

$$L' = 3\left(\frac{40}{2} - 18.0\right) = 6.0 \text{ ft.}$$

The bearing capacity $q_c = 3000 \times \min(10, 6/2) = 9,000 \text{ psf} = 9.0 \text{ ksf}$.

The design bearing capacity $\phi q_c = 0.6(9.0 \text{ ksf}) = 5.4 \text{ ksf} < 11.5 \text{ ksf}$. NG

Using an elastic distribution of soil pressures, the foundation fails the bearing capacity check (although stability is satisfied). Try the plastic distribution. Using this approach, the bearing pressure over the entire contact area is assumed to be equal to the design bearing capacity. In order to satisfy vertical equilibrium, the contact area times the design bearing capacity must equal the applied vertical load P . Because the bearing capacity used in this example is a function of the contact area and the value of P changes with the size, the most convenient calculation is iterative.

By iteration, the length of contact area $L' = 4.39 \text{ ft}$.

The bearing capacity $q_c = 3000 \times \min(10, 4.39) = 13,170 \text{ psf} = 13.2 \text{ ksf}$. (No adjustment to L' is needed as the pressure is uniform.)

The design bearing capacity $\phi q_c = 0.6(13.2 \text{ ksf}) = 7.92 \text{ ksf}$.

$(7.92)(4.39)(10) = 348 \text{ kips} \approx 346 \text{ kips}$, so equilibrium is satisfied; the difference is rounded off.

The resisting moment, $M_R = P(L/2 - L'/2) = 346(40/2 - 4.39/2) = 6160 \text{ ft-kip} \approx 6240 \text{ ft-kip}$. OK

Therefore, using a plastic distribution of soil pressures, the foundation satisfies overturning and bearing capacity checks.

The calculation of demands on concrete sections for strength checks should use the same soil stress distribution as the overturning check. Using a plastic distribution of soil stresses defines the upper limit of static loads for which the foundation remains stable, but the extreme concentration of soil bearing tends to drive up shear and flexural demands on the concrete section. It should be noted that the foundation may remain stable for larger loads if they are applied dynamically; even in that case, the strength demands on the concrete section will not exceed those computed on the basis of the plastic distribution.

For the sliding check, initially consider base traction only. The sliding demand is:

$$V = \sqrt{V_x^2 + V_y^2} = \sqrt{(-7.49)^2 + (-167)^2} = 167.2 \text{ kips}.$$

As calculated previously, the total compression force at the bottom of the foundation is 346 kips. The design sliding resistance is:

$$\phi V_c = \phi \times \text{friction coefficient} \times P = 0.8(0.65)(346 \text{ kips}) = 180 \text{ kips} > 167.2 \text{ kips}. \quad \text{OK}$$

If base traction alone had been insufficient, resistance due to passive pressure on the leading face could be included. Sec. 4.2.2.2 below illustrates passive pressure calculations for a pile cap.

4.1.3.4 Design Results

The calculations performed in Sec. 4.1.3.2 and 4.1.3.3 are repeated for combined footings at middle and side locations. Figure 4.1-6 shows the results.

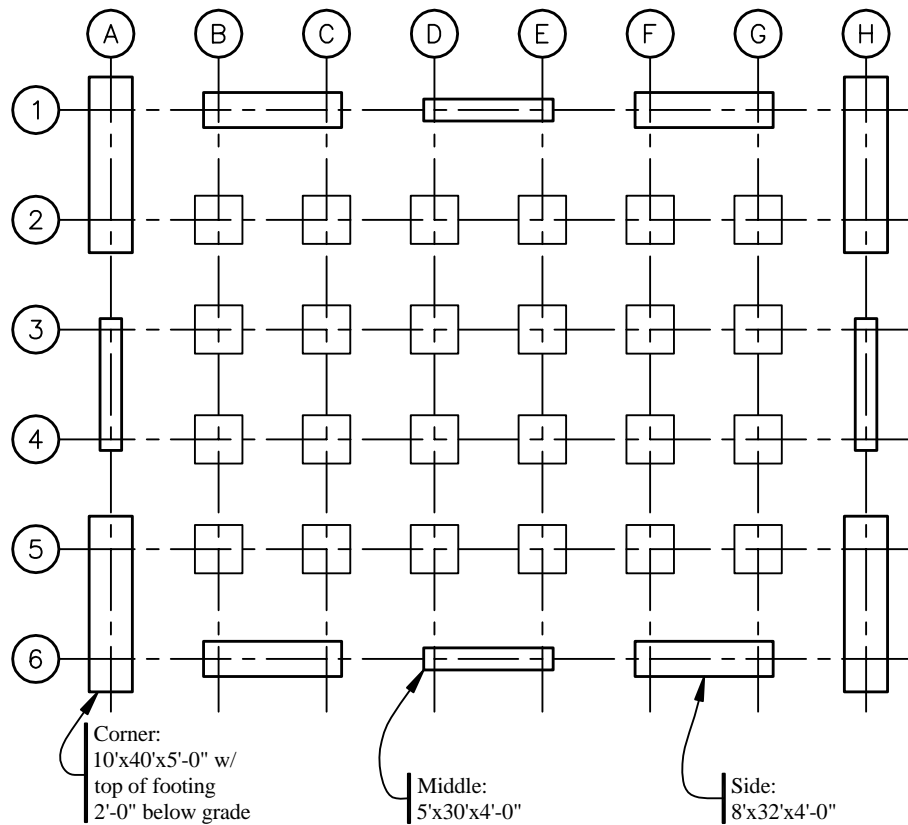


Figure 4.1-6 Foundation plan for moment-resisting frame system.

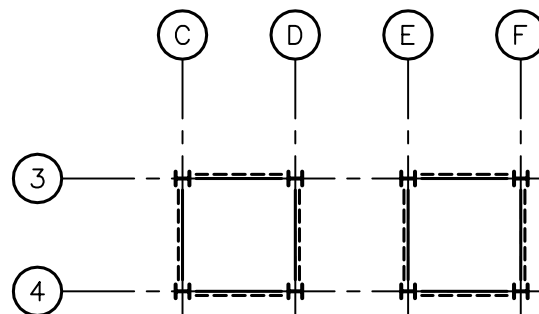


Figure 4.1-7 Framing plan for concentrically braced frame system.

One last check of interest is to compare the flexural stiffness of the footing with that of the steel column, which is needed because the steel frame design was based upon flexural restraint at the base of the columns. Using an effective moment of inertia of 50 percent of the gross moment of inertia and also using the distance between columns as the effective span, the ratio of EI/L for the smallest of the combined footings is more than five times the EI/h for the steel column. This is satisfactory for the design assumption.

4.1.4 Design for Concentrically Braced Frame System

Framing Alternate B in Sec. 5.2 of this volume of design examples employs a concentrically braced frame system at a central core to provide resistance to seismic loads. A framing plan for the system is shown in Figure 4.1-7.

4.1.4.1 Check Mat Size for Overturning

Uplift demands at individual columns are so large that the only practical shallow foundation is one that ties together the entire core. The controlling load combination for overturning has minimum vertical loads (which help to resist overturning), primary overturning effects (M_{xx}) due to loads applied parallel to the short side of the core, and smaller moments about a perpendicular axis (M_{yy}) due to orthogonal effects. Assume mat dimensions of 45 ft by 95 ft by 7 ft thick with the top of the mat 3'-6" below grade. Combining the factored loads applied to the mat by all eight columns and including the weight of the foundation and overlying soil produces the following loads at the foundation-soil interface:

$$\begin{aligned} P &= -7,849 \text{ kips} \\ M_{xx} &= -148,439 \text{ ft-kips} \\ M_{yy} &= -42,544 \text{ ft-kips} \\ V_x &= -765 \text{ kips} \\ V_y &= -2,670 \text{ kips} \end{aligned}$$

Figure 4.1-8 shows the soil pressures that result from application in this controlling case, depending on the soil distribution assumed. In both cases the computed uplift is significant. In Part a of the figure the contact area is shaded. The elastic solution shown in Part b was computed by modeling the mat in RISA 3D with compression only soil springs (with the stiffness of edge springs doubled as recommended by Bowles). For the elastic solution the average width of the contact area is 11.1 ft and the maximum soil pressure is 16.9 ksf.

The bearing capacity $q_c = 3000 \times \min(95, 11.1/2) = 16,650 \text{ psf} = 16.7 \text{ ksf}$.

The design bearing capacity $\phi q_c = 0.6(16.7 \text{ ksf}) = 10.0 \text{ ksf} < 16.9 \text{ ksf}$.

NG

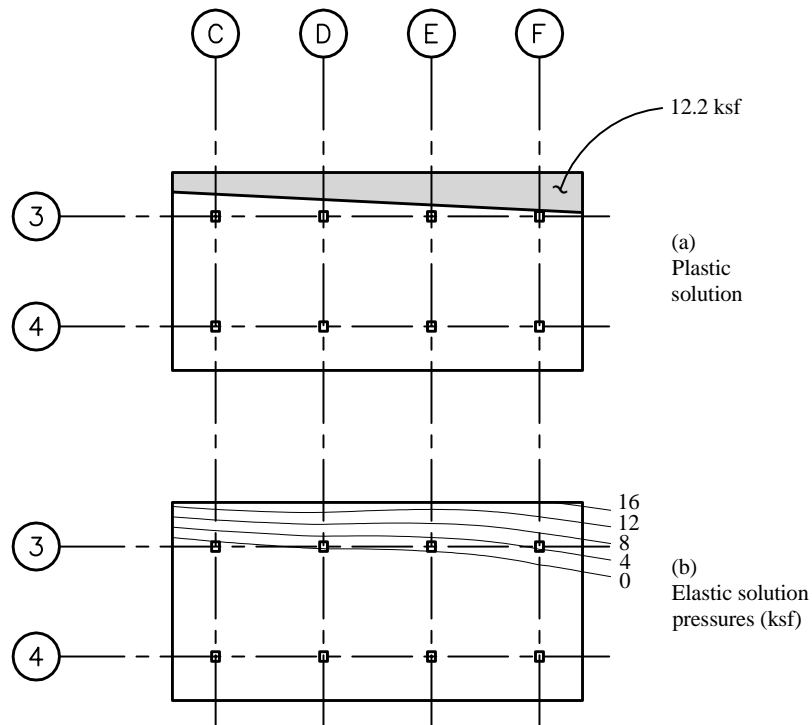


Figure 4.1-8 Soil pressures for controlling bidirectional case.

As was done in Sec. 4.1.3.3 above, try the plastic distribution. The present solution has an additional complication as the off-axis moment is not negligible. The bearing pressure over the entire contact area is assumed to be equal to the design bearing capacity. In order to satisfy vertical equilibrium, the contact area times the design bearing capacity must equal the applied vertical load P . The shape of the contact area is determined by satisfying equilibrium for the off-axis moment. Again the calculations are iterative.

Given the above constraints, the contact area shown in Figure 4.1-8 is determined. The length of the contact area is 4.46 ft at the left side and 9.10 ft at the right side. The average contact length, for use in determining the bearing capacity, is $(4.46 + 9.10)/2 = 6.78$ ft. The distances from the center of the mat to the centroid of the contact area are

$$\bar{x} = 5.42 \text{ ft}$$

$$\bar{y} = 18.98 \text{ ft}$$

The bearing capacity $q_c = 3000 \times \min(95, 6.78) = 20,340 \text{ psf} = 20.3 \text{ ksf}$.

The design bearing capacity $\phi q_c = 0.6(20.3 \text{ ksf}) = 12.2 \text{ ksf}$.

$$(12.2)(6.78)(95) = 7,858 \text{ kips} \approx 7,849 \text{ kips, confirming equilibrium for vertical loads.}$$

$$(7,849)(5.42) = 42,542 \text{ ft-kips} \approx 42,544 \text{ ft-kips, confirming equilibrium for off-axis moment.}$$

The resisting moment, $M_{R,xx} = P \bar{y} = 7849(18.98) = 148,974 \text{ ft-kips} > 148,439 \text{ ft-kips}$.

OK

So, the checks of stability and bearing capacity are satisfied. The mat dimensions are shown in Figure 4.1-9.

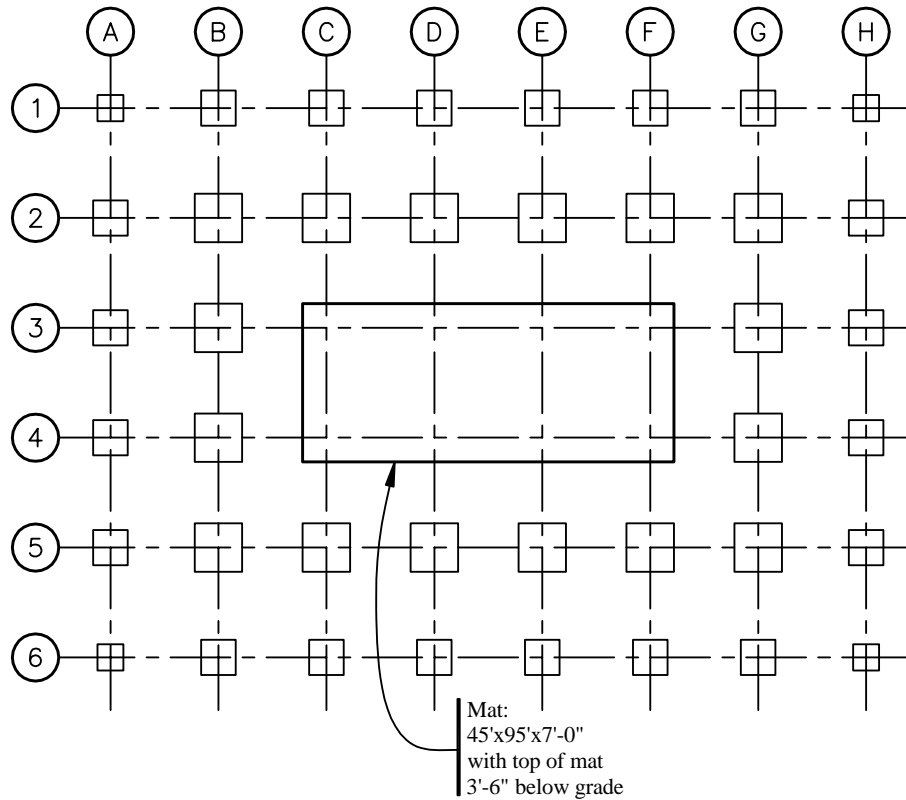


Figure 4.1-9 Foundation plan for concentrically braced frame system.

4.1.4.2 Design Mat for Strength Demands

As was previously discussed, the computation of strength demands for the concrete section should use the same soil pressure distribution as was used to satisfy stability and bearing capacity. Because dozens of load combinations were considered and “hand calculations” were used for the plastic distribution checks, the effort required would be considerable. The same analysis used to determine elastic bearing pressures yields the corresponding section demands directly. One approach to this dilemma would be to compute an additional factor that must be applied to selected elastic cases to produce section demands that are consistent with the plastic solution. Rather than provide such calculations here, design of the concrete section will proceed using the results of the elastic analysis. This is conservative for the demand on the concrete for the same reason that it was unsatisfactory for the soil: the edge soil pressures are high (that is, we are designing the concrete for a peak soil pressure of 16.9 ksf, even though the plastic solution gives 12.2 ksf).

[Note that Sec. 7.2.3 of the 2003 *Provisions* requires consideration of parametric variation for soil properties where foundations are modeled explicitly. This example does not illustrate such calculations.]

Concrete mats often have multiple layers of reinforcement in each direction at the top and bottom of their thickness. Use of a uniform spacing for the reinforcement provided in a given direction greatly increases the ease of construction. The minimum reinforcement requirements defined in Sec. 10.5 of ACI 318 were discussed in Sec. 4.1.1.3 above. Although all of the reinforcement provided to satisfy Sec. 7.12 of ACI 318 may be provided near one face, for thick mats it is best to compute and provide the amount of required reinforcement separately for the top and bottom halves of the section. Using a bar spacing of 10 in. for this 7-ft-thick mat and assuming one or two layers of bars, the section capacities indicate in Table 4.1-4 (presented in order of decreasing strength) may be precomputed for use in design. The amount of

reinforcement provided for marks B, C, and D are less than the basic minimum for flexural members, so the demands should not exceed three-quarters of the design strength where those reinforcement patterns are used. The amount of steel provided for Mark D is the minimum that satisfies ACI 318 Sec. 7.12.

Table 4.1-4 Mat Foundation Section Capacities

Mark	Reinforcement	A_s (in. ² per ft)	ϕM_n (ft-kip/ft)	$3/4 \phi M_n$ (ft-kip/ft)
A	2 layers of #10 bars at 10 in. o.c.	3.05	899	not used
B	2 layers of #9 bars at 10 in. o.c.	2.40	not used	534
C	2 layers of #8 bars at 10 in. o.c.	1.90	not used	424
D	#8 bars at 10 in. o.c.	0.95	not used	215

Note: Where the area of steel provided is less than the minimum reinforcement for flexural members as indicated in ACI 318 Sec. 10.5.1, demands are compared to $3/4$ of ϕM_n as permitted in Sec. 10.5.3.

To facilitate rapid design the analysis results are processed in two additional ways. First, the flexural and shear demands computed for the various load combinations are enveloped. Then the enveloped results are presented (see Figure 4.1-10) using contours that correspond to the capacities shown for the reinforcement patterns noted in Table 4.1-4.

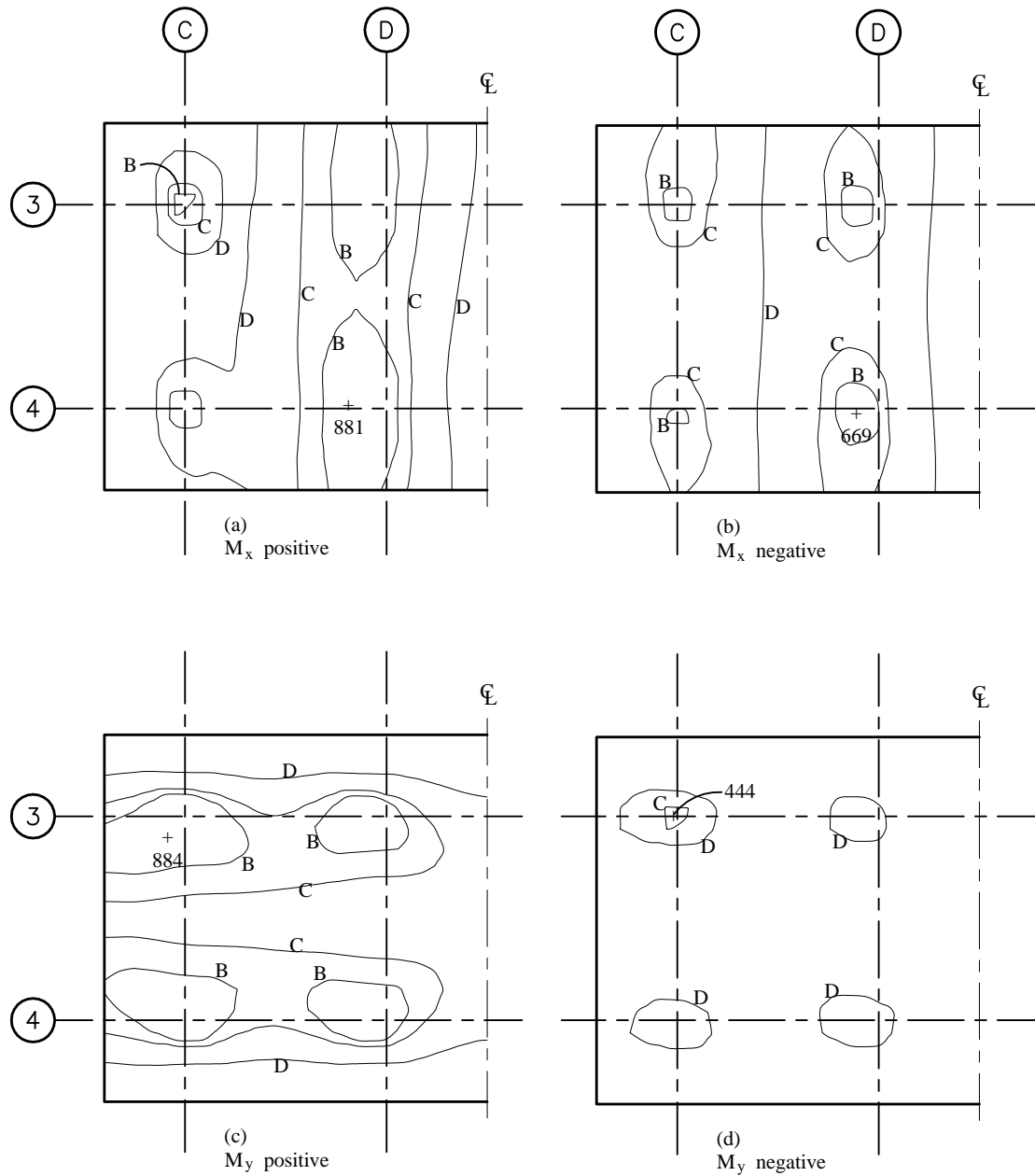


Figure 4.1-10 Envelope of mat foundation flexural demands.

Using the noted contours permits direct selection of reinforcement. The reinforcement provided within a contour for a given mark must be that indicated for the next higher mark. For instance, all areas within Contour B must have two layers of #10 bars. Note that the reinforcement provided will be symmetric about the centerline of the mat in both directions. Where the results of finite element analysis are used in the design of reinforced concrete elements, averaging of demands over short areas is appropriate. In Figure 4.1-11, the selected reinforcement is superimposed on the demand contours. Figure 4.1-12 shows a section of the mat along Gridline C.

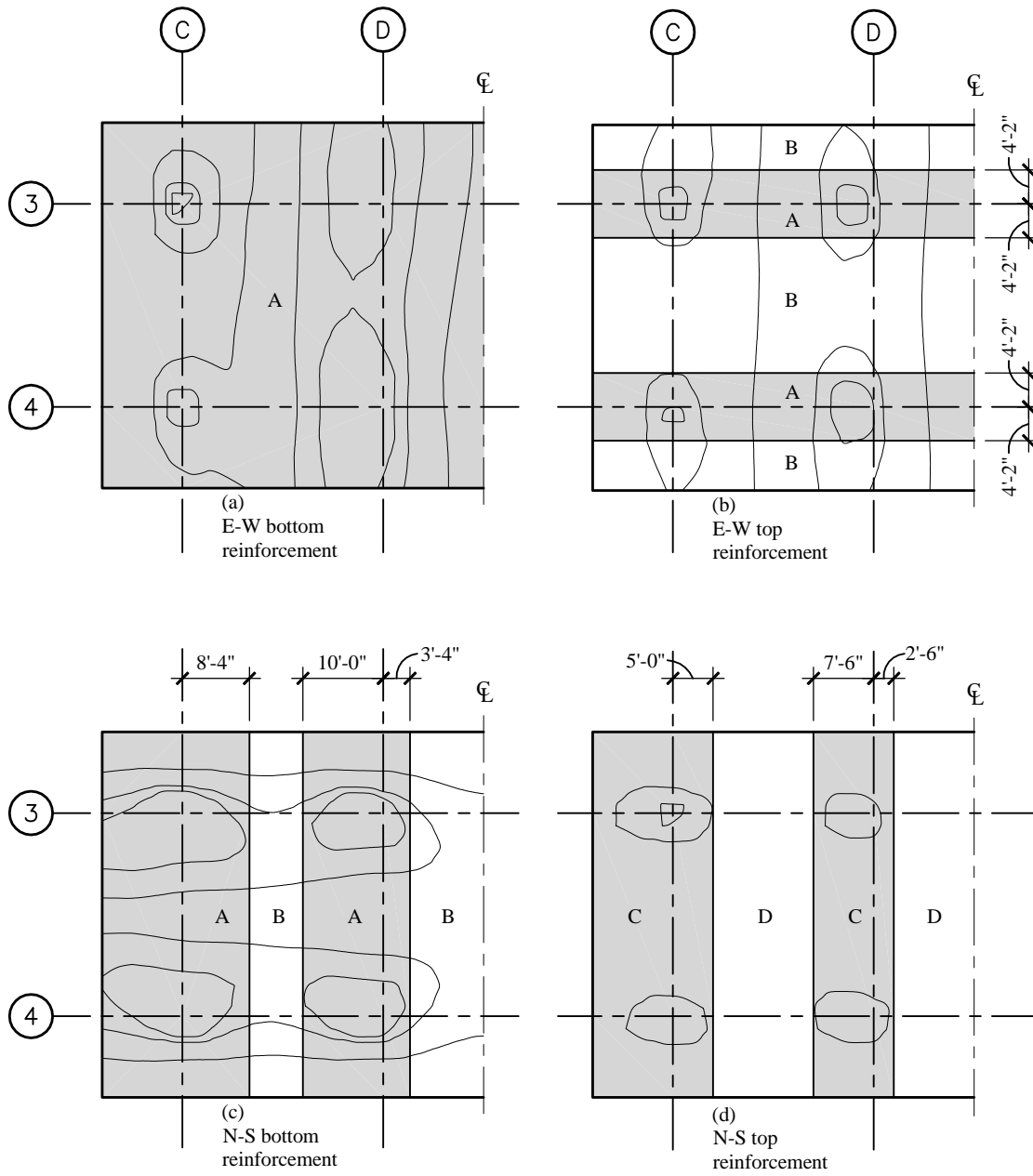


Figure 4.1-11 Mat foundation flexural reinforcement.

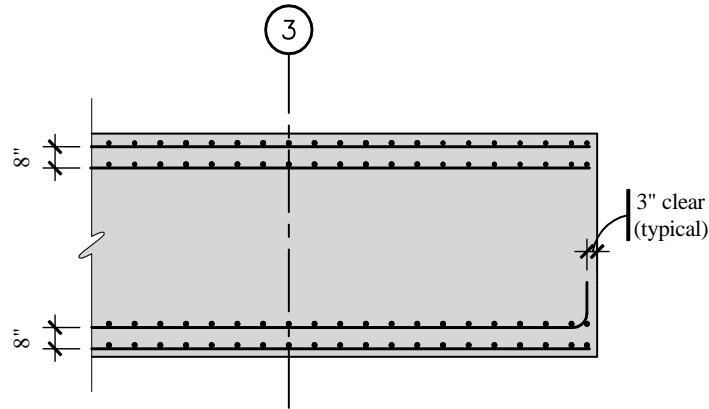


Figure 4.1-12 Section of mat foundation.

Figure 4.1-13 presents the envelope of shear demands. The contours used correspond to the design strengths computed assuming $V_s = 0$ for one-way and two-way shear. In the hatched areas the shear stress exceeds $\phi 4\sqrt{f'_c}$ and in the shaded areas it exceeds $\phi 2\sqrt{f'_c}$. The critical sections for two-way shear (as discussed in Sec. 4.1.1.3 also are shown. The only areas that need more careful attention (to determine whether they require shear reinforcement) are those where the hatched or shaded areas are outside the critical sections. At the columns on Gridline D, the hatched area falls outside the critical section, so closer inspection is needed. Because the perimeter of the hatched area is substantially smaller than the perimeter of the critical section for punching shear, the design requirements of ACI 318 are satisfied.

One-way shears at the edges of the mat exceed the $\phi 2\sqrt{f'_c}$ criterion. Note that the high shear stresses are not produced by loads that create high bearing pressures at the edge. Rather they are produced by loads that created large bending stresses parallel to the edge. The distribution of bending moments and shears is not uniform across the width (or breadth) of the mat, primarily due to the torsion in the seismic loads and the orthogonal combination. It is also influenced by the doubled spring stiffnesses used to model the soil condition. However, when the shears are averaged over a width equal to the effective depth (d), the demands are less than the design strength.

In this design, reinforcement for punching or beam shear is not required. If shear reinforcement cannot be avoided, bars may be used both to chair the upper decks of reinforcement and provide resistance to shear in which case they may be bent thus: .

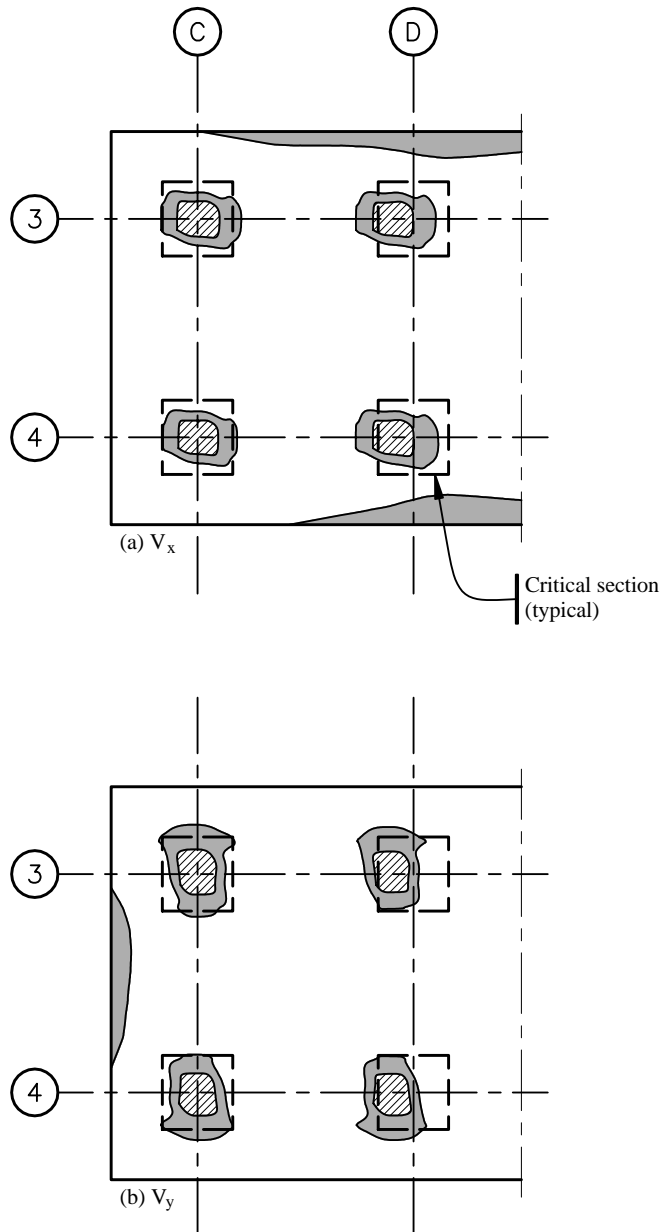


Figure 4.1-13 Critical sections for shear and envelope of mat foundation shear demands.

4.1.5 COST COMPARISON

Table 4.1-5 provides a summary of the material quantities used for all of the foundations required for the various conditions considered. Corresponding preliminary costs are assigned. The gravity-only condition does not represent a realistic case because design for wind loads would require changes to the foundations; it is provided here for discussion. It is obvious that design for lateral loads adds cost as compared to a design that neglects such loads. However, it is also worth noting that braced frame systems usually have substantially more expensive foundation systems than do moment frame systems. This condition occurs for two reasons. First, braced frame systems are stiffer, which produces shorter periods and higher design forces. Second, braced frame systems tend to concentrate spatially the demands on the

foundations. In this case the added cost amounts to about \$0.80/ft², which is an increase of perhaps 4 or 5 percent to the cost of the structural system.

Table 4.1-5 Summary of Material Quantities and Cost Comparison

Design Condition	Concrete at Gravity Foundations	Concrete at Lateral Foundations	Total Excavation	Total Cost
Gravity only (see Figure 4.1-4)	310 cy at \$150/cy = \$46,500		310 cy at \$15/cy = \$4,650	\$ 51,150
Moment frame (see Figure 4.1-6)	233 cy at \$150/cy = \$34,950	537 cy at \$180/cy = \$96,660	800 cy at \$15/cy = \$12,000	\$143,610
Braced frame (see Figure 4.1-9)	233 cy at \$150/cy = \$34,950	1108 cy at \$180/cy = \$199,440	1895 cy at \$15/cy = \$28,425	\$262,815

4.2 DEEP FOUNDATIONS FOR A 12-STORY BUILDING, SEISMIC DESIGN CATEGORY D

This example features the analysis and design of deep foundations for a 12-story reinforced concrete moment-resisting frame building similar to that described in Chapter 6 of this volume of design examples.

4.2.1 Basic Information

4.2.1.1 Description

Figure 4.2-1 shows the basic design condition considered in this example. A 2×2 pile group is designed for four conditions: for loads delivered by a corner and a side column of a moment-resisting frame system for Site Classes C and E. Geotechnical parameters for the two sites are given in Table 4.2-1.

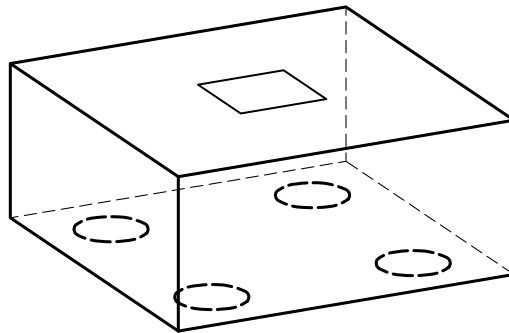


Figure 4.2-1 Design condition: column of concrete moment resisting frame supported by pile cap and cast-in-place piles.

Table 4.2-1 Geotechnical Parameters

Depth	Class E Site	Class C Site
0 to 3 ft	Loose sand/fill $\gamma = 110$ pcf angle of internal friction = 28 deg soil modulus parameter, $k = 25$ pci neglect skin friction neglect end bearing	Loose sand/fill $\gamma = 110$ pcf angle of internal friction = 30 deg soil modulus parameter, $k = 50$ pci neglect skin friction neglect end bearing
3 to 30 ft	Soft clay $\gamma = 110$ pcf undrained shear strength = 430 psf soil modulus parameter, $k = 25$ pci strain at 50 percent of maximum stress, $\epsilon_{50} = 0.01$ skin friction (ksf) = 0.3 neglect end bearing	Dense sand (one layer: 3 to 100 ft depth) $\gamma = 130$ pcf angle of internal friction = 42 deg soil modulus parameter, $k = 125$ pci
30 to 100 ft	Medium dense sand $\gamma = 120$ pcf angle of internal friction = 36 deg soil modulus parameter, $k = 50$ pci skin friction (ksf)* = $0.9 + 0.025/\text{ft} \leq 2$ end bearing (ksf)* = $40 + 0.5/\text{ft} \leq 100$	skin friction (ksf)* = $0.3 + 0.03/\text{ft} \leq 2$ end bearing (ksf)* = $65 + 0.6/\text{ft} \leq 150$
Pile cap resistance	300 pcf, ultimate passive pressure	575 pcf, ultimate passive pressure
Resistance factor for capacity checks (ϕ) = 0.75. Safety factor for settlement checks = 2.5.		[In the 2003 <i>Provisions</i> , ϕ factors for cohesive and cohesionless soils are explicitly defined; for vertical, lateral and rocking resistance, the values would be 0.8 for the clay layer and 0.7 for the sand layers.]

*Skin friction and end bearing values increase (up to the maximum value noted) for each additional foot of depth below the top of the layer. (The values noted assume a minimum pile length of 20 ft.)

The structural material properties assumed for this example are as follows:

$$f'_c = 3,000 \text{ psi}$$

$$f_y = 60,000 \text{ psi}$$

4.2.1.2 Provisions Parameters

Site Class = C and E (both conditions considered in this example)

$$S_{DS} = 0.9$$

Seismic Design Category = D (for both conditions)

4.2.1.3 Demands

The unfactored demands from the moment frame system are shown in Table 4.2-2.

Table 4.2-2 Gravity and Seismic Demands

Location	Load	R_x	R_y	R_z	M_{xx}	M_{yy}
Corner	D			-351.0		
	L			-36.0		
	V_x	40.7	0.6	142.5	4.8	439.0
	V_y	0.8	46.9	305.6	489.0	7.0
	AT_x	1.2	2.6	12.0	27.4	12.9
	AT_y	3.1	6.7	31.9	70.2	33.0
Side	D			-702.0		
	L			-72.0		
	V_x	29.1	0.5	163.4	3.5	276.6
	V_y	0.8	59.3	18.9	567.4	6.5
	AT_x	0.1	3.3	8.7	31.6	1.3
	AT_y	0.4	8.4	22.2	80.8	3.4

Note: Units are kips and feet. Load V_x is for loads applied toward the east. AT_x is the corresponding accidental torsion case. Load V_y is for loads applied toward the north. AT_y is the corresponding accidental torsion case.

Using ASCE 7 Load Combinations 5 and 7, E as defined in *Provisions* Sec. 5.2.7 [4.2.2] (with $0.2S_{DS}D = 0.18D$ and taking $\rho = 1.0$), considering orthogonal effects as required for Seismic Design Category D, and including accidental torsion, the following 32 load conditions must be considered. [Although the redundancy factor is changed substantially in the 2003 *Provisions*, it is expected that this system would still satisfy the conditions needed for $\rho = 1.0$, so these load combinations would not change.]

$$1.38D + 0.5L \pm 1.0V_x \pm 0.3V_y \pm \max(1.0AT_x, 0.3AT_y)$$

$$1.38D + 0.5L \pm 0.3V_x \pm 1.0V_y \pm \max(0.3AT_x, 1.0AT_y)$$

$$0.72D \pm 1.0V_x \pm 0.3V_y \pm \max(1.0AT_x, 0.3AT_y)$$

$$0.72D \pm 0.3V_x \pm 1.0V_y \pm \max(0.3AT_x, 1.0AT_y)$$

4.2.1.4 Design Approach

For typical deep foundation systems resistance to lateral loads is provided by both piles and pile cap. Figure 4.2-2 shows a simple idealization of this condition. The relative contributions of these piles and pile cap depend on the particular design conditions, but often both effects are significant. Resistance to vertical loads is assumed to be provided by the piles alone regardless of whether their axial capacity is primarily due to end bearing, skin friction, or both. Although the behavior of foundation and superstructure are closely related, they typically are modeled independently. Earthquake loads are applied to a model of the superstructure, which is assumed to have fixed supports. Then the support reactions are seen as demands on the foundation system. A similar substructure technique is usually applied to the foundation system itself, whereby the behavior of pile cap and piles are considered separately. This section describes that typical approach.

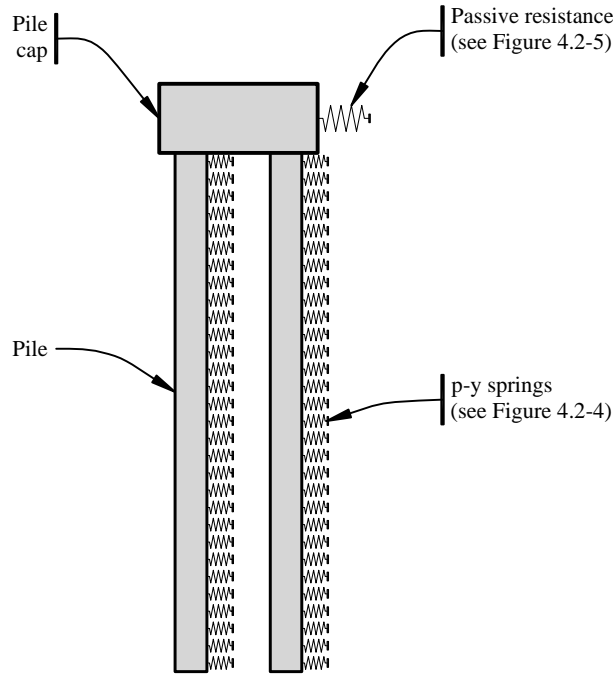


Figure 4.2-2 Schematic model of deep foundation system.

4.2.1.4.1 Pile Group Mechanics

With reference to the free body diagram (of a 2×2 pile group) shown in Figure 4.2-3, demands on individual piles as a result of loads applied to the group may be determined as follows:

$V = \frac{V_{group} - V_{passive}}{4}$ and $M = V \times \ell$, where ℓ is a characteristic length determined from analysis of a laterally loaded single pile.

$P_{ot} = \frac{V_{group} h + M_{group} + 4M - h_p V_{passive}}{2s}$, where s is the pile spacing, h is the height of the pile cap, and h_p is the height of $V_{passive}$ above Point O.

$P_p = \frac{P_{group}}{4}$ and $P = P_{ot} + P_p$

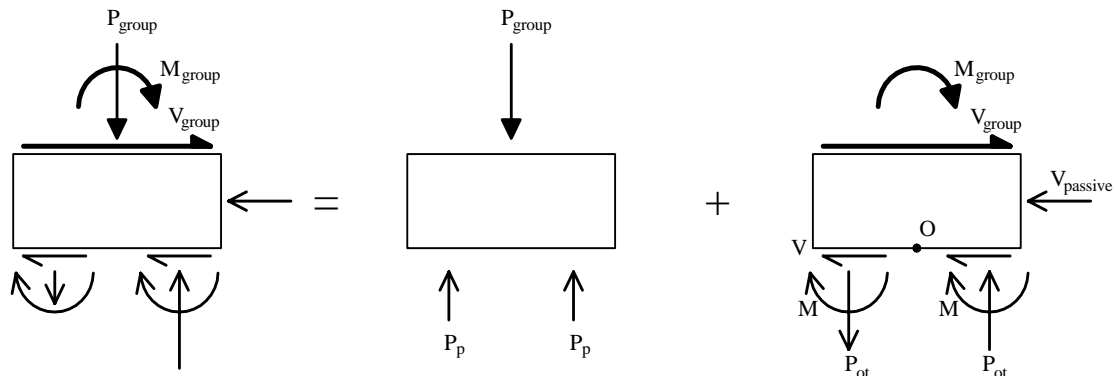


Figure 4.2-3 Pile cap free body diagram.

4.2.1.4.2 Contribution of Piles

The response of individual piles to lateral loads is highly nonlinear. In recent years it has become increasingly common to consider that nonlinearity directly. Based on extensive testing of full-scale specimens and small-scale models for a wide variety of soil conditions, researchers have developed empirical relationships for the nonlinear p - y response of piles that are suitable for use in design. Representative p - y curves (computed for a 22 in. diameter pile) are shown in Figure 4.2-4. The stiffness of the soil changes by an order of magnitude for the expected range of displacements (the vertical axis uses a logarithmic scale). The p - y response is sensitive to pile size (an effect not apparent in the figure which is based on a single pile size); soil type and properties; and, in the case of sands, vertical stress, which increases with depth. Pile response to lateral loads, like the p - y curves on which the calculations are based, is usually computed using computer programs like LPILE.

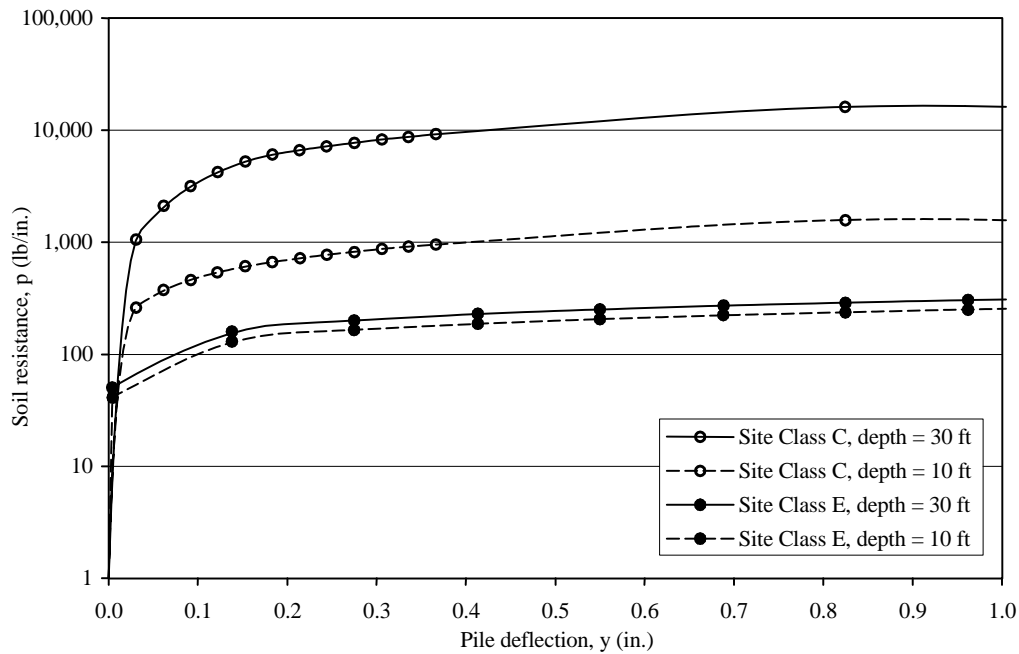


Figure 4.2-4 Representative p - y curves (note that a logarithmic scale is used on the vertical axis).

4.2.1.4.3 Contribution of Pile Cap

Pile caps contribute to the lateral resistance of a pile group in two important ways: directly as a result of passive pressure on the face of the cap that is being pushed into the soil mass and indirectly by producing a fixed head condition for the piles, which can significantly reduce displacements for a given applied lateral load. Like the p - y response of piles, the passive pressure resistance of the cap is nonlinear. Figure 4.2-5 shows how the passive pressure resistance (expressed as a fraction of the ultimate passive pressure) is related to the imposed displacement (expressed as a fraction of the minimum dimension of the face being pushed into the soil mass).

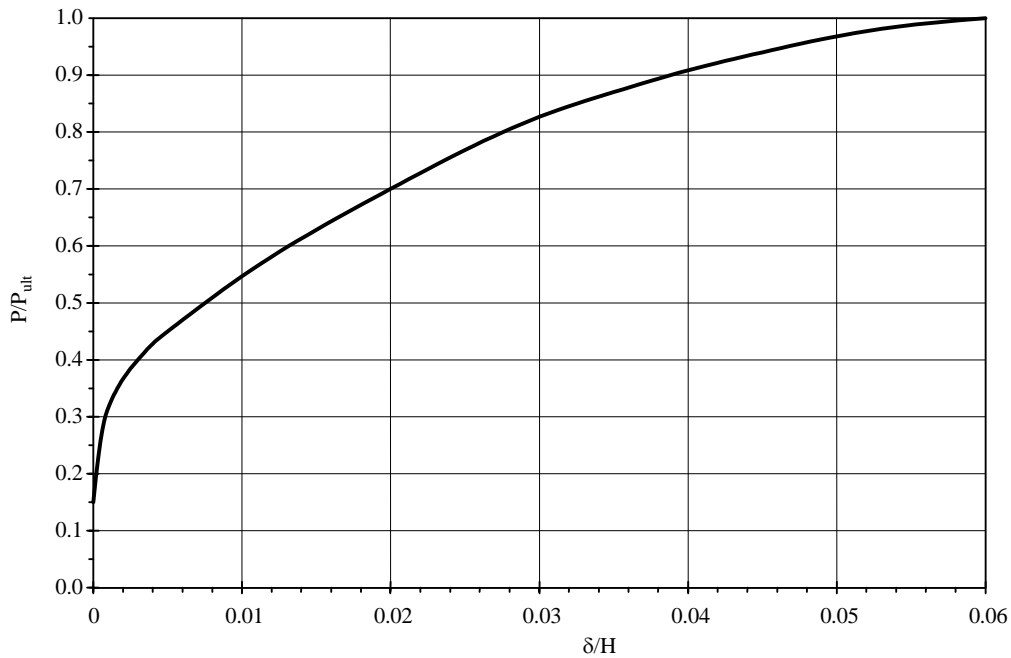


Figure 4.2-5 Passive pressure mobilization curve (after FEMA 356).

4.2.1.4.4 Group Effect Factors

The response of a group of piles to lateral loading will differ from that of a single pile due to pile-soil-pile interaction. (Group effect factors for axial loading of very closely spaced piles may also be developed, but are beyond the scope of the present discussion.) A useful discussion of this “group effect” may be found in PoLam Sec. 2.6.4, from which the following observations are taken:

The pile group effect has been a popular research topic within the geotechnical community for almost 50 years. At present, there is no common consensus on the approach for group effects. Full-size and model tests by a number of authors show that in general, the lateral capacity of a pile in a pile group versus that of a single pile (termed “efficiency”) is reduced as the pile spacing is reduced. . . .

[The experimental research reported in Brown 1987, Brown 1988, and other publications] . . . yielded information that largely corroborated each other on the following aspects:

- (1) Most of these experiments first used the single pile data to verify the validity of the widely used Reese’s and Matlock’s benchmark p-y criteria and all concluded that the Reese and Matlock p-y criteria provide reasonable solutions.
- (2) The observed group effects appeared to be associated with shadowing effects and the various researchers found relatively consistent pile group behavior in that the leading piles would be loaded more heavily than the trailing piles when all piles are loaded to the same deflection. . . . All referenced researchers recommended to modify the single pile p-y curves by adjusting the resistance value on the single pile p-y curves (i.e. p-multiplier). . . .

The experiments reported by McVay also included data for pile center-to-center spacing of 5D which showed p-multipliers of 1.0, 0.85, and 0.7 for the front, middle and back row piles, respectively. For such multipliers, the group stiffness efficiency would be about 95% and group effects would be practically negligible.

The basis of the calculation procedure for group effect factors that is shown below is described in Chapter 6 of GROUP. In these expressions, D is the pile diameter and s is the center-to-center spacing between the piles in question. In the equation for each efficiency factor, where s/D equals or exceeds the noted upper limit, the corresponding value of β is 1.0.

For piles that are side by side with respect to the applied load, a factor to reflect the reduction in efficiency, β_a , may be calculated as:

$$\beta_a = 0.5292 \left(\frac{s}{D} \right)^{0.5659} \quad \text{for } 1 \leq \frac{s}{D} < 3.28 .$$

For piles that are in-line with respect to the applied load, a factor to reflect the reduction in efficiency (β_b) may be calculated as follows:

$$\text{Leading piles: } \beta_{bL} = 0.7309 \left(\frac{s}{D} \right)^{0.2579} \quad \text{for } 1 \leq \frac{s}{D} < 3.37 .$$

$$\text{Trailing piles: } \beta_{bT} = 0.5791 \left(\frac{s}{D} \right)^{0.3251} \quad \text{for } 1 \leq \frac{s}{D} < 5.37 .$$

For piles that are skewed (neither in line nor side by side) with respect to the applied load, a factor to reflect the reduction in efficiency (β_s) may be calculated as:

$$\beta_s = \sqrt{\beta_a^2 \cos^2 \theta + \beta_b^2 \sin^2 \theta}$$

where β_a and β_b are calculated as defined above using s equal to the center-to-center distance along the skew and setting θ equal to the angle between the direction of loading and a line connecting the two piles.

If a group contains more than two piles, the effect of each pile on each other pile must be considered. If the effect of pile j on pile i is called β_{ji} and it is noted that $\beta_{ji} = 1.0$ when $j = i$ (as this is a single pile condition), the p -reduction factor for any given pile i is

$$f_{mi} = \prod_{j=1}^n \beta_{ji} .$$

Because the direction of loading varies during an earthquake and the overall efficiency of the group is the primary point of interest, the average efficiency factor is commonly used for all members of a group in the analysis of any given member. In that case, the average p -reduction factor is:

$$\bar{f}_m = \frac{1}{n} \sum_{i=1}^n \prod_{j=1}^n \beta_{ji} .$$

For a 2x2 pile group thus  with $s = 3D$, the group effect factor is calculated as:

$$\beta_{11} = 1.0,$$

$$\beta_{21} = \beta_a \beta_b = 0.5292 \left(\frac{3}{1} \right)^{0.5659} \times 1.0 = 0.985 ,$$

$$\beta_{31} = \beta_a \beta_b = 1.0 \times 0.7309 \left(\frac{3}{1} \right)^{0.2579} = 0.970 , \text{ and}$$

$$\beta_{41} = \beta_a \beta_b = (1.0)(1.0) = 1.0 \text{ (because } s/D = 4.24).$$

$$\text{Thus, } f_{m1} = \beta_{11} \times \beta_{21} \times \beta_{31} \times \beta_{41} = (1.00)(0.985)(0.970)(1.00) = 0.955 \approx 0.96.$$

By similar calculations, $f_{m2} = 0.96$, $f_{m3} = 0.79$, and $f_{m4} = 0.79$.

$$\text{And finally, } \bar{f}_m = \frac{0.96 + 0.96 + 0.79 + 0.79}{4} = 0.87 .$$

Figure 4.2-6 shows the group effect factors that are calculated for square pile groups of various sizes with piles at several different spacings.

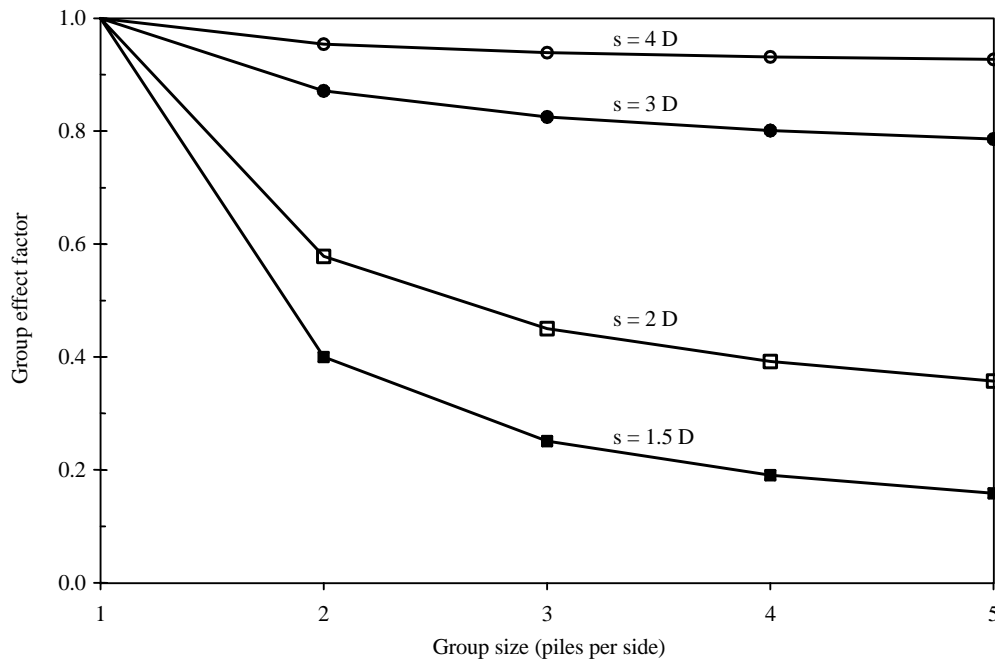


Figure 4.2-6 Calculated group effect factors.

4.2.2 Pile Analysis, Design, and Detailing

4.2.2.1 Pile Analysis

For this design example it is assumed that all piles will be fixed-head, 22-in.-diameter, cast-in-place piles arranged in 2×2 pile groups with piles spaced at 66 inches center-to-center. The computer program LPILE Plus 3.0 is used to analyze single piles for both soil conditions shown in Table 4.2-1 assuming a

length of 50 ft. Pile flexural stiffness is modeled using one-half of the gross moment of inertia because of expected flexural cracking. The response to lateral loads is affected to some degree by the coincident axial load. The full range of expected axial loads was considered in developing this example, but in this case the lateral displacements, moments, and shears were not strongly affected; the plots in this section are for zero axial load. A p -multiplier of 0.87 for group effects (as computed at the end of Sec. 4.2.1.4) is used in all cases. Figures 4.2-7, 4.2-8, and 4.2-9 show the variation of shear, moment, and displacement with depth (within the top 30 ft) for an applied lateral load of 15 kips on a single pile with the group reduction factor. It is apparent that the extension of piles to depths beyond 30 ft for the Class E site (or about 25 ft for the Class C site) does not provide additional resistance to lateral loading; piles shorter than those lengths would have reduced lateral resistance. The trends in the figures are those that should be expected. The shear and displacement are maxima at the pile head. Because a fixed-head condition is assumed, moments are also largest at the top of the pile. Moments and displacements are larger for the soft soil condition than for the firm soil condition.

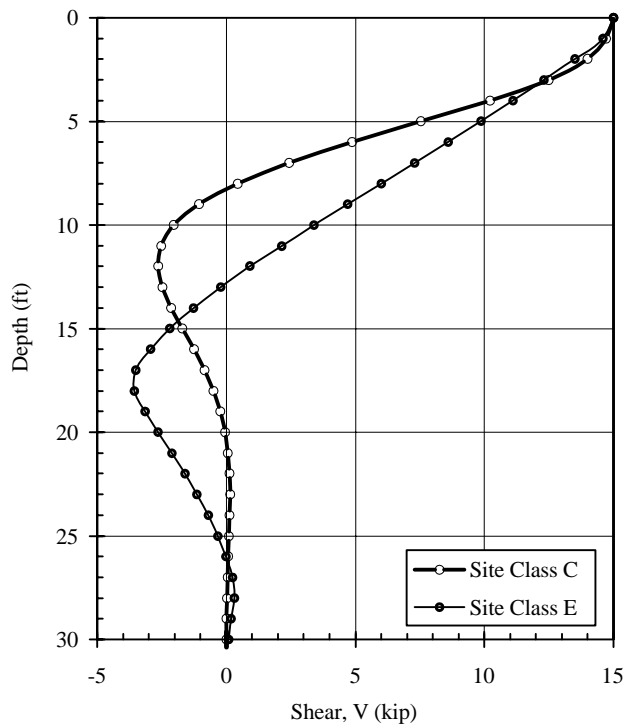


Figure 4.2-7 Results of pile analysis – shear versus depth (applied lateral load is 15 kips).

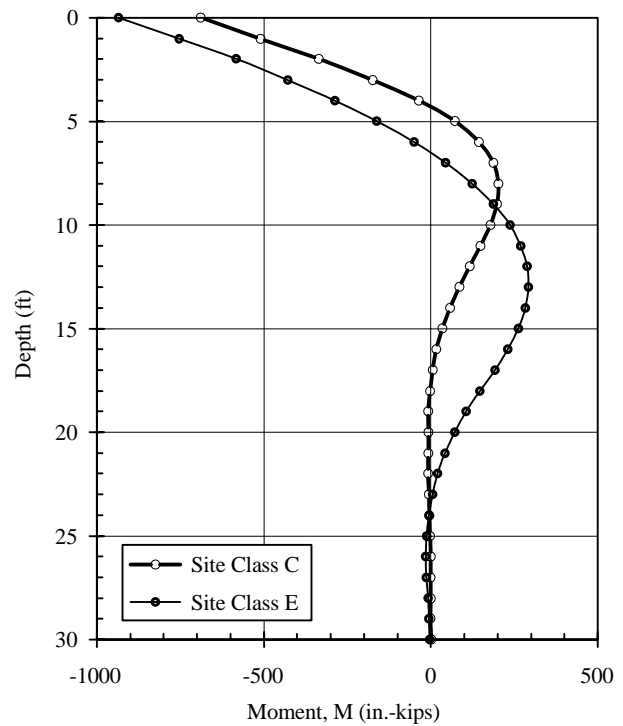


Figure 4.2-8 Results of pile analysis – moment versus depth (applied lateral load is 15 kips).

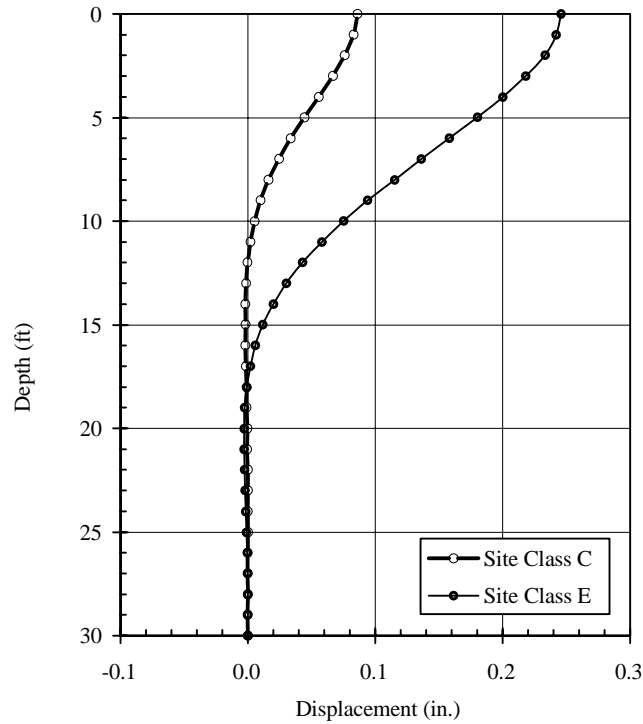


Figure 4.2-9 Results of pile analysis – displacement versus depth (applied lateral load is 15 kips)

The analyses performed to develop Figures 4.2-7 through 4.2-9 are repeated for different levels of applied lateral load. Figures 4.2-10 and 4.2-11 show how the moment and displacement at the head of the pile are related to the applied lateral load. It may be seen from Figure 4.2-10 that the head moment is related to the applied lateral load in a nearly linear manner; this is a key observation. Based on the results shown, the slope of the line may be taken as a characteristic length that relates head moment to applied load. Doing so produces the following:

$\ell = 46$ in. for the Class C site

$\ell = 70$ in. for the Class E site

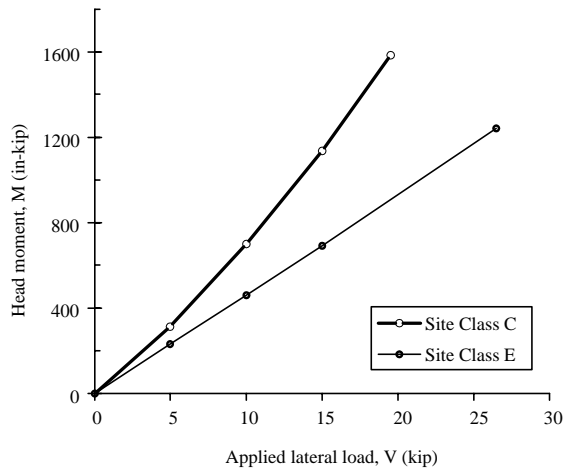


Figure 4.2-10 Results of pile analysis – applied lateral load versus head moment.

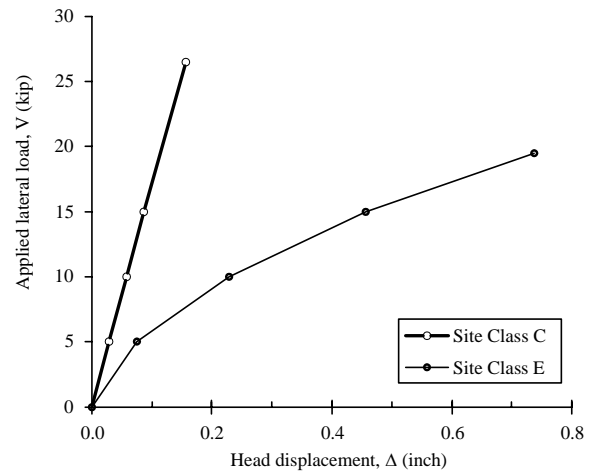


Figure 4.2-11 Results of pile analysis – head displacement versus applied lateral load.

A similar examination of Figure 4.2-11 leads to another meaningful insight. The load-displacement response of the pile in Site Class C soil is essentially linear. The response of the pile in Site Class E soil is somewhat nonlinear, but for most of the range of response a linear approximation is reasonable (and useful). Thus, the effective stiffness of each individual pile is:

$$k = 175 \text{ kip/in. for the Class C site}$$

$$k = 40 \text{ kip/in. for the Class E site}$$

4.2.2.2 Pile Group Analysis

The combined response of the piles and pile cap and the resulting strength demands for piles are computed using the procedure outlined in Sec. 4.2.1.4 for each of the 32 load combinations discussed in Sec. 4.2.1.3. Assume that each 2×2 pile group has a 9'-2" × 9'-2" × 4'-0" thick pile cap that is placed 1'-6" below grade.

Check the Maximum Compression Case under a Side Column in Site Class C

Using the sign convention shown in Figure 4.2-3, the demands on the group are:

$$P = 1097 \text{ kip}$$

$$M_{yy} = 93 \text{ ft-kips}$$

$$V_x = 10 \text{ kips}$$

$$M_{yy} = 659 \text{ ft-kips}$$

$$V_y = 69 \text{ kips}$$

From preliminary checks, assume that the displacements in the x and y directions are sufficient to mobilize 15 percent and 30 percent, respectively, of the ultimate passive pressure:

$$V_{passive,x} = 0.15(575) \left(\frac{18}{12} + \frac{48}{2(12)} \right) \left(\frac{48}{12} \right) \left(\frac{110}{12} \right) \left(\frac{1}{1000} \right) = 11.0 \text{ kips}$$

and

$$V_{passive,y} = 0.30(575) \left(\frac{18}{12} + \frac{48}{2(12)} \right) \left(\frac{48}{12} \right) \left(\frac{110}{12} \right) \left(\frac{1}{1000} \right) = 22.1 \text{ kips}$$

and conservatively take $h_p = h/3 = 16$ in.

Since $V_{passive,x} > V_x$, passive resistance alone is sufficient for this case in the x direction. However, in order to illustrate the full complexity of the calculations, reduce $V_{passive,x}$ to 4 kips and assign a shear of 1.5 kips to each pile in the x direction. In the y direction the shear in each pile is:

$$V = \frac{69 - 22.1}{4} = 11.7 \text{ kips .}$$

The corresponding pile moments are:

$$M = 1.5(46) = 69 \text{ in.-kips for x-direction loading}$$

and

$$M = 11.7(46) = 538 \text{ in.-kips for y-direction loading.}$$

The maximum axial load due to overturning for x-direction loading is:

$$P_{ot} = \frac{10(48) + 93(12) + 4(69) - 16(4)}{2(66)} = 13.7 \text{ kips}$$

and for y-direction loading (determined similarly) $P_{ot} = 98.6$ kips.

The axial load due to direct loading is $P_p = 1097/4 = 274$ kips.

Therefore the maximum load effects on the most heavily loaded pile are:

$$P_u = 13.7 + 98.6 + 274 = 386 \text{ kips}$$

$$M_u = \sqrt{(69)^2 + (538)^2} = 542 \text{ in.-kips .}$$

The expected displacement in the y direction is computed as:

$$\delta = V/k = 11.7/175 = 0.067 \text{ in., which is 0.14\% of the pile cap height } (h).$$

Reading Figure 4.2-5 with $\delta H = 0.0014$, $P/P_{ult} \approx 0.34$, so the assumption that 30 percent of P_{ult} would be mobilized was reasonable.

4.2.2.3 Design of Pile Section

The calculations shown in Sec. 4.2.2.2 are repeated for each of the 32 load combinations under each of the four design conditions. The results are shown in Figures 4.2-12 and 4.2-13. In these figures, circles indicate demands on piles under side columns and squares indicate demands on piles under corner columns. Also plotted are the ϕP - ϕM design strengths for the 22-in.-diameter pile sections with various amounts of reinforcement (as noted in the legends). The appropriate reinforcement pattern for each design condition may be selected by noting the innermost capacity curve that envelops the corresponding demand points. The required reinforcement is summarized in Table 4.2-4, following calculation of the required pile length.

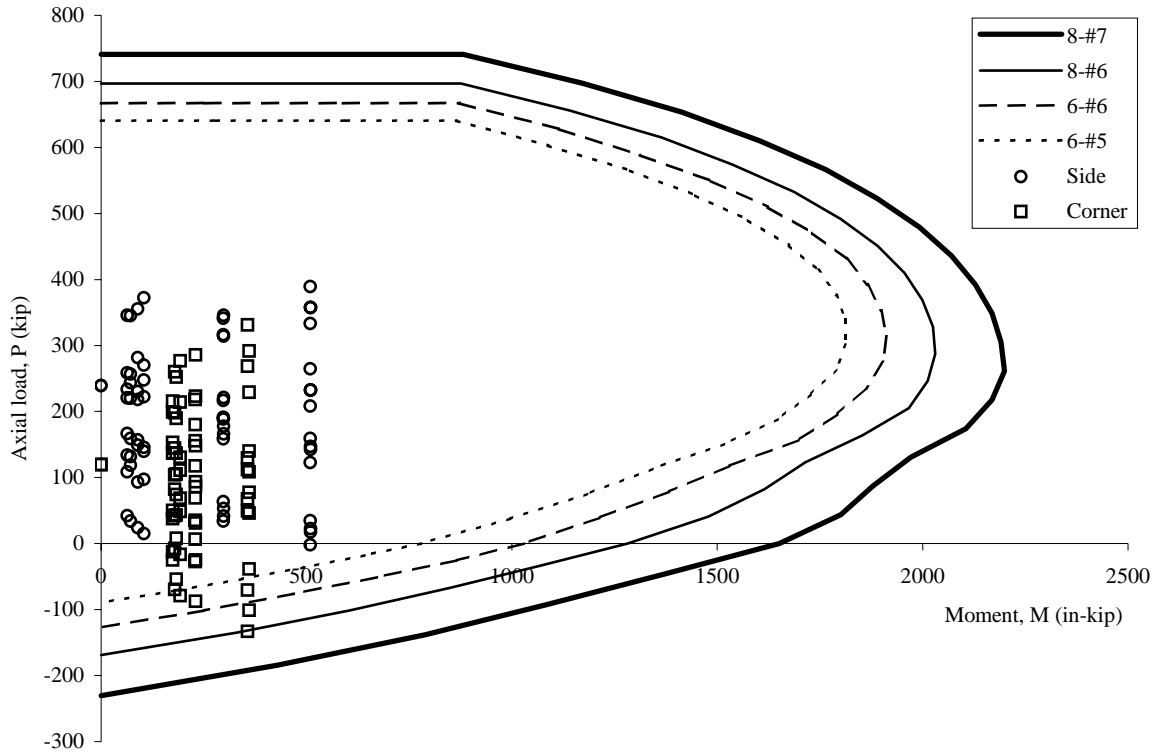


Figure 4.2-12 P-M interaction diagram for Site Class C.

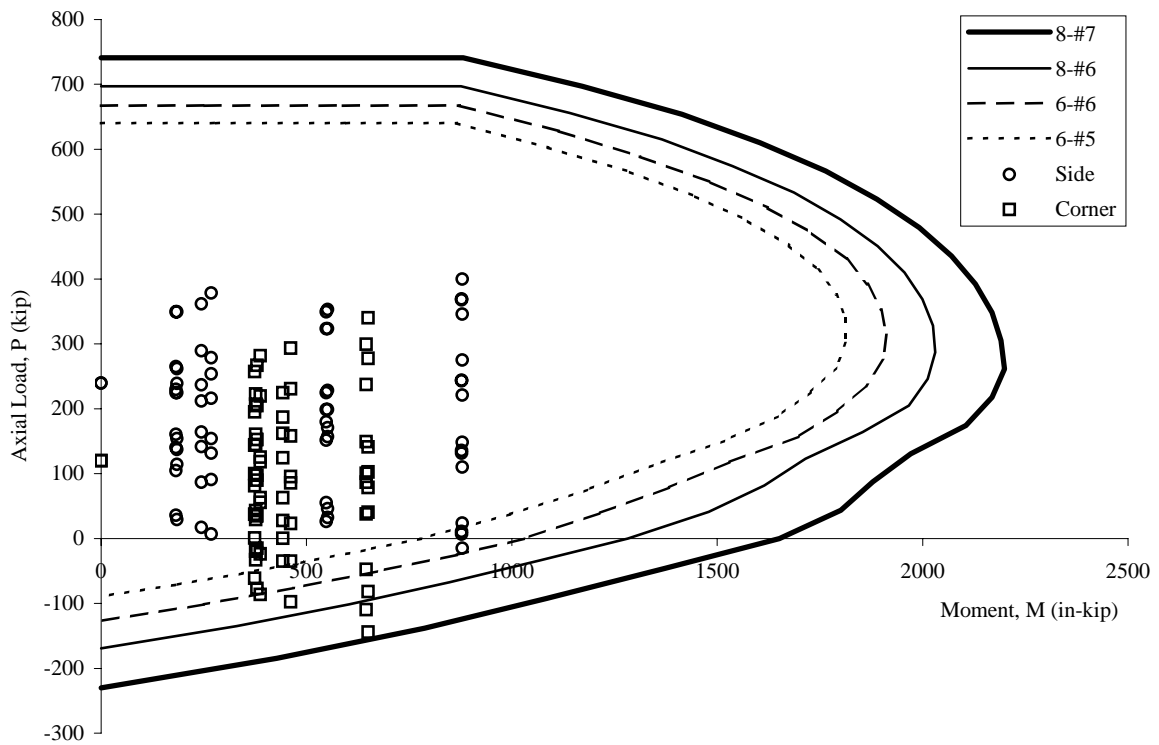


Figure 4.2-13 P-M interaction diagram for Site Class E.

4.2.2.4 Pile Length for Axial Loads

For the calculations that follow, recall that skin friction and end bearing are neglected for the top three feet in this example. (In these calculations, the pile cap depth is ignored – effectively assuming that piles begin at the ground surface. Because the soil capacity increases with depth and the resulting pile lengths are applied below the bottom of the pile cap, the results are slightly conservative.)

4.2.2.4.1 Length for Settlement

Service loads per pile are calculated as $P = (P_D + P_L)/4$.

Check pile group under side column in Site Class C, assuming $L = 47$ ft:

$$P = (702 + 72)/4 = 194 \text{ kips.}$$

$$P_{skin} = \text{average friction capacity} \times \text{pile perimeter} \times \text{pile length for friction} \\ = 0.5[0.3 + 0.3 + 44(0.03)]\pi(22/12)(44) = 243 \text{ kips.}$$

$$P_{end} = \text{end bearing capacity at depth} \times \text{end bearing area} \\ = [65 + 44(0.6)](\pi/4)(22/12)^2 = 241 \text{ kips.}$$

$$P_{allow} = (P_{skin} + P_{end})/S.F. = (243 + 241)/2.5 = 194 \text{ kips} = 194 \text{ kips (demand).} \quad \text{OK}$$

Check pile group under corner column in Site Class E, assuming $L = 43$ ft:

$$P = (351 + 36)/4 = 97 \text{ kips.}$$

$$P_{skin} = [\text{friction capacity in first layer} + \text{average friction capacity in second layer}] \times \text{pile perimeter} \\ = [27(0.3) + (13/2)(0.9 + 0.9 + 13[0.025])]\pi(22/12) = 126 \text{ kips.}$$

$$P_{end} = [40 + 13(0.5)](\pi/4)(22/12)^2 = 123 \text{ kips.}$$

$$P_{allow} = (126 + 123)/2.5 = 100 \text{ kips} > 97 \text{ kips.} \quad \text{OK}$$

4.2.2.4.2 Length for Compression Capacity

All of the strength-level load combinations (discussed in Sec. 4.2.1.3) must be considered.

Check pile group under side column in Site Class C, assuming $L = 50$ ft:

As seen in Figure 4.1-12, the maximum compression demand for this condition is $P_u = 390$ kips.

$$P_{skin} = 0.5[0.3 + 0.3 + 47(0.03)]\pi(22/12)(47) = 272 \text{ kips.}$$

$$P_{end} = [65 + 47(0.6)](\pi/4)(22/12)^2 = 246 \text{ kips.}$$

$$\phi P_n = \phi(P_{skin} + P_{end}) = 0.75(272 + 246) = 389 \text{ kips} \approx 390 \text{ kips.} \quad \text{OK}$$

Check pile group under corner column in Site Class E, assuming $L = 64$ ft:

As seen in Figure 4.2-13, the maximum compression demand for this condition is $P_u = 340$ kips.

$$P_{skin} = [27(0.3) + (34/2)(0.9 + 0.9 + 34[0.025])] \pi(22/12) = 306 \text{ kips.}$$

$$P_{end} = [40 + 34(0.5)](\pi/4)(22/12)^2 = 150 \text{ kips.}$$

$$\phi P_n = \phi(P_{skin} + P_{end}) = 0.75(306 + 150) = 342 \text{ kips} > 340 \text{ kips.} \quad \text{OK}$$

4.2.2.4.3 Length for Uplift Capacity

Again, all of the strength-level load combinations (discussed in Sec. 4.2.1.3) must be considered.

Check pile group under side column in Site Class C, assuming $L = 5$ ft:

As seen in Figure 4.2-12, the maximum tension demand for this condition is $P_u = -1.9$ kips.

$$P_{skin} = 0.5[0.3 + 0.3 + 2(0.03)] \pi(22/12)(2) = 3.8 \text{ kips.}$$

$$\phi P_n = \phi(P_{skin}) = 0.75(3.8) = 2.9 \text{ kips} > 1.9 \text{ kips.} \quad \text{OK}$$

Check pile group under corner column in Site Class E, assuming $L = 52$ ft.

As seen in Figure 4.2-13, the maximum tension demand for this condition is $P_u = -144$ kips.

$$P_{skin} = [27(0.3) + (22/2)(0.9 + 0.9 + 22[0.025])] \pi(22/12) = 196 \text{ kips.}$$

$$\phi P_n = \phi(P_{skin}) = 0.75(196) = 147 \text{ kips} > 144 \text{ kips.} \quad \text{OK}$$

4.2.2.4.4 Graphical Method of Selecting Pile Length

In the calculations shown above, the adequacy of the soil-pile interface to resist applied loads is checked once a pile length is assumed. It would be possible to generate mathematical expressions of pile capacity as a function of pile length and then solve such expressions for the demand conditions. However, a more practical design approach is to precalculate the capacity for piles for the full range of practical lengths and then select the length needed to satisfy the demands. This method lends itself to graphical expression as shown in Figures 4.2-14 and 4.2-15.

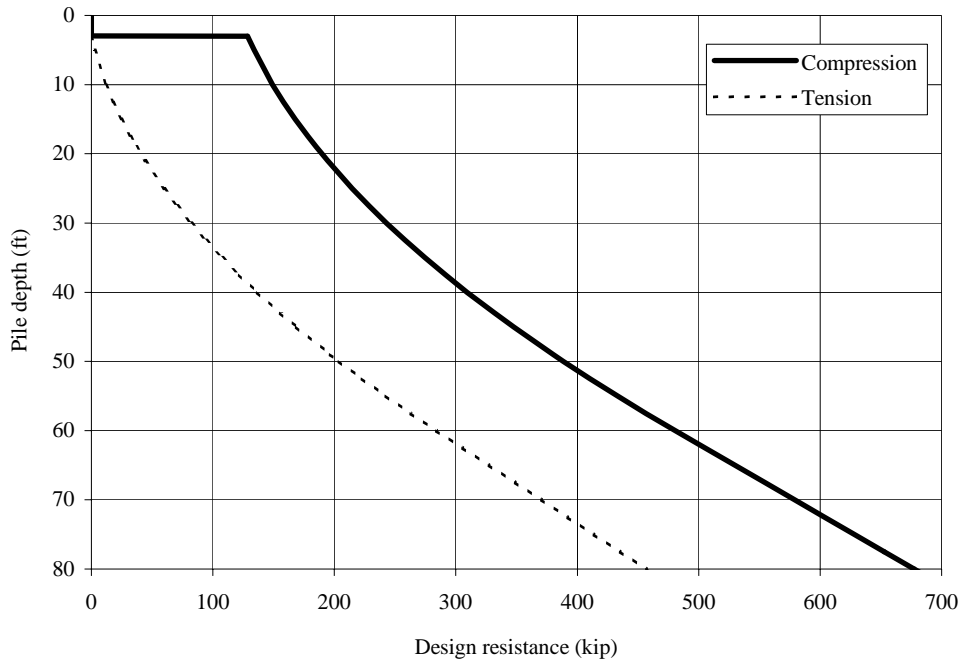


Figure 4.2-14 Pile axial capacity as a function of length for Site Class C.

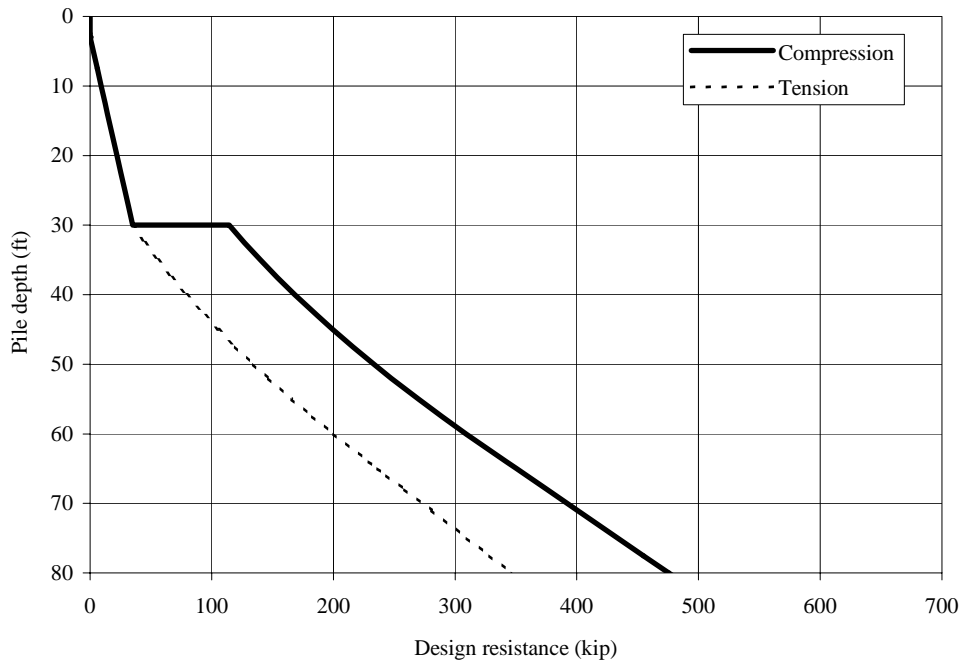


Figure 4.2-15 Pile axial capacity as a function of length for Site Class E.

4.2.2.4.5 Results of Pile Length Calculations

Detailed calculations for the required pile lengths are provided above for two of the design conditions. Table 4.2-3 summarizes the lengths required to satisfy strength and serviceability requirements for all four design conditions.

Table 4.2-3 Pile Lengths Required for Axial Loads

	Piles Under Corner Column			Piles Under Side Column		
	Condition	Load	Min Length	Condition	Load	Min Length
Site Class C	Compression	331 kip	43 ft	Compression	390 kip	50 ft
	Uplift	133 kip	40 ft	Uplift	1.9 kip	5 ft
	Settlement	97 kip	19 ft	Settlement	194 kip	47 ft
Site Class E	Compression	340 kip	64 ft	Compression	400 kip	71 ft
	Uplift	144 kip	52 ft	Uplift	14.7 kip	14 ft
	Settlement	97 kip	43 ft	Settlement	194 kip	67 ft

4.2.2.5 Design Results

The design results for all four pile conditions are shown in Table 4.2-4. The amount of longitudinal reinforcement indicated in the table is that required at the pile-pile cap interface and may be reduced at depth as discussed in the following section.

Table 4.2-4 Summary of Pile Size, Length, and Longitudinal Reinforcement

	Piles Under Corner Column	Piles Under Side Column
Site Class C	22 in. diameter by 43 ft long 8-#6 bars	22 in. diameter by 50 ft long 6-#5 bars
Site Class E	22 in. diameter by 64 ft long 8-#7 bars	22 in. diameter by 71 ft long 6-#6 bars

4.2.2.6 Pile Detailing

Provisions Sec. 7.4.4 and 7.5.4, respectively, contain special pile requirements for structures assigned to Seismic Design Category C or higher and D or higher. In this section, those general requirements and the specific requirements for uncased concrete piles that apply to this example are discussed. Although the specifics are affected by the soil properties and assigned site class, the detailing of the piles designed in this example focuses on consideration of the following fundamental items:

1. All pile reinforcement must be developed in the pile cap (*Provisions* Sec. 7.4.4).
2. In areas of the pile where yielding might be expected or demands are large, longitudinal and transverse reinforcement must satisfy specific requirements related to minimum amount and maximum spacing.
3. Continuous longitudinal reinforcement must be provided over the entire length resisting design tension forces (ACI 318 Sec. 21.8.4.2 [21.10.4.2]).

The discussion that follows refers to the detailing shown in Figures 4.2-16 and 4.2-17.

4.2.2.6.1 *Development at the Pile Cap*

Where neither uplift nor flexural restraint are required, the development length is the full development length for compression (*Provisions* Sec. 7.4.4). Where the design relies on head fixity or where resistance to uplift forces is required (both of which are true in this example), pile reinforcement must be fully developed in tension unless the section satisfies the overstrength load condition or demands are limited by the uplift capacity of the soil-pile interface (*Provisions* Sec. 7.5.4). For both site classes considered in this example, the pile longitudinal reinforcement is extended straight into the pile cap a distance that is sufficient to fully develop the tensile capacity of the bars. In addition to satisfying the requirements of the *Provisions*, this approach offers two advantages. By avoiding lap splices to field-placed dowels where yielding is expected near the pile head (although such would be permitted by *Provisions* Sec. 7.4.4), more desirable inelastic performance would be expected. Straight development, while it may require a thicker pile cap, permits easier placement of the pile cap's bottom reinforcement followed by the addition of the spiral reinforcement within the pile cap. Note that embedment of the entire pile in the pile cap facilitates direct transfer of shear from pile cap to pile, but is not a requirement of the *Provisions*.

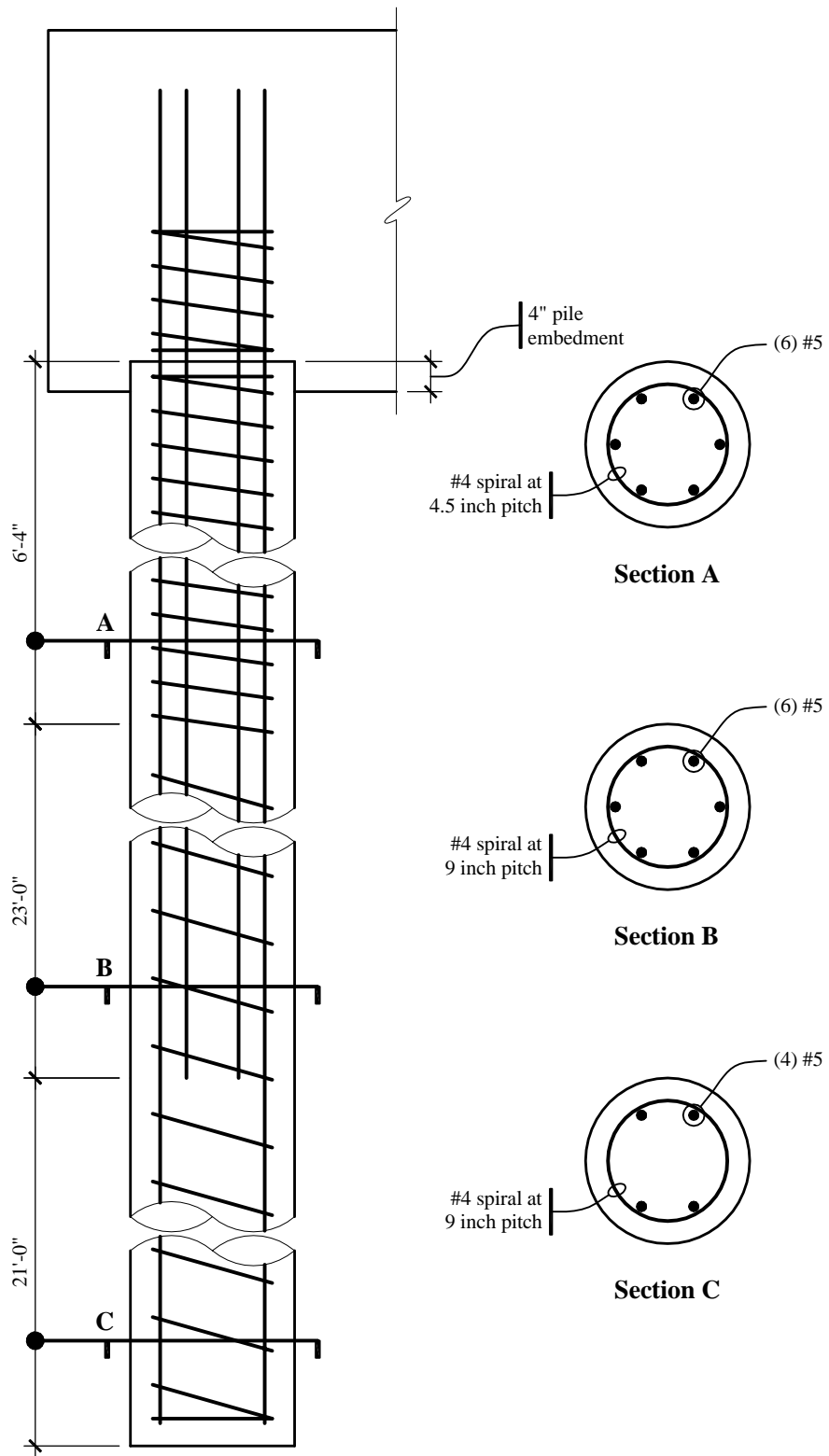


Figure 4.2-16 Pile detailing for Site Class C (under side column).

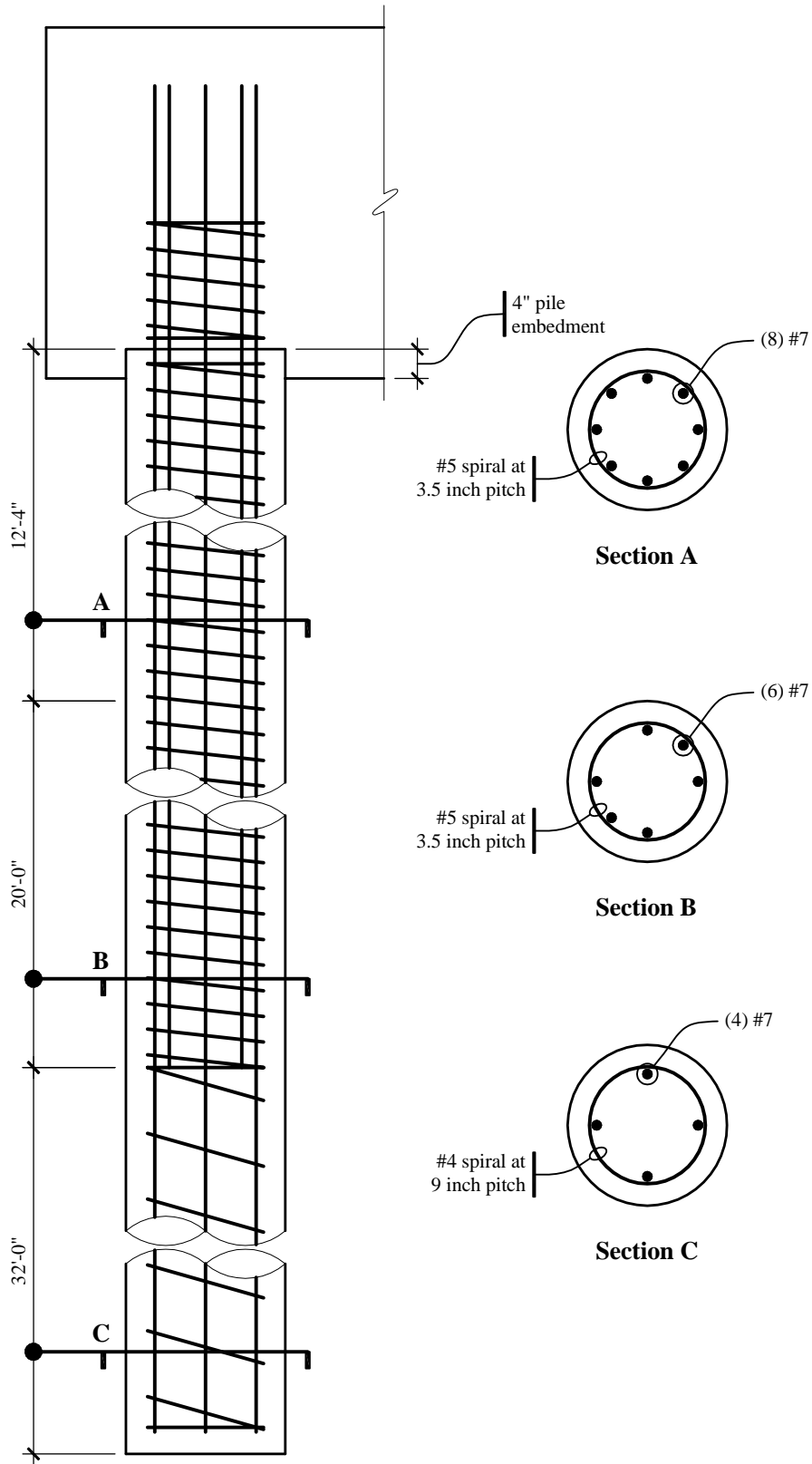


Figure 4.2-17 Pile detailing for Site Class E (under corner column).

4.2.2.6.2 Longitudinal and Transverse Reinforcement Where Demands Are Large

Requirements for longitudinal and transverse reinforcement apply over the entire length of pile where demands are large. For uncased concrete piles in Seismic Design Category D at least four longitudinal bars (with a minimum reinforcement ratio of 0.005) must be provided over the largest region defined as follows: the top one-half of the pile length, the top 10 ft below the ground, or the flexural length of the pile. The flexural length is taken as the length of pile from the cap to the lowest point where 0.4 times the concrete section cracking moment (see ACI 318 Sec. 9.5.2.3) exceeds the calculated flexural demand at that point. [A change made in Sec. 7.4.4.1 of the 2003 *Provisions* makes it clear that the longitudinal reinforcement must be developed beyond this point.] For the piles used in this example, one-half of the pile length governs. (Note that “providing” a given reinforcement ratio means that the reinforcement in question must be developed at that point. Bar development and cutoff are discussed in more detail in Chapter 6 of this volume of design examples.) Transverse reinforcement must be provided over the same length for which minimum longitudinal reinforcement requirements apply. Because the piles designed in this example are larger than 20 in. in diameter, the transverse reinforcement may not be smaller than 0.5 in. diameter. For the piles shown in Figures 4.2-16 and 4.2-17 the spacing of the transverse reinforcement in the top half of the pile length may not exceed the least of: $12d_b$ (7.5 in. for #5 longitudinal bars and 10.5 in. for #7 longitudinal bars), $22/2 = 11$ in., or 12 in.

Where yielding may be expected, even more stringent detailing is required. For the Class C site, yielding can be expected within three diameters of the bottom of the pile cap ($3D = 3 \times 22 = 66$ in.). Spiral reinforcement in that region must not be less than one-half of that required in ASCE 318 Sec. 21.4.4.1(a) of ACI 318 (since the site is not Class E, F, or liquefiable) and the requirements of Sec. 21.4.4.2 and 21.4.4.3 must be satisfied. Note that Sec. 21.4.4.1(a) refers to Eq. (10-6) [10-5], which often will govern. In this case, the minimum volumetric ratio of spiral reinforcement is one-half that determined using ACI 318 Eq. (10-6) [10-5]. In order to provide a reinforcement ratio of 0.01 for this pile section, a #4 spiral must have a pitch of no more than 4.8 in., but the maximum spacing permitted by Sec. 21.4.4.2 is $22/4 = 5.5$ in. or $6d_b = 3.75$ in., so a #4 spiral at 3.75 in. pitch is used.

For the Class E site, the more stringent detailing must be provided “within seven diameters of the pile cap and of the interfaces between strata that are hard or stiff and strata that are liquefiable or are composed of soft to medium-stiff clay” (*Provisions* Sec. 7.5.4). The author interprets “within seven diameters of . . . the interface” as applying in the direction into the softer material, which is consistent with the expected location of yielding. Using that interpretation, the *Provisions* does not indicate the extent of such detailing into the firmer material. Taking into account the soil layering shown in Table 4.2-1 and the pile cap depth and thickness, the tightly spaced transverse reinforcement shown in Figure 4.2-17 is provided within $7D$ of the bottom of pile cap and top of firm soil and is extended a little more than $3D$ into the firm soil. Because the site is Class E, the full amount of reinforcement indicated in ACI 318 Sec. 21.4.4.1 must be provided. In order to provide a reinforcement ratio of 0.02 for this pile section, a #5 spiral must have a pitch of no more than 3.7 in. The maximum spacing permitted by Sec. 21.4.4.2 is $22/4 = 5.5$ in. or $6d_b = 5.25$ in., so a #5 spiral at 3.5 in. pitch is used.

4.2.2.6.3 Continuous Longitudinal Reinforcement for Tension

Table 4.2-3 shows the pile lengths required for resistance to uplift demands. For the Site Class E condition under a corner column (Figure 4.2-17), longitudinal reinforcement must resist tension for at least the top 52 ft (being developed at that point). Extending four longitudinal bars for the full length and providing widely spaced spirals at such bars reflect the designer’s judgment (not specific requirements of the *Provisions*). For the Site Class C condition under a side column (Figure 4.2-16), design tension due to uplift extends only about 5 ft below the bottom of the pile cap. Therefore, a design with Section C of Figure 4.2-16 being unreinforced would satisfy the *Provisions* requirements, but the author has decided to extend very light longitudinal and nominal transverse reinforcement for the full length of the pile.

4.2.3 Other Considerations

4.2.3.1 Foundation Tie Design and Detailing

Provisions Sec. 7.4.3 requires that individual pile caps be connected by ties. Such ties are often grade beams, but the *Provisions* would permit use of a slab (thickened or not) or calculations that demonstrate that the site soils (assigned to Site Class A, B, or C) provide equivalent restraint. For this example, a tie beam between the pile caps under a corner column and a side column will be designed. The resulting section is shown in Figure 4.2-18.

For pile caps with an assumed center-to-center spacing of 32 ft in each direction, and given $P_{group} = 1121$ kips under a side column and $P_{group} = 812$ kips under a corner column, the tie is designed as follows.

As indicated in *Provisions* Sec. 7.4.3, the minimum tie force in tension or compression equals the product of the larger column load times S_{DS} divided by 10 = $1121(0.90)/10 = 101$ kips.

The design strength for five # 6 bars is $\phi A_s f_y = 0.8(5)(0.44)(60) = 106$ kips > 101 kips. OK

According to ACI 318 Sec. 21.8.3.2 [21.10.3.2], the smallest cross-sectional dimension of the tie beam must not be less than the clear spacing between pile caps divided by 20 = $(32'-0" - 9'-2")/20 = 13.7$ in. Use a tie beam that is 14 in. wide and 16 in. deep. ACI 318 Sec. 21.8.3.2 [21.10.3.2] further indicates that closed ties must be provided at a spacing of not more than one-half the minimum dimension = $14/2 = 7$ in.

Assuming that the surrounding soil provides restraint against buckling, the design strength of the tie beam concentrically loaded in compression is:

$$\begin{aligned} \phi P_n &= 0.8\phi[0.85f'_c(A_g - A_{st}) + f_y A_{st}] \\ &= 0.8(0.65)[0.85(3)(16)(14) + 60(5)(0.44)] = 366 \text{ kips} > 101 \text{ kips.} \end{aligned} \quad \text{OK}$$

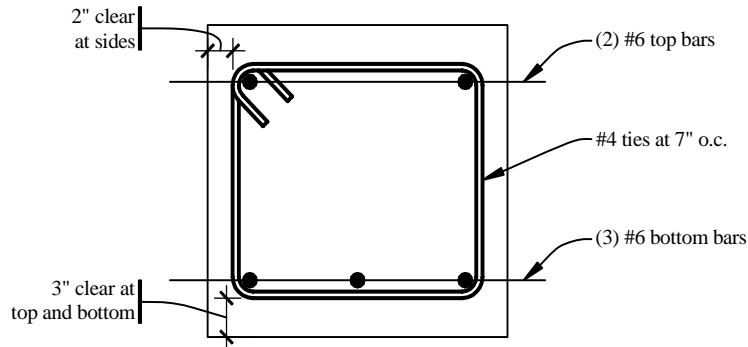


Figure 4.2-18 Foundation tie section.

4.2.3.2 Liquefaction

For Seismic Design Categories C, D, E and F, *Provisions* Sec. 7.4.1 requires that the geotechnical report address potential hazards due to liquefaction. For Seismic Design Categories D, E and F, *Provisions* Sec. 7.5.1 and 7.5.3 [7.5.1 and 7.5.2] further require that the geotechnical report describe the likelihood and potential consequences of liquefaction and soil strength loss (including estimates of differential settlement, lateral movement, and reduction in foundation soil-bearing capacity) and discuss mitigation measures. [In the 2003 *Provisions*, Sec. 7.5.2 also requires that the geotechnical report describe lateral loads on foundations, increases in lateral pressures on retaining walls, and flotation of embedded

structures.] During the design of the structure, such measures (which can include ground stabilization, selection of appropriate foundation type and depths, and selection of appropriate structural systems to accommodate anticipated displacements [and forces in the 2003 *Provisions*]) must be considered. *Commentary* Section 7.4.1 contains a calculation procedure that can be used to evaluate the liquefaction hazard, but readers should refer to Youd for an update of the methods described in the *Commentary*. [Sec. 7.4.1 of the 2003 *Commentary* has been updated to reflect Youd and other recent references.]

4.2.3.3 Kinematic Interaction

Piles are subjected to curvature demands as a result of two different types of behavior: inertial interaction and kinematic interaction. The term *inertial interaction* is used to describe the coupled response of the soil-foundation-structure system that arises as a consequence of the mass properties of those components of the overall system. The structural engineer's consideration of inertial interaction is usually focused on how the structure *loads* the foundation and how such loads are transmitted to the soil (as shown in the pile design calculations that are the subject of most of this example) but also includes assessment of the resulting foundation movement. The term *kinematic interaction* is used to describe the manner in which the stiffness of the foundation system impedes development of free-field ground motion. Consideration of kinematic interaction by the structural engineer is usually focused on assessing the strength and ductility demands imposed directly on piles by movement of the soil. Although it is rarely done in practice, the first two sentences of *Provisions* Sec. 7.5.4 require consideration of kinematic interaction for foundations of structures assigned to Seismic Design Category D, E, or F. Kramer discusses kinematic and inertial interaction and the methods of analysis employed in consideration of those effects, and demonstrates "that the solution to the entire soil-structure interaction problem is equal to the sum of the solutions of the kinematic and inertial interaction analyses."

One approach that would satisfy the requirements of the *Provisions* would be as follows:

1. The geotechnical consultant performs appropriate kinematic interaction analyses considering free-field ground motions and the stiffness of the piles to be used in design.
2. The resulting pile demands, which generally are greatest at the interface between stiff and soft strata, are reported to the structural engineer.
3. The structural engineer designs piles for the sum of the demands imposed by the vibrating superstructure and the demands imposed by soil movement.

A more practical, but less rigorous, approach would be to provide appropriate detailing in regions of the pile where curvature demands imposed directly by earthquake ground motions are expected to be significant. Where such a judgment-based approach is used, one must decide whether to provide only additional transverse reinforcement in areas of concern to improve ductility or whether additional longitudinal reinforcement should also be provided to increase strength. The third sentence of *Provisions* Sec. 7.5.4, which defines a specific instance in which this second method is to be employed to define areas requiring additional transverse reinforcement, helps to make an argument for general application of this practical approach.

4.2.3.4 Design of Pile Cap

Design of pile caps for large pile loads is a very specialized topic for which detailed treatment is beyond the scope of this volume of design examples. CRSI notes that "most pile caps are designed in practice by various short-cut rule-of-thumb procedures using what are hoped to be conservative allowable stresses." Wang & Salmon indicates that "pile caps frequently must be designed for shear considering the member as a deep beam. In other words, when piles are located inside the critical sections d (for one-way action)

or $d/2$ (for two-way action) from the face of column, the shear cannot be neglected.” They go on to note that “there is no agreement about the proper procedure to use.” Direct application of the special provisions for deep flexural members as found in ACI 318 is not possible as the design conditions are somewhat different. CRSI provides a detailed outline of a design procedure and tabulated solutions, but the procedure is developed for pile caps subjected to concentric vertical loads only (without applied overturning moments or pile head moments). Strut-and-tie models (as described in Appendix A of the 2002 edition of ACI 318) may be employed, but their application to elements with important three-dimensional characteristics (such as pile caps for groups larger than 2×1) is so involved as to preclude hand calculations.

4.2.3.5 Foundation Flexibility and Its Impact on Performance

4.2.3.5.1 Discussion

Most engineers routinely use fixed-base models. Nothing in the *Provisions* prohibits that common practice; the consideration of soil-structure interaction effects (*Provisions* Sec. 5.8 [5.6]) is “permitted” but not required. Such fixed-base models can lead to erroneous results, but engineers have long assumed that the errors are usually conservative. There are two obvious exceptions to that assumption: soft soil site-resonance conditions (e.g., as in the 1985 Mexico City earthquake) and excessive damage or even instability due to increased displacement response.

Site resonance can result in significant amplification of ground motion in the period range of interest. For sites with a fairly long predominant period, the result is spectral accelerations that increase as the structural period approaches the site period. However, the shape of the general design spectrum used in the *Provisions* does not capture that effect; for periods larger than T_0 , accelerations remain the same or decrease with increasing period. Therefore, increased system period (as a result of foundation flexibility) always leads to lower design forces where the general design spectrum is used. Site-specific spectra may reflect long-period site-resonance effects, but the use of such spectra is required only for Class F sites.

Clearly, an increase in displacements, caused by foundation flexibility, does change the performance of a structure and its contents – raising concerns regarding both stability and damage. Earthquake-induced instability of buildings has been exceedingly rare. The analysis and acceptance criteria in the *Provisions* are not adequate to the task of predicting real stability problems; calculations based on linear, static behavior cannot be used to predict instability of an inelastic system subjected to dynamic loading. While *Commentary* Sec. 5.2.8 [4.5.1] indicates that structural stability was considered in arriving at the “consensus judgment” reflected in the drift limits, such considerations were qualitative. In point of fact, the values selected for the drift limits were selected considering damage to nonstructural systems (and, perhaps in some cases, control of structural ductility demands). For most buildings, application of the *Provisions* is intended to satisfy performance objectives related to life safety and collapse prevention, not damage control or post-earthquake occupancy. Larger design forces and more stringent drift limits are applied to structures assigned to Seismic Use Group II or III in the hope that those measures will improve performance without requiring explicit consideration of such performance. Although foundation flexibility can affect structural performance significantly, the fact that all consideration of performance in the context of the *Provisions* is approximate and judgment-based has made it difficult to define how such changes in performance should be characterized. Explicit consideration of performance measures also tends to increase engineering effort substantially, so mandatory performance checks are often resisted by the user community.

The engineering framework established in FEMA 356 is more conducive to explicit use of performance measures. In that document (Sec. 4.4.3.2.1 and 4.4.3.3.1), the use of fixed-based structural models is prohibited for “buildings being rehabilitated for the Immediate Occupancy Performance Level that are

sensitive to base rotations or other types of foundation movement.” In this case the focus is on damage control rather than structural stability.

4.2.3.5.2 Example Calculations

To assess the significance of foundation flexibility, one may compare the dynamic characteristics of a fixed-base model to those of a model in which foundation effects are included. The effects of foundation flexibility become more pronounced as foundation period and structural period approach the same value. For this portion of the example, use the Site Class E pile design results from Sec. 4.2.2.1 and consider the north-south response of the concrete moment frame building located in Berkeley (Sec. 6.2) as representative for this building.

Stiffness of the Structure. Calculations of the effect of foundation flexibility on the dynamic response of a structure should reflect the overall stiffness of the structure (e.g., that associated with the fundamental mode of vibration), rather than the stiffness of any particular story. Table 6-2 shows that the total weight of the structure is 36,462 kips. Table 6-5 shows that the calculated period of the fixed-base structure is 2.50 seconds, and Table 6-4 indicates that 80.2 percent of the mass participates in that mode. Using the equation for the undamped period of vibration of a single-degree-of-freedom oscillator, the effective stiffness of the structure is:

$$K = \frac{4\pi^2 M}{T^2} = \frac{4\pi^2 ((0.802)36,462/386.1)}{2.50^2} = 478 \text{ kip/in.}$$

Foundation Stiffness. As seen in Figure 6-1 there are 36 moment frame columns. Assume that a 2×2 pile group supports each column. As shown in Sec. 4.2.2.1, the stiffness of each pile is 40 kip/in. Neglecting both the stiffness contribution from passive pressure resistance and the flexibility of the beam-slab system that ties the pile caps, the stiffness of each pile group is $4 \times 40 = 160$ kip/in. and the stiffness of the entire foundation system is $36 \times 160 = 5760$ kip/in.

Effect of Foundation Flexibility. Because the foundation stiffness is more than 10 times the structural stiffness, period elongation is expected to be minimal. To confirm this expectation the period of the combined system is computed. The total stiffness for the system (springs in series) is:

$$K_{combined} = \frac{1}{\frac{1}{K_{structure}} + \frac{1}{K_{fdn}}} = \frac{1}{\frac{1}{478} + \frac{1}{5760}} = 441 \text{ kip/in.}$$

Assume that the weight of the foundation system is 4000 kips and that 100 percent of the corresponding mass participates in the new fundamental mode of vibration. The period of the combined system is

$$T = 2\pi \sqrt{\frac{M}{K}} = 2\pi \sqrt{\frac{[(0.802)(36,462) + (1.0)(4000)]/386.1}{441}} = 2.78 \text{ sec}$$

which is an 11percent increase over that predicted by the fixed-base model. For systems responding in the constant-velocity portion of the spectrum, accelerations (and thus forces) are a function of $1/T$ and relative displacements are a function of T . Therefore, with respect to the fixed-based model, the combined system would have forces that are 10 percent smaller and displacements that are 11 percent larger. In the context of earthquake engineering, those differences are not significant.

STRUCTURAL STEEL DESIGN

James R. Harris, P.E., Ph.D., Frederick R. Rutz, P.E., Ph.D., and Teymour Manzouri, P.E., Ph.D.

This chapter illustrates how the 2000 *NEHRP Recommended Provisions* (hereafter the *Provisions*) is applied to the design of steel framed buildings. The three examples include:

1. An industrial warehouse structure in Astoria, Oregon;
2. A multistory office building in Los Angeles, California; and
3. A low-rise hospital facility in the San Francisco Bay area of California.

The discussion examines the following types of structural framing for resisting horizontal forces:

1. Concentrically braced frames,
2. Intermediate moment frames,
3. Special moment frames,
4. A dual system consisting of moment frames and concentrically braced frames, and
5. Eccentrically braced frames.

For determining the strength of steel members and connections, the 1993 [1999] *Load and Resistance Factor Design Specification for Structural Steel Buildings*, published by the American Institute of Steel Construction, is used throughout. In addition, the requirements of the 1997 [2002] *AISC Seismic Provisions for Structural Steel Buildings* are followed where applicable.

The examples only cover design for seismic forces in combination with gravity, and they are presented to illustrate only specific aspects of seismic analysis and design such as, lateral force analysis, design of concentric and eccentric bracing, design of moment resisting frames, drift calculations, member proportioning, and detailing.

All structures are analyzed using three-dimensional static or dynamic methods. The SAP2000 Building Analysis Program (Computers & Structures, Inc., Berkeley, California, v.6.11, 1997) is used in Example 5.1, and the RAMFRAME Analysis Program (RAM International, Carlsbad, California, v. 5.04, 1997) is used in Examples 5.2 and 5.3.

In addition to the 2000 *NEHRP Recommended Provisions*, the following documents are referenced:

AISC LRFD American Institute of Steel Construction. 1999. *Load and Resistance Factor Design Specification for Structural Steel Buildings*.

AISC Manual	American Institute of Steel Construction. 2001. <i>Manual of Steel Construction, Load and Resistance Factor Design</i> , 3rd Edition.
AISC Seismic	American Institute of Steel Construction. 2000. [2002] <i>Seismic Provisions for Structural Steel Buildings</i> , 1997, including Supplement No. 2.
IBC	International Code Council, Inc. 2000. <i>2000 International Building Code</i> .
FEMA 350	SAC Joint Venture. 2000. <i>Recommended Seismic Design Criteria for New Steel Moment-Frame Buildings</i> .
AISC SDGS-4	AISC Steel Design Guide Series 4. 1990. <i>Extended End-Plate Moment Connections</i> , 1990.
SDI	Luttrell, Larry D. 1981. <i>Steel Deck Institute Diaphragm Design Manual</i> . Steel Deck Institute.

The symbols used in this chapter are from Chapter 2 of the *Provisions*, the above referenced documents, or are as defined in the text. Customary U.S. units are used.

Although these design examples are based on the 2000 *Provisions*, it is annotated to reflect changes made to the 2003 *Provisions*. Annotations within brackets, [], indicate both organizational changes (as a result of a reformat of all of the chapters of the 2003 *Provisions*) and substantive technical changes to the 2003 *Provisions* and its primary reference documents. While the general concepts of the changes are described, the design examples and calculations have not been revised to reflect the changes to the 2003 *Provisions*.

The most significant change to the steel chapter in the 2003 *Provisions* is the addition of two new lateral systems, buckling restrained braced frames and steel plate shear walls, neither of which are covered in this set of design examples. Other changes are generally related to maintaining compatibility between the *Provisions* and the 2002 edition of AISC Seismic. Updates to the reference documents, in particular AISC Seismic, have some effects on the calculations illustrated herein.

Some general technical changes in the 2003 *Provisions* that relate to the calculations and/or design in this chapter include updated seismic hazard maps, changes to Seismic Design Category classification for short period structures and revisions to the redundancy requirements, new Simplified Design Procedure would not be applicable to the examples in this chapter.

Where they affect the design examples in this chapter, other significant changes to the 2003 *Provisions* and primary reference documents are noted. However, some minor changes to the 2003 *Provisions* and the reference documents may not be noted.

It is worth noting that the 2002 edition of AISC Seismic has incorporated many of the design provisions for steel moment frames contained in FEMA 350. The design provisions incorporated into AISC Seismic are similar in substance to FEMA 350, but the organization and format are significantly different. Therefore, due to the difficulty in cross-referencing, the references to FEMA 350 sections, tables, and equations in this chapter have not been annotated. The design professional is encouraged to review AISC Seismic for updated moment frame design provisions related to the examples in this chapter.

5.1 INDUSTRIAL HIGH-CLEARANCE BUILDING, ASTORIA, OREGON

This example features a transverse steel moment frame and a longitudinal steel braced frame. The following features of seismic design of steel buildings are illustrated:

1. Seismic design parameters,
2. Equivalent lateral force analysis,
3. Three-dimension (3-D) modal analysis,
4. Drift check,
5. Check of compactness and brace spacing for moment frame,
6. Moment frame connection design, and
7. Proportioning of concentric diagonal bracing.

5.1.1 Building Description

This industrial building has plan dimensions of 180 ft by 90 ft and a clear height of approximately 30 ft. It includes a 12-ft-high, 40-ft-wide mezzanine area at the east end of the building. The structure consists of 10 gable frames spanning 90 ft in the transverse (N-S) direction. Spaced at 20 ft o.c., these frames are braced in the longitudinal (EW) direction in two bays at the east end. The building is enclosed by nonstructural insulated concrete wall panels and is roofed with steel decking covered with insulation and roofing. Columns are supported on spread footings.

The elevation and transverse sections of the structure are shown in Figure 5.1-1. Longitudinal struts at the eaves and the mezzanine level run the full length of the building and, therefore, act as collectors for the distribution of forces resisted by the diagonally braced bays and as weak-axis stability bracing for the moment frame columns.

The roof and mezzanine framing plans are shown in Figure 5.1-2. The framing consists of a steel roof deck supported by joists between transverse gable frames. Because the frames resist lateral loading at each frame position, the steel deck functions as a diaphragm for distribution of the effects of eccentric loading caused by the mezzanine floor when the building is subjected to loads acting in the transverse direction.

The mezzanine floor at the east end of the building is designed to accommodate a live load of 125 psf. Its structural system is composed of a concrete slab over steel decking supported by floor beams spaced 10 ft o.c. The floor beams are supported on girders continuous over two intermediate columns spaced approximately 30 ft apart and are attached to the gable frames at each end.

The member sizes in the main frame are controlled by serviceability considerations. Vertical deflections due to snow were limited to 3.5 in. and lateral sway due to wind was limited to 2 in. (which did not control). These serviceability limits are not considered to control any aspect of the seismic-resistant design. However, many aspects of seismic design are driven by actual capacities so, in that sense, the serviceability limits do affect the seismic design.

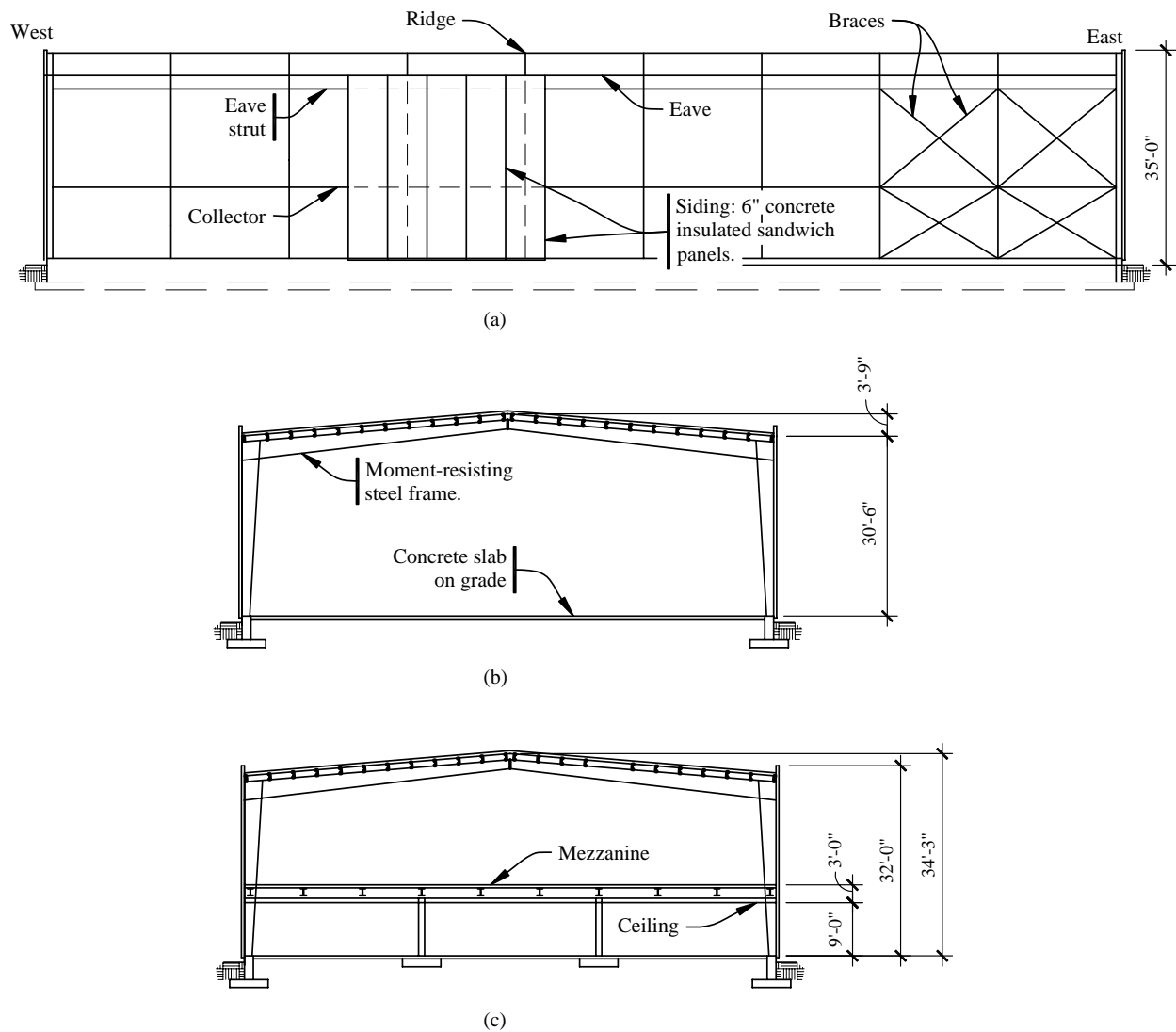


Figure 5.1-1 Framing elevation and sections (1.0 in. = 25.4 mm, 1.0 ft = 0.3048 m).

Earthquake rather than wind governs the lateral design due to the mass of the insulated concrete panels. The panels are attached with long pins perpendicular to the concrete surface. These slender, flexible pins avoid shear resistance by the panels. (This building arrangement has been intentionally contrived to illustrate what can happen to a tapered-moment frame building if high seismic demands are placed on it. More likely, if this were a real building, the concrete panels would be connected directly to the steel frame, and the building would tend to act as a shear wall building. But for this example, the connections have been arranged to permit the steel frame to move at the point of attachment in the in-plane direction of the concrete panels. This was done to cause the steel frame to resist lateral forces and, thus, shear-wall action of the panels does not influence the frames.)

The building is supported on spread footings based on moderately deep alluvial deposits (i.e., medium dense sands). The foundation plan is shown in Figure 5.1-3. Transverse ties are placed between the footings of the two columns of each moment frame to provide restraint against horizontal thrust from the moment frames. Grade beams carrying the enclosing panels serve as ties in the longitudinal direction as well as across the end walls. The design of footings and columns in the braced bays requires consideration of combined seismic loadings. The design of foundations is not included here.

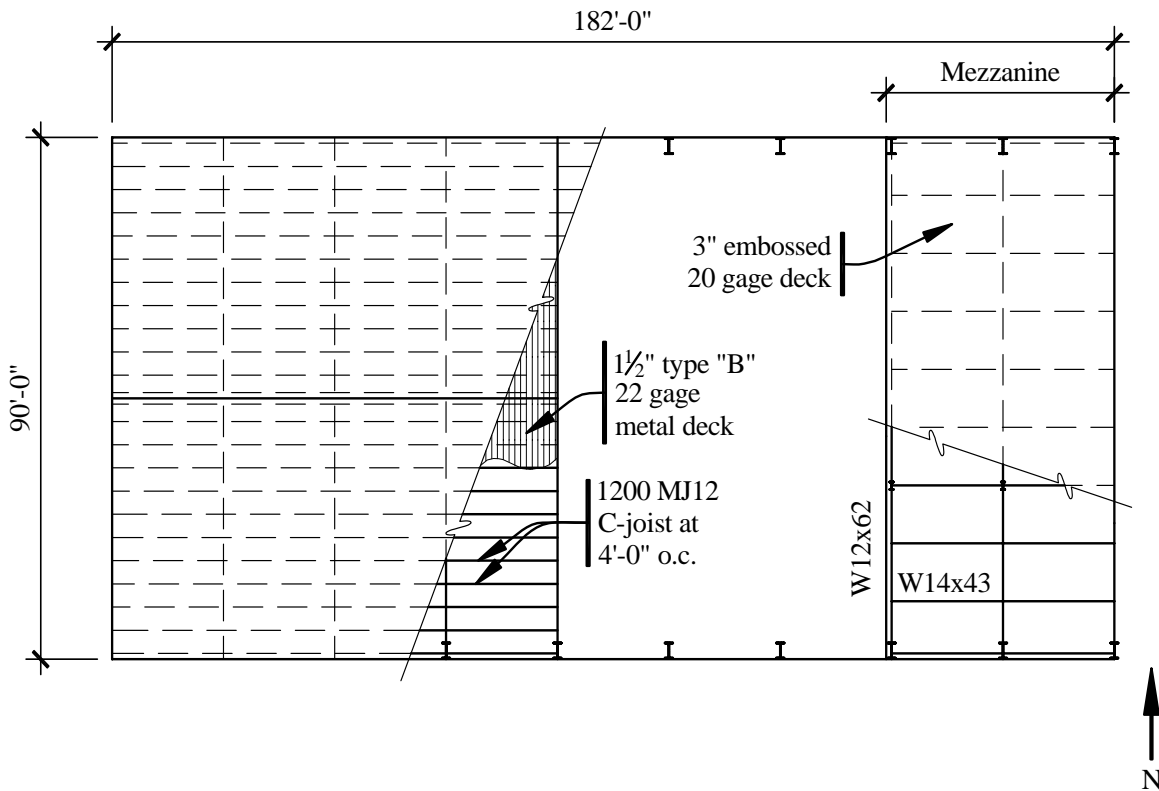


Figure 5.1-2 Roof framing and mezzanine framing plan (1.0 in. = 25.4 mm, 1.0 ft = 0.3048 m).

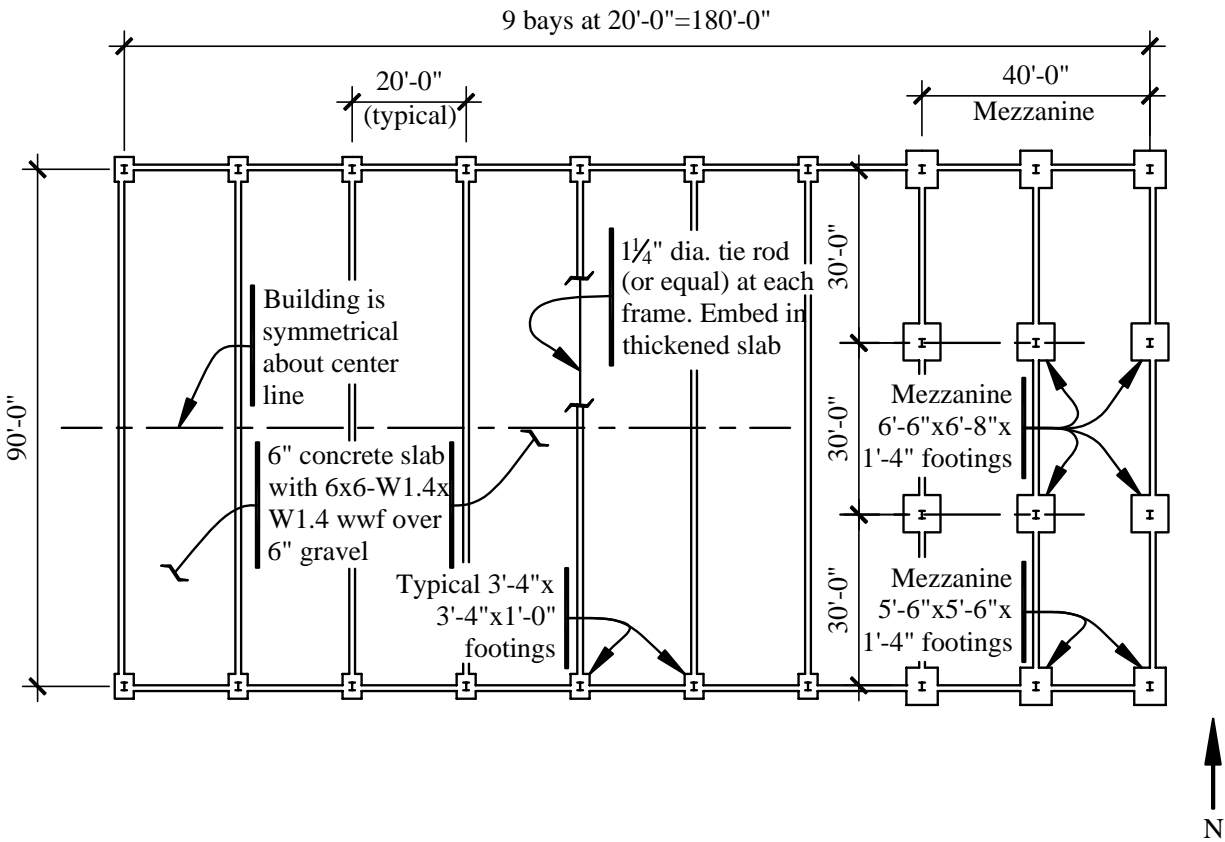


Figure 5.1-3 Foundation plan (1.0 in. = 25.4 mm, 1.0 ft = 0.3048 m).

5.1.2 Design Parameters

5.1.2.1 Provisions Parameters

Site Class	= D (<i>Provisions</i> Sec. 4.1.2.1[3.5])
S_S	= 1.5 (<i>Provisions</i> Map 9 [Figure 3.3-1])
S_I	= 0.6 (<i>Provisions</i> Map 10 [Figure 3.3-2])
F_a	= 1.0 (<i>Provisions</i> Table 4.1.2.4a [3.3-1])
F_v	= 1.5 (<i>Provisions</i> Table 4.1.2.4b [3.3-2])
$S_{MS} = F_a S_S$	= 1.5 (<i>Provisions</i> Eq. 4.1.2.4-1 [3.3-1])
$S_{MI} = F_v S_I$	= 0.9 (<i>Provisions</i> Eq. 4.1.2.4-2 [3.3-2])
$S_{DS} = 2/3 S_{MS}$	= 1.0 (<i>Provisions</i> Eq. 4.1.2.5-1 [3.3-3])
$S_{DI} = 2/3 S_{MI}$	= 0.6 (<i>Provisions</i> Eq. 4.1.2.5-2 [3.3-4])
Seismic Use Group	= I (<i>Provisions</i> Sec. 1.3 [1.2])
Seismic Design Category	= D (<i>Provisions</i> Sec. 4.2.1 [1.4])

[The 2003 *Provisions* have adopted the 2002 USGS probabilistic seismic hazard maps, and the maps have been added to the body of the 2003 *Provisions* as figures in Chapter 3 (instead of the previously used separate map package).]

Note that *Provisions* Table 5.2.2 [4.3-1] permits an ordinary moment-resisting steel frame for buildings that do not exceed one story and 60 feet tall with a roof dead load not exceeding 15 psf. This building would fall within that restriction, but the intermediate steel moment frame with stiffened bolted end plates is chosen to illustrate the connection design issues.

[The height and tributary weight limitations for ordinary moment-resisting frames have been revised in the 2003 *Provisions*. In Seismic Design Category D, these frames are permitted only in single-story structures up to 65 feet in height, with field-bolted end plate moment connections, and roof dead load not exceeding 20 psf. Refer to 2003 *Provisions* Table 4.3-1, footnote h. The building in this example seems to fit these criteria, but the presence of the mezzanine could be questionable. Similarly, the limitations on intermediate moment-resisting frames in Seismic Design Category D have been revised. The same single-story height and weight limits apply, but the type of connection is not limited.]

N-S direction:

Moment-resisting frame system	= intermediate steel moment frame
R	= 4.5 (<i>Provisions</i> Table 5.2.2 [4.3-1])
\mathcal{Q}_0	= 3 (<i>Provisions</i> Table 5.2.2 [4.3-1])
C_d	= 4 (<i>Provisions</i> Table 5.2.2 [4.3-1])

E-W direction:

Braced frame system	= ordinary steel concentrically braced frame (<i>Provisions</i> Table 5.2.2 [4.3-1])
R	= 5 (<i>Provisions</i> Table 5.2.2 [4.3-1]) ¹
\mathcal{Q}_0	= 2 (<i>Provisions</i> Table 5.2.2 [4.3-1])
C_d	= 4.5 (<i>Provisions</i> Table 5.2.2 [4.3-1])

¹ R must be taken as 4.5 in this direction, due to *Provisions* Sec. 5.2.2.2.1 [4.3.1.2], which states that if the value of R in either direction is less than 5, the smaller value of R must be used in both directions. If the ordinary steel moment frame were chosen for the N-S direction, this R factor would change to 3.5.

5.1.2.2 Loads

Roof live load (L), snow	= 25 psf
Roof dead load (D)	= 15 psf
Mezzanine live load, storage	= 125 psf
Mezzanine slab and deck dead load	= 69 psf
Weight of wall panels	= 75 psf

Roof dead load includes roofing, insulation, metal roof deck, purlins, mechanical and electrical equipment, and that portion of the main frames that is tributary to the roof under lateral load. For determination of the seismic weights, the weight of the mezzanine will include the dead load plus 25 percent of the storage load (125 psf) in accordance with *Provisions* Sec. 5.3 [5.2.1]. Therefore, the mezzanine seismic weight is $69 + 0.25(125) = 100$ psf.

5.1.2.3 Materials

Concrete for footings	$f'_c = 2.5$ ksi
Slabs-on-grade	$f'_c = 4.5$ ksi
Mezzanine concrete on metal deck	$f'_c = 3.0$ ksi
Reinforcing bars	ASTM A615, Grade 60
Structural steel (wide flange sections)	ASTM A992, Grade 50
Plates	ASTM A36
Bolts	ASTM A325

5.1.3 Structural Design Criteria

5.1.3.1 Building Configuration

Because there is a mezzanine at one end, the building might be considered vertically irregular (*Provisions* Sec. 5.2.3.3 [4.3.2.3]). However, the upper level is a roof, and the *Provisions* exempts roofs from weight irregularities. There also are plan irregularities in this building in the transverse direction, again because of the mezzanine (*Provisions* Sec. 5.2.3.2 [4.3.2.2]).

5.1.3.2 Redundancy

For a structure in Seismic Design Category D, *Provisions* Eq. 5.2.4.2 [not applicable in the 2003 *Provisions*] defines the reliability factor (ρ) as:

$$\rho = 2 - \frac{20}{r_{max_x} \sqrt{A_x}}$$

where the roof area (A_x) = 16,200 sq ft.

To checking ρ in an approximate manner. In the N-S (transverse) direction, there are (2 adjacent columns)/(2 x 9 bays) so:

$$r_{max_x} = 0.11 \text{ and } \rho = 0.57 < 1.00.$$

Therefore, use $\rho = 1.00$.

In the E-W (longitudinal) direction, the braces are equally loaded (ignoring accidental torsion), so there is (1 brace)/(4 braces) so

$$r_{max_x} = 0.25 \text{ and } \rho = 1.37 .$$

Thus, the reliability multiplier is 1.00 in the transverse direction and 1.37 in the longitudinal direction. The reliability factor applies only to the determination of forces, not to deflection calculations.

[The redundancy requirements have been substantially changed in the 2003 *Provisions*. For a building assigned to Seismic Design Category D, $\rho = 1.0$ as long as it can be shown that failure of beam-to-column connections at both ends of a single beam (moment frame system) or failure of an individual brace (braced frame system) would not result in more than a 33 percent reduction in story strength or create an extreme torsional irregularity. Therefore, the redundancy factor would have to be investigated in both directions based on the new criteria in the 2003 *Provisions*.]

5.1.3.3 Orthogonal Load Effects

A combination of 100 percent seismic forces in one direction plus 30 percent seismic forces in the orthogonal direction must be applied to the structures in Seismic Design Category D (*Provisions* Sec. 5.2.5.2.3 and 5.2.5.2.2 [4.4.2.3 and 4.4.2.2, respectively]).

5.1.3.4 Structural Component Load Effects

The effect of seismic load (*Provisions* Eq. 5.2.7-1 and 5.2.7-2 [4.2-1 and 4.2-2, respectively]) is:

$$E = \rho Q_E \pm 0.2 S_{DS} D.$$

Recall that $S_{DS} = 1.0$ for this example. The seismic load is combined with the gravity loads as follows:

$$1.2D + 1.0L + 0.2S + E = 1.2D + 1.0L + \rho Q_E + 0.2D = 1.4D + 1.0L + 0.2S + \rho Q_E.$$

Note $1.0L$ is for the storage load on the mezzanine; the coefficient on L is 0.5 for many common live loads:

$$0.9D + E = 0.9D + \rho Q_E - 0.2D = 0.7D + \rho Q_E.$$

5.1.3.5 Drift Limits

For a building in Seismic Use Group I, the allowable story drift (*Provisions* 5.2.8 [4.5-1]) is:

$$\Delta_a = 0.025 h_{sx}.$$

At the roof ridge, $h_{sx} = 34 \text{ ft-3 in.}$ and $\Delta_a = 10.28 \text{ in.}$

At the hip (column-roof intersection), $h_{sx} = 30 \text{ ft-6 in.}$ and $\Delta_a = 9.15 \text{ in.}$

At the mezzanine floor, $h_{sx} = 12 \text{ ft}$ and $\Delta_a = 3.60 \text{ in.}$

Footnote b in *Provisions* Table 5.2.8 [4.5-1, footnote c] permits unlimited drift for single-story buildings with interior walls, partitions, etc., that have been designed to accommodate the story drifts. See Sec. 5.1.4.3 for further discussion. The main frame of the building can be considered to be a one-story

building for this purpose, given that there are no interior partitions except below the mezzanine. (The definition of a story in building codes generally does not require that a mezzanine be considered a story unless its area exceeds one-third the area of the room or space in which it is placed; this mezzanine is less than one-third the footprint of the building.)

5.1.3.6 Seismic Weight

The weights that contribute to seismic forces are:

	<u>E-W direction</u>	<u>N-S direction</u>
Roof D and $L = (0.015)(90)(180) =$	243 kips	243 kips
Panels at sides $= (2)(0.075)(32)(180)/2 =$	0 kips	437 kips
Panels at ends $= (2)(0.075)(35)(90)/2 =$	224 kips	0 kips
Mezzanine slab $= (0.100)(90)(40) =$	360 kips	360 kips
Mezzanine framing $=$	35 kips	35 kips
Main frames $=$	<u>27 kips</u>	<u>27 kips</u>
Seismic weight $=$	889 kips	1,102 kips

The weight associated with the main frames accounts for only the main columns, because the weight associated with the remainder of the main frames is included in roof dead load above. The computed seismic weight is based on the assumption that the wall panels offer no shear resistance for the structure but are self-supporting when the load is parallel to the wall of which the panels are a part.

5.1.4 Analysis

Base shear will be determined using an equivalent lateral force (ELF) analysis; a modal analysis then will examine the torsional irregularity of the building. The base shear as computed by the ELF analysis will be needed later when evaluating the base shear as computed by the modal analysis (see *Provisions* Sec. 5.5.7 [5.3.7]).

5.1.4.1 Equivalent Lateral Force Procedure

In the longitudinal direction where stiffness is provided only by the diagonal bracing, the approximate period is computed using *Provisions* Eq. 5.4.2.1-1 [5.2-6]:

$$T_a = C_p h_n^x = (0.02)(34.25^{0.75}) = 0.28 \text{ sec}$$

In accordance with *Provisions* Sec. 5.4.2 [5.2.2], the computed period of the structure must not exceed:

$$T_{max} = C_u T_a = (1.4)(0.28) = 0.39 \text{ sec.}$$

The subsequent 3-D modal analysis finds the computed period to be 0.54 seconds.

In the transverse direction where stiffness is provided by moment-resisting frames (*Provisions* Eq. 5.4.2.1-1 [5.2-6]):

$$T_a = C_p h_n^x = (0.028)(34.25^{0.8}) = 0.47 \text{ sec}$$

and

$$T_{max} = C_u T_a = (1.4)(0.47) = 0.66 \text{ sec.}$$

Also note that the dynamic analysis found a computed period of 1.03 seconds.

The seismic response coefficient (C_s) is computed in accordance with *Provisions* Sec. 5.4.1.1 [5.2.1.1]. In the longitudinal direction:

$$C_s = \frac{S_{DS}}{R/I} = \frac{1.0}{4.5/1} = 0.222$$

but need not exceed

$$C_s = \frac{S_{DI}}{T(R/I)} = \frac{0.6}{(0.39)(4.5/1)} = 0.342$$

Therefore, use $C_s = 0.222$ for the longitudinal direction.

In the transverse direction (*Provisions* Eq. 5.4.1.1-1 and 5.4.1.1-2 [5.2-2 and 5.2-3, respectively]):

$$C_s = \frac{S_{DS}}{R/I} = \frac{1.0}{4.5/1} = 0.222$$

but need not exceed

$$C_s = \frac{S_{DI}}{T(R/I)} = \frac{0.6}{(0.66)(4.5/1)} = 0.202$$

Therefore, use $C_s = 0.202$ for the transverse direction.

In both directions the value of C_s exceeds the minimum value (*Provisions* Eq. 5.4.1.1-3 [not applicable in the 2003 *Provisions*]) computed as:

$$C_s = 0.044I S_{DS} = (0.044)(1)(1.0) = 0.044$$

[This minimum C_s value has been removed in the 2003 *Provisions*. In its place is a minimum C_s value for long-period structures, which is not applicable to this example.]

The seismic base shear in the longitudinal direction (*Provisions* Eq. 5.4.1 [5.2-1]) is:

$$V = C_s W = (0.222)(889 \text{ kips}) = 197 \text{ kips.}$$

The seismic base shear in the transverse direction is:

$$V = C_s W = (0.202)(1,102 \text{ kips}) = 223 \text{ kips.}$$

The seismic force must be increased by the reliability factor as indicated previously. Although this is not applicable to the determination of deflections, it is applicable in the determination of required strengths. The reliability multiplier (ρ) will enter the calculation later as the modal analysis is developed. If the ELF method was used exclusively, the seismic base shear in the longitudinal direction would be increased by ρ now:

$$V = \rho (197) \\ V = (1.37)(197) = 270 \text{ kips}$$

[See Sec. 5.1.3.2 for discussion of the changes to the redundancy requirements in the 2003 *Provisions*.]

Provisions Sec. 5.4.3 [5.2.3] prescribes the vertical distribution of lateral force in a multilevel structure. Even though the building is considered to be one story for some purposes, it is clearly a two-level structure. Using the data in Sec. 5.1.3.6 of this example and interpolating the exponent k as 1.08 for the period of 0.66 sec, the distribution of forces for the N-S analysis is shown in Table 5.1-1.

Table 5.1-1 ELF Vertical Distribution for N-S Analysis

Level	Weight (w_x)	Height (h_x)	$w_x h_x^k$	C_{vx}	F_x
Roof	707 kips	30.5 ft.	28340	0.83	185 kips
Mezzanine	395 kips	12 ft.	5780	0.17	38 kips
Total	1102 kips		34120		223 kips

It is not immediately clear as to whether the roof (a 22-gauge steel deck with conventional roofing over it) will behave as a flexible or rigid diaphragm. If one were to assume that the roof were a flexible diaphragm while the mezzanine were rigid, the following forces would be applied to the frames:

Typical frame at roof (tributary basis) = 185 kips / 9 bays = 20.6 kips

End frame at roof = 20.6/2 = 10.3 kips

Mezzanine frame at mezzanine = 38 kips/3 frames = 12.7 kips

If one were to assume the roof were rigid, it would be necessary to compute the stiffness for each of the two types of frames and for the braced frames. For this example, a 3-D model was created in SAP 2000.

5.1.4.2 Three-Dimension Static and Modal Response Spectrum Analyses

The 3-D analysis is performed for this example to account for:

1. The significance of differing stiffness of the gable frames with and without the mezzanine level,
2. The significance of the different centers of mass for the roof and the mezzanine,
3. The relative stiffness of the roof deck with respect to the gable frames, and
4. The significance of braced frames in controlling torsion due to N-S ground motions.

The gabled moment frames, the tension bracing, the moment frames supporting the mezzanine, and the diaphragm chord members are explicitly modeled using 3-D beam-column elements. The collector at the hip level is included as are those at the mezzanine level in the two east bays. The mezzanine diaphragm is modeled using planar shell elements with their in-plane rigidity being based on actual properties and dimensions of the slab. The roof diaphragm also is modeled using planar shell elements, but their in-plane rigidity is based on a reduced thickness that accounts for compression buckling phenomena and for the fact that the edges of the roof diaphragm panels are not connected to the wall panels. SDI's *Diaphragm Design Manual* is used for guidance in assessing the stiffness of the roof deck. The analytical model includes elements with one-tenth the stiffness of a plane plate of 22 gauge steel.

The ELF analysis of the 3-D model in the transverse direction yields two important results: the roof diaphragm behaves as a rigid diaphragm and the displacements result in the building being classified as torsionally irregular. The forces at the roof are distributed to each frame line in a fashion that offsets the center of force 5 percent of 180 ft (9 ft) to the west of the center of the roof. The forces at the mezzanine are similarly distributed to offset the center of the mezzanine force 5 percent of 40 ft to the west of the

center of the mezzanine. Using grid locations numbered from west to east, the applied forces and the resulting displacements are shown in Table 5.1-2.

Table 5.1-2 ELF Analysis in N-S Direction

Grid	Roof Force, kips	Mezzanine Force, kips	Roof Displace- ment, in.
1	13.19		4.56
2	25.35		4.45
3	23.98		4.29
4	22.61		4.08
5	21.24		3.82
6	19.87		3.53
7	18.50		3.21
8	17.13	14.57	2.86
9	15.76	12.67	2.60
10	7.36	10.77	2.42
Totals	184.99	38.01	

The average of the extreme displacements is 3.49 in. The displacement at the centroid of the roof is 3.67 in. Thus, the deviation of the diaphragm from a straight line is 0.18 in. whereas the average frame displacement is about 20 times that. Clearly then, the behavior is as a rigid diaphragm. The ratio of maximum to average displacement is 1.31, which exceeds the 1.2 limit given in *Provisions* Table 5.2.3.2 [4.3-2] and places the structure in the category “torsionally irregular.” *Provisions* Table 5.2.5.1 [4.4-1] then requires that the seismic force analysis be any one of several types of dynamic analysis. The simplest of these is the modal response spectrum (MRS) analysis.

The MRS is an easy next step once the 3-D model has been assembled. A 3-D dynamic design response spectrum analysis is performed per *Provisions* Sec. 5.5 [5.3] using the SAP 2000 program. The design response spectrum is based on *Provisions* Sec. 4.1.2.6 [3.3.4] and is shown in Figure 5.1-4. [Although it has no affect on this example, the design response spectrum has been changed for long periods in the 2003 *Provisions*. See the discussion in Chapter 3 of this volume of design examples.]

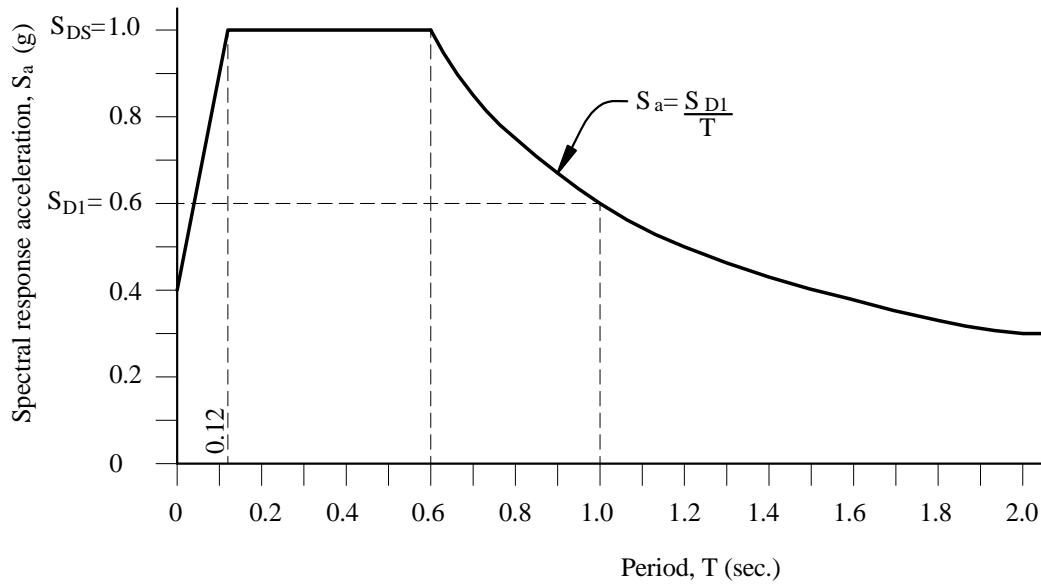


Figure 5.1-4 Design response spectrum.

The modal seismic response coefficient (*Provisions* Eq. 5.5.4-3 [5.3-3]) is $C_{sm} = \frac{S_{am}}{R/I}$. The design response spectra expressed in units of g and ft/sec² are shown in Table 5.1-3.

Table 5.1-3 Design Response Spectra

T (sec)	S_a (g) $S_{am} = S_a$ (g)	$C_{sm} = \frac{S_{am}}{(R/I)}$ $R = 4.5$	C_{sm} (ft/sec ²)
0.0	0.4	0.089	2.862
0.12	0.9	0.222	7.155
0.6	1.0	0.222	7.155
0.7	0.857	0.190	6.132
0.8	0.750	0.167	5.367
0.9	0.666	0.148	4.766
1.0	0.600	0.133	4.293
1.1	0.545	0.121	3.900
1.2	0.500	0.111	3.578
1.3	0.461	0.102	3.299
1.4	0.429	0.095	3.070

1.0 ft = 0.3048 m.

With this model, the first 24 periods of vibration and mode shapes of the structure were computed using the SAP2000 program. The first mode had a period of vibration of 1.03 seconds with predominantly transverse participation. The third mode period was 0.54 seconds with a predominantly longitudinal participation. The first 24 modes accounted for approximately 98 percent of the total mass of the

structure in the transverse direction and approximately 93 percent in the longitudinal direction, both of which are is greater than the 90 percent requirement of *Provisions* Sec. 5.5.2 [5.3.2].

The design value for modal base shear (V_i) is determined by combining the modal values for base shear. The SAP 2000 program uses the complete quadratic combination (CQC) of the modal values, which accounts for coupling of closely spaced modes. In the absence of damping, the CQC is simply the square root of the sum of the squares (SRSS) of each modal value. Base shears thus obtained are:

$$\begin{aligned} \text{Longitudinal } V_i &= 159.5 \text{ kips} \\ \text{Transverse } V_i &= 137.2 \text{ kips} \end{aligned}$$

In accordance with *Provisions* Sec. 5.5.7 [5.3.7], compare the design values of modal base shear to the base shear determined by the ELF method. If the design value for modal base shear is less than 85 percent of the ELF base shear calculated using a period of $C_u T_a$, a factor to bring the modal base shear up to this comparison ELF value must be applied to the modal story shears, moments, drifts, and floor deflections. According to *Provisions* Eq. 5.5.7.1 [5.3-10]:

$$\text{Modification factor} = 0.85 (V/V_i)$$

$$\begin{aligned} \text{E-W modification factor} &= 0.85(V/V_i) = (0.85)(197 \text{ kips}/159.5 \text{ kips}) = 1.05 \\ \text{N-S modification factor} &= 0.85(V/V_i) = (0.85)(223 \text{ kips}/137.2 \text{ kips}) = 1.38 \end{aligned}$$

The response spectra for the 3-D modal analysis is then revised by the above modification factors:

$$\begin{aligned} \text{E-W} & (1.0)(1.05)(\text{x-direction spectrum}) \\ \text{N-S} & (1.0)(1.38)(\text{y-direction spectrum}) \end{aligned}$$

The model is then run again.

The maximum lateral displacements at the ridge due to seismic loads (i.e., design response spectra as increased by the modification factors above) from the second analysis are:

$$\begin{aligned} \text{E-W deflection} & \delta_{xe} = 0.84 \text{ in.} \\ \text{N-S deflection} & \delta_{ye} = 2.99 \text{ in. at the first frame in from the west end} \end{aligned}$$

where δ_{xe} and δ_{ye} are deflections determined by the elastic modal analysis. Those frames closer to the mezzanine had smaller N-S lateral deflections in much the same fashion as was shown for the ELF analysis. Before going further, the deflections should be checked as discussed in Sec. 5.1.4.3 below.

The response spectra for the 3-D modal analysis are combined to meet the orthogonality requirement of *Provisions* Sec. 5.2.5.2.2a [4.4.2.3]:

$$\begin{aligned} \text{E-W} & (1.0)(\text{E-W direction spectrum}) + (0.3)(\text{N-S direction spectrum}) \\ \text{N-S} & (0.3)(\text{E-W direction spectrum}) + (1.0)(\text{N-S direction spectrum}) \end{aligned}$$

Finally, the design response spectra for the 3-D modal analysis is again revised by increasing the E-W direction response by the reliability factor, $\rho = 1.37$. Note that ρ is equal to unity in the N-S direction. Thus, the factors on the basic spectrum for the load combinations become:

$$\begin{aligned} \text{E-W} & (1.0)(1.05)(1.37)(\text{E-W direction spectrum}) + (0.3)(1.38)(1.00)(\text{N-S direction spectrum}) \\ \text{N-S} & (0.3)(1.05)(1.37)(\text{E-W direction spectrum}) + (1.0)(1.38)(1.00)(\text{N-S direction spectrum}) \end{aligned}$$

and the model is run once again to obtain the final result for design forces, shears, and moments. From this third analysis, the final design base shears are obtained. Applying the ρ factor (1.37) is equivalent to increasing the E-W base shear from $(0.85 \times 197 \text{ kips}) = 167.5 \text{ kips}$ to 230 kips.

5.1.4.3 Drift

The lateral deflection cited previously must be multiplied by $C_d = 4$ to find the transverse drift:

$$\delta_x = \frac{C_d \delta_{xe}}{I} = \frac{4.0(2.99)}{1.0} = 12.0 \text{ in.}$$

This exceeds the limit of 10.28 in. computed previously. However, there is no story drift limit for single-story structures with interior wall, partitions, ceilings, and exterior wall systems that have been designed to accommodate the story drifts. (The heavy wall panels were selected to make an interesting example problem, and the high transverse drift is a consequence of this. Some real buildings, such as refrigerated warehouses, have heavy wall panels and would be expected to have high seismic drifts. Special attention to detailing the connections of such features is necessary.)

In the longitudinal direction, the lateral deflection was much smaller and obviously is within the limits. Recall that the deflection computations do not consider the reliability factor. This value must be multiplied by a C_d factor to find the transverse drift. The tabulated value of C_d is 4.5, but this is for use when design is based upon $R = 5$. The *Provisions* does not give guidance for C_d when the system R factor is overridden by the limitation of *Provisions* Sec. 5.2.2.1 [4.3.1.2]. The authors suggest adjusting by a ratio of R factors.

5.1.4.4 P-delta

The AISC LRFD Specification requires P-delta analyses for frames. This was investigated by a 3-D P-delta analysis, which determined that secondary P-delta effect on the frame in the transverse direction was less than 1 percent of the primary demand. As such, for this example, P-delta was considered to be insignificant and was not investigated further. (P-delta may be significant for a different structure, say one with higher mass at the roof. P-delta should always be investigated for unbraced frames.)

5.1.4.5 Force Summary

The maximum moments and axial forces caused by dead, live, and earthquake loads on the gable frames are listed in Tables 5.1-2 and 5.1-3. The frames are symmetrical about their ridge and the loads are either symmetrical or can be applied on either side on the frame because the forces are given for only half of the frame extending from the ridge to the ground. The moments are given in Table 5.1-4 and the axial forces are given in Table 5.1-5. The moment diagram for the combined load condition is shown in Figure 5.1-5. The load combination is $1.4D + L + 0.2S + \rho Q_E$, which is used throughout the remainder of calculations in this section, unless specifically noted otherwise.

The size of the members is controlled by gravity loads, not seismic loads. The design of connections will be controlled by the seismic loads.

Forces in and design of the braces are discussed in Sec. 5.1.5.5 of this chapter.

Table 5.1-4 Moments in Gable Frame Members

Location	D (ft-kips)	L (ft-kips)	S (ft-kips)	Q_E (ft-kips)	Combined* (ft-kips)
1- Ridge	61	0	128	0	112 (279)
2- Knee	161	0	333	162	447 (726)
3- Mezzanine	95	83	92	137	79
4- Base	0	0	0	0	0

* Combined Load = $1.4D + L + 0.2S + \rho Q_E$ (or $1.2D + 1.6S$). Individual maximums are not necessarily on the same frame; combined load values are maximum for any frame.
 1.0 ft = 0.3048 m, 1.0 kip = 1.36 kN-m.

Table 5.1-5 Axial Forces in Gable Frames Members

Location	D (ft-kips)	L (ft-kips)	S (ft-kips)	ρQ_E (ft-kips)	Combined* (ft-kips)
1- Ridge	14	3.5	25	0.8	39
2- Knee	16	4.5	27	7.0	37
3- Mezzanine	39	39	23	26	127
4- Base	39	39	23	26	127

* Combined Load = $1.4D + L + 0.2S + \rho Q_E$. Individual maximums are not necessarily on the same frame; combined load values are maximum for any frame.
 1.0 ft = 0.3048 m, 1.0 kip = 1.36 kN-m.

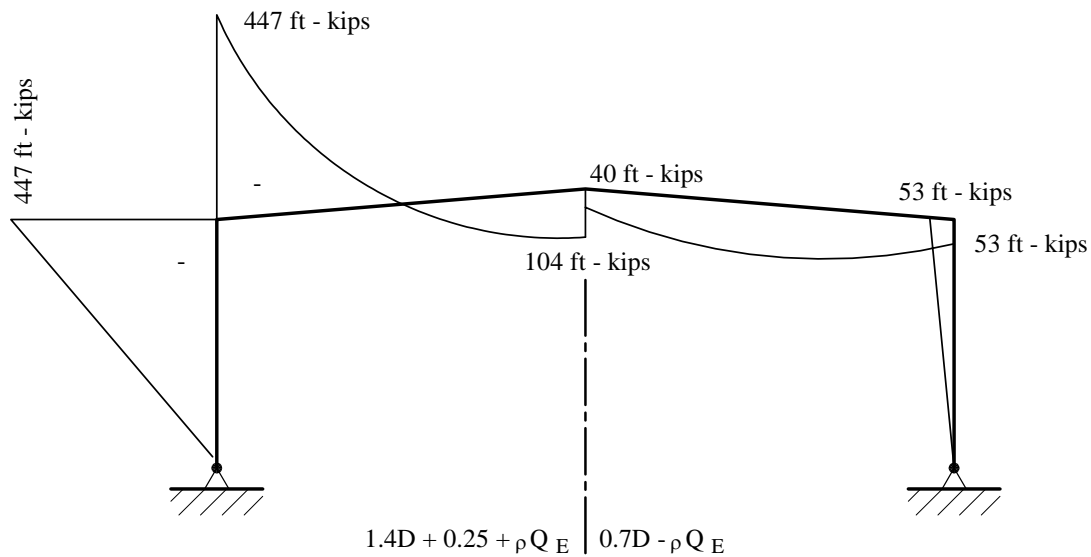


Figure 5.1-5 Moment diagram for seismic load combinations (1.0 ft-kip = 1.36 kN-m).

5.1.5 Proportioning and Details

The gable frame is shown schematically in Figure 5.1-6. Using load combinations presented in Sec. 5.1.3.4 and the loads from Tables 5.1-2 and 5.1-3, the proportions of the frame are checked at the roof beams and the variable-depth columns (at the knee). The mezzanine framing, also shown in Figure 5.1-1, was proportioned similarly. The diagonal bracing, shown in Figure 5.1-1 at the east end of the building, is proportioned using tension forces determined from the 3-D modal analysis.

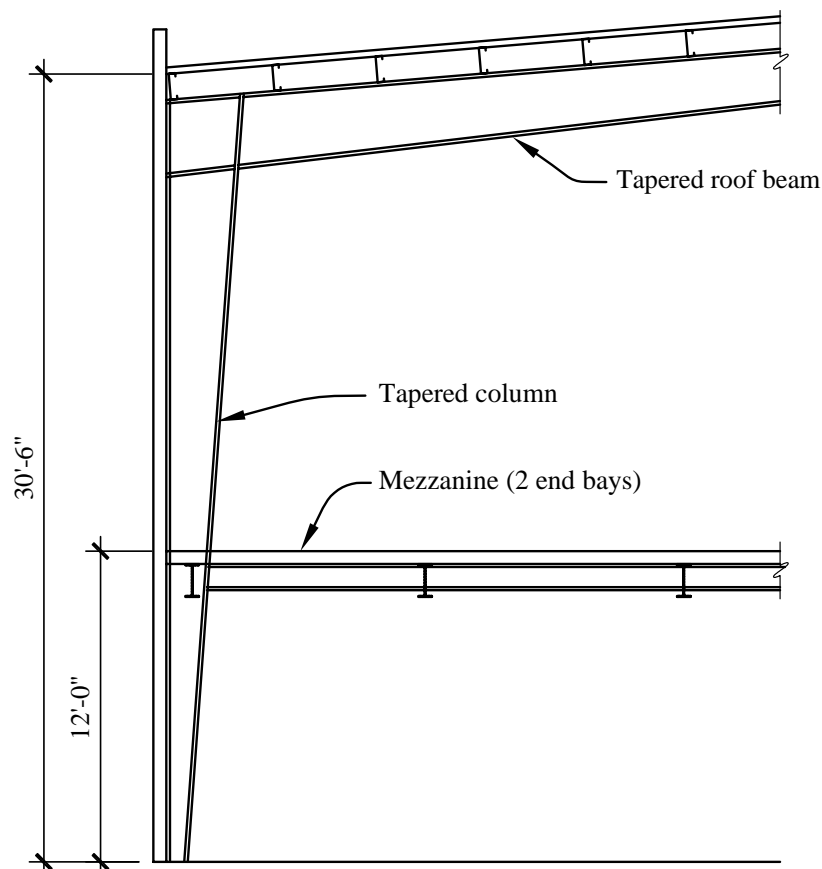


Figure 5.1-6 Gable frame schematic: Column tapers from 12 in. at base to 36 in. at knee; roof beam tapers from 36 in. at knee to 18 in. at ridge; plate sizes are given in Figure 5.1-8 (1.0 in. = 25.4+ mm).

5.1.5.1 Frame Compactness and Brace Spacing

According to *Provisions* Sec. 8.4 [8.2.2], steel structures assigned to Seismic Design Categories D, E, and F must be designed and detailed (with a few exceptions) per AISC Seismic. For an intermediate moment frame (IMF), AISC Seismic Part I, Section 1, “Scope,” stipulates that those requirements are to be applied in conjunction with AISC LRFD. Part I, Section 10 of AISC Seismic itemizes a few exceptions from AISC LRFD for intermediate moment frames, but otherwise the intermediate moment frames are to be designed per the AISC LRFD Specification.

Terminology for moment-resisting frames varies among the several standards; Table 5.1-6 is intended to assist the reader in keeping track of the terminology.

Table 5.1-6 Comparison of Standards

Total Rotation (story drift angle)	Plastic Rotation	AISC Seismic (1997)	FEMA 350	AISC Seismic (Supplement No. 2)	<i>Provisions</i>
0.04	0.03	SMF	SMF	SMF	SMF
0.03	0.02	IMF	Not used	Not used	Not used
0.02	0.01*	OMF	OMF	IMF	IMF
Not defined	Minimal	Not used	Not used	OMF	OMF

*This is called “limited inelastic deformations” in AISC Seismic.

SMF = special moment frame.

IMF = intermediate moment frame.

OMF = ordinary moment frame.

For this example, IMF per the *Provisions* corresponds to IMF per AISC Seismic.

[The terminology in the 2002 edition of AISC Seismic is the same as Supplement No. 2 to the 1997 edition as listed in Table 5.1-6. Therefore, the terminology is unchanged from the 2000 *Provisions*.]

Because AISC Seismic does not impose more restrictive width-thickness ratios for IMF, the width-thickness ratios of AISC LRFD, Table B5.1, will be used for our IMF example. (If the frame were an SMF, then AISC Seismic would impose more restrictive requirements.)

The tapered members are approximated as short prismatic segments; thus, the adjustments of AISC LRFD Specification for web-tapered members will not affect the results of the 3-D SAP 2000 analysis.

All width-thickness ratios are less than the limiting λ_p from AISC LRFD Table B5.1. All P-M ratios (combined compression and flexure) were less than 1.00. This is based on proper spacing of lateral bracing.

Lateral bracing is provided by the roof joists and wall girts. The spacing of lateral bracing is illustrated for the high moment area of the tapered beam near the knee. The maximum moment at the face of the column under factored load combinations is less than the plastic moment, but under the design seismic ground motion the plastic moment will be reached. At that point the moment gradient will be higher than under the design load combinations (the shear will be higher), so the moment gradient at design conditions will be used to compute the maximum spacing of bracing. The moment at the face of the column is 659 ft.-kip, and 4.0 ft away the moment is 427 ft.-kip. The member is in single curvature here, so the sign on the ratio in the design equation is negative (AISC LRFD Eq. F1-17):

$$L_{pd} = \left[0.12 + 0.076 \left(\frac{M_1}{M_2} \right) \right] \left(\frac{E}{F_y} \right) r_y$$

$$L_{pd} \left[0.12 + 0.076 \left(\frac{-488}{659} \right) \right] \left(\frac{29,000}{50} \right) (1.35) = 49.9 \text{ in.} > 48 \text{ in.} \quad \text{OK}$$

Also, per AISC LRFD Eq. F1-4:

$$L_p = 300r_y / \sqrt{F_{yf}}$$

$$L_p = (300)(1.35) / \sqrt{50} = 57 \text{ in.} > 48 \text{ in.}$$

OK

At the negative moment regions near the knee, lateral bracing is necessary on the bottom flange of the beams and inside the flanges of the columns (Figure 5.1-7).

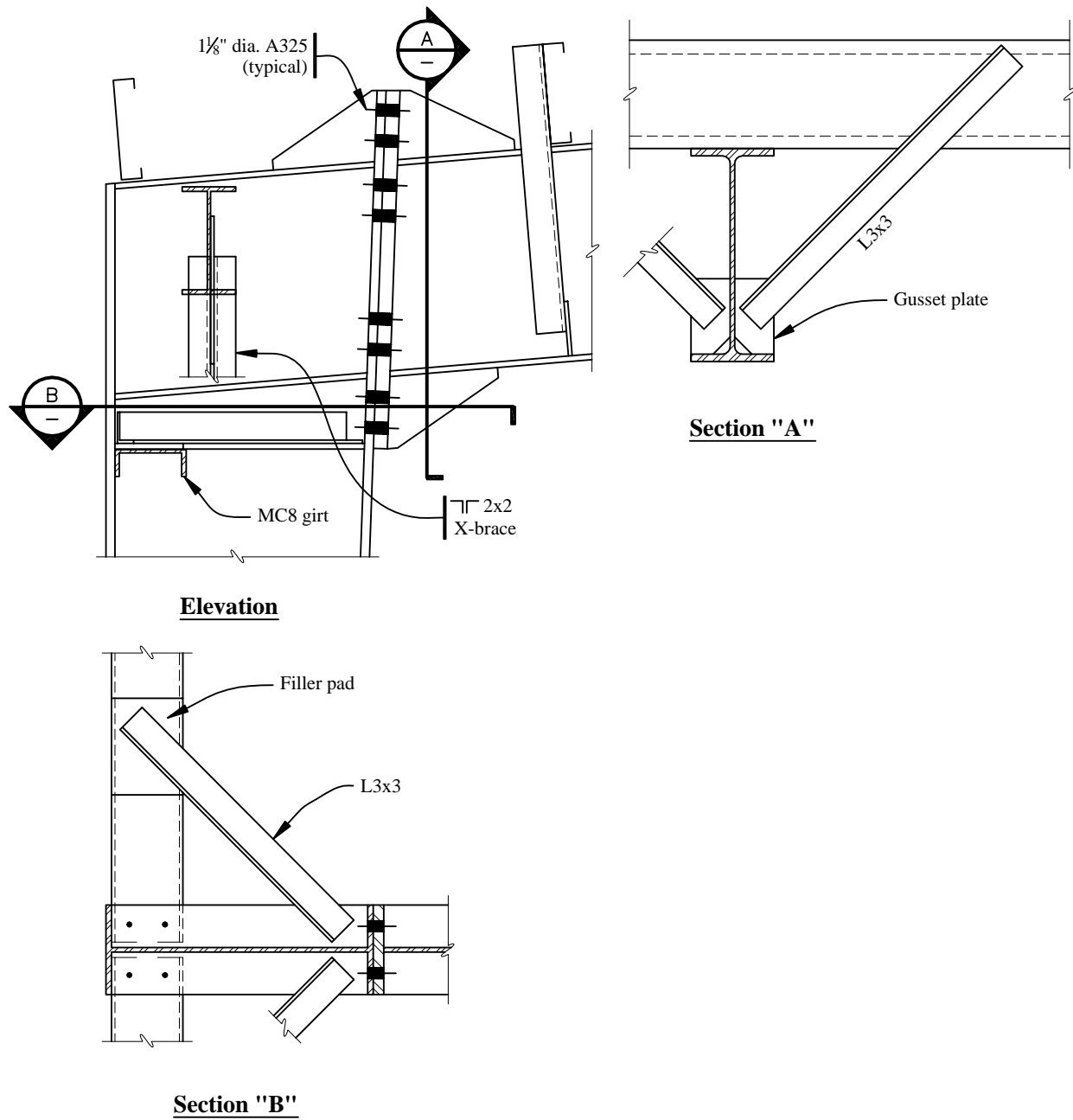


Figure 5.1-7 Arrangement at knee (1.0 in. = 25.4 mm).

5.1.5.2 Knee of the Frame

The knee detail is shown in Figures 5.1-7 and 5.1-8. The vertical plate shown near the upper left corner in Figure 5.1-7 is a gusset providing connection for X-bracing in the longitudinal direction. The beam to column connection requires special consideration. The method of FEMA 350 for bolted, stiffened end plate connections is used for a design guide here. (FEMA 350 has design criteria for specific connection details. The connection for our moment frame, which has a tapered column and a tapered beam is not one of the specific details per FEMA 350. However, FEMA 350 is used as a guide for this example because it is the closest design method developed to date for such a connection.) Refer to Figure 5.1-8 for configuration. Highlights from this method are shown for this portion of the example. Refer to FEMA 350 for a discussion of the entire procedure. AISC SDGS-4 is also useful.

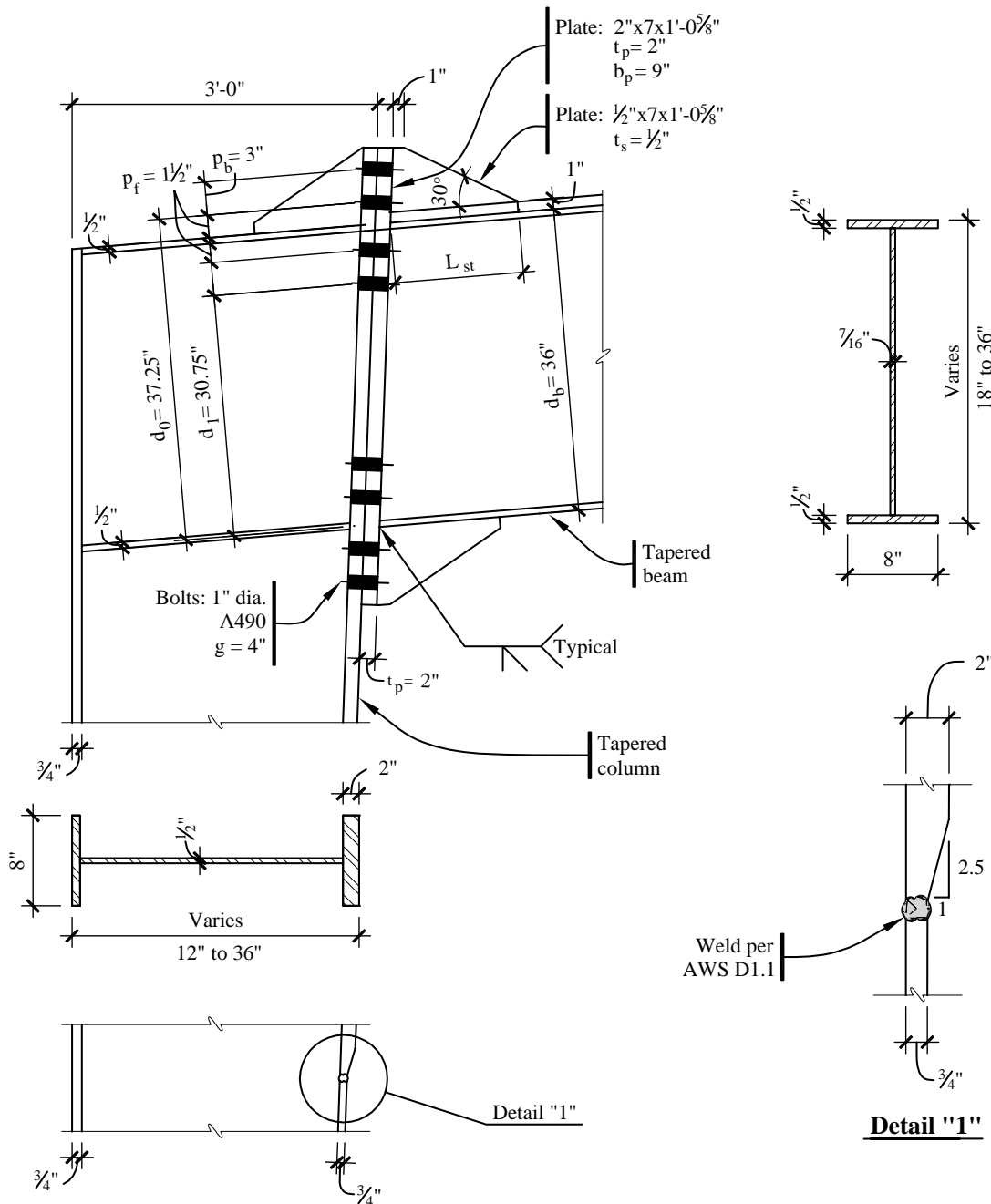


Figure 5.1-8 Bolted stiffened connection at knee (1.0 in. = 25.4 mm, 1.0 ft = 0.3048 m).

The FEMA 350 method for bolted stiffened end plate connection requires the determination of the maximum moment that can be developed by the beam. The steps in FEMA 350 for bolted stiffened end plates follow:

Step 1. The location of the plastic hinge is distance x from the face of the column. The end plate stiffeners at the top and bottom flanges increase the local moment of inertia of the beam, forcing the plastic hinge to occur away from the welds at the end of beam/face of column. The stiffeners should be long enough to force the plastic hinge to at least $d/2$ away from the end of the beam. With the taper of the section, the depth will be slightly less than 36 inches at the location of the hinge, but that reduction will be ignored here. The probable maximum moment (M_{pr}) at the plastic hinge is computed (FEMA 350 Eq. 3-1) as follows:

$$M_{pr} = C_{pr} R_y Z_e F_y.$$

Per FEMA 350 Eq. 3-2:

$$C_{pr} = \frac{F_y + F_u}{2F_u} = \frac{(50 + 65)}{(2)(50)} = 1.15 \quad .$$

AISC Seismic Table I-6-1 indicates:

$$\begin{aligned} R_y &= 1.1 \\ Z_e &= 267 \text{ in.}^3 \text{ at } d/2 \text{ from the end plate (the plastic hinge location)} \\ F_y &= 50 \text{ ksi} \end{aligned}$$

Therefore, $M_{pr} = (1.15)(1.1)(267)(50) = 16,888 \text{ in.-kips.} = 1,407 \text{ ft-kips.}$

The moment at the column flange, M_f , which drives the connection design, is determined from FEMA 350 Figure 3-4 as:

$$M_f = M_{pr} + V_p x$$

where

V_p = Shear at location of plastic hinge, assuming the frame has formed two hinges, one near each column.

$$V_p = w_g \frac{l}{2} + \frac{M_{pr1} + M_{pr2}}{l} = (0.52 \text{ klf}) \left(\frac{81 \text{ ft}}{2} \right) + \frac{1407 + 1407 \text{ ft-k}}{81 \text{ ft}} = 55.8 \text{ kips}$$

$l = 81 \text{ ft}$ comes from the 90 ft out-to-out dimension of the frame, less the column depth and distance to the hinge at each end. Where the gravity moments are a large fraction of the section capacity, the second hinge to form, which will be in positive moment, may be away from the column face, which will reduce l and usually increase V_p . That is not the circumstance for this frame.

$$x = d_b/2 = 18 \text{ in.} = 1.5 \text{ ft}$$

Thus, $M_f = 1407 + (55.8)(1.5) = 1491 \text{ ft-kips}$

In a like manner, the moment at the column centerline is found:

$$M_c = M_{pr} + V_p \left(x + \frac{d_c}{2} \right) = 1407 + 55.8(1.5 + 1.5) = 1574 \text{ ft-kips}$$

Step 2. Find bolt size for end plates. For a connection with two rows of two bolts inside and outside the flange, FEMA 350 Eq. 3-31 indicates:

$$\begin{aligned} M_f &< 3.4 T_{ub}(d_o + d_i) \\ (1491)(12) &< 3.4 T_{ub}(37.25 \text{ in.} + 30.75 \text{ in.}) \\ 77.38 &< T_{ub} \\ 77.38 &< 113 A_b \text{ (for A490 bolts)} \\ 0.685 \text{ in.}^2 &< A_b \end{aligned}$$

Use 1 in. Diameter A490 bolts.

Now confirm that T_{ub} satisfies FEMA 350 Eq. 3-32:

$$T_{ub} \geq \frac{0.00002305 p_f^{0.591} F_{fu}^{2.583}}{t_p^{0.895} d_{bt}^{1.909} t_s^{0.327} b_p^{0.965}} + T_b$$

where:

- p_f = dimension from top of flange to top of first bolt = 1.5 in.
- t_p = end plate thickness = 2 in. (Trial t_p)
- d_{bt} = bolt diameter = 1 in.
- t_s = thickness of stiffener plate = 0.44 in.
- b_p = width of end plate = 9 in.
- T_b = bolt pretension per AISC LRFD Table J3.1
- $T_{ub} = 113 A_b = (113)(0.785) = 88.7 \text{ kips}$

$$T_{ub} \geq \frac{(0.00002305)(1.5)^{0.591} (504)^{2.583}}{(2)^{0.895} (1)^{1.909} (0.44)^{0.327} (9)^{0.965}} + 64$$

$$T_{ub} = 88.7 \text{ kips} > 87.5 \text{ kips}$$

OK

Therefore, a 2-in.-thick end plate is acceptable.

Step 3. Check the bolt size to preclude shear failure. This step is skipped here because 16 bolts will obviously carry the shear for our example.

Step 4. Determine the minimum end plate thickness necessary to preclude flexural yielding by comparing the thickness determined above against FEMA 350 Eq. 3-34:

$$t_p \geq \frac{0.00609 p_f^{0.9} g^{0.6} F_{fu}^{0.9}}{d_{bt}^{0.9} t_s^{0.1} b_p^{0.7}}$$

$$t_p \geq \frac{(0.00609)(1.5)^{0.9} (4)^{0.6} (504)^{0.9}}{(1)^{0.9} (0.44)^{0.1} (9)^{0.7}}$$

$$2 \text{ in.} > 1.27 \text{ in.}$$

OK

and against FEMA 350 Eq. 3-35:

$$t_p \geq \frac{0.00413 p_f^{0.25} g^{0.15} F_{fu}}{d_{bt}^{0.7} t_s^{0.15} b_p^{0.3}}$$

$$t_p \geq \frac{(0.00413)(1.5)^{0.25} (4)^{0.15} (504)}{(1)^{0.7} (0.44)^{0.15} (9)^{0.3}}$$

2 in. > 1.66 in.

OK

Therefore, use a 2-in.-thick end plate.

Step 5. Determine the minimum column flange thickness required to resist beam flange tension using FEMA 350 Eq. 3-37:

$$t_{cf} > \sqrt{\frac{\alpha_m F_{fu} C_3}{0.9 F_{yc} (3.5 p_b + c)}}$$

where

$$C_3 = \frac{g}{2} - d_{bt} - k_1 = \frac{4}{2} - \frac{1}{4} - 0.75 = 1.00 \text{ in.}$$

(For purposes of this example, k_1 is taken to be the thickness of the column web, 0.5 in. and an assumed 0.25 in. fillet weld for a total of 0.75 in.).

Using FEMA 350 Eq. 3-38:

$$\alpha_m = C_a \left(\frac{A_f}{A_w} \right)^{\frac{1}{3}} \frac{C_3}{(d_{bt})^{\frac{1}{4}}} = (1.48) \left(\frac{(2)(8)(0.5)}{(35)(0.44)} \right)^{\frac{1}{3}} \frac{1}{(1)^{0.25}} = 1.19$$

$$t_{cf} > \sqrt{\frac{(1.19)(504)(1.00)}{(0.9)(50)[(3.5)(3) + (3.5)]}} = 0.95 \text{ in.}$$

Minimum $t_{cf} = 0.95$ in. but this will be revised in Step 7.

Step 6. Check column web thickness for adequacy for beam flange compression. This is a check on web crippling using FEMA 350 Eq. 3-40:

$$t_{wc} = \frac{M_f}{(d_b - t_{fb})(6k + 2t_p + t_{fb})F_{yc}} = \frac{(1491)(12)}{(36 - 0.5)[(6)(0.75) + (2)(2) + (0.5)](50)} = 1.44 \text{ in.}$$

$$t_{wc \text{ reqd}} = 1.44 \text{ in.} > 0.5 \text{ in.} = t_{wc}$$

OK

Therefore, a continuity plate is needed at the compression flange. See FEMA 350 Sec. 3.3.3.1 for continuity plate sizing. For one-sided connections, the necessary thickness of the continuity plate is $0.5(t_{bf} + t_{bf}) = 0.5$ in.

Step 7. Because continuity plates are required, t_{cf} must be at least as thick as the end plate thickness t_p . Therefore, $t_{cf} = 2$ in. For this column, the 2-in.-thick flange does not need to be full height but must continue well away from the region of beam flange compression and the high moment

portion of the column knee area. Some judgment is necessary here. For this case, the 2-in. flange is continued 36 in. down from the bottom of the beam, where it is welded to the 0.75-in.- thick flange. This weld needs to be carefully detailed.

Step 8. Check the panel zone shear in accordance with FEMA 350, Sec. 3.3.3.2. For purposes of this check, use $d_b = 35.5 + 1.5 + 3 + 1.5 = 41.5$ in. Per FEMA 350 Eq. 3-7:

$$t \geq \frac{C_y M_c \left(\frac{h-d_b}{h} \right)}{(0.9)(0.6F_y)R_{yc}d_c(d_b-t_{fb})}$$

where, according to FEMA 350 Eq. 3-4:

$$C_y = \frac{1}{C_{pr} \frac{Z_{be}}{S_b}} = \frac{1}{1.15 \left(\frac{267}{218} \right)} = 0.71$$

$$t_{cw} \geq \frac{(0.71)(1574 \times 12) \left(\frac{366-41.5}{366} \right)}{(0.9)(0.6)(50)(1.1)(36)(36-0.5)} = 0.31 \text{ in.}$$

$$t_{cw \text{ required}} = 0.31 \text{ in.} < 0.50 \text{ in.} = t_{cw}$$

OK

5.1.5.3 Frame at the Ridge

The ridge joint detail is shown in Figure 5.1-9. An unstiffened bolted connection plate is selected.

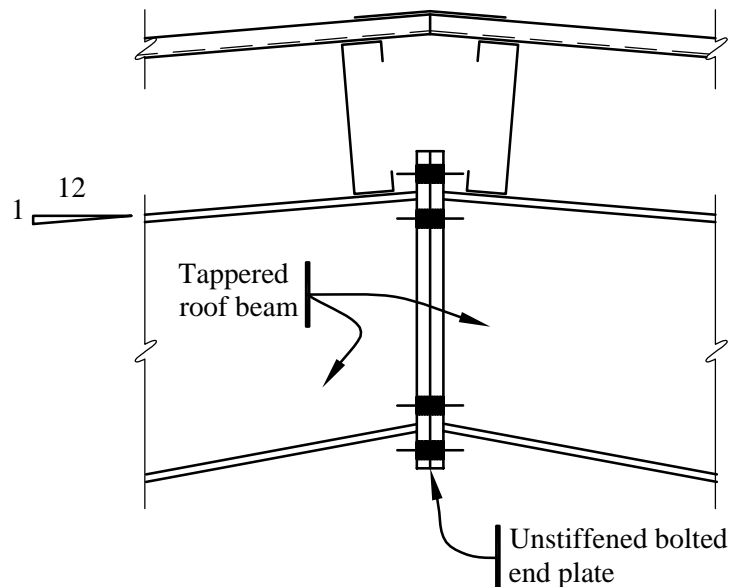


Figure 5.1-9 End plate connection at ridge.

This is an AISC LRFD designed connection, not a FEMA 350 designed connection because there should not be a plastic hinge forming in this vicinity. Lateral seismic force produces no moment at the ridge until yielding takes place at one of the knees. Vertical accelerations on the dead load do produce a

moment at this point; however, the value is small compared to all other moments and does not appear to be a concern. Once lateral seismic loads produce yielding at one knee, further lateral displacement produces some positive moment at the ridge. Under the condition on which the FEMA 350 design is based (a full plastic moment is produced at each knee), the moment at the ridge will simply be the static moment from the gravity loads less the horizontal thrust times the rise from knee to ridge. If one uses $1.2D + 0.2S$ as the load for this scenario, the static moment is 406 ft-kip and the reduction for the thrust is 128 ft-kip, leaving a net positive moment of 278 ft-kip, coincidentally close to the design moment for the factored gravity loads.

5.1.5.4 Design of Mezzanine Framing

The design of the framing for the mezzanine floor at the east end of the building is controlled by gravity loads. The concrete filled 3-in., 20-gauge steel deck of the mezzanine floor is supported on steel beams spaced at 10 ft and spanning 20 ft (Figure 5.1-2). The steel beams rest on three-span girders connected at each end to the portal frames and supported on two intermediate columns (Figure 5.1-1). The girder spans are approximately 30 ft each. The design of the mezzanine framing is largely conventional as seismic loads do not predominate. Those lateral forces that are received by the mezzanine are distributed to the frames and diagonal bracing via the floor diaphragm. A typical beam-column connection at the mezzanine level is provided in Figure 5.1-10. The design of the end plate connection is similar to that at the knee, but simpler because the beam is horizontal and not tapered.

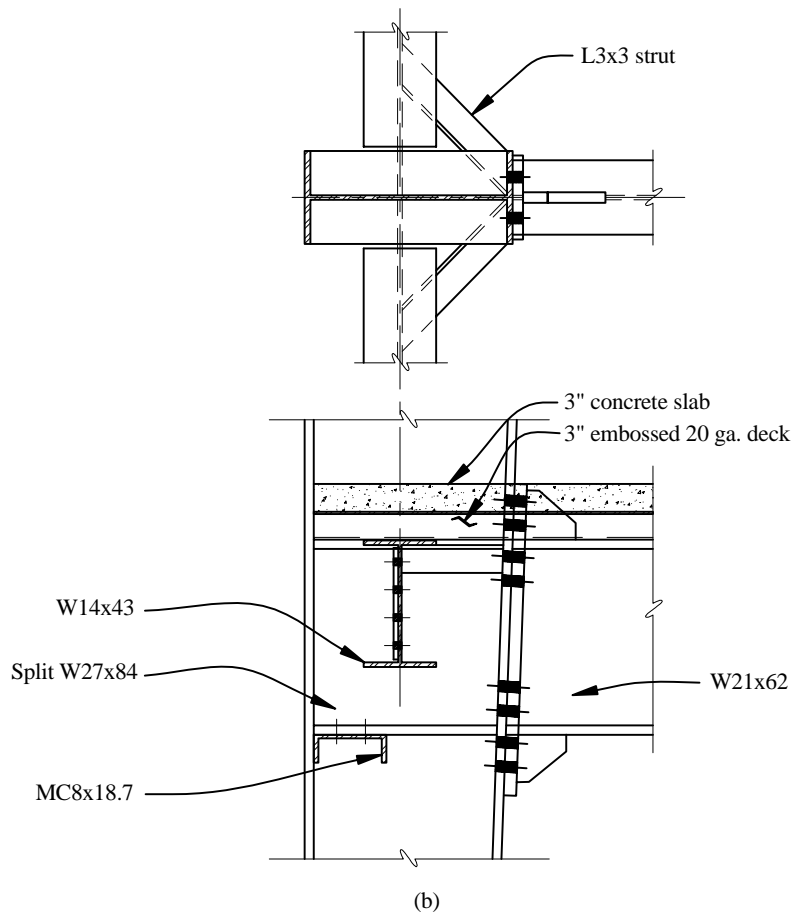


Figure 5.1-10 Mezzanine framing (1.0 in. = 25.4 mm).

5.1.5.5 Braced Frame Diagonal Bracing

Although the force in the diagonal X braces can be either tension or compression, only the tensile value is considered because it is assumed that the diagonal braces are capable of resisting only tensile forces.

See AISC Seismic Sec. 14.2 (November 2000 Supplement) for requirements on braces for OCBFs. The strength of the members and connections, including the columns in this area but excluding the brace connections, shall be based on AISC Seismic Eq. 4-1.

$$1.2D + 0.5L + 0.2S + \Omega_0 Q_E$$

Recall that a 1.0 factor is applied to L when the live load is greater than 100 psf (AISC Seismic Sec. 4.1). For the case discussed here, the “tension only” brace does not carry any live load so the load factor does not matter. For the braced design, $\Omega_0 = 2$.

However, *Provisions* Sec. 5.2.7.1, Eq. 5.2.7.1-1 and -2 [4.2-3 and 4.2-4, respectively] requires that the design seismic force on components sensitive to overstrength shall be defined by:

$$E = \Omega_0 Q_E \pm 0.2S_{DS}D$$

Given that the *Provisions* is being following, the AISC Seismic equation will be used but E will be substituted for Q_E . Thus, the load combination for design of the brace members reduces to:

$$1.4D + 0.5L + 0.2S + \Omega_0 Q_E$$

[The special load combinations have been removed from the 2002 edition of AISC Seismic to eliminate inconsistencies with other building codes and standards but the design of ordinary braced frames is not really changed because there is a reference to the load combinations including “simplified seismic loads.” Therefore, 2003 *Provisions* Eq. 4.2-3 and 4.2-4 should be used in conjunction with the load combinations in ASCE 7 as is done here.]

From analysis using this load combination, the maximum axial force in the X brace located at the east end of the building is 66 kips computed from the combined orthogonal earthquake loads (longitudinal direction predominates). With the Ω_0 factor, the required strength becomes 132 kips. All braces will have the same design. Using A36 steel for angles:

$$T_n = \phi F_y A_g$$

$$A_g = \frac{P_n}{\phi F_y} = \frac{132}{(0.9)(36)} = 4.07 \text{ in.}^2$$

Try (2) L4 × 3 × 3/8:

$$A_g = (2)(2.49) = 4.98 \text{ in.}^2 > 4.07 \text{ in.}^2$$

OK

AISC Seismic Sec. 14.2 requires the design strength of the brace connections to be based on the expected tensile strength:

$$R_y F_y A_g = (1.5)(36 \text{ ksi})(4.98 \text{ in.}^2) = 269 \text{ kips.}$$

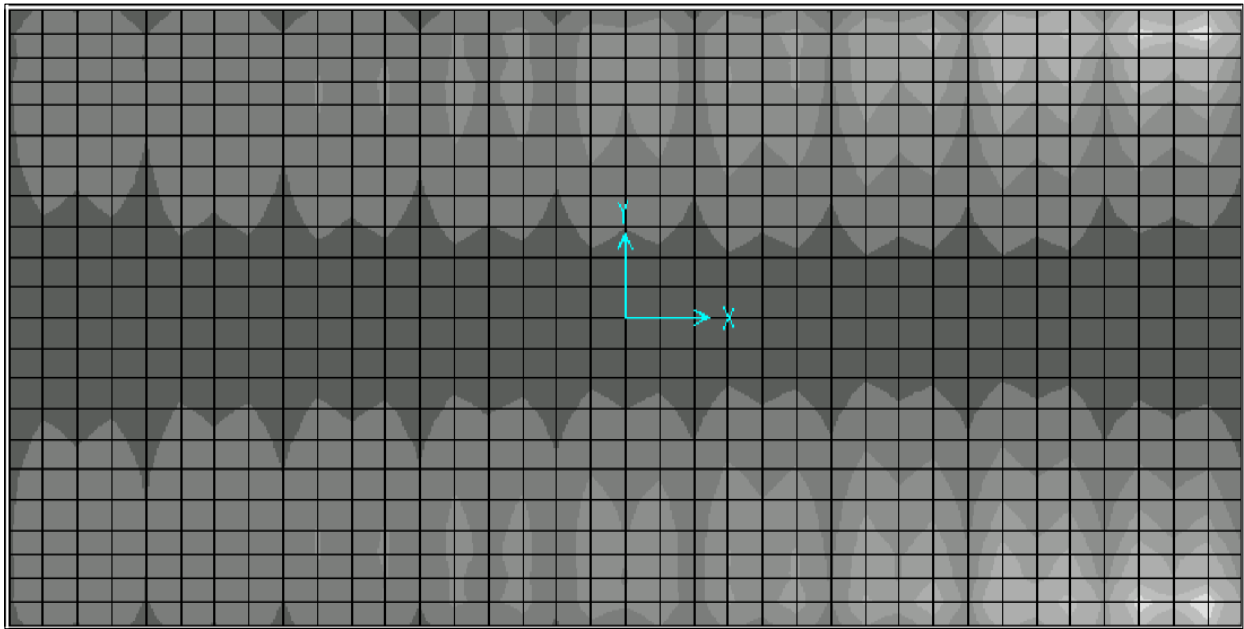
Also be sure to check the eave strut at the roof. The eave strut, part of the braced frame, has to carry compression and that compression is determined using the overstrength factor.

The kl/r requirement of AISC Seismic Sec. 14.2 does not apply because this is not a V or an inverted V

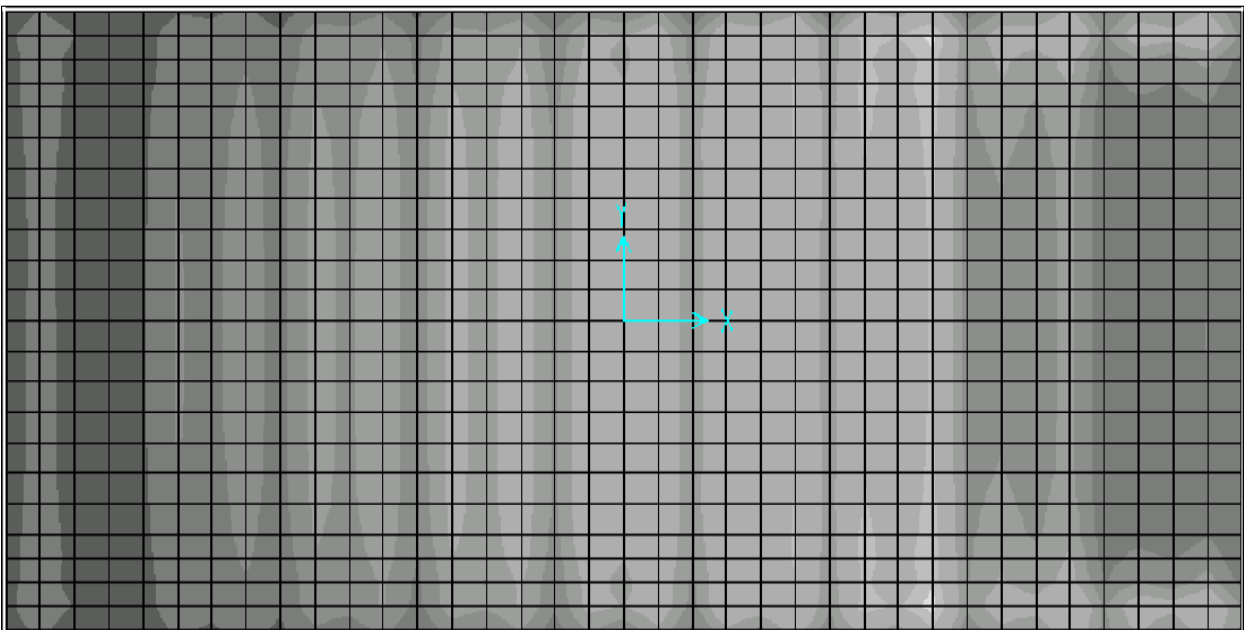
configuration.

5.1.5.6 Roof Deck Diaphragm

Figure 5.1-11 shows the in-plane shear force in the roof deck diaphragm for both seismic loading conditions. There are deviations from simple approximations in both directions. In the E-W direction, the base shear is 230 kips (Sec. 5.1.4.2) with 83 percent or 191 kips at the roof. Torsion is not significant so a simple approximation is to take half the force to each side and divide by the length of the building, which yields $(191,000/2)/180 \text{ ft.} = 530 \text{ plf}$. The plot shows that the shear in the edge of the diaphragm is significantly higher in the two braced bays. This is a shear lag effect; the eave strut in the 3-D model is a HSS 6x6x1/4. In the N-S direction, the shear is generally highest in the bay between the mezzanine frame and the first frame without the mezzanine. This might be expected given the significant change in stiffness. There does not appear to be any particularly good simple approximation to estimate the shear here without a 3-D model. The shear is also high at the longitudinal braced bays because they tend to resist the horizontal torsion. The shear at the braced bays is lower than observed for the E-W motion, however.



Roof diaphragm shear, East-West motion, pound per foot.



Roof diaphragm shear, North-South motion, pound per foot.



Figure 5.1-11 Shear force in roof deck diaphragm; upper diagram is for E-W motion and lower is for N-S motion (1.0 lb. /ft. = 14.59 N/M).

5.2 SEVEN-STORY OFFICE BUILDING, LOS ANGELES, CALIFORNIA

Three alternative framing arrangements for a seven-story office building are illustrated.

5.2.1 Building Description

5.2.1.1 General Description

This seven-story office building of rectangular plan configuration is 177 ft, 4 in. long in the E-W direction and 127 ft, 4 in. wide in the N-S direction (Figure 5.2-1). The building has a penthouse. It extends a total of 118 ft, 4 in. above grade. It is framed in structural steel with 25-ft bays in each direction. The story height is 13 ft, 4 in. except for the first story which is 22 ft, 4 in. high. The penthouse extends 16 ft above the roof level of the building and covers the area bounded by gridlines C, F, 2, and 5 in Figure 5.2-1. Floors consist of 3-1/4 in. lightweight concrete placed on composite metal deck. The elevators and stairs are located in the central three bays. The building is planned for heavy filing systems (350 psf) covering approximately four bays on each floor.

5.2.1.2 Alternatives

This example features three alternatives – a steel moment-resisting frame, concentrically braced frame, and a dual system with a moment-resisting frame at the perimeter and a concentrically braced frame at the core area – as follows:

1. Alternative A – Seismic force resistance is provided by special moment frames located on the perimeter of the building (on lines A, H, 1, and 6 in Figure 5.2-1, also illustrated in Figure 5.2-2).
2. Alternative B – Seismic force resistance is provided by four special concentrically braced frames in each direction. They are located in the elevator core walls between columns 3C and 3D, 3E and 3F, 4C and 4D, and 4E and 4F in the E-W direction and between columns 3C and 4C, 3-D and 4D, 3E and 4E, and 3F and 4F in the N-S direction (Figure 5.2-1). The braced frames in an X configuration are designed for both diagonals being effective in tension and compression. The braced frames are not identical, but are arranged to accommodate elevator door openings. Braced frame elevations are shown in Figure 5.2-3.
3. Alternative C – Seismic force resistance is provided by a dual system with the special moment frames at the perimeter of the building and a special concentrically braced frames at the core. The moment frames are shown in Figure 5.2-2 and the braced frames are shown in Figure 5.2-3.

5.2.1.3 Scope

The example covers:

1. Seismic design parameters
2. Analysis of perimeter moment frames
3. Beam and column proportioning
4. Analysis of concentrically braced frames
5. Proportioning of braces
6. Analysis and proportioning of the dual system

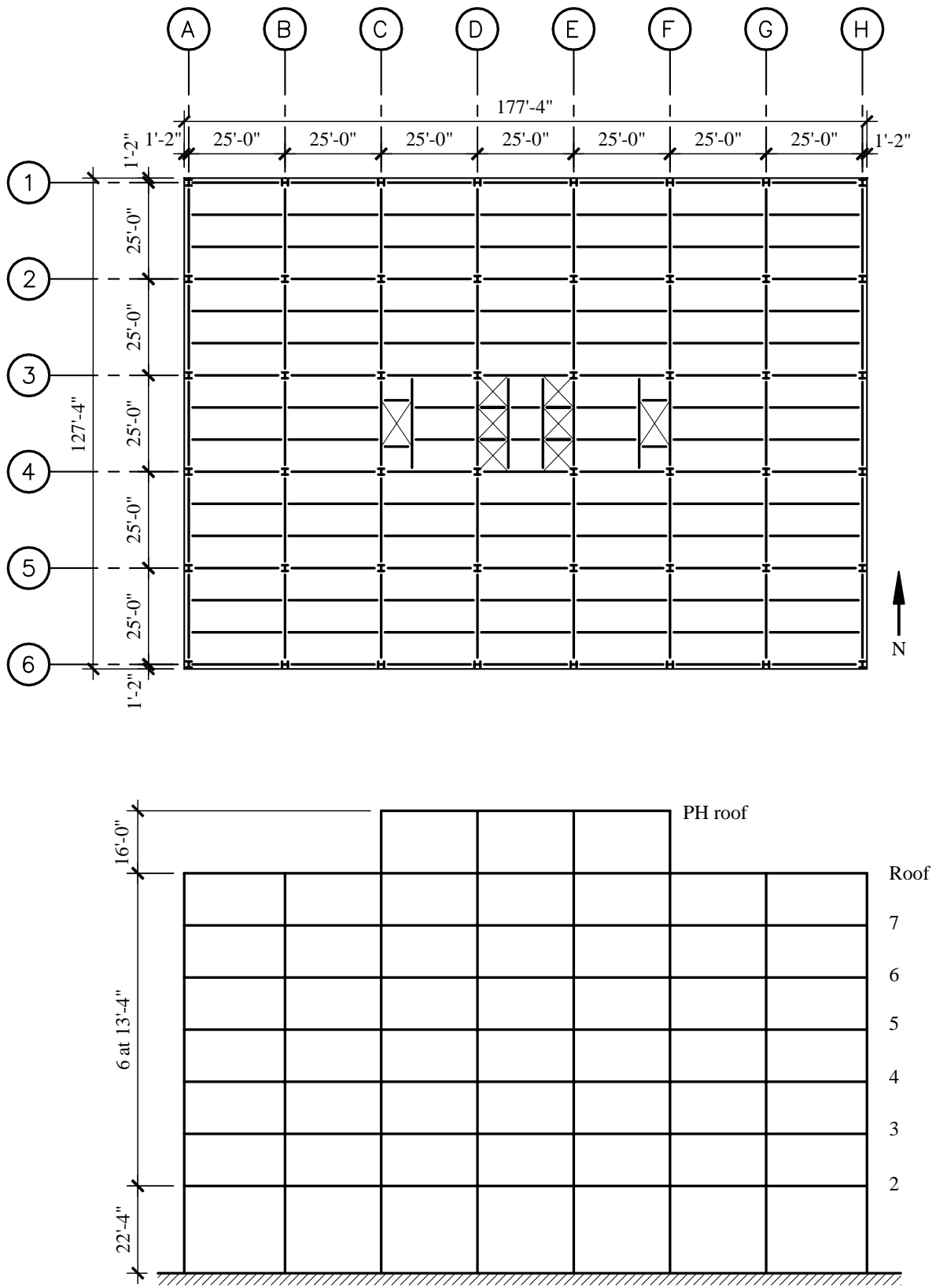


Figure 5.2-1 Typical floor framing plan and building section (1.0 in. = 25.4 mm, 1.0 ft = 0.3048 m).

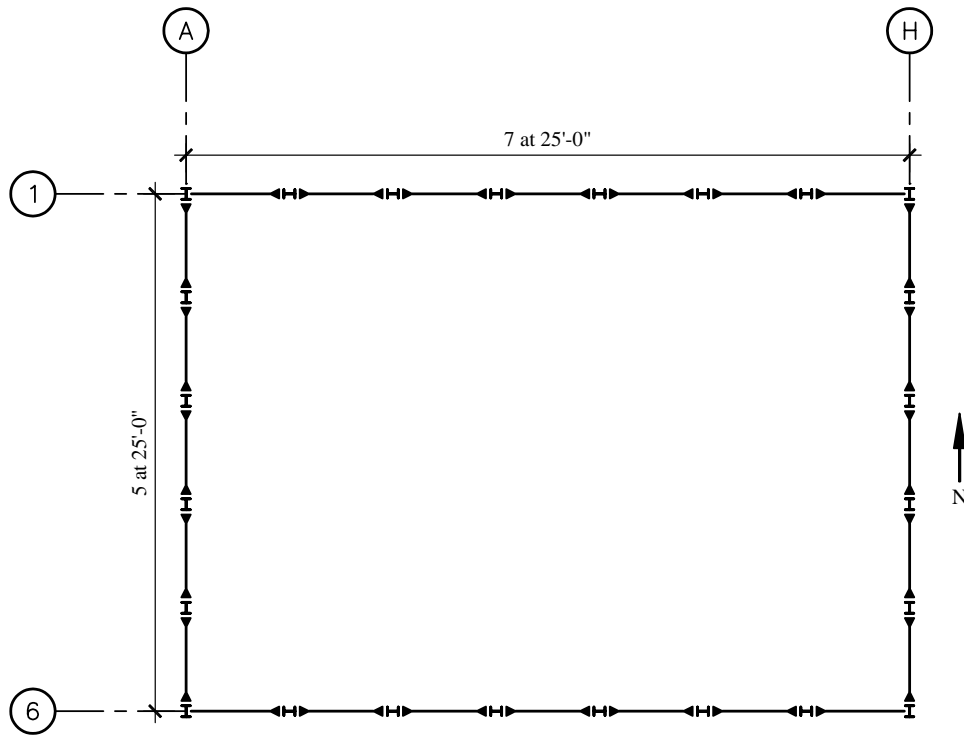


Figure 5.2-2 Framing plan for special moment frame (1.0 in. = 25.4 mm, 1.0 ft = 0.3048 m).

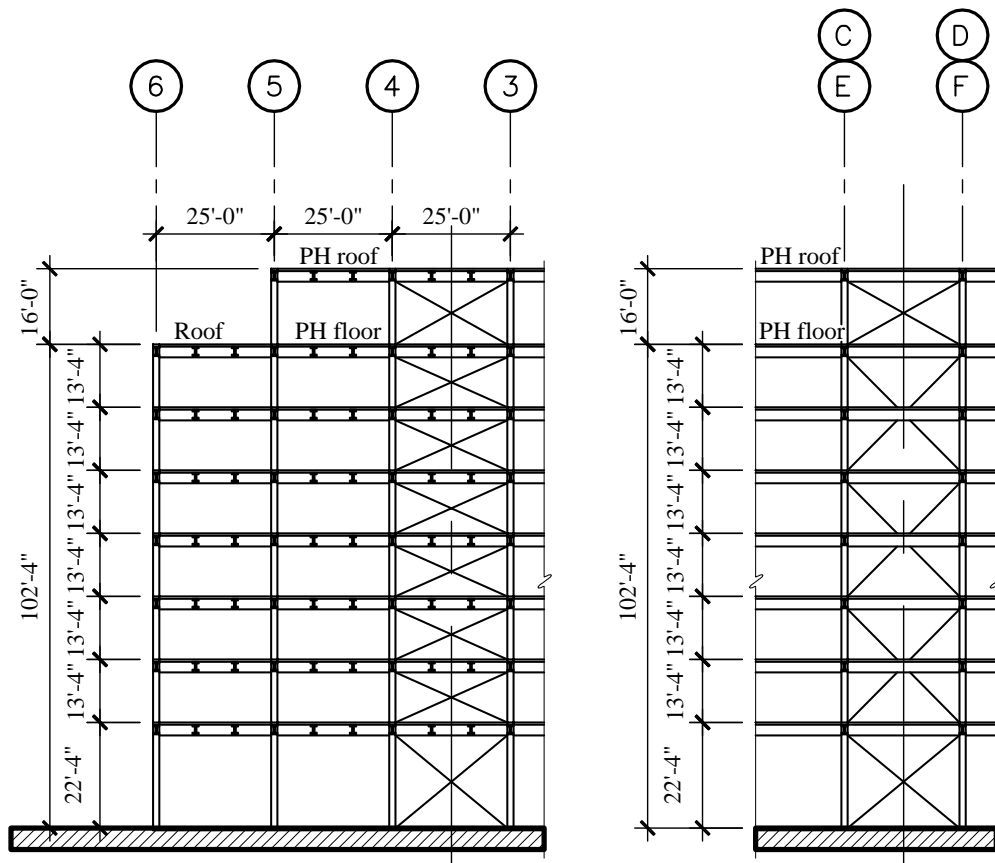


Figure 5.2-3 Concentrically braced frame elevations (1.0 in. = 25.4 mm, 1.0 ft = 0.3048 m).

5.2.2 Basic Requirements

5.2.2.1 Provisions Parameters

Site Class = D	(Provisions Sec. 4.1.2.1 [3.5])
$S_S = 1.5$	(Provisions Map 9 [Figure 3.3-3])
$S_I = 0.6$	(Provisions Map 10 [Figure 3.3-4])
$F_a = 1.0$	(Provisions Table 4.1.2.4a [3.3-1])
$F_v = 1.5$	(Provisions Table 4.1.2.4b [3.3-2])
$S_{MS} = F_a S_S = 1.5$	(Provisions Eq. 4.1.2.4-1 [3.3-1])
$S_{MI} = F_v S_I = 0.9$	(Provisions Eq. 4.1.2.4-2 [3.3-2])
$S_{DS} = 2/3 S_{MS} = 1.0$	(Provisions Eq. 4.1.2.5-1 [3.3-3])
$S_{DI} = 2/3 S_{MI} = 0.6$	(Provisions Eq. 4.1.2.5-2 [3.3-4])
Seismic Use Group = I	(Provisions Sec. 1.3 [1.2])
Seismic Design Category = D	(Provisions Sec. 4.2.1 [1.4])

Alternative A, Special Steel Moment Frame (Provisions Table 5.2.2 [4.3-1])

$$R = 8$$

$$\Omega_o = 3$$

$$C_d = 5.5$$

Alternative B, Special Steel Concentrically Braced Frame (Provisions Table 5.2.2 [4.3-1])

$$R = 6$$

$$\Omega_o = 2$$

$$C_d = 5$$

Alternative C, Dual System of Special Steel Moment Frame Combined with Special Steel Concentrically Braced Frame (Provisions Table 5.2.2 [4.3-1])

$$R = 8$$

$$\Omega_o = 2.5$$

$$C_d = 6.5$$

5.2.2.2 Loads

Roof live load (L)	= 25 psf
Penthouse roof dead load (D)	= 25 psf
Exterior walls of penthouse	= 25 psf of wall
Roof DL (roofing, insulation, deck beams, girders, fireproofing, ceiling, M&E)	= 55 psf
Exterior wall cladding	= 25 psf of wall
Penthouse floor D	= 65 psf
Floor L	= 50 psf
Floor D (deck, beams, girders, fireproofing, ceiling, M&E, partitions)	= 62.5 psf
Floor L reductions per the IBC	

5.2.2.3 Materials

Concrete for drilled piers	$f'_c = 5$ ksi, normal weight (NW)
Concrete for floors	$f'_c = 3$ ksi, lightweight (LW)

All other concrete	$f'_c = 4$ ksi, NW
Structural steel	
Wide flange sections	ASTM A992, Grade 50
HSS	ASTM A500, Grade B
Plates	ASTM A36

5.2.3 Structural Design Criteria

5.2.3.1 Building Configuration

The building is considered vertically regular despite the relatively tall height of the first story. The exception of *Provisions* Sec. 5.2.3.3 [4.3.2.3] is taken in which the drift ratio of adjacent stories are compared rather than the stiffness of the stories. In the 3-D analysis, it will be shown that the first story drift ratio is less than 130 percent of the story above. Because the building is symmetrical in plan, plan irregularities would not be expected. Analysis reveals that Alternatives B and C are torsionally irregular, which is not uncommon for core-braced buildings.

5.2.3.2 Redundancy

According to *Provisions* Sec. 5.2.4.2 [not applicable in the 2003 *Provisions*], the reliability factor, (ρ) for a Seismic Design Category D structure is:

$$\rho = 2 - \frac{20}{r_{\max_x} \sqrt{A_x}}$$

In a typical story, the floor area, $A_x = 22,579$ ft.²

The ratio of the design story shear resisted by the single element carrying the most shear force in the story to the total story shear is r_{\max_x} as defined in *Provisions* Sec. 5.2.4.2.

Preliminary ρ factors will be determined for use as multipliers on design force effects. These preliminary ρ factors will be verified by subsequent analyses.

[The redundancy requirements have been substantially changed in the 2003 *Provisions*. For a building assigned to Seismic Design Category D, $\rho = 1.0$ as long as it can be shown that failure of beam-to-column connections at both ends of a single beam (moment frame system) or failure of an individual brace (braced frame system) would not result in more than a 33 percent reduction in story strength or create an extreme torsional irregularity. Alternatively, if the structure is regular in plan and there are at least two bays of perimeter framing on each side of the structure in each orthogonal direction, it is permitted to use $\rho = 1.0$. Per 2003 *Provisions* Sec. 4.3.1.4.3, special moment frames in Seismic Design Category D must be configured such that the structure satisfies the criteria for $\rho = 1.0$. There are no reductions in the redundancy factor for dual systems. Based on the preliminary design, $\rho = 1.0$ for Alternative A because it has a perimeter moment frame and is regular. The determination of ρ for Alternatives B and C (which are torsionally irregular) requires the evaluation of connection and brace failures per 2003 *Provisions* Sec. 4.3.3.2.]

5.2.3.2.1 Alternative A (moment frame)

For a moment-resisting frame, r_{max_x} is taken as the maximum of the sum of the shears in any two adjacent columns divided by the total story shear. The final calculation of ρ will be deferred until the building frame analysis, which will include the effects of accidental torsion, is completed. At that point, we will know the total shear in each story and the shear being carried by each column at every story. See Sec. 5.2.4.3.1.

Provisions Sec. 5.2.4.2 requires that the configuration be such that ρ shall not exceed 1.25 for special moment frames. [1.0 in the 2003 *Provisions*] (There is no limit for other structures, although ρ need not be taken larger than 1.50 in the design.) Therefore, it is a good idea to make a preliminary estimate of ρ , which was done here. In this case, ρ was found to be 1.11 and 1.08 in the N-S and E-W directions, respectively. A method for a preliminary estimate is explained in Alternative B.

Note that ρ is a multiplier that applies only to the force effects (strength of the members and connections), not to displacements. As will be seen for this moment-resisting frame, drift, and not strength, will govern the design.

5.2.3.2.2 Alternative B (centrically braced frame)

Again, the following preliminary analysis must be refined by the final calculation. For the braced frame system, there are four braced-bay braces subject to shear at each story, so the direct shear on each line of braces is equal to $V_x/4$. The effects of accidental torsion will be estimated as:

$$\text{The torsional moment } M_{ta} = (0.05)(175)(V_x) = 8.75V_x.$$

$$\text{The torsional force applied to either grid line C or F is } V_t = M_{ta}Kd / \Sigma Kd^2.$$

Assuming all frame rigidity factors (K) are equal:

$$V_t = \frac{M_{ta}(37.5)}{[(2)(37.5)^2 + (6)(12.5)^2]} = 0.01M_{ta}$$

$$V_t = (0.01)(8.75 V_x) = 0.0875V_x$$

The amplification of torsional shear (A_x) must be considered in accordance with *Provisions* Sec. 5.4.4.1.3 [5.2.4.3]. Without dynamic amplification of torsion, the direct shear applied to each line of braces is $V_x/4$ and the torsional shear, $V_t = 0.0875 V_x$. Thus, the combined shear at Grid C is $0.25V_x - 0.0875V_x = 0.1625V_x$, and the combined shear at Grid F is $0.25V_x + 0.0875V_x = 0.3375V_x$. As the torsional deflections will be proportional to the shears and extrapolating to Grids A and H, the deflection at A can be seen to be proportional to $0.250V_x + (0.0875V_x)(87.5/37.5) = 0.454V_x$. Likewise, the deflection at H is proportional to $0.250V_x - (0.0875V_x)(87.5/37.5) = 0.046V_x$. The average deflection is thus proportional to $[(0.454 + 0.046)/2]V_x = 0.250V_x$. These torsional effects are illustrated in Figure 5.2-4.

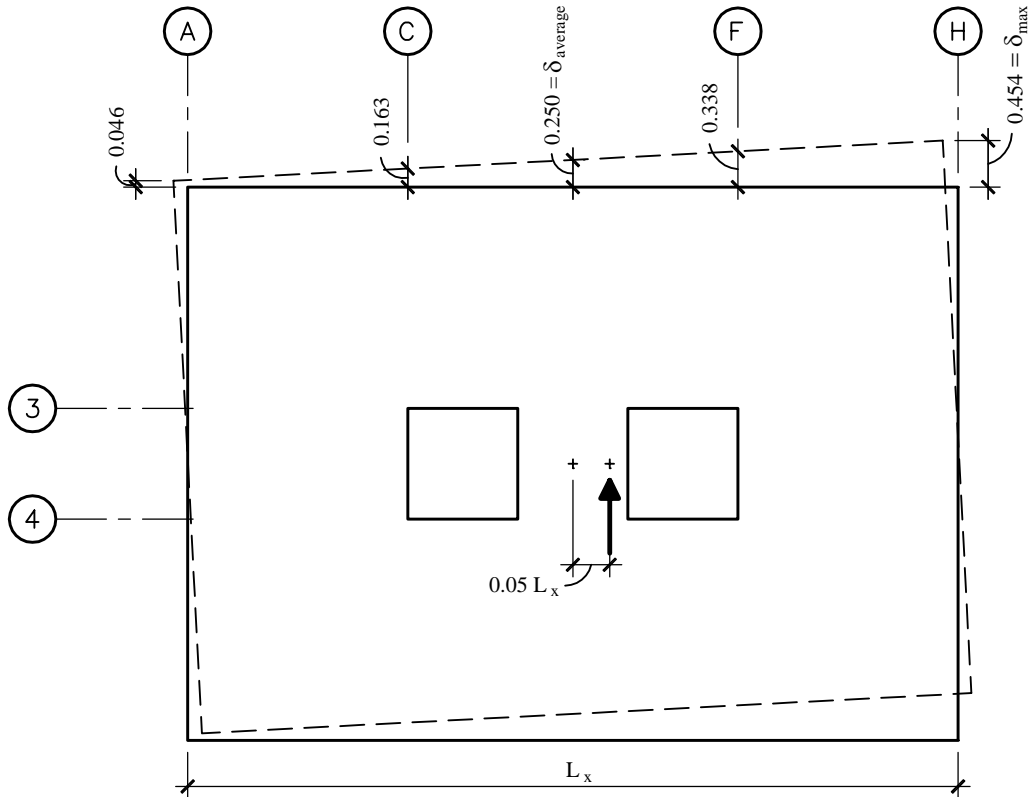


Figure 5.2-4 Approximate effect of accidental of torsion (1.0 in. = 25.4 mm).

From the above estimation of deflections, the torsional amplification can be determined per Provisions Eq. 5.4.4.1.3.1 [5.2-13] as:

$$A_x = \left(\frac{\delta_{max}}{1.2 \delta_{avg}} \right)^2 = \left(\frac{0.454}{(1.2)(0.250)} \right)^2 = 2.29$$

The total shear in the N-S direction on Gridlines C or F is the direct shear plus the amplified torsional shear equal to:

$$V_x/4 + A_x V_t = [0.250 + (2.29)(0.0875)]V_x = 0.450V_x$$

As there are two braces in each braced bay (one in tension and the other in compression):

$$r_{max_x} = \frac{0.450}{2} = 0.225$$

and

$$\rho = 2 - \frac{20}{r_{max_x} \sqrt{A_x}} = 2 - \frac{20}{(0.225)\sqrt{22,579}} = 1.41$$

Therefore, use $\rho = 1.41$ for the N-S direction. In a like manner, the ρ factor for the E-W direction is determined to be $\rho = 1.05$. These preliminary values will be verified by the final calculations.

5.2.3.2.3 Alternative C (dual system)

For the dual system, the preliminary value for ρ is taken as 1.0. The reason for this decision is that, with the dual system, the moment frame will substantially reduce the torsion at any story, so torsional amplification will be low. The combined redundancy of the braced frame combined with the moment frame (despite the fact that the moment frame is more flexible) will reduce ρ from either single system. Finally, *Provisions* Sec. 5.2.4.2 [not applicable in the 2003 *Provisions*] calls for taking only 80 percent of the calculated ρ value when a dual system is used. Thus, we expect the final value to fall below 1.0, for which we will take $\rho = 1.0$. This will be verified by analysis later.

5.2.3.3 Orthogonal Load Effects

A combination of 100 percent of the seismic forces in one direction with 30 percent seismic forces in orthogonal direction is required for structures in Seismic Design Category D (*Provisions* Sec. 5.2.5.2.3 and 5.2.5.2.2 [4.4.2.2]).

5.2.3.4 Structural Component Load Effects

The effect of seismic load is be defined by *Provisions* Eq, 5.2.7-1 [4.2-1] as:

$$E = \rho Q_E + 0.2 S_{DS} D$$

Recall that $S_{DS} = 1.0$. As stated above, ρ values are preliminary estimates to be checked and, if necessary, refined later.

For Alternative A

$$\begin{array}{ll} \text{N-S direction} & E = (1.11)Q_E \pm (0.2)D \\ \text{E-W direction} & E = (1.08)Q_E \pm (0.2)D \end{array}$$

Alternative B

$$\begin{array}{ll} \text{N-S direction} & E = (1.41)Q_E \pm (0.2)D \\ \text{E-W direction} & E = (1.05)Q_E \pm (0.2)D \end{array}$$

Alternative. C

$$\begin{array}{ll} \text{N-S direction} & E = (1.00)Q_E \pm (0.2)D \\ \text{E-W direction} & E = (1.00)Q_E \pm (0.2)D \end{array}$$

5.2.3.5 Load Combinations

Load combinations from ASCE 7 are:

$$1.2D + 1.0E + 0.5L + 0.2S$$

and

$$0.9D + 1.0E + 1.6H$$

To each of these load combinations, substitute E as determined above, showing the maximum additive and minimum negative. Recall that Q_E acts both east and west (or north and south):

Alternative A

$$\begin{array}{ll} \text{N-S} & 1.4D + 1.11Q_E + 0.5L \text{ and } 0.7D + 1.11Q_E \\ \text{E-W} & 1.4D + 1.08Q_E + 0.5L \text{ and } 0.7D + 1.08Q_E \end{array}$$

Alternative B

$$\begin{array}{ll} \text{N-S} & 1.4D + 1.41Q_E + 0.5L \text{ and } 0.7D + 1.41Q_E \\ \text{E-W} & 1.4D + 1.05Q_E + 0.5L \text{ and } 0.7D + 1.05Q_E \end{array}$$

Alternative C

$$\begin{array}{ll} \text{N-S} & 1.4D + Q_E + 0.5L \text{ and } 0.7D + Q_E \\ \text{E-W} & 1.4D + Q_E + 0.5L \text{ and } 0.7D + Q_E \end{array}$$

5.2.3.6 Drift Limits

The allowable story drift per *Provisions* Sec. 5.2.8 [4.5-1] is $\Delta_a = 0.02h_{sx}$.

The allowable story drift for the first floor is $\Delta_a = (0.02)(22.33 \text{ ft})(12 \text{ in./ft}) = 5.36 \text{ in.}$

The allowable story drift for a typical story is $\Delta_a = (0.02)(13.33 \text{ ft})(12 \text{ in./ft}) = 3.20 \text{ in.}$

Remember to adjust calculated story drifts by the appropriate C_d factor from Sec. 5.2.2.1.

Consider that the maximum story drifts summed to the roof of the seven-story building, (102 ft-4 in. main roof/penthouse floor) is 24.56 in.

5.2.3.7 Basic Gravity Loads

Penthouse roof

$$\begin{array}{ll} \text{Roof slab} = (0.025)(75)(75) & = 141 \text{ kips} \\ \text{Walls} = (0.025)(8)(300) & = 60 \text{ kips} \\ \text{Columns} = (0.110)(8)(16) & = \underline{14 \text{ kips}} \\ \text{Total} & = 215 \text{ kips} \end{array}$$

Lower roof

$$\begin{array}{ll} \text{Roof slab} = (0.055)[(127.33)(177.33) - (75)^2] & = 932 \text{ kips} \\ \text{Penthouse floor} = (0.065)(75)(75) & = 366 \text{ kips} \\ \text{Walls} = 60 + (0.025)(609)(6.67) & = 162 \text{ kips} \\ \text{Columns} = 14 + (0.170)(6.67)(48) & = 68 \text{ kips} \\ \text{Equipment (allowance for mechanical} & \\ \quad \text{equipment in penthouse)} & = \underline{217 \text{ kips}} \\ \text{Total} & = 1,745 \text{ kips} \end{array}$$

Typical floor

$$\begin{aligned}\text{Floor} &= (0.0625)(127.33)(177.33) &&= 1,412 \text{ kips} \\ \text{Walls} &= (0.025)(609)(13.33) &&= 203 \text{ kips} \\ \text{Columns} &= (0.285)(13.33)(48) &&= 182 \text{ kips} \\ \text{Heavy storage} &= (0.50)(4)(25 \times 25)(350) &&= \underline{438 \text{ kips}} \\ \text{Total} &&&= 2,235 \text{ kips}\end{aligned}$$

$$\text{Total weight of building} = 215 + 1,745 + 6(2,235) = 15,370 \text{ kips}$$

Note that this office building has heavy storage in the central bays of 280 psf over five bays. Use 50 percent of this weight as effective seismic mass. (This was done to add seismic mass to this example thereby making it more interesting. It is not meant to imply that the authors believe such a step is necessary for ordinary office buildings.)

5.2.4 Analysis

5.2.4.1 Equivalent Lateral Force Analysis

The equivalent lateral force (ELF) procedure will be used for each alternative building system. The seismic base shear will be determined for each alternative in the following sections.

5.2.4.1.1 ELF Analysis for Alternative A, Moment Frame

First determine the building period (T) per *Provisions* Eq. 5.4.2.1-1 [5.2-6]:

$$T_a = C_r h_n^x = (0.028)(102.3)^{0.8} = 1.14 \text{ sec}$$

where h_n , the height to the main roof, is conservatively taken as 102.3 ft. The height of the penthouse (the penthouse having a smaller contribution to seismic mass than the main roof or the floors) will be neglected.

The seismic response coefficient (C_s) is determined from *Provisions* Eq. 5.4.1.1-1 [5.2-2] as:

$$C_s = \frac{S_{DS}}{R/I} = \frac{1}{(8/1)} = 0.125$$

However, *Provisions* Eq. 5.4.1.1-2 [5.2-3] indicates that the value for C_s need not exceed:

$$C_s = \frac{S_{D1}}{T(R/I)} = \frac{0.6}{1.14(8/1)} = 0.066$$

and the minimum value for C_s per *Provisions* Eq. 5.4.1.1-3 [not applicable in the 2003 *Provisions*] is:

$$C_s = 0.044I S_{DS} = (0.044)(1)(1) = 0.044$$

Therefore, use $C_s = 0.066$.

Seismic base shear is computed per *Provisions* Eq. 5.4.1 [5.2-1] as:

$$V = C_s W = (0.066)(15,370) = 1014 \text{ kips}$$

5.2.4.1.2 ELF Analysis for Alternative B, Braced Frame

As above, first find the building period (T) using *Provisions* Eq. 5.4.2.1-1 [5.2-6]:

$$T_a = C_r h_n^x = (0.02)(102.3)^{0.75} = 0.64 \text{ sec}$$

The seismic response coefficient (C_s) is determined from *Provisions* Eq. 5.4.1.1-1 [5.2-2] as:

$$C_s = \frac{S_{DS}}{R/I} = \frac{1}{(6/1)} = 0.167$$

However, *Provisions* Eq. 5.4.1.1-2 [5.2-3] indicates that the value for C_s need not exceed:

$$C_s = \frac{S_{DI}}{T(R/I)} = \frac{0.6}{(0.64)(6/1)} = 0.156$$

and the minimum value for C_s per *Provisions* Eq. 5.4.1.1-3 [not applicable in 2003 *Provisions*] is:

$$C_s = 0.044 I S_{DS} = (0.044)(1)(1) = 0.044$$

Use $C_s = 0.156$.

Seismic base shear is computed using *Provisions* Eq. 5.4.1 [5.2-1] as:

$$V = C_s W = (0.156)(15,370) = 2,398 \text{ kips}$$

5.2.4.1.3 ELF Analysis for Alternative C, Dual System

The building period (T) is the same as for the braced frame (*Provisions* Eq. 5.4.2.1-1 [5.2-6]):

$$T_a = C_r h_n^x = (0.02)(102.3)^{0.75} = 0.64 \text{ sec}$$

The seismic response coefficient (C_s) is determined as (*Provisions* Eq. 5.4.1.1-1 [5.2-2]):

$$C_s = \frac{S_{DS}}{R/I} = \frac{1}{(8/1)} = 0.125$$

However, the value for C_s need not exceed (*Provisions* Eq. 5.4.1.1-2 [5.2-3]):

$$C_s = \frac{S_{DI}}{T(R/I)} = \frac{0.6}{(0.64)(8/1)} = 0.117$$

and the minimum value for C_s is (*Provisions* Eq. 5.4.1.1-3 [not applicable in the 2003 *Provisions*]):

$$C_s = 0.044 I S_{DS} = (0.044)(1)(1) = 0.044$$

Therefore, use $C_s = 0.117$.

Seismic base shear is computed as (*Provisions* Eq. 5.4.1 [5.2-1]):

$$V = C_s W = (0.117)(15,370) = 1,798 \text{ kips}$$

5.2.4.2 Vertical Distribution of Seismic Forces

Provisions Sec. 5.4.3 [5.2.3] provides the procedure for determining the portion of the total seismic load that goes to each floor level. The floor force F_x is calculated using *Provisions* Eq. 5.4.3-1 [5.2-10] as:

$$F_x = C_{vx} V$$

where (*Provisions* Eq. 5.4.3-2 [5.2-11])

$$C_{vx} = \frac{w_x h_x^k}{\sum_{i=1}^n w_i h_i^k}$$

For Alternative A

$$T = 1.14 \text{ secs, thus } k = 1.32$$

For Alternatives B and C

$$T = 0.64 \text{ sec, thus } k = 1.07$$

Using *Provisions* Eq. 5.4.4 [5.2-12], the seismic design shear in any story is computed as:

$$V_x = \sum_{i=x}^n F_i$$

The story overturning moment is computed from *Provisions* Eq. 5.4.5 [5.2-14]:

$$M_x = \sum_{i=x}^n F_i (h_i - h_x)$$

The application of these equations for the three alternative building frames is shown in Tables 5.2-1, 5.2-2, and 5.1-3.

Table 5.2-1 Alternative A, Moment Frame Seismic Forces and Moments by Level

Level (x)	W_x (kips)	h_x (ft)	$W_x h_x^k$ (ft-kips)	C_{vx}	F_x (kips)	V_x (kips)	M_x (ft-kips)
PH Roof	215	118.33	117,200	0.03	32	32	514
Main roof	1,745	102.33	785,200	0.21	215	247	3,810
Story 7	2,235	89.00	836,500	0.23	229	476	10,160
Story 6	2,235	75.67	675,200	0.18	185	661	18,980
Story 5	2,235	62.33	522,700	0.14	143	805	29,710
Story 4	2,235	49.00	380,500	0.10	104	909	41,830
Story 3	2,235	35.67	250,200	0.07	69	977	54,870
Story 2	<u>2,235</u>	22.33	<u>134,800</u>	<u>0.04</u>	<u>37</u>	1,014	77,520
Σ	15,370		3,702,500	1.00	1,014		

1.0 kip = 4.45 kN, 1.0 ft = 0.3048 m.

Table 5.2-2 Alternative B, Braced Frame Seismic Forces and Moments by Level

Level (x)	W_x (kips)	h_x (ft)	$W_x h_x^k$ (ft-kips)	C_{vx}	F_x (kips)	V_x (kips)	M_x (ft-kips)
PH Roof	215	118.33	35,500	0.03	67	67	1,070
Main roof	1,745	102.33	246,900	0.19	463	530	8,130
Story 7	2,235	89.00	272,300	0.21	511	1,041	22,010
Story 6	2,235	75.67	228,900	0.18	430	1,470	41,620
Story 5	2,235	62.33	186,000	0.15	349	1,819	65,870
Story 4	2,235	49.00	143,800	0.11	270	2,089	93,720
Story 3	2,235	35.67	102,400	0.08	192	2,281	124,160
Story 2	<u>2,235</u>	22.33	<u>62,000</u>	<u>0.05</u>	<u>116</u>	2,398	177,720
Σ	15,370		1,278,000	1.00	2,398		

1.0 kip = 4.45 kN, 1.0 ft = 0.3048 m.

Table 5.2-3 Alternative C, Dual System Seismic Forces and Moments by Level

Level (x)	W_x (kips)	h_x (ft)	$W_x h_x^k$ (ft-kips)	C_{vx}	F_x (kips)	V_x (kips)	M_x (ft-kips)
PH Roof	215	118.33	35,500	0.03	50	50	800
Main roof	1,745	102.33	246,900	0.19	347	397	6,100
Story 7	2,235	89.00	272,350	0.21	383	781	16,500
Story 6	2,235	75.67	228,900	0.18	322	1,103	31,220
Story 5	2,235	62.33	186,000	0.15	262	1,365	49,400
Story 4	2,235	49.00	143,800	0.11	202	1,567	70,290
Story 3	2,235	35.67	102,386	0.08	144	1,711	93,120
Story 2	<u>2,235</u>	22.33	<u>62,000</u>	<u>0.05</u>	<u>87</u>	1,798	133,270
Σ	15,370		1,278,000	1.00	1,798		

1.0 kip = 4.45 kN, 1.0 ft = 0.3048 m.

Be sure to note that the seismic mass at any given level, which includes the lower half of the wall above that level and the upper half of the wall below that level, produces the shear applied at that level and that shear produces the moment which is applied at the top of the next level down. Resisting the overturning moment is the weight of the building above that level combined with the moment resistance of the framing at that level. Note that the story overturning moment is applied to the level below the level that receives the story shear. (This is illustrated in Figure 9.2-4 in the masonry examples.)

5.2.4.3 Size Members

At this point we are ready to select the sizes of the framing members. The method for each alternative is summarized below.

Alternative A, Special Moment Frame:

1. Select preliminary member sizes
2. Check deflection and drift *(Provisions Sec. 5.2.8 [5.4.1])*
3. Check torsional amplification *(Provisions Sec. 5.4.4.1.3 [5.2.4.3])*
4. Check the column-beam moment ratio rule *(AISC Seismic Sec. 9.6)*
5. Check shear requirement at panel-zone *(AISC Seismic Sec. 9.3; FEMA 350 Sec. 3.3.3.2)*
6. Check redundancy *(Provisions Sec. 5.2.4.2 [5.3.3])*
7. Check strength

Reportion member sizes as necessary after each check. The most significant criteria for the design are drift limits, relative strengths of columns and beams, and the panel-zone shear.

Alternative B, Special Concentrically Braced Frame:

1. Select preliminary member sizes
2. Check strength
3. Check drift (Provisions Sec. 5.2.8 [4.5.1])
4. Check torsional amplification (Provisions Sec. 5.4.4.1 [5.2.4.3])
5. Check redundancy (Provisions Sec. 5.2.4.2 [4.3.3])

Reportion member sizes as necessary after each check. The most significant criteria for this design is torsional amplification.

Alternative C, Dual System:

1. Select preliminary member sizes
2. Check strength of moment frame for 25 percent of story shear (Provisions Sec. 5.2.2.1 [4.3.1.1])
3. Check strength of braced frames
4. Check drift for total building (Provisions Sec. 5.2.8 [4.5.1])
5. Check torsional amplification (Provisions Sec. 5.4.4.1 [5.2.4.3])
6. Check redundancy (Provisions Sec. 5.2.4.2 [4.3.3])

Reportion member sizes as necessary after each check.

5.2.4.3.1 Size Members for Alternative A, Moment Frame

1. Select Preliminary Member Sizes – The preliminary member sizes are shown for the moment frame in the X-direction (7 bays) in Figure 5.2-5 and in the Y direction (5 bays) in Figure 5.2-6.

Check Local Stability – Check beam flange stability in accordance with AISC Seismic Table I-9-1 [I-8-1] (same as FEMA 350 Sec. 3.3.1.1) and beam web stability in accordance with AISC Seismic Table I-9-1 [I-8-1]. (FEMA 350 Sec.3.3.1.2 is more restrictive for cases with low $P_u/\phi_b P_y$, such as in this example.) Beam flange slenderness ratios are limited to $52/\sqrt{F_y}$ and beam web height-to-thickness ratios are limited to $418/\sqrt{F_y}$.

[The terminology for local stability has been revised in the 2002 edition of AISC Seismic. The limiting slenderness ratios in AISC Seismic use the notation λ_{ps} (“seismically compact”) to differentiate them from λ_p in AISC LRFD. In addition, the formulas appear different because the elastic modulus, E_s , has been added as a variable. Both of these changes are essentially editorial, but Table I-8-1 in the 2002 edition of AISC Seismic has also been expanded to include more elements than in the 1997 edition.]

Be careful because certain shapes found in the AISC Manual will not be permitted for Grade 50 steel (but may have been permitted for Grade 36 steel) because of these restrictions. For Grade 50, b/t is limited to 7.35.

Further note that for columns in special steel moment frames such as this example, AISC Seismic 9.4b [I-8-1] requires that when the column moment strength to beam moment strength ratio is less than or equal to 2.0, the more stringent λ_p requirements apply for b/t , and when $P_u/\phi_b P_y$ is less than or equal to 0.125, the more stringent h/t requirements apply.

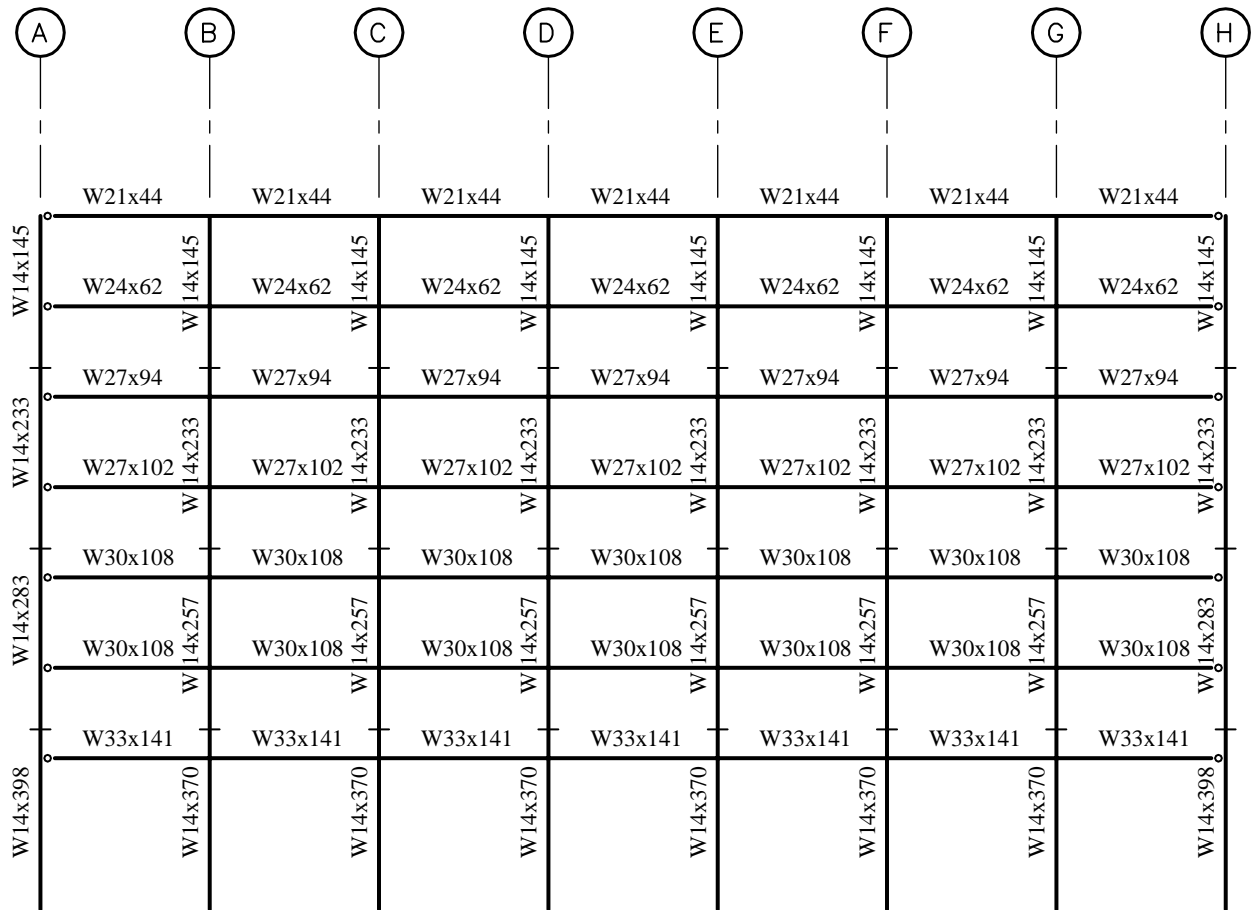


Figure 5.2-5 SMRF frame in E-W direction (penthouse not shown).

2. Check Drift – Check drift in accordance with *Provisions* Sec. 5.2.8 [4.5.1]. The building was modeled in 3-D using RAMFRAME. Displacements at the building centroid are used here because the building is not torsionally irregular (see the next paragraph regarding torsional amplification). Calculated story drifts and C_d amplification factors are summarized in Table 5.2-4. P-delta effects are included.

All story drifts are within the allowable story drift limit of $0.020h_{sx}$ per *Provisions* Sec. 5.2.8 [4.5.1] and Sec. 5.2.3.6 of this chapter.

As indicated below, the first story drift ratio is less than 130 percent of the story above (*Provisions* Sec. 5.2.3.3 [4.3.2.3]):

$$\frac{C_d \Delta_{x \text{ story 2}}}{C_d \Delta_{x \text{ story 3}}} = \frac{\left(\frac{5.17 \text{ in.}}{268 \text{ in.}} \right)}{\left(\frac{3.14 \text{ in.}}{160 \text{ in.}} \right)} = 0.98 < 1.30$$

Therefore, there is no vertical irregularity.

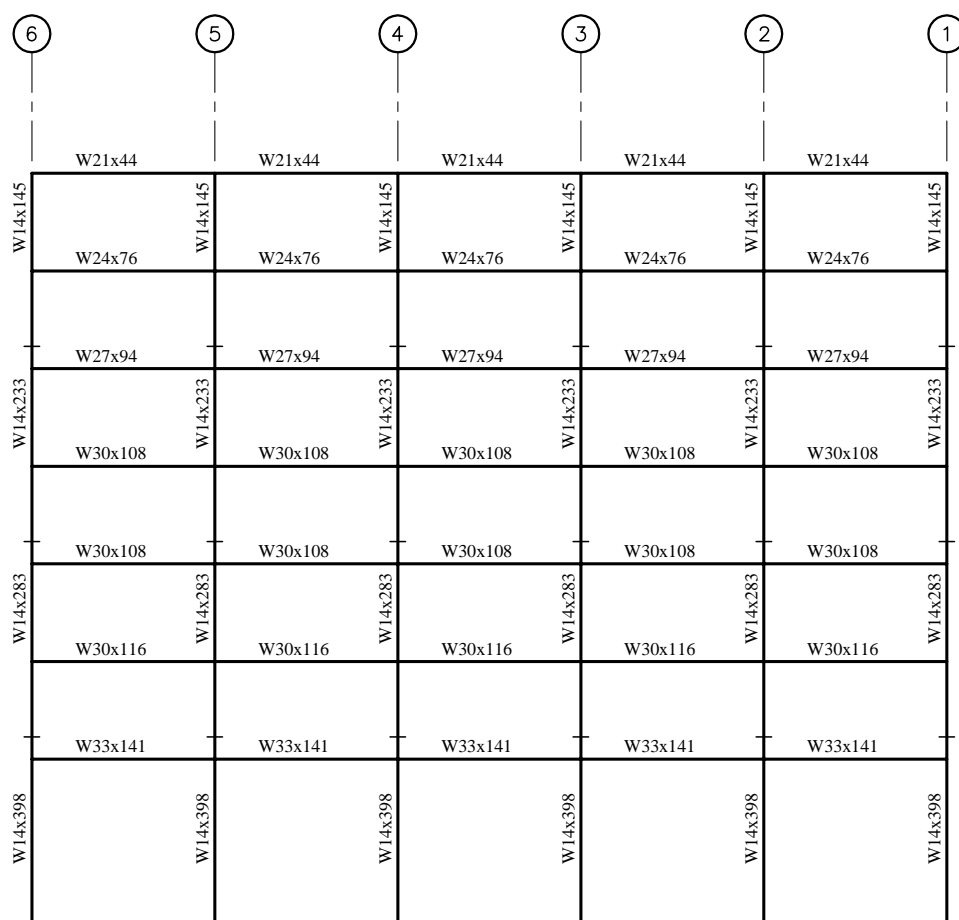


Figure 5.2-6 SMRF frame in N-S direction (penthouse not shown).

Table 5.2-4 Alternative A (Moment Frame) Story Drifts under Seismic Loads

	Total Displacement at Building Centroid (86.5, 62.5)		Story Drift from 3-D Elastic Analysis at Building Centroid		C_d	$(C_d) \times$ (Elastic Story Drift)		Allowable Story Drift
	$\Delta E-W$ (in.)	$\Delta N-S$ (in.)	$\Delta E-W$ (in.)	$\Delta N-S$ (in.)		$\Delta E-W$ (in.)	$\Delta N-S$ (in.)	
Roof	4.24	4.24	0.48	0.47	5.5	2.64	2.59	3.20
Floor 7	3.76	3.77	0.57	0.58	5.5	3.14	3.19	3.20
Floor 6	3.19	3.19	0.54	0.53	5.5	2.97	2.92	3.20
Floor 5	2.65	2.66	0.57	0.58	5.5	3.14	3.19	3.20
Floor 4	2.08	2.08	0.57	0.58	5.5	3.14	3.19	3.20
Floor 3	1.51	1.50	0.57	0.57	5.5	3.14	3.14	3.20
Floor 2	0.94	0.93	0.94	0.93	5.5	5.17	5.12	5.36

1.0 in. = 25.4 mm.

3. Check Torsional Amplification – The torsional amplification factor per *Provisions* Eq. 5.4.4.1.3-1 [5.2-13] is:

$$A_x = \left(\frac{\delta_{max}}{1.2\delta_{avg}} \right)^2$$

If $A_x < 1.0$, then torsional amplification need not be considered. It is readily seen that if the ratio of $\delta_{max}/\delta_{avg}$ is less than 1.2, then torsional amplification will not be necessary.

The 3-D analysis provided the story deflections listed in Table 5.2-5. Because none of the ratios for $\delta_{max}/\delta_{avg}$ exceed 1.2, torsional amplification of forces is not necessary for the moment frame alternative.

Table 5.2-5 Alternative A Torsional Analysis

	Torsion Checks			
	$\delta_{EW_{max}}$ (in.) (175,0)	$\delta_{NS_{max}}$ (in.) (125,0)	$\delta_{EW_{max}}/\delta_{EW_{avg}}$	$\delta_{NS_{max}}/\delta_{NS_{avg}}$
Roof	4.39	4.54	1.04	1.07
Story 7	3.89	4.04	1.04	1.07
Story 6	3.30	3.42	1.04	1.07
Story 5	2.75	2.85	1.03	1.07
Story 4	2.16	2.23	1.04	1.07
Story 3	1.57	1.62	1.04	1.08
Story 2	0.98	1.00	1.04	1.08

1.0 in. = 25.4 mm.

Member Design Considerations – Because $P_u/\phi P_n$ is typically less than 0.4 for the columns (re: AISC Seismic Sec. 8.2 [8.3]), combinations involving Ω_0 factors do not come into play for the special steel moment frames. In sizing columns (and beams) for strength we will satisfy the most severe value from interaction equations. However, this frame is controlled by drift. So, with both strength and drift requirements satisfied, we will check the column-beam moment ratio and the panel zone shear.

4. Check the Column-Beam Moment Ratio – Check the column-beam moment ratio per AISC Seismic Sec. 9.6. For purposes of this check, the plastic hinge was taken to occur at $0.5d_b$ from the face or the column in accordance with FEMA 350 for WUF-W connections (see below for description of these connections). The expected moment strength of the beams were projected from the plastic hinge location to the column centerline per the requirements of AISC Seismic Sec. 9.6. This is illustrated in Figure 5.2-7. For the columns, the moments at the location of the beam flanges is projected to the column-beam intersection as shown in Figure 5.2-8.

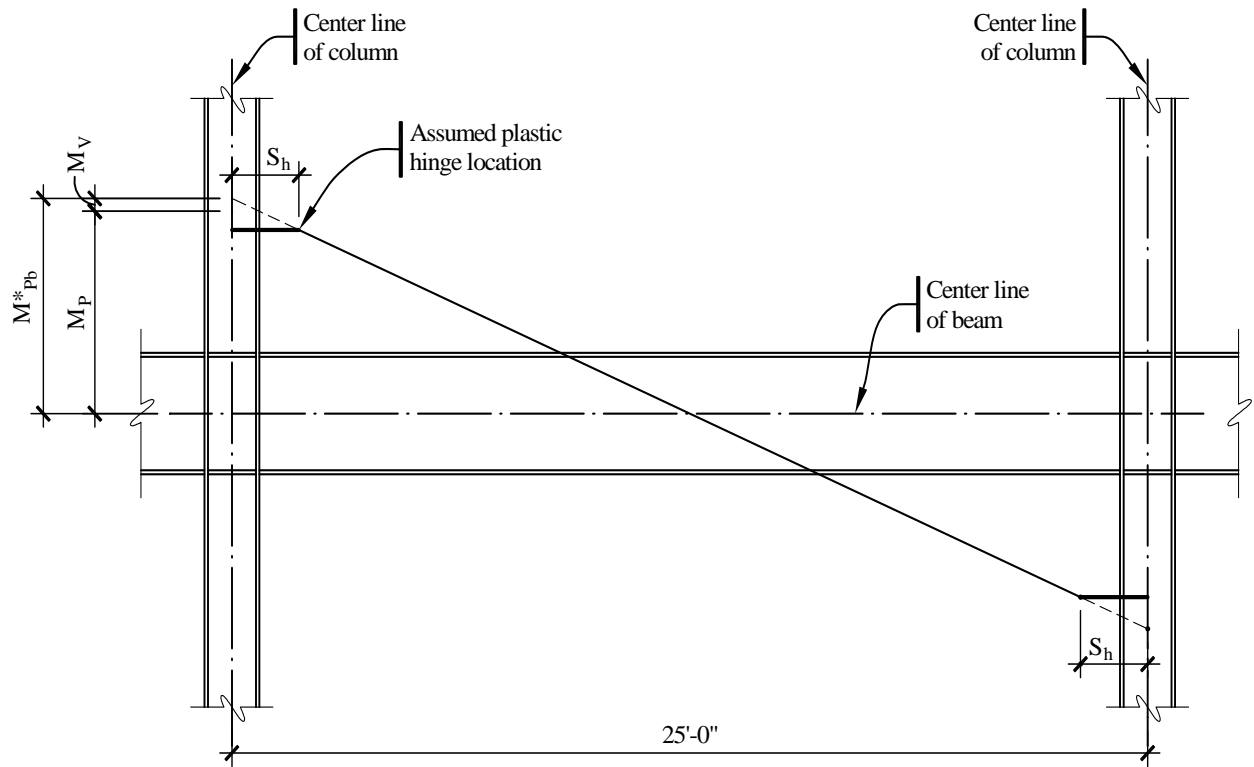


Figure 5.2-7 Projection of expected moment strength of beam (1.0 in. = 25.4 mm, 1.0 ft = 0.3048 m).

The column-beam strength ratio calculation is illustrated for the lower level in the E-W direction, Level 2, at gridline G (W14×370 column and W33×141 beam). For the columns:

$$\Sigma M_{pc}^* = \Sigma Z_c \left(F_{yc} - \frac{P_{uc}}{A_g} \right)$$

$$\Sigma M_{pc}^* = 2 \left[736 \text{ in.}^3 \left(50 \text{ ksi} - \frac{500 \text{ kips}}{109 \text{ in.}^2} \right) \right] = 66,850 \text{ ft-kips}$$

Adjust this by the ratio of average story height to average clear height between beams, or $(268 + 160) / (251.35 + 128.44) = 1.13$. Therefore, $\Sigma M_{pc}^* = (1.13)(66,850) = 75,300 \text{ ft-kips}$. For the beams,

$$\Sigma M_{pb}^* = \Sigma (1.1R_y M_p + M_v)$$

where

$R_y = 1.1$ for Grade 50 steel

$M_p = F_y Z = (50)(514) = 25,700 \text{ in.-kips}$

$M_v = V_p S_h$

$S_h = \text{Distance from column centerline to plastic hinge} = d_c/2 + d_b/2 = 25.61 \text{ in.}$

$V_p = \text{Shear at plastic hinge location}$

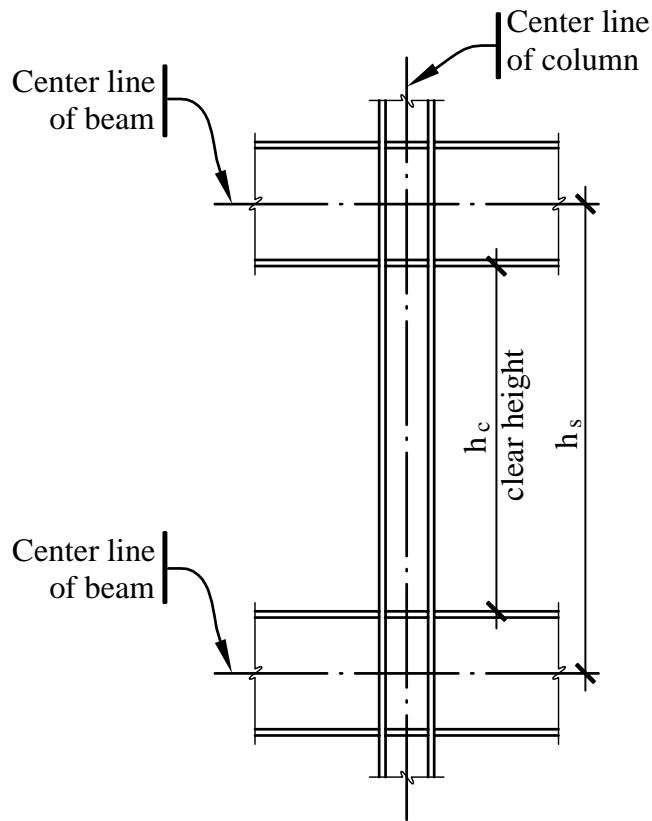


Figure 5.2-8 Story height and clear height.

The shear at the plastic hinge (Figure 5.2-9) is computed as:

$$V_p = [2M_p + (wL'^2/2)] / L'$$

where

$$\begin{aligned} L' &= \text{Distance between plastic hinges} = 248.8 \text{ in.} \\ w &= \text{Factored uniform gravity load along beam} \\ w &= 1.4D + 0.5L = 1.4(0.0625 \text{ ksf})(12.5 \text{ ft}) \\ &\quad + 0.5(0.050 \text{ ksf})(12.5 \text{ ft}) = 1.406 \text{ klf} \end{aligned}$$

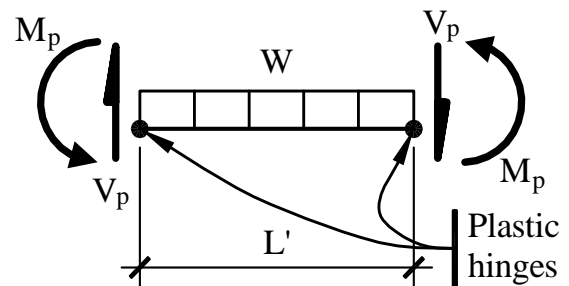


Figure 5.2-9 Free body diagram bounded by plastic hinges.

Therefore,

$$V_p = \frac{2M_p + \frac{wL'^2}{2}}{L'} = \frac{(2)(25,700) + \left(\frac{(1.406)(248.8)^2}{2}\right)}{248.8} = 221.2 \text{ kips}$$

and

$$M_v = V_p S_h = (221.2)(25.61) = 5,665 \text{ in.-kips}$$

$$\text{Finally, } \Sigma M_{pb}^* = \Sigma(1.1R_y M_p + M_v) = 2[(1.1)(1.1)(25,700) + 5,665] = 73,500 \text{ in.-kips.}$$

The ratio of column moment strengths to beam moment strengths is computed as:

$$\text{Ratio} = \frac{\Sigma M_{pc}^*}{\Sigma M_{pb}^*} = \frac{76,900}{73,500} = 1.05 > 1.0 \quad \text{OK}$$

The column-beam strength ratio for all the other stories is determined in a similar manner. They are summarized in Table 5.2-4 for the E-W direction (seven-bay) frame and in Table 5.2-5 for the N-S direction (five-bay) frame. All cases are acceptable because the column-beam moment ratios are all greater than 1.00.

Table 5.2-4 Column-Beam Moment Ratios for Seven-Bay Frame (N-S Direction)

Story	Member	ΣM_{pc}^* (in.-kips)	ΣM_{pb}^* (in.-kips)	Column- Beam Ratio
7	column W14×145 beam W24×62	29,000	21,300	1.36
5	column W14×233 beam W27×102	40,000	42,600	1.15
3	column W14×257 beam W30×108	53,900	48,800	1.11
2	column W14×370 beam W33×141	75,300	73,500	1.02

For levels with the same size column, the one with the larger beam size will govern; only these are shown. 1.0 in.-kip = 0.113 kN-m.

Table 5.2-5 Column-Beam Moment Ratios for Five-Bay Frame (N-S Direction)

Story	Member	ΣM_{pc}^* (in.-kips)	ΣM_{pb}^* (in.-kips)	Column- Beam Ratio
7	column W14×145 beam W24×76	29,400	27,700	1.06
5	column W14×233 beam W30×108	50,700	48,700	1.04
3	column W14×283 beam W30×116	63,100	53,900	1.17
2	column W14×398 beam W33×141	85,900	74,100	1.16

For levels with the same size column, the one with the larger beam size will govern; only these are shown. 1.0 in.-kip = 0.113 kN-m.

5. Check Panel Zone – The *Provisions* defers to AISC Seismic for the panel zone shear calculation. Because the two methods for calculating panel zone shear (AISC Seismic and FEMA 350) differ, both are illustrated below.

AISC Seismic Method

Check the shear requirement at the panel zone in accordance with AISC Seismic Sec. 9.3. The factored shear R_u is determined from the flexural strength of the beams connected to the column. This depends on the style of connection. In its simplest form, the shear in the panel zone (R_u) is

$$R_u = \sum \frac{M_f}{d_b - t_{fb}}$$

M_f is the moment at the column face determined by projecting the expected moment at the plastic hinge points to the column faces (see Figure 5.2-10).

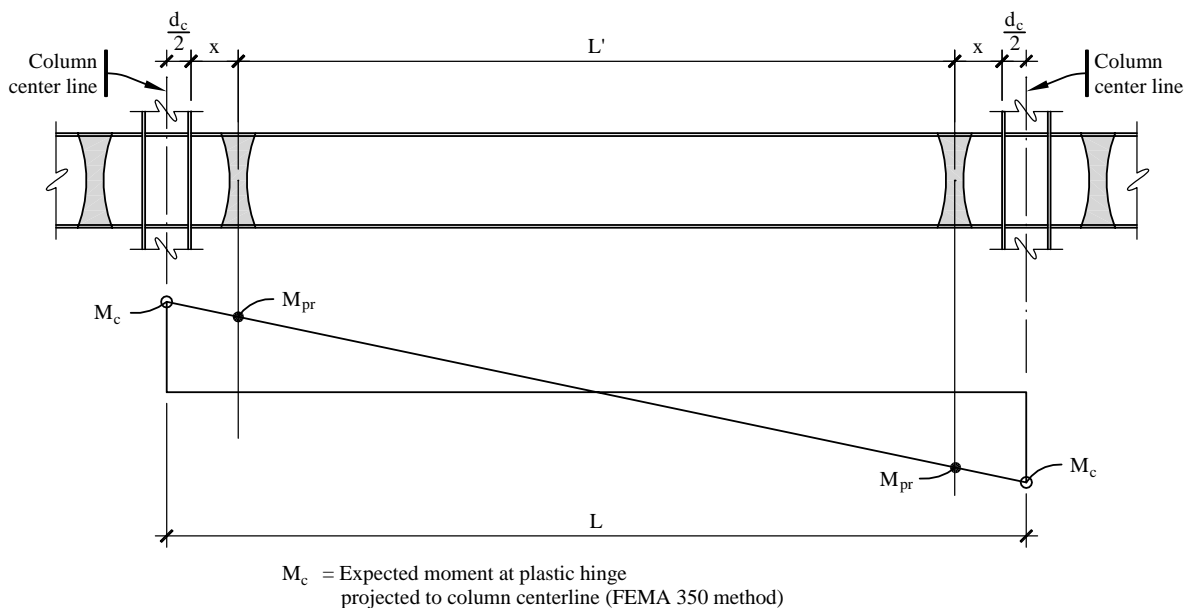
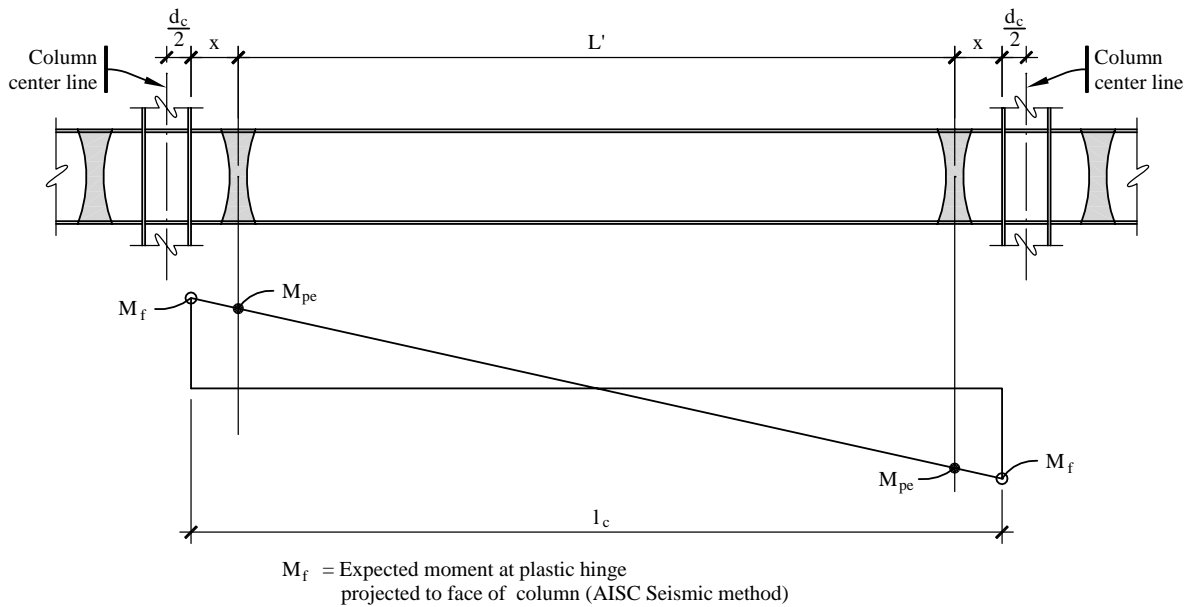


Figure 5.2-10 Illustration of AISC Seismic vs. FEMA 350 methods for panel zone shear.

For a column with equal beams of equal spans framing into opposite faces (such as on Grids C, D, E, F, 2, 3, 4, and 5), the effect of gravity loads offset, and

$$\Sigma M_f = 2R_y F_y Z_x \left[\frac{l_c}{l_c - 2x} \right]$$

where l_c = the clear span and x = distance from column face to plastic hinge location.

For Grids 1 and 6, only one beam frames into the column; at Grids B and G, the distance x is different on one side; at Grids A and H, there is no moment because the beams are pin-connected to the corner columns. For all these cases, the above relationship needs to be modified accordingly.

For W33×141 beams framing into each side of a W14×370 column (such as Level 2 at Grid F):

$$\Sigma M_f = (2)(1.1)(50)(514) \left[\frac{282.1}{282.1 - (2)(16.55)} \right] = 64,056 \text{ in.-kips}$$

$$R_u = \frac{64,056}{33.30 - 0.96} = 1,981 \text{ kips}$$

The shear transmitted to the joint from the story above opposes the direction of R_u and may be used to reduce the demand. From analysis, this is 98 kips at this location. Thus the frame $R_u = 1,981 - 98 = 1,883$ kips.

The panel zone shear calculation for Story 2 of the frame in the E-W direction at Grid F (column: W14×370; beam: W33×141) is from AISC Seismic Eq. 9-1:

$$R_v = 0.6F_y d_c t_p \left[1 + \frac{3b_{cf} t_{cf}^2}{d_p d_c t_p} \right]$$

$$R_v = (0.6)(50)(17.92)(t_p) \left[1 + \frac{(3)(16.475)(2.660)^2}{(33.30)(17.92)(t_p)} \right]$$

$$R_v = 537.6t_p \left[1 + \frac{0.586}{t_p} \right]$$

$$R_v = 537.6t_p + 315$$

The required total (web plus doubler plate) thickness is determined by:

$$R_v = \phi R_u$$

Therefore, $537.6t_p + 315 = (1.0)(1883)$ and $t_p = 2.91$ in.

Because the column web thickness is 1.655 in., the required doubler plate thickness is 1.26 in. Use a plate thickness of 1-1/4 in.

Both the column web thickness and the doubler plate thickness are checked for shear buckling during inelastic deformations by AISC Seismic Eq. 9-2. If necessary, the doubler plate may be plug-welded to the column web as indicated by AISC Seismic Commentary Figure C-9.2. For this case, the minimum individual thickness as limited by local buckling is:

$$t \geq (d_z + w_z) / 90$$

$$t \geq \frac{(31.38 + 12.6)}{90} = 0.49 \text{ in.}$$

Because both the column web thickness and the doubler plate thicknesses are greater than 0.49 in., plug welding of the doubler plate to the column web is not necessary.

In the case of thick doubler plates, to avoid thick welds, two doubler plates (each of half the required thickness) may be used, one on each side of the column web. For such cases, buckling also must be checked using AISC Seismic Eq. 9-2 as doubler plate buckling would be a greater concern. Also, the detailing of connections that may be attached to the (thinner) doubler plate on the side of the weld needs to be carefully reviewed for secondary effects such as undesirable out-of-plane bending or prying.

FEMA 350 Method

For the FEMA 350 method, see FEMA 350 Sec. 3.3.3.2, "Panel Zone Strength," to determine the required total panel zone thickness (t):

$$t = \sum \frac{C_y M_c \left[\frac{h - d_b}{h} \right]}{(0.9)(0.6) F_{yc} R_{yc} d_c (d_b - t_{fb})}$$

(Please note the Σ ; its omission from FEMA 350 Eq. 3-7 is an inadvertent typographical error.)

The term M_c refers to the expected beam moment projected to the centerline of the column; whereas AISC Seismic uses the expected beam moment projected to the face of the column flange. (This difference is illustrated in Figure 5.2-10.) The term $\left[\frac{h - d_b}{h} \right]$ is an adjustment similar to reducing R_u by the direct shear in the column, where h is the average story height. C_y is a factor that adjusts the force on the panel down to the level at which the beam begins to yield in flexure (see FEMA 350 Sec. 3.2.7) and is computed from FEMA 350 Eq. 3-4:

$$C_y = \frac{1}{C_{pr} \frac{Z_{be}}{S_b}}$$

C_{pr} , a factor accounting for the peak connection strength, includes the effects of strain hardening and local restraint, among others (see FEMA 350 Sec. 3.2.4) and is computed from FEMA 350 Eq. 3-2:

$$C_{pr} = \frac{(F_y + F_u)}{2F_y}$$

For the case of a W33×141 beam and W14×370 column (same as used for the above AISC Seismic method), values for the variables are:

Distance from column centerline to plastic hinge, $S_h = d_c/2 + d_b/2 = 17.92/2 + 33.30/2 = 25.61$ in.

Span between plastic hinges, $L' = 25 \text{ ft} - 2(25.61 \text{ in.})/12 = 20.73$ ft

$M_{pr} = C_{pr}R_yZ_eF_y$ (FEMA 350 Figure 3-4)

$M_{pr} = (1.2)(1.1)(514)(50) = 33,924$ in.-kips (FEMA 350, Figure 3-4)

$$V_p = \frac{\left[2M_{pr} + \left(\frac{wL'^2}{2} \right) \right]}{L'}$$

$$V_p = \frac{\left[(2)(33,924) + \left(\frac{(1.266)(20.73)^2}{(12)(2)} \right) \right]}{(20.73)(12)} = 273 \text{ kips}$$

$M_c = M_{pr} + V_p(x + d_c/2)$ (FEMA 350 Figure 3-4)

$M_c = 33,924 + (273)(17.92/2 + 25.61/2) = 40,916$ in.-kips

$$C_y = \frac{1}{C_{pr} \frac{Z_{be}}{S_b}} = \frac{1}{(1.2) \frac{514}{448}} = 0.73$$

Therefore,

$$t = 2 \left[\frac{(0.73)(40,916) \left[\frac{(214) - (33.30)}{(214)} \right]}{(0.9)(0.6)(50)(1.1)(17.92)(33.30 - 0.96)} \right] = 2.93 \text{ in.}$$

The required doubler plate thickness is equal to $t - t_{cw} = 2.93 \text{ in.} - 1.655 \text{ in.} = 1.27 \text{ in.}$ Thus, the doubler plate thickness for 1.27 in. by FEMA 350 is close to the thickness of 1.26 by AISC Seismic.

6. Check Redundancy – Return to the calculation of r_x for the moment frame. In accordance with *Provisions* Sec. 5.2.4.2 [not applicable in the 2003 *Provisions*], r_{max_x} is taken as the maximum of the sum of the shears in any two adjacent columns in the plane of a moment frame divided by the story shear. For columns common to two bays with moment resisting connections on opposite sides of the column at the level under consideration, 70 percent of the shear in that column may be used in the column shear summation (Figures 5.2-11 and 5.2-12).

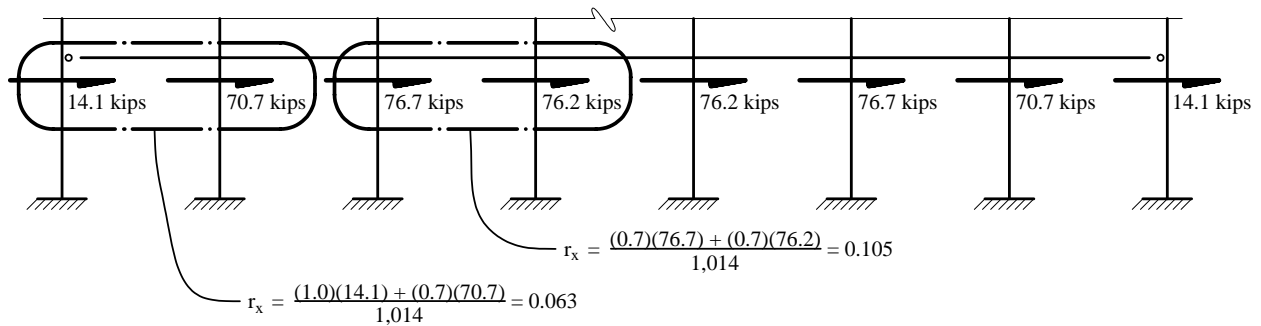


Figure 5.2-11 Column shears for E-W direction (partial elevation, Level 2) (1.0 kip = 4.45 kN).

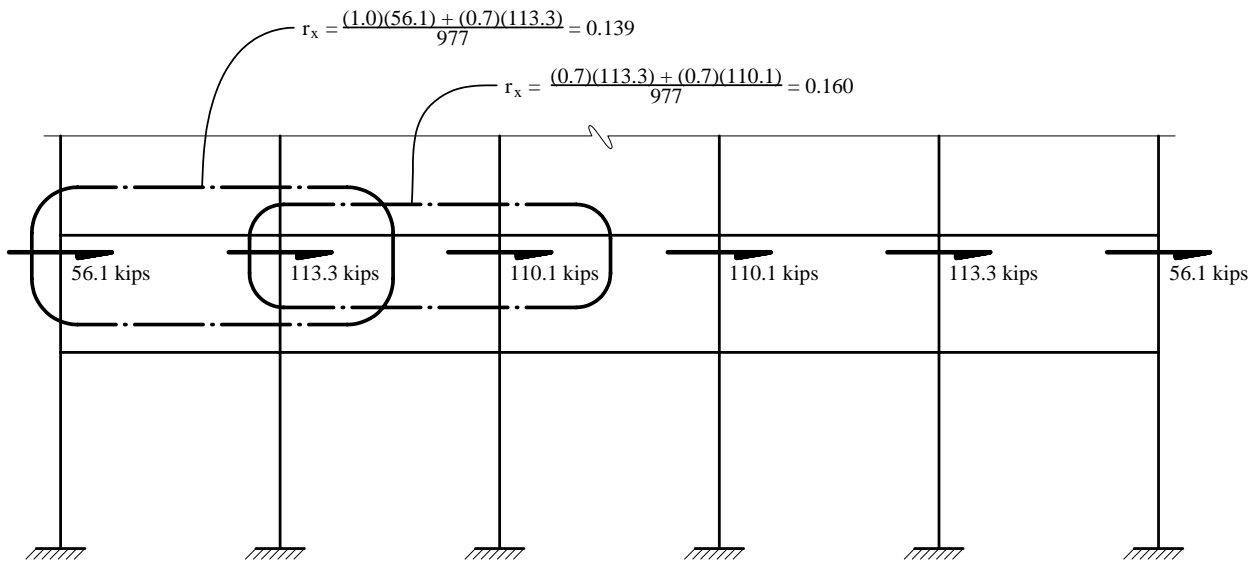


Figure 5.2-12 Column shears for N-S direction (partial elevation, Level 3) (1.0 kip = 4.45 kN).

For this example, r_x was computed for every column pair at every level in both directions. The shear carried by each column comes from the RAMFRAME analysis, which includes the effect of accidental torsion. Selected results are illustrated in the figures. The maximum value of r_{max_x} in the N-S direction is 0.160, and ρ is now determined using *Provisions* Eq.5.2.4.2 [not applicable in the 2003 *Provisions*]:

$$\rho = 2 - \frac{20}{r_{max_x} \sqrt{A_x}}$$

$$\rho = 2 - \frac{20}{0.160 \sqrt{21,875 \text{ ft}^2}} = 1.15$$

Because 1.15 is less than the limit of 1.25 for special moment frames per the exception in the *Provisions* Sec. 5.2.4.2 [not applicable in the 2003 *Provisions*], use $\rho = 1.15$. (If $\rho > 1.25$, then the framing would have to be reconfigured until $\rho < 1.25$.)

In the E-W direction, $r_{max_x} = 0.105$ and $\rho = 0.71$, which is less than 1.00, so use $\rho = 1.00$. All design force effects (axial force, shear, moment) obtained from analysis must be increased by the ρ factors. (However, drift controls the design in this example. Drift and deflections are not subject to the ρ factor.)

7. Connection Design – One beam-to-column connection for the moment-resisting frame is now designed to illustrate the FEMA 350 method for a prequalified connection. The welded unreinforced flanges-welded web (WUF-W) connection is selected because it is prequalified for special moment frames with members of the size used in this example. FEMA 350 Sec. 3.5.2 notes that the WUF-W connection can perform reliably provided all the limitations are met and the quality assurance requirements are satisfied. While the discussion of the design procedure below considers design requirements, remember that the quality assurance requirements are a vital part of the total requirements and must be enforced.

Figure 5.2-13 illustrates the forces at the beam-to-column connection.

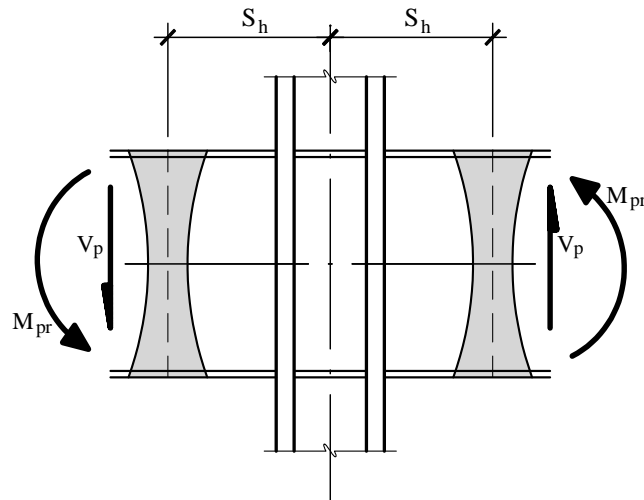


Figure 5.2-13 Forces at beam/column connection.

First review FEMA 350 Table 3-3 for prequalification data. Our case of a W36×135 beam connected to a W14×398 column meets all of these. (Of course, here the panel zone strength requirement is from FEMA 350, not the AISC Seismic method.)

The connection, shown in Figure 5.2-14, is based on the general design shown in FEMA 350 Figure 3-8. The design procedure outlined in FEMA 350 Sec. 3.5.2.1 for this application is reviewed below. All other beam-to-column connections in the moment frame will be similar.

The procedure outlined above for the FEMA 350 method for panel zone shear is repeated here to determine S_h , M_{pr} , V_p , M_c , C_y and the required panel zone thickness.

Continuity plates are required in accordance with FEMA 350 Sec. 3.3.3.1:

$$t_{cf} < 0.4 \sqrt{1.8 b_f t_f \frac{F_{yb} R_{yb}}{F_{yc} R_{yc}}}$$

$$t_{cf} < 0.4 \sqrt{(1.8)(11.950)(0.790) \frac{(50)(1.1)}{(50)(1.1)}} = 1.65 \text{ in. required}$$

$$t_{cf} = 2.845 \text{ in.} > \text{actual}$$

OK

Therefore, continuity plates are not necessary at this connection because the column flange is so thick. But we will provide them anyway to illustrate continuity plates in the example. At a minimum, continuity plates should be at least as thick as the beam flanges. Provide continuity plates of 7/8 in. thickness, which is thicker than the beam flange of 0.79 in.

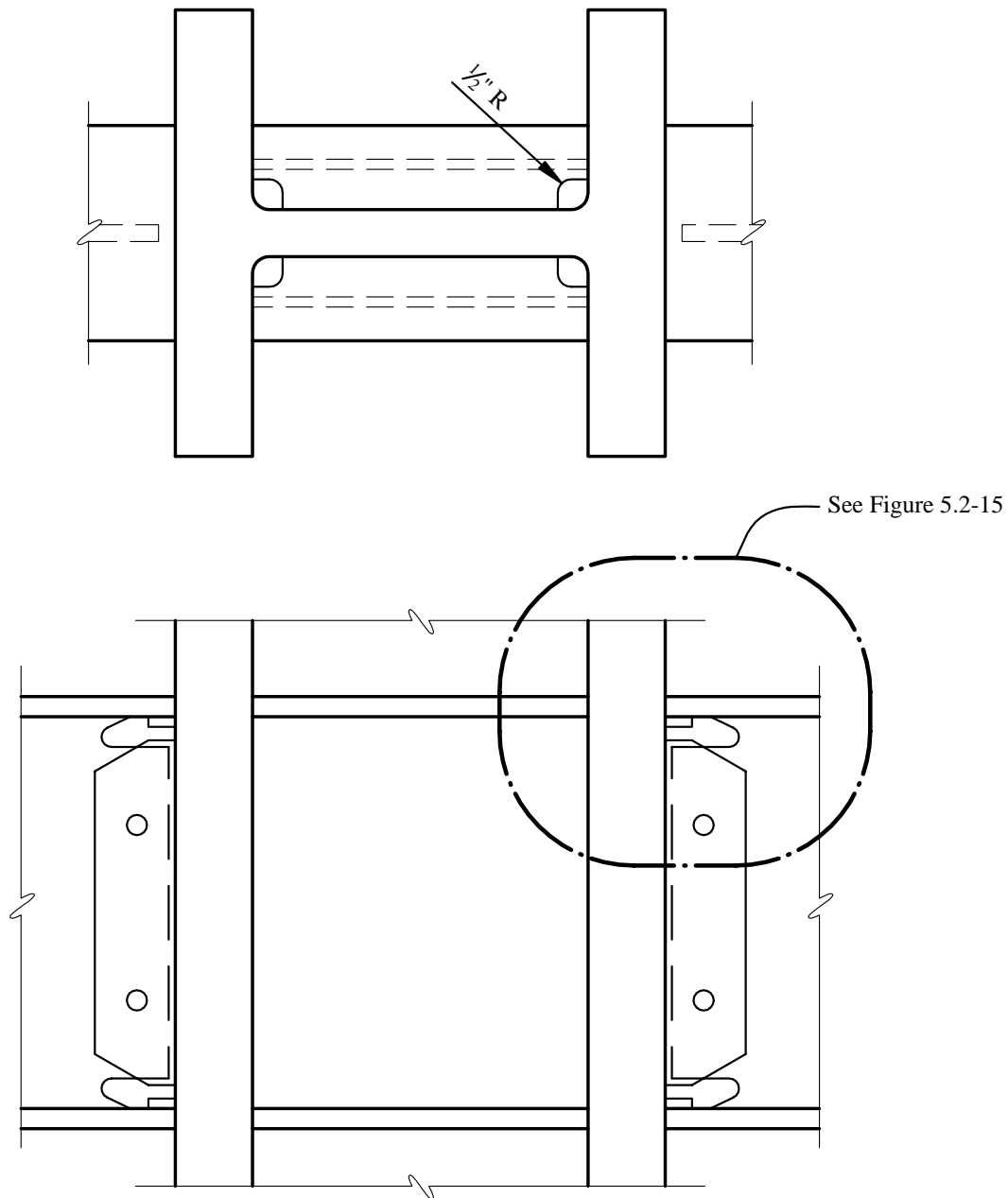


Figure 5.2-14 WUF-W connection, Second level, NS-direction (1.0 in. = 25.4 mm).

Check AISC LRFD K1.9:

$$\text{Width of stiffener} + \frac{t_{cw}}{2} \geq \frac{b_{bf}}{3}$$

$$\left(5 + \frac{1.77}{2}\right) = 5.88 \text{ in.} > 3.98 \text{ in.} = \frac{11.950}{3}$$

OK

$$t_{stiffener} \geq \frac{b_f}{2}$$

$$0.875 \text{ in.} > 0.395 \text{ in.} = \frac{0.79}{2}$$

OK

$$t_{stiffener} > w_{stiffener} \frac{\sqrt{F_y}}{95}$$

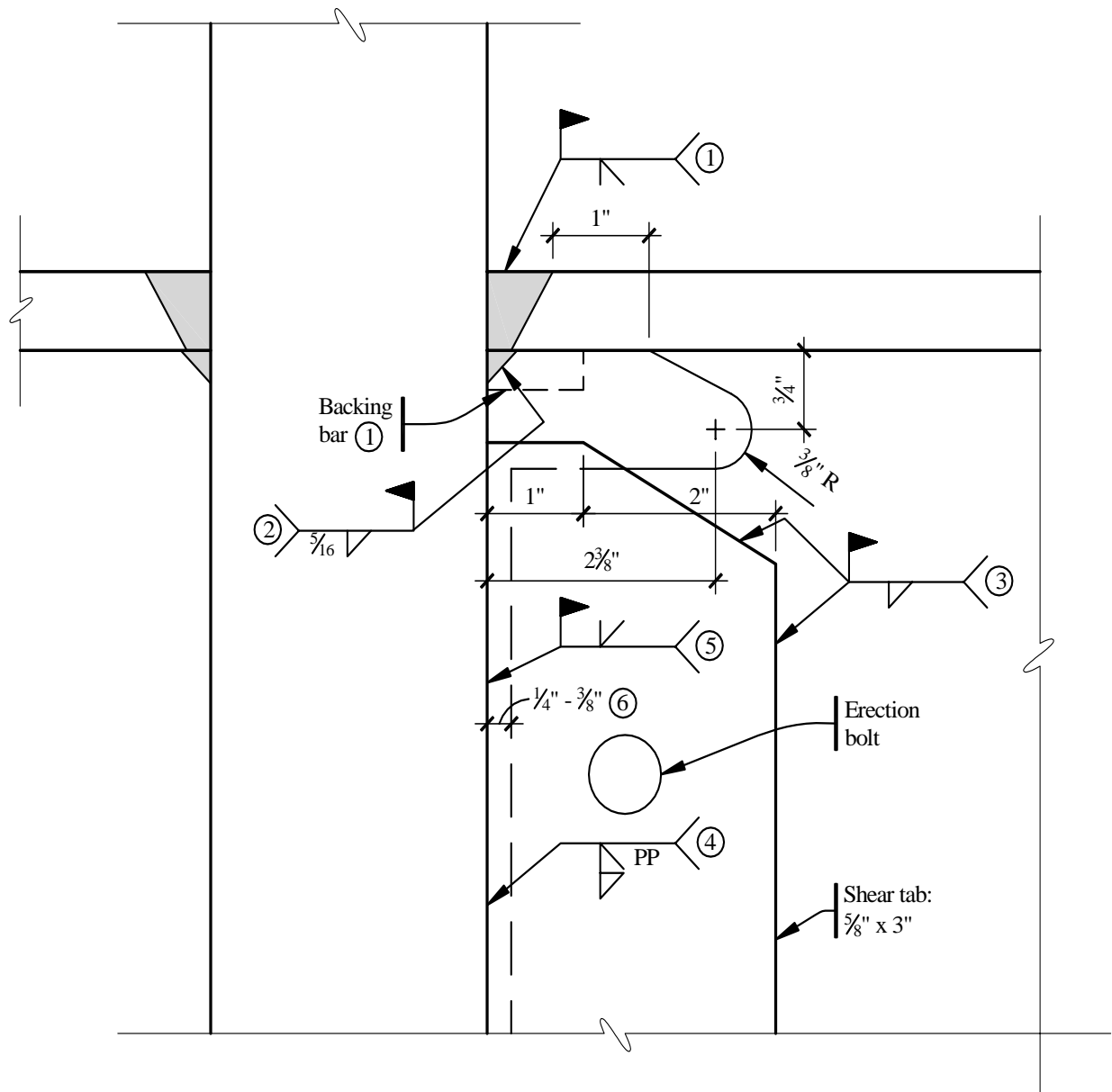


Figure 5.2-15 WUF-W weld detail (1.0 in. = 25.4 mm).

$$0.875 \text{ in.} > 0.37 \text{ in.} = (5) \left(\frac{\sqrt{50}}{95} \right) \quad \text{OK}$$

The details shown in Figures 5.2-14 and 5.2-15 conform to the requirements of FEMA 350 for a WUF-W connection in a special moment frame.

Notes for Figure 5.2-15 (indicated by circles in the figure) are:

1. CJP groove weld at top and bottom flanges, made with backing bar.
2. Remove backing bar, backgouge, and add fillet weld.
3. Fillet weld shear tab to beam web. Weld size shall be equal to thickness of shear tab minus 1/16 in. Weld shall extend over the top and bottom third of the shear tab height and extend across the top and bottom of the shear tab.
4. Full depth partial penetration weld from far side. Then fillet weld from near side. These are shop welds of shear tab to column.
5. CJP groove weld full length between weld access holes. Provide non-fusible weld tabs, which shall be removed after welding. Grind end of weld smooth at weld access holes.
6. Root opening between beam web and column prior to starting weld 5.

See also FEMA 350 Figure 3-8 for more elaboration on the welds.

5.2.4.3.2 Size Members for Alternative B, Braced Frame

1. Select Preliminary Member Sizes – The preliminary member sizes are shown for the braced frame in the E-W direction (seven bays) in Figure 5.2-16 and in the N-S direction (five bays) in Figure 5.2-17. The arrangement is dictated by architectural considerations regarding doorways into the stairwells.
2. Check Strength – First, check slenderness and width-to-thickness ratios – the geometrical requirements for local stability. In accordance with AISC Seismic Sec. 13.2, bracing members must satisfy

$$\frac{kl}{r} \leq \frac{1000}{\sqrt{F_y}} = \frac{1000}{\sqrt{50}} = 141$$

The columns are all relatively heavy shapes, so kl/r is assumed to be acceptable and is not examined in this example.

Wide flange members and channels must comply with the width-to-thickness ratios contained in AISC Seismic Table I-9-1 [I-8-1]. Flanges must satisfy:

$$\frac{b}{2t} \leq \frac{52}{\sqrt{F_y}} = \frac{52}{\sqrt{50}} = 7.35$$

Webs in combined flexural and axial compression (where $P_u/\phi_b P_y < 0.125$, which is the case in this example) must satisfy:

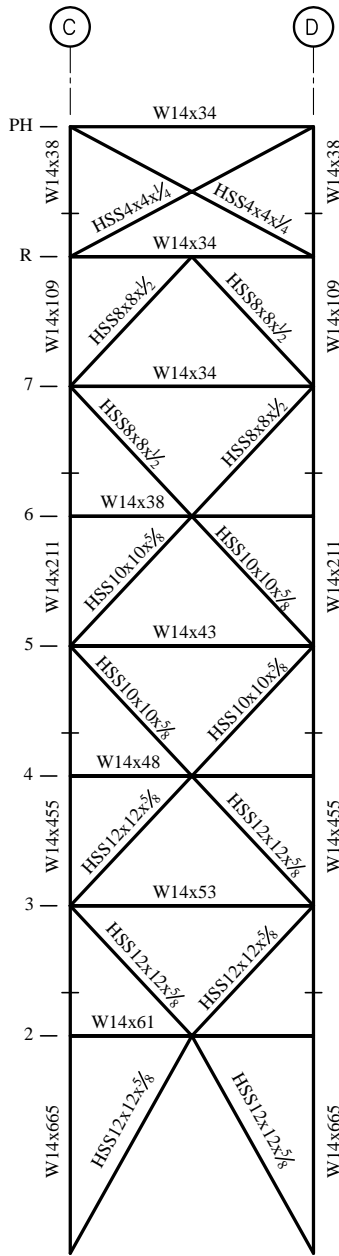


Figure 5.2-16 Braced frame in E-W direction.

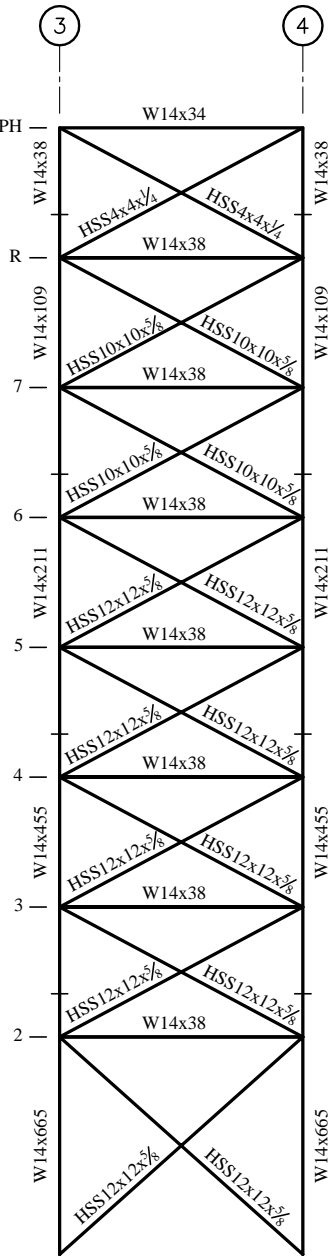
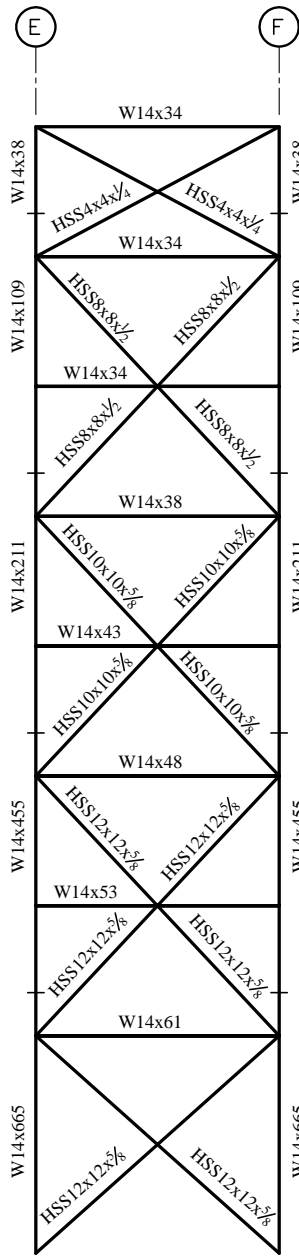


Figure 5.2-17 Braced frame in N-S direction.

$$\frac{h_c}{t_w} \leq \frac{520}{\sqrt{F_y}} \left[1 - 1.54 \frac{P_u}{\phi_b P_y} \right]$$

Rectangular HSS members must satisfy:

$$\frac{b}{t} \leq \frac{110}{\sqrt{F_y}} = \frac{110}{\sqrt{46}} = 16.2$$

Selected members are checked below:

W14×38: $b/2t = 6.6 < 7.35$ OK

W14×34: $b/2t = 7.4 > 7.35$, but is acceptable for this example. Note that the W14×34 is at the penthouse roof, which is barely significant for this braced frame.

HSS12×12×5/8: $\frac{kl}{r} = \frac{(1)\left(\frac{28.33 \times 12}{2}\right)}{4.62} = 36.8 < 141$ OK

$\frac{b}{t} = \frac{9.4}{0.581} = 16.17 < 16.2$ OK

Also note that t for the HSS is actual, not nominal. The corner radius of HSS varies somewhat, which affects the dimension b . The value of b used here, 9.40 in., depends on a corner radius slightly larger than $2t$, and it would have to be specified for this tube to meet the b/t limit.

3. Check Drift – Check drift in accordance with *Provisions* Sec. 5.2.8 [4.5]. The building was modeled in 3-D using RAMFRAME. Maximum displacements at the building corners are used here because the building is torsionally irregular. Displacements at the building centroid are also calculated because these will be the average between the maximum at one corner and the minimum at the diagonally opposite corner. Use of the displacements at the centroid as the average displacements is valid for a symmetrical building. Calculated story displacements are used to determine A_x , the torsional amplification factor. This is summarized in Table 5.2-6. P-delta effects are included.

Table 5.2-6 Alternative B Amplification of Accidental Torsion

	Average Elastic Displacement = Displacement at Building Centroid (in.)		Maximum Elastic Displacement at Building Corner* (in.)		$\frac{\delta_{max}}{\delta_{avg}}$ **		Torsional Amplification Factor = $A_x = \left(\frac{\delta_{max}}{1.2\delta_{avg}} \right)^2$		Amplified Eccentricity = $A_x(0.05 L)$ *** (ft)	
	E-W	N-S	E-W	N-S	E-W	N-S	E-W	N-S	E-W	N-S
R	2.38	2.08	3.03	3.37	1.28	1.62	1.13	1.82	7.08	15.95
7	2.04	1.79	2.62	2.93	1.29	1.64	1.15	1.88	7.20	16.41
6	1.65	1.47	2.15	2.44	1.30	1.67	1.18	1.93	7.37	16.86
5	1.30	1.16	1.70	1.96	1.32	1.69	1.2	1.99	7.52	17.41
4	0.95	0.86	1.27	1.48	1.33	1.72	1.23	2.06	7.71	17.99
3	0.66	0.59	0.89	1.03	1.34	1.75	1.25	2.14	7.80	18.70
2	0.39	0.34	0.53	0.60	1.35	1.79	1.26	2.23	7.89	19.57

* These values are taken directly from the analysis. Accidental torsion is not amplified here.

** Amplification of accidental torsion is required because this term is greater than 1.2 (*Provisions* Table 5.2.3.2 Item 1a [4.3-2, Item 1a]). The building is *torsionally irregular* in plan. *Provisions* Table 5.2.5.1 [4.4-1] indicates that an ELF analysis is “not permitted” for torsionally irregular structures. However, given rigid diaphragms and symmetry about both axes, a modal analysis will not give any difference in results than an ELF analysis insofar as accidental torsion is concerned unless one arbitrarily offsets the center of mass. The *Provisions* does not require an arbitrary offset for center of mass in dynamic analysis nor is it common practice to do so. One reason for this is that the computed period of vibration would lengthen, which, in turn, would reduce the overall seismic demand. See Sec. 9.2 and 9.3 of this volume of design examples for a more detailed examination of this issue.

*** The initial eccentricities of 0.05 in the E-W and N-S directions are multiplied by A_x to determine the amplified eccentricities. These will be used in the next round of analysis.

1.0 in. = 25.4 mm, 1.0 ft = 0.3048 m.

4. Check Torsional Amplification – A second RAMFRAME 3-D analysis was made, using the amplified eccentricity for accidental torsion instead of merely 0.05L for accidental torsion. The results are summarized in Table 5.2-7.

Table 5.2-7 Alternative B Story Drifts under Seismic Load

	Max. Elastic Displacement at Building Corners (in.)		Elastic Story Drift at Location of Max. Displacement (at corners) (in.)		C_d	$(C_d) \times$ (Elastic Story Drift) (in.)		Allowable Story Drift (in.)
	E-W	N-S	Δ E-W	Δ N-S		Δ E-W	Δ N-S	
R	3.14	4.50	0.42	0.55	5	2.10	2.75	3.20
7	2.72	3.95	0.49	0.64	5	2.46	3.19	3.20
6	2.23	3.32	0.45	0.63	5	2.27	3.16	3.20
5	1.77	2.68	0.45	0.64	5	2.25	3.18	3.20
4	1.32	2.05	0.40	0.61	5	1.98	3.07	3.20
3	0.93	1.43	0.38	0.59	5	1.89	2.93	3.20
2	0.55	0.85	0.55	0.85	5	2.75	4.24	5.36

1.0 in. = 25.4 mm

All story drifts are within the allowable story drift limit of $0.020h_{sx}$ in accordance with *Provisions* Sec. 5.2.8 [4.5-1] and the allowable deflections for this building from Sec. 5.2.3.6 above. This a good point to reflect on the impact of accidental torsion and its amplification on the design of this core-braced structure. The sizes of members were increased substantially to bring the drift within the limits (note how close the N-S direction drifts are). For the final structure, the elastic displacements at the main roof are:

At the centroid = 2.08 in.
 At the corner with accidental torsion = 3.37 in.
 At the corner with amplified accidental torsion = 4.50 in.

The two effects of torsional irregularity (in this case, it would more properly be called torsional flexibility) of amplifying the accidental torsion and checking the drift limits at the corners combine to create a demand for substantially more stiffness in the structure. Even though many braced frames are controlled by strength, this is an example of how the *Provisions* places significant stiffness demands on some braced structures.

5. Check Redundancy – Now return to the calculation of r_x for the braced frame. Per *Provisions* Sec. 5.2.4.2 [not applicable in the 2003 *Provisions*], r_{max_x} for braced frames is taken as the lateral force component in the most heavily loaded brace element divided by the story shear (Figure 5.2-18).

A value for r_x was determined for every brace element at every level in both directions. The lateral component carried by each brace element comes from the RAMFRAME analysis, which includes the effect of amplified accidental torsion. Selected results are illustrated in the figures. The maximum r_x was found to be 0.223 below Level 7 in the NS-direction. The reliability factor (ρ) is now determined using *Provisions* Eq. 5.2.4.2 [not applicable in the 2003 *Provisions*]:

$$\rho = 2 - \frac{20}{r_{max_x} \sqrt{A_x}} = 2 - \frac{20}{0.223 \sqrt{21,875 \text{ ft}^2}} = 1.39$$

In the N-S direction, all design force effects (axial forces, shears, moments) obtained from analysis must be increased by the ρ factor of 1.39. Similarly, for the E-W-direction, r_{max_x} and ρ are found to be 0.192 and 1.26, respectively. (However drift controls the design for this problem. Drift and deflection are not subject to the ρ factor.)

[See Sec. 5.2.3.2 for a discussion of the significant changes to the redundancy requirements in the 2003 *Provisions*.]

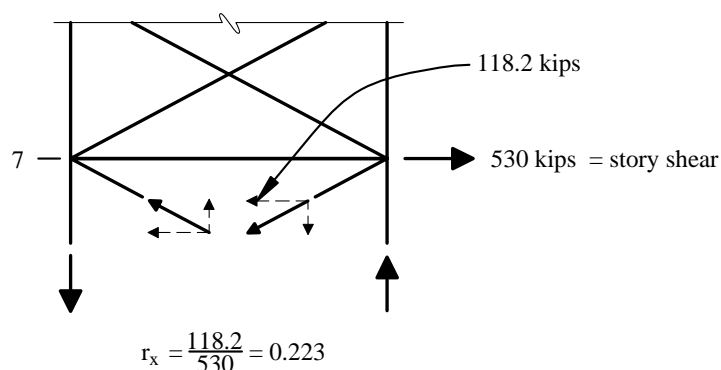


Figure 5.2-18 Lateral force component in braces for N-S direction – partial elevation, Level 7 (1.0 kip = 4.45 kN).

6. Braced Frame Member Design Considerations – The design of members in the special concentrically braced frame (SCBF) needs to satisfy AISC Seismic Sec. 13 and columns also need to satisfy AISC Seismic Sec. 8. When $P_u/\phi P_n$ is greater than 0.4, as is the predominant case here, the required axial strength needs to be determined from AISC Seismic Eq. 4-1 and 4-2 [*Provisions* Eq. 4.2-3 and 4.2-4]. These equations are for load combinations that include the Ω_0 , or overstrength, factors. Moments are generally small for the braced frame so load combinations with Ω_0 can control column size for strength considerations but, for this building, drift controls because of amplified accidental torsion. Note that ρ is not used where Ω_0 is used (see *Provisions* Sec. 5.2.7 [4.2.2.2]).

Bracing members have special requirements as well, although Ω_0 factors do not apply to braces in a SCBF. Note in particular AISC Seismic Sec. 13.2c, which requires that both the compression brace and the tension brace share the force at each level (as opposed to the “tension only” braces of Example 5.1). AISC Seismic Sec. 13.2 also stipulates a kl/r limitation and local buckling (width-thickness) ratio limits.

Beams in many configurations of braced frames have small moments and forces, which is the case here. V and inverted V (chevron) configurations are an exception to this. There is a panel of chevron bracing at the top story of one of the braced frames (Figure 5.2-16). The requirements of AISC Seismic Sec. 13.4 should be checked although, in this case, certain limitations of AISC Seismic do not apply because the beam is at the top story of a building. (The level above in Figure 5.2-16 is a minor penthouse that is not considered to be a story.) If the chevron bay were not at the top story, the size of the braces must be known in order to design the beam. The load combination for the beam is modified using a Q_b factor defined in AISC Seismic Sec. 13.4a. Basically, the beam must be able to

carry a concentrated load equal to the difference in vertical force between the post-buckling strength of the compression brace and the yield strength of the tension brace (i.e., the compression brace has buckled, but the tension brace has not yet yielded). The prescribed load effect is to use $0.3\phi_c P_n$ for the compression brace and P_y for the tension brace in order to determine a design vertical force to be applied to the beam.

7. Connection Design – Figure 5.2-19 illustrates a typical connection design at a column per AISC Seismic Sec. 13. First, check the slenderness and width-to-thickness ratios (see above). The bracing members satisfy these checks.

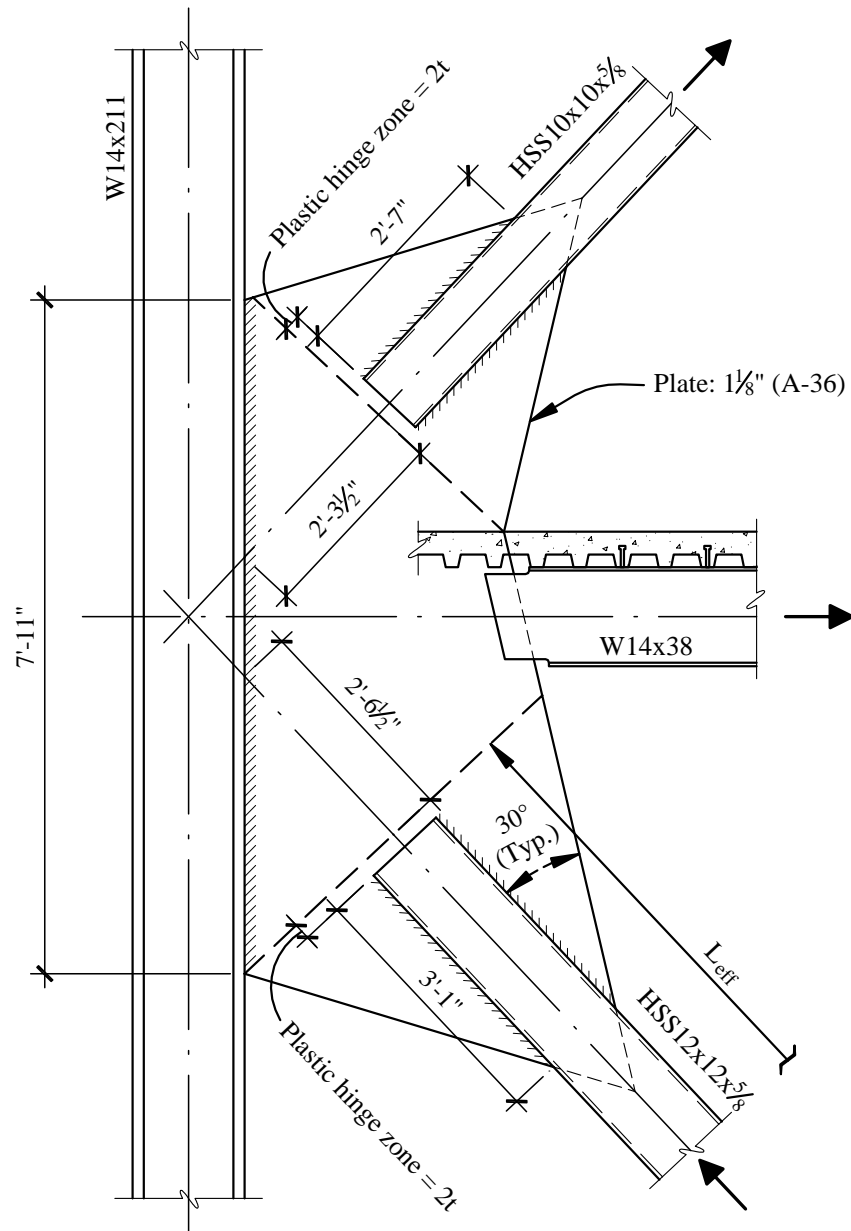


Figure 5.2-19 Bracing connection detail (1.0 in. = 25.4 mm, 1.0 ft = 0.3048 m).

Next, design the connections. The required strength of the connection is to be the nominal axial tensile strength of the bracing member. For an HSS12×12×5/8, the nominal axial tensile strength is computed using AISC Seismic Sec. 13.3a:

$$P_n = R_y F_y A_g = (1.3)(46 \text{ ksi})(27.4 \text{ in.}^2) = 1,639 \text{ kips}$$

The area of the gusset is determined using the plate thickness and the Whitmore section for effective width. See Figure 5.2-20 for the determination of this dimension.

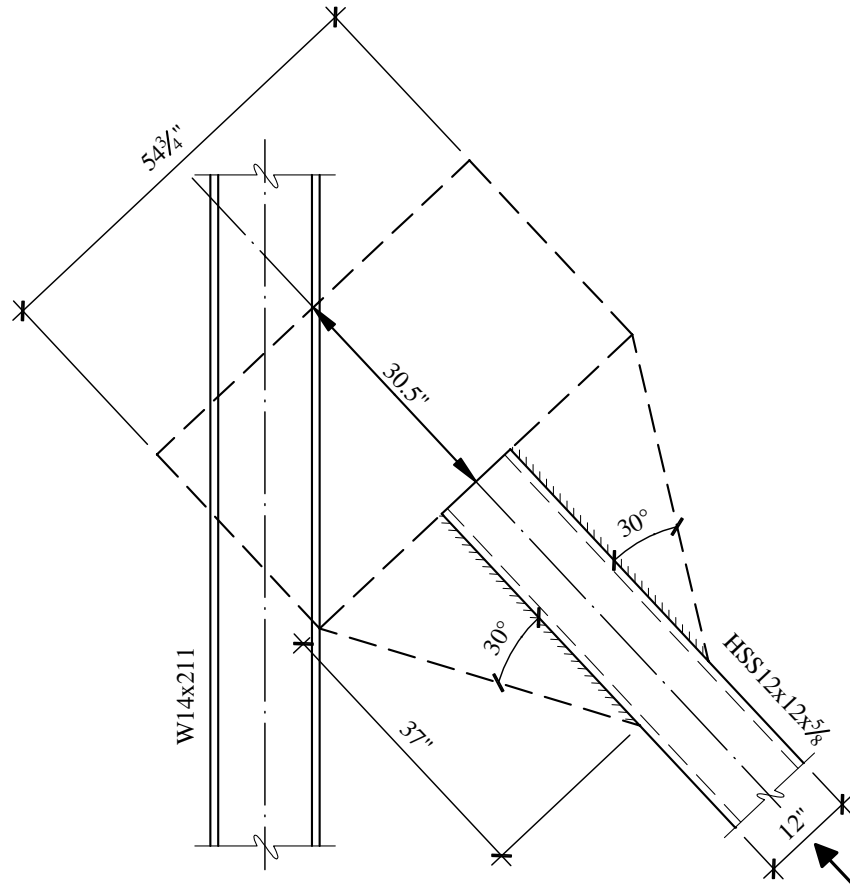


Figure 5.2-20 Whitmore section (1.0 in. = 25.4 mm, 1.0 ft = 0.3048 m).

For tension yielding of the gusset plate:

$$\phi T_n = \phi F_y A_g = (0.90)(36 \text{ ksi})(1.125 \text{ in.} \times 54.7 \text{ in.}) = 1,993 \text{ kips} > 1,639 \text{ kips} \quad \text{OK}$$

For fracture in the net section:

$$\phi T_n = \phi F_u A_n = (0.75)(58 \text{ ksi})(1.125 \text{ in.} \times 54.7 \text{ in.}) = 2,677 \text{ kips} > 1,639 \text{ kips} \quad \text{OK}$$

Since 1,933 kips is less than 2,677 kips, yielding (ductile behavior) governs over fracture.

For a tube slotted to fit over a connection plate, there will be four welds. The demand in each weld will be $1,639 \text{ kips}/4 = 410 \text{ kips}$. The design strength for a fillet weld per AISC LRFD Table J2.5 is:

$$\phi F_w = \phi(0.6F_{exx}) = (0.75)(0.6)(70 \text{ ksi}) = 31.5 \text{ ksi}$$

For a 1/2 in. fillet weld, the required length of weld is determined to be:

$$L_w = \frac{410 \text{ kips}}{(0.707)(0.5 \text{ in.})(31.5 \text{ ksi})} = 37 \text{ in.}$$

In accordance with the exception of AISC Seismic Sec. 13.3c, the design of brace connections need not consider flexure if the connections meet the following criteria:

- a. Inelastic rotation associated with brace post-buckling deformations: The gusset plate is detailed such that it can form a plastic hinge over a distance of $2t$ (where t = thickness of the gusset plate) from the end of the brace. The gusset plate must be permitted to flex about this hinge, unrestrained by any other structural member. See also AISC Seismic C13.3c. With such a plastic hinge, the compression brace may buckle out-of-plane when the tension braces are loaded. Remember that during the earthquake, there will be alternating cycles of compression to tension in a single bracing member and its connections. Proper detailing is imperative so that tears or fractures in the steel do not initiate during the cyclic loading.
- b. The connection design strength must be at least equal to the nominal compressive strength of the brace.

Therefore, the connection will be designed in accordance with these criteria. First, determine the nominal compressive strength of the brace member. The effective brace length (L_{eff}) is the distance between the plastic hinges on the gusset plates at each end of the brace member. For the brace being considered, $L_{eff} = 169 \text{ in.}$ and the nominal compressive strength is determined using AISC LRFD Eq. E2-4:

$$\lambda_c = \frac{kl}{r\pi} \sqrt{\frac{F_y}{E}} = \frac{(1)(169)}{(4.60)\pi} \sqrt{\frac{46}{29,000}} = 0.466$$

Since $\lambda_c < 1.5$, use AISC LRFD Eq. E2-2:

$$F_{cr} = (0.658^{\lambda_c^2}) F_y = (0.658^{0.217})(46) = 42.0 \text{ ksi}$$

$$P_{cr} = A_g F_{cr} = (27.4)(42.0) = 1,151 \text{ kips}$$

Now, using a design compressive load from the brace of 1,151 kips, determine the buckling capacity of the gusset plate using the Whitmore section method. By this method, illustrated by Figure 5.2-20, the compressive force per unit length of gusset plate is $(1,151 \text{ kips}/54.7 \text{ in.}) = 21.04 \text{ kips/in.}$

Try a plate thickness of 1.125 in.

$$f_a = P/A = 21.04 \text{ kips}/(1 \text{ in.} \times 1.25 \text{ in.}) = 18.7 \text{ ksi}$$

The gusset plate is modeled as a 1 in. wide by 1.125 in. deep rectangular section, pinned at one end (the plastic hinge) and fixed at the other end where welded to column (see Whitmore section diagram). The effective length factor (k) for this “column” is 0.8.

Per AISC LRFD Eq. E2-4:

$$\lambda_c = \frac{kl}{r\pi} \sqrt{\frac{F_y}{E}} = \frac{(0.8)(30.5)}{(0.54)\pi} \sqrt{\frac{36}{29,000}} = 0.51$$

Since $\lambda_c < 1.5$, use AISC LRFD Eq. E2-2:

$$F_{cr} = (0.658^{\lambda_c^2}) F_y = (0.658^{0.257})(36) = 32.3 \text{ ksi}$$

$$\phi F_{cr} = (0.85)(32.3) = 27.4 \text{ ksi}$$

$$\phi F_{cr} = 27.4 \text{ ksi} > 18.7 \text{ ksi}$$

OK

Now consider the brace-to-brace connection shown in Figure 5.2-21. The gusset plate will experience the same tension force as the plate above, and the Whitmore section is the same. However, the compression length is much less, so a thinner plate may be adequate.

Try a 15/16 in. plate. Again, the effective width is shown in Figure 5.2-20. For tension yielding of the gusset plate:

$$\phi T_n = \phi F_y A_g = (0.90)(36 \text{ ksi})(0.9375 \text{ in.} \times 54.7 \text{ in.}) = 1,662 \text{ kips} > 1,639 \text{ kips} \quad \text{OK}$$

For fracture in the net section:

$$\phi T_n = \phi F_u A_n = (0.75)(58 \text{ ksi})(0.9375 \text{ in.} \times 54.7 \text{ in.}) = 2,231 \text{ kips} > 1,639 \text{ kips} \quad \text{OK}$$

Since 1,662 kips is less than 2,231 kips, yielding (ductile behavior) governs over fracture.

For compression loads, the plate must be detailed to develop a plastic hinge over a distance of $2t$ from the end of the brace. The effective length for buckling of this plate will be $k[12" + (2)(2t + \text{weld length})]$. For this case, the effective length is $0.65[12 + (2)(2 \times 15/16 + 5/16)] = 9.2 \text{ in.}$ Compression in the plate over this effective length is acceptable by inspection and will not be computed here.

Next, check the reduced section of the tube, which has a 1 1/4 in. wide slot for the gusset plate (at the column). The reduction in HSS12×12×5/8 section due to the slot is $(0.581 \times 1.25 \times 2) = 1.45 \text{ in.}^2$, and the net section, $A_{net} = (25.7 - 1.45) = 24.25 \text{ in.}^2$

Compare yield in the gross section with fracture in the net section:

$$\text{Yield} = F_y A_g = (46 \text{ ksi})(25.7 \text{ in.}^2) = 1,182 \text{ kips} \quad \text{OK}$$

$$\text{Fracture} = F_u A_n = (58 \text{ ksi})(24.25 \text{ in.}^2) = 1,406 \text{ kips} \quad \text{OK}$$

AISC Seismic 13.3b could be used to require design fracture strength ($0.75 \times 1,406 = 1,055 \text{ kips}$) to exceed probable tensile yield (1,639 kips), but this is clearly impossible, even if the net area equaled the gross area. This design is considered satisfactory.

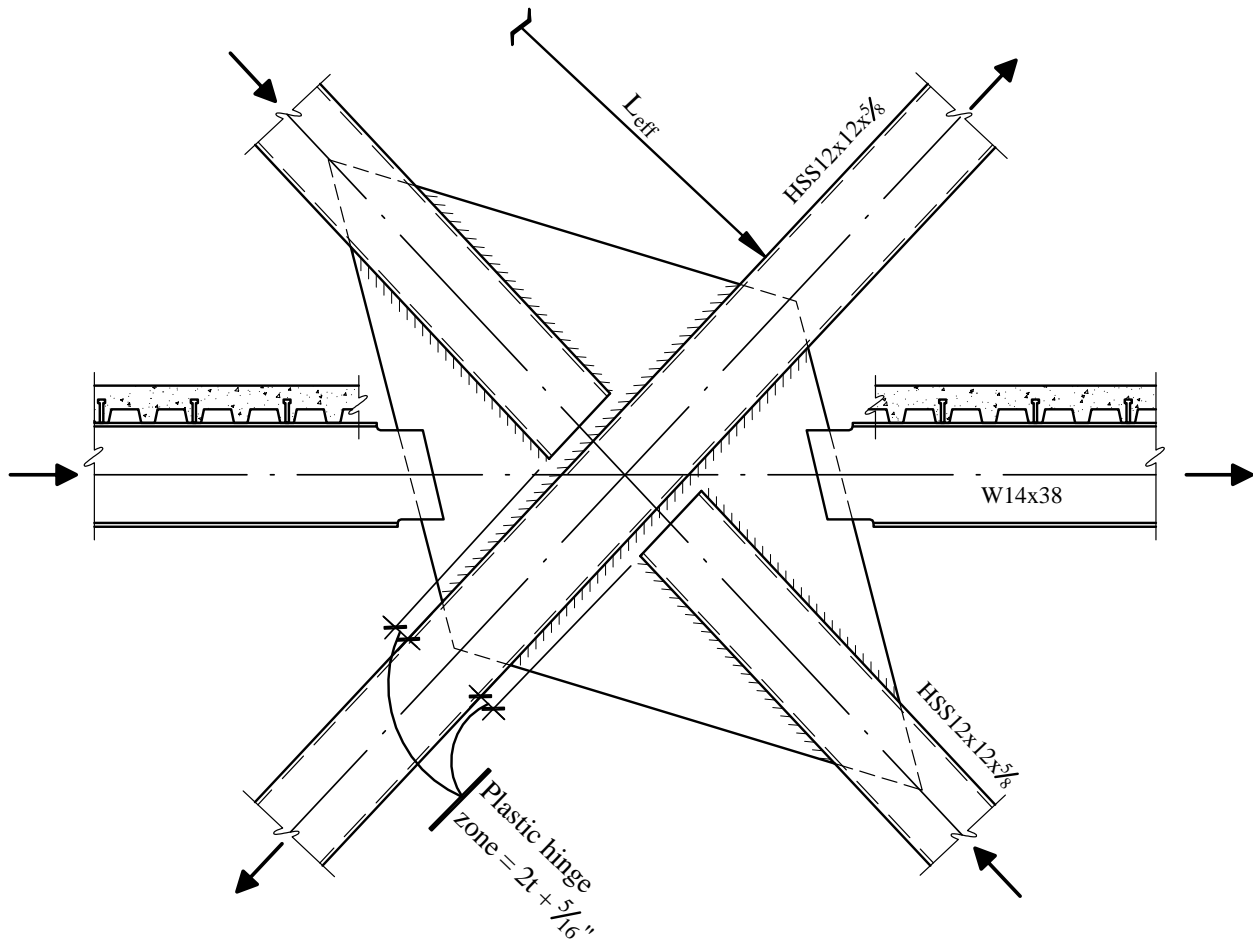


Figure 5.2-21 Brace-to-brace connection (1.0 in. = 25.4 mm).

5.2.4.3.3 Size Members for Alternative C, Dual System

1. Select Preliminary Member Sizes – A dual system is a combination of a moment-resisting frame with either a shear wall or a braced frame. In accordance with the building systems listed in *Provisions* Table 5.2.2 [4.3-1], a dual system consisting of special moment frames at the perimeter and special concentrically braced frames at the core will be used.
2. Check Strength of Moment Frame – The moment frame is required to have sufficient strength to resist 25 percent of the design forces by itself (*Provisions* Sec. 5.2.2.1 [4.3.1]). This is a good place to start a design. Preliminary sizes for the perimeter moment frames are shown in Figures 5.2-22 and 5.2-23. It is designed for strength using 25 percent of the design lateral forces. All the design requirements for special moment frames still apply (flange and web width-to-thickness ratios, column-beam moment ratio, panel zone shear, drift, and redundancy) and all must be checked; however, it may be prudent to defer some of the checks until the design has progressed a bit further. The methodology for the analysis and these checks is covered in Sec. 5.2.4.3.1, so they will not be repeated here.

For some buildings this may present an opportunity to design the columns without doubler plates because the strength requirement is only 25 percent of the total. However, for the members used in this example, doubler plates will still be necessary. The increase in column size to avoid doubler plates is substantial, but feasible. The sequence of column sizes that is shown is W 14×132 - 82 - 68 -

53 and would become W14×257 - 233 - 211 - 176 to avoid doubler plates. The beams in Figures 5.2-22 and 5.2-23 are controlled by strength because drift is not a criterion.

Note that $P_u/\phi P_n > 0.4$ for a few of the columns when analyzed without the braced frame so the overstrength requirements of AISC Seismic Sec. 8.2 [8.3] apply to these columns. Because the check using $\Omega_0 E$ is for axial capacity only and the moment frame columns are dominated by bending moment, the sizes are not controlled by the check using $\Omega_0 E$.

3. Check the Strength of the Braced Frames – The next step is to select the member sizes for the braced frame. Because of the presence of the moment frame, the accidental torsion on the building will be reduced as compared to a building with only a braced core. In combination with the larger R factor (smaller design forces), this should help to realize significant savings in the braced frame member sizes. A trial design is selected, followed by analysis of the entire dual system. All members need to be checked for width-thickness ratios and the braces need to be checked for slenderness. Note that columns in the braced frame will need to satisfy the overstrength requirements of AISC Seismic Sec. 8.2 [8.3] because $P_u/\phi P_n > 0.4$. This last requirement causes a significant increase in column sizes, except in the upper few stories.

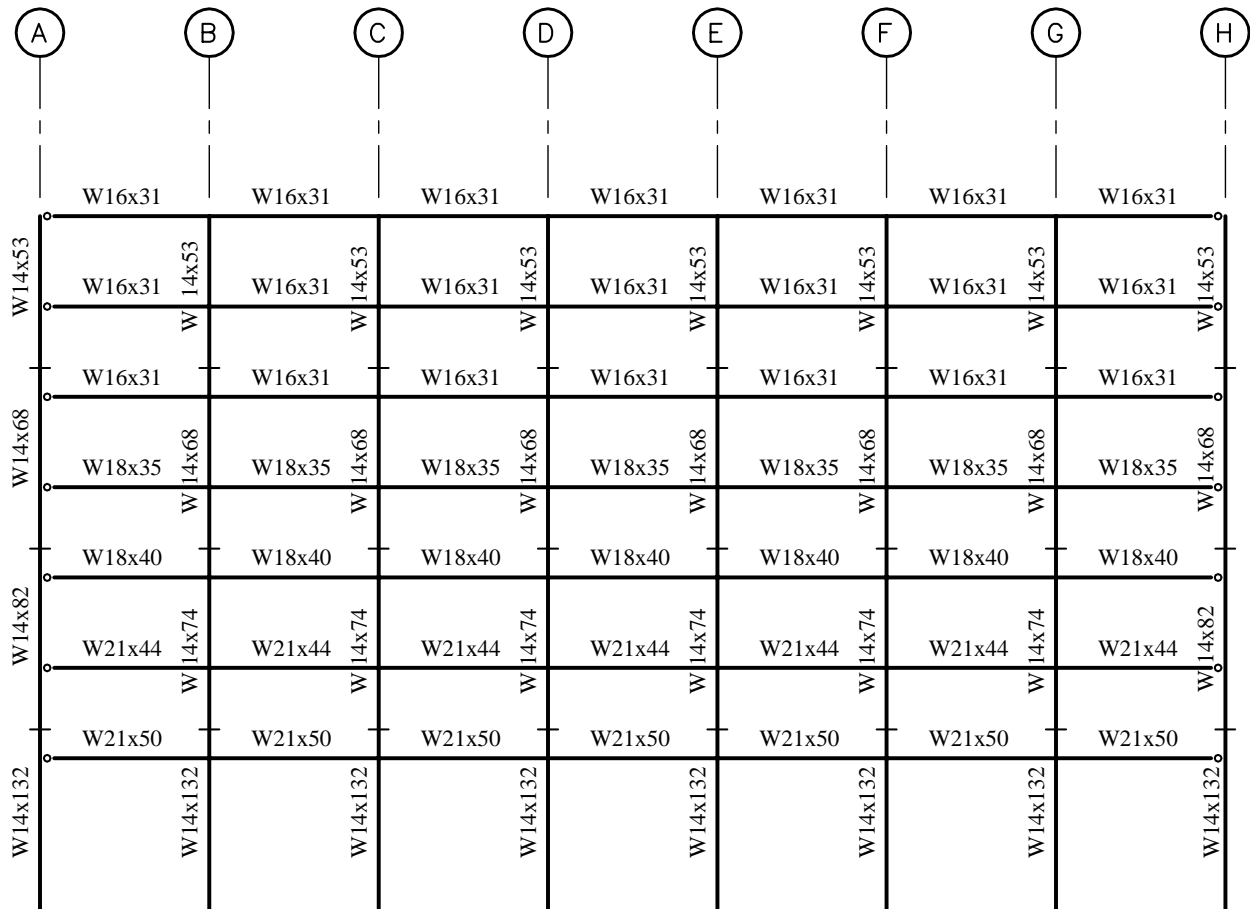


Figure 5.2-22 Moment frame of dual system in E-W direction.

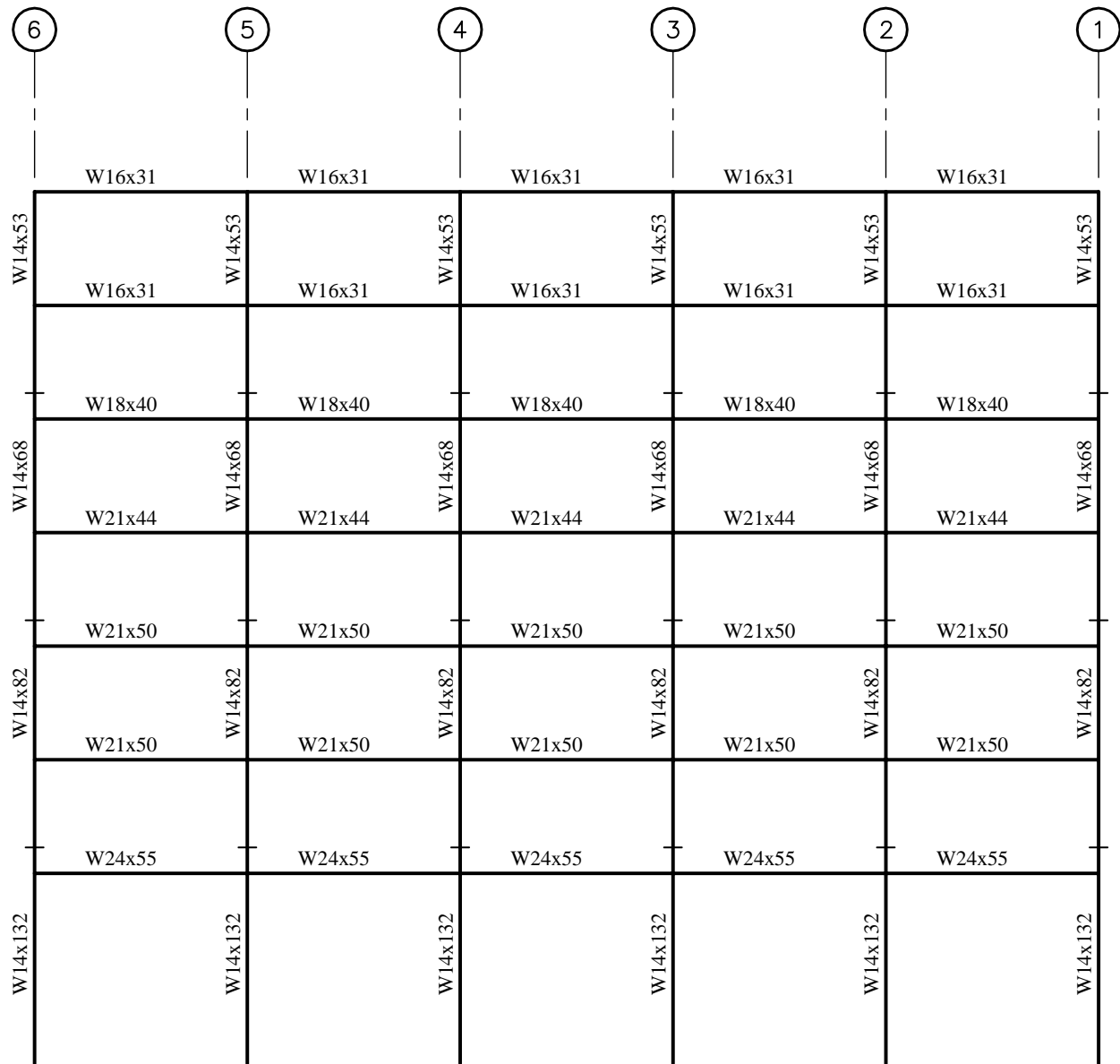


Figure 5.2-23 Moment frame of dual system in N-S direction.

4. Check Drift – Check drift in accordance with *Provisions* Sec. 5.2.8 [4.5]. The building was modeled in three dimensions using RAMFRAME. Maximum displacements at the building corners are used here because the building is torsionally irregular. Displacements at the building centroid are also calculated because these will be the average between the maximum at one corner and the minimum at the diagonally opposite corner. Use of the displacements at the centroid as the average displacements is valid for a symmetrical building.
5. Check Torsional Amplification – Calculated story drifts are used to determine A_p , the torsional amplification factor (Table 5.2-8). P-delta effects are included.

Table 5.2-8 Alternative C Amplification of Accidental Torsion

	Average Elastic Displacement = Displacement at Building Centroid (in.)		Maximum Elastic Displacement at Building Corner* (in.)		$\frac{\delta_{\max}}{\delta_{\text{avg}}}$ **		Torsional Amplification Factor = $A_x = \left(\frac{\delta_{\max}}{1.2\delta_{\text{avg}}} \right)^2$		Amplified Eccentricity = $A_x(0.05L)^{***}$ (ft.)	
	E-W	N-S	E-W	N-S	E-W	N-S	E-W	N-S	E-W	N-S
R	2.77	2.69	3.57	3.37	1.29	1.25	1.15	1.09	7.19	9.54
7	2.45	2.34	3.15	3.00	1.28	1.28	1.14	1.14	7.14	10.01
6	2.05	1.91	2.63	2.50	1.28	1.31	1.13	1.20	7.07	10.46
5	1.64	1.51	2.10	2.01	1.28	1.33	1.13	1.23	7.08	10.8
4	1.22	1.11	1.56	1.50	1.28	1.35	1.14	1.27	7.13	11.15
3	0.81	0.75	1.05	1.03	1.29	1.38	1.16	1.31	7.25	11.50
2	0.43	0.41	0.57	0.57	1.32	1.40	1.20	1.37	7.52	11.98

* These values are directly from the analysis. Accidental torsion is not amplified here.

** Amplification of accidental torsion is required because this term is greater than 1.2 (*Provisions* Table 5.2.3.2, Item 1a [4.3-2, Item 1a]). The building is *torsionally irregular* in plan. See discussion in footnote ** of Table 5.2.6.

*** The initial eccentricities of $0.05L$ in the E-W and N-S directions are multiplied by A_x to determine the amplified eccentricities. These will be used in the next round of analysis.

1.0 in. = 25.4 mm, 1.0 ft = 0.3048 m.

The design that yielded the displacements shown in Table 5.2-8 does not quite satisfy the drift limits, even without amplifying the accidental torsion. That design was revised by increasing various brace and column sizes and then re-analyzing using the amplified eccentricity instead of merely $0.05L$ for accidental torsion. After a few iterations, a design that satisfied the drift limits was achieved. These member sizes are shown in Figures 5.2-24 and 5.2-25. That structure was then checked for its response using the standard $0.05L$ accidental eccentricity in order to validate the amplifiers used in design. The amplifier increased for the E-W direction but decreased for the N-S direction, which was the controlling direction for torsion. The results are summarized in Table 5.2-9.

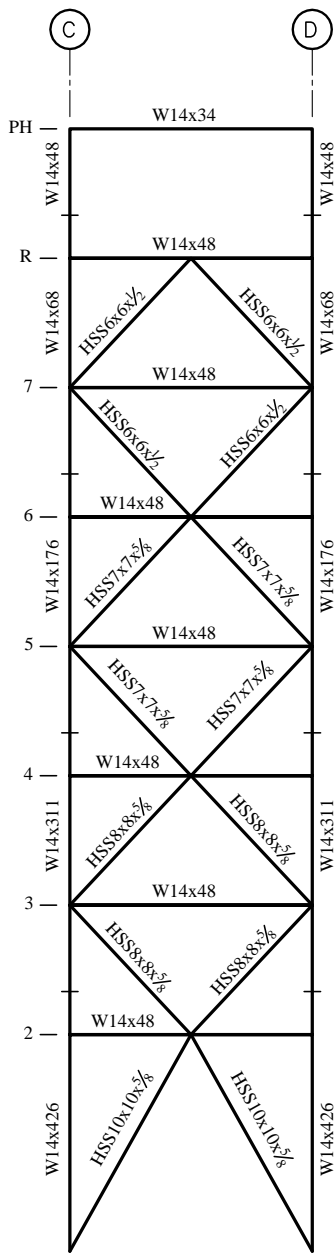


Figure 5.2-24 Braced frame of dual system in E-W-direction.

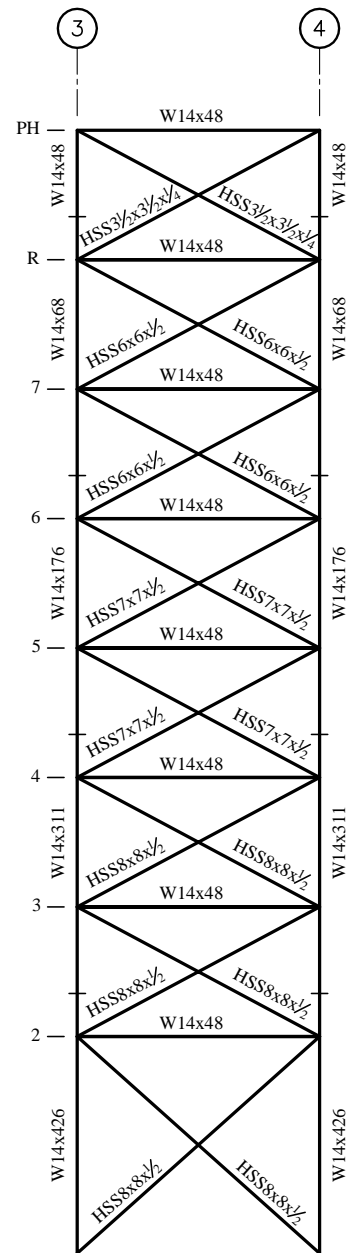
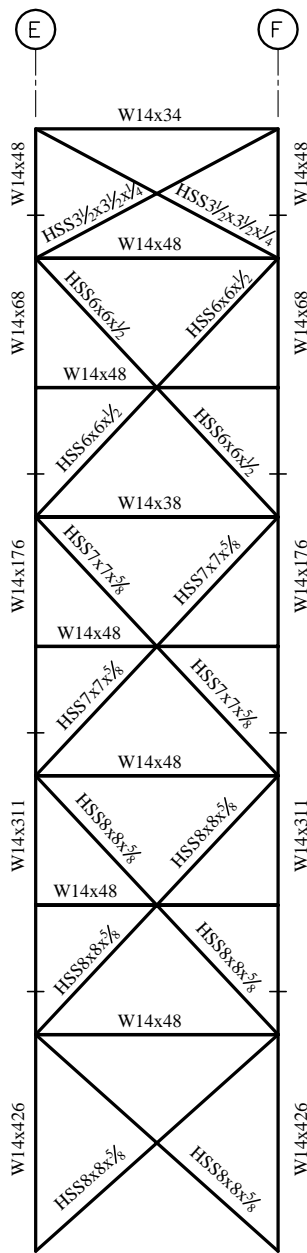


Figure 5.2-25 Braced frame of dual system in N-S direction.

Table 5.2-9 Alternative C Story Drifts under Seismic Load

	Max. Elastic Displacement at Building Corners (in.)		Elastic Story Drift at Location of Max. Displacement (at corners) (in.)		C_d	$(C_d) \times$ (Elastic Story Drift) (in.)		Allowable Story Drift (in.)
	E-W	N-S	Δ E-W	Δ N-S		Δ E-W	Δ N-S	
R	3.06	3.42	0.37	0.37	6.5	2.43	2.42	3.20
7	2.69	3.05	0.45	0.47	6.5	2.94	3.05	3.20
6	2.24	2.58	0.45	0.49	6.5	2.89	3.17	3.20
5	1.79	2.09	0.45	0.51	6.5	2.93	3.30	3.20
4	1.34	1.58	0.41	0.48	6.5	2.66	3.09	3.20
3	0.93	1.11	0.39	0.46	6.5	2.55	3.01	3.20
2	0.54	0.64	0.54	0.64	6.5	3.52	4.17	5.36

1.0 in. = 25.4 mm

The story drifts are within the allowable story drift limit of $0.020h_{sx}$ as per *Provisions* Sec. 5.2.8 [4.5.1]. Level 5 has a drift of 3.30 in. > 3.20 in. but the difference of only 0.1 in. is considered close enough for this example.

6. Check Redundancy – Now return to the calculation of r_x for the braced frame. In accordance with *Provisions* Sec. 5.2.4.2 [not applicable in the 2003 *Provisions*], r_{max_x} for braced frames is taken as the lateral force component in the most heavily loaded brace element divided by the story shear. This is illustrated in Figure 5.2-18 for Alternative B.

For this design, r_x was determined for every brace element at every level in both directions. The lateral component carried by each brace element comes from the RAMFRAME analysis, which includes the effect of amplified accidental torsion. The maximum value was found to be 0.1762 at the base level in the N-S direction. Thus, ρ is now determined to be (see Sec. 5.2.4.2):

$$\rho = 0.8 \left[2 - \frac{20}{r_{max_x} \sqrt{A_x}} \right] = 0.8 \left[2 - \frac{20}{0.1762 \sqrt{21,875 \text{ ft.}^2}} \right] = 0.986$$

The 0.8 factor comes from *Provisions* Sec. 5.2.4.2 [not applicable in the 2003 *Provisions*]. As ρ is less than 1.0, $\rho = 1.0$ for this example.

In the E-W direction, r_{max} is less; therefore, ρ will be less, so use $\rho = 1.0$ for both directions.

[See Sec. 5.2.3.2 for a discussion of the significant changes to the redundancy requirements in the 2003 *Provisions*.]

7. Connection Design – Connections for both the moment frame and braced frames may be designed in accordance with the methods illustrated in Sec. 5.2.4.3.1 and 5.2.4.3.2.

5.2.5 Cost Comparison

Material takeoffs were made for the three alternatives. In each case, the total structural steel was estimated. The takeoffs are based on all members, but do not include an allowance for plates and bolts at connections. The result of the material takeoffs are:

Alternative A, Special Steel Moment Resisting Frame	593 tons
Alternative B, Special Steel Concentrically Braced Frame	640 tons
Alternative C, Dual System	668 tons

The higher weight of the systems with bracing is primarily due to the placement of the bracing in the core, where resistance to torsion is poor. Torsional amplification and drift limitations both increased the weight of steel in the bracing. The weight of the moment-resisting frame is controlled by drift and the strong column rule.

5.3 TWO-STORY BUILDING, OAKLAND, CALIFORNIA

This example features an eccentrically braced frame (EBF) building. The following items of seismic design of steel-framed buildings are illustrated:

1. Analysis of eccentrically braced frames
2. Design of bracing members
3. Brace connections

5.3.1 Building Description

This two-story hospital, 120 ft by 140 ft in plan, is shown in Figure 5.3-1. The building has a basement and two floors. It has an unusually high roof load because of a plaza with heavy planters on the roof.

The vertical-load-carrying system consists of concrete fill on steel deck floors supported by steel beams and girders that span to steel columns and to the perimeter basement walls. The bay spacing is 20 ft each way. Floor beams are spaced three to a bay. The beams and girders on the column lines are tied to the slabs with stud connectors.

The building is founded on a thick mat. The foundation soils are deep stable deposits of sands, gravels, and stiff clays overlying rock.

The lateral-force-resisting system for Stories 1 and 2 consists of EBFs on Gridlines 1, 8, B, and F as

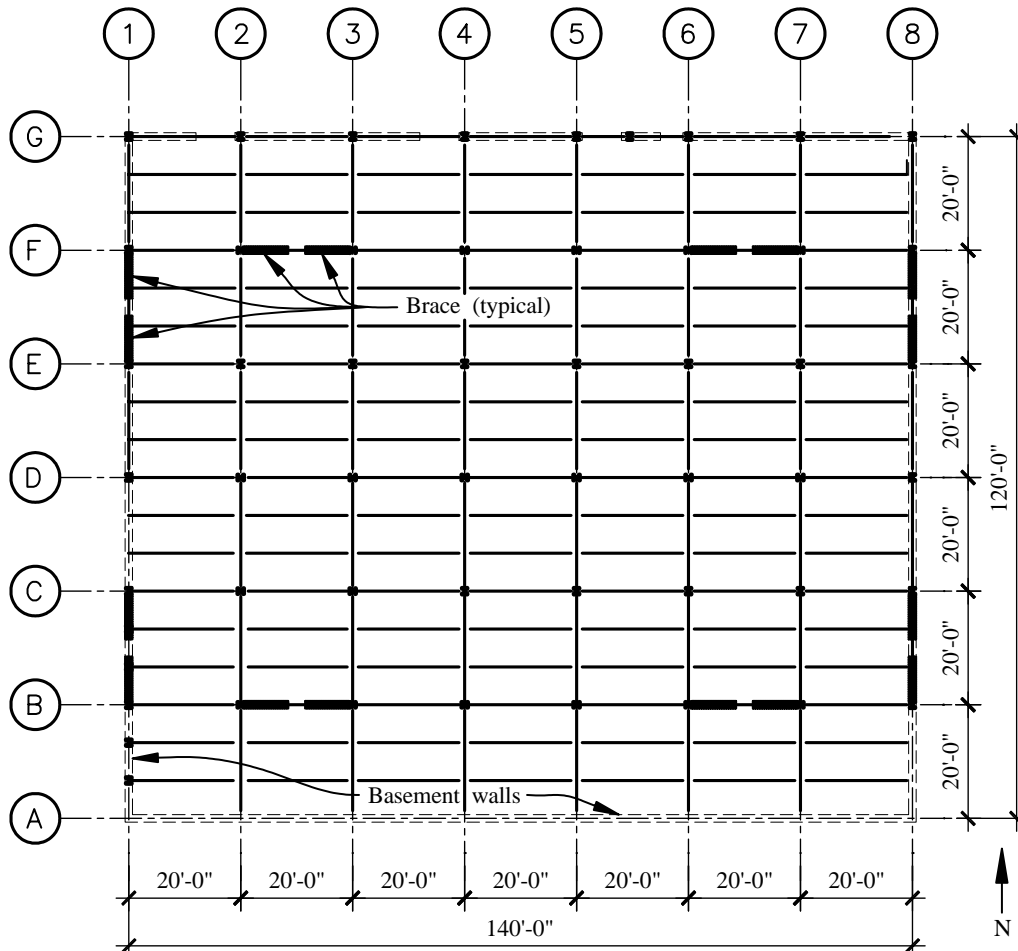


Figure 5.3-1 Main floor framing plan (1.0 in. = 25.4 mm, 1.0 ft = 0.3048 m).

shown in Figure 5.3-1. A typical bracing elevation is shown in Figure 5.3-2. These EBFs transfer lateral loads to the main floor diaphragm. The braced frames are designed for 100 percent of lateral load and their share of vertical loads. EBFs have been selected for this building because they provide high stiffness and a high degree of ductility while permitting limited story-to-story height.

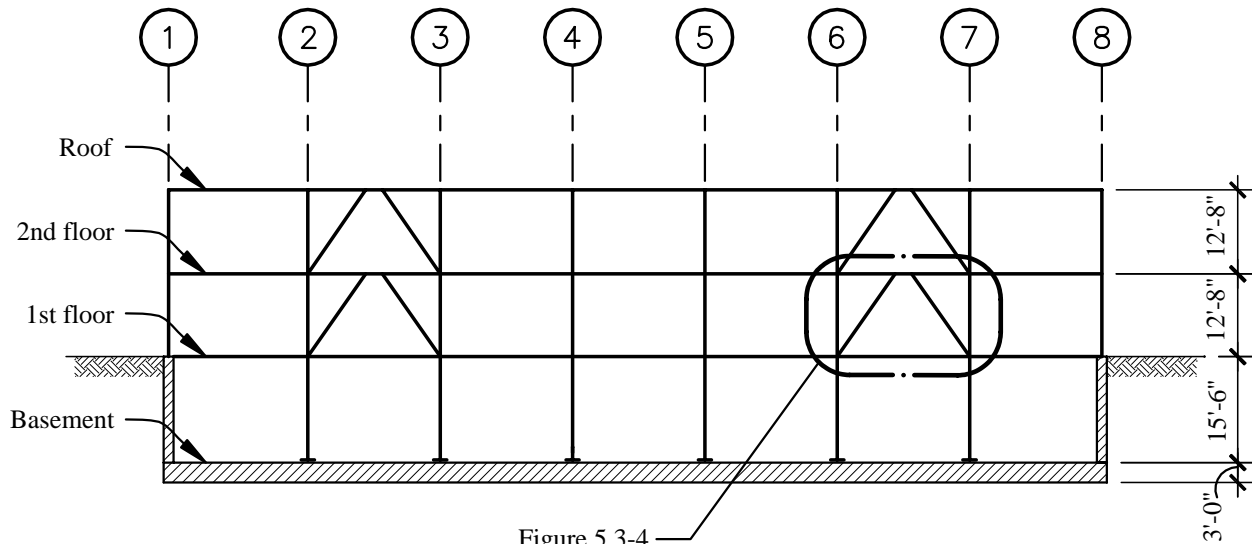


Figure 5.3-2 Section on Grid F (1.0 in. = 25.4 mm, 1.0 ft = 0.3048 m).

The structure illustrates a common situation for low-rise buildings with basements. The combination of the basement walls and the first floor diaphragm is so much stiffer that the superstructure that the *base* (see *Provisions* Chapter 2 [4.1.3] for definition) of the building is the first floor, not the foundation. Therefore, the diagonal braces do not extend into the basement because the horizontal force is in the basement walls (both in shear parallel to the motion considered and in direct pressure on perpendicular walls). This has a similarity to the irregularity Type 4 “out-of-plane offsets” defined in *Provisions* Table 5.2.3.2 [4.3-2], but because it is below the base that classification does not apply. However, the columns in the basement that are part of the EBFs must be designed and detailed as being the extension of the EBF that they are. This affects width-thickness ratios, overstrength checks, splice requirements, and so on. Column design for an EBF is illustrated later in this example.

5.3.2 Method

The method for determining basic parameters is similar to that for other examples. It will not be repeated here; rather the focus will be on the design of a specific example of an EBF starting with the forces in the frame as obtained from a linear analysis. Keep in mind that the load path is from the floor diaphragm to the beam to the braces. The fundamental concept behind the eccentric braced frame is that seismic energy is absorbed by yielding of the link. Yielding in shear is more efficient than yielding in flexure, although either is permitted. A summary of the method is as follows:

1. Select member preliminary sizes.
2. Perform an elastic analysis of the building frame. Compute elastic drift (δ_e) and forces in the members.
3. Compute the inelastic displacement as the product of C_d times δ_e . The inelastic displacement must be within the allowable story drift from *Provisions* Table 5.2.8 [4.5-1].

4. Compute the link rotation angle (α) and verify that it is less than 0.08 radians for yielding dominated by shear in the link or 0.02 radians for yielding dominated by flexure in the link. (See Figure 5.3-4 for illustration of α). The criteria is based on the relationship between M_p and V_p as related to the length of the link.
5. To meet the link rotation angle requirement, it may be necessary to modify member sizes, but the more efficient approach is to increase the link length. (The trade-off to increasing the link length is that the moment in the link will increase. Should the moment become high enough to govern over shear yielding, then α will have to be limited to 0.02 radians instead of 0.08 radians.)
6. The braces and building columns are to remain elastic. The portions of the beam outside the link are to remain elastic; only the link portion of the beam yields.
7. For this case, there are moment-resisting connections at the columns. Therefore from *Provisions* Table 5.2.2 [4.3-1], $R = 8$, $C_d = 4$, and $\Omega_0 = 2$. (Neither the *Provisions* nor AISC Seismic offer very much detailed information about requirements for moment-resisting connections for the beam to column connection in an EBF. There are explicit requirements for the connection from a link to a column. The EBF system will not impose large rotational demands on a beam to column connection; the inelastic deformations are confined to the link. Therefore, without further detail, it is the authors' interpretation that an ordinary moment resisting frame connection will be adequate).

5.3.3 Analysis

Because the determination of basic provisions and analysis are so similar to those of other examples, they will not be presented here. An ELF analysis was used.

5.3.3.1 Member Design Forces

The critical forces for the design of individual structural elements, determined from computer analysis, are summarized in Table 5.3-1.

Table 5.3-1 Summary of Critical Member Design Forces

Member	Force Designation	Magnitude
Link	P_{link}	5.7 kips
	V_{link}	85.2 kips
	M_{left}	127.9 ft-kips
	M_{right}	121.3 ft-kips
Brace	P_{brace}	120.0 kips
	M_{top}	15.5 ft-kips
	M_{bot}	9.5 ft-kips

1.0 kip = 4.45 kN, 1.0 ft-kip = 1.36 kN-m.

The axial load in the link at Level 2 may be computed directly from the second-floor forces. The force from the braces coming down from the roof level has a direct pass to the braces below without affecting the link. The axial forces in the link and brace may be determined as follows:

Total second-story shear (determined elsewhere) = 535.6 kips

Second-story shear per braced line = $535.6/2 = 267.8$ kips
Second-story shear per individual EBF = $267.8/2 = 133.9$ kips
Second-story shear per brace = $133.9/2 = 66.95$ kips
Axial force per brace = $66.95 (15.25 \text{ ft}/8.5 \text{ ft}) = 120.0$ kips

Second-story shear per braced line = 267.8 kips
Second-story shear per linear foot = $267.8 \text{ kips}/140 \text{ ft} = 1.91$ klf
Axial force in link = $(1.91 \text{ klf})(3 \text{ ft}) = 5.7$ kips

5.3.3.2 Drift

From the linear computer analysis, the elastic drift was determined to be 0.247 inches. The total inelastic drift is computed as:

$$C_d \delta_c = (4)(0.247) = 0.99 \text{ in.}$$

The link rotation angle is computed for a span length, $L = 20$ ft, and a link length, $e = 3$ ft as follows:

$$\alpha = \left(\frac{L}{e}\right)\theta = \left(\frac{20 \text{ ft}}{3 \text{ ft}}\right)\left(\frac{0.99 \text{ in.}}{(12.67 \text{ ft})(12)}\right) = 0.043 \text{ radians}$$

The design is satisfactory if we assume that shear yielding governs because the maximum permissible rotation is 0.08 radians (AISC Seismic Sec. 15.2g [15.2]). For now, we will assume that shear yielding of the link governs and will verify this later.

5.3.4 Design of Eccentric Bracing

Eccentric bracing adds two elements to the frame: braces and links. As can be seen in Figure 5.3-3, two eccentric braces located in one story of the same bay intersect the upper beam a short distance apart, thus creating a link subject to high shear. In a severe earthquake, energy is dissipated through shear yielding of the links while diagonal braces and columns remain essentially elastic.

The criteria for the design of eccentric bracing are given in AISC Seismic Sec. 15. All section sizes and connection details are made similar for all braced bays. The following sections have been selected as a preliminary design:

Typical girders	W16×57
Typical columns	W14×132
Typical braces	HSS 8×8×5/8

Since all members of the braced frames are to be essentially the same, further calculations deal with the braced frames on Line F, shown in Figures 5.3-3 and 5.3-4.

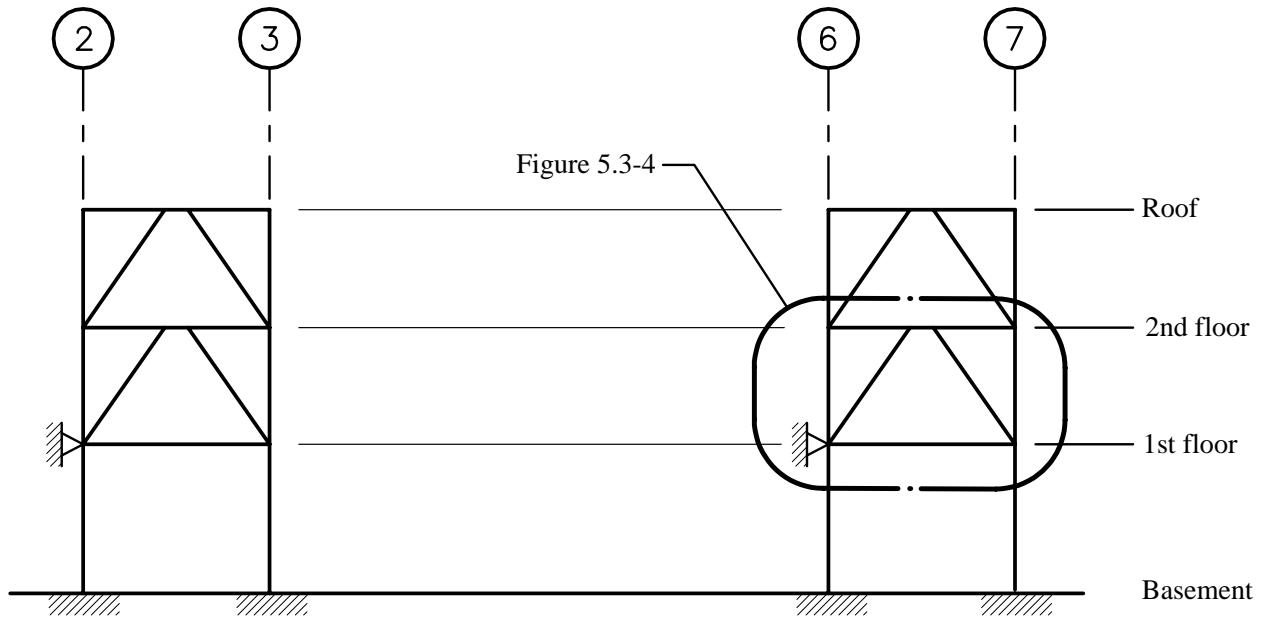


Figure 5.3-3 Diagram of eccentric braced frames on Grid F.

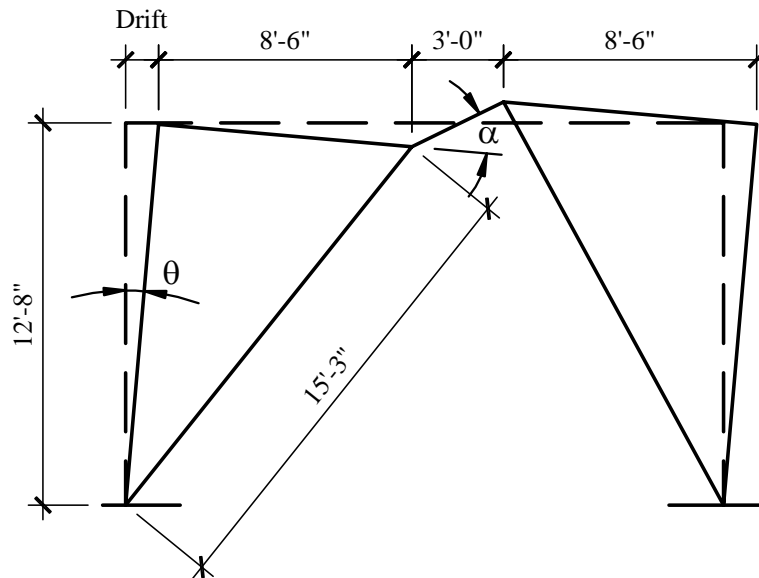


Figure 5.3-4 Typical eccentric braced frame
(1.0 in. = 25.4 mm, 1.0 ft = 0.3048 m).

5.3.4.1 Link Design

The first-story eccentric braced frame (identified in Figure 5.3-2) is examined first. The shear force and end moments in the link (W16x57 beam section) are listed in Table 5.3-1 and repeated below:

$$\begin{aligned}
 P_{link} &= 5.7 \text{ kips} \\
 V_{link} &= 85.2 \text{ kips} \\
 M_{left} &= 127.9 \text{ ft-kips} \\
 M_{right} &= 121.3 \text{ ft-kips}
 \end{aligned}$$

5.3.4.1.1 Width-Thickness Ratio

The links are first verified to conform to AISC Seismic Sec. 15.2a [15.2], which refers to AISC Seismic Table I-9-1 [I-8-1].

First, check the beam flange width-thickness ratio. For the selected section, $b/t = 4.98$, which is less than the permitted b/t ratio of :

$$\frac{52}{\sqrt{F_y}} = \frac{52}{\sqrt{50}} = 7.35 \quad \text{OK}$$

The permitted web slenderness is dependent on the level of axial stress. The level of axial stress is determined as:

$$\frac{P_u}{\phi_b P_y} = \frac{5.8}{(0.9)(16.8 \times 50)} = 0.008$$

It is less than 0.125; therefore, the ratio $t_w/h_c = 33.0$ for the selected section is less than the limiting width-to-thickness ratio computed as:

$$\frac{253}{\sqrt{F_y}} = \frac{253}{\sqrt{50}} = 35.7 \quad \text{OK}$$

5.3.4.1.2 Link Shear Strength

The forces V_{link} , M_{left} , and M_{right} must not exceed member strength computed from AISC Seismic Sec. 15.2d [15.2]. That section specifies that the required shear strength of the link (V_u) must not exceed the design shear strength ϕV_n , where $V_u = V_{link} = 85.2$ kips and V_n is the nominal shear strength of link. The nominal shear strength of the link is defined as the lesser of:

$$V_p = (0.60F_y)(d-2t_f)t_w$$

and

$$\frac{2M_p}{e}$$

For the W16×57 section selected for the preliminary design:

$$V_p = (0.60)(50)[16.43 - (2)(0.715)](0.430) = 193.5 \text{ kips}$$

and

$$M_p = \phi M_n = 0.9F_y Z_x = (0.9)(50)(105) = 4725 \text{ in.-kips}$$

$$\frac{2M_p}{e} = \frac{(2)(4725)}{(3 \times 12)} = 262.5 \text{ kips}$$

Therefore,

$$V_n = 193.5 \text{ kips}$$

$$\phi V_n = (0.9)(193.5) = 174.2 \text{ ft-kips} > 85.2 \text{ kips} \quad \text{OK}$$

5.3.4.1.3 Link Axial Strength

In accordance with AISC Seismic Sec. 15.2e [15.2], the link axial strength is examined:

$$P_y \text{ of the link} = F_y A_g = (50 \text{ ksi})(16.8 \text{ in}) = 840 \text{ kips}$$

$$0.15P_y \text{ of the link} = (0.15)(840) = 126 \text{ kips}$$

Since the axial demand of 5.7 kips is less than 126 kips, the effect of axial force on the link design shear strength need not be considered. Further, because $P_u < P_y$, the additional requirements of AISC Seismic Sec. 15.f [15.2] do not need to be invoked.

5.3.4.1.4 Link Rotation Angle

In accordance with AISC Seismic Sec. 15.2g [15.2], the link rotation angle is not permitted to exceed 0.08 radians for links $1.6M_p/V_p$ long or less. Therefore, the maximum link length is determined as:

$$1.6M_p/V_p = (1.6)(4725)/(193.5) = 39.1 \text{ in.}$$

Since the link length (e) of 36 in. is less than $1.6M_p/V_p$, the link rotation angle is permitted up to 0.08 radians. From Sec. 5.3.3.2, the link rotation angle, α , was determined to be 0.043 radians, which is acceptable.

5.3.4.1.5 Link Stiffeners

AISC Seismic Sec. 15.3a [15.3] requires full-depth web stiffeners on both sides of the link web at the diagonal brace ends of the link. These serve to transfer the link shear forces to the reacting elements (the braces) as well as restrain the link web against buckling.

Because the link length (e) is less than $1.6M_p/V_p$, intermediate stiffeners are necessary in accordance with AISC Seismic Sec. 15.3b [15.3]. Interpolation of the stiffener spacing based on the two equations presented in AISC Seismic Sec. 15.3b.1 [15.3] will be necessary. For a link rotation angle of 0.08 radians:

$$\text{Spacing} = (30t_w - d/5) = (30 \times 0.430 - 16.43/5) = 9.6 \text{ in.}$$

For link rotation angle of 0.02 radians:

$$\text{Spacing} = (52t_w - d/5) = (52 \times 0.430 - 16.43/5) = 19.1 \text{ in.}$$

For our case the link rotation angle is 0.043 radians, and interpolation results in a spacing requirement of 15.4 in. Therefore, use a stiffener spacing of 12 in. because it conforms to the 15.4 in. requirement and also fits nicely within the link length of 36 in.

In accordance with AISC Seismic Sec. 15.3a [5.3], full depth stiffeners must be provided on both sides of the link, and the stiffeners must be sized as follows:

Combined width at least $(b_f - 2t_w) = (7.120 - 2 \times 0.430) = 6.26$ in. Use 3.25 in. each.
 Thickness at least $0.75t_w$ or 3/8 in. Use 3/8 in.

5.3.4.1.6 Lateral Support of Link

The spacing of the lateral bracing of the link must not exceed the requirement of AISC LRFD Eq. F1-17, which specifies a maximum unbraced length of:

$$L_{pd} = \frac{[3,600 + 2,200(M_1/M_2)]r_y}{F_y} = \frac{[3,600 + 2,200(121.3/127.9)](1.60)}{50} = 182 \text{ in.}$$

Accordingly, lateral bracing of beams with one brace at each end of the link (which is required for the link design per AISC Seismic Sec. 15.5) is sufficient.

In accordance with AISC Seismic Sec. 15.5, the end lateral supports must have a design strength computed as:

$$0.06R_y F_y b_{tf} = (0.06)(1.1)(50)(7.120)(0.715) = 16.8 \text{ kips}$$

While shear studs on the top flange are expected to accommodate the transfer of this load into the concrete deck, the brace at the bottom flange will need to be designed for this condition. Figure 5.3-5 shows angle braces attached to the lower flange of the link. Such angles will need to be designed for 16.8 kips tension or compression.

5.3.4.2 Brace Design

For the design equations used below, see Chapter E. of the AISC LRFD Specification. The braces, determined to be 8×8×5/8 in. tubes with $F_y = 46$ ksi in the preliminary design, are subjected to a calculated axial seismic load of 120 kips (from elastic analysis in Table 5.3-1). Taking the length of the brace conservatively as the distance between panel points, the length is 15.26 feet. The slenderness ratio is

$$\frac{kl}{r} = \frac{(1)(15.26)(12)}{2.96} = 61.9$$

(k has been conservatively taken as 1.0, but is actually lower because of restraint at the ends.)

Using AISC LRFD E2-4 for $F_y = 46$ ksi:

$$\lambda_c = \frac{kl}{r\pi} \sqrt{\frac{F_y}{E}} = \frac{(1)(15.26 \times 12)}{2.96\pi} \sqrt{\frac{50}{29,000}} = 0.817$$

$$F_{cr} = (0.658^{\lambda_c^2}) F_y = (0.658^{0.817^2})(46) = 34.8 \text{ ksi}$$

The design strength of the brace as an axial compression element is:

$$P_{br} = \phi_c A_g F_{cr} = (0.85)(17.4)(34.8) = 514 \text{ kips}$$

AISC Seismic Sec. 15.6a [15.6] requires that the design axial and flexural strength of the braces be those resulting from the expected nominal shear strength of the link (V_n) increased by R_y and a factor of 1.25.

Thus, the factored V_n is equal to $(193.5 \text{ kips})(1.1)(1.25) = 266 \text{ kips}$. The shear in the link, determined from elastic analysis, is 85.2 kips. Thus, the increase is $266/85.2 = 3.12$. Let us now determine the design values for brace axial force and moments by increasing the values determined from the elastic analysis by the same factor:

$$\text{Design } P_{brace} = (3.12)(120) = 374 \text{ kips}$$

$$\text{Design } M_{top} = (3.12)(15.5) = 48.4 \text{ ft-kips}$$

$$\text{Design } M_{bot} = (3.12)(9.5) = 29.6 \text{ ft-kips}$$

The design strength of the brace, 514 kips, exceeds the design demand of 374 kips, so the brace is adequate for axial loading. However, the brace must also be checked for combined axial and flexure using AISC LRFD Chapter H. For axial demand-to-capacity ratio greater than 0.20, axial and flexure interaction is governed by AISC LRFD H1-1a:

$$\frac{P_u}{\phi P_n} + \frac{8}{9} \left(\frac{M_u}{\phi_b M_n} \right) \leq 1.0$$

where

$$P_u = 374 \text{ kips}$$

$$P_n = 514 \text{ kips}$$

$$M_n = ZF_y = (105)(50) = 5250 \text{ in.-kips}$$

The flexural demand, M_u , is computed in accordance with AISC LRFD Chapter C and must account for second order effects. For a braced frame only two stories high and having several bays, the required flexural strength in the brace to resist lateral translation of the frame only (M_{lt}) is negligible. Therefore, the required flexural strength is computed from AISC LRFD C1-1 as:

$$M_u = B_1 M_{nt}$$

where $M_{nt} = 48.4 \text{ ft-kips}$ as determined above and, per AISC LRFD C1-2:

$$B_1 = \frac{C_m}{1 - P_u/P_e} \geq 1.0$$

$$P_e = \frac{A_g F_y}{\lambda_c^2} = \frac{(17.4)(46)}{(0.817)^2} = 1,199 \text{ kips}$$

$$C_m = 0.6 - 0.4 \left(\frac{M_1}{M_2} \right) = 0.6 - 0.4 \left(\frac{29.6}{48.4} \right) = 0.36$$

Therefore,

$$M_u = B_1 M_{nt} = \frac{C_m M_{nt}}{1 - \frac{P_u}{P_e}} = \frac{(0.36)(48.4)}{1 - \frac{374}{1,199}} = (0.52)(48.4) = 25.3 \text{ ft-kips}$$

and

$$\frac{P_u}{\phi P_n} + \frac{8}{9} \left(\frac{M_u}{\phi_b M_n} \right) = \frac{374}{(0.85)(514)} + \frac{8}{9} \left(\frac{(25.3)(12)}{(0.9)(4,830)} \right) = 0.92 < 1.00 \quad \text{OK}$$

The design of the brace is satisfactory.

5.3.4.3 Brace Connections at Top of Brace

AISC Seismic Sec. 15.6 requires that, like the brace itself, the connection of the brace to the girder be designed to remain elastic at yield of the link. The required strength of the brace-to-beam connection must be at least as much as the required strength of the brace. Because there is a moment at the top of the brace, the connections must also be designed as a fully restrained moment connection. The beam, link, and brace centerlines intersect at a common work point, and no part of this connection shall extend over the link length.

The tube may be attached to the girder with a gusset plate welded to the bottom flange of the girder and to the tube with fillet welds. The design of the gusset and connecting welds is conventional except that cutting the gusset short of the link may require adding a flange. (Such a flange is shown in Figure 5.3-5.) Adding a similar flange on the other side of the brace will keep the joint compact. In such a case, it may be required, or at least desirable, to add another stiffener to the beam opposite the flange on the gusset. It also should be remembered that the axial force in the brace may be either tension or compression reflecting the reversal in seismic motions.

In addition to the design of the gusset and the connecting welds, a check should be made of stiffener requirements on the beam web opposite the gusset flanges (if any) and the panel zone in the beam web above the connection. All of these calculations are conventional and need no explanation here. Details of the link and adjacent upper brace connection are shown in Figure 5.3-5.

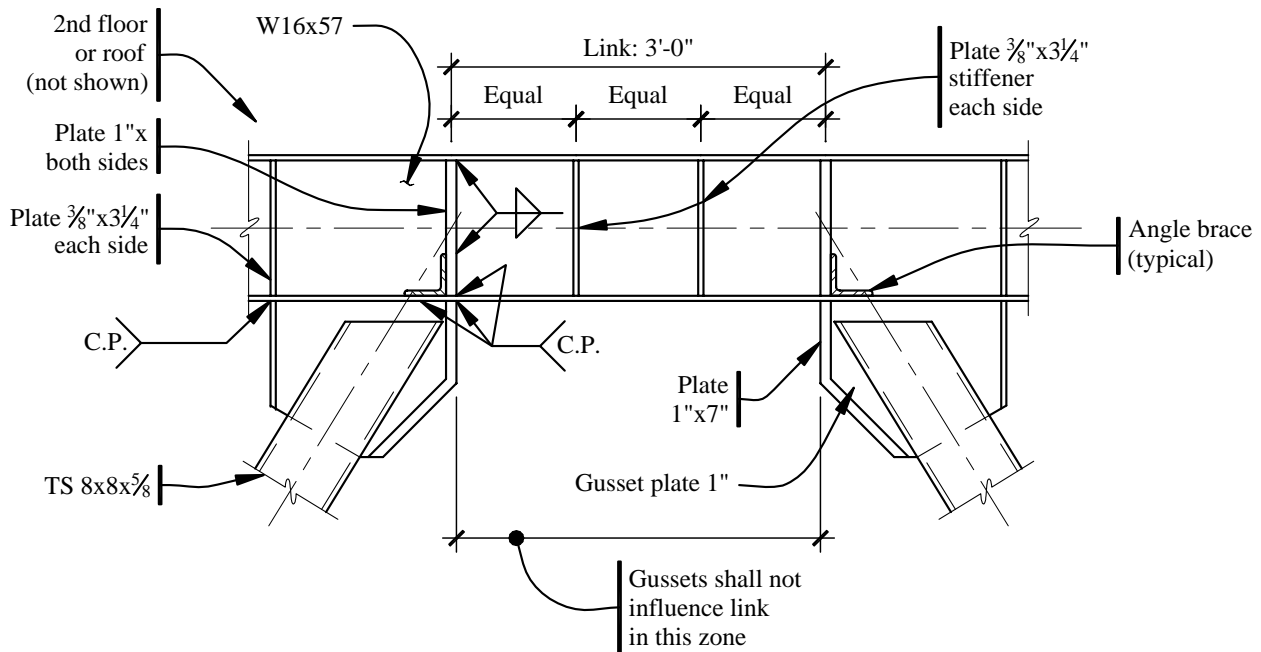


Figure 5.3-5 Link and upper brace connection (1.0 in. = 25.4 mm, 1.0 ft = 0.3048 m).

5.3.4.4 Brace Connections at Bottom of Brace

These braces are concentric at their lower end, framing into the column-girder intersection in a conventional manner.

The design of the gusset plate and welds is conventional. Details of a lower brace connection are shown in Figure 5.3-6. In order to be able to use $R = 8$, moment connections are required at the ends of the link beams (at the roof and second floor levels). Moment connections could be used, but are not required, outside of the EBF (e.g., the left beam in Figure 5.3-6) or at the bottom of the brace at the first floor (e.g., the right beam in Figure 5.3-6 if it is at the first floor level). The beam on the left in Figure 5.3-6 could be a collector. If so, the connection must carry the axial load (force from floor deck to collector) that is being transferred through the beam to column connection to the link beam on the right side, as well as beam vertical loads.

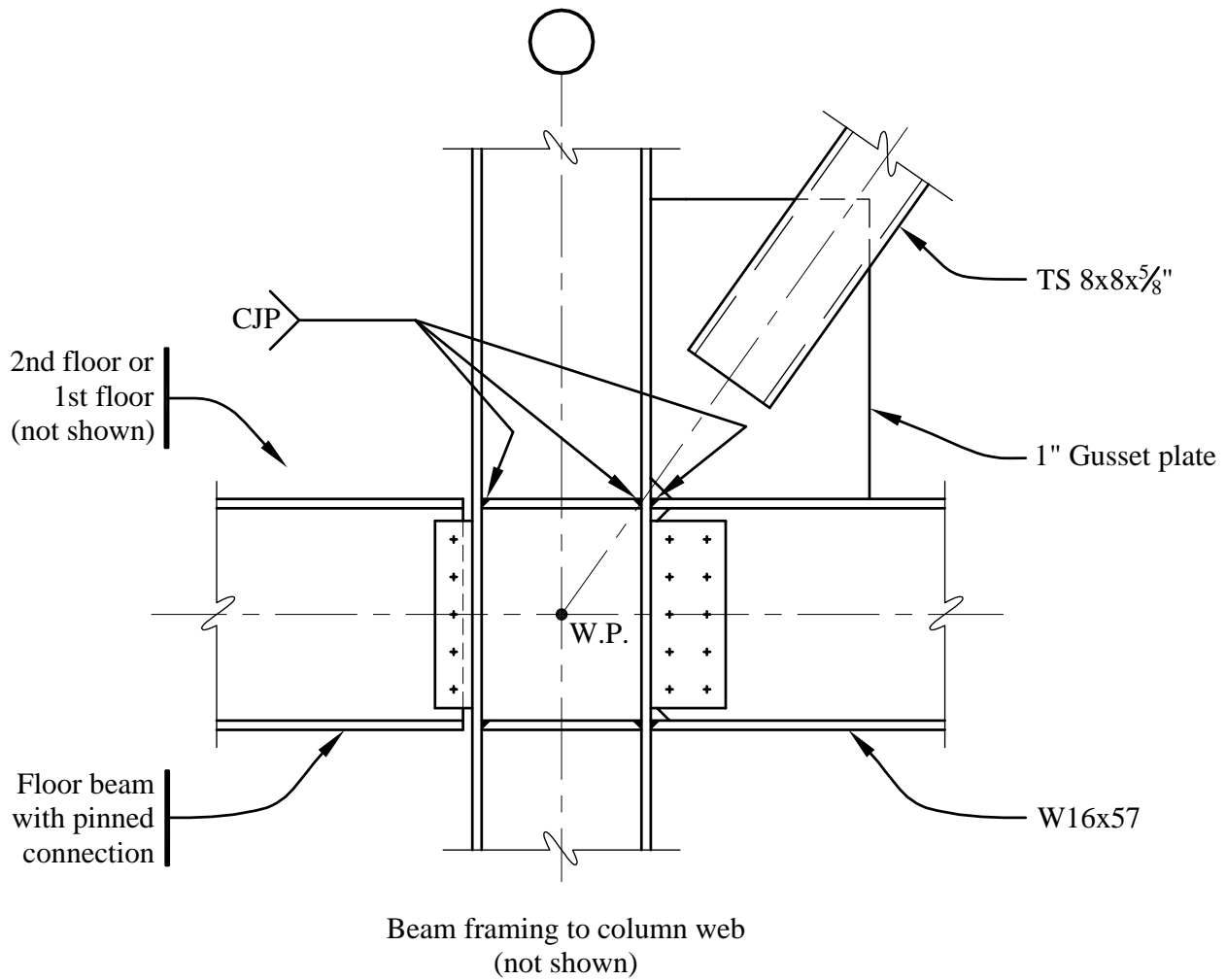


Figure 5.3-6 Lower brace connections (1.0 in. = 25.4 mm).

5.3.4.5 Beam and Column Design

Refer to AISC Seismic Sec. 15.6 for design of the beam outside the link and AISC Seismic Sec. 15.8 for design of the columns. The philosophy is very similar to that illustrated for the brace: the demand becomes the forces associated with expected yield of the link. Although the moment and shear are less in the beam than in the link, the axial load is substantially higher.